

**Engineering of Cytochrome P450
Monooxygenases for the Chemo-, Regio-, and
Stereoselective Oxidation of Complex
Substrates**

Inaugural-Dissertation

zur Erlangung des Doktorgrades
der Mathematisch-Naturwissenschaftlichen Fakultät
der Heinrich-Heine-Universität Düsseldorf

vorgelegt von

Ansgar Bokel
aus Rheda-Wiedenbrück

Mannheim, Juni 2021

aus dem Institut für Biochemie, Lehrstuhl II
der Heinrich-Heine-Universität Düsseldorf

Gedruckt mit der Genehmigung der
Mathematisch-Naturwissenschaftlichen Fakultät der
Heinrich-Heine-Universität Düsseldorf

Berichterstattende:

1. Prof. Dr. Vlada B. Urlacher

2. Prof. Dr. Karl-Erich Jäger

Tag der mündlichen Prüfung:

22. November 2021

Eidesstattliche Erklärung

Ich, Herr Ansgar Bokel, versichere an Eides statt, dass die vorliegende Dissertation „Engineering of Cytochrome P450 Monooxygenases for the Chemo-, Regio-, and Stereoselective Oxidation of Complex Substrates“ von mir selbstständig und ohne unzulässige fremde Hilfe unter Beachtung der „Grundsätze zur Sicherung guter wissenschaftlicher Praxis an der Heinrich-Heine-Universität Düsseldorf“ erstellt worden ist.

Diese Dissertation wurde weder in dieser noch in ähnlicher Form bei einer anderen Fakultät eingereicht. Bisher habe ich keine erfolglosen oder erfolgreichen Promotionsversuche unternommen.

Ansgar Bokel

„Ich will keine Antwort haben
Denn Antworten begraben
Nur all die schönen Fragen unter sich“

Fabian Römer

For Lili.

It's not what I have but who I have in my life that matters most.

I. Conference Contributions

Bokel, A., Le-Huu, P., Petrović, D., Strodel, B., & Urlacher, V. B. Multiple selective hydroxylation of the macrocyclic diterpenoid β -cembrenediol catalyzed by P450 BM3 mutants. *International Conference on Cytochrome P450 (ICCP)*. Düsseldorf, Germany, August 27-31, 2017.

Bokel, A., & Urlacher, V. B. Engineering of a CYP154 Family Member for Regio- and Stereoselective Hydroxylation of Ketamine. *International Symposium on Cytochrome P450 Biodiversity and Biotechnology*. York, Great Britain, July 15-19, 2018.

Poster was awarded with a poster prize

Bokel, A., & Urlacher, V. B. Engineering of CYP154E1 Monooxygenase for highly Regio- and Stereoselective Hydroxylation of (S)-Ketamine. *International Symposium on Biocatalysis and Biotransformations (BioTrans)*. Groningen, Netherlands, July 7-11, 2019.

II. List of Publications

Petrović, D., **Bokel, A.**, Allan, M., Urlacher, V. B., & Strodel, B. (2018). Simulation-guided design of cytochrome P450 for chemo- and regioselective macrocyclic oxidation. *Journal of chemical information and modeling*, 58(4), 848-858.

Le-Huu, P. *, Rekow, D. *, Krüger, C., **Bokel, A.**, Heidt, T., Schaubach, S., Claasen, B., Hölzel, S., Frey, W. & Urlacher, V. B. (2018). Chemoenzymatic route to oxyfunctionalized cembranoids facilitated by substrate and protein engineering. *Chemistry—A European Journal*, 24(46), 12010-12021.

*both authors contributed equally.

Bokel, A., Rühlmann, A., Hutter, M. C., & Urlacher, V. B. (2020). Enzyme-mediated two-step regio- and stereoselective synthesis of potential rapid-acting antidepressant (2*S*,6*S*)-hydroxynorketamine. *ACS Catalysis*, 10(7), 4151-4159.

Bokel, A., Hutter, M. C., & Urlacher, V. B. (2021). Molecular evolution of a cytochrome P450 for the synthesis of potential antidepressant (2*R*,6*R*)-hydroxynorketamine. *Chemical Communications*, 57(4), 520-523.

Publication that is not included in this work

Bakkes, P. J., Biemann, S., **Bokel, A.**, Eickholt, M., Girhard, M., & Urlacher, V. B. (2015). Design and improvement of artificial redox modules by molecular fusion of flavodoxin and flavodoxin reductase from *Escherichia coli*. *Scientific Reports*, 5, 12158.

Luelf, U. J., Reiss, G. J., **Bokel, A.**, & Urlacher, V. B. (2021). Selective Biocatalytic Synthesis and Crystal Structure of (2*R*,6*R*)-Hydroxyketaminium Chloride, C₁₃H₁₇Cl₂NO₂. *Zeitschrift für Kristallographie-New Crystal Structures*. <https://doi.org/10.1515/ncrs-2021-0055>.

III. Table of Contents

| | |
|---|------|
| I. Conference Contributions | V |
| II. List of Publications..... | VI |
| III. Table of Contents | VIII |
| IV. Zusammenfassung..... | X |
| V. Abstract..... | XII |
| 1. Introduction..... | 1 |
| 1.1 Biocatalysis | 1 |
| 1.1.1 Advantages of Biocatalysts over Chemocatalysts | 3 |
| 1.2 Cytochrome P450 Monooxygenases | 5 |
| 1.2.1 Redox Partner Systems of P450 | 5 |
| 1.2.2 P450 Catalytic Mechanism | 7 |
| 1.2.3 P450 Structure..... | 11 |
| 1.2.4 CYP154 Family..... | 14 |
| 1.2.5 CYP102A1 – P450 BM3 | 15 |
| 1.2.6 Industrial Applications of P450s | 16 |
| 1.2.7 Limitations of P450s and Engineering of Selectivity | 19 |
| 1.3 Objective of the Thesis | 26 |
| 2. Results..... | 28 |
| 2.1 Chapter I | 29 |
| 2.2 Chapter II | 39 |
| 2.3 Chapter III | 44 |
| 2.4 Chapter IV..... | 56 |
| 3. General Discussion and Outlook | 69 |

| | |
|--|-----|
| 3.1 Semirational Protein Design for the Selective Oxidation of (<i>S</i>)- and (<i>R</i>)-Ketamine | 70 |
| 3.2 Comparison of CYP154E1 QAA and TQA – Enantiodivergency | 72 |
| 3.3 Whole-Cell Biocatalysis..... | 74 |
| 3.4 Rational Protein Design for the Selective Oxidation of β -Cembrenediol | 77 |
| 3.5 Substrate Engineering for the Selective Oxidation of Macrocycles | 79 |
| 3.6 Comparison between Chemical and Biocatalytic Syntheses..... | 82 |
| 3.7 Conclusion | 85 |
| 4. Bibliography | 86 |
| 5. Abbreviations..... | 101 |
| 6. Acknowledgments | 102 |
| 7. Supplementary Data Chapter I-IV..... | 105 |

IV. Zusammenfassung

Die selektive Oxidation inerter, nicht-aktivierter Kohlenwasserstoffverbindungen ist eine grundlegende Reaktion bei der Funktionalisierung von organischen Verbindungen. Cytochrom P450 Monooxygenasen (P450 oder CYPs) gehören zu den wenigen Enzymen, die diese anspruchsvolle Reaktion an (zyklischen) Alkanen, Terpenoiden, oder anderen industriell bedeutsamen Verbindungen katalysieren können und stellen somit eine der vielversprechendsten Enzyme im Bereich der Biokatalyse dar. Allerdings findet nur ein Bruchteil aller P450 Anwendung in der industriellen Biokatalyse. Einer der Gründe liegt darin, dass P450 mit nicht-natürlichen Substraten oftmals nur geringe bis moderate Selektivitäten und Aktivitäten zeigen. Mit Beginn der zweiten Welle der Biokatalyse nach Bornscheuer sind eine Vielzahl an Methoden und Strategien im Bereich des Protein Engineerings verfügbar geworden, um Enzyme durch eben diese Steigerung der Selektivität und Aktivität für die industrielle Nutzbarkeit zu optimieren.

In dieser Arbeit kamen verschiedene Strategien des Protein Engineerings zum Einsatz, um gezielt die Selektivität und Aktivität der Monooxygenasen CYP154E1 und CYP102A1 (P450 BM3) bei der Oxidation von Ketamine beziehungsweise Cembranoiden zu steigern und deren Anwendung für die Biokatalyse zu demonstrieren.

Schwere depressive Störung ist eine ernste und weltweit verbreitete Erkrankung. Dementsprechend hoch ist der Bedarf an wirksamen Antidepressiva. In **Kapitel I** und **II** werden CYP154E1 Varianten beschrieben, die durch die Mutagenese von Aminosäuren in der „first-sphere“ des aktiven Zentrums erzeugt wurden und die ausgehend von (*S*)- und (*R*)-Ketamin äußerst selektiv in einem Zweistufenprozess die potentiellen Antidepressiva (*2S,6S*)- (**Kapitel I**) und (*2R,6R*)-Hydroxynorketamine (**Kapitel II**) synthetisieren.

Unter der Annahme, dass die Regioselektivität einer P450-katalysierten Reaktion maßgeblich durch die Bindung des Substrates im aktiven Zentrum beeinflusst wird, wird in **Kapitel III** die Entwicklung eines simulations-unterstützten Arbeitsablaufs zum Design chemo- und regioselektiver P450 BM3 Varianten für die Oxidation des pharmazeutisch interessanten Cembranoids β -Cembrenediol beschrieben. In **Kapitel IV** wird die Beschreibung der Oxyfunktionalisierung von Cembranoiden durch P450 BM3 fortgeführt. Darin wird sowohl die chemische mit der enzymatischen Synthese,
X

als auch das Substrat- mit dem „first-sphere“ Protein Engineering vereint. Auf diese Weise wurde eine P450 BM3 Variante erzeugt, die 100% Diastereoselektivität bei der Hydroxylierung eines Cembranoid-Derivats zeigte.

Zusammenfassend untermauert diese Arbeit die Effektivität der „first-sphere“ Mutagenese zur Selektivitäts- und Aktivitätssteigerung und erweitert die Eignung von P450 Monooxygenasen für die Biokatalyse.

V. Abstract

The selective oxidation of inert, non-activated hydrocarbon compounds is a fundamental reaction in the functionalization of organic molecules. Cytochrome P450 monooxygenases (P450s or CYPs) belong to the few enzymes which can catalyze this challenging reaction on both cyclic and linear alkanes, terpenoids, or other industrially important compounds and are therefore among the most promising enzymes in the field of biotechnology. However, only a fraction of all P450s finds its application in such an environment. One of the reasons is that P450s often exhibit only low to moderate selectivities and activities with non-natural substrates. Since the beginning of the so-called second wave of biocatalysis according to Bornscheuer, various protein engineering methods and strategies have become available to optimize enzymes for industrial utility, including increasing their selectivity and activity.

In this thesis, various protein engineering strategies were employed to specifically enhance the selectivity and activity of the two monooxygenases CYP154E1 and CYP102A1 (P450 BM3) in the oxidation of ketamine and cembranoids, respectively, and to demonstrate their application in biocatalysis.

Major depressive disorder is a severe and globally prevalent mental disorder, and the need for effective antidepressants is accordingly high. **Chapter I** and **II** describe the construction of two CYP154E1 variants by using first-sphere active site mutagenesis. These variants enable the highly chemo-, regio- and stereoselective two-step oxidation either of (S)- or (R)-ketamine, yielding the potential antidepressants (2*S*,6*S*) (**Chapter I**), and (2*R*,6*R*)-hydroxynorketamine (**Chapter II**).

Assuming that the regioselectivity of a P450-catalyzed reaction is significantly influenced by the binding of the substrate in the active site, a simulation-based workflow was developed and applied for the design of P450 BM3 variants for the chemo- and regioselective oxidation of the pharmaceutically interesting cembranoid β -cembrenediol as examples, as described in **Chapter III**. **Chapter IV** describes an approach combining substrate engineering of various cembranoid compounds with first-sphere active site mutagenesis of P450 BM3 to achieve highly selective hydroxylation. The result was a P450 BM3 variant with absolute diastereoselectivity in the hydroxylation of a cembranoid derivative.

In summary, this thesis demonstrates the effectiveness of the first-sphere mutagenesis for selectivity and activity enhancement and extends the suitability of P450 monooxygenases for biocatalysis.

1. Introduction

1.1 Biocatalysis

Biocatalysis can be defined as the application of microbes and enzymes thereof in synthetic chemistry.^{1, 2} Enzymes catalyze reactions essential in all living systems to maintain life and reproduction.³ The seminal discovery that they can also act independently from the living cell, which occurred in the late 19th century to the early 20th century, initiated the first wave of biocatalysis proposed by Bornscheuer *et al.*¹ In 1894, when it had not yet been established that enzymes are proteins, Emil Fischer proposed the “lock and key” concept between enzymes and their substrates, thereby introducing specificity as a variable in enzyme characteristics.⁴ In analogy to a key, only a substrate with a suitable form can fit into the respective active site, which acts as the keyhole or lock.⁵ This model was extended in 1958 by the “induced-fit model”, which states that substrate binding causes a three-dimensional alteration of the enzyme and brings the catalytic residues into proper alignment with the substrate.^{6, 7} Simultaneously, the impact of enzymes on industry and everyday life started to increase steadily. At the end of the 19th century, isomaltose, used in food and beverage production, was synthesized enzymatically, and, in the early 20th century, pancreatic proteases were utilized in the leather industry. Around the middle of the 20th century, detergent proteases were developed, and enzymes emerged in the pharmaceutical industry with the synthesis of penicillin derivatives,⁴ just to mention a few examples.

From the middle until the end of the 20th century, biocatalysis experienced another extension through the inventions arising from several revolutionary discoveries and technologies in molecular biology: the decoding of the DNA structure by James Watson and Franklin Crick in 1953,⁸ the discovery and usage of restriction enzymes,^{9, 10} the construction of the first recombinant plasmid,¹¹ Sanger sequencing,¹² as well as the application of the polymerase chain reaction (PCR). These molecular technologies enabled the cloning for virtually every protein found in nature and subsequently its production in significant amounts¹³ and paved the way for the second wave of biocatalysis and modern biotechnology.

During the second wave of biocatalysis that, according to Bornscheuer *et al.* 2012,¹ lasted 15 – 20 years between the 1980s and the 1990s, knowledge of the three-dimensional protein structure combined with DNA manipulation techniques led to the

development of the first methods of protein engineering. Protein engineering was successfully applied in broadening the substrate spectrum of enzymes towards non-physiological substrates, thereby expanding their use to synthesize of, for example, pharmaceutical intermediates and fine chemicals.¹

The work of Pim Stemmer and Francis Arnold in the 1990s instigated the third and current wave of biocatalysis. The molecular biology methods of that time, nowadays called directed evolution, made the power of Darwinian evolution accessible to the scientific community and resulted in the rapid modification of biocatalysts towards desired properties without the need for knowledge about three-dimensional protein structure.¹ Generally, directed evolution starts with the creation of a library consisting of randomly mutated genes. The resulting protein variants are then screened for improvements in the desired property or properties, and the respective gene(s) is (are) iteratively selected for additional cycles of random mutagenesis and screening (for a detailed description, see Section 1.2.7).¹⁴ Directed evolution enabled rapid enzyme engineering for higher thermal and solvent stability, or enhanced activity and selectivity, turning biocatalysts into attractive alternatives to chemocatalysts in industrial processes. The significance of this invention was recently honored by awarding the Nobel Prize in chemistry to Frances H. Arnold, George P. Smith, and Gregory Winter for making use of the power of evolution for protein engineering.¹⁵

At this point, it is speculative to question what the fourth wave of biocatalysis will bring, but it is almost certain to come sooner or later.¹⁶ For instance, Arnold and colleagues recently brought “silicon to life” (Kan *et al.*, 2016)¹⁷ by engineering a cytochrome c from *Rhodothermus marinus* to catalyze the formation of carbon-silicon bonds – a bond that is entirely unknown in nature.¹⁷ Alternatively, the fourth wave might include stepping further from (re-)engineering existing enzymes to designing enzymes with new functions *de novo*.¹⁸ A methodology based on the physical principles that underly protein folding to generate/design new proteins unrelated to nature and is “coming of age” due to advances in computational methods and power.¹⁹ For example, Donnelly *et al.* recently designed Syn-F4, a synthetic ferric enterobactin esterase that hydrolyzes ferric enterobactin and thereby releases vital iron for the cell. Syn-F4 is the first *de novo* enzyme catalytically active *in vitro* and *in vivo*, key for synthetic biology.²⁰ But already several years before, Baker and colleagues *de novo* designed an enzyme capable of the catalyzation of a bimolecular Diels-Alder reaction, a reaction that no natural enzyme has been described to catalyze before.²¹

1.1.1 Advantages of Biocatalysts over Chemocatalysts

Biocatalysis has been successfully integrated into various industrial branches, and the field of biocatalysis permanently evolves as outlined in the market forecast for biocatalysis.^a In comparison to chemocatalysts, biocatalysts offer several advantages: First of all, biocatalysts are environmentally friendly since they are sustainably produced from renewable sources, usually non-toxic, and fully biodegradable.²²

Secondly, biocatalysts usually operate in an aqueous environment under mild reaction conditions such as physiological temperature and pH, which reduces the use of toxic solvents and might decrease energy consumption during biocatalytic processes.²³ Nevertheless, it is worthwhile to mention that some biocatalytic reactions require the use of organic solvents because of poor substrate solubility in aqueous media or harsher reaction conditions (e.g., enzymes as detergent additives need to be active at 60°C and pH 9-11).²⁴ Therefore, enzymes from extreme environments (extremophilic enzymes) represent excellent candidates for industrial application.²⁵

Thirdly, biocatalysts often possess broad substrate spectra or are at least not restricted to just one substrate.²³ In addition to the more than 8,000 different enzyme types known to date,^b this circumstance highlights their enormous biological variety and potential.

Finally, biocatalysts often exhibit high chemo-, regio-, and stereoselectivity. On the contrary, chemocatalysts often do not display such high selectivities, which makes the introduction of protecting groups during chemical syntheses often necessary though not desired. The use of highly selective enzymes makes the use of protection/deprotection manipulations redundant.^{22, 26} Higher selectivity also means fewer side products, which simplifies the product's recovery. Furthermore, enzymes are biopolymers that are composed of many amino acids. By replacing specific amino acids or even entire protein elements through protein engineering, its properties can be changed according to the desired needs.²²

^a World Biocatalysis & Biocatalyst Market Analysis to 2024 - Market Forecast to Grow at a CAGR of 15% from 2019 to 2024; <https://www.globenewswire.com/news-release/2020/06/17/2049282/0/en/World-Biocatalysis-Biocatalyst-Market-Analysis-to-2024-Market-Forecast-to-Grow-at-a-CAGR-of-15-from-2019-to-2024.html>

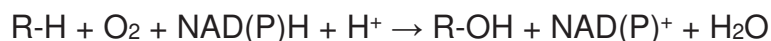
^b All enzymes in BRENDA™; https://www.brenda-enzymes.org/all_enzymes.php

In 2002, biocatalysts were involved in more than 134 biotechnological processes – with an upward tendency.²⁷ The analysis of the enzymes, which were utilized in these processes, revealed a discrepancy in the distribution of the enzyme classes and therefore revealed limitations of biocatalysts for industrial application. Enzymes are categorized in seven classes, namely oxidoreductases (EC 1.x.x.x), transferases (EC 2.x.x.x), hydrolases (EC 3.x.x.x), lyases (EC 4.x.x.x), isomerases (EC 5.x.x.x), ligases (EC 6.x.x.x), and translocases (EC 7.x.x.x). Among all classes, hydrolases already contribute to almost 50% of the 134 biotechnological processes.²⁷ They are highly attractive enzymes for synthetic chemistry due to their independence on cofactors, often the commercial availability and tolerance for organic solvents.²⁸ In contrast, cytochrome P450 monooxygenases (P450s or CYPs), belonging to the enzyme class of oxidoreductases (EC 1.14.-.-), are recognized as “potentially amongst the most useful of all enzymes to exploit as industrial biocatalysts” (Lundemo and Woodley, 2015),²⁹ but play only a subordinate role in biotechnological processes. Their dependency on costly cofactors, low activity, and stability are limiting factors that prevent P450s from being fully exploited as biocatalysts.^{27, 30}

However, P450 enzymes can be engineered and improved for biotechnological approaches in terms of higher activity, stability, and overall process efficiency. For instance, Arnold and colleagues engineered the P450 BM3, and Wong and colleagues engineered the P450_{cam}, for hydroxylation of small alkanes,^{31, 32} an essential step in the conversion of gas to fuels and chemicals,³³ or Fasan and colleagues engineered P450 BM3 for selective C6 and C7 hydroxylation of the antimalarial artemisinin to potentially increase its half-life in the human body,³⁴ just to mention a few out of the vast number of examples of beneficial P450 engineering. Despite the achievements in the engineering of P450 enzymes, highly stereo- and particularly regioselective oxidations at predetermined positions of a substrate with several equivalent positions for oxidation remains a challenging task. Moreover, the complex organization of P450 enzymes (discussed in the next chapters) requires much effort, time, and expense, and each approach (enzyme, substrate, demand) needs to be investigated individually. Therefore, I hereby demonstrate different protein engineering strategies with different P450 enzymes and substrates to contribute to the overall progress made in protein engineering and to reveal the potential of P450s in biocatalysis. The following chapters of the introduction will provide a short overview of cytochrome P450 monooxygenases and how they can be improved for biocatalysis.

1.2 Cytochrome P450 Monooxygenases

Cytochrome P450 monooxygenases (P450s or CYPs) are heme b containing oxidoreductases (EC 1.14.-.-) found in all kingdoms of life³⁵ and even in viruses.³⁶ Heme is a protoporphyrin IX with four nitrogen atoms coordinating a central iron ion. Heme is linked to the protein in the active center via coordination of the iron ion via an axial, highly conserved cysteine residue (see Section 1.2.2). When carbon monoxide (CO) binds to the reduced heme iron as the distal, sixth ligand, a Soret peak at around 450 nm appears. This characteristic in absorption is eponymous for P450s, where “P” stands for pigment.³⁷ P450s are versatile biocatalysts that catalyze the reductive cleavage of molecular oxygen by introducing one oxygen atom into the substrate, whereas the second oxygen atom is reduced to water (Scheme 1). The most commonly observed reactions are the chemically challenging non-activated C-H bond hydroxylation (Scheme 1) or C=C double bond epoxidation. However, depending on the substrate’s nature, reactions like sulfoxidation, oxidative deamination, and *N*- or *O*-dealkylation can occur.³⁸ The cofactors NADH or NADPH ultimately provide electrons required for this reaction and, in most cases, are transferred via redox proteins to the catalytic heme iron.



Scheme 1. General equation of a hydroxylation catalyzed by cytochrome P450 monooxygenases.

The functions of P450s in various organisms are diverse. These enzymes are involved in the metabolism of endo- and exogenous xenobiotics, in C-source assimilation, and the synthesis of secondary metabolites.^{39, 40} Especially in the latter case, P450s are well known for their ability to catalyze these reactions with high regio- and stereoselectivity, which makes them very attractive biocatalysts in biotechnology.

1.2.1 Redox Partner Systems of P450

As already mentioned above, P450s require electrons for the reductive cleavage of molecular oxygen and subsequent substrate monooxygenation. To achieve this, most P450s interact with one or more redox partner proteins to receive the required electrons from NAD(P)H.⁴¹ Depending on the organization of the electron transfer

system, P450s are categorized in ten different classes and consist either of a three-, two-, or one-component P450 system.⁴² In relevance for this thesis, only the three-component P450 system of class III and the one-component P450 system of class VIII are described in the following (Figure 1).

A three-component P450 system is characteristic for most bacterial and mitochondrial P450s.⁴² The three-component P450 system of class III includes, besides the P450, a flavin adenine dinucleotide (FAD) containing reductase and a flavin mononucleotide (FMN) containing flavodoxin. The electron transfer happens in the order of the donor NAD(P)H via the reductase to the flavodoxin from which the electrons are transferred to the cytochrome P450. All components are soluble and localized in the cytosol.⁴² For the herein reported CYP154E1, an artificial class III, three-component system consisting of the flavodoxin reductase (FdR) from *E. coli* and the flavodoxin (YkuN) from *Bacillus subtilis*⁴³ were used in this thesis to compensate for the lack of physiological redox partners. Yet, CYP154E1 cannot be clearly categorized into class III since there are other reports available demonstrating electron acceptance via class I ferredoxin (putidaredoxin) or even class II cytochrome P450 reductase (CPR, diflavin redox protein containing both FAD and FMN).⁴⁴

The one-component P450 system of class VIII can be found in prokaryotes and lower eukaryotes and constitutes of a NAD(P)H-dependent diflavin cytochrome P450 reductase (CPR) fused via a linker to the C-terminus of the heme domain. The first and well-known example of this class is P450 BM3 (CYP102A1) (Section 1.2.5) from *Bacillus megaterium* and the second P450 enzyme of this thesis.⁴⁵

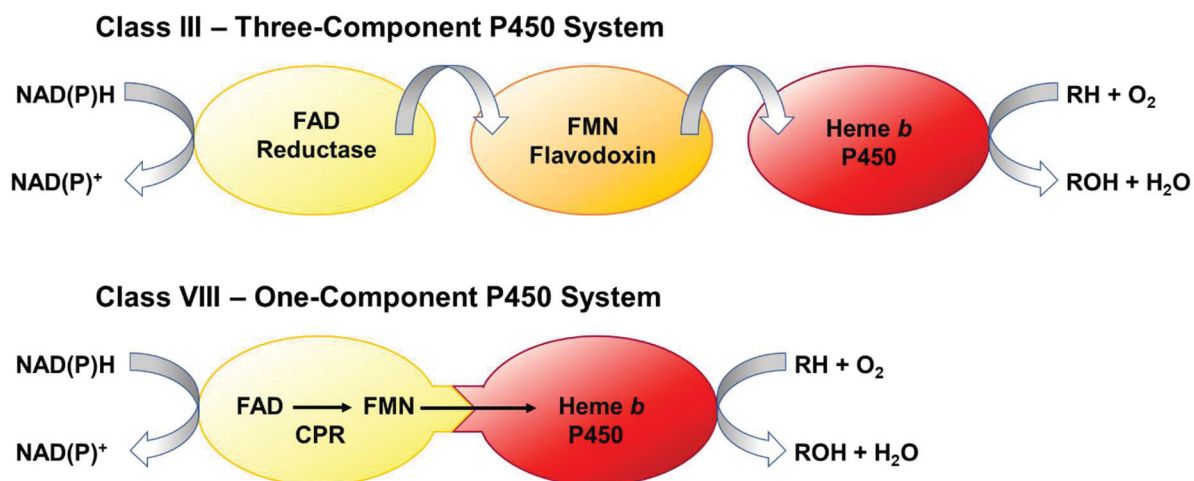


Figure 1. Schematic organization of class III (Three-Component P450 System) and class VIII (One-Component P450 System) adapted from Urlacher and Girhard 2012.⁴⁶ Class III: redox system consisting of a flavin adenine dinucleotide (FAD) containing reductase, a flavin mononucleotide (FMN) containing flavodoxin, and a heme b containing P450 enzyme. Class VIII: Fusion between a diflavin reductase (CPR, cytochrome P450 reductase) and a P450.

1.2.2 P450 Catalytic Mechanism

The classical mechanism for P450-catalyzed substrate hydroxylation is shown in Figure 2 and includes nine states. At the beginning of the catalytic cycle, the P450 is in a resting state, and the active site is filled with a hydrogen bonding cluster of several water molecules.⁴⁷ The heme iron is in a ferric Fe³⁺ form and coordinated by four nitrogen atoms of the porphyrin, an axial sulfur atom provided by the conserved cysteine residue (see Section 1.2.3), and a water molecule as the distal ligand. In this state, heme iron is in a low-spin configuration **(1)**. Upon binding, the substrate displays the distal water, which destabilizes the iron-water coordination and leaves the iron in a five-coordinated, high-spin configuration **(2)**.⁴⁸ This shift in spin state causes alterations in optical absorption spectra, shifting the absorption maximum from 415-417 nm in the low-spin configuration to 390-394 nm in the high-spin configuration.⁴⁸ This characteristic is used to record substrate binding by the titration of P450 with a substrate, which gives the Type I spectrum.

The switch in spin-states also increases the redox potential of the iron and therefore enables the first single electron reduction of ferric (Fe³⁺) form to a ferrous (Fe²⁺) high-spin complex **(3)**.⁴⁹ Dioxygen binding leads to species designated as ferrous dioxygen (Fe²⁺-OO) or a ferric superoxide (Fe³⁺-OO⁻) complex **(4)**.⁵⁰ After the second single electron reduction, the ferrous peroxy complex (Fe³⁺-OO²⁻) **(5)** is formed, whose

protonation results in the ferric hydroperoxo complex, also referred to as *compound 0* (**6**). The second protonation of the distal oxygen results in a heterolytic cleavage of the O-O bond, thereby yielding one water molecule and the highly reactive intermediate Fe-IV-Oxo-porphyrin-radical complex (**7**). This reactive intermediate, also referred to as *compound I*, has the outstanding ability to activate inert C-H bonds.⁵¹ At this stage, the actual substrate oxidation via the commonly accepted oxygen rebound mechanism begins. Groves and McClusky initially proposed this mechanism in 1976.⁵² *Compound I* abstracts a hydrogen radical from the substrate resulting in a Fe-IV-Hydroxo complex (*compound II*) (**8**), leaving behind the substrate with a carbon radical. Via radical recombination, the hydroxylated product is formed (**9**), whose release regenerates the low-spin ferric enzyme (**1**).⁵³⁻⁵⁵

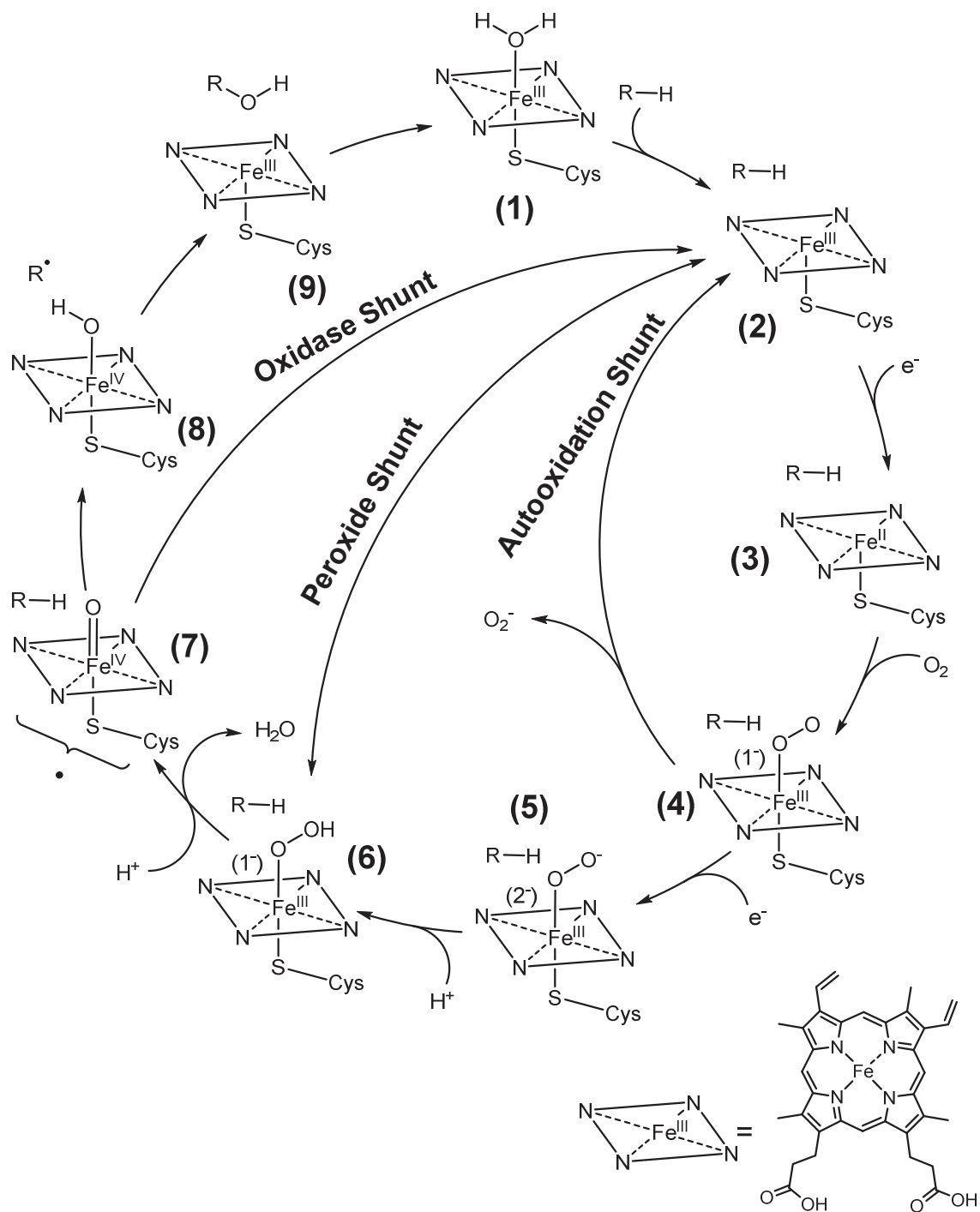


Figure 2. Catalytic reaction cycle of P450 monooxygenases adapted from Krest et al. 2013.⁵⁶ (1) Resting state (low-spin) ferric. (2) Substrate displays water ligand inducing structural alterations, which lead to a high-spin ferric species (transition between spin states causes alterations in absorption properties). (3) Firstly, one-electron reduction results in a ferrous high-spin complex (4) enabling binding of molecular oxygen. (5) Secondly, one-electron reduction forms the ferrous peroxo complex, whose protonation results in the ferric hydroperoxo complex (*compound 0*) (6). Second protonation and water cleavage form the catalytically active *compound I* (7). Abstracting a hydrogen radical from the substrate results in *compound II* (Fe-IV-Hydroxo complex) and a substrate radical (8). The latter rebounds to the hydroxo-complex and exits the active site as the hydroxylated product (9), leaving the heme iron in its resting state (1).

Besides the aliphatic hydroxylation, *N*-dealkylation of amines is another essential reaction of P450s. The P450 catalyzed *N*-dealkylation of amines (described in chapters I and II) involves two steps (Figure 3 A). During the first enzymatic step (Figure 3 A, Step 1), the amine is converted into a hemiaminal which is then, in a second non-enzymatic step, decomposed to a carbonyl derivate and an amine with a by one reduced alkylation stage (Figure 3 A, Step 2).⁵⁷ In the case of ketamine's methylamino group in chapters I and II, formaldehyde is formed as the carbonyl derivate. For the P450-catalyzed *N*-dealkylation, two mechanisms have been debated in the literature. The single electron transfer (SET) mechanism starts with initial one-electron oxidation of the amine, thereby generating a radical cation of the nitrogen. Subsequent deprotonation leads to an α -amino radical, which rebounds to form the hydroxylated product, whose release regenerates the enzymes' resting state.⁵⁸⁻⁶⁰ The second mechanism starts with an initial hydrogen atom transfer (HAT), directly producing the α -amino radical.⁶¹⁻⁶³ The remaining steps of the mechanism resemble those of the SET mechanism.

C=C double bond epoxidation also belongs to the repertoire of P450s (described in chapter III). Starting with *compound I*, the first step of C-O bond formation is rate determining.⁶⁴ This step forms a radical at the second carbon of the initial C=C double bond (Figure 3 B). Subsequent ring closure between the radical and the oxygen forms the epoxide product, which, after its release, leaves the Fe-III complex resting state behind.^{64, 65}

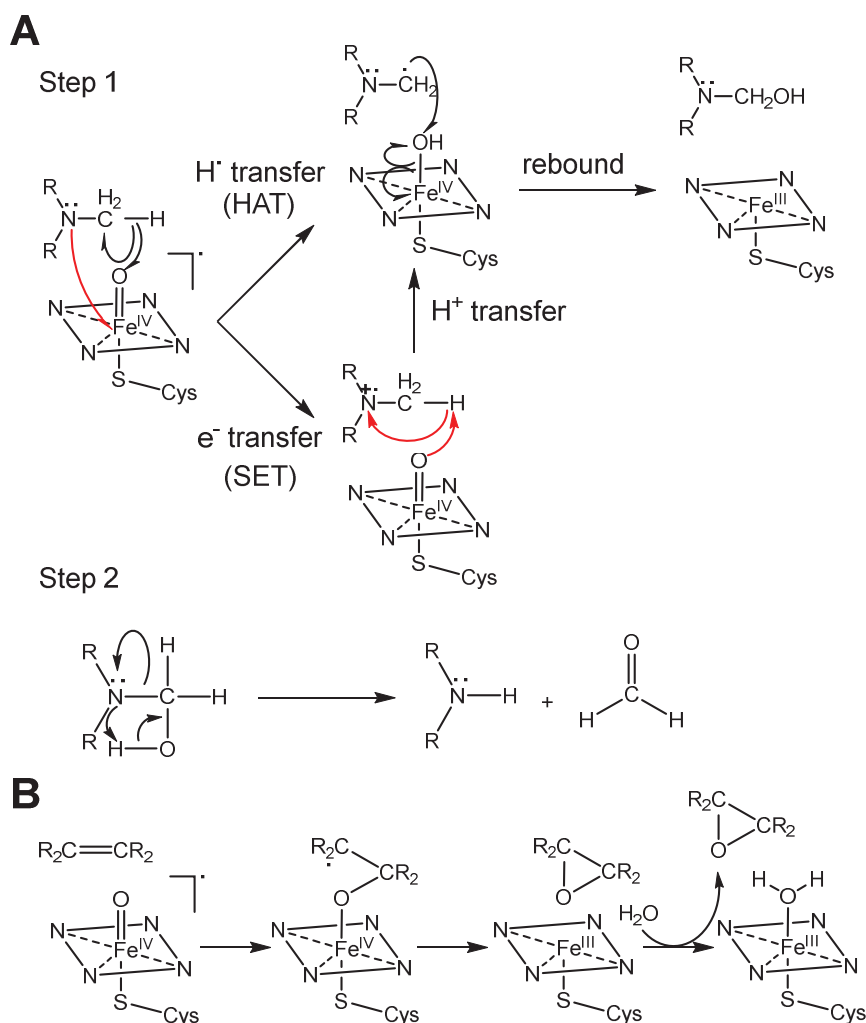


Figure 3. Mechanism of *N*-demethylation mechanism (A) adapted from Wang et al.⁵⁷ and C=C double bond epoxidation (B) adapted from Kumar et al..⁶⁴ HAT: hydrogen atom transfer; SET: single electron transfer. Red arrows describe the SET mechanism.

The catalytic cycle of P450s contains three branches on which side reactions can occur that uncouple the NAD(P)H consumption from substrate oxidation. These *shunt pathways* are the autoxidation of species (4) with the release of a superoxide anion (O_2^-), the dissociation of hydrogen peroxide from (6) in the peroxide shunt, and the release of water from (7) in the oxidase shunt.⁵⁰ All of those side reactions transfer the P450 back into its resting state (1).

1.2.3 P450 Structure

All P450s maintain an overall conserved three-dimensional structure – the so-called P450 fold. This P450 fold basically contains 13 α -helices (α A, α B, α B' and α C-L) and 4-5 β -sheets (β 1 - β 5) (Figure 4). β -sheets are often numbered with two Arabic

numerals, which are separated by a dash [e.g., β 4-1], whereby the first number represents the occurrence in the structure from N-terminus to C-terminus, and the latter represents the strain. Although the overall fold is conserved, individual structural elements may differ significantly.⁶⁶ These variations mainly occur in regions controlling the substrate specificity. For instance, comparing the structures of P450_{cam} from *Pseudomonas putida* and P450_{eryF} from *Saccharopolyspora erythraea*, the α B' helix is rotated by about 90°,⁶⁶ or in other cases, this helix is replaced by a loop like in the human CYP2C9.⁶⁷ At the same time, these variable structural elements, especially α B', α F, and α G helices, are highly flexible and can undergo substantial movements enabling substrate entrance and product release.⁶⁸ The closer to the heme group, the more conserved the P450 structure. Essential elements which need to be mentioned here are related to the heme binding. Firstly, the helices α I and α L, which directly contact the heme, retaining it in its place, and secondly the conserved cysteine residue found in the so-called “P450-signature” (Phe-XX-Gly-X_b-XX-Cys-X-Gly) in the Cys-pocket.⁶⁰ This cysteine residue acts as the fifth axial ligand to the central heme iron and is responsible for the spectroscopic and catalytic characteristics of P450 enzymes.

Of particular importance for P450 engineering is the knowledge regarding the structural elements involved in the recognition and binding of substrates and which are therefore the basis of altering substrate specificity, chemo-, regio-, and stereoselectivity of any P450. The first and still often cited study^c on such so-called “substrate recognition sites” (SRS),⁶⁹ was implemented by Osamu Gotoh in 1992. By comparing the sequences of CYP2 family members with the sequence of the, at that time already crystallized CYP101A1 (P450_{cam}), Gotoh identified six SRS.⁶⁹ The SRS are numbered according to their appearance, starting at the N-terminus (Figure 4). They contain amino acid residues pointing towards the active site and are therefore responsible for substrate recognition and binding. Positions located in these SRSs are recognized as hotspots for improving activity, selectivity, and specificity by protein engineering.^{69, 70} For instance, SRS-4 is located in the I-helix, directly above the heme group, and substitutions of SRS-4 residues have been reported to influence the activity and selectivity of certain P450 enzymes.⁷¹⁻⁷⁵

Like SRS-4, SRS-5 is located close to the heme group. It extends from the C-terminal end of the α K helix to the β 1-4 strand and is only a few amino acids downstream of the

^c 195 citations since 2016, according to Google Scholar (29th December 2020).

conserved ExxR motif. The location of SRS-5 close to the heme makes residues in this SRS likely to be involved in the control of regioselectivity.⁷⁰ Two positions in SRS-5, namely position 5 and 9-11 downstream of the ExxR motif, are especially important in this respect. In a comprehensive investigation of 6379 P450 sequences and several 3D structures, Seifert and Pleiss found, that in 98.4%, residues at position 5 downstream of the highly conserved ExxR motif are closest to the heme group and are most likely affecting the regio- and stereoselectivity.^{70, 76, 77} Substitution of residues at position 9-11 downstream of the ExxR motif (positions 7 and 8 may also have such effect) have also been reported to alter enzyme regioselectivity.⁷⁶⁻⁷⁸

Although SRS-1 to SRS-3 define the most probable ligand access channel, another ligand access channel is built by the β 4 sheet of SRS-6.⁷⁹ SRS-6 forms a corner top part of the active site, and the amino acid residue sizes and polarities in SRS-6 can restrict or lose the degree of substrate flexibility, depending on its shape and size. These changes of the space available for the substrate have been shown to impact P450's activity, substrate specificity,⁸⁰ regio-, and stereoselectivity.^{81, 82}

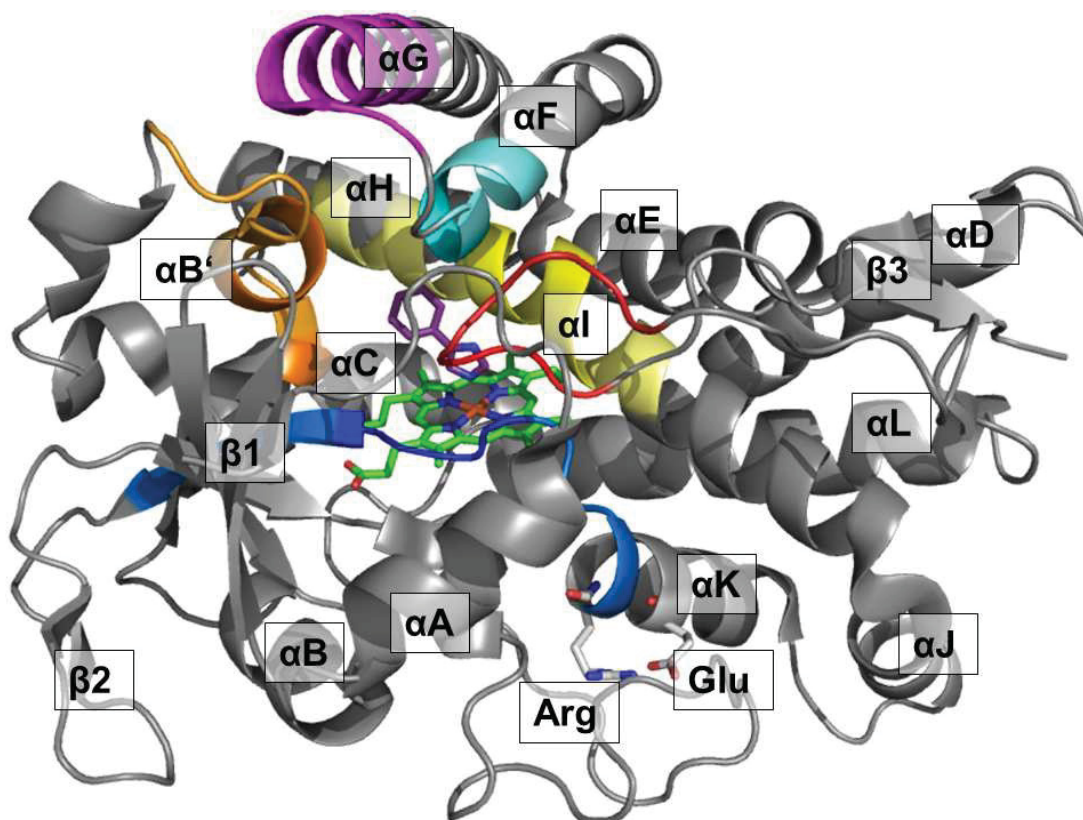


Figure 4. Illustration of the crystal structure of CYP154A8 (PDB-code: 1ODO) in complex with 4-phenyl-imidazole. α -helices, β -sheets, and the glutamate and arginine of the highly conserved ExxR motif are labeled. The prosthetic heme group is colored in green, and the 4-phenyl-imidazole ligand is purple. Substrate recognition sites are highlighted in orange (SRS-1), turquoise (SRS-2), violet (SRS-3), yellow (SRS-4), blue (SRS-5), and red (SRS-6).

1.2.4 CYP154 Family

The CYP154 family currently contains 35 bacterial P450 enzymes subdivided into 17 subfamilies (A-S, subfamily I and O missing; Nelson, DR [2009] The Cytochrome P450 Homepage; April 2021). 27 out of the 35 members were found in different *Streptomyces* species, and 4 of them were found in *Thermobifida fusca*. All originating bacteria species belong to the phylum of actinobacteria, which are of high relevance because of their comprehensive secondary metabolism. Around two-thirds of naturally derived antibiotics in clinical use, anticancer, anthelmintic, and antifungal compounds are produced by actinobacteria.⁸³ Bacterial cytochrome P450 monooxygenases play a pivotal role in many secondary metabolism pathways⁸⁴ making them promising target enzymes for biotechnological applications.

Actinobacteria, however, contain many *cyp* genes that are not involved in the clusters for secondary metabolic pathways like CYP154 family members. Their physiological roles remain uncertain. So far, an endogenous substrate has only been found for CYP154A1 from *Streptomyces coelicolor* A3(2). It catalyzes the rearrangement of a dipentaenone – hypothesized to be necessary for the stability of the bacterium – without the usually mandatory redox partners or nicotine amide cofactors.⁸⁵ The crystal structure elucidation of CYP154A1 (PDB-code: 1ODO)⁸⁶ revealed another unique property of this P450 enzyme: Compared to most P450s, the heme in CYP154A1 is in an orientation flipped by 180 degrees, which might contribute to the observed unusual catalytic property.⁸⁵

Besides CYP154A1, six other P450s of this family have been studied concerning their substrate spectra and catalytic activity. The data revealed that the members of the CYP154 family accept chemically diverse substrates of various sizes and structures. CYP154C1 from *Streptomyces coelicolor* A3(2) oxidizes large antibiotic macrolides like the 14-membered narbomycin to pikromycin and the 12-membered YC-17 to neomethymycin.⁸⁷ Hence, it was hypothesized that CYP154C1 is involved in the defense of *Streptomyces coelicolor* against other bacteria. CYP154C3 from *Streptomyces griseus* and CYP154C5 from *Nocardia farcinica* catalyze the regio- and stereoselective hydroxylation of steroids like testosterone and progesterone at position C-16 α , which defines them as steroid D-ring 16 α -specific hydroxylases.^{88, 89} CYP154H1 accepts smaller aromatic compounds, such as ethylbenzene, styrene, or indole derivatives.⁹⁰ CYP154H1 originates from the moderate thermophilic bacterium

Thermobifida fusca, whose optimal growth temperature ranges from 50-55°C. Thermostable P450s are barely described in the literature, and those from bacteria even less. CYP154H1 has a melting temperature of 67°C and is still active after incubation at 80°C.⁹⁰ *T. fusca* possesses three other CYP154 enzymes, namely CYP154E1, CYP154F1, and CYP154G1. Although no physiological substrate could yet be found for CYP154G1, CYP154E1, and CYP154F1, they have been characterized regarding their substrate preferences. While CYP154F1 accepts comparatively small and mostly linear substrates like octan-2-ol or geraniol, CYP154E1 is promiscuous. It catalyzes the oxidation of various substrates with higher activity.⁹¹ von Bühler *et al.* found that CYP154E1 accepted 33 out of 51 substrates with varying size and shape, such as linear alkanolic acids, cyclic substrates like camphor, and the largest alkaloid pergolide mesylate.⁹² Furthermore, in almost all cases, CYP154E1 showed higher activity compared to CYP154A8 from *Nocardia farcinica*, which was also characterized in the same study. Along with the relatively high activity and the broad substrate spectrum of CYP154E1, it displays high selectivities. The highest regioselectivity of 100% was found during the hydroxylation of geraniol and nerol, leading to 8-hydroxygeraniol or 8-hydroxyneryl,⁹³ or of (*E*)-stilbene leading to (*E*)-4,4'-dihydroxystilbene.⁷¹

Members of the CYP154 family are very diverse in their reactions, making them interesting candidates for biocatalysis and are worth investigating the so far uncharacterized CYP154 members. Among the characterized CYP154s, CYP154E1 is of particular interest because of its broad substrate spectrum, the relatively high activity compared to other members of the CYP154 family, its high selectivity, and potentially moderate thermostability. A current disadvantage of CYP154E1 is the lack of its crystal structure and the information about the physiological redox partners. The crystal structures of only four family members, CYP154A1 (PDB-code: 1ODO),⁸⁶ CYP154C1 (PDB-code: 1GWI),⁸⁷ CYP154C4 (PDB code: 6A7I),⁹⁴ and CYP154C5 (PDB-codes: 4J6B, 4J6C, 4J6D, and 4JB5)⁹⁵ have been solved so far.

1.2.5 CYP102A1 – P450 BM3

Since its discovery in 1974, P450 BM3 (CYP102A1) from *Bacillus megaterium* “has become one of the most intensively studied of all enzymes” (Whitehouse, Bell, & Wong,

2012).⁹⁶ A literature search for “P450 BM3” generates about 5000 hits^d and the number is still increasing (809 hits since 2019 and 467 hits since 2020). P450 BM3 is a soluble enzyme consisting of a heme-containing monooxygenase domain (BMP, 55 kDa) fused to a flavin adenine dinucleotide (FAD) and flavin mononucleotide (FMN) containing reductase domain (BMR, 65 kDa). This unique organization makes P450 BM3 catalytically self-sufficient because substrate oxidation requires only the cofactor NADPH and oxygen. The well evolved natural fusion between the catalytic and reductase domains in P450 BM3 is proposed to support a rapid electron transfer of electrons from NADPH to the heme iron, resulting in a highly active P450.⁹⁷ With a k_{cat} of $17,100 \text{ min}^{-1}$, the hydroxylation of arachidonic acid catalyzed by P450 BM3 is considered the fastest P450-catalyzed reaction described so far.⁹⁸ Putting all this together, self-sufficiency, solubility, high activity, and its easy expression in *E. coli* makes P450 BM3 probably the most promising P450 for biotechnological applications.⁹⁶ This P450 has become the obvious and most often used target for protein engineering with medium- to high-throughput screening assays *in vitro*. Other P450s that rely on separate redox partners often require *in vivo* screening systems to reduce the practical effort to generate these additional proteins.

1974, Fulco *et al.* identified P450 BM3 as a medium- to long-chain length fatty acid hydroxylase with the preference for hydroxylation at ω -1, ω -2, and ω -3 positions.⁹⁹ Since then, many mutagenesis studies have been executed to extend the substrate spectrum of P450 BM3 towards non-natural substrates until 2011, P450 BM3 has earned the designation “Swiss Army Knife” (Wong, 2011).¹⁰⁰ By now, the substrate spectrum ranges from gaseous alkanes,^{31, 33} cyclic alkanes,¹⁰¹ (a)cyclic monoterpenes^{102, 103} and sesquiterpenes^{34, 102, 104} up to alkaloids¹⁰⁵ and steroids.¹⁰⁵⁻¹⁰⁷ Besides the extension of the substrate spectrum of P450 BM3, many engineering attempts have also been undertaken to improve stability¹⁰⁸, activity¹⁰⁹, and in particular selectivity.¹¹⁰⁻¹¹²

1.2.6 Industrial Applications of P450s

Cytochrome P450 monooxygenases possess the extraordinary capability to catalyze the chemically demanding hydroxylation of non-activated C-H bonds in a wide variety

^d Google Scholar: Search Item: P450 BM3 (accessed 7th April 2021)

of organic molecules, often with high regio- and stereoselectivity, which makes P450s potential candidates for use in biotechnology and synthetic chemistry.

However, due to some disadvantages attributed to these enzymes (see Section 1.2.7), industrial applications are scarce and mainly limited to the production of drug metabolites, pharmaceuticals, and fine chemicals like fragrances and flavors.¹¹³ Nevertheless, many efforts have been, and are still being, undertaken to identify and control P450s for their commercial usage.¹¹⁴ Their value in late-stage oxyfunctionalization has been particularly recognized in organic chemistry. Late-stage oxyfunctionalization describes an approach in which first, simple and minimally oxidized building blocks are assembled to a hydrocarbon skeleton and oxidized at a later stage of the synthesis.^{115, 116} Such late-stage reactions are generally challenging to perform via classical chemical means and require the use of tedious functional group protection chemistry.^{110, 117} Selective enzymatic late-stage oxyfunctionalization is basically addressed in every chapter of this thesis.

Although the examples of P450 involved biocatalytic processes in industry are scarce, the hydroxylation of steroids belongs to the very first large-scale biotransformations in the pharmaceutical industry and date back to the late 1940s.¹¹⁸ The large-scale production of steroids are nowadays well-established commercial applications of P450s. Two processes that need to be named are, firstly hydroxylation of 11-desoxycortisol to cortisol catalyzed by P450_{lun} in *Curvularia lunata*^{119, 120} (established by Schering AG; Figure 5B) and secondly, the hydroxylation of progesterone to 11 α -hydroxyprogesterone by utilizing species from *Rhizopus* (established by the Upjohn Company).¹²¹ Instead of multistep chemical syntheses, both reactions involve only one single-reaction step.¹²²

Another example of P450 in the industry is the CYP105A3 catalyzed regioselective and stereoselective 6 β -hydroxylation of compactin to the cholesterol-lowering drug pravastatin (Figure 5B) in *Streptomyces carbophilus* (Daiichi Sankyo Inc. and Bristol-Myers Squibb).^{123, 124}

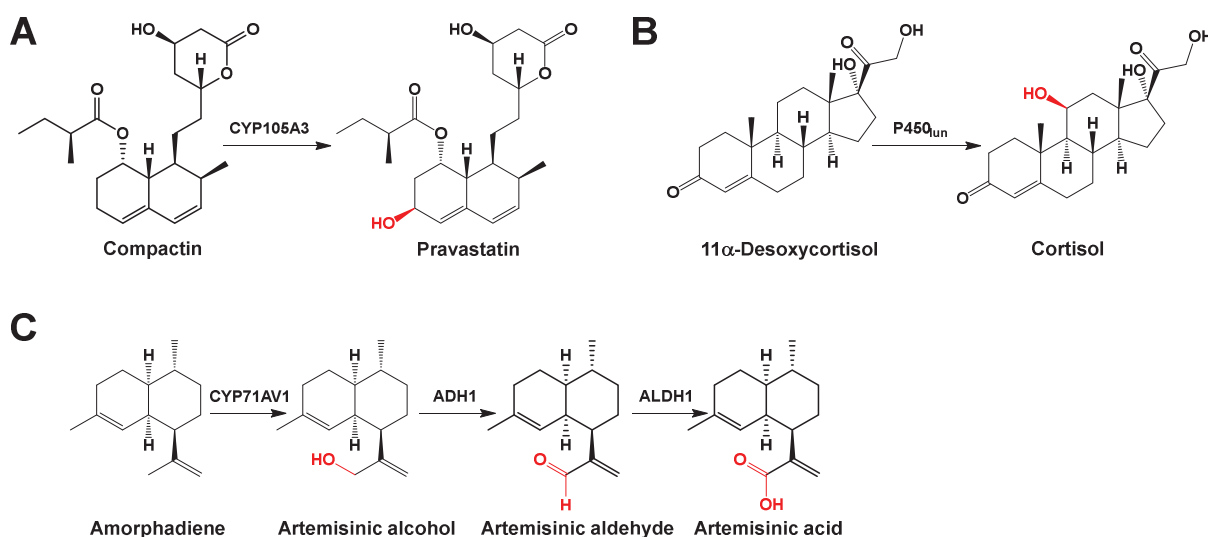


Figure 5. Examples of P450s implemented in industrial processes. **A** Pravastatin synthesis in *Streptomyces carbophilus*. CYP105A3 catalyzes the hydroxylation of compactin at position 6 to pravastatin. **B** P450_{11β} catalyzed hydroxylation of 11α-desoxycortisol to cortisol. **C** Extract from the biosynthesis of artemisinin. CYP71AV1 catalyzes the first oxidation of amorpha-2,6-diene to artemisinic alcohol. Subsequent oxidation of artemisinic alcohol is catalyzed by artemisinic alcohol dehydrogenase (ADH1) and artemisinic aldehyde dehydrogenase (ALDH1). The oxidation sites are marked in red.

Secondary metabolites from plants and microorganisms are sources of new pharmaceuticals.^{125, 126} However, they are often produced in low amounts in the original organism and/or require tedious isolation procedures. Alternatively, the reconstitution of biosynthetic pathways in recombinant microorganisms represents a promising field of synthetic biology, as demonstrated by the *de novo* synthesis of artemisinic acid, a precursor of the anti-malaria drug artemisinin, in engineered *Saccharomyces cerevisiae*. Artemisinin is a secondary metabolite of the plant *Artemisia annua*. Significant parts of the biosynthetic pathway (from simple sugars to the artemisinin precursor of artemisinic acid), including the gene of *cyp71AV1*, were integrated into *Saccharomyces cerevisiae*. CYP71AV1 is responsible for the oxidation of amorpha-2,6-diene to the respective artemisinic alcohol. Artemisinic alcohol dehydrogenase (ADH1) and artemisinic aldehyde dehydrogenase (ALDH1) catalyze the subsequent oxidation of artemisinic alcohol to artemisinic acid (Figure 5C),^{127, 128} which is then further converted to the final artemisinin by chemical means.¹²⁹ This engineered yeast strain was commercialized by Sanofi, producing 2013 ~35 metric tons of artemisinin with an uprising tendency. But, two years later Sanofi stopped producing semi-synthetic artemisinin mainly due to the lower price of naturally extracted artemisinin from *A. annua*.^{130, 131} Despite the end of production, the *de novo*

biosynthesis of artemisinin remains the pioneering and one of the most prominent examples of synthetic biology.¹²⁸

The synthesis of pharmaceuticals is not the only scope of P450s, rather also the drug metabolism. Hepatic P450s metabolize roughly 75% of all drugs and xenobiotics in the human body.¹³² Therefore, P450 conducted drug biotransformations are essential in evaluating the pharmacological profile of a drug and its metabolites (toxicity, drug-drug interactions, or alternate biological activities)¹³³⁻¹³⁵ before commercial usage. The synthesis of human drug metabolites with the selective metabolism of the antidepressant ketamine is addressed in this thesis in chapters I and II.

1.2.7 Limitations of P450s and Engineering of Selectivity

As already stated above, P450s are among the most valuable enzymes for biotechnological applications.²⁹ Nevertheless, the relatively confined number of examples of cytochrome P450s in industrial applications still evidently show their limitations.

One of the limitations is related to uncoupling reactions (shunt pathways, see Section 1.2.2) in the P450 cycle, during which the enzymes themselves form hydrogen peroxide or other reactive oxygen species. The formation of such might lead to the bleaching of the heme cofactor or inactivation of the apoprotein. Most P450s are dependent on separate redox partner proteins for the electron transfer from the cofactor NAD(P)H to the heme iron, which needs to be considered for the set-up of an industrial process (redox protein process stability, solvent tolerance, etc.). Moreover, P450s obtain the electrons needed for the catalytic cycle from stoichiometric amounts of the expensive nicotinamide cofactor NAD(P)H. To make the P450 catalyzed reaction economically feasible, cofactor regeneration is required, which further increases the system's complexity.

As mentioned above, human hepatic P450s involved in drug metabolism are important biocatalysts for the pharmaceutical industry. In the production of recombinant P450s, *E. coli* is one of the most commonly used hosts.⁴⁶ However, most eukaryotic P450s are membrane-bound enzymes, which results in low expression levels when recombinant bacterial expression hosts such as *E. coli* are used. Thus, the modification of the *N*-terminal membrane-associated anchor and the co-expression of chaperones are

necessary, which increases the expression burden on the host organism and hampers their use as biocatalysts.^{46, 109, 136} On the other hand, soluble prokaryotic P450s, which are easier to express in prokaryotic hosts and possess higher activity than their eukaryotic counterparts, usually possess a narrower substrate spectrum.¹³⁷

Another limitation is related to the substrates of P450 enzymes. P450s mostly catalyze the oxidation of hydrophobic substances like fatty acids, terpenes, and alkanes, which are often poorly soluble in aqueous media and reduce the productivity of a biocatalyst. The addition of solubilizer increases the substrate solubility but such a solubilizer (often water-miscible organic solvents) often negatively affects enzyme stability due to water molecule abstraction.

The fastest P450 catalyzed oxidation reaction reported so far is the hydroxylation of arachidonic acid catalyzed by P450 BM3 with a turnover number (k_{cat}) of 17,000 min^{-1} . However, most P450s have much lower activities with turnover numbers between 1- 300 min^{-1} .¹³⁸ In contrast, other commercially used enzymes like the penicillin amidase from *Alcaligenes faecalis*, detergent-stable serine alkaline protease from *Caldicoprobacter guelmensis* or L-asparaginase from *Escherichia coli* B possess higher turnover numbers of 4.800 min^{-1} ¹³⁹ (penicillin G), 26.925 min^{-1} ¹⁴⁰ (casein), and 89.500 min^{-1} ¹⁴¹ (L-asparagine) instead, to mention a few examples.

These limitations do not belittle the potential of cytochrome P450 monooxygenases but demonstrate the obstacles linked with their widespread applications.

This thesis focuses on a yet not mentioned drawback of P450-catalyzed reactions: low selectivity. Although P450s are often attributed with high regio- and stereoselectivity, this is not always the case, particularly when non-natural substrates or P450s with broad substrate spectra are used.^{96, 137} The control of selectivity is mandatory for enzyme implementation into biotechnological processes.¹⁴² However, given the fact that many organic molecules can be oxidized at several different sites⁹⁶ and “partly because individual mutations do not have predictable or generic effects, meaning that substrates must generally be dealt with on a case-by-case basis” (Whitehouse, Bell, & Wong, 2012),⁹⁶ control of P450s selectivity is challenging. Engineering has played a pivotal role in designing P450s with improved selectivity. The three main strategies of either directed evolution, rational, or semi-rational design have thereby been used.¹⁴³

Directed Evolution – Directed evolution describes a process that imitates natural evolution by repeating cycles (the best variant of the first cycle serves as the template for the next cycle, etc.) of random mutagenesis (e.g., by error-prone PCR or DNA shuffling) followed by the screening of these randomly created variants for the desired property. Since the process of mutagenesis occurs – equal to natural evolution – randomly, no structural information about a protein is required, and every position might be potentially targeted. Over the years, directed evolution has been proven to be a powerful tool in protein engineering and has often been applied to engineering P450 monooxygenases. Thereby, enzyme activity and stability could be increased, and/or the substrate spectrum broadened or amended. However, studies explicitly targeting regio- or stereoselectivity with pure directed evolution are rare. It is widely accepted that selectivity is influenced by those residues in direct contact with the substrate. Compared to the whole sequential space, these residues are massively underrepresented and hence less likely to be altered by directed evolution. These residues are rather specifically targeted by rational or semi-rational protein design to improve the enzyme's selectivity (see below).

Another drawback of directed evolution, is the large number of mutants in libraries that need to be screened for an enzyme variant with the appropriate property. Considering a sequence space of 400 amino acids (CYP154E1, for example, consists of 402 amino acids), 20^{400} ($\approx 10^{520}$) possible variants exist, which exceeds clearly, what modern ultra-high-throughput assays can handle ($>10^7$ variants). Screening of mutant libraries ideally requires an (ultra-) high-throughput assay on a small scale which accurately fits into the new property desired for an enzyme.¹⁴⁴ However, creating such an ideal screening system may become difficult, especially when P450's regio- and stereoselectivity are the properties that need to be evolved.^{106, 145, 146} Such screening for selectivity is often executed using HPLC, LC-MS, or GC-MS, which reduces the high-throughput to a medium- or low-throughput of about 10^2 - 10^4 clones instead, or, for example, up to 10^6 clones with a solid phase screening system (e.g., agar plate screening).¹⁴⁶

Nevertheless, mimicking nature's evolution and delivering it to the world's laboratories was a milestone in protein engineering – and was honored with the Nobel Prize for Chemistry in 2018. Directed evolution is still a powerful tool to alter the enzyme's characteristics, especially when no structural information is available or when it is combined with rational design (see below, Semirational Design).

Rational Protein Design – Rational protein design is based on the information regarding a protein's sequence, structure, and function guided by computational algorithms.¹⁴⁷ This knowledge-driven engineering extends the pre-laboratory work of sequence and structure analysis or *in silico* modeling but reduces the laboratory work to a minimum since only a handful of mutants are constructed by site-directed mutagenesis and tested for the desired properties.

Due to the steadily increasing number of identified P450s in all kingdoms of life and habitats, over 60 years of research on P450s and their structure-function relationship, the overall conserved fold, and the biotechnological importance, P450s are ideal target enzymes for rational design studies. One of the groundbreaking works in sequence-function and structure-function analysis in P450s was identifying the substrate recognition sites (SRS) by Osamu Gotoh in 1992⁶⁹ and is described in detail in Section 1.2.3. The presence of SRS in all P450s was extended by other research to find universal residues for determining selectivity in all cytochrome P450 monooxygenases.^{70, 148} This universal knowledge in the structure-function relationship for all P450s resulted in many successful attempts for rationally engineering the selectivity of P450s. For example, Seifert *et al.* created an enriched P450 BM3 library of only 24 variants with mutations on two SRS positions and strongly improved regio- or stereoselectivity during oxidation of terpenes such as limonene or valencene, whose oxidized products are valuable aromatics or fragrances.¹⁰² In another study, Carmichael and Wong utilized site-directed mutagenesis on active site residues (SRS residues) to oxidize polycyclic aromatic hydrocarbons (PAHs), an important step in environmental bioremediation.¹⁴⁹

What sequence-based or structure-based protein engineering alone does not consider are the dynamics of proteins and substrates. Protein and substrate can possess several conformational stages, and substrates can bind in different binding modes to the active site. The elemental forces that determine protein interactions between protein and solvent, and protein and substrate include van der Waals interactions, electrostatic interactions, hydrogen bonds, and the hydrophobic effect.¹⁵⁰ A typical approach that predicts these forces for small ligands (substrate) and receptors (protein) is molecular docking. During molecular docking, the conformations or poses of the ligand in the binding site or active site are initially predicted. The binding energies between ligand and receptor are subsequently calculated and ranked accordingly for each of those poses.¹⁵¹ The top-ranked pose should then reflect the correct binding of

the substrate. Assuming that the substrate binding to the active site is determinant for the reaction selectivity,¹⁵² it can subsequently be altered accordingly using the docking information to reshape the active site. Molecular docking was applied in all studies of this thesis. In search of a novel semi-biosynthetic route for artemisinin production (biosynthetic pathway in Section 1.2.6), epoxidation of amorpha-4,11-diene to artemisinic-11S,12-epoxide was required as the initial step in the synthesis. P450 BM3 was selected for this reaction, but the wild type showed no activity. Docking of amorpha-4,11-diene into the active site revealed key residues around the heme group, whose subsequent mutagenesis led to increased activity against amorpha-4,11-diene. The P450 BM3 mutant G4 (with the four mutations of F87A, R47L, Y51F, and A328L) generated the desired product artemisinic-11S,12-epoxide with titer above 250 mg/L.¹⁵³

Most of the docking programs have adopted the methodology of a flexible ligand in a rigid receptor.¹⁵⁴ Only to a limited extent, molecular docking has been used to address the issues under consideration of protein flexibility. For a detailed view regarding the protein motions, molecular dynamic (MD) simulations need to be combined with the molecular docking approach.

Semi-rational Design – The term “semi-rational design” indicates a combination of knowledge-based (rational) hotspot identification combined with random mutagenesis of the identified specific residues. The focus on specific residues, instead of the whole sequence space (as in directed evolution), drastically reduces the library size, making these libraries amenable to screening systems other than high-throughput ones (e.g., low- to medium-throughput HPLC and GC based screenings).¹⁴⁷ Many mutagenesis studies have revealed that improvements in substrate specificity, catalytic activity, or selectivity, often derive from mutations of amino acids at positions located in or close to the enzyme’s active site.^{155, 156} Studies of rational engineering therefore mainly focus on these active site residues, whereas random mutagenesis methods often create distant mutations far away from the active site (due to the lower number of amino acids around the active site compared to the total number of amino acids).¹⁵⁷ Consequently, focusing random mutagenesis to the hotspot residues in and around the active site – semi-rational design – combines the benefits of both directed evolution and rational design.¹⁵⁶ In such cases, saturation mutagenesis (SM) techniques, where all 20 canonical amino acids are tested at one position, are often implemented at identified hotspots. Comparable to repeated cycles of random mutagenesis in directed evolution,

saturation mutagenesis at different positions can be performed iteratively (iterative saturation mutagenesis, ISM). In ISM, the best variant of the previous cycle of saturation mutagenesis at multiple positions serves as the template for the next cycle. Bernhardt and colleagues utilized a combination of site-directed and saturation mutagenesis to efficiently alter the regioselectivity of CYP106A2 from C15- to C11-hydroxylation of progesterone. Their approach enabled the highly selective synthesis of 11 α -hydroxyprogesterone, a pharmaceutical compound with anti-androgenic and blood-pressure regulating activity.¹⁵⁸ Saturation mutagenesis at multiple positions can either be performed in parallel, where each position is mutated independently of the other positions, or in combination, where two or more positions are mutated simultaneously. The latter harbors one of the most significant advantages of semi-rational design compared to directed evolution or rational design: the probability of obtaining synergistic mutations.¹⁵⁶ The effects of two mutations can interact with each other as additive, partially additive, synergistic, antagonistic, or with no additional effect. The synergistic effect means that the effect of two combined mutations is higher than the expected effect created by the addition of each mutation.¹⁵⁹ Based on this potential for synergistic mutations, Reetz and colleagues created the method of combinatorial active-site saturation test (CAST), which is focused on saturation mutagenesis of two or more amino acid positions simultaneously in a single library.¹⁶⁰ Using CASTing, P450 BM3 variants were successfully engineered for the highly regio- and stereoselective oxidation of testosterone and progesterone.¹⁰⁶

Substrate Engineering – So far, the methods and examples dealt with the engineering of one reactant, the biocatalyst. However, selectivity upon the reaction can also be driven by altering the substrate, which is widely used in synthetic chemistry and adopted by Griengl and colleagues for enzymes.¹⁶¹ For P450-catalyzed hydroxylations, the concept of “docking and protecting” (d/p) groups were elaborated to “anchor” the substrate in a particular orientation in the active site for selective hydroxylation.^{162, 163} The approach of docking and protecting groups was picked up and combined with protein engineering by Arnold and coworkers for the enantioselective hydroxylation of 2-arylacetic acids.¹⁶⁴ They predicted that the size and charge of the substrate’s carboxyl groups prevent sufficient catalysis by P450 BM3 and therefore “masked” them with esters of a different size.¹⁶⁴ The combination of protein and substrate engineering resulted in the synthesis of propyl mandelate with 93% enantiomeric excess, 88% regioselectivity, and a total turnover number (TTN) of 1640.

Variations of masking ester residues clearly alter the activity and selectivity for the same P450 BM3 variant. In another attempt, carboxylated 2-nitrophenylsulfonamides d/p groups and protein engineering were combined with the bioinformatic tools of docking and molecular dynamics to enhance the activity and regioselectivity of P450 BM3 for the late-stage oxyfunctionalization of vabicaserin. As a positive side effect, the introduction of the d/p group increased the substrate's solubility in the aqueous media, which evades some of the limitations connected with P450 reactions (see the section above) and might therefore be deployable for other biocatalytic applications.¹⁶⁵

Despite the advances in P450 engineering for improved selectivity, the control of selectivity remains a challenging task, and each enzyme-substrate-combination still needs to be investigated as necessity arises.⁹⁶

1.3 Objective of the Thesis

In a time where sustainability, environmental friendliness and conservation of resources are increasingly becoming in the focus of society and industry, the development of bio-based alternative production routes starts to emerge in every industry field.

Owing to their unique and, at the same time, chemically challenging reaction of non-active C-H bond oxidation and the extensive knowledge gained during sixty years of research,¹⁶⁶ cytochrome P450 monooxygenases are promising biocatalysts for biotechnological purposes. Concerning substrate spectra, hepatic P450s have the edge over bacterial P450s because they are responsible for the metabolism of drugs and other xenobiotics and hence oxidize interesting compounds for the pharmaceutical industry. However, due to generally higher activity and higher expression levels in recombinant host organisms such as *E. coli*, soluble bacterial P450s seem to be more applicable for biotechnological applications. Their most significant drawbacks are their narrow substrate spectrum and low selectivity in reactions with non-natural substrates possessing several chemically equivalent positions for oxidation.

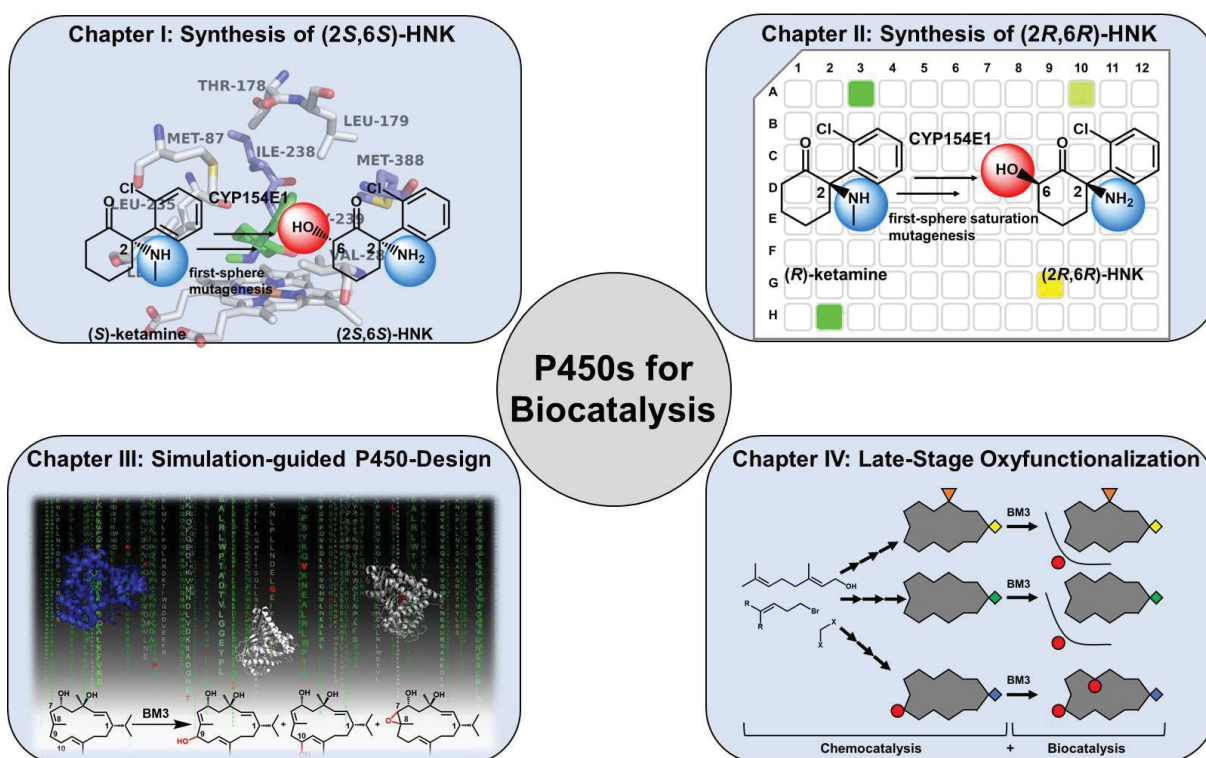
The aim of this thesis was, by developing and using different methods of protein engineering, to construct bacterial P450 enzymes with high activity, regioselectivity, stereoselectivity, and chemoselectivity during late-stage oxidation of complex substrates.

For this purpose, two very promising P450s, the thermotolerant CYP154E1 from *T. fusca* YX with an unusually broad substrate spectrum and the well-studied highly evolvable self-sufficient P450 BM3 from *B. megaterium*, were selected. The objective was their engineering to achieve i) the highly regio-, chemo-, and stereoselective synthesis of (2*S*,6*S*)- and (2*R*,6*R*)-hydroxynorketamine, human metabolites and potentially safer antidepressants of the likewise antidepressant ketamine – and ii) the chemically challenging highly selective late-stage oxyfunctionalization of cembranoids – terpenoids with anticancerogenic effects. In order to implement these set objectives, out of the vast and rapidly increasing number of strategies for protein engineering, four different strategies were tested for their efficiency in turning a P450 into an active and highly selective version of its own: i) first-sphere active site-directed mutagenesis, ii) first-sphere active site saturation mutagenesis, iii) computer-guided rational design, and iv) substrate engineering.

In this way, the pool of biotechnologically applicable P450 variants is extended while more information about protein engineering strategies is subsequently gained.

2. Results

This section contains four published manuscripts in peer-reviewed journals in order to describe the results of this thesis. Starting with the “Synthesis of (2*S*,6*S*)-Hydroxynorketamine and (2*R*,6*R*)-Hydroxynorketamine” (chapters I and II), to “Simulation-guided P450-Design” (chapter III) and “Late-Stage Oxyfunctionalization” (chapter IV), all chapters contain different protein engineering strategies to design P450s for biocatalysis. The own contribution to each manuscript is provided at the beginning of each chapter.



2.1 Chapter I

Enzyme-Mediated Two-Step Regio- and Stereoselective Synthesis of Potential Rapid-Acting Antidepressant (2*S*,6*S*)-Hydroxynorketamine

Ansgar Bokel, Ansgar Rühlmann, Michael C. Hutter, and Vlada B. Urlacher*

*corresponding author

ACS Catalysis, 2020, 10(7), 4151-4159

Own contribution (80%): AB and AR designed the project. AB planned and performed all the experimental work. AB and VBU wrote the manuscript.

Expression, purification, and enzyme assays for all enzymes (GDH, YkuN, FdR, CYP154E1) were executed by AB. AB implemented the cloning for the *E. coli* based whole-cell system. AB created all CYP154E1 variants, expressed them, measured their concentration, and performed the *in vitro* and *in vivo* reactions. AB implemented GC-MS and LC-MS method development, measurements, and analysis. AB also implemented method development for the chiral HPLC and sample measuring. AB executed characterization of the CYP154E1 QAA triple mutant (substrate-binding spectra and kinetics). Upscaling of the (*S*)-ketamine conversion, product isolation, and NMR analysis was implemented by AB. NMR samples were measured by the NMR facility (HHU).

In cooperation with MCH, AB created the homology model and executed docking experiments to identify the hot spot position for mutagenesis and explain the experimental outcome.

Reprinted with permission from Bokel, A., Rühlmann, A., Hutter, M. C., & Urlacher, V. B. (2020). Enzyme-Mediated Two-Step Regio- and Stereoselective Synthesis of Potential Rapid-Acting Antidepressant (2*S*,6*S*)-Hydroxynorketamine. *ACS Catalysis*, 10(7), 4151-4159. Copyright 2020 American Chemical Society.

Enzyme-Mediated Two-Step Regio- and Stereoselective Synthesis of Potential Rapid-Acting Antidepressant (2*S*,6*S*)-Hydroxynorketamine

Ansgar Bokel, Ansgar Rühlmann, Michael C. Hutter, and Vlada B. Urlacher*

Cite This: *ACS Catal.* 2020, 10, 4151–4159

Read Online

ACCESS |

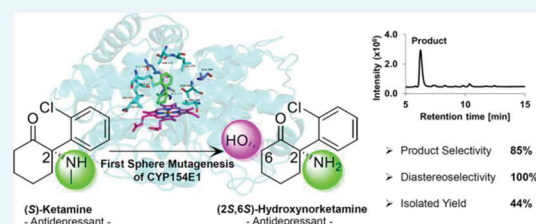
Metrics & More

Article Recommendations

Supporting Information

ABSTRACT: Recently, the anesthetic (*S*)-ketamine has been approved as a rapid-acting and long-lasting antidepressant. Its metabolite, (2*S*,6*S*)-hydroxynorketamine, has been found to have a similar antidepressant effect but with less undesirable side effects, which make this compound an interesting target for synthesis. Using the first-sphere mutagenesis of the cytochrome P450 154E1 from *Thermobifida fusca* YX, we constructed a triple mutant that enables the effective production of (2*S*,6*S*)-hydroxynorketamine from (*S*)-ketamine. This engineered P450 monooxygenase catalyzes the consecutive oxidative N-demethylation and highly regio- and stereoselective C6-hydroxylation reactions leading directly to the desired product with 85% product selectivity. The integration of this selective monooxygenase into an *Escherichia coli* whole-cell biocatalyst allowed the production of (2*S*,6*S*)-hydroxynorketamine at a semipreparative scale. The metabolite was purified and its structure was confirmed by NMR spectroscopy.

KEYWORDS: cytochrome P450, protein engineering, ketamine, N-demethylation, hydroxylation, regioselectivity, stereoselectivity



INTRODUCTION

Ketamine, a noncompetitive *N*-methyl-D-aspartate (NMDA) receptor antagonist, was synthesized more than 50 years ago and since then has been widely used as an anesthetic agent for the management of acute and chronic pain, often in emergency cases, because of its rapid effect.¹ In the early 2000s, ketamine was found to have an unexpected antidepressant effect on patients with treatment-resistant major depression.² A major depressive disorder is a common illness that affects more than 300 million people worldwide (about 4% of the world population according to the report of World Health Organization, March 2018) and is a major cause for suicidal behavior.³ Obviously, there is a demand for efficient antidepressants for the treatment of this disorder. Recent findings demonstrate that ketamine is a promising candidate to meet this demand.⁴ This drug has a rapid onset effect, often within 1 h, that can also last up to 1 week.⁵ For comparison, currently applied therapeutics need weeks to months until a positive response in patients occurs.^{5,6} This high potential of ketamine is underlined by the count of patents secured during the last years.⁷

However, ketamine has a number of side effects like blurred vision, dizziness, dissociation, elevated blood pressure, and headache.⁸ Moreover, the mechanism of its rapid and long-lasting antidepressant effect remains elusive. Although superior and longer-lasting effects of (*R*)-ketamine have been demonstrated only in animal models, clinical studies are only available for racemic and (*S*)-ketamine so far.^{9–11} Interestingly, the therapeutic effect of ketamine lasts up to 1 week, whereas

the half-life of this drug is only 2–3 h. In humans, ketamine is metabolized by several liver microsomal cytochromes P450. Thereby, the major metabolic pathway follows N-demethylation to form norketamine, which is further oxidized at various positions of the cyclohexanone ring, resulting in hydroxylated norketamine metabolites (Scheme 1, Route A). The reverse reaction order, ketamine hydroxylation followed by N-demethylation, was also suggested and leads to identical metabolites (Scheme 1, Route B).^{12,13} Among the identified metabolites, (2*R*,6*R*)-hydroxynorketamine and (2*S*,6*S*)-hydroxynorketamine have attracted particular interest, as they exhibit a longer half-life than ketamine and were recently supposed to be essentially involved in the antidepressant mechanism or at least support the ketamine activity.^{10,14,15} Since then, the mode of ketamine action has been intensively debated in the literature, and the scientific community seems to be at the very beginning of understanding how the antidepressant effect of ketamine and its metabolites are correlated to each other.

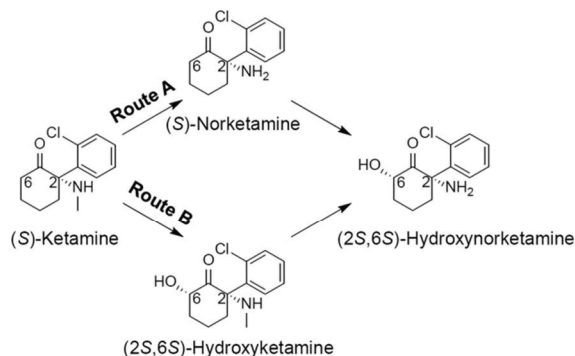
In 2019, (*S*)-ketamine (esketamine) nasal spray (SPRAVATO) was approved in the United States for the therapy of treatment-resistant patients with major depression.¹⁶ This

Received: December 12, 2019

Revised: February 21, 2020

Published: March 6, 2020

Scheme 1. Oxidation of (*S*)-Ketamine to (*2S,6S*)-Hydroxynorketamine via *N*-Demethylation and Hydroxylation at Position C6 of the Cyclohexanone Ring



development and the potential of (*2S,6S*)-hydroxynorketamine ((*2S,6S*)-HNK) as a rapid-onset antidepressant that is devoid of the negative side effects of ketamine,¹⁵ makes this metabolite a target of synthetic approaches. Han et al. reported a chemical route toward (*2S,6S*)-HNK starting with 1-*o*-chlorophenylcyclohexene and resulting in an isolated yield of around 30%.¹⁷ In another chemical synthesis, reported by Zanos et al., the overall yield of (*2S,6S*)-HNK reached 5% when the process was started with racemic norketamine. If the first step, the chiral resolution of racemic norketamine with a 9% yield, is not taken into account, the isolated yield reaches 54%. It is important to mention that in this route, demethylation of ketamine was avoided and norketamine was used as a starting material.¹⁰

The shortcomings of the chemical routes to (*2S,6S*)-HNK prompted us to seek a selective enzymatic route starting from (*S*)-ketamine via oxidative *N*-demethylation and C6-hydroxylation. Basically, both C–H bond hydroxylation and *N*-demethylation reactions belong to the repertoire of cytochrome P450 monooxygenases (P450s or CYPs).¹⁸ P450s are heme-containing enzymes that catalyze the reductive scission of molecular oxygen. One atom of oxygen is introduced into the substrate molecule, whereas the second oxygen atom is reduced to water. The activation of molecular oxygen occurs via a number of steps that lead to the formation of a reactive heme iron–oxygen complex Fe(IV) = O, generally referred to as compound I.^{19–21} Generally, P450 enzymes enable regio-, chemo-, and stereospecific oxidations of chemically diverse organic molecules in the presence of NAD(P)H. Among several hepatic P450s involved in ketamine metabolism, the formation of (*2S,6S*)-HNK is primarily attributed to CYP2A6 and CYP2B6.¹² The use of those eukaryotic enzymes for the synthesis of (*2S,6S*)-HNK is however limited by their low regioselectivity. Along with (*2S,6S*)- and (*2R,6R*)-HNKs, these human P450s also produce (*2S,4S*)-, (*2S,4R*)-, (*2S,5S*)-, (*2S,5R*)-HNK, and their respective enantiomers as well as non-demethylated hydroxyketamine products.^{12,13,22}

We focused our attempts on bacterial P450s because they are generally easier to express in recombinant hosts and possess higher activity than their eukaryotic counterparts. Our ultimate goal was to identify and/or engineer a P450 enzyme that enables both *N*-demethylation and C6-hydroxylation of (*S*)-ketamine to directly form the target product (*2S,6S*)-HNK. Compound I was suggested to mediate the C–H bond hydroxylation and *N*-demethylation,^{23,24} which suggests that

both reactions can be catalyzed by one P450 enzyme at one substrate. However, although hydroxylation and *N*-demethylation have been extensively studied, reports describing both reactions catalyzed by one P450 enzyme at the same substrate molecule are rare.

Herein, we report the construction, characterization, and application of a triple mutant of CYP154E1 from *Thermobifida fusca* YX that enables both the *N*-demethylation and C6-hydroxylation of (*S*)-ketamine with high chemo-, regio-, and stereoselectivity to furnish the desired product (*2S,6S*)-HNK.

■ RESULT AND DISCUSSION

CYP154E1 Mutagenesis. In preliminary experiments, an in-house collection of bacterial cytochrome P450 enzymes and their mutated variants available in our laboratory were tested with (*S*)-ketamine as a substrate. CYP154E1 from *T. fusca* YX, which demonstrated activity toward (*S*)-ketamine, even though resulting in only 2% conversion, was selected for further experiments. This bacterial P450 enzyme is an interesting candidate because it accepts a broad diversity of substrates, possesses high stability, has been used for preparative scale transformations, and its enzymatic properties could be effectively improved by mutagenesis.^{25–30} Most P450s rely on NAD(P)H and redox partner proteins for their activity. Since physiological redox partners for CYP154E1 remain unknown, the flavodoxin YkuN from *Bacillus subtilis* and the flavodoxin reductase FdR from *Escherichia coli* were used for electron delivery.^{28,30}

P450 enzymes have been extensively studied and engineered for the selective oxidation of diverse substrates for synthetic applications.^{31–34} Along with wild-type P450s, which are capable of regio- and stereoselective oxidations with high activity,^{35,36} these enzymes were successfully optimized by means of protein engineering. Engineered P450 variants were constructed using directed evolution,^{37,38} site-directed mutagenesis,^{39–41} site-saturation mutagenesis,^{42–44} and combinatorial active-site saturation tests (CASTs).^{45,46} In our attempt to increase the CYP154E1 activity toward (*S*)-ketamine and simultaneously construct a highly selective variant, we applied first-sphere mutagenesis focusing on amino acid substitutions at positions located at a distance of fewer than 15 Å from the heme iron. The first-sphere mutagenesis has been successfully used by our and other research groups to increase the activity and selectivity of different P450 enzymes.^{27,47–52} This strategy is based on the hypothesis that positions in the first sphere of the heme iron are likely to interact with any substrate and hence influence its orientation and thereby the regio- and stereoselectivity of the enzyme. Based on a homology model constructed using CYP154A1 from *Streptomyces coelicolor* (PDB: 1ODO) as a template, and the molecular docking of (*S*)-ketamine and (*S*)-norketamine in all possible conformations in the active site of the wild-type CYP154E1, we identified nine first-sphere amino acid residues for mutagenesis (Figure S1).

Several single CYP154E1 mutants with substitutions at the identified positions were already available in our in-house collection (Table S2). Due to the relatively polar nature of ketamine and, common for most P450s, rather nonpolar CYP154E1 active site, fifteen additional single mutants were constructed with polar amino acids at most identified positions. Especially the positions L235 and I238, located in the I-helix, directly above the heme, seemed appropriate to stabilize the keto and amino groups of ketamine via hydrogen

bonding to the newly introduced polar amino acid residues (Figure S1). Hydrogen bonding between substrate and enzyme can be crucial for determining the selectivity of P450 as demonstrated for P450cam (CYP101A1) and P450cin (CYP108).⁵³ Presence or absence of H-bonds can influence the orientation and stabilization of the substrate in the active site, which then alters product formation.⁵³

Twenty-two out of 25 tested CYP154E1 variants showed similar or lower activity toward (S)-ketamine as compared to the wild-type enzyme (Figure 1). Only three variants catalyzed

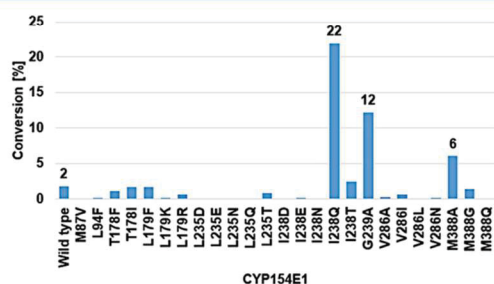


Figure 1. Screening of CYP154E1 mutants with (S)-ketamine. The numbers above the bars represent substrate conversion in %. The conversion was calculated by the ratio of the product peaks to the sum of all peak areas. Product analysis was carried out by GC/MS.

the oxidation of this substrate with higher activity. Replacement of I238 located in the I-helix above the heme by glutamine resulted in 12-fold improved substrate conversion. Interestingly, such a positive effect was achieved only by introducing glutamine at position 238. Substitution of I238 with glutamate and asparagine led to the complete loss of enzyme activity, which indicates that charged amino acids at this position are strongly disfavored and the length of the side

chain does matter as well. Glutamine at position 238 might serve as a hydrogen-bond donor for stabilizing (S)-ketamine in the orientation, where the amino group is located close to the heme iron, which is not the case in the wild-type enzyme and might explain the initial low activity (Figure S1).

Another substitution with a pronounced effect on (S)-ketamine conversion is G239A. By introducing alanine at position 239, the AGxxT motif conserved among many P450s was reconstituted,⁵⁴ which resulted in a 7-fold increased conversion. In our previous study, the G239A substitution in CYP154E1 had a positive effect on stilbene hydroxylation.²⁷ In the same study, again position 238 was in the focus of mutagenesis but, because of relatively nonpolar stilbene nature, isoleucine at position 238 was replaced by valine.

Substrate conversion was enhanced by a factor of 3 also by the M388A mutation. The relatively long side chain of methionine lies in a potential substrate-binding channel and might hinder the access of (S)-ketamine to the heme group.⁵⁵ Thus, its removal can be advantageous for heme accessibility for the substrate.

Remarkably, the three best CYP154E1 single mutants I238Q, G239A, and M388A did not only demonstrated higher activity but also produced, in contrast to all other variants, hydroxynorketamine in detectable amounts (Figure 2, Tables 1 and S2). This means that those CYP154E1 variants catalyze both N-demethylation and C6-hydroxylation at the same molecule.

In the next step, the mutations I238Q, G239A, and M388A were combined to the respective double and triple mutants. Each combination led to higher conversion and regioselectivity for C6-hydroxylation compared to the best single mutant I238Q (Figure 2).

Although the M388A single mutant showed only minor improvements compared to the wild-type enzyme, the integration of this mutation into the double and triple mutants

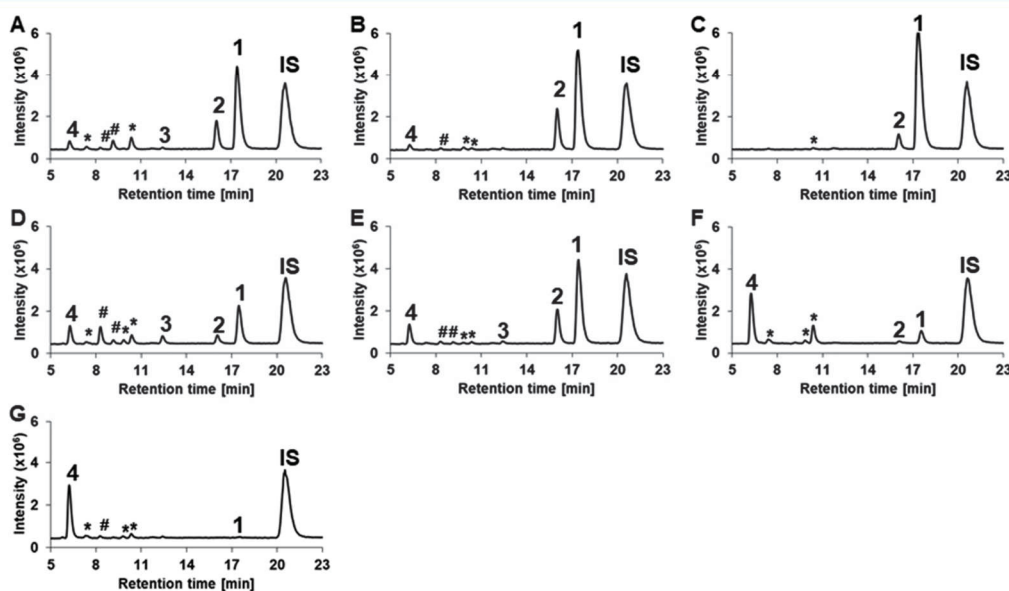


Figure 2. LC/MS chromatograms of (S)-ketamine oxidation catalyzed by CYP154E1 I238Q (A), G239A (B), M388A (C), I238Q G239A (D), G239A M388A (E), I238Q M388A (F), and QAA (G). IS: xylazine as internal standard, 1: ketamine, 2: norketamine, 3: dehydronorketamine, 4: (2S,6S)-hydroxynorketamine (identified by comparing with authentic standards, MS fragmentation pattern and NMR analysis), *: unknown hydroxyketamine (assigned by MS fragmentation pattern); #: unknown hydroxynorketamine (assigned by MS fragmentation pattern).

Table 1. (*S*)-Ketamine Oxidation Catalyzed by CYP154E1 Variants^a

| mutant | conv. [%] | product distribution [%] | | | | | |
|----------------------------------|-----------|--------------------------|------|-------------------------|-------------------------|---------------------|---------------------|
| | | NK | DHNK | Rt 8.2 min ^b | Rt 9.1 min ^b | (2 <i>S</i> ,6)-HNK | others ^c |
| I238Q | 49 ± 2 | 52 | 2 | 2 | 11 | 13 | 20 |
| G239A | 28 ± 3 | 81 | 2 | 2 | 1 | 8 | 6 |
| M388A | 6 ± 0.5 | 85 | | 1 | 1 | 3 | 10 |
| I238Q G239A | 85 ± 2 | 15 | 11 | 23 | 5 | 27 | 19 |
| G239A M388A | 49 ± 4 | 60 | 3 | 3 | 2 | 27 | 5 |
| I238Q M388A | 97 ± 2 | 1 | | | 1 | 70 | 28 |
| I238Q G239A M388A (QAA) | >99 | | | 3 | 1 | 85 | 11 |

^aNK: norketamine; DHNK: dehydronorketamine; (2*S*,6)-HNK: (2*S*,6)-hydroxynorketamine. ^bProducts with retention times of 8.2 and 9.1 min had mass fragmentation equivalent to that of (2*S*,6)-HNK, indicating either configuration or constitutional isomer. ^cProducts with mass fragmentation equivalent to that of HK (hydroxyketamine) underwent hydroxylation but no N-demethylation occurred.

was crucial for high conversion and selectivity. The combination of I238Q and M388A drastically increased the conversion to 97% (vs ~49% conversion with the single mutant I238Q). In addition, although none of the depicted single mutants exhibited high regioselectivity, the I238Q and M388A double mutant produced up to 70% C6-hydroxylated product. Introduction of the G239A mutation in the I238Q and M388A double mutant reduced the ratio of undesired products and thus boosted the product selectivity further to above 85%, demonstrated by the triple mutant QAA. Simultaneously, the triple mutant demonstrated the highest activity and caused quantitative conversions of (*S*)-ketamine and the intermediate (*S*)-norketamine (Figure 2G). Generally, it seems that all three mutations are responsible for the increased selectivity toward (2*S*,6*S*)-HNK.

In an attempt to further enhance the product selectivity of the QAA variant, T243 was replaced with asparagine, glutamine, and serine. Substitutions of this highly conserved threonine located at the distal part of the I-helix in other P450s

influenced various enzyme properties, including regio- and stereoselectivity.⁵⁶ Another position selected for mutagenesis was L234 because its substitution was found to be advantageous for the oxidation of other substrates.²⁷ None of the constructed quadruple mutants demonstrated higher activity or product selectivity (Figure S2). Thus, the triple CYP154E1 mutant QAA remained the enzyme of choice that demonstrated the highest activity and the highest product selectivity among all the constructed CYP154E1 variants.

What all CYP154E1 variants listed in Table 1 have in common is that they are able to perform both reactions, N-demethylation and hydroxylation, at the same (*S*)-ketamine molecule to furnish hydroxynorketamine. This capability of performing these two reactions by one P450 enzyme is rather uncommon. In vitro studies with a set of hepatic P450s have revealed that N-demethylation of ketamine to norketamine was catalyzed with the highest efficiency by CYP2B6 and hydroxylation of norketamine to hydroxynorketamines by CYP2A6. Although both enzymes were shown to catalyze both reactions, direct conversion of ketamine to hydroxynorketamine(s) with only one of those P450s has not been reported.^{12,13} Most studies on drug metabolism including those regarding ketamine metabolism in humans revealed that several P450 enzymes are responsible for hydroxylation and demethylation reactions on the same molecule.⁵⁷ Alternatively, one P450 is capable of both reactions but not on the same substrate molecule.⁵⁸

Characterization and Application of CYP154E1 QAA.

Starting with (*S*)-ketamine as a substrate, two stereoisomers, namely, (2*S*,6*S*)-hydroxynorketamine and its diastereomer (2*S*,6*R*)-hydroxynorketamine, can be formed. To better distinguish between the two diastereomers and to analyze the stereoselectivity of CYP154E1 variants during C6-hydroxylation of (*S*)-ketamine, all reactions were analyzed via HPLC on a chiral column (Figure S3). Identification of (2*S*,6*S*)-HNK product occurred via spiking with the authentic (2*S*,6*S*)-HNK standard (Figure S4). Except for (2*S*,6*S*)-hydroxynorketamine, no further respective standards were available and the side product formation was too low for NMR analysis. The chiral HPLC analysis of the QAA-catalyzed (*S*)-ketamine conversion revealed the (2*S*,6*S*)-HNK product peak whose shape is absolutely identical to the peak shape of the authentic standard (Figure S4). This observation indicates a 100% diastereoselectivity of this mutant. Even if one takes all

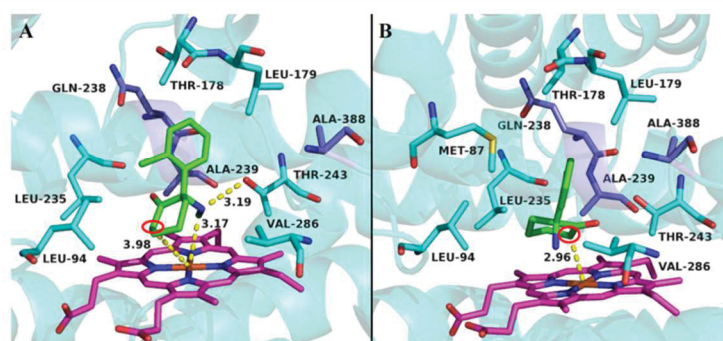


Figure 3. Best scored rigid docking poses of (*S*)-ketamine (green, A) and (*S*)-norketamine (green, B) in the active site of CYP154E1 QAA. Position C6 of the cyclohexanone ring is marked by red circle. Dashed yellow lines indicate distances between atoms. The numerical distance is given in Å.

other peaks into consideration, diastereoselectivity would only decrease to 92%.

These results were supported by docking studies (Figure 3). The best docking poses of (*S*)-ketamine and (*S*)-norketamine into the active site of CYP154E1 QAA demonstrated that the cyclohexanone ring in both substrates is located above and almost parallel to the heme group. This position favors the *syn*-attack, leading to the highly diastereoselective formation of (2*S*,6*S*)-hydroxynorketamine.

To complete the characterization of the best mutant QAA, the enzyme was purified to homogeneity and characterized regarding substrate binding and reaction kinetics. Upon (*S*)-ketamine titration, spectral changes of the Soret band occurred (Figures S5 and S6). The observed type I binding spectrum is typical for most P450 substrates. The binding constant K_D of 232 μM is however higher than the K_D values estimated for wild-type CYP154E1 and other mutants with other reported substrates, such as stilbene, geraniol, nerol, and fatty acids.^{27,28} Nevertheless, a direct comparison is somewhat questionable because small changes in the active site of P450 and in the substrate structure might lead to substantial perturbation during binding.

When comparing the kinetic parameters for the CYP154E1 QAA variant (Figure S7) with those found in the literature for human P450s, one recognizes that the K_M of $452 \pm 67 \mu\text{M}$ is in the same order of magnitude as that for ketamine oxidizing hepatic P450s.⁵⁹ On the other hand, the k_{cat} value of $56.2 \pm 4.7 \text{ min}^{-1}$ calculated for the QAA variant during (*S*)-ketamine conversion was in all cases higher. For example, the k_{cat} values for the three most active human P450s, CYP2B6, CYP2C9, and CYP3A4 are at least two times and up to six times lower compared to that of QAA.^{13,59,60}

Time-course studies have revealed that the first detected product of (*S*)-ketamine oxidation was (*S*)-norketamine, whereas (2*S*,6*S*)-HNK appeared later. This finding allowed us to suggest that demethylation and C6-hydroxylation occur in a consecutive manner according to Route A (Scheme 1), and the overall process is a two-step, four-electron oxidation of (*S*)-ketamine. According to substrate docking (Figure 3), the (*S*)-norketamine molecule is rotated about 90° clockwise around the vertical axis as compared to (*S*)-ketamine. This change in orientation brings position C6 1 Å closer to the heme iron (3.0 vs 4.0 Å for norketamine compared to ketamine), which makes this position more favorable for hydroxylation after demethylation. However, the MS analysis of the side products (Table 1) revealed the presence of low amounts of non-demethylated hydroxyketamine. Even after prolonged reaction times, N-demethylation of this hydroxyketamine occurred at a very low extent. Docking of (2*S*,6*S*)-hydroxyketamine (Figure S8) revealed that in this case the amine group of the substrate is located quite far away from the heme iron (7.09 Å), which could explain the observed low demethylation activity of the enzyme toward this metabolite. Thus, the presence of hydroxylated but not demethylated co-product may be due to more complex kinetics, which requires further detailed investigations.

For product isolation and testing the applicability of the CYP154E1 QAA variant for (2*S*,6*S*)-HNK production, we increased the reaction volume from 125 μL to 10 mL and the substrate concentrations from 500 μM to 5 mM. This reaction was performed using an *E. coli* based whole-cell biocatalyst harboring the *cyp154E1* QAA gene and the genes encoding the heterologous redox partners as described in the Experimental

Section. Within 6 h, (*S*)-ketamine HCl at a concentration of up to 1.16 g/L was converted (Figure S9) and (2*S*,6*S*)-hydroxynorketamine at a concentration of 935 mg/L was produced. In comparison to the CYP154E1 QAA, a maximum concentration of 201.6 $\mu\text{g/L}$ of (2,6)-HNK produced from the direct precursor (2,6)-hydroxyketamine was achieved in the reaction catalyzed by human CYP2B6. The formation of (2,6)-HNK with other human CYPs was even lower.¹²

The main product was isolated and purified via silica column with a yield of 44% (19.55 mg with 99% purity after conversion of 44.29 mg (*S*)-ketamine) and was confirmed as (2*S*,6*S*)-HNK via spiking experiment with respective standard and NMR analysis (Figures S10–S13).

CONCLUSIONS

Ketamine has been recognized as a promising antidepressant for the treatment of major depressive disorder and some other mental diseases. Since 2016, when the antidepressant effects of (2*S*,6*S*)- and (2*R*,6*R*)-hydroxynorketamines were first reported,¹⁰ their modes of action have been steadily discussed in the literature. Very recently, ketamine was suggested to be a prodrug that is metabolized to hydroxynorketamines with the desired antidepressant effect.⁴ In this context, the development of new effective synthetic routes of hydroxynorketamines are of high importance.

Herein, we report a new direct enzymatic route for (2*S*,6*S*)-hydroxynorketamine. The first-sphere mutagenesis at several positions located in close proximity to the heme group of CYP154E1, followed by combining the best mutations, led to the QAA triple mutant that possesses high product selectivity. In numbers, the conversion was increased from 2% with the wild-type enzyme to >99%. The engineered P450 enzyme is able to catalyze both the N-demethylation and the C6-hydroxylation reactions in a consecutive manner with high regio- and stereoselectivity leading to the desired product (2*S*,6*S*)-hydroxynorketamine at a ratio of 85%. In combination with the heterologous redox partners YkuN and FdR, this P450 turned out to be very efficient for the selective synthesis of (2*S*,6*S*)-hydroxynorketamine not only in vitro but also in the form of the whole-cell biocatalyst. The developed direct enzymatic route provides an efficient alternative to the chemical synthesis developed by Han et al. in 2017.¹⁷ In the chemical four-step approach, overall yield of around 30% was reached. In our CYP154E1 QAA-mediated process starting with (*S*)-ketamine, (2*S*,6*S*)-hydroxynorketamine with 99% purity was formed with an isolated yield of 44%. This P450-catalyzed reaction can further be combined with a simple chemical kinetic resolution of *rac*-ketamine with tartaric acid,⁶¹ which would reduce the overall production costs.

EXPERIMENTAL SECTION

Cloning. Mutagenesis, expression, and purification of enzymes are described in the Supporting Information and Table S1.

Docking Study. The homology model of CYP154E1 was created using the SWISS-MODEL^{62–65} server and the crystal structure of CYP154A1 (PDB: IODO) as a template. The coordinates of the heme were manually integrated into the homology model. The analysis of the homology model was done as described by Petrović and Zlatović in 2015.⁶⁶ The 3D structures of (*S*)-ketamine and (*S*)-norketamine in all stereoisomeric forms were obtained from the Cambridge

Structural Database. Rigid docking was performed using Autodock 4.0.^{67–70} Parameters files were created using AutoDockTools. Visualization of the results was carried out with PyMOL software.

Oxidation Reaction on an Analytical Scale. All reactions were performed in 100 mM potassium phosphate buffer with pH 7.5. Enzyme screening reactions were performed in 125 μL volume using *E. coli* cell lysate at 25 $^{\circ}\text{C}$ and 600 rpm. The reaction mixture consisted of 500 μM (*S*)-ketamine (dissolved in water), 2.5 μM P450 (crude cell lysate), 2.5 μM purified FdR, 25 μM purified YkuN, and 200 μM NADPH. NADPH recycling was supported by 5 U/mL GDH in the presence of 20 mM glucose. The decomposition of the potentially formed hydrogen peroxide due to P450 uncoupling reactions was achieved by adding 600 U/mL catalase. Reactions were stopped after 17 h by adding 125 μL of 1 M Na_2CO_3 . The extraction of the reaction mixtures was done twice with 200 μL of ethyl acetate each. The combined organic phases were evaporated to dryness and resolved in 100 μL of acetonitrile (for LC/MS analysis) or 100 μL of ethanol (for HPLC analysis). Substrate conversion in the screening experiments was based on the ratio between the sum of product peak areas compared to the sum of all peak areas. For all reactions other than the screening, 222 μM xylazine hydrochloride served as an internal standard for quantification and was added directly before the reaction was stopped by adding 1 M Na_2CO_3 .

Oxidation Reaction for Product Isolation. For reaction at higher scale, an in vivo two-plasmid whole-cell biotransformation system was created. Therefore, the genes of the redox proteins YkuN and FdR were cloned into the first and, respectively, second multiple cloning sites of the pCOLA Duet vector system. The P450 gene was cloned into pET22b as a second vector system. Expression was done in autoinduction medium using lactose as an inducer once glucose is consumed as a preferred carbon source. Overall expression was carried out in 500 mL flasks containing 100 mL of medium, initially at 37 $^{\circ}\text{C}$ and 180 rpm until OD_{600} of 1.0 was reached. Afterward, the cultures were stirred for another 20 h at 25 $^{\circ}\text{C}$ and 120 rpm before harvesting the cells. *E. coli* cells were washed once with reaction buffer (containing) and subsequent cell density was adjusted to 50 mg/mL cell density (cell wet weight) in the reaction buffer before the suspension was frozen at -80°C for at least 24 h. (*S*)-Ketamine (2 mM of 5 mM final concentration, dissolved in water) was added to 10 mL of thawed *E. coli* cell suspensions (50 mg/mL) and the reaction mixture was incubated in round-bottom flasks at 25 $^{\circ}\text{C}$ and 230 rpm. Extraction was done similar to the extraction procedure at an analytical scale except that volumes of 1 M Na_2CO_3 and ethyl acetate were adjusted to 1 mL and twice 7.5 mL, respectively. Organic layers were combined, dried over NaSO_4 , and removed under reduced pressure. The main product (2*S,6S*)-HNK was isolated with flash chromatography on a silica column using a mobile phase comprising 60% chloroform, 35% ethyl acetate, 5% methanol, and 0.1% ammonium hydroxide. Fractions were first analyzed via TLC using the same mobile phase and those with products were further analyzed via LC/MS and NMR (for details, see below).

Product Analysis. Screening of CYP154E1 mutant minimal library was carried out via GC/MS on a GCMS QP-2010 Plus GC/MS equipment (Shimadzu, Duisburg, Germany) with an FS-Supreme-5ms (30 m \times 0.25 mm \times 0.25 μm) column and helium as a carrier gas. The samples

were injected at an injection temperature of 300 $^{\circ}\text{C}$. Starting with a column oven temperature of 170 $^{\circ}\text{C}$ held for 2 min, the temperature then increased at the rate of 20 $^{\circ}\text{C}/\text{min}$ till 300 $^{\circ}\text{C}$ and held again for another 4 min.

LC/MS analysis was performed on a LCMS-2020 (Shimadzu) on a Chromolith Performance RP-8e 100–4.6 mm (Merck Millipore) column, equipped with a Chromolith RP-8e 5–4.6 mm guard cartridge using xylazine (222 μM concentration) as an internal standard. Elution occurred on a gradient between water (supplemented with 0.1% formic acid) and acetonitrile.

Stereoselectivity was analyzed using a LC-2020 (Shimadzu) HPLC system equipped with the chiral column Chiralpak IB (0.46 cm \varnothing \times 25 cm, Chiral Technologies Europe) and an isocratic elution mode consisting of 97% *n*-hexane and 3% ethanol.

Products and substrates were identified by their retention times and mass fragmentation patterns (GC/MS and LC/MS) compared to the corresponding values of authentic reference compounds and literature.⁷¹ Conversions were determined either via substrate depletion compared to the negative control or via internal standard quantification using xylazine as the internal standard.

Structure Elucidation. (2*S,6S*)-Hydroxynorketamine (**4**): ¹H NMR (600 MHz, chloroform-*d*) (Figure S10): δ 7.62–7.57 (m, 2H), 7.41–7.26 (m, 2H), 4.20 (dd, $J = 11.7, 6.9$ Hz, 1H), 2.93–2.86 (m, 1H), 2.39–2.31 (m, 1H), 2.03 (s, 2H), 1.74–1.64 (m, 2H), 1.67–1.54 (m, 1H), 1.51–1.40 (m, 1H). ¹³C NMR (151 MHz, chloroform-*d*) (Figure S11): δ 214.65, 138.17, 133.79, 131.58, 129.86, 128.78, 127.78, 73.75, 67.28, 42.19, 40.02, 19.40. Further structure elucidation was done by 2D-NMR (Figures S12 and S13).

Kinetic Studies. The reaction conditions and mixture were similar to those for analytical conversions. Instead of cell-free lysate, purified CYP154E1 QAA in a final concentration of 0.5 μM was used. The concentrations of purified FdR and YkuN were adjusted to 0.5 and 20 μM , respectively. To calculate the kinetic constants, the initial activity of CYP154E1 QAA was monitored at (*S*)-ketamine concentrations ranging from 50 to 2000 μM . The reactions were stopped after 5–20 min by adding 1 M sodium carbonate and xylazine (222 μM) as the internal standard. Conversions were analyzed on a LCMS-2020 (as described in the Product Analysis). For the calculation of k_{cat} and K_M , the data were fitted according to the equation of Michaelis–Menten by nonlinear regression using RStudio software (Figure S7) (RStudio Team (2015); RStudio: Integrated Development for R. RStudio, Inc., Boston, MA; <http://www.rstudio.com/>).

Determination of Substrate Dissociation Constant (K_D). Upon substrate binding in the P450 active site, spectral changes related to the changes in the heme iron spin state, were determined using a Lambda 35 double beam UV–vis spectrometer (Perkin-Elmer, Germany) equipped with two tandem quartz cuvettes (Hellma, Germany). The procedure was done according to Rühlmann et al. 2017.²⁷ One micromolar purified P450 enzyme buffered in 100 mM potassium phosphate buffer of pH 7.5 was used. Volumes of 0.5–10 μL of (*S*)-ketamine stock solutions were added successively. For the calculation of K_D , the data were fitted according to Michaelis–Menten-like hyperbolic equation by nonlinear regression using RStudio software (RStudio Team (2015); RStudio: Integrated Development for R. RStudio, Inc., Boston, MA; <http://www.rstudio.com/>).

■ ASSOCIATED CONTENT

Supporting Information

The Supporting Information is available free of charge at <https://pubs.acs.org/doi/10.1021/acscatal.9b05384>.

Experimental details, enzyme assays, chromatographic and spectral data, and NMR spectra (PDF)

■ AUTHOR INFORMATION

Corresponding Author

Vlada B. Urlacher – Institute of Biochemistry, Heinrich Heine University Düsseldorf, 40225 Düsseldorf, Germany;
 ● orcid.org/0000-0003-1312-4574; Email: Vlada.Urlacher@uni-duesseldorf.de

Authors

Ansgar Bokel – Institute of Biochemistry, Heinrich Heine University Düsseldorf, 40225 Düsseldorf, Germany

Ansgar Rühlmann – Institute of Biochemistry, Heinrich Heine University Düsseldorf, 40225 Düsseldorf, Germany

Michael C. Hutter – Center for Bioinformatics, Saarland University, 66123 Saarbrücken, Germany; ● orcid.org/0000-0003-3168-6554

Complete contact information is available at: <https://pubs.acs.org/doi/10.1021/acscatal.9b05384>

Notes

The authors declare no competing financial interest.

■ ACKNOWLEDGMENTS

We wish to thank Sebastian Hölzel, Heinrich Heine University Düsseldorf, Germany, for technical assistance. Generous financial support by the Federal Ministry of Education and Research to Heinrich Heine University Düsseldorf (grant number 031A223A) is gratefully acknowledged.

■ REFERENCES

- (1) Domino, E. F.; Chodoff, P.; Corssen, G. Pharmacologic Effects of CI-581, a New Dissociative Anesthetic, in Man. *Clin. Pharmacol. Ther.* **1965**, *6*, 279–291.
- (2) Berman, R. M.; Cappiello, A.; Anand, A.; Oren, D. A.; Heninger, G. R.; Charney, D. S.; Krystal, J. H. Antidepressant Effects of Ketamine in Depressed Patients. *Biol. Psychiatry* **2000**, *47*, 351–354.
- (3) Eikelenboom, M.; Beekman, A. T. F.; Penninx, B. W. J. H.; Smit, J. H. A 6-Year Longitudinal Study of Predictors for Suicide Attempts in Major Depressive Disorder. *Psychol. Med.* **2019**, *49*, 911–921.
- (4) Torjesen, I. Ketamine Could Be First of New Generation of Rapid Acting Antidepressants, say Experts. *BMJ* **2019**, *366*, No. 14714.
- (5) Monteggia, L. M.; Zarate, C., Jr. Antidepressant Actions of Ketamine: From Molecular Mechanisms to Clinical Practice. *Curr. Opin. Neurobiol.* **2015**, *30*, 139–143.
- (6) Scheuing, L.; Chiu, C.-T.; Liao, H.-M.; Chuang, D.-M. Antidepressant Mechanism of Ketamine: Perspective from Preclinical Studies. *Front. Neurosci.* **2015**, *9*, No. 249.
- (7) 22 Patents from 2006 to 2019 (Google Patents: Search Item: Ketamine or Esketamine; Search Item: Depression or Disorder (accessed Oct 24, 2019)).
- (8) Short, B.; Fong, J.; Galvez, V.; Shelker, W.; Loo, C. K. Side-Effects Associated with Ketamine Use in Depression: A Systematic Review. *Lancet Psychiatry* **2018**, *5*, 65–78.
- (9) Zanos, P.; Gould, T. D. Intracellular Signaling Pathways Involved in (S)- and (R)-Ketamine Antidepressant Actions. *Biol. Psychiatry* **2018**, *83*, 2–4.
- (10) Zanos, P.; Moaddel, R.; Morris, P. J.; Georgiou, P.; Fischell, J.; Elmer, G. I.; Alkondon, M.; Yuan, P.; Pribut, H. J.; Singh, N. S.;

Dossou, K. S.; Fang, Y.; Huang, X. P.; Mayo, C. L.; Wainer, I. W.; Albuquerque, E. X.; Thompson, S. M.; Thomas, C. J.; Zarate, C. A., Jr.; Gould, T. D. NMDAR Inhibition-Independent Antidepressant Actions of Ketamine Metabolites. *Nature* **2016**, *533*, 481–486.

(11) Zhang, J.-C.; Li, S.-X.; Hashimoto, K. R.-(-)-Ketamine Shows Greater Potency and Longer Lasting Antidepressant Effects Than S-(+)-Ketamine. *Pharmacol., Biochem. Behav.* **2014**, *116*, 137–141.

(12) Desta, Z.; Moaddel, R.; Ogburn, E. T.; Xu, C.; Ramamoorthy, A.; Venkata, S. L.; Sanghvi, M.; Goldberg, M. E.; Torjman, M. C.; Wainer, I. W. Stereoselective and Regiospecific Hydroxylation of Ketamine and Norketamine. *Xenobiotica* **2012**, *42*, 1076–1087.

(13) Portmann, S.; Kwan, H. Y.; Theurillat, R.; Schmitz, A.; Mevissen, M.; Thormann, W. Enantioselective Capillary Electrophoresis for Identification and Characterization of Human Cytochrome P450 Enzymes Which Metabolize Ketamine and Norketamine in Vitro. *J. Chromatogr. A* **2010**, *1217*, 7942–7948.

(14) Paul, R. K.; Singh, N. S.; Khadeer, M.; Moaddel, R.; Sanghvi, M.; Green, C. E.; O’Loughlin, K.; Torjman, M. C.; Bernier, M.; Wainer, I. W. R,S-Ketamine Metabolites (R,S)-Norketamine and (2S,6S)-Hydroxynorketamine Increase the Mammalian Target of Rapamycin Function. *Anesthesiology* **2014**, *121*, 149–159.

(15) Singh, N. S.; Zarate, C. A., Jr.; Moaddel, R.; Bernier, M.; Wainer, I. W. What Is Hydroxynorketamine and What Can It Bring to Neurotherapeutics? *Expert Rev. Neurother.* **2014**, *14*, 1239–1242.

(16) Johnson + Johnson Janssen Submits European Marketing Authorisation Application for Esketamine Nasal Spray for Treatment-Resistant Depression. <https://www.jnj.com/janssen-submits-european-marketing-authorisation-application-for-esketamine-nasal-spray-for-treatment-resistant-depression> (accessed Oct 22, 2019).

(17) Han, Y.; Mahender Reddy, K.; Corey, E. J. Simple Enantioselective Syntheses of (2R,6R)-Hydroxynorketamine and Related Potential Rapid-Onset Antidepressants. *Org. Lett.* **2017**, *19*, 5224–5227.

(18) Bernhardt, R.; Urlacher, V. B. Cytochromes P450 as Promising Catalysts for Biotechnological Application: Chances and Limitations. *Appl. Microbiol. Biotechnol.* **2014**, *98*, 6185–6203.

(19) Rittle, J.; Green, M. T. Cytochrome P450 Compound I: Capture, Characterization, and C-H Bond Activation Kinetics. *Science* **2010**, *330*, 933–937.

(20) Grant, J. L.; Hsieh, C. H.; Makris, T. M. Decarboxylation of Fatty Acids to Terminal Alkenes by Cytochrome P450 Compound I. *J. Am. Chem. Soc.* **2015**, *137*, 4940–4943.

(21) Groves, J. T.; Subramanian, D. V. Hydroxylation by Cytochrome-P-450 and Metalloporphyrin Models - Evidence for Allylic Rearrangement. *J. Am. Chem. Soc.* **1984**, *106*, 2177–2181.

(22) Moaddel, R.; Venkata, S. L.; Tanga, M. J.; Bupp, J. E.; Green, C. E.; Iyer, L.; Furimsky, A.; Goldberg, M. E.; Torjman, M. C.; Wainer, I. W. A Parallel Chiral-Achiral Liquid Chromatographic Method for the Determination of the Stereoisomers of Ketamine and Ketamine Metabolites in the Plasma and Urine of Patients with Complex Regional Pain Syndrome. *Talanta* **2010**, *82*, 1892–1904.

(23) Karki, S. B.; Dinnocenzo, J. P.; Jones, J. P.; Korzekwa, K. R. Mechanism of Oxidative Aminodealkylation of Substituted N,N-Dimethylanilines by Cytochrome P450 - Application of Isotope Effect Profiles. *J. Am. Chem. Soc.* **1995**, *117*, 3657.

(24) Dubey, K. D.; Wang, B.; Vajpai, M.; Shaik, S. MD Simulations and QM/MM Calculations Show that Single-Site Mutations of Cytochrome P450 BM3 Alter the Active Site’s Complexity and the Chemoselectivity of Oxidation without Changing the Active Species. *Chem. Sci.* **2017**, *8*, 5335–5344.

(25) Bogazkaya, A. M.; von Buhler, C. J.; Kriening, S.; Busch, A.; Seifert, A.; Pleiss, J.; Laschat, S.; Urlacher, V. B. Selective Allylic Hydroxylation of Acyclic Terpenoids by CYP154E1 from *Thermobifida fusca* YX. *Beilstein J. Org. Chem.* **2014**, *10*, 1347–1353.

(26) Hernández-Martín, A.; von Buhler, C. J.; Tieves, F.; Fernandez, S.; Ferrero, M.; Urlacher, V. B. Whole-Cell Biotransformation with Recombinant Cytochrome P450 for the Selective Oxidation of Grundmann’s Ketone. *Bioorg. Med. Chem.* **2014**, *22*, 5586–5592.

- (27) Rühlmann, A.; Antovic, D.; Müller, T. J. J.; Urlacher, V. B. Regioselective Hydroxylation of Stilbenes by Engineered Cytochrome P450 from *Thermobifida fusca* YX. *Adv. Synth. Catal.* **2017**, *359*, 984–994.
- (28) von Bühler, C. J.; Le-Huu, P.; Urlacher, V. B. Cluster Screening: An Effective Approach for Probing the Substrate Space of Uncharacterized Cytochrome P450s. *ChemBioChem* **2013**, *14*, 2189–2198.
- (29) von Bühler, C. J.; Urlacher, V. B. A Novel P450-Based Biocatalyst for the Selective Production of Chiral 2-Alkanols. *Chem. Commun.* **2014**, *50*, 4089–4091.
- (30) Tieves, F.; Erenburg, I. N.; Mahmoud, O.; Urlacher, V. B. Synthesis of Chiral 2-Alkanols from *n*-Alkanes by a *P. putida* Whole-Cell Biocatalyst. *Biotechnol. Bioeng.* **2016**, *113*, 1845–1852.
- (31) Girvan, H. M.; Munro, A. W. Applications of Microbial Cytochrome P450 Enzymes in Biotechnology and Synthetic Biology. *Curr. Opin. Chem. Biol.* **2016**, *31*, 136–145.
- (32) Wei, Y.; Ang, E. L.; Zhao, H. Recent Developments in the Application of P450 Based Biocatalysts. *Curr. Opin. Chem. Biol.* **2018**, *43*, 1–7.
- (33) Urlacher, V. B.; Girhard, M. Cytochrome P450 Monooxygenases in Biotechnology and Synthetic Biology. *Trends Biotechnol.* **2019**, *37*, 882–897.
- (34) Zhang, R. K.; Huang, X.; Arnold, F. H. Selective CH Bond Functionalization with Engineered Heme Proteins: New Tools to Generate Complexity. *Curr. Opin. Chem. Biol.* **2019**, *49*, 67–75.
- (35) Manning, J.; Tavanti, M.; Porter, J. L.; Kress, N.; De Visser, S. P.; Turner, N. J.; Flitsch, S. L. Regio- and Enantio-Selective Chemo-Enzymatic C-H-Lactonization of Decanoic Acid to (*S*)- δ -Decalactone. *Angew. Chem., Int. Ed.* **2019**, *58*, 5668–5671.
- (36) Matthews, S.; Tee, K. L.; Rattray, N. J.; McLean, K. J.; Leys, D.; Parker, D. A.; Blankley, R. T.; Munro, A. W. Production of Alkenes and Novel Secondary Products by P450 OleTJE Using Novel H₂O₂-Generating Fusion Protein Systems. *FEBS Lett.* **2017**, *591*, 737–750.
- (37) Gillam, E. M. Engineering Cytochrome P450 Enzymes. *Chem. Res. Toxicol.* **2008**, *21*, 220–231.
- (38) Jung, S. T.; Lauchli, R.; Arnold, F. H. Cytochrome P450: Taming a Wild Type Enzyme. *Curr. Opin. Biotechnol.* **2011**, *22*, 809–817.
- (39) Li, Q. S.; Ogawa, J.; Schmid, R. D.; Shimizu, S. Engineering Cytochrome P450 BM-3 for Oxidation of Polycyclic Aromatic Hydrocarbons. *Appl. Environ. Microbiol.* **2001**, *67*, 5735–5739.
- (40) Ost, T. W.; Miles, C. S.; Murdoch, J.; Cheung, Y.; Reid, G. A.; Chapman, S. K.; Munro, A. W. Rational Re-Design of the Substrate Binding Site of Flavocytochrome P450 BM3. *FEBS Lett.* **2000**, *486*, 173–177.
- (41) Xu, F.; Bell, S. G.; Rao, Z.; Wong, L. L. Structure-Activity Correlations in Pentachlorobenzene Oxidation by Engineered Cytochrome P450cam. *Protein Eng., Des. Sel.* **2007**, *20*, 473–480.
- (42) Dennig, A.; Weingartner, A. M.; Kardashliev, T.; Müller, C. A.; Tassano, E.; Schürmann, M.; Ruff, A. J.; Schwaneberg, U. An Enzymatic Route to A-Tocopherol Synthons: Aromatic Hydroxylation of Pseudocumene and Mesitylene with P450 BM3. *Chem. - Eur. J.* **2017**, *23*, 17981–17991.
- (43) Holec, C.; Hartrampf, U.; Neufeld, K.; Pietruszka, J. P450 BM3-Catalyzed Regio- and Stereoselective Hydroxylation Aiming at the Synthesis of Phthalides and Isocoumarins. *ChemBioChem* **2017**, *18*, 676–684.
- (44) Wang, S.; Liu, Z. Oxygenation Cascade Analysis in Conversion of *n*-Octane Catalyzed by Cytochrome P450 CYP102A3 Mutants at the P331 Site. *Biotechnol. Appl. Biochem.* **2017**, *64*, 14–19.
- (45) Acevedo-Rocha, C. G.; Gamble, C. G.; Lonsdale, R.; Li, A. T.; Nett, N.; Hoebenreich, S.; Lingnau, J. B.; Wirtz, C.; Fares, C.; Hinrichs, H.; Deege, A.; Mulholland, A. J.; Nov, Y.; Leys, D.; McLean, K. J.; Munro, A. W.; Reetz, M. T. P450-Catalyzed Regio- and Diastereoselective Steroid Hydroxylation: Efficient Directed Evolution Enabled by Mutability Landscaping. *ACS Catal.* **2018**, *8*, 3395–3410.
- (46) Kille, S.; Zilly, F. E.; Acevedo, J. P.; Reetz, M. T. Regio- and Stereoselectivity of P450-Catalyzed Hydroxylation of Steroids Controlled by Laboratory Evolution. *Nat. Chem.* **2011**, *3*, 738–743.
- (47) Kolev, J. N.; O'Dwyer, K. M.; Jordan, C. T.; Fasan, R. Discovery of Potent Parthenolide-Based Antileukemic Agents Enabled by Late-Stage P450-Mediated C-H Functionalization. *ACS Chem. Biol.* **2014**, *9*, 164–173.
- (48) Le-Huu, P.; Petrović, D.; Strodel, B.; Urlacher, V. B. One-Pot Two-Step Hydroxylation of the Macrocyclic Diterpenoid β -Cembrene diol Catalyzed by P450 BM3 Mutants. *ChemCatChem* **2016**, *8*, 3755–3761.
- (49) Zhang, K.; Shafer, B. M.; Demars, M. D., II; Stern, H. A.; Fasan, R. Controlled Oxidation of Remote sp³ C-H Bonds in Artemisinin Via P450 Catalysts with Fine-Tuned Regio- and Stereoselectivity. *J. Am. Chem. Soc.* **2012**, *134*, 18695–18704.
- (50) Li, Y.; Wong, L. L. Multi-Functional Oxidase Activity of CYP102A1 (P450BM3) in the Oxidation of Quinolines and Tetrahydroquinolines. *Angew. Chem., Int. Ed.* **2019**, *58*, 9551–9555.
- (51) O'Hanlon, J. A.; Ren, X. K.; Morris, M.; Wong, L. L.; Robertson, J. Hydroxylation of Anilides by Engineered Cytochrome P450(BM3). *Org. Biomol. Chem.* **2017**, *15*, 8780–8787.
- (52) Seifert, A.; Antonovici, M.; Hauer, B.; Pleiss, J. An Efficient Route to Selective Bio-Oxidation Catalysts: An Iterative Approach Comprising Modeling, Diversification, and Screening, Based on CYP102A1. *ChemBioChem* **2011**, *12*, 1346–1351.
- (53) Slessor, K. E.; Stok, J. E.; Chow, S.; De Voss, J. J. Significance of Protein-Substrate Hydrogen Bonding for the Selectivity of P450-Catalyzed Oxidations. *Chem. - Eur. J.* **2019**, *25*, 4149–4155.
- (54) Mestres, J. Structure Conservation in Cytochromes P450. *Proteins* **2005**, *58*, 596–609.
- (55) Wade, R. C.; Winn, P. J.; Schlichting, I.; Sudarko, A. Survey of Active Site Access Channels in Cytochromes P450. *J. Inorg. Biochem.* **2004**, *98*, 1175–1182.
- (56) Clark, J. P.; Miles, C. S.; Mowat, C. G.; Walkinshaw, M. D.; Reid, G. A.; Daff, S. N.; Chapman, S. K. The Role of Thr268 and Phe393 in Cytochrome P450 BM3. *J. Inorg. Biochem.* **2006**, *100*, 1075–1090.
- (57) Jiang, Z.-P.; Shu, Y.; Chen, X.-P.; Huang, S.-L.; Zhu, R.-H.; Wang, W.; He, N.; Zhou, H.-H. The Role of CYP2C19 in Amitriptyline *N*-Demethylation in Chinese Subjects. *Eur. J. Clin. Pharmacol.* **2002**, *58*, 109–113.
- (58) Olesen, O. V.; Linnet, K. Hydroxylation and Demethylation of the Tricyclic Antidepressant Nortriptyline by cDNA-Expressed Human Cytochrome P-450 Isozymes. *Drug Metab. Dispos.* **1997**, *25*, 740–744.
- (59) Hijazi, Y.; Bouliou, R. Contribution of CYP3A4, CYP2B6, and CYP2C9 Isoforms to *N*-Demethylation of Ketamine in Human Liver Microsomes. *Drug Metab. Dispos.* **2002**, *30*, 853–858.
- (60) Yanagihara, Y.; Kariya, S.; Ohtani, M.; Uchino, K.; Aoyama, T.; Yamamura, Y.; Iga, T. Involvement of CYP2B6 in *N*-Demethylation of Ketamine in Human Liver Microsomes. *Drug Metab. Dispos.* **2001**, *29*, 887–890.
- (61) Steiner, K.; Gangkofner, S.; Grunenwald, J.-M. Racemic Separation of Ketamine. U.S. Patent US6,040,479, March 31, 2000.
- (62) Arnold, K.; Bordoli, L.; Kopp, J.; Schwede, T. The SWISS-MODEL Workspace: A Web-Based Environment for Protein Structure Homology Modelling. *Bioinformatics* **2006**, *22*, 195–201.
- (63) Biasini, M.; Bienert, S.; Waterhouse, A.; Arnold, K.; Studer, G.; Schmidt, T.; Kiefer, F.; Gallo Cassarino, T.; Bertoni, M.; Bordoli, L.; Schwede, T. SWISS-MODEL: Modelling Protein Tertiary and Quaternary Structure Using Evolutionary Information. *Nucleic Acids Res.* **2014**, *42*, W252–W258.
- (64) Guex, N.; Peitsch, M. C.; Schwede, T. Automated Comparative Protein Structure Modeling with SWISS-MODEL and Swiss-PdbViewer: A Historical Perspective. *Electrophoresis* **2009**, *30*, S162–S173.
- (65) Kiefer, F.; Arnold, K.; Kunzli, M.; Bordoli, L.; Schwede, T. The SWISS-MODEL Repository and Associated Resources. *Nucleic Acids Res.* **2009**, *37*, D387–D392.

(66) Petrović, D.; Zlatović, M. Modeling Human Serum Albumin Tertiary Structure to Teach Upper-Division Chemistry Students Bioinformatics and Homology Modeling Basics. *J. Chem. Educ.* **2015**, *92*, 1233–1237.

(67) Goodsell, D. S.; Olson, A. J. Automated Docking of Substrates to Proteins by Simulated Annealing. *Proteins* **1990**, *8*, 195–202.

(68) Morris, G. M.; Goodsell, D. S.; Halliday, R. S.; Huey, R.; Hart, W. E.; Belew, R. K.; Olson, A. J. Automated Docking Using a Lamarckian Genetic Algorithm and an Empirical Binding Free Energy Function. *J. Comput. Chem.* **1998**, *19*, 1639–1662.

(69) Morris, G. M.; Goodsell, D. S.; Huey, R.; Olson, A. J. Distributed Automated Docking of Flexible Ligands to Proteins: Parallel Application of AutoDock 2.4. *J. Comput.-Aided Mol. Des.* **1996**, *10*, 293–304.

(70) Morris, G. M.; Huey, R.; Lindstrom, W.; Sanner, M. F.; Belew, R. K.; Goodsell, D. S.; Olson, A. J. AutoDock4 and AutoDockTools4: Automated Docking with Selective Receptor Flexibility. *J. Comput. Chem.* **2009**, *30*, 2785–2791.

(71) Wu, C. H.; Huang, M. H.; Wang, S. M.; Lin, C. C.; Liu, R. H. Gas Chromatography-Mass Spectrometry Analysis of Ketamine and Its Metabolites—a Comparative Study on the Utilization of Different Derivatization Groups. *J. Chromatogr. A* **2007**, *1157*, 336–351.

2.2 Chapter II

Molecular Evolution of a Cytochrome P450 for the Synthesis of Potential Antidepressant (2*R*,6*R*)-Hydroxynorketamine

Ansgar Bokel, Michael C. Hutter, and Vlada B. Urlacher*

*corresponding author

Chemical Communications, 2021, 57, 520-523

Own contribution (85%): AB designed the project. AB planned and performed all the experimental work. AB and VBU wrote the manuscript.

AB executed isolation of (*R*)-ketamine from racemic ketamine. Expression, purification, and enzyme assays for all enzymes (GDH, YkuN, FdR, CYP154E1) was executed by AB. AB developed the deep-well cultivation and GC-MS-based screening procedure. AB implemented analysis and selection of hits. AB created all CYP154E1 variants, expressed them, measured their concentration, and performed the *in vitro* and *in vivo* reactions. Kinetics of the CYP154E1 TQA triple mutant were measured and evaluated by AB. Upscaling of the (*R*)-ketamine conversion, method development for the semi-preparative HPLC, product isolation, and NMR analysis was implemented by AB. NMR samples were measured by the NMR facility (HHU).

In cooperation with MCH, AB created the homology model and executed the docking experiments to identify the hot spot position for mutagenesis.

Bokel, A., Hutter, M. C., & Urlacher, V. B. (2021). Molecular evolution of a cytochrome P450 for the synthesis of potential antidepressant (2*R*,6*R*)-hydroxynorketamine. *Chemical Communications*, 57, 520-523. - Reproduced by permission of The Royal Society of Chemistry.

Cite this: *Chem. Commun.*, 2021, 57, 520Received 9th October 2020,
Accepted 3rd December 2020

DOI: 10.1039/d0cc06729f

rsc.li/chemcomm

Molecular evolution of a cytochrome P450 for the synthesis of potential antidepressant (2*R*,6*R*)-hydroxynorketamine†

Ansgar Bokel,^a Michael C. Hutter^b and Vlada B. Urlacher^{†*}

Saturation mutagenesis at seven first-sphere residues of the cytochrome P450 monooxygenase 154E1 (CYP154E1) from *Thermobifida fusca* YX was applied to construct a variant with only three substitutions that enabled the effective two-step synthesis of the potential antidepressant (2*R*,6*R*)-hydroxynorketamine. A recombinant *E. coli* whole-cell system was essential for GC/MS based medium-throughput screening and at the same time facilitated the oxidation of the substrate (*R*)-ketamine at a higher scale for product isolation and subsequent NMR analysis.

Since the microbial regio- and stereoselective oxidation of Reichstein S to hydrocortisone¹ and the stereo- and regiospecific hydroxylation of compactin to pravastatin² have been implemented at industrial scale, cytochromes P450 (P450) that catalyze these reactions are recognized as unsurpassed oxidizing biocatalysts for the production of pharmaceuticals and high-value building blocks. In the presence of molecular oxygen and NAD(P)H these heme containing enzymes catalyze various oxidation reactions like hydroxylation of non-activated C–H bonds, sulfoxidation, and *N*- or *O*-dealkylation which are often challenging for chemical synthesis.³ For their activity, most P450s require redox partners like flavin reductases, ferredoxin or flavodoxins, which transfer electrons from NAD(P)H to the ferric heme iron. In the last two decades, many P450 enzymes have been characterized, engineered by means of directed evolution and rational protein design regarding improved activity, selectivity, altered substrate scope, and introduced in cascade reactions or whole-cell biocatalysts.⁴ Despite these achievements, engineering of P450 enzymes for highly regio- and stereospecific oxidations at predetermined positions of a substrate molecule with several potential positions for oxidation remains a challenging task.⁵ Along with uncertainties in the effect of the predicted amino acid substitutions on reaction outcome, practical difficulties in screening of

thousands of mutants generated *via e.g.* directed evolution are associated with the requirement for separate redox partner proteins for most P450s.

In this work, we aimed to achieve efficient enzyme-mediated regio- and stereoselective oxidation of ketamine. Originally synthesized in 1962 as an alternative to the anaesthetic phencyclidine,⁶ ketamine is also known since 2000 as a rapid-acting and long-lasting antidepressant in the therapy of treatment-resistant major depressive disorder and some other mental diseases.⁷ Recent studies have revealed that not ketamine alone, but its metabolites and particularly (2*R*,6*R*)-hydroxynorketamine are responsible for the antidepressant effects after ketamine intake.⁸ Moreover, (2*R*,6*R*)-hydroxynorketamine does not induce negative side effects related to ketamine and thus is considered as a potential antidepressant drug.^{8a}

Chemical syntheses of (2*R*,6*R*)-hydroxynorketamine either involve several steps or start with already demethylated norketamine.^{8a,9} These circumstances prompted us to construct a P450 enzyme capable of catalyzing both *N*-demethylation and the stereoselective C6-hydroxylation of (*R*)-ketamine **1** to form (2*R*,6*R*)-hydroxynorketamine **4** (Scheme in Table 1).

For this purpose, we chose CYP154E1 from *Thermobifida fusca* YX, which possesses a broad substrate spectrum and was optimized by means of protein engineering for higher activity and selectivity towards different substrates.¹⁰ First, (*R*)-**1** was isolated from racemic ketamine according to the previously reported protocol,¹¹ with 37% isolated yield and 99% purity (ESI,† Fig. S1) and tested with the wild type enzyme. As CYP154E1 wild type showed almost no activity towards (*R*)-**1** (ESI,† Fig. S2), we applied a semi-rational approach in which rational design was combined with saturation mutagenesis at positions located in the first sphere around the heme aiming (i) to increase activity towards (*R*)-**1** and (ii) to achieve high degree of *N*-dealkylation in combination with regio- and stereoselective C6-hydroxylation to ultimately get to (2*R*,6*R*)-**4**.

Our previous studies on CYP154E1 engineering demonstrated that both activity and selectivity can be “induced” by replacing the isoleucine at position 238.^{10b,12} I238 is located in

^a Institute of Biochemistry, Heinrich-Heine University Düsseldorf, Universitätsstr. 1, Düsseldorf 40225, Germany. E-mail: Vlada.Urlacher@uni-duesseldorf.de

^b Center for Bioinformatics, Saarland University, Campus E2.1, Saarbruecken 66123, Germany

† Electronic supplementary information (ESI) available: Experimental methods, docking, and NMR data. See DOI: 10.1039/d0cc06729f

Table 1 (*R*)-Ketamine oxidation catalyzed by CYP154E1 mutants. HNK: hydroxynorketamine; HK: hydroxyketamine; NK: norketamine. Reaction conditions: 2.5 μM CYP, 2.5 μM FdR, 25 μM YkuN, 500 μM (*R*)-ketamine, 200 μM NADPH, 20 mM glucose, 600 U mL^{-1} catalase, 5 U mL^{-1} GDH, 100 mM potassium phosphate buffer pH 7.5, total volume of 125 μL . Incubation at 25 $^{\circ}\text{C}$ and 600 rpm (Eppendorf ThermoMixer) for 20 hours

| | Mutations | Conversion [%] | Product distribution [%] | | | | | TTN ^f | |
|---|------------------|----------------|------------------------------------|-----------------------------------|---|--|-------------------|------------------|--------------------|
| | | | (2 <i>R</i> ,6)-HNK 4 ^a | (2 <i>R</i> ,6)-HK 3 ^b | (2 <i>R</i> ,4 <i>S</i>)-HK ^c | (2 <i>R</i> ,4 <i>S</i>)-HNK ^d | (<i>R</i>)-NK 2 | | Other ^e |
| Starting variant | I238Q/M388A (QA) | 97 | 9 | 12 | 15 | 47 | 1 | 16 | n.d. |
| | M87V/QA | 92 | 11 | 13 | 12 | 40 | 13 | 10 | n.d. |
| | L94P/QA | > 99 | 10 | 14 | 17 | 45 | — | 14 | 3333 |
| | T243S/QA | > 99 | 11 | 21 | 37 | 16 | — | 16 | 2275 |
| Mutants selected from the site-saturation sub-libraries | V286G/QA | 99 | 22 | 45 | — | 11 | 14 | 8 | n.d. |
| | L289A/QA | > 99 | 84 | 5 | — | — | — | 11 | 4891 |
| | L289G/QA | > 99 | 81 | 4 | — | — | — | 15 | 3075 |
| | L289P/QA | > 99 | 70 | 7 | — | — | — | 23 | 3817 |
| | L289T/QA | > 99 | 85 | 10 | — | — | — | 5 | 7090 |

^a Structure was elucidated *via* NMR analysis (ESI, Fig. S7–S10) and comparison with authentic standards. ^b Structure was elucidated *via* NMR analysis (ESI, Fig. S11–S14). ^c Structure was solved previously.¹⁷ ^d Conversion of (2*R*,4*S*)-HK resulted in a single product corresponding to the mass of a hydroxynorketamine (ESI, Fig. S6). ^e “Other” are those products whose structures have not yet been solved. However, MS data indicate that they are unknown hydroxyketamines and hydroxynorketamines. ^f For the calculation of TTN for the mutants with the quantitative conversion of 500 μM (*R*)-1, 1 μM P450 and 5 mM or 10 mM (*R*)-1 were used; n.d. not determined.

the I-helix directly above the heme and is likely to interact with any substrate (Fig. 1). In order to identify a suitable starting variant with activity towards (*R*)-1, we performed saturation mutagenesis at this position. Replacement of isoleucine 238 by alanine, glycine, glutamine or serine induced enzyme activity leading to a substrate conversion of 65–98%, and to formation

of (2*R*,6)-4 but at a low ratio (ESI,† Fig. S2). Another “hotspot” for mutagenesis was M388 that lies in the potential substrate binding channel and might hinder the access to the heme (Fig. 1). The M388A mutation has been found to drastically enhance enzyme activity and selectivity.¹² Thus, the M388A mutation was introduced into the four best I238 single mutants. The double mutants I238A/M388A and I238Q/M388A were equally efficient with respect to substrate conversion and desired product formation (ESI,† Fig. S3). They differed, however, in their regioselectivity; while the I238A/M388A mutant demonstrated a slight preference for C4-hydroxylation, the I238Q/M388A mutant possessed a 2-fold higher regioselectivity for C6-hydroxylation.

To identify further “hotspot” positions for saturation mutagenesis, we used a homology model based on the crystal structure of CYP154A1 from *Streptomyces coelicolor* (PDB 1ODO) and molecular docking. Seven positions in the first sphere located within 13 Å from the heme were selected, because their side chains interact with the substrate (Fig. 1). Thus, we hypothesized that their mutations might affect enzyme selectivity. The NNK codon degeneracy, encoding all 20 canonical amino acids, was introduced at each of the selected positions individually in the starting mutant

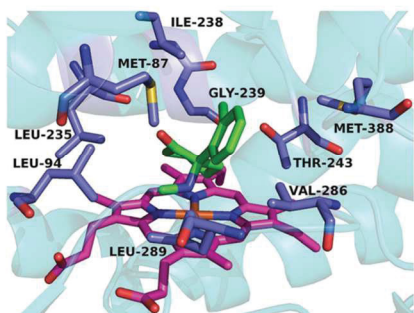


Fig. 1 Best scored docking pose of (*R*)-ketamine **1** (green) in the active site of CYP154E1. The heme group is shown in purple. Residues of the first-sphere pointing towards the substrate are shown in blue and labelled.

I238Q/M388A, resulting in seven site-saturation mutagenesis sub-libraries. The initially constructed libraries generated with the standard QuikChange method did not result in sufficient mutant diversity. For this reason, the site-saturation sub-libraries with high diversity were constructed using the improved PCR method reported by Sanchis *et al.* (see ESI†).¹³ Screening of 180 colonies per site (instead of 94, suggested by tools for saturation mutagenesis, to cover 95% of a given library [CASTER 2.0]¹⁴) was estimated sufficient to compensate small discrepancies in codon/amino acid distribution at a given position.

In order to reduce practical efforts, the mutated genes were cloned in an *E. coli* strain, additionally expressing two redox partner proteins to ensure P450 activity (see the ESI†). The generated *E. coli* cell-based sub-libraries were screened with (*R*)-1 for increased activity and/or C6-selectivity using GC/MS analysis. LC/MS analysis was subsequently used for the verification of the identified hits after reactions with isolated enzymes.

Screening revealed that saturation mutagenesis at G239 and L235 did not improve the enzyme selectivity. At all other positions, substitutions had minor to major effects on product selectivity (Table 1). Generally, in all mutants with enhanced regioselectivity towards C6, the wild type amino acids were replaced by smaller amino acids, providing more space in the active site. Furthermore, none of the new substitutions drastically decreased the activity of the starting mutant. Even the replacement of the highly conserved threonine 243 located at the distal part of the I-helix, which has often caused dramatic loss of activity in other P450s,¹⁵ did not affect conversion but enzyme regioselectivity. Specifically, the T243S/I238Q/M388A mutant led to double the amount of (2*R*,6)-3 (hydroxylation at C6 but no dealkylation), whereas the desired product (2*R*,6)-4 was produced in similar amounts as with the starting variant. This result means an enhancement of the regioselectivity for C6-hydroxylation from 21% (9% (2*R*,6)-4 + 12% (2*R*,6)-3 achieved with the starting variant) to 32% (11% (2*R*,6)-4 + 21% (2*R*,6)-3 with T243S/I238Q/M388A) (Table 1). The influence of this conserved position on regioselectivity has been reported for other P450s as well.¹⁶

The most profound effect on the formation of (2*R*,6)-4 had substitutions at positions V286 and L289. The V286G mutation increased (2*R*,6)-4 formation by a factor of 3 compared to the starting variant. The substitutions L289P and L289T increased the (2*R*,6)-4 ratio 8- or 9-times, respectively. Thus, the L289T/I238Q/M388A mutant demonstrated 95% regioselectivity for C6-hydroxylation – resulting from 10% (2*R*,6)-3 and 85% (2*R*,6)-4 (Table 1). The obtained high amount of (2*R*,6)-4 also means that besides high regioselectivity, L289T/I238Q/M388A efficiently catalyzes, subsequent or prior to the C6-hydroxylation, the *N*-demethylation reaction. Since six mutants resulted in a quantitative conversion of 500 μM (*R*)-1, they were also tested with 5 mM and 10 mM substrate concentrations. Total turnover numbers (TTNs) ranging between 2000 and 7000 reflect the middle to high catalytic performance of these mutants (Table 1).

To minimize further screening efforts using GC/MS, the variants V286G/I238Q/M388A and L289T/I238Q/M388A were then directly combined to a quadruple mutant. Conversion was not affected by the introduction of the fourth mutation

but the product distribution pattern drastically changed. While the triple mutant L289T/I238Q/M388A produced 85% (2*R*,6)-4, this value dropped to 32% for the quadruple mutant V286G/L289T/I238Q/M388A.

On the other hand, the formation of non-demethylated (2*R*,6)-3 increased from roughly 10% (with L289T/I238Q/M388A) to almost 67% (ESI† Table S2). Thus, although the amount of (2*R*,6)-4 decreased, the regioselectivity towards C6 increased from 95% (10% (2*R*,6)-3 + 85% (2*R*,6)-4) to 99% (67% (2*R*,6)-3 + 32% (2*R*,6)-4). This change in the product pattern indicates that V286G either negatively influences the substrate orientation for the *N*-demethylation reaction or positively influences C6-hydroxylation after which subsequent *N*-demethylation is somehow more difficult. This latter assumption is supported by the results obtained with the triple mutant V286G/I238Q/M388A, which also preferentially produced (2*R*,6)-3 (45% among all products) lacking *N*-demethylation.

For the assessment of the effect of each mutation in the optimal L289T/I238Q/M388A mutant that resulted in the highest ratio of (2*R*,6*R*)-4, the L289T single mutant and all possible double mutants (L289T/I238Q and L289T/M388A, in addition to I238Q/M388A) were constructed and investigated (ESI† Table S2). The L289T mutant led to slightly higher conversion than wild type, but *N*-demethylation was the only observed reaction. By combining L289T and I238Q, the conversion of both (*R*)-ketamine 1 and (*R*)-norketamine 2 as well as regioselectivity during C6-hydroxylation was improved: the L289T/I238Q mutant enabled quantitative conversion, and the regioselectivity for C6 increased up to 91% (30% (2*R*,6)-3 + 61% (2*R*,6)-4). The introduction of M388A further enhanced the demethylation reaction leading to a 1.4-fold higher amount of (2*R*,6)-4 (ESI† Table S2). Thus, all three substitutions – I238Q, L289T and M388A – contribute to higher substrate dealkylation and C6-hydroxylation, ultimately leading to quantitative conversion of (*R*)-1 (99%) and resulting in 85% (2*R*,6)-4. The product was isolated and analyzed by NMR, which confirmed that (2*R*,6)-hydroxynorketamine 4 was produced. The k_M value of $709 \pm 71 \mu\text{M}$, k_{cat} of $71.8 \pm 4.8 \text{ min}^{-1}$ and k_{cat}/k_M of $0.1 \mu\text{M}^{-1} \text{ min}^{-1}$ were estimated for the triple mutant L289T/I238Q/M388A (ESI† Fig. S4). In the course of the kinetic experiments, (*R*)-norketamine was detected as the first product of (*R*)-ketamine oxidation.

Furthermore, this triple mutant was analyzed regarding its stereoselectivity. Potentially, two stereoisomers of (2*R*,6)-4 can be formed – (2*R*,6*S*)- and (2*R*,6*R*)-hydroxynorketamine, whereas the latter is the herein desired isomer 4. The reaction catalyzed by L289T/I238Q/M388A was analyzed *via* chiral HPLC by spiking with an authentic (2*R*,6*R*)-hydroxynorketamine standard. This analysis revealed a single product peak corresponding to the peak of the authentic (2*R*,6*R*)-4 (ESI† Fig. S5). Thus, it can be concluded that the L289T/I238Q/M388A mutant catalyzes hydroxylation at position C6 with 100% diastereoselectivity.

Next, *E. coli* cells expressing this triple mutant were used at a higher scale (10 ml volume) to oxidize (*R*)-1 at a concentration of 5 mM for product isolation. 11.86 mg (1.186 g L^{-1}) substrate were converted to 10 mg (1 g L^{-1}) of the desired product (2*R*,6*R*)-4. The product was isolated in 49.8% yield and analyzed by NMR (ESI† Fig. S7–S10).

To rationalize the observed regio- and stereoselectivity, a homology model of the L289T/I238Q/M388A mutant was generated on the basis of the crystal structure of CYP154A1 from *S. coelicolor* A3(2) (PDB 1ODO). Visual inspection of the residues that outline the binding pocket suggested that an alternative side chain rotamer of G238 leads to a better local hydrogen-bonding network. Likewise, a different conformer of the side chain of M87 was chosen to make more space for ligands. Thus, two homology models were used as receptors for substrate docking: the originally obtained homology model (denoted model A) and the refined model B that contained the modified side chains. The energetically most favourable conformations of (*R*)-ketamine 1 (ESI,† Fig. S15B) and (*R*)-norketamine 2 (ESI,† Fig. S15C) obtained by docking into the refined receptor model B of the L289T/I238Q/M388A mutant show the cyclohexanone ring in close distance (<3.1 Å) to the heme iron and oriented for (6*R*)-hydroxylation, respectively. In both poses, the modified side chain of M87 avoids steric clashes with the aromatic ring that would be occurring when using the original homology model A. Conversely, docking into model A yields as the energetically most favourable pose a conformation of (*R*)-ketamine 1 that has the methyl group pointing towards the heme iron (2.98 Å distance), enabling also the experimentally observed *N*-demethylation (ESI,† Fig. S15A). Thus, reorientation of the side chain of M87 upon ligand binding seems likely.

In summary, we have turned the poorly active wild type CYP154E1 into a highly active, regio- and stereoselective variant with only three mutations in the first sphere in the active site. To achieve this, we applied a focused mutagenesis approach by constructing and screening of seven individual site-saturation sub-libraries. For screening, we used an *E. coli* whole-cell system which might also be applicable for other P450s making the addition of redox proteins redundant. The same *E. coli* cells expressing the “best” mutant enabled simple reaction upscaling with subsequent product isolation.

V. B. U. thanks the Federal Ministry of Education and Research for financial support [grant number 031A223A] and Prof. C. Czekelius and U. J. Lülff for their assistance in the synthesis of the substrate and product analysis.

Conflicts of interest

There are no conflicts to declare.

Notes and references

- 1 K. Petzoldt, K. Annen, H. Laurent and R. Wiechert, *US Pat.* 4353985, 1982, 353, 985.
- 2 J.-W. Park, J.-K. Lee, T.-J. Kwon, D.-H. Yi, Y.-J. Kim, S.-H. Moon, H.-H. Suh, S.-M. Kang and Y.-I. Park, *Biotechnol. Lett.*, 2003, 25, 1827–1831.
- 3 M. Sono, M. P. Roach, E. D. Coulter and J. H. Dawson, *Chem. Rev.*, 1996, 96, 2841–2887.
- 4 (a) V. Steck, J. N. Kolev, X. Ren and R. Fasan, *J. Am. Chem. Soc.*, 2020, 142, 10343–10357; (b) Y. Ensari, G. de Almeida Santos, A. J. Ruff and U. Schwaneberg, *Enzyme Microb. Technol.*, 2020, 138, 109555; (c) O. Shoji, Y. Aiba and Y. Watanabe, *Acc. Chem. Res.*, 2019, 52, 925–934; (d) J. Manning, M. Tavanti, J. L. Porter, N. Kiess, S. P. De Visser, N. J. Turner and S. L. Flitsch, *Angew. Chem., Int. Ed.*, 2019, 58, 5668–5671; (e) O. F. Brandenberg, D. C. Miller, U. Markel, A. O. Chaib and F. H. Arnold, *ACS Catal.*, 2019, 9, 8271–8275; (f) S. D. Munday, O. Shoji, Y. Watanabe, L. L. Wong and S. G. Bell, *Chem. Commun.*, 2016, 52, 1036–1039.
- 5 A. Li, C. G. Acevedo-Rocha, L. D'Amore, J. Chen, Y. Peng, M. Garcia-Borrás, C. Gao, J. Zhu, H. Rickerby, S. Osuna, J. Zhou and M. T. Reetz, *Angew. Chem., Int. Ed.*, 2020, 59, 12499–12505.
- 6 E. F. Domino, P. Chodoff and G. Corssen, *Clin. Pharmacol. Ther.*, 1965, 6, 279–291.
- 7 R. M. Berman, A. Cappiello, A. Anand, D. A. Oren, G. R. Heninger, D. S. Charney and J. H. Krystal, *Biol. Psychiatry*, 2000, 47, 351–354.
- 8 (a) P. Zanos, R. Moaddel, P. J. Morris, P. Georgiou, J. Fischell, G. I. Elmer, M. Alkondon, P. Yuan, H. J. Pribut, N. S. Singh, K. S. Dossou, Y. Fang, X. P. Huang, C. L. Mayo, I. W. Wainer, E. X. Albuquerque, S. M. Thompson, C. J. Thomas, C. A. Zarate, Jr. and T. D. Gould, *Nature*, 2016, 533, 481–486; (b) T. H. Pham, C. Defaix, X. Xu, S. X. Deng, N. Fabresse, J. C. Alvarez, D. W. Landry, R. A. Brachman, C. A. Denny and A. M. Gardier, *Biol. Psychiatry*, 2018, 84, e3–e6; (c) P. Zanos, J. N. Highland, B. W. Stewart, P. Georgiou, C. E. Jenne, J. Lovett, P. J. Morris, C. J. Thomas, R. Moaddel, C. A. Zarate and T. D. Gould, *Proc. Natl. Acad. Sci. U. S. A.*, 2019, 116, 6441–6450.
- 9 Y. Han, K. M. Reddy and E. J. Corey, *Org. Lett.*, 2017, 19, 5224–5227.
- 10 (a) C. von Bühler, P. Le-Huu and V. B. Urlacher, *ChemBioChem*, 2013, 14, 2189–2198; (b) A. Rühlmann, D. Antovic, T. J. J. Müller and V. B. Urlacher, *Adv. Synth. Catal.*, 2017, 359, 984–994.
- 11 V. F. T. Russo and E. M. D. S. Russo, US6743949B2, 2004.
- 12 A. Bokel, A. Rühlmann, M. C. Hutter and V. B. Urlacher, *ACS Catal.*, 2020, 10, 4151–4159.
- 13 J. Sanchis, L. Fernandez, J. D. Carballeira, J. Drone, Y. Gumulya, H. Hobenreich, D. Kahakeaw, S. Kille, R. Lohmer, J. J. Peyralans, J. Podtetenieff, S. Prasad, P. Soni, A. Taglieber, S. Wu, F. E. Zilly and M. T. Reetz, *Appl. Microbiol. Biotechnol.*, 2008, 81, 387–397.
- 14 (a) M. T. Reetz and J. D. Carballeira, *Nat. Protoc.*, 2007, 2, 891–903; (b) M. T. Reetz, *CASTER 2.0*, <http://www.kofo.mpg.de/de/forschung/biocatalysis>.
- 15 M. J. Cryle and J. J. De Voss, *ChemBioChem*, 2008, 9, 261–266.
- 16 (a) J. P. Clark, C. S. Miles, C. G. Mowat, M. D. Walkinshaw, G. A. Reid, S. N. Daff and S. K. Chapman, *J. Inorg. Biochem.*, 2006, 100, 1075–1090; (b) Y. T. Mehareenna, K. E. Slessor, S. M. Cavaignac, T. L. Poulos and J. J. De Voss, *J. Biol. Chem.*, 2008, 283, 10804–10812.
- 17 G. J. Reiss, V. B. Urlacher and U. J. Lülff, *Z. Kristallogr. - New Cryst. Struct.*, 2020, 235, 1037–1039.

2.3 Chapter III

Simulation-guided Design of Cytochrome P450 for Chemo-and Regioselective Macrocyclic Oxidation

Dušan Petrović*, Ansgar Bokel, Matthew Allan, Vlada B. Urlacher, and Birgit Strodel

*corresponding author

Journal of Chemical Information and Modeling, 2018, 58(4), 848-858

Own contribution (35%): AB performed all the experimental work and writing part of the manuscript. AB created and expressed all P450 BM3 variants in *E. coli*. AB determined the concentration of all P450 BM3 variants and tested their activity *in vitro*. AB created the LC-MS programs, and AB supervised the measurements. AB wrote parts of the manuscript containing experimental details.

Reprinted with permission from Petrović, D., Bokel, A., Allan, M., Urlacher, V. B., & Strodel, B. (2018). Simulation-guided design of cytochrome P450 for chemo-and regioselective macrocyclic oxidation. *Journal of chemical information and modeling*, 58(4), 848-858. Copyright (2018) American Chemical Society.

Simulation-Guided Design of Cytochrome P450 for Chemo- and Regioselective Macrocyclic Oxidation

 Dušan Petrović,^{*,†,‡,§,||} Ansgar Bokel,[‡] Matthew Allan,^{†,§} Vlada B. Urlacher,[‡] and Birgit Strodel^{*,†,||}
[†]Institute of Complex Systems: Structural Biochemistry, Forschungszentrum Jülich, 52425 Jülich, Germany

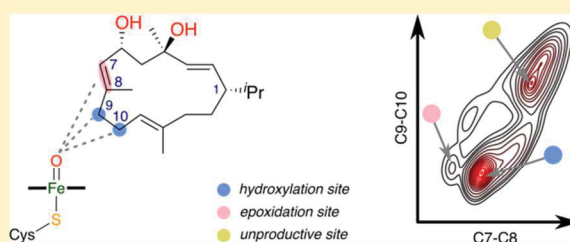
[‡]Institute of Biochemistry, Heinrich Heine University Düsseldorf, Universitätsstraße 1, 40225 Düsseldorf, Germany

[§]Schreyer Honors College, The Pennsylvania State University, University Park, Pennsylvania 16802, United States

^{||}Institute of Theoretical and Computational Chemistry, Heinrich Heine University Düsseldorf, Universitätsstraße 1, 40225 Düsseldorf, Germany

S Supporting Information

ABSTRACT: Engineering high chemo-, regio-, and stereo-selectivity is a prerequisite for enzyme usage in organic synthesis. Cytochromes P450 can oxidize a broad range of substrates, including macrocycles, which are becoming popular scaffolds for therapeutic agents. However, a large conformational space explored by macrocycles not only reduces the selectivity of oxidation but also impairs computational enzyme design strategies based on docking and molecular dynamics (MD) simulations. We present a novel design workflow that uses enhanced-sampling Hamiltonian replica exchange (HREX) MD and focuses on quantifying the substrate binding for suggesting the mutations to be made. This computational approach is applied to P450 BM3 with the aim to shift regioselectivity toward one of the numerous possible positions during β -cembrenediol oxidation. The predictions are experimentally tested and the resulting product distributions validate our design strategy, as single mutations led up to 5-fold regioselectivity increases. We thus conclude that the HREX-MD-based workflow is a promising tool for the identification of positions for mutagenesis aiming at P450 enzymes with improved regioselectivity.



INTRODUCTION

The selective oxidation of an unactivated C–H bond for many years presented a major problem for chemists.^{1,2} Even today, an environmentally friendly chemo-, regio-, and stereoselective oxidation of hydrocarbons is a challenging task.^{3,4} Nature, however, has evolved umpteen enzyme catalysts for this purpose.^{5,6} The heme-containing monooxygenases (i.e., cytochromes P450 or CYPs) use the electrophilic oxyferryl radical of heme, commonly known as the *compound I* (CI),^{7–9} to insert one atom of molecular oxygen into a hydrocarbon skeleton, such as a fatty acid or steroid. A CYP from *Bacillus megaterium*, namely CYP102A1 or P450 BM3, typically performs subterminal hydroxylation of saturated and hydroxylation/epoxidation of (poly)unsaturated fatty acids. Due to a number of attractive features, P450 BM3 is commonly used as the CYP scaffold to engineer catalysts for oxidation of novel substrates.^{6,7,10}

To bind unnatural substrates, especially bulky ones, enzymes often require an active site overhaul.¹¹ Exchanging Phe87, which is located in the active site, with a residue with a smaller side chain allows for the extension of the P450 BM3 binding pocket and enables a bulky substrate to bind in the vicinity of heme.¹² On the other hand, engineering overly spacious active sites can lead to a high substrate mobility that is often reflected as enzyme promiscuity.^{13,14} In a simplified view of P450

engineering, there should be enough space in the active site for a substrate to bind in a desired, transition-state-like pose, but not more than that, which would allow alternative binding modes.¹⁵ In addition to the shape and size match, the proper electrostatic complementarity between the substrate and the active site and the existence of a geometrically precise H-bond network can lead to better-performing enzymes.^{16,17}

The mutation of P450 BM3 first-shell residues around a substrate has a strong impact on the substrate selectivity and activity.¹⁸ Many P450 BM3 variants have been engineered for the selective oxidation of different classes of organic molecules, such as alkanes (e.g., *n*-octane and cyclododecane),¹⁹ polycyclic aromatic hydrocarbons (e.g., naphthalene²⁰ and anthracene²¹), alkaloids (e.g., thebaine and dextromethorphan),²² steroids (e.g., testosterone²³ and norandrostenedione²⁴), and terpenes (e.g., geranylacetone,²⁵ (+)-valencene,²⁶ and artemisinin²⁷). Macrocycles have been recognized as potential scaffolds for therapeutic agents,^{28–30} and we recently studied the P450 BM3-catalyzed transformations of (1*S*,2*E*,4*R*,6*R*,7*E*,11*E*)-4,6-dihydroxycembra-2,7,11-triene or β -cembrenediol (**1**)³¹ and its oxidation products (**2–4**)³² (Figure 1). A monocyclic diterpenoid isolated from *Nicotiana tabacum*, **1**, is characterized

Received: January 25, 2018

Published: March 9, 2018

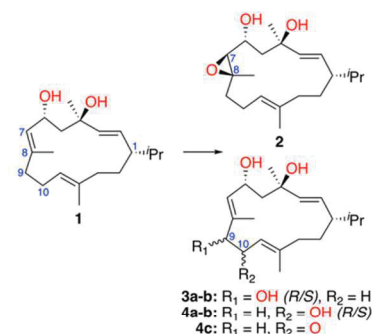


Figure 1. Common oxidation products of β -cembrenediol (**1**) by P450 BM3 mutants.^{31,32}

by a 14-membered macrocyclic ring. β -Cembrenediol (**1**) is a challenging substrate for selective oxidation as well as for rational design, as it is flexible and bears seven potential allylic and six nonallylic hydroxylation sites, as well as three epoxidation sites. While the conversion of **1** by the wild-type P450 BM3 is lower than 2%, the Phe87 mutations create more spacious active sites leading to higher conversion rates (i.e., 6% for the F87A and 59% for the F87G mutation).³¹ However, the increased conversion rate of **1** by the F87G mutant comes at the cost of low chemo-, regio-, and stereoselectivities. Additional mutations to either F87A or F87G P450 BM3 mutants typically increase the conversion rates, with unpredictable implications on the product selectivity.³¹

In this study, we present a computational workflow to predict positions influencing the regioselectivity of P450 BM3 for oxidation of the flexible macrocycle β -cembrenediol, which bears numerous potential oxidation sites. The P450 BM3 double mutant V78A/F87A was used as a parent enzyme for improvement due to its decent conversion rate of **1** but poor chemo-, regio-, and stereoselectivities.³¹ Shaik and co-workers, among others, argued that the selectivity of CYP-catalyzed monooxygenation is, in fact, a combination of *electronic* (i.e., substrate activation) and *classical* factors (i.e., substrate binding and interactions with the active site pocket).³³ While electronic factors can explain why some potential oxidation sites are nonreactive (e.g., high activation energies),³⁴ substrate binding is a very important factor for determining regio- and stereoselectivities of CYPs with fast cI activation of a substrate.^{33,35–38} To this end, we aimed to test if solely optimizing the binding of β -cembrenediol would lead to changes in regioselectivity. Our strategy involves substrate docking by Hamiltonian replica exchange (HREX) molecular dynamics (MD) simulations to elucidate how **1** binds to the enzyme, which allowed us to adjust the shape and electrostatic complementarity at selected binding hotspots by introducing mutations with the aim to shift product distribution. The quality of our models is validated by experimentally measured product distributions.

METHODS

Unliganded Enzyme MD. The starting structure of the parent enzyme (V78A/F87A P450 BM3) was prepared from the 1.65 Å resolution crystal structure of the wild-type enzyme (PDB ID: 1JPZ³⁹) by truncating the side chains of Val78 and Phe87 to alanine. The 1JPZ crystal structure contains *N*-palmitoylglycine, which was removed prior to simulations. The mutated protein was relaxed in MD simulations performed

in GROMACS 5.0.4,⁴⁰ using the Amber 99SB*-ILDN force field^{41,42} with TIP3P water.⁴³ The heme parameters for the cI state were adopted from Cheatham and co-workers.⁴⁴ The protein was centered in a dodecahedral box and positioned at least 10 Å away from any box edge. The protonation states were assigned to all titratable protein residues based on the PROPKA 3.1⁴⁵ analysis at a pH of 7.5. The total charge was neutralized by adding sodium ions to the solvated system, followed by minimization of the system in two steps: steepest descent (force convergence criterion of 500 kJ mol⁻¹ nm⁻¹) and conjugate gradient (force convergence criterion of 100 kJ mol⁻¹ nm⁻¹). The system was modeled under periodic boundary conditions where electrostatic interactions were treated with the particle mesh Ewald method.⁴⁶ The short-range nonbonded interactions were calculated within a cutoff of 9 Å. An integration step of 2.0 fs was used, while bond lengths were constrained using the LINCS algorithm.⁴⁷ The minimized system was gradually heated to 298 K and equilibrated using the v-rescale thermostat⁴⁸ for 200 ps, with the protein α atoms restrained using a positional restraint force constant of 1000 kJ mol⁻¹ nm⁻². An NPT equilibration was subsequently carried out for 2.8 ns, over which the restraint forces were gradually reduced to 10 kJ mol⁻¹ nm⁻², and the pressure was kept constant at 1 bar using the Berendsen barostat.⁴⁹ The 200 ns unrestrained production MD was performed in the NPT ensemble using the Parrinello–Rahman barostat⁵⁰ at 1 bar and the v-rescale thermostat at 298 K. The coordinates of the system were collected every 10 ps. The unliganded enzyme was stable during both MD simulations (Figure S1). All simulation snapshots were clustered based on the backbone conformation, using the Daura algorithm,⁵¹ to produce representative enzyme structures. The structures of the two most populated clusters were used for the subsequent simulations.

Molecular Docking. The conformational ensemble of **1** was generated using the OMEGA 2.5.1.4 software,⁵² which employs fragment libraries with a subsequent exhaustive knowledge-based scan of rotatable bonds. Energies were estimated using the MMFF94s force field *in vacuo*.⁵³ Conformations with root-mean-square deviations (RMSDs) of atomic coordinates of less than 0.5 Å were considered to be identical and only the lowest energy conformer from the set of identical structures was kept. A set of 20 conformers was generated with energies up to 42 kJ mol⁻¹ higher than the lowest energy conformer, which were subsequently employed in rigid docking using the FRED 3.0.1 tool from the OEDocking suite.⁵⁴ The receptor active site was defined as a 20 Å × 20 Å × 20 Å box that encompasses cI. For each of the two protein models obtained from clustering, 100 binding poses of **1** were generated. From these, four binding modes, with different geometries but similar binding affinities were selected for further MD simulations.

Enzyme–Substrate MD. The topology of **1** was created using ACPYPE⁵⁵ and Antechamber.⁵⁶ The restrained electrostatic potential (RESP) charges, shown in Figure S2, were determined at the HF/6-31G*/B3LYP/6-31G* level of theory in Gaussian 09.⁵⁷ The MD simulations of the enzyme–substrate systems were prepared and run in the same manner as the MD simulations of the unliganded enzyme. Each of the four production simulations was 200 ns long.

The Hamiltonian replica exchange simulations were initiated from the same starting structures as the enzyme–substrate complex MD simulations. HREX-MD was performed in GROMACS 4.6.7 patched with the PLUMED 2.1 plugin.^{58,59}

To enhance the conformational sampling of β -cembrenediol, six replicas were simulated for each of the four binding modes, where the energy term (i.e., the Hamiltonian) for the substrate's nonbonded interactions was scaled to effectively correspond to temperatures between 300 and 600 K (the exact λ scaling factors were 1.00, 0.87, 0.76, 0.66, 0.57, and 0.50). The chosen λ range of 1.0–0.5 should be sufficient to enhance the conformational sampling of β -cembrenediol, while at the same time achieving optimal exchange rates (i.e., 30–70%) with a low number of replicas. In the GROMACS/PLUMED implementation of HREX-MD,⁵⁹ charges of all “hot” atoms (i.e., the substrate in the present case) were scaled by a factor $\sqrt{\lambda}$, while the depth of the Lennard-Jones potentials (ϵ) and the torsional potentials were scaled by a factor λ .

The exchange between replicas was attempted every 2 ps, giving exchange rates of around 55%. Coordinates were saved every 5 ps during the 115 ns simulation per replica, giving a total of $\sim 2.8 \mu\text{s}$ sampling time (6 replicas \times 115 ns \times 4 binding modes). The initial 15 ns of each replica were discarded as equilibration, and data analysis was performed on the replicas with the unperturbed Hamiltonian (i.e., the scaling factor of 1). Binding density surfaces were produced from the HREX-MD data, showing the binding preferences of **1** along selected enzyme–substrate distances or angles.

MM/PBSA Calculations. After the alignment of the protein backbone, the snapshots from the combined HREX-MD trajectories were clustered based on the orientation of **1** in the active site using the Daura algorithm with a cutoff of 1.5 Å. The representative structures of each cluster were projected onto the binding density surfaces and the clusters at or close to binding density maxima considered for further analysis. For each of the selected six clusters, a set of 30 short MD simulations was performed for the molecular mechanics/Poisson–Boltzmann surface area (MM/PBSA) calculations. In each simulation, the initial velocities were randomized and the system was equilibrated in the NPT ensemble for 0.5 ns, followed by a 2 ns production sampling run. We confirmed that each simulation sampled only a narrow region around its initial binding mode. The MM/PBSA calculations were performed for each cluster on a combined 60 ns trajectory (30 simulations of 2 ns) with the *g_mmpbsa* tool,⁶⁰ assuming a solute dielectric constant of 4. The binding free energy was decomposed on a per-residue basis.

Simulation Analysis. Data analysis was performed using GROMACS 5.0.4 tools, MDAnalysis,⁶¹ and VMD.⁶² Shown structures were rendered with PyMOL.⁶³

Experimental Reagents. β -Cembrenediol was purchased from Santa Cruz Biotechnology (Dallas, USA). Ethyl acetate and methanol were from Fisher Chemical (Waltham, USA) in either analytical grade (ethyl acetate) or certified ACS reagent grade (methanol).

Cloning and Expression. The pET28a plasmid (Novagen) with the integrated gene encoding P450 BM3 (GenBank J04832) from *B. megaterium* was already available in our laboratory. Mutants of P450 BM3 were created following a modified protocol of Edelheit et al.⁶⁴ and expressed as described elsewhere.³¹ Glucose dehydrogenase (GDH) from *B. megaterium* (*gdhIV*, GenBank D10626) was used for NADPH cofactor regeneration, which was available in our laboratory in pET22b vector. Expression was done using *E. coli* BL21(DE3) cells. First, precultures comprising 5 mL Lysogeny Broth (LB) medium, containing $100 \mu\text{g mL}^{-1}$ ampicillin, were inoculated with single colonies and incubated overnight at 37

°C and 180 rpm. For the main cultures, 400 mL TB medium in 2 L flasks, supplemented with $100 \mu\text{g mL}^{-1}$ ampicillin, were inoculated with the preculture to O.D.₆₀₀ 0.05 and incubated at 37 °C and 180 rpm until O.D.₆₀₀ 0.6–0.8 was reached. Gene expression was then induced by adding 0.25 mM isopropyl- β -D-thiogalactopyranoside (IPTG) and cultures were further kept at 25 °C and 140 rpm for 20 h. Harvested cells were resuspended in 50 mM potassium phosphate buffer (pH 7.5, 0.5 M NaCl) supplemented with $100 \mu\text{M}$ phenylmethylsulfonyl fluoride (PMSF) and disrupted by sonification on ice. Afterward, cell debris was removed by centrifugation.

Enzyme Assays. The concentrations of all P450 BM3 variants were calculated from CO difference spectra using the extinction coefficient $\epsilon_{450-490} = 91 \text{ mM}^{-1}$.⁶⁵ Since the spectra were not recorded under the exclusion of oxygen, reduction with sodium dithionite followed after bubbling with CO. Absorbance spectra were recorded from 400–500 nm at least three times successively. The NADP⁺ reduction activity of GDH was measured by the increase of absorbance at 340 nm ($\epsilon_{340} = 6.22 \text{ mM}^{-1} \text{ cm}^{-1}$) over a period of 1 min. The reaction solutions contained 100 mM glucose and 100 μL of diluted, cell-free sample in 900 μL 50 mM potassium phosphate buffer, pH 7.5. The reaction was started by adding 100 μL NADP⁺ (1 mM).

LC/MS Analysis of Product Distribution. For the experimental validation of the reaction selectivity of the suggested P450 BM3 mutants, the following reaction setup in a total volume of 500 μL was used. The reaction mixture contained 100 μM β -cembrenediol (**1**) dissolved in ethanol (reaction finally contained 2% (v/v) ethanol), 2.5 μM P450 BM3 mutants, and 200 μM NADPH. The latter was regenerated by addition of 5 U mL^{-1} GDH and 20 mM glucose. Removal of hydrogen peroxide, which might arise from uncoupling reactions, was accomplished by adding 600 U mL^{-1} catalase from bovine liver (Sigma-Aldrich). The reactions were performed in potassium phosphate buffer (50 mM, pH 7.5) at 25 °C and 500 rpm (ThermoShaker) for 17 h. Prior the extraction (twice with 300 μL ethyl acetate), 25 μM dioctyl phthalate was added as internal standard. The combined ethyl acetate phases were evaporated to dryness and resolved in methanol for liquid chromatography/mass spectrometry (LC/MS) analysis.

LC/MS analysis was carried out on a Prominence/LCMS 2020 instrument (Shimadzu, Duisburg, Germany) equipped with a Chromolith RP-18e 100-4.6 column (Merck, Darmstadt, Germany). Oven temperature was set to 30 °C and a flow rate of 1 mL min^{-1} was chosen. The following solvent gradient of 0.1% formic acid (A) and methanol (B) was used: increasing B from 50% to 70% B within the first 25 min, and further increasing it to 100% within another 10 min, finally holding for 2 min. Mass spectroscopy was done in the positive scan mode measuring electrospray ionization (ESI) and atmospheric pressure chemical ionization (APCI) in the dual ionization mode at the same time.³²

To minimize the cell extract background, negative controls were done with crude extract of *E. coli* carrying the pET28a empty vector (vector does not contain the CYP102A1 encoding gene). The products were identified by comparison of retention times of the corresponding peaks and *m/z* values with published data.³¹ The conversion was calculated using a calibration curve with dioctyl phthalate as internal standard. The product distribution was calculated based on the observed product peak areas under the assumption that the ionization of

the metabolites is similar. All reactions were performed in triplicate.

RESULTS

β -Cembrenediol Docking. The first objective of this study was to investigate how **1** binds to the parent enzyme, bearing in mind that the binding mode can dictate reaction selectivity. A typical approach to study a small molecule binding to a protein is molecular docking. Substrate docking and classical MD simulations have been successfully used to predict the selectivity of P450 BM3 for alkanes and fatty acids, see e.g., ref 66, but fatty acids are native substrates for P450 BM3 and there are several substrate-bound crystal structures that can assist in docking. A combination of short MD simulations (3 ns) to study binding and quantum mechanical (QM) calculations to obtain transition state geometries and reaction barriers was used to understand the reaction selectivity of P450 2D6 for the antipsychotic drug thioridazine.⁶⁷ More exhaustive sampling (500 ns) was recently used by Houk and co-workers to engineer the desired reactivity in PikC monooxygenase for menthol derivatives.⁶⁸

Macrocycle docking is, however, a more challenging task because of the larger conformational space than that accessible to small organic molecules.⁶⁹ This problem usually requires a thorough conformational analysis of the substrate and docking of a predefined substrate conformational library to a rigid protein.⁷⁰ To this end, we performed the conformational analysis of **1** using OMEGA. We recently showed that this procedure gives reasonable coordinates for molecules **2** and **3**, which enabled us to study their NMR spectra.³² Furthermore, one of the conformers of **1** that was generated in this work corresponds to the crystal structure of β -cembrenediol (Figure S3).⁷¹

To account for protein flexibility in substrate docking,^{72,73} we introduced the mutations to P450 BM3 (V78A and F87A), performed MD simulations to relax the protein, and clustered the conformations to identify representative structures. The two most populated clusters were selected, and the pregenerated conformational ensemble of **1** was docked into each instance of the rigid parent enzyme. Figure 2 shows that the regiopreferences from docking, which we define here based on the closest contact of the axial oxygen of Cl and the carbon atoms of the substrate, are not fully corresponding to the

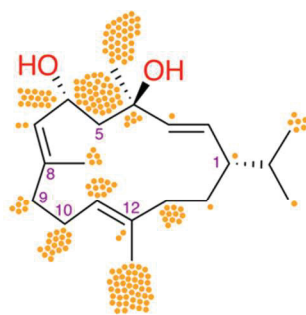


Figure 2. Rigid ensemble docking of **1** to the parent enzyme models. Data points indicate the closest contact between the axial oxygen of Cl and C atoms of **1** in the binding modes resulting from docking. Only poses with FRED scores⁵² ≤ -4 are shown. Most of the observed docking poses would not lead to oxidation of C atoms that were identified experimentally, i.e., C7/C8, C9, and C10 atoms.

experimentally identified products of **1** by the parent enzyme (i.e., P450 BM3 V78A/F87A).³¹ Karlén et al. identified three requirements in rigid ensemble docking that commonly lead to inaccurate results if one or more of these requirements are not fulfilled: (1) proper *conformational analysis of the substrate*, and especially the generation of “protein-bound-like” conformations, (2) *exhaustive search of the substrate binding poses*, and (3) accurate *scoring* and ordering of the binding modes.⁷⁰ Since the discrepancies between simulated and experimental data can result from inaccuracies at any of these steps in β -cembrenediol docking, we turned to MD simulations to more thoroughly sample the conformational space of both the protein and the substrate.

To study the substrate dynamics, we selected four binding modes of **1** obtained from docking. The selected binding modes, numbered 1–4 in Figure S4, had similar docking scores but substantially different orientations in the active site. For structurally complex substrates, at commonly employed nanosecond time scales, unbiased MD simulations are incapable of crossing high free energy barriers that connect several metastable substrate binding modes. This is confirmed by the results obtained from our 200 ns MD simulations of the enzyme–substrate complex (see the ESI for details, including Figures S5 and S6). To overcome the barriers and describe the complete binding process, μ s-long unbiased MD simulations are needed.⁷⁴ An alternative is applying enhanced-sampling MD approaches, e.g., adaptive biasing force MD,⁷⁵ alchemical transformations,⁷⁶ or computationally expensive 2D umbrella sampling (US) MD.⁷⁷ We increased the conformational sampling of **1** using HREX-MD, which we have recently shown to provide a level of conformational sampling comparable to that of US-MD.⁷⁸ While the substrate was very stable in the unbiased simulations (i.e., rather constant RMSD, Figure S5), it was quite flexible in the HREX-MD simulations, which is indicated by noisier RMSD profiles exceeding 7 Å from the initial structure. In addition, the substrate often visited three to four different regions in the RMSD space of each simulation (Figure S7), indicating that **1** was exhaustively exploring the active site in the HREX-MD simulations.

Binding Density Surfaces. To rationalize the selectivity of the parent enzyme based on binding preferences, we chose any two oxidation products and used their corresponding reaction coordinates to investigate the binding density surface (BDS), which we define as the 2D representation of two probability density functions. For the selection of the reaction coordinates we considered that the allylic C9- or C10-hydroxylation of **1** by the parent enzyme follows a mechanistic pathway that begins with the abstraction of a hydrogen atom from β -cembrenediol by the axial oxygen of Cl,^{8,9} while the initial Cl attack for epoxidation is on the C7–C8 π -bond of the substrate.⁷⁹ To investigate the regiopreference of the substrate binding, we assumed that the corresponding position of **1** (i.e., C7, C8, C9, or C10) needs to be sufficiently close to the active oxygen species for the reaction to occur. Mulholland et al. suggested a common cutoff of 4 Å for the $C_{\text{substrate}}-O_{\text{Cl}}$ contact in the reactant state, which would lead to a model that resembles the transition state as closely as possible.⁸⁰ In addition, Houk et al. showed, based on QM calculations, that the $H_{\text{substrate}}-O_{\text{Cl}}$ distance is often ~ 2.5 Å longer in the reactant than at the transition state leading to hydroxylation.⁶⁸

We assumed that the chemo- and regioselectivity of C7,C8-epoxidation versus C9/C10-hydroxylation would be deter-

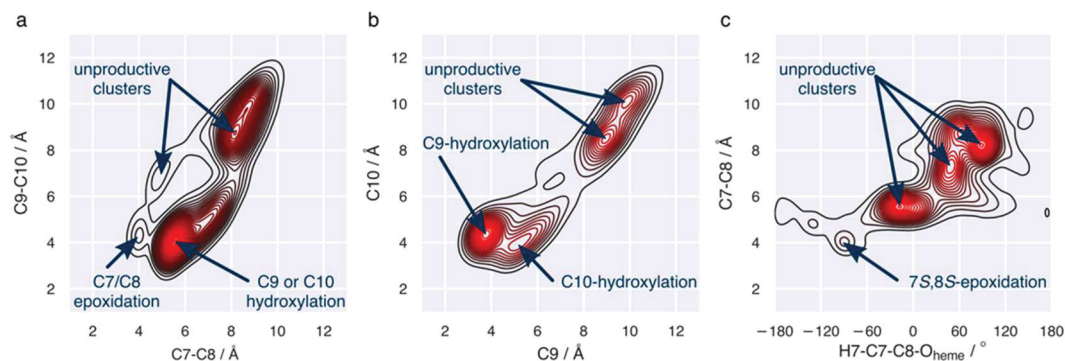


Figure 3. Binding density surfaces underpinning chemo-, regio-, and stereoselectivity of the parent enzyme with **1**. (a) Chemo- and regioselectivity are preferential for C9/C10-hydroxylation rather than for C7/C8-epoxidation. (b) Hydroxylation at C9 is preferred to that at C10. (c) C7/C8-epoxidation is *S,S*-stereoselective.

mined by the distance from the *cl* oxygen atom to the centroids (i.e., the centers of mass) of the C7–C8 and C9–C10 bonds, respectively (Figure 3a). Several local maxima can be identified on the corresponding BDS of the parent enzyme, two of which place carbon atoms of the substrate sufficiently close to the *cl* oxygen to lead to product formation. Binding is more favorable for C9/C10-hydroxylation, as it is characterized by a broader and higher maximum, which is supported experimentally by the high yield (>60%) of hydroxylation products.³¹ Although other maxima on the plot exist, they place the relevant atoms of **1** too far from *cl* to allow proton abstraction and are thus denoted *unproductive* for the specified reactivity.

After showing that the BDS approach resembles the experimental preference for hydroxylation over epoxidation, we investigated its ability to predict regioselectivity of hydroxylation of the parent enzyme at C9 vs C10. Two productive and two unproductive maxima could be identified on this BDS (Figure 3b). The maximum corresponding to C10-hydroxylation is lower and narrower than the one for the C9-hydroxylation, indicating a geometrically smaller window of opportunity for C10 to react. The preference for C9-hydroxylation on the BDS agrees qualitatively with the experimentally observed product distribution for P450 BM3 V78A/F87A.

The BDS approach also allows to describe the stereoselectivity of the hydroxylation and epoxidation reactions. For epoxidation, the dihedral angle criterion distinguishes the oxygen to attack from either the *re*- or *si*- side of the substrate (Figure 3c). However, only one maximum on this BDS is at a distance short enough for the reaction to occur, which corresponds to the sterically less restricted 7*S*,8*S*-epoxidation product (**2**). For understanding the stereoselectivity of the C9- and C10-hydroxylations, we constructed the BDSs using distances from the *pro-R* and *pro-S* H atoms to *cl* (Figure S8).

Selection of Mutagenesis Hotspots from Binding Free Energy Analysis. Once we generally understood how **1** binds to the parent enzyme, we identified hotspot residues whose mutation would lead to a shift in selectivity. For this, we focused on two main properties: enzyme–substrate interaction energies and H-bond networks. However, constructing one binding surface that encompasses all reaction coordinates for chemo-, regio-, and stereoselectivity would require a highly multidimensional analysis and would not be practical. In order to simultaneously consider all the coordinates, we needed to identify structural and geometric similarities between different

positions on the BDSs (Figures 3 and S8). To this end, we performed geometrical clustering of substrate positions over the HREX-MD simulation trajectory and projected the six dominant cluster representatives to BDSs shown in Figure S9.

The interaction free energies between the enzyme and substrate were investigated for different clusters using the MM/PBSA method. To this end, we ran a set of short MD simulations starting from each of the six clusters and ensured that they remained in their respective binding modes (Figure S10). From these simulations, we calculated the binding free energies and decomposed them per residue to identify important amino acids capable of stabilizing or destabilizing the substrate binding mode in each cluster. Although the MM/PBSA method is not the most accurate method for calculating the binding free energies, it works sufficiently well (see e.g., ref 81) and it is faster than other, more precise methods (e.g., alchemical transformations),^{82,83} allowing it to be incorporated in an enzyme design strategy. The selection strategy for mutagenesis hotspots, based on the MM/PBSA results, is described in detail in the ESI. Figure 4 summarizes the identified stabilizing and destabilizing residues for several potential selectivity goals: regioselective C10-hydroxylation vs C7,C8-epoxidation and stereoselective C9-hydroxylation.

The Euler diagrams (Figure 4a,b) help to visualize that a hotspot for a given goal cannot be stabilizing and destabilizing at the same time. However, the hotspots for one goal do not necessarily depend on those for another. For example, while C7,C8-epoxidation is stabilized by Met185, destabilized by Ile263, and unaffected by Ala330, these three residues all stabilize C10-hydroxylation (Figure 4a). Interestingly, for the stereoselectivity of C9-hydroxylation, all positions that stabilize the *R*-epimer are destabilizing for the *S*, and *vice versa* (Figure 4b). Figure 4c compares all four goals at the same time and was used to make suggestions for mutation.

Identification of Promising Mutations. To identify the most beneficial mutations for each hotspot, we considered the structural and physicochemical properties of alternative amino acids at the hotspots. In testing for steric interactions, we performed *in silico* mutations. In the case where all rotamers (taken from the Dynameomics rotamer library⁸⁴) of an amino acid were clashing with the substrate or the rest of the protein, that mutation was discarded. If we, for example, wanted to mutate Ala to an amino acid able to form an H-bond, we tested those amino acids with the matching properties. Based on these considerations, the most promising one or two mutations for a

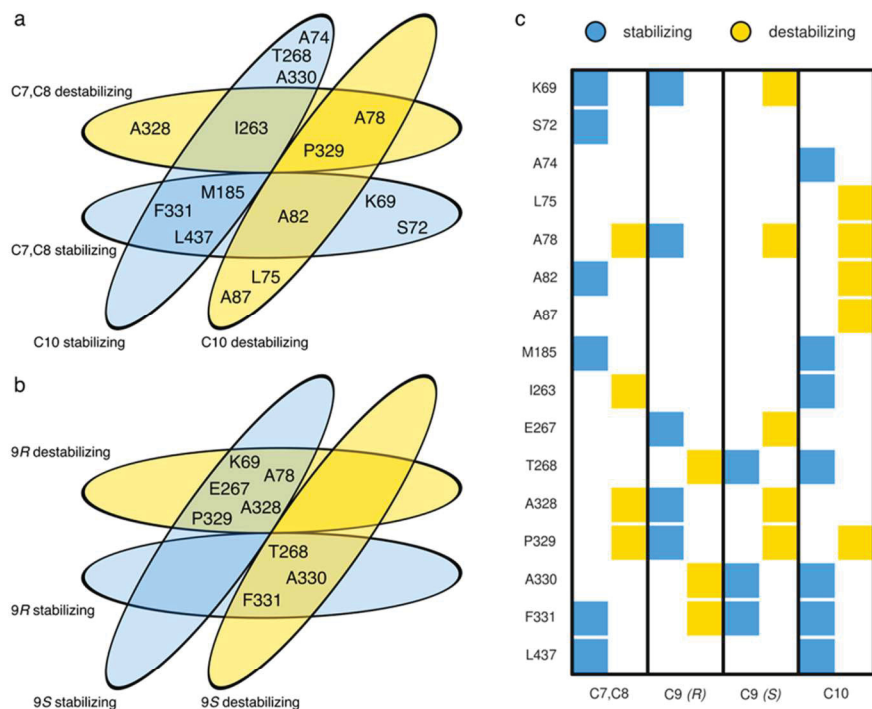


Figure 4. Identification of the V78A/F87A P450 BM3 amino acid residues that stabilize or destabilize β -cembrenediol for a desired selectivity. Euler diagrams for (a) C7,C8-epoxidation vs C10-hydroxylation and (b) 9R- vs 9S-hydroxylation. (c) Combined diagram connecting all four goals.

Table 1. Selected Hotspots and Mutations for the V78A/F87A P450 BM3 Mutant

| hotspot | mutation | goal | reason |
|---------|---------------|-----------------------|--|
| Lys69 | Arg | reduce C9 | identified as stabilizing for C7,C8-epoxidation known to coordinate the propionate groups of heme K69R maintains heme coordination and at the same time destabilizes 1 in a mode productive for C9-hydroxylation |
| Ser72 | Ala, Ile, Leu | increase C10 | identified as stabilizing for C7,C8-epoxidation too far from the substrate to form H-bond (Figure 5a) adding a bulky hydrophobic residue (e.g., Leu) fills the void between the enzyme and substrate and locks it in a binding mode productive for C10-hydroxylation (Figure 5b) |
| Leu75 | Ala | increase C10 | identified as destabilizing only for the C10-hydroxylation clashes with the substrate in its productive conformation for C10-hydroxylation (Figure 5c) L75A mutant removes that clash and anchors the substrate in the appropriate position, which increases the likelihood of this substrate conformation to be sampled |
| Thr268 | Ala, Ser | increase C10 C7,C8 | identified as stabilizing for C10-hydroxylation as the methyl group stabilizes the necessary binding mode of 1 T268A mutation preserves the methyl group but removes the H-bonding capability, favoring C10-hydroxylation T268S mutation preserves the H-bond network with the axial oxygen of 1 and OH-group on C6 of the substrate but removes the anchoring methyl group, which stabilizes the mode for epoxidation |
| Ala328 | Ser | increase C7,C8 | identified as destabilizing for epoxidation due to shape and polarity mismatch, i.e., methyl group positioned between the OH groups of the substrate (Figure 5e) A238S mutation introduces an H-bond to the OH-group of C6 of the substrate (Figure 5f), which is suitable for epoxidation also suitable for 9S-hydroxylation, but it geometrically prevents 9R-hydroxylation |
| Phe331 | Tyr, Thr | increase C10 | identified as stabilizing for epoxidation and hydroxylation located close to the C6 OH-group of the substrate mutation to a polar residue stabilizes 1 by an H-bond in a position suitable for C10-hydroxylation |

certain goal were suggested per hotspot, which are summarized in Table 1.

Experimental Validation of Suggested Mutations. The conversions of **1** and the oxidation product distributions were measured for the parent enzyme (P450 BM3 V78A/F87A mutant) and the triple mutants, suggested in Table 1, to investigate the quality of the computational redesigns. For the parent mutant we observed the products **2** (24%), **3** (42%),

and **4** (12%), as well as a 22% of other products (Figure 6). Comparing the experimentally observed distributions of the products **2**, **3**, and **4** of the double and triple mutants (Figure 6) with our computational predictions (Table 1), we notice a qualitatively good agreement.

We should first note that for six out of ten tested triple mutants (i.e., V78A/F87A/S72A, V78A/F87A/L75A, V78A/F87A/T268A, V78A/F87A/T268S, V78A/F87A/F331Y, and

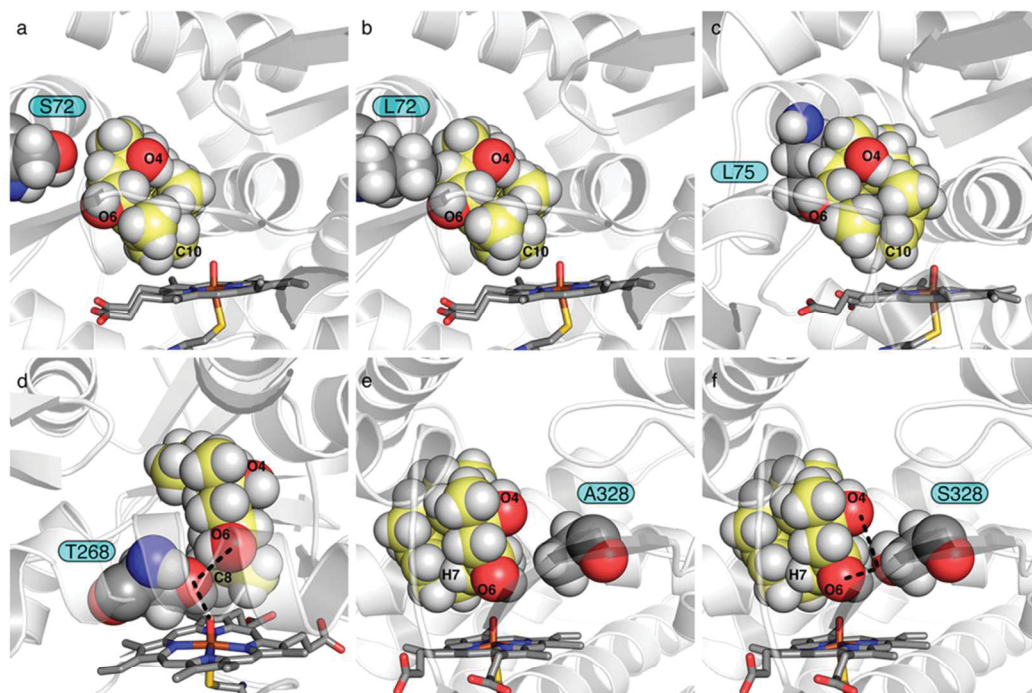


Figure 5. β -Cembrene-1–P450 BM3 interactions. The protein is shown in gray; protein hotspots and the substrate are shown as spheres; the C atoms of **1** are colored in light yellow; O and N atoms are colored in red and blue, respectively. H-bonds are indicated by dashed black lines. (a) S72 is too far away to form H-bonds with the substrate. (b) The S72L mutant could fill the void present in the productive mode for C10-hydroxylation. (c) L75 clashes with the substrate binding mode for C10-hydroxylation. (d) T268 forms an H-bond network with the substrate and cI. (e) A328 has a polarity mismatch for C7,C8-epoxidation. (f) The A328S mutation can form an H-bond with the substrate.

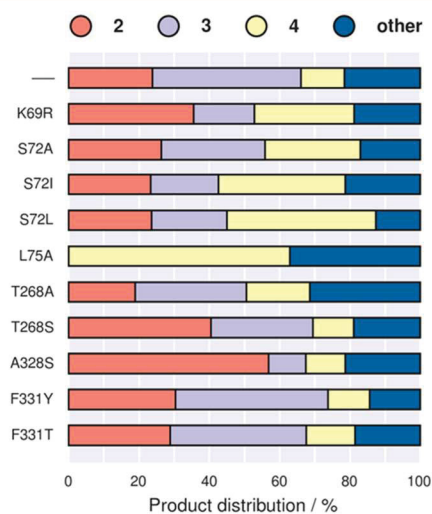


Figure 6. Experimental distribution of β -cembrene-1 (**1**) oxidation products 2–4 for the parent enzyme and its designed mutants. For the detailed product distribution and conversion rates, consult Table S1.

V78A/F87A/F331T) we observed a similar level of substrate conversion of around 80–99%, indicating that those mutations are not detrimental for the activity. The remaining four mutants (i.e., V78A/F87A/K69R, V78A/F87A/S72I, V78A/F87A/S72L, and V78A/F87A/A328S) had significantly lower conversion rates (11–24%), suggesting that further optimization is needed. When comparing the ratio of a certain product

formed with the parent and triple mutant, for six of the ten suggested mutations we obtain at least 2-fold gain in the product intended by the given goal (i.e., V78A/F87A/K69R, V78A/F87A/S72A, V78A/F87A/S72I, V78A/F87A/S72L, and V78A/F87A/L75A for the C-10 hydroxylation (**4**) and V78A/F87A/A328S for the C7,C8-epoxidation (**2**)). While the K69R mutation was identified as beneficial for C10-hydroxylation, this mutant has a very low conversion rate; mutations at this position usually deteriorate catalytic parameters.^{22,85} Another mutation that significantly decreases substrate conversion is A328S. This mutation, however, introduces a new H-bond between the enzyme and substrate and relatively enriches the C7,C8-epoxidation product in the mixture. In addition, this binding mode impedes the abstraction of the *pro-R* H atom at C9, preventing the formation of the **3a** product for this mutant. However, the benefit of the shift in product distribution for this mutant is significantly challenged by the low substrate conversion. The L75A mutation increases regioselective C10-hydroxylation over 5-fold (counting products **4a**, **4b**, and **4c**), completely removing the C9-hydroxylation and C7,C8-epoxidation products. This mutant also forms 37% of other uncharacterized products, identified at lower retention times. Two mutants showed modest improvements, enriching C10-hydroxylation (V78A/F87A/T268A) and C7,C8-epoxidation (V78A/F87A/T268S). Finally, only two mutants (V78A/F87A/F331Y and V78A/F87A/F331T) did not lead to a noteworthy change in the product distribution. Phe331 is located in the vicinity of the OH-group on C6 of the substrate, and these mutations were anticipated to form an H-bond with **1**, which apparently did not happen.

DISCUSSION AND CONCLUSIONS

P450 BM3 Design Workflow. Some CYPs show a remarkably high promiscuity in substrate binding. While in nature enzyme promiscuity is of great importance because it can lead to the evolution of new function, selectivity is one of the critical properties demanded from enzymes as biocatalysts in synthetic chemistry.¹⁴ In this work, we addressed the challenging task of shifting product distribution for oxidation of macrocyclic substrates by P450 BM3 variants, by developing an *in silico* engineering methodology based on the assumption that the binding of the substrate determines reaction selectivity,^{33,35–37} which is summarized in Figure 7.

In previous studies, substrate binding was investigated using various computational methods, including docking as well as unbiased and enhanced MD simulations.^{66–68,75,77} Macrocycles are often more flexible than other substrates and, hence,

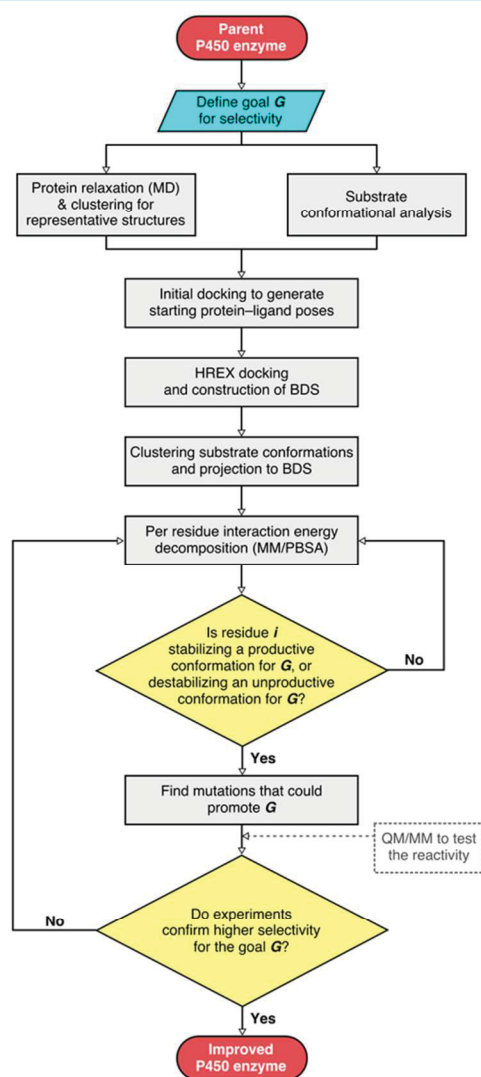


Figure 7. Flowchart overview for the P450 design process used in the present study. A possibility where quantum mechanics/molecular mechanics (QM/MM) calculations could be included is shown in dotted gray field.

particularly complicated to model.^{69,70} To this end, we employed HREX-MD simulations to thoroughly explore the conformational ensemble of **1** in the active site of the parent enzyme (i.e., P450 BM3 V78A/F87A).^{31,32} Based on the HREX-MD data, we constructed binding density surfaces along reaction coordinates representing the different chemo- and regioselectivities, which enabled us to identify productive and unproductive orientations of the substrate for a particular reaction. These were then submitted to MM/PBSA calculations for the mutagenesis hotspot selection, and mutations at hotspots were proposed to further stabilize the productive binding mode, or destabilize the unproductive ones.

The suggested mutations were evaluated through experiments and the resulting product distributions validated our computational workflow. Out of the ten predicted mutations, eight showed enhanced selectivity for either the C7,C8-epoxidation (**2**) or the C10-hydroxylation (**4**). In particular, the L75A/V78A/F87A mutant converts >99% of the substrate and mainly produces C10-hydroxylation products **4**, while **2–3** were not detected (the remainder are unidentified products). The V78A/F87A/A328S mutant increases the selectivity for **2** 2-fold; yet, at the cost of lowering the substrate conversion rate. However, it should be noted that enzyme activity was not considered during our design protocol, a problem which would require further QM/MM calculations.

Further Directions. At the current state, the BDS approach gives only a qualitative description of the binding. The conformational space would need to be sampled even more thoroughly than we already did with HREX-MD to obtain accurate binding free energies for each substrate orientation, which is beyond the scope of this manuscript. We use HREX-MD to study relative populations and propose that this limited approach is appropriate for enzyme design purposes, where identifying that a mutation leads to an increase (or decrease) in selectivity is more important than exactly quantifying this change with very expensive and time-consuming computational methods. Mulholland and co-workers successfully applied a similar approach using MD simulations to determine the distance between the substrate and residues important for its positioning to infer about reactivity and specificity of glutamate mutase.⁸⁶ However, it should be noted that, while in certain cases the substrate proximity is the leading factor in determining P450 selectivity, the proximity alone is not always enough to rationalize enzyme selectivity.^{34,87,88} In such instances, further QM/MM⁸⁰ or empirical valence bond (EVB)⁸⁹ calculations would be necessary to investigate the effects of mutations on reactivity and selectivity.

The primary goal of the present study was to shift product distribution, which this *in silico* protocol demonstrated. Considering the ease of use and relatively low computational cost of HREX-MD simulations⁷⁸ (compared to other enhanced-sampling MD methods or QM/MM), the presented workflow could be incorporated in enzyme design strategies to reduce the screening efforts. While promising already, its performance could be further improved by involving QM/MM calculations to investigate chemical steps, which would help in selecting the mutations with high conversion rates (i.e., low activation barriers). The present study focuses on inverting the already observed product ratio; however, in future work it would be interesting to explore β -cembrene diol conformations currently designated unproductive, which would potentially introduce new reactivities. As other potentially reactive C-atoms were found sufficiently close to cI, addition of QM/MM

calculations would reveal if high activation barriers prevent such reactions from occurring, which could guide further P450 design strategies.

■ ASSOCIATED CONTENT

Supporting Information

The Supporting Information is available free of charge on the ACS Publications website at DOI: 10.1021/acs.jcim.8b00043.

Additional methodology description, including RESP charges for β -cembrenediol and mutagenesis hotspot selection. Supporting simulation results: RMSD and distance profiles, additional BDS profiles, and clustering for MM/PBSA. Supporting experimental validation results on substrate conversion by the designed mutants (PDF)

■ AUTHOR INFORMATION

Corresponding Authors

*E-mail: dusan.petrovic@icm.uu.se (D.P.).

*E-mail: b.strodel@fz-juelich.de (B.S.).

ORCID

Dušan Petrović: 0000-0002-1834-7358

Birgit Strodel: 0000-0002-8734-7765

Present Address

[†]D.P.: Department of Cell and Molecular Biology, Uppsala University, BMC Box 596, 751 24 Uppsala, Sweden.

Notes

The authors declare no competing financial interest.

■ ACKNOWLEDGMENTS

The project was funded by “Strategischer Forschungsfond” of the Heinrich-Heine University Düsseldorf (F2014/730-11) and by the Heinrich-Heine International Graduate School of Protein Science and Technology (iGRASPseed). D.P. is financially supported by the Jürgen Manchot Foundation. M.A. acknowledges the support from the Deutscher Akademischer Austauschdienst via the DAAD RISE Germany program. The authors gratefully acknowledge the computing time granted by the JARA-HPC Vergabegremium and VSR commission on the supercomputer JURECA (project ICS69) at Forschungszentrum Jülich. Further computational infrastructure was provided by the Center for Information and Media Technology (ZIM) at the Heinrich-Heine University Düsseldorf.

■ REFERENCES

- (1) Newhouse, T.; Baran, P. S. If C–H Bonds Could Talk: Selective C–H Bond Oxidation. *Angew. Chem., Int. Ed.* **2011**, *50*, 3362–3374.
- (2) Hartwig, J. F. Catalyst-Controlled Site-Selective Bond Activation. *Acc. Chem. Res.* **2017**, *50*, 549–555.
- (3) Roduner, E.; Kaim, W.; Sarkar, B.; Urlacher, V. B.; Pleiss, J.; Gläser, R.; Einicke, W.-D.; Sprenger, G. A.; Beifuß, U.; Klemm, E.; Liebner, C.; Hieronymus, H.; Hsu, S.-F.; Plietker, B.; Laschat, S. Selective Catalytic Oxidation of C–H Bonds with Molecular Oxygen. *ChemCatChem* **2013**, *5*, 82–112.
- (4) Hönig, M.; Sondermann, P.; Turner, N. J.; Carreira, E. M. Enantioselective Chemo- and Biocatalysis: Partners in Retrosynthesis. *Angew. Chem., Int. Ed.* **2017**, *56*, 8942–8973.
- (5) Lewis, J. C.; Coelho, P. S.; Arnold, F. H. Enzymatic Functionalization of Carbon–Hydrogen Bonds. *Chem. Soc. Rev.* **2011**, *40*, 2003–2021.
- (6) Fasan, R. Tuning P450 Enzymes as Oxidation Catalysts. *ACS Catal.* **2012**, *2*, 647–666.
- (7) Warman, A. J.; Roitel, O.; Neeli, R.; Girvan, H. M.; Seward, H. E.; Murray, S. A.; McLean, K. J.; Joyce, M. G.; Toogood, H.; Holt, R. A.; Leys, D.; Scrutton, N. S.; Munro, A. W. Flavocytochrome P450 BM3: An Update on Structure and Mechanism of a Biotechnologically Important Enzyme. *Biochem. Soc. Trans.* **2005**, *33*, 747–753.
- (8) Shaik, S.; Cohen, S.; Wang, Y.; Chen, H.; Kumar, D.; Thiel, W. P450 Enzymes: Their Structure, Reactivity, and Selectivity. *Chem. Rev.* **2010**, *110*, 949–1017.
- (9) Shaik, S.; Chen, H.; Usharani, D.; Thiel, W. QM/MM Studies of Structure and Reactivity of Cytochrome P450 Enzymes: Methodology and Selected Applications. In *Drug metabolism prediction*; Kirchmair, J., Ed.; Wiley-VCH Verlag GmbH & Co. KGaA: Weinheim, Germany, 2014; pp 133–178.
- (10) Lewis, J. C.; Arnold, F. H. Catalysts on Demand: Selective Oxidations by Laboratory-Evolved Cytochrome P450 BM3. *Chimia* **2009**, *63*, 309–312.
- (11) Ebert, M. C.; Pelletier, J. N. Computational Tools for Enzyme Improvement: Why Everyone Can – and Should – Use Them. *Curr. Opin. Chem. Biol.* **2017**, *37*, 89–96.
- (12) Whitehouse, C. J. C.; Bell, S. G.; Wong, L.-L. P450_{BM3} (CYP102A1): Connecting the Dots. *Chem. Soc. Rev.* **2012**, *41*, 1218–1260.
- (13) Toscano, M. D.; Woycechowsky, K. J.; Hilvert, D. Minimalist Active-Site Redesign: Teaching Old Enzymes New Tricks. *Angew. Chem., Int. Ed.* **2007**, *46*, 3212–3236.
- (14) Wang, J.; Li, G.; Reetz, M. T. Enzymatic Site-Selectivity Enabled by Structure-Guided Directed Evolution. *Chem. Commun.* **2017**, *53*, 3916–3928.
- (15) Huang, W.-C.; Westlake, A. C. G.; Maréchal, J.-D.; Joyce, M. G.; Moody, P. C. E.; Roberts, G. C. K. Filling a Hole in Cytochrome P450 BM3 Improves Substrate Binding and Catalytic Efficiency. *J. Mol. Biol.* **2007**, *373*, 633–651.
- (16) Hammes-Schiffer, S. Catalysts by Design: The Power of Theory. *Acc. Chem. Res.* **2017**, *50*, 561–566.
- (17) Tinberg, C. E.; Khare, S. D.; Dou, J.; Doyle, L.; Nelson, J. W.; Schena, A.; Jankowski, W.; Kalodimos, C. G.; Johnsson, K.; Stoddard, B. L.; Baker, D. Computational Design of Ligand-Binding Proteins with High Affinity and Selectivity. *Nature* **2013**, *501*, 212–216.
- (18) Urlacher, V. B.; Schmid, R. D. Protein Engineering of the Cytochrome P450 Monooxygenase from *Bacillus megaterium*. *Methods Enzymol.* **2004**, *388*, 208–224.
- (19) Weber, E.; Seifert, A.; Antonovici, M.; Geinitz, C.; Pleiss, J.; Urlacher, V. B. Screening of a Minimal Enriched P450 BM3 Mutant Library for Hydroxylation of Cyclic and Acyclic Alkanes. *Chem. Commun.* **2011**, *47*, 944–946.
- (20) Whitehouse, C. J. C.; Bell, S. G.; Tufton, H. G.; Kenny, R. J. P.; Ogilvie, L. C. I.; Wong, L.-L. Evolved CYP102A1 (P450_{BM3}) Variants Oxidise a Range of Non-Natural Substrates and Offer New Selectivity Options. *Chem. Commun.* **2008**, 966–968.
- (21) Appel, D.; Lutz-Wahl, S.; Fischer, P.; Schwaneberg, U.; Schmid, R. D. A P450 BM-3 Mutant Hydroxylates Alkanes, Cycloalkanes, Arenes and Heteroarenes. *J. Biotechnol.* **2001**, *88*, 167–171.
- (22) Lewis, J. C.; Mantovani, S. M.; Fu, Y.; Snow, C. D.; Komor, R. S.; Wong, C.-H.; Arnold, F. H. Combinatorial Alanine Substitution Enables Rapid Optimization of Cytochrome P450_{BM3} for Selective Hydroxylation of Large Substrates. *ChemBioChem* **2010**, *11*, 2502–2505.
- (23) Kille, S.; Zilly, F. E.; Acevedo, J. P.; Reetz, M. T. Regio- and Stereoselectivity of P450-Catalysed Hydroxylation of Steroids Controlled by Laboratory Evolution. *Nat. Chem.* **2011**, *3*, 738–743.
- (24) Venkataraman, H.; te Poele, E. M.; Rosloniec, K. Z.; Vermeulen, N.; Commandeur, J. N. M.; van der Geize, R.; Dijkhuizen, L. Biosynthesis of a Steroid Metabolite by an Engineered *Rhodococcus erythropolis* Strain Expressing a Mutant Cytochrome P450 BM3 Enzyme. *Appl. Microbiol. Biotechnol.* **2015**, *99*, 4713–4721.
- (25) Watanabe, Y.; Laschat, S.; Budde, M.; Affolter, O.; Shimada, Y.; Urlacher, V. B. Oxidation of Acyclic Monoterpenes by P450 BM-3 Monooxygenase: Influence of the Substrate E/Z-Isomerism on

Enzyme Chemo- and Regioselectivity. *Tetrahedron* **2007**, *63*, 9413–9422.

(26) Sowden, R. J.; Yasmin, S.; Rees, N. H.; Bell, S. G.; Wong, L.-L. Biotransformation of the Sesquiterpene (+)-Valencene by Cytochrome P450_{cam} and P450_{BM-3}. *Org. Biomol. Chem.* **2005**, *3*, 57–64.

(27) Dietrich, J. A.; Yoshikuni, Y.; Fisher, K. J.; Woolard, F. X.; Ockey, D.; McPhee, D. J.; Renninger, N. S.; Chang, M. C. Y.; Baker, D.; Keasling, J. D. A Novel Semi-Biosynthetic Route for Artemisinin Production Using Engineered Substrate-Promiscuous P450 BM3. *ACS Chem. Biol.* **2009**, *4*, 261–267.

(28) Driggers, E. M.; Hale, S. P.; Lee, J.; Terrett, N. K. The Exploration of Macrocycles for Drug Discovery — an Underexploited Structural Class. *Nat. Rev. Drug Discovery* **2008**, *7*, 608–624.

(29) Giordanetto, F.; Kihlberg, J. Macrocyclic Drugs and Clinical Candidates: What Can Medicinal Chemists Learn from Their Properties? *J. Med. Chem.* **2014**, *57*, 278–295.

(30) Marsault, E.; Peterson, M. L. Macrocycles Are Great Cycles: Applications, Opportunities, and Challenges of Synthetic Macrocycles in Drug Discovery. *J. Med. Chem.* **2011**, *54*, 1961–2004.

(31) Le-Huu, P.; Heidt, T.; Claasen, B.; Laschat, S.; Urlacher, V. B. B. Chemo-, Regio-, and Stereoselective Oxidation of the Monocyclic Diterpenoid β -Cembrenediol by P450 BM3. *ACS Catal.* **2015**, *5*, 1772–1780.

(32) Le-Huu, P.; Petrović, D.; Strodel, B.; Urlacher, V. B. One-Pot, Two-Step Hydroxylation of the Macrocyclic Diterpenoid β -Cembrenediol Catalyzed by P450 BM3 Mutants. *ChemCatChem* **2016**, *8*, 3755–3761.

(33) de Visser, S. P.; Ogliaro, F.; Sharma, P. K.; Shaik, S. What Factors Affect the Regioselectivity of Oxidation by Cytochrome P450? A DFT Study of Allylic Hydroxylation and Double Bond Epoxidation in a Model Reaction. *J. Am. Chem. Soc.* **2002**, *124*, 11809–11826.

(34) Oláh, J.; Mulholland, A. J.; Harvey, J. N. Understanding the Determinants of Selectivity in Drug Metabolism Through Modeling of Dextromethorphan Oxidation by Cytochrome P450. *Proc. Natl. Acad. Sci. U. S. A.* **2011**, *108*, 6050–6055.

(35) Dubey, K. D.; Wang, B.; Shaik, S. Molecular Dynamics and QM/MM Calculations Predict the Substrate-Induced Gating of Cytochrome P450 BM3 and the Regio- and Stereoselectivity of Fatty Acid Hydroxylation. *J. Am. Chem. Soc.* **2016**, *138*, 837–845.

(36) Ramanan, R.; Dubey, K. D.; Wang, B.; Mandal, D.; Shaik, S. Emergence of Function in P450-Proteins: A Combined Quantum Mechanical/Molecular Mechanical and Molecular Dynamics Study of the Reactive Species in the H₂O₂-Dependent Cytochrome P450_{SPR} and Its Regio- and Enantioselective Hydroxylation of Fatty Acids. *J. Am. Chem. Soc.* **2016**, *138*, 6786–6797.

(37) Dubey, K. D.; Wang, B.; Vajpai, M.; Shaik, S. MD Simulations and QM/MM Calculations Show That Single-Site Mutations of Cytochrome P450 BM3 Alter the Active Site's Complexity and the Chemoselectivity of Oxidation Without Changing the Active Species. *Chem. Sci.* **2017**, *8*, 5335–5344.

(38) Poulos, T. L. Heme Enzyme Structure and Function. *Chem. Rev.* **2014**, *114*, 3919–3962.

(39) Haines, D. C.; Tomchick, D. R.; Machius, M.; Peterson, J. A. Pivotal Role of Water in the Mechanism of P450BM-3. *Biochemistry* **2001**, *40*, 13456–13465.

(40) Hess, B.; Kutzner, C.; van der Spoel, D.; Lindahl, E. GROMACS 4: Algorithms for Highly Efficient, Load-Balanced, and Scalable Molecular Simulation. *J. Chem. Theory Comput.* **2008**, *4*, 435–447.

(41) Best, R. B.; Hummer, G. Optimised Molecular Dynamics Force Fields Applied to the Helix–Coil Transition of Polypeptides. *J. Phys. Chem. B* **2009**, *113*, 9004–9015.

(42) Lindorff-Larsen, K.; Piana, S.; Palmo, K.; Maragakis, P.; Klepeis, J. L.; Dror, R. O.; Shaw, D. E. Improved Side-Chain Torsion Potentials for the Amber ff99SB Protein Force Field. *Proteins: Struct., Funct., Genet.* **2010**, *78*, 1950–1958.

(43) Jorgensen, W. L.; Chandrasekhar, J.; Madura, J. D.; Impey, R. W.; Klein, M. L. Comparison of Simple Potential Functions for Simulating Liquid Water. *J. Chem. Phys.* **1983**, *79*, 926.

(44) Shahrokh, K.; Orendt, A.; Yost, G. S.; Cheatham, T. E. Quantum Mechanically Derived AMBER-Compatible Heme Parameters for Various States of the Cytochrome P450 Catalytic Cycle. *J. Comput. Chem.* **2012**, *33*, 119–133.

(45) Sondergaard, C. R.; Olsson, M. H. M.; Rostkowski, M.; Jensen, J. H. Improved Treatment of Ligands and Coupling Effects in Empirical Calculation and Rationalization of pKa Values. *J. Chem. Theory Comput.* **2011**, *7*, 2284–2295.

(46) Darden, T.; York, D.; Pedersen, L. Particle Mesh Ewald: An $N \log(N)$ Method for Ewald Sums in Large Systems. *J. Chem. Phys.* **1993**, *98*, 10089.

(47) Hess, B. P-LINCS: A Parallel Linear Constraint Solver for Molecular Simulation. *J. Chem. Theory Comput.* **2008**, *4*, 116–122.

(48) Bussi, G.; Donadio, D.; Parrinello, M. Canonical Sampling Through Velocity Rescaling. *J. Chem. Phys.* **2007**, *126*, 14101.

(49) Berendsen, H. J. C.; Postma, J. P. M.; van Gunsteren, W. F.; DiNola, A.; Haak, J. R. Molecular Dynamics With Coupling to an External Bath. *J. Chem. Phys.* **1984**, *81*, 3684.

(50) Parrinello, M.; Rahman, A. Polymorphic Transitions in Single Crystals: A New Molecular Dynamics Method. *J. Appl. Phys.* **1981**, *52*, 7182.

(51) Daura, X.; Gademann, K.; Jaun, B.; Seebach, D.; van Gunsteren, W. F.; Mark, A. E. Peptide Folding: When Simulation Meets Experiment. *Angew. Chem., Int. Ed.* **1999**, *38*, 236–240.

(52) Hawkins, P. C. D.; Skillman, A. G.; Warren, G. L.; Ellingson, B. A.; Stahl, M. T. Conformer Generation with OMEGA: Algorithm and Validation Using High Quality Structures from the Protein Databank and Cambridge Structural Database. *J. Chem. Inf. Model.* **2010**, *50*, 572–584.

(53) Halgren, T. A. MMFF VI. MMFF94s Option for Energy Minimization Studies. *J. Comput. Chem.* **1999**, *20*, 720–729.

(54) McGann, M. FRED Pose Prediction and Virtual Screening Accuracy. *J. Chem. Inf. Model.* **2011**, *51*, 578–596.

(55) Sousa da Silva, A. W.; Vranken, W. F. ACPYPE — AnteChamber Python Parser interface. *BMC Res. Notes* **2012**, *5*, 367.

(56) Wang, J.; Wang, W.; Kollman, P. A.; Case, D. A. Automatic Atom Type and Bond Type Perception in Molecular Mechanical Calculations. *J. Mol. Graphics Modell.* **2006**, *25*, 247–260.

(57) Frisch, M. J.; Trucks, G. W.; Schlegel, H. B.; Scuseria, G. E.; Robb, M. A.; Cheeseman, J. R.; Scalmani, G.; Barone, V.; Mennucci, B.; Petersson, G. A.; Nakatsuji, H.; Caricato, M.; Li, X.; Hratchian, H. P.; Izmaylov, A. F.; Bloino, J.; Zheng, G.; Sonnenberg, J. L.; Hada, M.; Ehara, M.; Toyota, K.; Fukuda, R.; Hasegawa, J.; Ishida, M.; Nakajima, T.; Honda, Y.; Kitao, O.; Nakai, H.; Vreven, T.; Montgomery, J. A., Jr.; Peralta, J. E.; Ogliaro, F.; Bearpark, M.; Heyd, J. J.; Brothers, E.; Kudin, K. N.; Staroverov, V. N.; Kobayashi, R.; Normand, J.; Raghavachari, K.; Rendell, A.; Burant, J. C.; Iyengar, S. S.; Tomasi, J.; Cossi, M.; Rega, N.; Millam, J. M.; Klene, M.; Knox, J. E.; Cross, J. B.; Bakken, V.; Adamo, C.; Jaramillo, J.; Gomperts, R.; Stratmann, R. E.; Yazyev, O.; Austin, A. J.; Cammi, R.; Pomelli, C.; Ochterski, J. W.; Martin, R. L.; Morokuma, K.; Zakrzewski, V. G.; Voth, G. A.; Salvador, P.; Dannenberg, J. J.; Dapprich, S.; Daniels, A. D.; Farkas, Ö.; Foresman, J. B.; Ortiz, J. V.; Cioslowski, J.; Fox, D. J. *Gaussian 09*, Revision A.02; Gaussian, Inc., Wallingford CT, 2009.

(58) Bonomi, M.; Branduardi, D.; Bussi, G.; Camilloni, C.; Provasi, D.; Raiteri, P.; Donadio, D.; Marinelli, F.; Pietrucci, F.; Broglia, R. A.; Parrinello, M. PLUMED: A Portable Plugin for Free-Energy Calculations with Molecular Dynamics. *Comput. Phys. Commun.* **2009**, *180*, 1961–1972.

(59) Bussi, G. Hamiltonian Replica Exchange in GROMACS: A Flexible Implementation. *Mol. Phys.* **2014**, *112*, 379–384.

(60) Kumari, R.; Kumar, R.; Lynn, A. G. mmpbsa — A GROMACS Tool for High-Throughput MM-PBSA Calculations. *J. Chem. Inf. Model.* **2014**, *54*, 1951–1962.

(61) Michaud-Agrawal, N.; Denning, E. J.; Woolf, T. B.; Beckstein, O. MDAnalysis: A Toolkit for the Analysis of Molecular Dynamics Simulations. *J. Comput. Chem.* **2011**, *32*, 2319–2327.

(62) Humphrey, W.; Dalke, A.; Schulten, K. VMD: Visual Molecular Dynamics. *J. Mol. Graphics* **1996**, *14*, 33–38.

- (63) *The PyMOL Molecular Graphics System*, Version 1.6; Schrödinger, LLC.
- (64) Edelheit, O.; Hanukoglu, A.; Hanukoglu, I. Simple and Efficient Site-Directed Mutagenesis Using Two Single-Primer Reactions in Parallel to Generate Mutants for Protein Structure-Function Studies. *BMC Biotechnol.* **2009**, *9*, 61.
- (65) Omura, T.; Sato, R. The Carbon Monoxide-Binding Pigment of Liver Microsomes: II. Solubilization, Purification, and Properties. *J. Biol. Chem.* **1964**, *239*, 2379–2385.
- (66) Feenstra, K. A.; Starikov, E. B.; Urlacher, V. B.; Commandeur, J. N. M.; Vermeulen, N. P. E. Combining Substrate Dynamics, Binding Statistics, and Energy Barriers to Rationalize Regioselective Hydroxylation of Octane and Lauric Acid by CYP102A1 and Mutants. *Protein Sci.* **2007**, *16*, 420–431.
- (67) Sasahara, K.; Mashima, A.; Yoshida, T.; Chuman, H. Molecular Dynamics and Density Functional Studies on the Metabolic Selectivity of Antipsychotic Thioridazine by Cytochrome P450 2D6: Connection with Crystallographic and Metabolic Results. *Bioorg. Med. Chem.* **2015**, *23*, 5459–5465.
- (68) Narayan, A. R. H.; Jiménez-Osés, G.; Liu, P.; Negretti, S.; Zhao, W.; Gilbert, M. M.; Ramabhadran, R. O.; Yang, Y.-F.; Furan, L. R.; Li, Z.; Podust, L. M.; Montgomery, J.; Houk, K. N.; Sherman, D. H. Enzymatic Hydroxylation of an Unactivated Methylene C–H Bond Guided by Molecular Dynamics Simulations. *Nat. Chem.* **2015**, *7*, 653–660.
- (69) Hawkins, P. C. D. Conformation Generation: The State of the Art. *J. Chem. Inf. Model.* **2017**, *57*, 1747–1756.
- (70) Alogheli, H.; Olanders, G.; Schaal, W.; Brandt, P.; Karlén, A. Docking of Macrocycles: Comparing Rigid and Flexible Docking in Glide. *J. Chem. Inf. Model.* **2017**, *57*, 190–202.
- (71) Begley, M. J.; Crombie, L.; McNamara, D.; Firth, D. F.; Smith, S.; Bevan, P. C. Cembrenediols in the Curing of Tobacco. X-Ray Crystal Structures of β -Cembrenediol and α -Cembreneketol. *Phytochemistry* **1988**, *27*, 1695–1703.
- (72) Elokely, K. M.; Doerksen, R. J. Docking Challenge: Protein Sampling and Molecular Docking Performance. *J. Chem. Inf. Model.* **2013**, *53*, 1934–1945.
- (73) Motta, S.; Bonati, L. Modeling Binding with Large Conformational Changes: Key Points in Ensemble-Docking Approaches. *J. Chem. Inf. Model.* **2017**, *57*, 1563–1578.
- (74) Buch, I.; Giorgino, T.; De Fabritiis, G. Complete Reconstruction of an Enzyme-Inhibitor Binding Process by Molecular Dynamics Simulations. *Proc. Natl. Acad. Sci. U. S. A.* **2011**, *108*, 10184–10189.
- (75) Ebert, M. C. C. J. C.; Guzman Espinola, J.; Lamoureux, G.; Pelletier, J. N. Substrate-Specific Screening for Mutational Hotspots Using Biased Molecular Dynamics Simulations. *ACS Catal.* **2017**, *7*, 6786–6797.
- (76) Capoferri, L.; Leth, R.; ter Haar, E.; Mohanty, A. K.; Grootenhuys, P. D. J.; Vottero, E.; Commandeur, J. N. M.; Vermeulen, N. P. E.; Jørgensen, F. S.; Olsen, L.; Geerke, D. P. Insights Into Regioselective Metabolism of Mefenamic Acid by Cytochrome P450 BM3 Mutants through Crystallography, Docking, Molecular Dynamics, and Free Energy Calculations. *Proteins: Struct., Funct., Genet.* **2016**, *84*, 383–396.
- (77) Yang, Y.; Wong, S. E.; Lightstone, F. C. Understanding a Substrate's Product Regioselectivity in a Family of Enzymes: A Case Study of Acetaminophen Binding in Cytochrome P450s. *PLoS One* **2014**, *9*, e87058.
- (78) Petrović, D.; Frank, D.; Kamerlin, S. C. L.; Hoffmann, K.; Strodel, B. Shuffling Active Site Substrate Populations Affects Catalytic Activity: The Case of Glucose Oxidase. *ACS Catal.* **2017**, *7*, 6188–6197.
- (79) Vaz, A. D. N.; McGinnity, D. F.; Coon, M. J. Epoxidation of Olefins by Cytochrome P450: Evidence from Site-Specific Mutagenesis for Hydroperoxo-Iron as an Electrophilic Oxidant. *Proc. Natl. Acad. Sci. U. S. A.* **1998**, *95*, 3555–3560.
- (80) Lonsdale, R.; Houghton, K. T.; Żurek, J.; Bathelt, C. M.; Foloppe, N.; de Groot, M. J.; Harvey, J. N.; Mulholland, A. J. Quantum Mechanics/Molecular Mechanics Modeling of Regioselectivity of Drug Metabolism in Cytochrome P450 2C9. *J. Am. Chem. Soc.* **2013**, *135*, 8001–8015.
- (81) Bonomo, S.; Jørgensen, F. S.; Olsen, L. Dissecting the Cytochrome P450 1A2- and 3A4-Mediated Metabolism of Aflatoxin B1 in Ligand and Protein Contributions. *Chem. - Eur. J.* **2017**, *23*, 2884–2893.
- (82) Shirts, M. R.; Mobley, D. L.; Brown, S. P. Free-Energy Calculations in Structure-Based Drug Design. In *Drug design: Structure- and ligand-based approaches*; Merz, K. M., Ringe, D., Reynolds, C. H., Eds.; Cambridge University Press: Cambridge, 2010; pp 61–86.
- (83) Aldeghi, M.; Bodkin, M. J.; Knapp, S.; Biggin, P. C. Statistical Analysis on the Performance of Molecular Mechanics Poisson–Boltzmann Surface Area Versus Absolute Binding Free Energy Calculations: Bromodomains as a Case Study. *J. Chem. Inf. Model.* **2017**, *57*, 2203–2221.
- (84) Scouras, A. D.; Daggett, V. The Dymeomics Rotamer Library: Amino Acid Side Chain Conformations and Dynamics from Comprehensive Molecular Dynamics Simulations in Water. *Protein Sci.* **2011**, *20*, 341–352.
- (85) Renata, H.; Lewis, R. D.; Sweredoski, M. J.; Moradian, A.; Hess, S.; Wang, Z. J.; Arnold, F. H. Identification of Mechanism-Based Inactivation in P450-Catalyzed Cyclopropanation Facilitates Engineering of Improved Enzymes. *J. Am. Chem. Soc.* **2016**, *138*, 12527–12533.
- (86) Román-Meléndez, G. D.; von Glehn, P.; Harvey, J. N.; Mulholland, A. J.; Marsh, E. N. G. Role of Active Site Residues in Promoting Cobalt–Carbon Bond Homolysis in Adenosylcobalamin-Dependent Mutases Revealed Through Experiment and Computation. *Biochemistry* **2014**, *53*, 169–177.
- (87) Lodola, A.; Mor, M.; Żurek, J.; Tarzia, G.; Piomelli, D.; Harvey, J. N.; Mulholland, A. J. Conformational Effects in Enzyme Catalysis: Reaction via a High Energy Conformation in Fatty Acid Amide Hydrolase. *Biophys. J.* **2007**, *92*, L20–22.
- (88) Lodola, A.; Sirirak, J.; Fey, N.; Rivara, S.; Mor, M.; Mulholland, A. J. Structural Fluctuations in Enzyme-Catalyzed Reactions: Determinants of Reactivity in Fatty Acid Amide Hydrolase from Multivariate Statistical Analysis of Quantum Mechanics/Molecular Mechanics Paths. *J. Chem. Theory Comput.* **2010**, *6*, 2948–2960.
- (89) Amrein, B. A.; Steffen-Munsberg, F.; Szeler, I.; Purg, M.; Kulkarni, Y.; Kamerlin, S. C. L. CADEE: Computer-Aided Directed Evolution of Enzymes. *IUCrJ* **2017**, *4*, 50–64.

2.4 Chapter IV

Chemoenzymatic Route to Oxyfunctionalized Cembranoids Facilitated by Substrate and Protein Engineering

Priska Le-Huu⁺, Dominik Rekow⁺, Claudia Krüger, Ansgar Bokel, Tanja Heidt, Sebastian Schaubach, Birgit Claasen, Sebastian Hölzel, Wolfgang Frey, Sabine Laschat*, and Vlada B. Urlacher*

⁺ these authors contributed equally to this work

* corresponding authors

Chemistry—A European Journal, 2018, 24(46), 12010-12021

Own contribution (10%): AB performed the molecular docking of the cembranoid enantiomers in the active site of P450 BM3. AB wrote the respective abstract of the manuscript.

Reprinted with permission from Le-Huu, P., Rekow, D., Krüger, C., Bokel, A., Heidt, T., Schaubach, S., Claasen, B., Hölzel, S., Frey, W., Laschat, S., & Urlacher, V. B. (2018). Chemoenzymatic route to oxyfunctionalized cembranoids facilitated by substrate and protein engineering. *Chemistry—A European Journal*, 24(46), 12010-12021. Copyright 2018 Wiley-VCH Verlag GmbH & Co. KGaA, Weinheim

Biochemistry

Chemoenzymatic Route to Oxyfunctionalized Cembranoids Facilitated by Substrate and Protein Engineering

 Priska Le-Huu⁺,^[a] Dominik Rekow⁺,^[b] Claudia Krüger,^[b] Ansgar Bokel,^[a] Tanja Heidt,^[b] Sebastian Schaubach,^[b] Birgit Claasen,^[b] Sebastian Hölzel,^[a] Wolfgang Frey,^[b] Sabine Laschat,^{*[b]} and Vlada B. Urlacher^{*[a]}

Abstract: Cembranoids constitute a large family of 14-membered oxygenated macrocyclic diterpenoids with potential as therapeutic agents. Selective late-stage oxidations of cembranoid scaffolds remain a challenge for chemical catalysts but can be accomplished by enzymes. Here, a new chemoenzymatic route to oxyfunctionalized 14-membered macrocycles including cembranoids is described. This route combines a metal-catalyzed ring-closing metathesis with a subsequent P450 BM3-catalyzed hydroxylation and delivers cembranoid-like analogues. Systematic substrate probing with a set of synthetic 14-membered macrocycles revealed

that the regioselectivity of a P450 BM3-based biocatalyst increased with increasing ring rigidity as well as size and polarity of the exocyclic substituents. Enzyme regioselectivity could further be improved by first-sphere active site mutagenesis. The V78A/F87A variant catalyzed hydroxylation of cembranoid-ol (9*S*/*R*)-**3d** with 90% regioselectivity for C5 position. Extensive NMR analysis of Mosher esters and single crystal X-ray structure determination revealed a remarkable diastereoselectivity of this P450 BM3 mutant depending on substrate stereochemistry, which led exclusively to the *syn*-cembranoid-diols (5*S*,9*S*)-**4** and (5*R*,9*R*)-**4**.

Introduction

Macrocyclic natural products have been recognized as potential candidates for drug development due to their pharmacological activities and diverse chemical structures.^[1] Analysis of a database of more than 130 000 natural products has revealed that a majority of macrocycles have a molecular weight of 300–400 g mol⁻¹ and occur as 14-membered compounds.^[2] Alongside macrolide antibiotics, macrocyclic diterpenoids of cembrane-type, referred to as cembranoids, build the vast majority of this group. Cembranoids originate from insects such as ants, and plants such as tobacco and conifers,^[3] but pre-

dominantly from marine invertebrates, particularly gorgonian and soft corals.^[3b] Approximately 300 naturally occurring cembranoids have been isolated and studied regarding their structures and biological activities.^[4] Cembranoids with antimalarial, cytotoxic, antiviral, neuroprotective, anti-inflammatory, Ca-antagonistic, and different target inhibitory activities have been reported.^[3b,5] These natural products share a common 14-membered carbocyclic structure, derived from cyclized geranylgeranyl diphosphate, which is decorated by various oxygen functions.^[3b,6] Due to the complex molecular architecture of cembranoids, as well as their potential as pharmacological agents, these natural products and their analogues have attracted much interest in the synthetic community.^[5,7] These compounds are usually synthesized in a chemical convergent approach, in which multiple, separately generated fragments are combined in the desired product. Functional groups, including oxygen functions, are introduced already at an early stage of the synthesis which requires laborious protecting group manipulations in the following steps.^[7,8]

Alternatively, a minimally oxidized hydrocarbon skeleton, synthesized from simple building blocks, can be oxidized at a later-stage of synthesis, which allows a more effective diversification. Inspired by terpene biosynthesis, Baran and co-workers introduced a biomimetic “two-phase” approach for the total synthesis of natural products and their analogues.^[9] A hydrocarbon skeleton synthesized in the first “cyclase phase”, is diversified through oxidation reactions and rearrangements in the second “oxidase phase”. This “two-phase” approach has successfully been applied to the synthesis of a taxol precursor (–)-taxuyunnanin D,^[10] and diterpenoid (–)-ingenol.^[11]

[a] Dr. P. Le-Huu,⁺ A. Bokel, S. Hölzel, Prof. Dr. V. B. Urlacher
Institute of Biochemistry
Heinrich-Heine University Düsseldorf
Universitätsstrasse 1
40225 Düsseldorf (Germany)
E-mail: vlada.urlacher@uni-duesseldorf.de

[b] D. Rekow,⁺ C. Krüger, Dr. T. Heidt, S. Schaubach, Dr. B. Claasen, Dr. W. Frey,
Prof. Dr. S. Laschat
Institute of Organic Chemistry
University Stuttgart
Pfaffenwaldring 55
70569 Stuttgart (Germany)
E-mail: sabine.laschat@oc.uni-stuttgart.de

[†] These authors contributed equally to this work.

Supporting information and the ORCID identification number(s) for the author(s) of this article can be found under:
<https://doi.org/10.1002/chem.201802250>.

Part of the Special Issue for the 7th EuCheMS Chemistry Congress consisting of contributions from selected speakers and conveners. To view the complete issue, visit Issue 46.

The aim of this study was to combine the recently reported synthesis of macrocyclic cembranoids^[12] with late-stage oxidation. However, despite advances in the development of chemical catalysts enabling selective oxidation,^[13] the feasibility of the two-phase approach seems to be limited by insufficient regioselectivity of C–H oxidations of complex compounds like cembranoids. Enzyme catalyzed selective oxidation of complex molecules, bearing several chemically equivalent positions, presents an alternative way to oxidized derivatives.

In nature, late-stage oxidation of cembranoids is proposed to be catalyzed by cytochrome P450 monooxygenases.^[14] Cytochrome P450 monooxygenases are heme containing NAD(P)H dependent enzymes found in virtually all organisms, where they are involved—amongst others—in secondary metabolism. It was shown that after the geranylgeranyl diphosphate cyclization step, CYP71D16 catalyzes the hydroxylation of cembra-2,7,11-trien-4-ol at position C6 to form the most abundant cembranoids in *Nicotiana tabacum*, α - and β -cembrenediols.^[15] No further naturally occurring P450 enzymes involved in cembranoids oxidation have been reported to date. The introduction of oxygen containing functionalities during biosynthesis of other cembranoids is much less investigated.^[6b] This is probably due to the fact that cembranoids are mainly originated from soft corals, whose biosynthetic pathways have not yet been fully elucidated.

This limitation can be overcome by enzyme engineering^[16] of known well-characterized P450 enzymes. Recently, we reported P450 BM3 variants that are capable of oxidizing β -cembrenediol ((1S,2E,4R,6R,7E,11E)-4,6-dihydroxycembra-2,7,11-triene) (Figure 1) from *N. tabacum*^[17] and its oxidized derivatives.^[18] P450 BM3 from *Bacillus megaterium* (CYP102A1) is catalytically self-sufficient because the electron transferring reduc-

tase domain is fused to the heme containing monooxygenase domain.^[19] It is a fatty acid hydroxylase^[20] that demonstrates high activity^[21] and can be applied on a large scale.^[22] P450 BM3 is highly 'evolvable' and was redesigned to accept a broad range of new substrates^[23] including sterically demanding compounds such as alkaloids,^[24] sesquiterpenoids,^[25] polycyclic aromatic hydrocarbons,^[26] steroids,^[27] and drugs.^[28]

While the wild-type enzyme led to approximately 2% conversion of β -cembrenediol, P450 BM3 variants with only two or three first-sphere mutations converted up to 99% of this compound with high regioselectivity of 97–100%.^[17] The effect of amino acid substitutions on the regioselectivity of P450 BM3-mediated cembranoid oxidation was studied in detail.^[29] However, the effect of substrate structure on the product selectivity remained unclear. Here, a set of 14-membered macrocycles (1–3, Figure 1) differing in the number of C=C double bonds and the polarity and size of the exocyclic substituents, was used to probe chemo- and regioselectivity of the P450-catalyzed oxidation. This substrate engineering approach allowed us to identify structural elements of the target macrocycles that affect enzyme regioselectivity. Subsequently, a P450 BM3 variant was constructed and applied in a chemoenzymatic process for the regioselective hydroxylation of one of the synthetic macrocycles, dimethyl (3E,7E,11E)-9-hydroxy-4,8-dimethylcyclotetradeca-3,7,11-triene-1,1-dicarboxylate (**3d**). The hydroxylated product was isolated and identified as dimethyl (3E,7E,11E)-5,9-dihydroxy-4,8-dimethylcyclotetradeca-3,7,11-triene-1,1-dicarboxylate (**4**). NMR analysis and single crystal X-ray structure determination revealed a remarkable diastereoselectivity of the P450 BM3-based biocatalyst depending on substrate stereochemistry, which led to (5S,9S)-**4** and (5R,9R)-**4**.

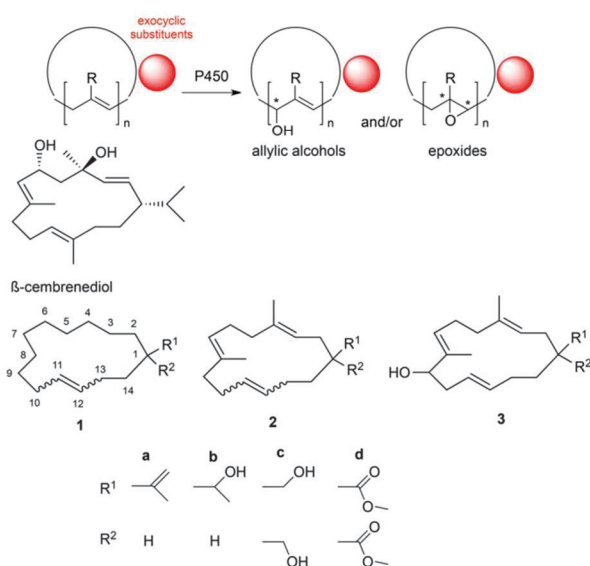


Figure 1. Set of synthetic 14-membered macrocycles (1–3) with various substituents at C1 (a–d) and β -cembrenediol. The numbering of the carbon atoms is different from IUPAC and was used uniformly for all macrocycles (1–3) and is given here for the macrocycle 1.

Results and Discussion

Probing various 14-membered macrocycles as P450 BM3 substrates

In enzyme-catalyzed reactions, an increase in regioselectivity can be achieved inter alia by forcing the substrate into a certain orientation via specific interactions with a P450 enzyme.^[30] For example, the desosamine glycoside moiety of the two natural CYP107L substrates – 14-membered macrolides YC-17 and narbomycin—was linked via an acetal linkage to a set of saturated carbon cycles with a ring size of 12–15 atoms.^[31] Acting as an anchor, the desosamine glycoside moiety facilitated substrate binding, which led to considerable regioselectivity of hydroxylation catalyzed by CYP107L. Furthermore, while the natural substrate YC-17 was hydroxylated by a mutant of CYP107L1 at positions C10 and C12 at a ratio of 1:1, its analogue containing 3-aminobenzoate instead of the desosamine glycoside anchoring group was preferably oxidized at C10 (> 20:1, C10/ C12).^[32]

We applied the substrate engineering approach and examined the hypothesis whether additional exocyclic substituents covalently bound to a macrocyclic substrate enable its specific interactions with the enzyme and thus affect the selectivity of

P450-catalyzed oxidation reactions. Furthermore, the influence of ring flexibilities on product selectivity was analyzed as well.

The model substrates **1**, **2** and **3** (Figure 1), were synthesized via ring closing metathesis (RCM) using Grubbs II catalyst, followed by subsequent functionalization of the exocyclic substituents. Synthesis of compounds **2d** and **3d** via RCM have recently been reported.^[12] Further details are described in the Supporting Information.

The simplest macrocycle cyclotetradec-11-ene (**1**) is the most flexible and non-polar with only one double bond (*E/Z*-ratio of 9:91). The two other macrocycles, dimethyl (3*E*,7*E*)-4,8-dimethylcyclotetradeca-3,7,11-triene (**2**) and dimethyl (3*E*,7*E*,11*E*)-9-hydroxy-4,8-dimethyl-cyclotetradeca-3,7,11-triene (**3**) have a similar cembranoid structure with three double bonds as well as two methyl groups but differ by an additional hydroxy group at C9 in the latter case. *E/Z*-ratio for cembranoid **2** was determined to be 89:11 and for compound **3**, 99:1.^[12] The exocyclic substituents (**a-d**) at position C1 vary in their polarity and size: the most nonpolar is isopropenyl group **a**; **b** and **c** with one or two hydroxy groups are more polar, while the diester-containing **d** represents the largest substituting group (Figure 1).

P450 BM3 wild type shows no activity with macrocycles **1–3**. Crystal structures of the monooxygenase domain demonstrate that phenylalanine 87, located directly over the heme group, can hinder the access of bulky compounds to the heme iron.^[33] It is one of the most frequently mutated positions that has often been exchanged by smaller residues, especially for large substrates.^[34] We assumed that for the oxidation of 14-membered macrocycles, F87 should be replaced by an amino acid that would offer the greatest possible spatial gain. Hence, all oxidations in the first set of experiments were performed using the F87G mutant. Indeed, this mutant accepted all synthetic macrocycles as substrates. Conversions and products formed were analyzed by LC/MS (see Figure S1 and S2 in the Supporting Information). Depending on the compound tested, conversions ranging from 15% to 100% were achieved and different numbers of products (5 to >16) were detected, with masses corresponding to single- to five-fold oxidized products. The results indicate that this monooxygenase can oxidize both pure hydrocarbon macrocycles and macrocycles carrying hydroxy or ester groups, which agrees with previous observations.^[35]

The influence of exocyclic substituents of different size and polarity on enzyme activity and selectivity was first studied with the same ring structure and different exocyclic groups (**1a–d** and **3c,d**). The oxidation of the predominantly saturated macrocycles **1** showed considerable differences depending on the exocyclic substituents **a–d** (Table 1 and Figure S1 in the Supporting Information). With increasing polarity and size of the exocyclic substituents conversion of macrocycles **1b–d** and the number of products decreased (**1b**: >15 (conv. 100%), **1c**: 8 (93%), **1d**: 5 (15%)). While **1a** was oxidized four to five times in a multi-step fashion, the macrocycles **1b** and **1c** with one or two alcohol functionalities, respectively, were oxidized each only at one or two positions. Further oxidation of a hydroxy to a ketone group was observed during oxidation

Table 1. P450 BM3 F87G-catalyzed oxidations of macrocycles **1a–d** and MS analysis of the products. Time: reaction time; Mw: molecular weight in g mol⁻¹; Δ*m*: mass difference to the substrate; Δ*A*: additional atoms compared to the substrate. n.d.—since a separation into individual product peaks was not possible for **1a** oxidation, no product number can be specified here. For details see Figures S1 in the Supporting Information. (11,12)-epoxides of **1c** and **1d** were identified by comparison with synthesized reference compounds.

| Substrate | Time [h] | Conversion [%] | Mw | Δ <i>m</i> | Number of products | Δ <i>A</i> | | |
|-----------|----------|----------------|-----|------------|---------------------|------------|---------------------|----|
| 1a | 0.5 | 40 ± 7 | 234 | 0 | | – | | |
| | 23 | 100 ± 1 | 282 | +48 | n.d. | +30 | | |
| | | | 296 | +62 | | +40, –2H | | |
| 1b | 0.5 | 100 ± 0 | 298 | +64 | | +40 | | |
| | | | 238 | 0 | | – | | |
| | | | 254 | +16 | >5 | +0 | | |
| | | | 270 | +32 | >6 | +20 | | |
| 1c | 0.5 | 93 ± 2 | 272 | +34 | 4 | +20, +2H | | |
| | | | 254 | 0 | | – | | |
| | | | 270 | +16 | 5 (incl. 1 epoxide) | +0 | | |
| | | | 284 | +30 | 1 | +20, –2H | | |
| | | | 286 | +32 | 1 | +20 | | |
| 1d | 0.5 | 15 ± 6 | 310 | 0 | | – | | |
| | | | 23 | 70 ± 2 | 326 | +16 | 5 (incl. 1 epoxide) | +0 |
| | | | | | | | | |

of **1c**. The macrocycle **1d**, which carries the largest exocyclic substituents with two ester functionalities, was oxidized only to mono-oxidized products. For **1c** and **1b** the corresponding (11,12)-epoxides were identified, which indicates that other products with a mass difference of +16 *m/z* compared to the substrate are presumably hydroxylated compounds.

Similar to the compound **1** with various exocyclic groups, the same tendency was observed for the oxidation of **3c** and **3d** (Table 2 and Figures S2b and S2c in the Supporting Information). While compound **3c** with a diol group was converted after 0.5 h to 50% to form eight products, compound **3d** with a diester group was converted to 36% resulting in four products. Similar to **1c** and **1d**, the products derived from **3c** and **3d** were identified as singularly hydroxylated or epoxidized derivatives.

In the next experiment, the influence of ring structure on the activity and product selectivity of P450 BM3 F87G was investigated with **1d** (*E/Z* ratio of 9:91) and **2d** (*E/Z* ratio of 89:11). The macrocycle **1d** with only one double bond and thus a more flexible ring, was converted to a lesser extent (15%, Table 1) as compared to the more rigid macrocycle **2d** (59%, Table 2). However, differences in enzyme activity might be due to differences in *E/Z* configuration of the C11/C12 double bond: While **2d** was predominantly *E*-configured (*E/Z* = 89:11), macrocycle **1d** was predominantly *Z*-configured (*E/Z* = 9:91). In the present study, the influence of the *E/Z*-configuration on the C11/C12 double bond was not systematically investigated. Our previous studies on geranylacetone and nerylacetone, respectively revealed that *E*- and *Z*-isomers were oxidized in the presence of a P450 BM3 mutant with different activity and regioselectivity.^[36] Although both macrocycles **1d** and **2d** were converted to a comparable number of products, the product spectrum of **2d** with three double bonds revealed

Table 2. P450 BM3 F87G-catalyzed oxidations of macrocycles **2d** and **3c,d** and MS-analysis of the products. Time: reaction time; Mw: molecular weight in g mol^{-1} ; Δm : mass difference to the substrate; ΔA : additional atoms compared to the substrate. For details see Figures S2 in the Supporting Information.

| Substrate | Time [h] | Conversion [%] | Mw | Δm | Number of products | ΔA |
|-----------|----------|----------------|-----|------------|--------------------|------------|
| 2d | 0.5 | 59 ± 5 | 334 | 0 | – | – |
| | | | 348 | +14 | 2 | +O, –2H |
| | | | 350 | +16 | 5 | +O |
| 3c | 0.5 | 50 ± 2 | 294 | 0 | – | – |
| | | | 308 | +14 | 1 | +O, –2H |
| | | | 310 | +16 | 7 | +O |
| 3d | 23 | 97 ± 0 | 350 | 0 | – | – |
| | | | 350 | 0 | – | – |
| | | | 364 | +14 | 1 | +O, –2H |
| | | | 366 | +16 | 3 | +O |

two main products, while the products of **1d** with one double bond were equally distributed (Figures S1d and S2a in the Supporting Information). Clearly, not only the exocyclic group but also ring flexibility influences enzyme regioselectivity. The products of both macrocycles had predominantly a mass difference of +16 m/z (compared to the substrate), suggesting single hydroxylation or epoxidation.

Comparison of cembranoid **2d** and cembranoid-ol **3d** demonstrated that the presence of an additional hydroxy group in **3d** at C9, located at a maximum distance from the exocyclic substituents, led to a lower conversion (**2d**: 59% and **3d**: 36%) and less products (**2d**: 7 products, **3d**: 4 products) (Table 2, Figures S2a and S2c in the Supporting Information). Here, again predominantly mono-oxidized products were found.

Our observations indicate that the regioselectivity of P450 BM3 F87G was influenced by size and polarity of the exocyclic substituents as well as by substrate flexibility, which in turn was affected by the number of double bonds. Both cembrene-type compounds **2** and **3** carrying three double bonds were oxidized by P450 BM3 F87G with higher regioselectivity than cyclotetradec-11-ene **1** with one double bond. The presence of the double bonds can affect the chemoselectivity of the enzyme catalyzed oxidation, because epoxidation competes

with allylic hydroxylation. Whereas this aspect could not be clarified for **2d**, **3c**, and **3d** because of lacking reference epoxides, (11,12)-epoxides of **1c** and **1d** were identified in the corresponding product mixtures along with 4 hydroxylated products obtained for each of the two substrates. For both substrates, the corresponding epoxide appeared as a minor product along with at least four hydroxylated products (Table 1, and Figures S1c and S1d in the Supporting Information).

Furthermore, cembranoid-ol **3d** was oxidized more selectively than cembranoid **2d**, which indicates that a hydroxy group on the ring has a significant influence on product selectivity. Although the interaction of all exocyclic substituents with the enzyme was not studied in detail, it can be proposed that polar groups at C1 direct positioning of the synthetic macrocycles in the active site of P450 BM3. With increasing size and polarity of directing exocyclic groups, enzyme regioselectivity increased and was accompanied by less multi-oxidized products but also lower enzyme activities.

Since the oxidation of cembranoid-ol **3d** led to the smallest number of products, this substrate was selected for further experiments to optimize the target reaction with regard to its chemo- and regioselectivity by means of protein engineering.

Engineering selective P450 BM3 variants

Cembranoid-ol **3d** possesses a multitude of potential oxidation sites: In addition to seven allylic positions and three positions for non-allylic hydroxylation, triene **3d** has three possible sites for epoxidation (Figure 2). Thus, a chemo- and regioselective oxidation of **3d** is a challenging task. Conversion of **3d** in the presence of P450 BM3 F87G achieved 33% (Table 3). Along with the main mono-oxidized product **4** with a retention time of 10.4 min (55%), two other products were detected with retention times of 11.4 min (24%) and 11.7 min

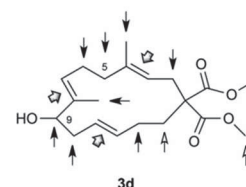


Figure 2. Potential oxidation sites of **3d**. Sites for epoxidation are marked with broad arrows. Potential allylic (filled arrows) and non-allylic (open arrows) hydroxylation sites are marked with thin arrows.

Table 3. Conversion and product distribution of **3d** oxidations catalyzed by P450 BM3 mutants. Product **4** was detected at a retention time (R_t) of 10.4 min. The products with a retention time of 11.4 min, 11.7 min and 12.8 min showed a mass difference of +16 to the substrate (MS). The experiments were performed with cell-free *E. coli* extract (1 μM final P450 concentration).

| Amino acid substitution | | | Conversion [%] | Product distribution [%] | | | | Other products |
|-------------------------|-----|-----|----------------|------------------------------|------------------|------------------|------------------|----------------|
| L75 | V78 | F87 | | 4 R_t 10.4 [min] | R_t 11.4 [min] | R_t 11.7 [min] | R_t 12.8 [min] | |
| A | G | G | 33 ± 8 | 55 | 24 | 21 | – | – |
| | | G | 85 ± 5 | 54 | 14 | – | – | 32 |
| | | G | 72 ± 4 | 17 | – | 38 | 35 | 10 |
| | | A | 50 ± 5 | 64 | 13 | 16 | 7 | – |
| A | G | A | 25 ± 7 | 100 | – | – | – | – |
| | | A | 87 ± 5 | 75 | 9 | – | – | 16 |
| | | A | 78 ± 1 | 90 | – | – | 5 | 5 |
| | | A | 84 ± 2 | 88 | 7 | – | – | 5 |

(21%). To increase enzyme activity and regioselectivity with minimal screening efforts, we first analyzed the results of our previous first-sphere mutagenesis study aiming at construction of P450 BM3 variants for selective hydroxylation of β -cembrene-diol.^[17] Besides F87 two other positions in the enzyme active site, namely V78 and L75 played an essential role in the selective oxidation of β -cembrene-diol. Thus, for the conversion of substrate **3d**, we tested P450 BM3 F87G/A single mutants as well as F87G- or F87A-based double mutants with an additional amino acid substitution at V78 or L75 (Table 3). The F87G-based double mutants led to higher conversions (50–85%) as compared to the parent mutant. However, a slight increase in regioselectivity for product **4** (64%) could only be achieved with the V78A/F87G variant.

Compared to the single F87G variant, the single F87A mutant demonstrated 100% selectivity for product **4**, but only 25% conversion. The introduction of additional amino acid substitutions at positions L75 or V78 into the parent mutant F87A resulted in 78–87% conversion but reduced regioselectivity (Table 3). The highest selectivity towards product **4** (88–90%) combined with high substrate conversion was observed after the introduction of glycine or alanine at position 78. The most active double mutant V78A/F87A that led to 84% conversion and gave product **4** with a regioselectivity of 88% (Figure 3), was used in preparative reactions. This enzyme demonstrates an NADPH oxidation rate of 60 min^{-1} , a coupling efficiency of 17% and a substrate oxidation rate of 10 min^{-1} which are comparable to the corresponding values assessed for β -cembrene-diol oxidation catalyzed by several P450 BM3 mutants.^[17]

The product **4** was prepared in a chemoenzymatic process starting with a metal-catalyzed ring-closing metathesis^[12] followed by the V78A/F87A-catalyzed hydroxylation. 160 mg of

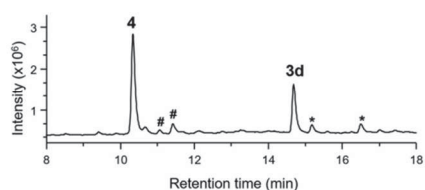
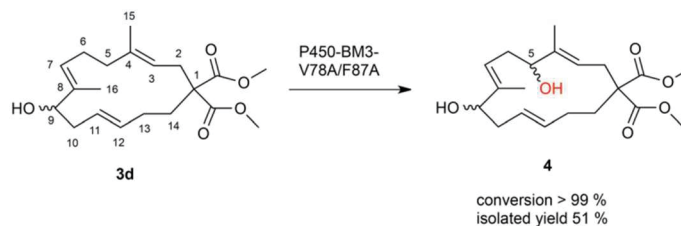


Figure 3. LC/MS chromatogram of **3d** oxidation catalyzed by the V78A/F87A variant. The main product was detected at retention time of 10.4 min. Additional products were detected at retention times of 11.1 and 11.4 min (#). Contaminations are marked with an asterisk (*). Intensity is shown as the total ion current in the positive ion mode.

3d were subjected to enzymatic reaction. In comparison to the screening experiments in small volume, higher agitation speed and reaction volume of the preparative reactions positively influenced substrate conversion which achieved > 99%. After complete substrate conversion the main product **4** was isolated by semi-preparative HPLC with a 51% yield and analyzed by NMR spectroscopy and mass spectrometry. Mass analysis of **4** confirmed the incorporation of one oxygen atom, suggesting hydroxylation or epoxidation of cembranoid-ol **3d**. Assignment of the ^1H and ^{13}C chemical shifts was achieved by analyzing their $^1\text{H}, ^1\text{H}$ -COSY, $^1\text{H}, ^{13}\text{C}$ -HSQC, and $^1\text{H}, ^{13}\text{C}$ -HMBC spectra (for details see Supporting Information). Compared to **3d** its oxidized product **4** showed an additional signal at 4.15 ppm in the ^1H NMR spectrum in the range of 3.8–5.6 ppm. Due to the presence of a complete set of olefinic signals an epoxide could be excluded. Thus, product **4** could be identified as dimethyl (3*E*,7*E*,11*E*)-5,9-dihydroxy-4,8-dimethylcyclotetradeca-3,7,11-triene-1,1-dicarboxylate (Scheme 1).

Docking cembranoid-ol **3d** to P450 BM3 active site

In attempt to rationalize the observed results we applied the molecular docking approach. For comparison a pre-generated conformation of **3d** with OH group at C9 either in *S*- or *R*-configuration was docked into the V78A/F87A and V78G/F87G variants. The molecular docking of both **3d** isomers into the V78G/F87G variant revealed several possible poses with equal scores, whereas with the V78A/F87A variant one pose was favored for each isomer (Figure 4). This is in good agreement with the results in Table 3, showing that V78G/F87G exhibits the lowest and V78A/F87A the highest regioselectivity. Although the overall orientation of both **3d** isomers in the active site of the V78A/F87A enzyme is similar, the exact orientation of the polar groups at C1 and C9 together with their stabilizing hydrogen-bond interactions are slightly different (Figure 4). In (9*S*)-**3d**, one exocyclic substituent at C1 is stabilized via H-bond between the keto oxygen of the ester group and the hydroxy group of S72 (2.16 Å). In the *R*-configuration, however, H-bond occurs between again hydroxy group of S72 and the methoxy group of the ester (2.35 Å). The second exocyclic ester group is stabilized via H-bonding to the backbone amide of A330. Here again, the distance between the exocyclic group of the *S*-configured isomer and the A330 amide backbone is shorter than for the (9*R*)-**3d**. Also the C9 hydroxy group seems to be stabilized by H-bonds, though weaker than the substituent at C1. Whereas the hydroxy group of the (9*S*)-



Scheme 1. Selective oxidation of **3d** on a preparative scale. The reaction was catalyzed by the V78A/F87A variant.

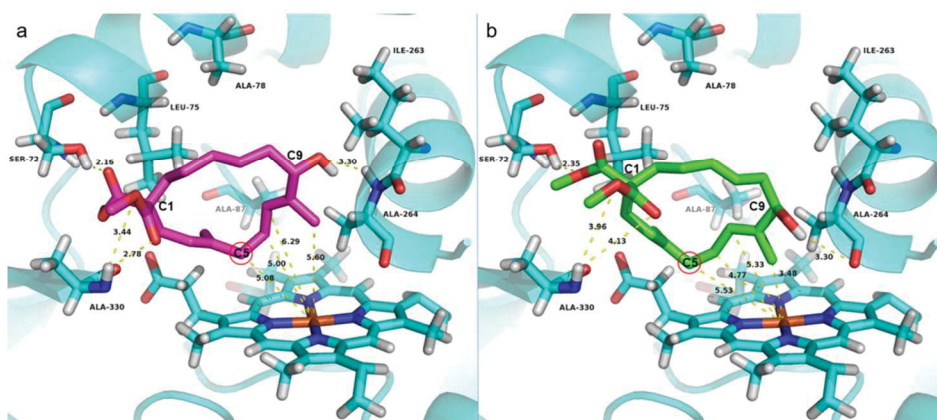


Figure 4. Best scored docking poses of (9*S*)-**3d** (purple, 4a) and (9*R*)-**3d** (green, 4b) in the active site of the V78A/F87A variant. Position C5 of both **3d** isomers is marked by red circle. Dashed yellow lines are indicating distances between atoms. The numerical distance is given in Å.

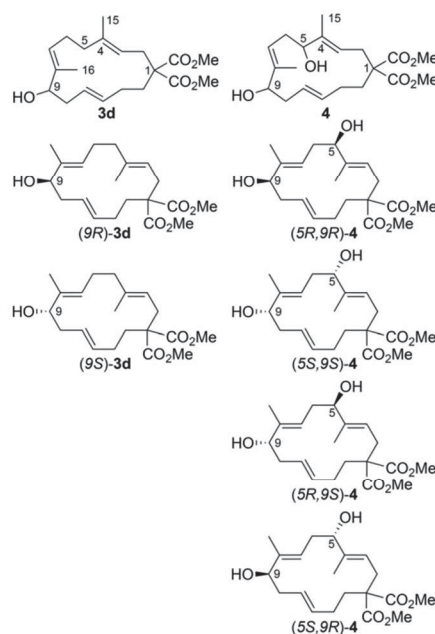
3d is at 3.30 Å distance to the backbone amide of A264, the C9 hydroxy group in (9*R*)-**3d** is again at 3.30 Å distance to the backbone carbonyl oxygen of the same residue A264. The substituents at C1 and C9 force the substrate in an orientation where C5, C6 and C7=C8 are located in close proximity to the heme. For (9*S*)-**3d**, position C5 (5.08 Å) and C6 (5.00 Å) are at equal distances from the heme iron whereas the distances to the C7-C8 double bond and to the methyl group at C8 are longer (Figure 4a). Based on this we can expect C6-oxidized product along with the identified C5-hydroxylated product. For (9*R*)-**3d**, the closest to heme iron is the methyl group at C8 position (3.48 Å). Generally, P450 BM3 tends to form secondary alcohols and does not catalyze oxidation at terminal positions because of high H-abstraction barriers as was demonstrated for saturated fatty acids.^[37] Furthermore, epoxidation reaction is usually preferred over primary allylic hydroxylation. Thus, methyl group hydroxylation at C8 of (9*R*)-**3d** is not expected. Further, the best scored pose revealed that positions C6 and C7 in (9*R*)-**3d** are with 4.77 Å and 5.33 Å a little bit closer to the heme iron than C5 (5.53 Å), which suggests that C6 hydroxylation and C7-C8 double bond epoxidation can also occur. Our experimental data revealed formation of two minor unidentified products along with C5-hydroxylated main product (Table 3), which is in agreement with the docking studies. However, as this macrocycle has a flexible structure which cannot be reflected using rigid docking, MD simulations are required to provide a more precise explanation for the obtained results.

Assignment of the relative and absolute configuration of cembranoid-diol **4**

To assess the stereoselectivity of the V78A/F87A variant towards C5, we sought to determine the absolute configuration of cembranoid-diol **4**. It should be noted that for better visibility of the stereochemical issues, the macrocyclic rings of cembranoid-ol **3d** and cembranoid-diol **4** are drawn in a different conformation as compared to the previously published struc-

ture of compounds **3d** and related cembranoids (Scheme 2).^[3b,12,17] Furthermore, it should be emphasized that stereoisomers resulting from the planar chirality of macrocyclic alkenes **3d** and **4** were not considered.^[38]

In order to assign the relative configuration of the two hydroxy groups in compound **4**, 2D-¹H-NOESY experiments were performed.^[39] However, due to the signal overlap of 5-H with 12-H and 9-H with 7-H respectively, no conclusive assignment regarding *syn*- or *anti*-configuration was possible (Figure S4 in the Supporting Information). Due to this ambiguous result, both relative and absolute configuration of cembranoid-diol **4**

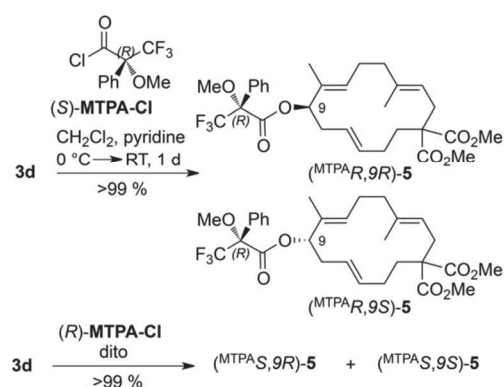


Scheme 2. Possible stereoisomers of cembranoid-ol **3d** and cembranoid-diol **4**. The structures are drawn in different perspectives for better visibility of the stereochemical issues.

were determined via the modified Mosher method as discussed below.

For assignment of the absolute configurations of cembranoid-ol **3d** the modified Mosher method by Kishikawa was used.^[40] Following the protocol by Hoye^[41] alcohol **3d** was treated in two parallel experiments with (*S*)-Mosher acid chloride (*S*)-(-)-MTPA-Cl and (*R*)-Mosher acid chloride (*R*)-(+)-MTPA-Cl in CH₂Cl₂ in the presence of pyridine at 0 °C for 30 min, respectively, then warmed to room temperature and stirred for 24 h. The Mosher esters **5** were first analyzed by ¹H NMR (Scheme 3, Figure 5a). In an initial experiment, incomplete conversion was observed, resulting in a (1:0.75) mixture of the Mosher esters **5** (Figure 5c). However, upon repeating the experiment and subsequent chromatographic purification >99% of the corresponding Mosher esters **5** were isolated, this time as a (1:1) mixture according to the ¹H NMR spectrum (Figure 5b,d), which confirmed the use of *racemic* starting material *rac*-**3d**. The Mosher esters **5** were analyzed by ¹H,¹³C-COSY, ¹H,¹³C-HSQC, ¹H,¹³C-HMBC and NOESY NMR experiments in CDCl₃.^[42]

Based on previous work by Kakisawa, who determined the absolute configuration of several marine diterpenoids and cembranoids via Mosher's method,^[40b] we expected pronounced chemical shift differences $\Delta\delta \approx 25$ Hz between the ¹H NMR signals of the (*R*)- and (*S*)-Mosher ester **5**. However, as can be seen upon comparison of diagnostic methyl signals (15-H, 16-H) of (^{MTPA}*R,R*)-**5**/^(MTPA)*R,S*-**5** (Figure 5b) with those of (^{MTPA}*S,S*)-**5**/^(MTPA)*S,R*-**5** (Figure 5d), derived from (*S*)- and (*R*)-Mosher acid chloride, respectively, the ¹H NMR spectra were



Scheme 3. Synthesis of Mosher esters **5** from cembranoid-ol **3d**.

almost identical. We surmised, that in case of a perfect equimolar mixture of enantiomeric alcohols (*9R*)-**3d**/*(9S)*-**3d** = 1:1, the Mosher method does not allow configurational assignment of the corresponding Mosher esters (^{MTPA}*R,R*)-**5**, (^{MTPA}*R,S*)-**5** and (^{MTPA}*S,S*)-**5**, (^{MTPA}*S,R*)-**5**, respectively. In order to validate this hypothesis, we synthesized the known Mosher esters of *D*- and *L*-menthol^[41] and *D,L*-menthol for comparison. Analysis of the ¹H NMR spectra showed, that the chemical shifts of *D*-menthyl-(^{MTPA}*R*) ester are identical with *L*-menthyl-(^{MTPA}*S*) ester (see Figures S3 and S4 in the Supporting Information for a detailed discussion). Therefore, further assignments were performed with the (1:0.75) mixture of Mosher esters **5** rather

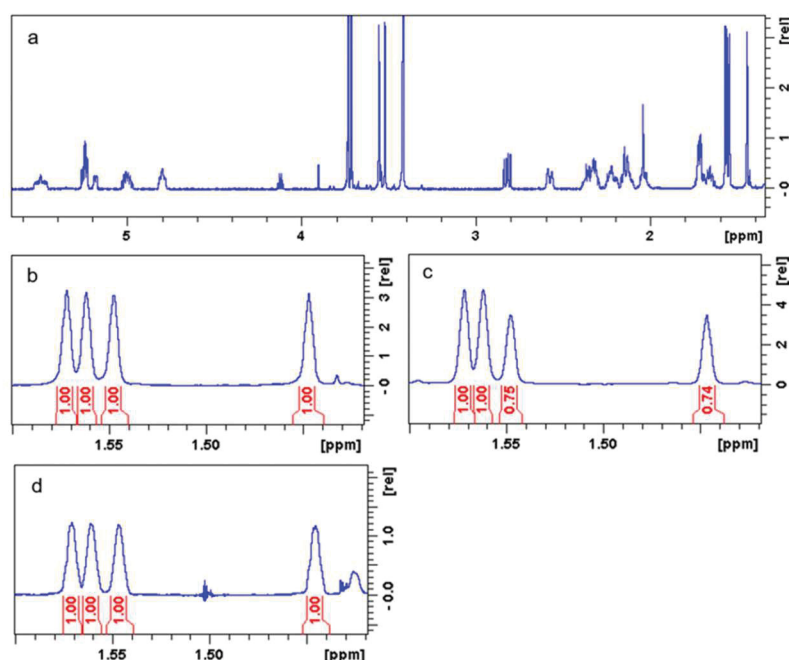
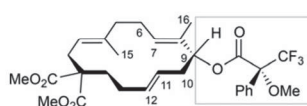


Figure 5. Section of the ¹H NMR spectrum (700 MHz, CDCl₃) of Mosher ester (^{MTPA}*R,R*)-**5**/^(MTPA)*R,S*-**5**. a) After complete conversion. b) Section of the ¹H NMR spectrum (700 MHz, CDCl₃) showing the methyl signals 15-H and 16-H of a (1:1) mixture of (^{MTPA}*R,R*)-**5**/^(MTPA)*R,S*-**5**. c) Methyl signals 15-H and 16-H of a (1:0.75) mixture of (^{MTPA}*R,R*)-**5**/^(MTPA)*R,S*-**5**; d) Methyl signals 15-H and 16-H of a (1:1) mixture of (^{MTPA}*S,S*)-**5**/^(MTPA)*S,R*-**5**.

than the (1:1) mixture. As an example 15-H, 16-H signals of a (1:0.75) mixture of (^{MTPA}R,9R)-5/ (^{MTPA}R,9S)-5 are shown in Figure 5c. In Table 4 the ¹H NMR chemical shifts δ of characteristic signals are summarized, which could be assigned to the Mosher esters **5** derived from cembranoid-ol **3d**.

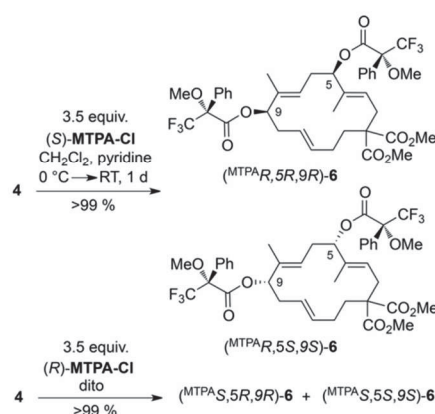
| 1H-NMR signal | Major product (^{MTPA} R,9R)-5 δ [ppm] | Minor product (^{MTPA} R,9S)-5 δ [ppm] | $\Delta\delta^{SR} = (\delta_S - \delta_R)$ | |
|-------------------|--|--|---|------------|
| | | | Major [Hz] | Minor [Hz] |
| 15-H | 1.56 | 1.55 | -10 | +10 |
| 16-H | 1.57 | 1.45 | -88 | +88 |
| 6-H _a | 2.14 | 2.12 | -29 | +29 |
| 6-H _b | 2.36 | 2.32 | -26 | +26 |
| 7-H | 5.26 | 5.18 | -52 | +52 |
| 10-H _a | 2.22 | 2.32 | +70 | -70 |
| 10-H _b | 2.33 | 2.37 | +35 | -35 |
| 12-H | 5.48 | 5.52 | +25 | -25 |
| 11-H | 5.01 | 5.01 | +10 | -10 |

According to the Mosher theory, H atoms located below the plane of the Mosher ester (Scheme 4, see Schemes S1, S2 in the Supporting Information for a detailed discussion) lead to negative $\Delta\delta^{SR}$ values, while H atoms located above the plane of the Mosher ester lead to positive $\Delta\delta^{SR}$ values. Therefore, for cembranoid-ol **4** nine proton signals could be assigned to a specific stereoisomer. For the remaining H atoms no detailed assignment was possible due to severe overlap of signals. In agreement with the Mosher theory the major isomer of the (1:0.75) mixture was assigned to (^{MTPA}R,9R)-5, while the minor isomer was assigned to (^{MTPA}R,9S)-5.



Scheme 4. Schematic drawing of the plane formed by the Mosher ester regarding **5**.

Cembranoid-diol **4** was converted with 3.5 equivalents of (*S*)-Mosher acid chloride (*S*)-(-)-MTPA-Cl and (*R*)-Mosher acid chloride (*R*)-(+)-MTPA-Cl, respectively to the corresponding Mosher diesters **6**, as described above (Scheme 5). Each reaction provided a mixture of only two isomers in a (1:0.75) ratio despite the four possible ones outlined in Scheme 5. In order to determine the relative configuration of the two hydroxy groups, NOESY experiments were performed with the (*S*)-(-)-MTPA-Cl and the (*R*)-(+)-MTPA-Cl derived Mosher esters **6**. However, as was already described for the parent cembranoid-diol **4**, no cross signal could be observed. Only cross signals between the overlapping protons 5-H/7-H or 9-H/12-H were apparent. Thus configurational assignment was performed



Scheme 5. Synthesis of the Mosher esters **6** from cembranoid-diol **4**.

solely on the basis of the modified Mosher method (Scheme 5). During parallel reaction of the cembranoid-diol **4** with (*R*)- and (*S*)-MTPA-Cl we noticed in the ¹H NMR spectrum, that the two isomers of Mosher esters **6** were not present in an equimolar mixture. Despite complete conversion of the respective MTPA chloride a (1:0.75) mixture of **6** was obtained (Figure 6). From this outcome we assumed, that the enzymatic oxidation proceeded not only regioselectively but also with some stereoselectivity. Nevertheless, detailed analysis of the signals turned out to be rather difficult. The designated ¹H NMR signals of the (^{MTPA}S)-esters shown in Figure 6 could be unambiguously assigned to a specific stereoisomer.

According to ¹H, ¹H-HSQC- and ¹H, ¹³C-COSY NMR spectra (700 MHz, CDCl₃) assignment of the H signals of major and minor isomer of (^{MTPA}S)-**6** could be achieved. The methyl groups 15-H and 16-H were determined from the HSQC NMR and the coupling pattern of the major and minor product could be detected (see Figure S5a in the Supporting Information). Subsequently, olefinic signals 3-H, 7-H were identified in the COSY NMR due to their coupling pattern, in particular *J*_{3,15} (Figure S5b). Next, signals 2-H (Figure S5c) and 6-H (Figure S5d) could be identified.

In Table 5 the chemical shifts δ of characteristic signals of the (^{MTPA}S)-Mosher diester (^{MTPA}S)-**6** are listed. As shown for the benchmark system D-, L-menthol and cembranoid-ol **3d** the H signals of similar chemical shifts δ are expected for both major (^{MTPA}S)-Mosher diester (^{MTPA}S)-**6** and minor (^{MTPA}R)-Mosher diester (^{MTPA}R)-**6**. Based on this analogy the difference $\Delta\delta^{SR}$ with respect to the major and minor product was determined for the Mosher diesters **6** derived from cembranoid-diol **4**. For these Mosher diesters **6** of cembranoid-diol **4** 11 signals could be assigned, while a detailed analysis of the remaining signals was not possible due to signal overlap or no significant influence of the Mosher ester unit on these protons. According to the Mosher theory the major isomer was determined as (^{MTPA}S,5S,9S)-**6** and the minor isomer was determined as (^{MTPA}S,5R,9R)-**6**.

Initial crystallization attempts of cembranoid-diol **4** in various solvents CH₂Cl₂, CHCl₃, 1,2-dichloroethane, nitrobenzene or

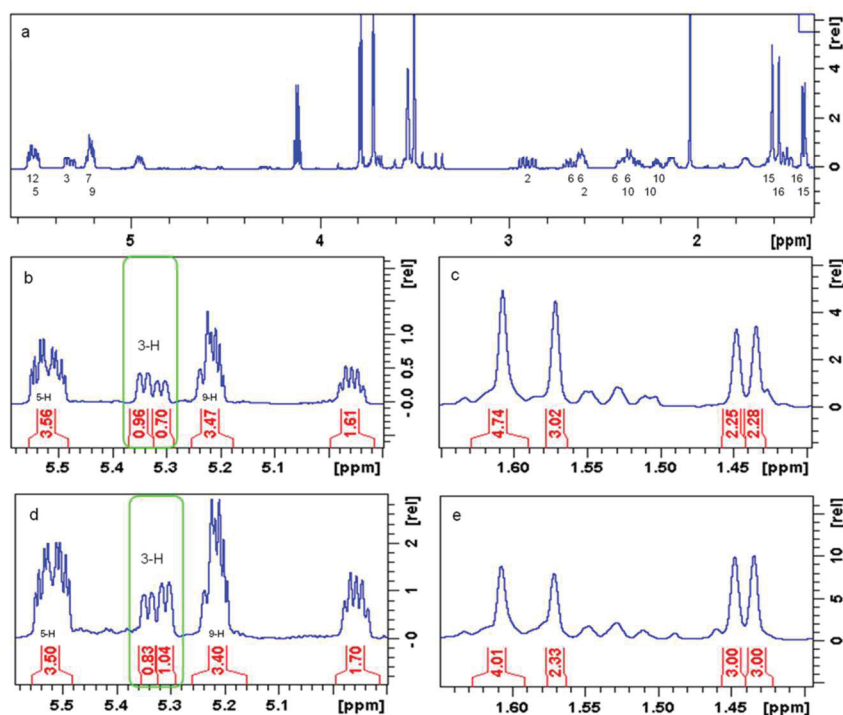


Figure 6. a) Section of the ^1H NMR spectrum (700 MHz, CDCl_3) of the Mosher esters **6** derived from cembranoid-diol **4** and (*R*)-MTPA-Cl; b) Section of the ^1H NMR spectrum of the (MTPA,S)-Mosher ester (MTPA,S)-**6**. Olefinic signals 7-H, 3-H and 12-H are overlapping with 5-H and 9-H; c) Methyl signals of the (MTPA,S)-Mosher ester (MTPA,S)-**6**, enabling determination of the isomeric ratio = 1:0.75; d) Olefinic signals of the (MTPA,R)-Mosher ester (MTPA,R)-**6**. In the green area the reversed ratio of major and minor product depending on the MTPA chloride is clearly visible. e) Methyl signals of the (MTPA,R)-Mosher ester (MTPA,R)-**6**.

| ^1H NMR signal | δ [ppm] | | $\Delta\delta^{\text{SR}} = (\delta_{\text{S}} - \delta_{\text{R}})$ | |
|-------------------------|--|--|--|---------------|
| | Major (MTPA,S)-diester 6 [ppm] | Minor (MTPA,S)-diester 5 [ppm] | Major [Hz] | Minor [Hz] |
| 2- H_a | 2.93 | 2.88 | +33 | -33 |
| 2- H_b | 2.62 | 2.60 | +11 | -11 |
| 3-H | 5.34 | 5.31 | +23 | -23 |
| 15-H | 1.61 | 1.44 | +122 | -122 |
| 6- H_a | 2.63 | 2.69 | -42 | +42 |
| 6- H_b | 2.37 | 2.41 | -28 | +28 |
| 7-H | 5.23 | 5.22 | +7 | -7 |
| 16-H | 1.57 | 1.45 | +87 | -87 |
| 10- H_a | 2.22 | 2.31 | -63 | +63 |
| 10- H_b | 2.35 | 2.39 | -28 | +28 |
| 12-H | 5.51 | 5.53 | -15 | +15 |

CH_3CN met with little success. Fortunately, slow evaporation of an ethyl acetate solution provided single crystals of **4** suitable for X-ray crystal structure determination (Figure 7). Cembranoid-diol **4** crystallized in the triclinic space group $P\bar{1}$ with lattice parameters $a = 9.1 \text{ \AA}$, $b = 13.3 \text{ \AA}$, $c = 20.0 \text{ \AA}$, $\alpha = 93.1^\circ$, $\beta = 101.8^\circ$, $\gamma = 105.4^\circ$ and a volume of $V = 2281 \text{ \AA}^3$. The number of molecules in the unit cell were $Z = 4$. The unit cell contains

two conformers, which differ in disordered units of the macrocycle. The space group $P\bar{1}$ indicates the presence of a center of inversion. Therefore, the crystalline solid contains a racemic mixture of the enantiomers (*5R,9R*)-**4** and (*5S,9S*)-**4**. It should be noted that only part of the solution crystallized, meaning that the observed (1:0.75) ratio of the solution might be changed during preferred crystallization of a racemate containing a (1:1) mixture of both enantiomers in the unit cell. It should be emphasized however, that the crystallographic results supports the assignment of the relative *syn*-configuration of the hydroxy groups via the Mosher method.

With regard to the P450 monooxygenase-catalyzed hydroxylation of cembranoid-ol **3d**, these results suggest that the orientation of the enantiomers (*9R*)-**3d** and (*9S*)-**3d** in the active site should differ, which leads to a stereoselective hydroxylation of the $(\text{C}5)\text{H}_2$ unit. Thus, the *syn*-cembranoid-diols (*5S,9S*)-**4** and (*5R,9R*)-**4** are exclusively produced. Only trace amounts of the corresponding *anti*-cembranoid-diols (*5R,9S*)-**4** and (*5S,9R*)-**4** ($\text{dr} > 95:5$) could be detected. Furthermore, the observed (1:0.75) ratio of the Mosher esters (MTPA,S,5S,9S)-**6**, (MTPA,S,5R,9R)-**6** suggests that there is a slight preference of the P450 monooxygenase in favor of the (*5S,9S*)-cembranoid-diol (*5S,9S*)-**4**.

Substrate docking revealed slight differences in positioning of (*9R*)-**3d** and (*9S*)-**3d** in the enzyme active site. Although both substrates show a distance of C5 atom to the Fe-heme

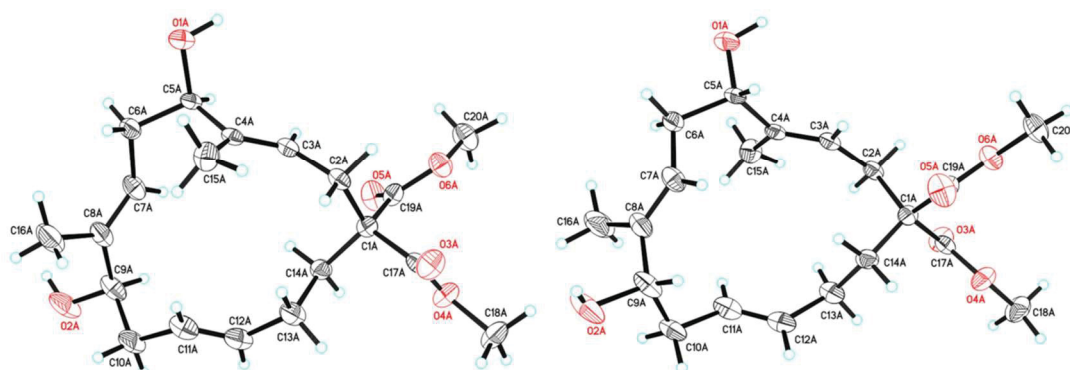


Figure 7. Structure of (5*R*,9*R*)-cembranoid-diol ((5*R*,9*R*)-4 (left) and the corresponding (5*S*,9*S*)-cembranoid-diol ((5*S*,9*S*)-4 (right)) in the solid state.^[43]

atom of 5.1–5.5 Å, they are differently stabilized by hydrogen bonds between the active site and both the substrates exocyclic ester group at C1 as well as the alcohol group at C9. Moreover, position C5 in (9*S*)-**3d** but not in (9*R*)-**3d** appears to be the closest to the heme iron. According to the substrates configuration and its defined orientation within the active site the hydroxylation occurs only in one stereochemical orientation. More detailed investigations such as co-crystallization with **3d** and MD simulations are needed to identify molecular determinants of the stereoselectivity of the V78A/F87A variant in this reaction.

Conclusions

Complex structural architecture of macrocyclic natural products with a broad range of functionalities presents a problem for their chemical de novo synthesis. As a result, total syntheses of natural products such as cembranoids include many steps and involve introduction and elimination of protecting groups. De novo biosynthesis in engineered microorganisms may serve as an attractive way to natural products, but in many cases biosynthetic pathways remain undeciphered or are very difficult to manipulate. Moreover, de novo biosynthesis is limited only to naturally occurring compounds. Chemoenzymatic synthetic approaches, combining advantages of both organic chemistry and enzyme catalysis,^[44] allow to overcome some bottlenecks: On the one hand, they enable production of highly functionalized natural products for which biosynthetic pathways are not known and, on the other hand they deliver also synthetic analogs not present in nature.

Reported chemoenzymatic total syntheses of complex natural compounds relying on selective oxidations often involve P450 enzymes from biosynthetic pathways.^[45] However, high substrate specificity and narrow substrate spectrum of such P450s limits their application in the oxidation of synthetic substrates. This limitation can be overcome either by using engineered P450 enzymes^[46] or via substrate engineering.^[31,32,47] Engineered P450s can successfully be applied for total synthesis of natural products as recently demonstrated for nigelladine A.^[48]

In this study we applied both, substrate engineering and protein engineering, to achieve high regioselectivity of bacterial P450 BM3 for the oxidation of a designed synthetic cembranoid analogue. Our previous results regarding P450-catalyzed oxidation of the natural cembranoid β -cembrenediol indicate that either isopropyl group at C1 or hydroxy groups in the ring or both ensure a substrate orientation which exclusively leads to hydroxylation at C9 and C10 or to C7=C8 epoxidation.^[17] The present work provides a systematic screening of different exocyclic groups and ring structures and confirms the role of ring rigidity and directing groups on the regioselectivity of P450-catalyzed oxidation of 14-membered macrocycles. Furthermore, we applied first-sphere active site mutagenesis of amino acids at only three positions to tune the regioselectivity of P450 BM3-catalyzed hydroxylation of **3d**. Our mutagenesis study demonstrates that small changes in the active site affect substrate orientation. Whereas the V78G/F87G mutant forms only 17% of the target product **4**, the V78A/F87A mutant prefers this position over others with a regioselectivity of 88%.

A detailed NMR and X-ray analysis of the produced stereoisomers of cembranoid-diol (5*S*,9*S*)-**4** and (5*R*,9*R*)-**4** revealed that the stereoselectivity of P450-catalyzed hydroxylation seems to depend on the stereochemistry of the hydroxy group at position C9 of the substrate **3d**. Co-crystallization of the V78A/F87A variant with **3d** and MD-simulations will provide more fundamental insights into how a directing group at C1 position and a hydroxy group of the substrate interact with the enzyme and influence its selectivity. Finally, the described chemoenzymatic route to oxyfunctionalized cembranoids open up the way towards completely new compounds which can further be diversified via functionalization of ester and hydroxy groups.

Experimental Section

General procedure for the ring closing metathesis, Mosher ester preparation and NMR analysis are described in the Supporting Information.

Strains, expression vectors, enzyme, and chemicals

E. coli strain DH5a was obtained from Takara Bio. *E. coli* strain BL21(DE3) and pET28a vector were purchased from Merck. All enzymes for cloning were from Thermo Fisher Scientific. All chemicals were purchased from Carl Roth, Sigma–Aldrich, Merck and Thermo Fisher Scientific and were of analytical grade or higher.

Cloning, mutagenesis, expression and purification of enzymes

The gene *cyp102a1* encoding P450 BM3 from *Bacillus megaterium* (GenBank J04832) was cloned in pET28a as previously described.^[49] Site-specific mutagenesis of P450 BM3 was performed following the QuikChange Mutagenesis method (Stratagene). Target mutations were introduced using complementary primers carrying target mutations.

Wild-type P450 BM3 and mutants thereof were heterologously expressed in the *E. coli* strain BL21(DE3) according to the previously reported procedure.^[17] Protein purification was done via Immobilized Metal Affinity Chromatography (IMAC) using Ni-NTA (Qiagen) column and performed according to the manufacturer's standard protocol. Affinity chromatography was facilitated by the N-terminal His-tag introduced during cloning as described elsewhere.^[17] Glucose dehydrogenase (GDH) from (GenBank D10626) was expressed and purified as previously described.^[17]

Enzyme-catalyzed reaction on an analytical scale

Concentrations of P450 BM3 variants were estimated from CO-difference spectra and calculated using the extinction coefficient $\epsilon_{450-490} = 91 \text{ mm}^{-1} \text{ cm}^{-1}$ as described previously.^[50] Standard reaction solutions contained P450 (1 μM), substrate 1–3 (200 μM), NADPH (200 μM), catalase (600 U mL^{-1}), glucose (20 mM), and GDH (3.5 U mL^{-1}) in a final volume of 500 μL . Substrates were dissolved in ethanol (final concentration 2% (v/v)). Catalase was added for removal of hydrogen peroxide, which can be formed in course of uncoupling reactions. GDH was used for NADPH regeneration during P450-catalyzed oxidation reactions. Reactions were performed in potassium phosphate buffer (50 mM , pH 7.5) at 25 °C for 0.5 h or 23 h. Before extraction an internal standard was added and the reactions were extracted with ethyl acetate (2 \times 300 μL). For compounds 1a and 1b cembrene (200 μM) and for compounds 1c, 1d, 2d, 3c, and 3d cyclotetradec-4-ene-1,1-diylbis(methylene)diacetate (50 μM) were used as internal standards. The combined organic phases were concentrated under reduced pressure and the residues were dissolved in methanol for LC/MS analysis (see Supporting Information).

Products were analyzed on the basis of their *m/z* values. Product distributions were calculated based on the detected peak areas. Conversions were calculated based on the consumed substrate in comparison to a control reaction with cell extracts of *E. coli* carrying the pET28a vector. All experiments were performed in triplicate.

Oxidation of cembranoid-ol 3d on a preparative scale and product purification

Preparative reactions were performed in potassium phosphate buffer (50 mM , pH 7.5) and contained 3d (2 mM), P450 BM3 V78A/F87A (5 μM), NADPH (1000 μM), 50 mM glucose, GDH (10 U mL^{-1}) and 600 (U mL^{-1}). Several reactions in a volume of 20–25 mL each were set in reaction vessels (100 mL) and run 16 h under luffing shaking at 25 °C. Reactions were extracted with ethyl acetate (3 \times

8 mL) and the organic phases of all reactions were combined. Before drying under reduced pressure, a sample was taken for LC/MS analysis. Product isolation was performed by semi-preparative HPLC with a methanol/H₂O gradient. The separation was carried out at a flow rate of 5 mL min^{-1} . Product 4 was isolated as a colorless solid with 51% yield. For product verification high-resolution mass spectrometry (HRMS), ¹H NMR and ¹³C NMR were performed as described in the Supporting Information.

Molecular modeling and docking study

The structures of (9*R*)-3d and (9*S*)-3d were generated using the Chem3D 16.0 software. Introduction of the mutations V78A and F87A was done using the crystal structure of the monooxygenase domain of P450 BM3 wild type (PDB Code: 1ZO9) as template and the mutagenesis function of PyMOL.^[51]

Rigid docking was performed with Autodock 4.0 and the AutoGrid^[52] and AutoDock parameter files were set using AutoDockTools. The active site encompassing the heme iron was defined by a grid box with the dimensions 60 \times 60 \times 70 (number of points in *x*-, *y*- and *z*-dimension). The search for the optimal ligand-receptor arrangement was done using the Lamarckian Genetic Algorithm (LGA). Visualization of the results was done using again PyMOL.^[51]

Acknowledgements

Generous financial support by the German Research Foundation (Deutsche Forschungsgemeinschaft, EXC 1028) (for V.U.), generous financial support by the Ministerium für Wissenschaft, Forschung und Kunst des Landes Baden-Württemberg (Landesgraduerten fellowship for T.H.) and the Artur Fischer Stiftung (Artur Fischer Prize for S.S.) is gratefully acknowledged.

Conflict of interest

The authors declare no conflict of interest.

Keywords: cembranoids · chemoenzymatic synthesis · protein engineering · regioselectivity · substrate engineering

- [1] a) E. M. Driggers, S. P. Hale, J. Lee, N. K. Terrett, *Nat. Rev. Drug Discovery* **2008**, *7*, 608–624; b) F. Giordanetto, J. Kihlberg, *J. Med. Chem.* **2014**, *57*, 278–295; c) E. Marsault, M. L. Peterson, *J. Med. Chem.* **2011**, *54*, 1961–2004; d) L. F. Tietze, H. P. Bell, S. Chandrasekhar, *Angew. Chem. Int. Ed.* **2003**, *42*, 3996–4028; *Angew. Chem.* **2003**, *115*, 4128–4160.
- [2] L. A. Wessjohann, E. Ruijter, D. Garcia-Rivera, W. Brandt, *Mol. Diversity* **2005**, *9*, 171–186.
- [3] a) J. R. Hanson, *Nat. Prod. Rep.* **2015**, *32*, 1654–1663; b) L. F. Liang, Y. W. Guo, *Chem. Biodiversity* **2013**, *10*, 2161–2196.
- [4] P. A. Ferchmin, O. R. Pagan, H. Ulrich, A. C. Szeto, R. M. Hann, V. A. Eterovic, *Toxicol.* **2009**, *54*, 1174–1182.
- [5] N. Yan, Y. M. Du, X. M. Liu, H. B. Zhang, Y. H. Liu, P. Zhang, D. P. Gong, Z. F. Zhang, *Ind. Crops Prod.* **2016**, *83*, 66–80.
- [6] a) R. A. Craig II, B. M. Stoltz, *Chem. Rev.* **2017**, *117*, 7878–7909; b) Y. Li, G. Pattenden, *Nat. Prod. Rep.* **2011**, *28*, 1269–1310.
- [7] J. M. Ellis, M. T. Crimmins, *Chem. Rev.* **2008**, *108*, 5278–5298.
- [8] A. J. Welford, I. Collins, *J. Nat. Prod.* **2011**, *74*, 2318–2328.
- [9] K. Chen, P. S. Baran, *Nature* **2009**, *459*, 824–828.
- [10] a) Y. Ishihara, A. Mendoza, P. S. Baran, *Tetrahedron* **2013**, *69*, 5685–5701; b) N. C. Wilde, M. Isomura, A. Mendoza, P. S. Baran, *J. Am. Chem. Soc.* **2014**, *136*, 4909–4912.

- [11] S. J. McKerrall, L. Jorgensen, C. A. Kuttruff, F. Ungeheuer, P. S. Baran, *J. Am. Chem. Soc.* **2014**, *136*, 5799–5810.
- [12] T. Heidt, A. Baro, A. Kohn, S. Laschat, *Chem. Eur. J.* **2015**, *21*, 12396–12404.
- [13] a) S. Das, C. D. Incarvito, R. H. Crabtree, G. W. Brudvig, *Science* **2006**, *312*, 1941–1943; b) J. T. Groves, R. Neumann, *J. Am. Chem. Soc.* **1989**, *111*, 2900–2909.
- [14] L. M. Podust, D. H. Sherman, *Nat. Prod. Rep.* **2012**, *29*, 1251–1266.
- [15] a) E. Wang, S. Gan, G. J. Wagner, *J. Exp. Bot.* **2002**, *53*, 1891–1897; b) E. Wang, G. J. Wagner, *Planta* **2003**, *216*, 686–691; c) E. Wang, R. Wang, J. DeParasis, J. H. Loughrin, S. Gan, G. J. Wagner, *Nat. Biotechnol.* **2001**, *19*, 371–374.
- [16] a) S. T. Jung, R. Lauchli, F. H. Arnold, *Curr. Opin. Biotechnol.* **2011**, *22*, 809–817; b) J. A. McIntosh, C. C. Farwell, F. H. Arnold, *Curr. Opin. Chem. Biol.* **2014**, *19*, 126–134.
- [17] P. Le-Huu, T. Heidt, B. Claasen, S. Laschat, V. B. Urlacher, *ACS Catal.* **2015**, *5*, 1772–1780.
- [18] P. Le-Huu, D. Petrovic, B. Strodel, V. B. Urlacher, *ChemCatChem* **2016**, *8*, 3755–3761.
- [19] L. O. Narhi, A. J. Fulco, *J. Biol. Chem.* **1986**, *261*, 7160–7169.
- [20] S. S. Boddupalli, R. W. Estabrook, J. A. Peterson, *J. Biol. Chem.* **1990**, *265*, 4233–4239.
- [21] J. H. Capdevila, S. Wei, C. Helvig, J. R. Falck, Y. Belosludtsev, G. Truan, S. E. Graham-Lorence, J. A. Peterson, *J. Biol. Chem.* **1996**, *271*, 22663–22671.
- [22] I. Kaluzna, T. Schmitges, H. Straatman, D. van Tegelen, M. Muller, M. Schurmann, D. Mink, *Org. Process Res. Dev.* **2016**, *20*, 814–819.
- [23] C. J. Whitehouse, S. G. Bell, L. L. Wong, *Chem. Soc. Rev.* **2012**, *41*, 1218–1260.
- [24] J. C. Lewis, S. M. Mantovani, Y. Fu, C. D. Snow, R. S. Komor, C. H. Wong, F. H. Arnold, *ChemBioChem* **2010**, *11*, 2502–2505.
- [25] a) K. Zhang, B. M. Shafer, M. D. Demars II, H. A. Stern, R. Fasan, *J. Am. Chem. Soc.* **2012**, *134*, 18695–18704; b) J. N. Kolev, K. M. O'Dwyer, C. T. Jordan, R. Fasan, *ACS Chem. Biol.* **2014**, *9*, 164–173.
- [26] A. B. Carmichael, L. L. Wong, *Eur. J. Biochem.* **2001**, *268*, 3117–3125.
- [27] a) S. Kille, F. E. Zilly, J. P. Acevedo, M. T. Reetz, *Nat. Chem.* **2011**, *3*, 738–743; b) J. Reinen, G. Vredenburg, K. Klaering, N. P. E. Vermeulen, J. N. M. Commandeur, M. Honing, J. C. Vos, *J. Mol. Catal. B* **2015**, *121*, 64–74.
- [28] a) B. M. van Vugt-Lussenburg, M. C. Damsten, D. M. Maasdijk, N. P. Vermeulen, J. N. Commandeur, *Biochem. Biophys. Res. Commun.* **2006**, *346*, 810–818; b) A. M. Sawayama, M. M. Chen, P. Kulanthaivel, M. S. Kuo, H. Hemmerle, F. H. Arnold, *Chem. Eur. J.* **2009**, *15*, 11723–11729.
- [29] D. Petrovic, A. Bokel, M. Allan, V. B. Urlacher, B. Strodel, *J. Chem. Inf. Model.* **2018**, *58*, 848–858.
- [30] a) A. de Raadt, H. Griengl, *Curr. Opin. Biotechnol.* **2002**, *13*, 537–542; b) R. Fasan, *ACS Catal.* **2012**, *2*, 647–666; c) V. Polic, K. Auclair, *Bioorg. Med. Chem.* **2014**, *22*, 5547–5554; d) E. A. Hall, M. R. Sarkar, J. H. Z. Lee, S. D. Munday, S. G. Bell, *ACS Catal.* **2016**, *6*, 6306–6317.
- [31] S. Li, M. R. Chalugain, A. R. Knauff, L. M. Podust, J. Montgomery, D. H. Sherman, *Proc. Natl. Acad. Sci. USA* **2009**, *106*, 18463–18468.
- [32] S. Negretti, A. R. Narayan, K. C. Chiou, P. M. Kells, J. L. Stachowski, D. A. Hansen, L. M. Podust, J. Montgomery, D. H. Sherman, *J. Am. Chem. Soc.* **2014**, *136*, 4901–4904.
- [33] a) K. G. Ravichandran, S. S. Boddupalli, C. A. Hasermann, J. A. Peterson, J. Deisenhofer, *Science* **1993**, *261*, 731–736; b) H. Li, T. L. Poulos, *Nat. Struct. Biol.* **1997**, *4*, 140–146.
- [34] a) Q. S. Li, J. Ogawa, R. D. Schmid, S. Shimizu, *Appl. Environ. Microbiol.* **2001**, *67*, 5735–5739; b) E. Vottero, V. Rea, J. Lastdrager, M. Honing, N. P. Vermeulen, J. N. Commandeur, *J. Biol. Inorg. Chem.* **2011**, *16*, 899–912.
- [35] S. S. Boddupalli, B. C. Pramanik, C. A. Slaughter, R. W. Estabrook, J. A. Peterson, *Arch. Biochem. Biophys.* **1992**, *292*, 20–28.
- [36] Y. Watanabe, S. Laschat, M. Budde, O. Afolter, Y. Shimada, V. B. Urlacher, *Tetrahedron* **2007**, *63*, 9413–9422.
- [37] K. A. Feenstra, E. B. Starikov, V. B. Urlacher, J. N. Commandeur, N. P. Vermeulen, *Protein Sci.* **2007**, *16*, 420–431.
- [38] a) W. S. Fyvie, M. W. Peczu, *Chem. Commun.* **2008**, 4028–4030; b) J. A. Marshall, T. H. Black, *J. Am. Chem. Soc.* **1980**, *102*, 7581–7583.
- [39] P. Tzvetkova, B. Luy, S. Simova, *Magn. Reson. Chem.* **2012**, *50*, S92–S101.
- [40] a) I. Ohtani, T. Kusumi, M. O. Ishitsuka, H. Kakisawa, *Tetrahedron Lett.* **1989**, *30*, 3147–3150; b) I. Ohtani, T. Kusumi, Y. Kashman, H. Kakisawa, *J. Am. Chem. Soc.* **1991**, *113*, 4092–4096; c) I. Ohtani, T. Kusumi, Y. Kashman, H. Kakisawa, *J. Org. Chem.* **1991**, *56*, 1296–1298.
- [41] T. R. Hoye, C. S. Jeffrey, F. Shao, *Nat. Protoc.* **2007**, *2*, 2451–2458.
- [42] T. Carlomagno, *Nat. Prod. Rep.* **2012**, *29*, 536–554.
- [43] Details of the X-ray crystal structure determination of cembranoid-diol 4 have been deposited at the Cambridge Crystallographic Data Centre. CCDC 1841002 contains the supplementary crystallographic data for this paper. These data can be obtained free of charge from the Cambridge Crystallographic Data Centre.
- [44] H. Gröger, W. Hummel, *Curr. Opin. Chem. Biol.* **2014**, *19*, 171–179.
- [45] a) E. King-Smith, C. R. Zwick III, H. Renata, *Biochemistry* **2018**, *57*, 403–412; b) A. N. Lowell, M. D. DeMars II, S. T. Slocum, F. Yu, K. Anand, J. A. Chemler, N. Korakavi, J. K. Priessnitz, S. R. Park, A. A. Koch, P. J. Schultz, D. H. Sherman, *J. Am. Chem. Soc.* **2017**, *139*, 7913–7920.
- [46] V. Tyagi, H. Alwaseem, K. M. O'Dwyer, J. Ponder, Q. Y. Li, C. T. Jordan, R. Fasan, *Bioorg. Med. Chem.* **2016**, *24*, 3876–3886.
- [47] H. Alwaseem, B. J. Frisch, R. Fasan, *Bioorg. Med. Chem.* **2018**, *26*, 1365–1373.
- [48] S. A. Loskot, D. K. Romney, F. H. Arnold, B. M. Stoltz, *J. Am. Chem. Soc.* **2017**, *139*, 10196–10199.
- [49] S. C. Maurer, H. Schulze, R. D. Schmid, V. Urlacher, *Adv. Synth. Catal.* **2003**, *345*, 802–810.
- [50] T. Omura, R. Sato, *J. Biol. Chem.* **1964**, *239*, 2379–2385.
- [51] The PyMOL Molecular Graphics System, Version 1.6, Schrödinger, LLC.
- [52] <http://autodock.scripps.edu/>.

Manuscript received: May 4, 2018
 Revised manuscript received: June 27, 2018
 Version of record online: July 19, 2018

3. General Discussion and Outlook

The development of P450-catalyzed reactions in biocatalysis is a complex process. In comparison to other enzymes, such as hydrolases, P450s usually possess relatively low activities. And even if a P450 with high activity is found, then most P450s are still dependent on the very costly cofactor NAD(P)H and redox proteins for the electron transfer, which, besides other limiting factors (see Section 1.2.7), contribute to the high complexity of P450-catalyzed reactions. Therefore, P450s are more suitable for the synthesis of high-value products, such as drug metabolites, pharmaceuticals, and fine chemicals. Since the synthesis and especially the late-stage oxyfunctionalization of these molecules are usually complex and stereochemically demanding, they are often challenging to perform with chemical catalysts. Hence, P450s are a considerable alternative. However, such molecules often have a large number of chemically equivalent oxidation sites, which is why the selectivity of the P450s in particular must be adapted.

In this thesis, I endeavor to turn the two prokaryotic P450s CYP154E1 and P450 BM3 into convincing biocatalysts capable of selectively synthesizing valuable, oxyfunctionalized molecules:

i) Major depressive disorder is a severe and globally prevalent mental disorder, and the need for effective antidepressants is accordingly high. Two potential candidates that might stand the demands on safe and effective antidepressants are (2*S*,6*S*)- and (2*R*,6*R*)-hydroxynorketamine. Their synthesis involves both *N*-demethylation and selective C6-hydroxylation of the starting enantiomers (*S*)- and (*R*)-ketamine.

ii) Cembranoids possess various biological activities, such as anti-inflammatory,¹⁶⁷ potential anti-HIV,¹⁶⁸ or anticarcinogenic¹⁶⁹ effects. Due to these diverse biological activities, cembranoids are of pharmacological interest. Since cembranoids often carry numerous oxygen-containing functional groups, they are complex compounds that are challenging to synthesize.

The complexity of the molecules required the development and application of different protein engineering strategies to achieve selective oxyfunctionalization and to demonstrate the potential cytochrome P450 monooxygenases possess in biocatalysis.

3.1 Semirational Protein Design for the Selective Oxidation of (*S*)- and (*R*)-Ketamine

A combination of random and rational design is often the preferred method of changing an enzyme's selectivity properties (chemo-, regio-, and stereoselectivity).¹⁷⁰ In chapter I (*Enzyme-Mediated Two-Step Regio- and Stereoselective Synthesis of Potential Rapid-Acting Antidepressant (2*S*,6*S*)-Hydroxynorketamine*) and chapter II (*Molecular Evolution of a Cytochrome P450 for the Synthesis of Potential Antidepressant (2*R*,6*R*)-Hydroxynorketamine*), I examined the efficiency of semi-rational first-sphere site-directed (saturation) mutagenesis on the selective conversion of antidepressant (*S*)-ketamine (chapter I), respectively (*R*)-ketamine (chapter II) into the potentially safer antidepressant (*2S,6S*)-, respectively (*2R,6R*)-hydroxynorketamine. At first sight, ketamine is allegedly a little complex substrate. However, the difficulty lies in the targeted synthesis of (*2S/R,6S/R*)-hydroxynorketamine starting from ketamine. This synthesis involves two consecutive steps – *N*-demethylation and C6-hydroxylation – requiring high chemo-, regio-, and stereoselectivity combined in one P450 enzyme. Homology modeling and rigid docking served as the foundation to identify residues of the first-sphere, which are close to the substrate and likely to be involved in the influence on selectivity. Different from chapter I ((*S*)-ketamine), in chapter II ((*R*)-ketamine), position L289 was also taken into consideration. This position is located close to the highly conserved ExxR motif in P450s (see Section 1.2.3). Seifert and Pleiss reported the importance of this position for a P450's selectivity,⁷⁰ but examples of successful selectivity alterations by mutation at the homologous positions in other P450s are scarce in the literature. One of the rare examples is human CYP2C8. An exchange of the small side chain of V366 by a bulkier leucine hereby reduced paclitaxel 6 α hydroxylation and therefore reduced the intrinsic clearance of the anticancerogenic paclitaxel.¹⁷¹ In chapter II, saturation mutagenesis at position 289, combined with the substitutions I238Q and M388A in CYP154E1, drastically improved product selectivity. Interestingly, independent from each other, in both chapters, substitution I238Q was found crucial for the highly selective conversion of ketamine to the respective hydroxynorketamine. In chapter I, I238 was only substituted against polar residues due to the polar character of ketamine and the potential of hydrogen bonding between the keto- or amine-group of ketamine and a polar amino acid residue. The results of chapter I indicate that glutamine at position 238 has just the right size and polarity to

stabilize (*S*)-ketamine in a productive binding pose (since substitutions against asparagine and glutamate did not have positive effects). Homology model and docking could neither disprove nor prove this assumption since no interaction between the glutamine residue and ketamine was found. In chapter II, saturation mutagenesis at position 238 revealed that either glutamine or smallest residues (alanine, glycine, or serine) seemed beneficial for converting (*R*)-ketamine in the first place. However, again homology model and docking were not able to explain the effect of glutamine on conversion and selectivity. Both studies on the ketamine enantiomers were guided by constructing a homology model for CYP154E1 based on the structure of CYP154A8 and binding the substrates into the active site via rigid docking. One reason might be that the homology model does not reflect the “real” structure of the active site. Although the P450 fold is well conserved, the sequence identity between CYP154E1 and the used template CYP154A8 (1ODO) is only 40%,^e a value that might cause deficiencies in modeling accuracy.¹⁷² 40% is the least sequence identity to assign two P450s to the same family. To overcome the limitations of a homology model, CYP154E1 was crystallized as part of this and a previous thesis.¹⁷³ However, neither of the X-ray diffraction data enabled the solution of the CYP154E1 structure. The potential reason might be the high flexibility of some structural regions, which prevents the growth of adequate regular crystals.¹⁷⁴ Therefore, without a proper enzyme model, the decision for certain amino acid residue substitutions “resembles more an educated guess than a purely rational choice” (Otten *et al.*, 2010).¹⁷⁰ Compared to rational design, semi-rational design often gives few indications of why certain mutations cause the effect they cause.

Further, although a crystal structure of CYP154E1 would be preferred over a homology model, it still represents the enzyme as a rigid construct, which it is not. So in extension to the two semi-rational studies of chapters I and II, it would be of great benefit to perform pure rational engineering – that considers protein and substrate flexibility – of CYP154E1 for selective ketamine metabolism. As described below in chapter III, the initial step in the protein design is to learn how the molecule binds to the enzyme. This can be done using classical MD simulations or, as in chapter III described, using a more thorough analysis of the binding modes. Once the molecule’s binding to the enzyme is understood, hotspot residues that either stabilize productive substrate-

^e <https://swissmodel.expasy.org/interactive/T5CHPM/templates/>

binding and/or destabilize unproductive substrate binding need to be identified. In this way, it would be interesting if the same positions, substitutions, and results of the semi-rational strategies in chapters I and II can either be confirmed or disputed. This situation will encounter us with the chapter “Simulation-Guided Design of Cytochrome P450 for Chemo- and Regioselective Macrocyclic Oxidation” and the study by Le-Huu *et al.*¹¹⁰ In both studies, the same P450 BM3 triple mutant L75A/V78A/F87A was constructed independently of each other. However, only the rational approach outlined in chapter III was able to explain the effects of the substitutions. Applying a fully rational approach according to “Simulation-Guided Design of Cytochrome P450 for Chemo- and Regioselective Macrocyclic Oxidation” on CYP154E1 might provide a more detailed explanation of why the substitutions caused the observed effects. This would be particularly useful for further studies on CYP154E1 and ketamine and how to further increase selectivity and activity. A fully randomized engineering strategy would probably not be sufficient since, as already mentioned in Section 1.2.7, the number of selectivity determining residues is greatly underrepresented compared to the whole sequence space. Hence, the analysis of disproportionately many clones and huge libraries would be necessary to identify variants with improved selectivity.

Nevertheless, the research conducted in chapters I and II confirmed that focused libraries of first-sphere site-directed mutagenesis and their extension by a higher degree of randomization via applying saturation mutagenesis on selected first-sphere residues could be a valid method for engineering P450s. Besides the previously known human P450s, such as CYP2A6, CYP2B6, or CYP3A4,^{175, 176} the two CYP154E1 variants QAA ((*S*)-ketamine) and TQA ((*R*)-ketamine) are the first reported bacterial P450s which can catalyze the metabolism of (*S*)- and (*R*)-ketamine into (2*S*,6*S*)- respectively (2*R*,6*R*)-hydroxynorketamine. They did so in a very selective manner of, in both cases, 85% product selectivity and 100% diastereoselectivity.

3.2 Comparison of CYP154E1 QAA and TQA – Enantiodivergency

As discussed in the previous section, two triple mutants of CYP154E1 were independently constructed for the selective two-step conversion of ketamine enantiomers: QAA for the selective oxidation of (*S*)-ketamine and TQA for the selective

oxidation of (*R*)-ketamine. But how do they perform with the opposite ketamine enantiomer? As demonstrated in Figure 6, QAA is selective in the double-oxidation of (*S*)-ketamine to (2*S*,6*S*)-HNK (Figure 6A) but less so with (*R*)-ketamine as substrate (Figure 6B). For CYP154E1 TQA, the results look different. TQA is selective with (*R*)-ketamine (Figure 6D), but, with (*S*)-ketamine as substrate (Figure 6C), the regioselectivity is still maintained although, switched from C6 to C4. 43% (2*S*,4)-hydroxyketamine and 44% (2*S*,4)-hydroxynorketamine were formed as the main products. However, although the regioselectivity was still high (in total, 87% for position C4), product selectivity is considerably lower since only half of the C4-hydroxylated product was also demethylated. Although both enzyme variants quantitatively convert both enantiomers and both variants differ only in the substitution of two residues (G239 and L289), each variant is selective with only one of the enantiomers. This behavior is formally known as enantiodivergency – enzymes that indicate no substrate enantioselectivity but product selectivity with a specific enantiomer. Drugs, like the herein synthesized antidepressants, develop their biological effects through interaction with proteins. For example, drugs can inhibit or activate enzymes or block a receptor protein. The chiral nature of proteins causes that different drug stereoisomers can interact differently with the same protein and can cause different – undesired (distomers) or desired (eutomers)¹⁷⁷ – biological effects.¹⁷⁸ Therefore, the pharmacokinetics of each stereoisomer should be tested, as already included in the guidelines of the United States Food and Drug Administration (FDA) in 1992.^{179, f} The development of enantiodivergent – or more generally stereodivergent – biocatalysts to access each stereoisomer is challenging but very useful and sought after in the synthesis of biologically active compounds.^{177, 180} With regard to this thesis, although not all stereoisomers of 2,6-HNK, the two enantiomers (2*S*,6*S*)- and (2*R*,6*R*)-HNK, which were described as potentially safer antidepressants compared to ketamine¹⁸¹, were accessed with two variants of the very same P450 enzyme.

^f <https://www.fda.gov/regulatory-information/search-fda-guidance-documents/development-new-stereoisomeric-drugs>

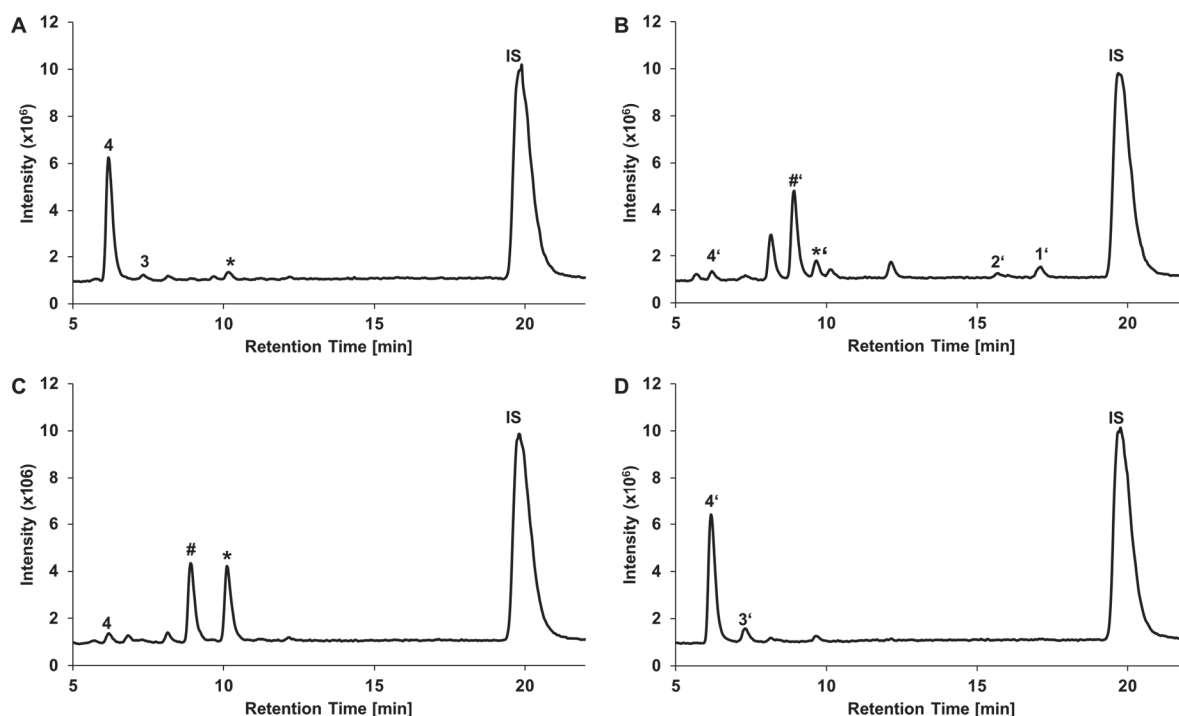


Figure 6. LC-MS Chromatograms of the oxidation of (*S*)-ketamine (A) and (*R*)-ketamine (B) by CYP154E1 QAA and (*S*)-ketamine (C) and (*R*)-ketamine (D) by CYP154E1 TQA. IS: Internal Standard (xylazine), 3: (2*S*,6)-hydroxyketamine, 4: (2*S*,6*S*)-hydroxynorketamine, *: (2*S*,4)-hydroxyketamine, #: (2*S*,4)-hydroxynorketamine, 1': (*R*)-ketamine. Peaks marked with ' represent the (*R*)-enantiomers. Identification of peaks due to representative standards or structure elucidation throughout this thesis.

3.3 Whole-Cell Biocatalysis

The results of chapters I and II have demonstrated that CYP154E1 QAA is well capable of (*S*)-ketamine oxidation to yield (2*S*,6*S*)-HNK with high selectivity, and that CYP154E1 TQA is capable of (*R*)-ketamine oxidation to yield (2*R*,6*R*)-HNK with high selectivity. Both reactions happened *in vitro* and at analytical scale. However, productivity at higher scale requires the upscaling of the reaction. The stoichiometric demand for the costly cofactor NAD(P)H (in this case NADPH) complicates the usage of P450s as *in vitro* biocatalysts, especially at higher scale.¹⁸² To compensate, the *in vitro* P450 reaction system can be expanded by an additional enzyme reaction for the cofactor regeneration, but this further increases the complexity of the system.¹⁸² Further, besides the P450 enzyme and redox proteins, the cofactor regeneration system adds another enzyme to the reaction that needs to be expressed and eventually purified prior to reaction. Instead, by using a whole-cell system, there is no need for enzyme isolation and the cellular metabolism provides reduced cofactor for the reaction.^{29, 43} Therefore, two whole-cell biocatalysts with the recombinant *E. coli* strain BL21(DE3) expressing YkuN and FdR (localized on one plasmid) together with

either CYP154E1 QAA or CYP154E1 TQA (localized on another plasmid) were developed to facilitate the upscaling of (*S*)- and (*R*)-ketamine oxidation from analytical to (semi)preparative scale for product isolation, and subsequent product structure elucidation. With both whole-cell systems, the maximum concentration of (*S*)- respectively (*R*)-ketamine, at which high conversion and selectivity were still maintained, was 5 mM. At concentrations higher than 5 mM, conversion and formation of (*2S,6S*)- respectively (*2R,6R*)-HNK drastically decreased. As explicitly outlined in chapters I and II, the production of hydroxynorketamine proceeding from ketamine involves two catalytic steps – hydroxylation and *N*-demethylation. The mechanism for the latter might provide a possible explanation for the decrease in conversion at specific ketamine concentrations. As described in Section 1.2.2 and depicted in Figure 3A, formaldehyde is produced in equimolar amounts during *N*-demethylation. Formaldehyde can damage the cell^{183, 184} or lead to alterations in protein structure¹⁸⁵ and reduce the efficiency of the catalytic process. This applies to higher ketamine concentrations in particular because they lead to higher formaldehyde concentrations. Metabolic engineering of the *E. coli* whole-cell system might turn this disadvantage of formaldehyde occurrence during the antidepressant production into an advantage: Toxic formaldehyde can be oxidized into lesser toxic formate by formaldehyde dehydrogenase (FDH). Simultaneously, depending on the nature of the FDH, the cofactor NAD(P)⁺ is reduced to NAD(P)H, which is then again accessible for the P450-catalytic cycle. *E. coli* already possesses intrinsic FDHs, but their expression and activity might not be enough when higher substrate concentrations than the tested 5-10 mM (*R/S*)-ketamine are used. Therefore, the integration of further FDH into *E. coli* or the optimization of the existing FDHs (expression and/or activity) might enhance the synthesis of (*2S,6S*)-HNK and (*2R,6R*)-HNK. The addition of a formate dehydrogenase can further expand this cofactor regenerative cycle. The formate dehydrogenase could also contribute to the regeneration of NAD(P)H by formate oxidation to gaseous CO₂, adding a further driving force to the catalytic process due to CO₂ release. This concept does not only work for CYP154E1 and ketamine but any P450-catalyzed demethylation reaction. For example for the demethylation of tricyclic antidepressants such as amitriptyline and derivatives thereof catalyzed by CYP107Z and CYP105D.¹⁸⁶ The potentially harmful effect of formaldehyde on the herein used whole-cell system or enzymes is, however, speculative and needs to be tested more closely in future studies.

Despite the potential effect of formaldehyde, embedding CYP154E1 QAA and CYP154E1 TQA in two *E. coli* whole-cell biocatalysts enabled the production of 0.935 g/L (2*S*,6*S*)- and 1 g/L (2*R*,6*R*)-HNK. These values are much higher than a previously reported value achieved with the human P450 CYP2B6.¹⁷⁶ Human P450s, such as CYP2A6 or CYP2B6, have been reported to metabolize ketamine in the human body. Among others, they produce (2*S*,6*S*)-HNK and (2*R*,6*R*)-HNK as the main metabolites.^{175, 176} CYP2B6 catalyzed the oxidation of (2,6)-hydroxyketamine – the product of ketamine hydroxylation at C6; subsequent *N*-demethylation results in (2,6)-HNK – to furnish (2,6)-HNK at a concentration of 201.6 µg/L.¹⁷⁶ That is about factor 5000 lower compared to what was achieved in both *E. coli* systems from chapters I and II. The formation of (2,6)-HNK with other human P450s was even lower.¹⁷⁶

Due to the novelty of the herein described biocatalytic synthesis of (2*S*,6*S*)- and (2*R*,6*R*)-HNK, other examples of their biocatalytic synthesis (despite the mentioned CYP2B6 catalyzed synthesis) are not available. But for the classification of the herein developed whole-cell system's productivity, it is necessary to compare it to other P450-involved preparative scale reactions. So how did the two *E. coli* systems from chapters I and II perform? Although many reports describe P450-catalyzed reactions only on an analytical scale,¹⁸⁷ several P450-catalyzed preparative scale reactions are described in the following to classify the productivity of the two *E. coli* whole-cell systems. In a study, also making use of first-sphere mutagenesis, evolved P450 BM3 variants were constructed for furnishing the hydroxylation of antimalaria agent artemisinin to both 7(*R*)- and 7(*S*)-hydroxyartemisinin with 100% stereoselectivity (100% ee). In *in vitro* preparative scale conversions, 138 mg/L 7(*S*)-hydroxyartemisinin and 100 mg/ml 7(*R*)-hydroxyartemisinin were produced.³⁴ In another study, the bacterial CYP199A2 F185L variant was utilized in an *E. coli* whole-cell biotransformation to catalyze the oxidation of *p*-coumaric acid to caffeic acid with a productivity of 2.8 g/L.¹⁸⁸ Using an *E. coli* whole-cell system very similar to that described in chapters I and II, Worsch *et al.* reported the oxidation of antimalarial agent amodiaquine by CYP107L from *Streptomyces platensis* at 200 mg/L (main product yielded 128 mg/L).¹⁸⁹ However, it has to be stated that the CYP107L wild type and no optimized variant was used for the oxidation of amodiaquine. In this thesis, the productivity of the two CYP154E1 variants is in the same order of magnitude and, in most cases, even higher compared to the mentioned examples. This demonstrates the applicability of CYP154E1 in the preparative scale production of (2*S*,6*S*)- and (2*R*,6*R*)-HNK.

3.4 Rational Protein Design for the Selective Oxidation of β -Cembrenediol

It is more than 40 years since site-directed mutagenesis was first used to alter the active site of an enzyme^{190, 191} and more than a quarter of a century since Pim Stemmer and Francis Arnold instigated the third and current wave of biocatalysis, according to Bornscheuer *et al.* 2012.^{1, 192, 193} Since then, impressive progress has been made in protein engineering: Saturation mutagenesis (SM) at residues of the active site, which can be extended by iterative cycles of SM; Combinatorial Active-Site Saturation Test (CAST) that allows finding synergistic effects between at least two mutations; theoretical, computer-based techniques such as molecular docking, MD simulations, or machine learning,¹⁹⁴ just to mention a very few examples of progress in protein engineering. Despite the impressive progress in protein engineering, “reliable prediction of the influence of even a single mutation on protein function remains difficult” (Acevedo-Rocha *et al.*, 2018),¹⁹⁵ and therefore the specific synthesis of a specific product remains difficult. To get closer to making reliable predictions of mutations and their effect on product synthesis, in chapter III (“*Simulation-guided design of cytochrome P450 for chemo-and regioselective macrocyclic oxidation*”), Petrović and coworkers presented a workflow for computational P450 design, and we supported its applicability by experimental results. The workflow was designed and tested for the P450 BM3 V78A/F87A and the cembranoid β -cembrenediol. Cembranoids constitute a 14-membered macrocycle and possess a multitude of potential oxidation sites.¹¹⁶ β -cembrenediol possesses three potential epoxidation, seven allylic, and six non-allylic hydroxylation sites. This high number of competing, chemically equivalent oxidation sites presents a challenge for selective oxidation and therefore is ideal for testing a computational protein design approach that predicts substitutions to shift product distribution.

Computational protein design generally relies on detailed knowledge about the structure and conformational flexibility of an enzyme and its substrate before modifications on the enzyme can be implemented. Assuming that substrate binding in the active site is a determinant for the regio- and stereoselectivity of a P450,¹⁵² then finding proper binding poses for the substrate is the initial step. Molecular docking and classical molecular dynamic (MD) simulations are standard methods, utilized to identify the binding and orientation of a substrate in the enzyme’s active site. Both molecular

docking and MD simulations have been used to predict the selectivity of P450 BM3, for example, with benzene¹⁹⁶ or fatty acids.¹⁹⁷ However, molecular docking with a macrocycle like β -cembrenediol is challenging compared to molecular docking with smaller molecules.¹⁹⁸ Macrocycles possess a larger conformational space than smaller molecules, and thus a thorough conformational analysis is required before docking.^{198, 199} Performing classical MD simulations is limited to specific low energy regions of the conformational space²⁰⁰ since the free energy barriers between different binding modes is too high to be crossed by classical MD simulations.²⁰¹ In particular for complex molecules that means that the complete binding process cannot be simulated. This was the case with β -cembrenediol, where four binding modes of β -cembrenediol were selected that differed substantially in their orientation. Further, classical MD simulations have often been used to investigate the origin of selectivity but rarely for guiding rational engineering.¹⁹⁵ Therefore, HREX-MD (Hamiltonian replica exchange molecular dynamics) simulations were required for a thorough analysis of the conformational space of both the substrate and the enzyme. In replica exchange molecular dynamics simulations, independent and parallel simulations of several replicas of the system are carried out, and neighboring replicas can be exchanged with a specific probability.^{200, 201} With that, a larger conformational space can be sampled and a better understanding of the binding of the molecule to the enzyme gained, which is essential in identification of hotspots for mutagenesis.

Two routes can be followed to identify hotspots for enhancing the regioselectivity for a specific position of β -cembrenediol: i) stabilization of the productive substrate conformation and/or ii) destabilization of the unproductive substrate conformations. Destabilizing or stabilizing interactions can be caused by enzyme–substrate interaction energies and H-bond networks.¹⁹⁹ Their calculations via molecular mechanics (MM) revealed six hotspot positions for increasing either C7,C8-epoxidation, or C9 hydroxylation, or C10 hydroxylation. As mentioned above are reliable predictions of mutations on the protein function still difficult and require the validation via experimental results. For instance, residue L75 was identified as destabilizing for hydroxylation at C10 due to clashes with the substrate in its productive orientation.¹⁹⁹ Replacing leucine at position 75 by the smaller residue of alanine was calculated to remove these clashes. Indeed, experimental results approved that the C10 oxidation of β -cembrenediol increased by factor 5 when the bulky residue of leucine was replaced by the small alanine in the P450 BM3 L75A/V78A/F87A triple mutant.

Interestingly, the same P450 BM3 triple mutant has also been constructed by Le-Huu *et al.* for the same purpose.¹¹⁰ Instead of an entirely rational protein design, they utilized semi-rational first-sphere active site mutagenesis. Unfortunately, other than in chapter III, Le-Huu *et al.* describe how they selected the positions for mutagenesis but neither how they selected the substitutions, nor explained their effects. However, this would be important for future attempts to increase the selectivity for C10 oxidation of β -cembrenediol further.

In summary, six out of the ten suggested mutations increased the formation of the intended product by at least factor 2. However, the results also demonstrate the complexity of predicting substitutions for shifting product distribution. Even though the selectivity in most cases could be increased, this happened at the expense of activity. For example, the substitution of alanine at position 328 by serine was calculated to stabilize a conformation of β -cembrenediol in which the C7,C8 epoxidation is favored. Indeed, C7,C8 epoxidation increased from 24% for the P450 BM3 V78A/F87A starting variant to 57% for P450 BM3 A328S/V78A/F87A. This is 1.5 times more selective for the C7,C8 epoxidation than the most selective C7,C8 epoxidizing P450 BM3 variant which was constructed by Le-Huu *et al.*¹¹⁰ However, at the time selectivity increased from 24% to 57%, conversion decreased from 98% to 11%.¹⁹⁹ This negative correlation of “high selectivity [that] is observed only at low substrate conversion, while high substrate conversion compromises selectivity” (Acevedo-Rocha *et al.*, 2018)¹⁹⁵ is still a challenge in engineering P450s.

3.5 Substrate Engineering for the Selective Oxidation of Macrocycles

The selectivity of an enzyme-catalyzed reaction is determined by the shape and size and the interactions between the substrate and active site. In general, there are two ways of altering these interactions, firstly by reshaping the enzyme (protein engineering), or secondly by altering the substrate by substrate engineering (without the use of mutagenesis). In chapter IV (“*Chemoenzymatic Route to Oxyfunctionalized Cembranoids Facilitated by Substrate and Protein Engineering*”), we combined organic synthesis and biocatalysis into a chemo-enzymatic route for late-stage oxyfunctionalization of cembranoids. In the first stage of chapter IV, substrate

engineering was applied. Several characteristics of the interplay between substrate and enzyme can be altered through substrate engineering, for example, substrate acceptance, regio-, or stereoselectivity.²⁰² The strategy of substrate engineering involves the addition of groups to the substrate that direct or anchor the engineered substrate in the enzyme's active site and facilitate binding in a productive orientation.^{162, 203} Besides testing varying anchoring or directing groups, chapter IV goes one step further, which is measuring the influence of substrate rigidity, polarity, and isomerism on the selectivity of P450 BM3 F87G. Therefore, three model macrocycles (Figure 7) with a set of four varying C1 substituents (anchoring/exocyclic groups) were chemically synthesized. The systematic comparison of the model macrocycles with different exocyclic groups revealed that with increasing size and polarity of the exocyclic substituent, the conversion decreased but regioselectivity increased (tested within the same ring structure but for different exocyclic groups; **1a-d** and **3c, d**).

In protein engineering, a protein variant is typically designed for the selective reaction with one specific substrate. In contrast, analyzing anchoring effects might enable the selective conversion of multiple different substrates (of comparable size and structure) with the same enzyme,²⁰⁴ because the different substrates share a joint anchoring group that directs their binding. Indeed, Sherman and colleagues investigated the anchoring functionality of the macrocycle YC-17's desosamine group in the active site of the P450 PikC. Linking the desosamine-anchoring group to different substrates enabled their oxidation by PikC.²⁰⁵ However, the results of chapter IV demonstrate that the commonality of an anchoring-group alone might not be sufficient for the selective oxidation of various substrates. Otherwise, oxidation of **1d**, **2d**, and **3d** in chapter IV would have been equally selective. Comparison of different ring structures but same anchoring-group demonstrated a positive correlation between rigidity and regioselectivity (tested with **1d**, **2d**, and **3d**). The highest regioselectivity (lowest number of products) was found with substrate **3d**, meaning that the anchor-group, rigidity and polarity of the substrate all together affect regioselectivity. The docking simulations of **3d** into the active of P450 BM3 V78A/F87A support that the interplay between anchor-group, rigidity, and polarity in **3d** anchors the substrate in the active site so that only a few transition state-like poses are generated. This leads to a reduced number of different products and subsequent higher selectivity. Hydrogen bonds between residues in the P450 BM3's I-helix and **3d**'s C9 hydroxy group and between

residues opposite to the I-helix (C-helix and SRS-5) and **3d**'s ester-anchor-group stabilize **3d** in a position, in which mainly position C5 is in close proximity to the heme.

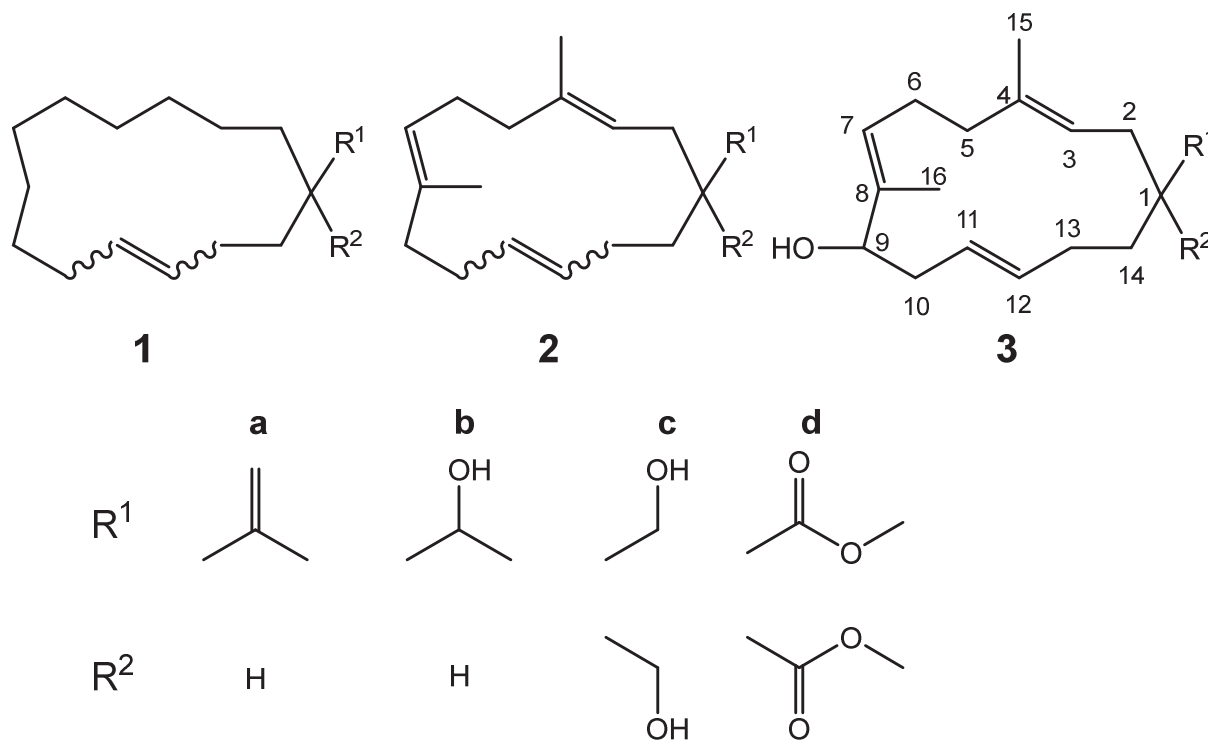


Figure 7. Synthetic macrocycles (1-3) with various exocyclic groups (a-d). Adapted from Le-Huu et al.¹¹⁶

Although in chapter IV effects of the substrate structure on P450 BM3 F87G's reaction selectivity were demonstrated, moderate regioselectivity of only 55% for the main product was found after the conversion of **3d**. The same applies with activity, as **3d** was converted to only 33%. Therefore, activity and regioselectivity were further improved by first-sphere active site mutagenesis. The highest regioselectivity of 88%, combined with the highest conversion of 84%, was observed for the variant P450 BM3 V78A/F87A. Further, this P450 BM3 variant showed remarkable diastereoselectivity depending on substrate stereochemistry, which led exclusively to the syn-products.¹¹⁶

Whereas classical substrate engineering allows the removal of the anchoring group after the biocatalytic process and eventually after the downstream processing,¹⁶³ this is not possible with the substrate engineering approach utilized in chapter IV. Instead, chapter IV demonstrates the synergy between substrate- and protein engineering. This synergy between substrate- and protein engineering has already been used in other studies^{164, 165} and offers a source of P450-catalyzed reactions for various non-native substrates with high value.¹⁶²

3.6 Comparison between Chemical and Biocatalytic Syntheses

P450s are often referred to as having the edge over pure chemical synthesis since P450s catalyze the challenging reaction of non-activated C-H bond oxidation, which is among the most challenging reactions in organic chemistry.²⁰⁶ But how did the P450s in this thesis perform compared to already existing chemical syntheses?

For (2*S*,6*S*)-HNK and (2*R*,6*R*)-HNK, two chemical syntheses have been described so far. The first chemical synthesis was described by Zanos *et al.* in 2016, starting from racemic norketamine¹⁸¹ and the second synthesis by Han *et al.* in 2017, starting from 1-*o*-chlorophenylcyclohexene.²⁰⁷ The latter synthesis can be regarded as an extension to the synthesis by Zanos *et al.* since three reaction steps were added prior to the formation of (*R*)-norketamine (Figure 8). From the synthesis of (*R*)-norketamine onwards, both chemical syntheses are almost the same and start with the activation of position C6 using the keto-enol tautomerism. Although only the synthesis of (2*R*,6*R*)-HNK HCl is shown in Figure 8, the synthesis of its enantiomer (2*S*,6*S*)-HNK follows the same scheme. Starting from (*R*)-norketamine, Zanos *et al.* calculated an isolated yield of 54%, which closely resembles the magnitude of the isolated yields for both (2*S*,6*S*)-HNK and (2*R*,6*R*)-HNK from the chapters I and II (44% and 50% isolated yield). Although the synthetic route after (*R*)-norketamine formation is almost identical between Zanos *et al.* and Han *et al.*, Han *et al.* calculated an isolated yield of 80%. Both isolated yields for the chemical syntheses are higher than for the enzymatic reactions. However, these values only describe the isolated yield when started with norketamine. Compared to the enzymatic synthesis, one step – the *N*-demethylation of ketamine to norketamine – is missing. The complete synthesis of (2*R*,6*R*)-HNK HCl from 1-*o*-chlorophenylcyclohexene yielded 31%.²⁰⁷

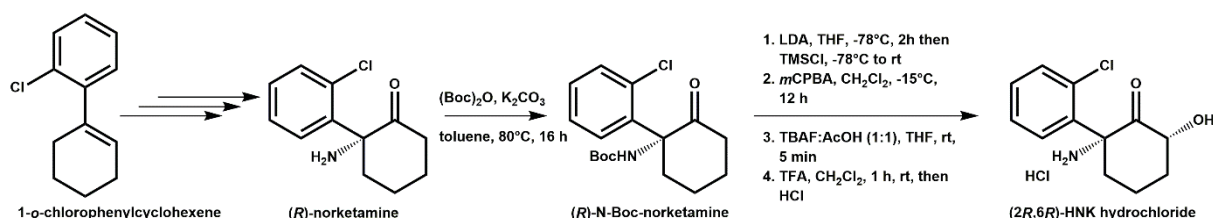


Figure 8. Chemical synthesis of (2*R*,6*R*)-HNK from 1-*o*-chlorophenylcyclohexene adapted from Han *et al.* 2017.²⁰⁷ Synthesis steps 1 to 3 are described in Han *et al.* 2017 in detail. LDA: Lithium diisopropylamide, THF: Tetrahydrofuran, TMSCl: Trimethylsilyl chloride; mCPBA: meta-Chloroperoxybenzoic acid, TBAF: Tetra-n-butylammonium fluoride, TFA: Trifluoroacetic acid.

Han *et al.* did not only synthesize the two HNK enantiomers. They also presented synthetic routes for the production of analogs or derivatives. They verified that their developed synthetic route could also be used to synthesize *o*-fluoro analogs of hydroxynorketamine.²⁰⁷ For future studies on CYP154E1 and ketamine, it would be interesting to test whether the CYP154E1 QAA and TQA maintain their high selectivities when fluoro ketamine analogs are used or, if that is not the case, whether CYP154E1 can be engineered to oxidize fluoro ketamine analogs selectively.

The selective introduction of a hydroxyl group at position C6 of the cyclohexanone ring in the chemical synthesis was possible due to the keto-enol tautomerism. The transition from the keto to the enol form activates C6 for the oxidation by a peroxy acid. Chemical selective hydroxylation at any position in the cyclohexanone ring other than C6 is more complex since it is non-activated.²⁰⁶ On the contrary, P450s are well known for the oxidation of such non-activated bonds. Indeed, the results of chapters I and II confirm that P450-catalyzed hydroxylation at positions other than C6 is feasible. Many CYP154E1 variants described in both chapters produced (2(*S/R*)/4(*S/R*))-hydroxyketamine and -hydroxynorketamine with high selectivity, hydroxy(nor)ketamine derivatives whose biological effects have not yet been described in the literature.

A drawback for both chemical syntheses is the necessity for many toxic and potentially carcinogenic solvents such as tetrahydrofuran (THF) and dichloromethane (CH₂Cl₂). The only solvents required for the fully enzymatic synthesis are ethyl acetate and acetonitrile.

For β -cembrenediol and cembranoids, this direct comparison of enzymatic versus chemical synthesis is not possible since the syntheses of the described oxygenated products has not been implemented in organic synthesis. However, Tietze *et al.* described an efficient total synthesis of a polyoxygenated cembrene with a total yield of 2.7%.²⁰⁸ In a ring-closing metathesis between dithiane and epoxide building blocks, they constructed a 14-membered macrocycle, at which oxy-groups were subsequently introduced at the late stage of the synthesis. As a drawback of this route, the authors mentioned the formation of two diastereomers in a ratio of 40:60 during epoxidation of a double-bond with dimethyldioxirane. Moreover, methylation and reduction of a keto group run with only moderate diastereoselectivity and led to two diastereomers in a ratio of 40:60 again.²⁰⁸ In contrast to that, the P450 BM3 V78A F78A variant described in chapter IV exhibited exclusive diastereoselectivity. Depending on the

stereochemistry of the substrate **3d**, only the *syn*-diol product of either (5*S*,9*S*) or (5*R*,9*R*) was observed. Furthermore, the P450 BM3 variants described in chapter III all produced only one out of two possible diastereomeric epoxides, which is again due to the absolute diastereoselectivity of the enzyme. Although substrate and product are different from those used for the total synthesis by Tietze *et al.*, the results of chapters III and IV highlight the advantages of the selective P450-catalyzed late-stage oxidation of the complex cembranoid scaffolds.

However, a great deal of progress has been achieved in the field of chemical late-stage oxidation with novel catalysts mimicking P450-catalyzed oxidations of non-activated C-H bonds.²⁰⁶ Before 2007, the paradigm stated that physical differences between aliphatic, non-directed C-H bonds are too small to address them selectively for oxidation. But, inspired by the biosynthesis of terpenes, Baran and coworkers developed a two-phase approach for the total synthesis of terpenoids.^{115, 209} During the first “cyclase phase”, a hydrocarbon skeleton is formed, which is then functionalized in the second “oxidase phase”. Using this biomimicking approach, they successfully synthesized, for example, the complex taxol precursor (-)-taxuyunnanine D,²¹⁰ or the diterpenoid (+)-ingenol.²¹¹ Alternatively, inspired by the nature of P450 and its active iron(IV)oxo (or ferryl) species, Chen and White furnished the Fe(PDP) catalyst (also known as White-Chen catalyst),²¹² which similar to the iron(IV)oxo species in the catalytic cycle of P450s, abstracts a hydrogen from the substrate to generate a Fe-OH intermediate and a substrate-carbon radical. Via a rebound mechanism, the hydroxylated product is furnished, and the Fe(PDP) catalyst is regenerated.²⁰⁶ The Fe(PDP) catalyst has proven its powerfulness in selective aliphatic C-H bond hydroxylation in many attempts.^{206, 213, 214}

Combining those options of selective C-H oxidation in chemical and enzymatic catalysts, like the P450s, opens many opportunities for the efficient synthesis of pharmaceuticals and value compounds. For instance, a reaction catalyzed by an engineered P450 BM3 variant produced 9-hydroxy artemisinin with 92% yield, whereas the same reaction catalyzed by a Fe(PDP) catalyst yielded only 52%. On the contrary, the results changed for 10-hydroxy artemisinin, for which the Fe(PDP) catalyst had the edge over a P450-catalyzed reaction.²⁰⁶

3.7 Conclusion

One of the main objectives when working with cytochrome P450 monooxygenases is to unfold their extraordinary potential as industrial biocatalysts. As outlined in this thesis, as high as their potential is, as high are the challenges attributed with P450s – their dependency on costly cofactors, often low stability and activity, or the reliance on an electron transport chain. Within this thesis, I have contributed to the status quo of P450s in science and biotechnology on different levels. Firstly, in collaboration with cooperation partners, I applied and investigated the efficiency of four different protein engineering strategies – site-directed mutagenesis, site-directed saturation mutagenesis, simulation-guided design, and substrate engineering – on two P450s for the selective metabolism of four main substrates. Secondly, in two of the outlined four studies, I created and utilized a whole-cell system that enabled product formation at a preparative scale. Thirdly, I underpinned the potential and broadened the usage of the CYP154E1, a thermotolerant, well expressible, broadly applicable prokaryotic but yet underrepresented P450.

These findings can thereby serve as an inspiration and starting point for future research on cytochrome P450 monooxygenases from a fundamental and applied perspective and initiate how to engineer and use these exceptional enzymes in biocatalysis effectively.

4. Bibliography

1. Bornscheuer, U. T.; Huisman, G. W.; Kazlauskas, R. J.; Lutz, S.; Moore, J. C.; Robins, K., Engineering the Third Wave of Biocatalysis. *Nature* **2012**, *485* (7397), 185-94.
2. Torrelo, G.; Hanefeld, U.; Hollmann, F., Biocatalysis. *Catal. Lett.* **2015**, *145* (1), 309-345.
3. Buchholz, K.; Kasche, V.; Bornscheuer, U. T., *Biocatalysts and Enzyme Technology*. Wiley-Blackwell: 2012.
4. Bornscheuer, U. T.; Buchholz, K., Highlights in Biocatalysis - Historical Landmarks and Current Trends. *Eng. Life Sci.* **2005**, *5* (4), 309-323.
5. Robinson, P. K., Enzymes: Principles and Biotechnological Applications. *Essays Biochem.* **2015**, *59*, 1-41.
6. Koshland Jr., D. E., Application of a Theory of Enzyme Specificity to Protein Synthesis. *PNAS* **1958**, *44* (2), 98-104.
7. Koshland Jr., D. E., The Key-Lock Theory and the Induced Fit Theory. *Angew. Chem. Int. Ed.* **1994**, *33* (23-24), 2375-2378.
8. Watson, J. D.; Crick, F. H., The Structure of DNA. *Cold Spring Harb. Symp. Quant. Biol.* **1953**, *18*, 123-131.
9. Kelly, T. J.; Smith, H. O., A Restriction Enzyme from *Hemophilus influenzae*: II. Base Sequence of the Recognition Site. *J. Mol. Biol.* **1970**, *51* (2), 393-409.
10. Smith, H. O.; Wilcox, K. W., A Restriction Enzyme from *Hemophilus influenzae*: I. Purification and General Properties. *J. Mol. Biol.* **1970**, *51* (2), 379-391.
11. Cohen, S. N.; Chang, A. C. Y.; Boyer, H. W.; Helling, R. B., Construction of Biologically Functional Bacterial Plasmids *in vitro*. *PNAS* **1973**, *70* (11), 3240-3244.
12. Sanger, F.; Nicklen, S.; Coulson, A. R., DNA Sequencing with Chain-Terminating Inhibitors. *PNAS* **1977**, *74* (12), 5463-5467.
13. Ulmer, K. M., Protein Engineering. *Science* **1983**, *219* (4585), 666-671.
14. Kuchner, O.; Arnold, F. H., Directed Evolution of Enzyme Catalysts. *Trends Biotechnol.* **1997**, *15* (12), 523-530.
15. AB, N. M. The Nobel Prize in Chemistry 2018. <https://www.nobelprize.org/prizes/chemistry/2018/summary/>.
16. Bornscheuer, U. T., The Fourth Wave of Biocatalysis Is Approaching. *Phil. Trans. R. Soc. A* **2018**, *376* (2110).
17. Kan, S. B. J.; Lewis, R. D.; Chen, K.; Arnold, F. H., Directed Evolution of Cytochrome C for Carbon-Silicon Bond Formation: Bringing Silicon to Life. *Science* **2016**, *354* (6315), 1048-1051.
18. Zanghellini, A., *de novo* Computational Enzyme Design. *Curr. Opin. Biotechnol.* **2014**, *29*, 132-138.
19. Huang, P.-S.; Boyken, S. E.; Baker, D., The Coming of Age of *de novo* Protein Design. *Nature* **2016**, *537* (7620), 320-327.

20. Donnelly, A. E.; Murphy, G. S.; Digianantonio, K. M.; Hecht, M. H., A *de novo* Enzyme Catalyzes a Life-Sustaining Reaction in *Escherichia coli*. *Nat. Chem. Biol.* **2018**, *14* (3), 253-255.
21. Siegel, J. B.; Zanghellini, A.; Lovick, H. M.; Kiss, G.; Lambert, A. R.; St. Clair, J. L.; Gallaher, J. L.; Hilvert, D.; Gelb, M. H.; Stoddard, B. L.; Houk, K. N.; Michael, F. E.; Baker, D., Computational Design of an Enzyme Catalyst for a Stereoselective Bimolecular Diels-Alder Reaction. *Science* **2010**, *329* (5989), 309-313.
22. Truppo, M. D., Biocatalysis in the Pharmaceutical Industry: The Need for Speed. *ACS Med. Chem. Lett.* **2017**, *8* (5), 476-480.
23. Loughlin, W. A., Biotransformation in Organic Synthesis. *Bioresour. Technol.* **2000**, *74* (1), 49-62.
24. Rigoldi, F.; Donini, S.; Redaelli, A.; Parisini, E.; Gautieri, A., Engineering of Thermostable Enzymes for Industrial Applications. *APL Bioeng.* **2018**, *2* (1), 011501
25. Littlechild, J. A., Enzymes from Extreme Environments and Their Industrial Applications. *Front. Bioeng. Biotechnol.* **2015**, *3*, 161.
26. Sheldon, R. A., Green Solvents for Sustainable Organic Synthesis: State of the Art. *Green Chem.* **2005**, *7* (5), 267-278.
27. Straathof, A. J. J.; Panke, S.; Schmid, A., The Production of Fine Chemicals by Biotransformations. *Curr. Opin. Biotechnol.* **2002**, *13* (6), 548-556.
28. Méndez-Sánchez, D.; López-Iglesias, M.; Gotor-Fernández, V., Hydrolases in Organic Chemistry. Recent Achievements in the Synthesis of Pharmaceuticals. *Curr. Org. Chem.* **2016**, *20* (11), 1186-1203.
29. Lundemo, M. T.; Woodley, J. M., Guidelines for Development and Implementation of Biocatalytic P450 Processes. *Appl. Microbiol. Biotechnol.* **2015**, *99* (6), 2465-2483.
30. Chefson, A.; Auclair, K., Progress Towards the Easier Use of P450 Enzymes. *Mol. Biosyst.* **2006**, *2* (10), 462-469.
31. Fasan, R.; Chen, M. M.; Crook, N. C.; Arnold, F. H., Engineered Alkane-Hydroxylating Cytochrome P450_{BM3} Exhibiting Nativelike Catalytic Properties. *Angew. Chem. Int. Ed.* **2007**, *46* (44), 8414-8418.
32. Xu, F.; Bell, S. G.; Lednik, J.; Insley, A.; Rao, Z.; Wong, L.-L., The Heme Monooxygenase Cytochrome P450_{cam} Can Be Engineered to Oxidize Ethane to Ethanol. *Angew. Chem.* **2005**, *117* (26), 4097-4100.
33. Meinhold, P.; Peters, M. W.; Chen, M. M.; Takahashi, K.; Arnold, F. H., Direct Conversion of Ethane to Ethanol by Engineered Cytochrome P450 BM3. *ChemBioChem* **2005**, *6* (10), 1765-1768.
34. Zhang, K.; Shafer, B. M.; Demars II, M. D.; Stern, H. A.; Fasan, R., Controlled Oxidation of Remote sp³ C-H Bonds in Artemisinin via P450 Catalysts with Fine-Tuned Regio- and Stereoselectivity. *J. Am. Chem. Soc.* **2012**, *134* (45), 18695-18704.
35. Nelson, D. R.; Nebert, D. W., Cytochrome P450 (CYP) Gene Superfamily. *eLS* **2011**, 1-19.

36. Lamb, D. C.; Lei, L.; Warrilow, A. G.; Lepesheva, G. I.; Mullins, J. G.; Waterman, M. R.; Kelly, S. L., The First Virally Encoded Cytochrome P450. *J. Virol.* **2009**, *83* (16), 8266-8269.
37. Omura, T.; Sato, R., The Carbon Monoxide-Binding Pigment of Liver Microsomes. *J. Biol. Chem.* **1964**, *239* (7), 2370-2378.
38. Sono, M.; Roach, M. P.; Coulter, E. D.; Dawson, J. H., Heme-Containing Oxygenases. *Chem. Rev.* **1996**, *96* (7), 2841-2887.
39. Nebert, D. W.; Russell, D. W., Clinical Importance of the Cytochromes P450. *Lancet* **2002**, *360* (9340), 1155-1162.
40. Urlacher, V. B.; Girhard, M., Cytochrome P450 Monooxygenases in Biotechnology and Synthetic Biology. *Trends Biotechnol.* **2019**, *37* (8), 882-897.
41. Li, S.; Du, L.; Bernhardt, R., Redox Partners: Function Modulators of Bacterial P450 Enzymes. *Trends Microbiol.* **2020**, *28* (6), 445-454.
42. Hannemann, F.; Bichet, A.; Ewen, K. M.; Bernhardt, R., Cytochrome P450 Systems—Biological Variations of Electron Transport Chains. *Biochim. Biophys. Acta* **2007**, *1770* (3), 330-344.
43. Hernández-Martin, A.; von Buhler, C. J.; Tieves, F.; Fernández, S.; Ferrero, M.; Urlacher, V. B., Whole-Cell Biotransformation with Recombinant Cytochrome P450 for the Selective Oxidation of Grundmann's Ketone. *Bioorg. Med. Chem.* **2014**, *22* (20), 5586-5592.
44. Girhard, M.; Tieves, F.; Weber, E.; Smit, M. S.; Urlacher, V. B., Cytochrome P450 Reductase from *Candida apicola*: Versatile Redox Partner for Bacterial P450s. *Appl. Microbiol. Biotechnol.* **2013**, *97* (4), 1625-1635.
45. Warman, A. J.; Roitel, O.; Neeli, R.; Girvan, H. M.; Seward, H. E.; Murray, S. A.; McLean, K. J.; Joyce, M. G.; Toogood, H.; Holt, R. A.; Leys, D.; Scrutton, N. S.; Munro, A. W., Flavocytochrome P450 BM3: An Update on Structure and Mechanism of a Biotechnologically Important Enzyme. *Biochem. Soc. Trans.* **2005**, *33* (4), 747-753.
46. Urlacher, V. B.; Girhard, M., Cytochrome P450 Monooxygenases: An Update on Perspectives for Synthetic Application. *Trends Biotechnol.* **2012**, *30* (1), 26-36.
47. Aissaoui, H.; Bachmann, R.; Schweiger, A.; Woggon, W.-D., On the Origin of the Low-Spin Character of Cytochrome P450_{cam} in the Resting State - Investigations of Enzyme Models with Pulse EPR and Endor Spectroscopy. *Angew. Chem. Int. Ed. Engl.* **1998**, *37* (21), 2998-3002.
48. Luthra, A.; Denisov, I. G.; Sligar, S. G., Spectroscopic Features of Cytochrome P450 Reaction Intermediates. *Arch. Biochem. Biophys.* **2012**, *507* (1), 26-35.
49. Sligar, S. G., Coupling of Spin, Substrate, and Redox Equilibria in Cytochrome P450. *Biochemistry* **1976**, *15* (24), 5399-5406.
50. Denisov, I. G.; Makris, T. M.; Sligar, S. G.; Schlichting, I., Structure and Chemistry of Cytochrome P450. *Chem. Rev.* **2005**, *105* (6), 2253-2277.
51. Rittle, J.; Green, M. T., Cytochrome P450 Compound I: Capture, Characterization, and C-H Bond Activation Kinetics. *Science* **2010**, *330* (6006), 933-937.

52. Groves, J. T.; McClusky, G. A., Aliphatic Hydroxylation via Oxygen Rebound. Oxygen Transfer Catalyzed by Iron. *J. Am. Chem. Soc.* **1976**, *98* (3), 859-861.
53. Ogliaro, F.; Harris, N.; Cohen, S.; Filatov, M.; De Visser, S. P.; Shaik, S., A Model "Rebound" Mechanism of Hydroxylation by Cytochrome P450: Stepwise and Effectively Concerted Pathways, and Their Reactivity Patterns. *J. Am. Chem. Soc.* **2000**, *122* (37), 8977-8989.
54. Auclair, K.; Hu, Z.; Little, D. M.; Ortiz de Montellano, P. R.; Groves, J. T., Revisiting the Mechanism of P450 Enzymes with the Radical Clocks Norcarane and Spiro[2,5]Octane. *J. Am. Chem. Soc.* **2002**, *124* (21), 6020-6027.
55. Filatov, M.; Harris, N.; Shaik, S., On the "Rebound" Mechanism of Alkane Hydroxylation by Cytochrome P450: Electronic Structure of the Intermediate and the Electron Transfer Character in the Rebound Step. *Angew. Chem. Int. Ed. Engl.* **1999**, *38* (23), 3510-3512.
56. Krest, C. M.; Onderko, E. L.; Yosca, T. H.; Calixto, J. C.; Karp, R. F.; Livada, J.; Rittle, J.; Green, M. T., Reactive Intermediates in Cytochrome P450 Catalysis. *J. Biol. Chem.* **2013**, *288* (24), 17074-17081.
57. Wang, Y.; Kumar, D.; Yang, C.; Han, K.; Shaik, S., Theoretical Study of *N*-Demethylation of Substituted *N,N*-Dimethylanilines by Cytochrome P450: The Mechanistic Significance of Kinetic Isotope Effect Profiles. *J. Phys. Chem. B* **2007**, *111* (26), 7700-7710.
58. Guengerich, F. P.; Yun, C.-H.; Macdonald, T. L., Evidence for a 1-Electron Oxidation Mechanism in *N*-Dealkylation of *N,N*-Dialkylanilines by Cytochrome P450 2B1. *J. Biol. Chem.* **1996**, *271* (44), 27321-27329.
59. Guengerich, F. P.; Macdonald, T. L., Mechanism of Cytochrome P-450 Catalysis. *The FASEB Journal* **1990**, *4* (8), 2453-2459.
60. Meunier, B.; De Visser, S. P.; Shaik, S., Mechanism of Oxidation Reactions Catalyzed by Cytochrome P450 Enzymes. *Chem. Rev.* **2004**, *104* (9), 3947-3980.
61. Bhakta, M. N.; Wimalasena, K., Microsomal P₄₅₀-Catalyzed *N*-Dealkylation of *N,N*-Dialkylanilines: Evidence for a C α -H Abstraction Mechanism. *J. Am. Chem. Soc.* **2002**, *124* (9), 1844-1845.
62. Karki, S. B.; Dinnocenzo, J. P.; Jones, J. P.; Korzekwa, K. R., Mechanism of Oxidative Aminedealkylation of Substituted *N,N*-Dimethylanilines by Cytochrome-P450 - Application of Isotope Effect Profiles. *J. Am. Chem. Soc.* **1995**, *117* (13), 3657-3657.
63. Manchester, J. I.; Dinnocenzo, J. P.; Higgins, L.; Jones, J. P., A New Mechanistic Probe for Cytochrome P450: An Application of Isotope Effect Profiles. *J. Am. Chem. Soc.* **1997**, *119* (21), 5069-5070.
64. Kumar, D.; Karamzadeh, B.; Sastry, G. N.; De Visser, S. P., What Factors Influence the Rate Constant of Substrate Epoxidation by Compound I of Cytochrome P450 and Analogous Iron(IV)-Oxo Oxidants? *J. Am. Chem. Soc.* **2010**, *132* (22), 7656-7667.
65. de Visser, S. P.; Ogliaro, F.; Shaik, S., Stereospecific Oxidation by Compound I of Cytochrome P450 Does Not Proceed in a Concerted Synchronous Manner. *Chem. Commun. (Camb.)* **2001**, (22), 2322-2323.

66. Poulos, T. L.; Johnson, E. F., Structures of Cytochrome P450 Enzymes. In *Cytochrome P450*, Springer: 2015; pp 3-32.
67. Nair, P. C.; McKinnon, R. A.; Miners, J. O., Cytochrome P450 Structure-Function: Insights from Molecular Dynamics Simulations. *Drug Metab. Rev.* **2016**, *48* (3), 434-452.
68. Poulos, T. L., Cytochrome P450 Flexibility. *PNAS* **2003**, *100* (23), 13121-13122.
69. Gotoh, O., Substrate Recognition Sites in Cytochrome P450 Family 2 (CYP2) Proteins Inferred from Comparative Analyses of Amino Acid and Coding Nucleotide Sequences. *J. Biol. Chem.* **1992**, *267* (1), 83-90.
70. Seifert, A.; Pleiss, J., Identification of Selectivity-Determining Residues in Cytochrome P450 Monooxygenases: A Systematic Analysis of the Substrate Recognition Site 5. *Proteins* **2009**, *74* (4), 1028-1035.
71. Rühlmann, A.; Antovic, D.; Müller, T. J. J.; Urlacher, V. B., Regioselective Hydroxylation of Stilbenes by Engineered Cytochrome P450 from *Thermobifida fusca* YX. *Adv. Synth. Catal.* **2017**, *359* (6), 984-994.
72. Syed, K.; Porollo, A.; Miller, D.; Yadav, J. S., Rational Engineering of the Fungal P450 Monooxygenase CYP5136A3 to Improve Its Oxidizing Activity toward Polycyclic Aromatic Hydrocarbons. *Protein Eng. Des. Sel.* **2013**, *26* (9), 553-557.
73. Meharena, Y. T.; Slessor, K. E.; Cavaignac, S. M.; Poulos, T. L.; De Voss, J. J., The Critical Role of Substrate-Protein Hydrogen Bonding in the Control of Regioselective Hydroxylation in P450cin. *J. Biol. Chem.* **2008**, *283* (16), 10804-10812.
74. Gober, J. G.; Rydeen, A. E.; Gibson-O'Grady, E. J.; Leuthaeuser, J. B.; Fetrow, J. S.; Brustad, E. M., Mutating a Highly Conserved Residue in Diverse Cytochrome P450s Facilitates Diastereoselective Olefin Cyclopropanation. *ChemBioChem* **2016**, *17* (5), 394-397.
75. Clark, J. P.; Miles, C. S.; Mowat, C. G.; Walkinshaw, M. D.; Reid, G. A.; Daff, S. N.; Chapman, S. K., The Role of Thr268 and Phe393 in Cytochrome P450 BM3. *J. Inorg. Biochem.* **2006**, *100* (5-6), 1075-1090.
76. He, Y. A.; He, Y. Q.; Szklarz, G. D.; Halpert, J. R., Identification of Three Key Residues in Substrate Recognition Site 5 of Human Cytochrome P450 3A4 by Cassette and Site-Directed Mutagenesis. *Biochemistry* **1997**, *36* (29), 8831-8839.
77. He, Y. Q.; He, Y. A.; Halpert, J. R., *Escherichia coli* Expression of Site-Directed Mutants of Cytochrome P450 2B1 from Six Substrate Recognition Sites: Substrates Specificity and Inhibitor Selectivity Studies. *Chem. Res. Toxicol.* **1995**, *8* (4), 574-579.
78. de Graaf, C.; Oostenbrink, C.; Keizers, P. H. J.; van Vugt-Lussenburg, B. M. A.; van Waterschoot, R. A. B.; Tschirret-Guth, R. A.; Commandeur, J. N. M.; Vermeulen, N. P. E., Molecular Modeling-Guided Site-Directed Mutagenesis of Cytochrome P450 2D6. *Curr. Drug Metab.* **2007**, *8* (1), 59-77.
79. Wade, R. C.; Winn, P. J.; Schlichting, I.; Sudarko, A Survey of Active Site Access Channels in Cytochromes P450. *J. Inorg. Biochem.* **2004**, *98* (7), 1175-1182.

80. He, Y. A.; Balfour, C. A.; Kedzie, K. M.; Halpert, J. R., Role of Residue 478 as a Determinant of the Substrate Specificity of Cytochrome P450 2B1. *Biochemistry* **1992**, *31* (38), 9220-9226.
81. Xue, L.; Zgoda, V. G.; Arison, B.; Correia, M. A., Structure-Function Relationships of Rat Liver CYP3A9 to Its Human Liver Orthologs: Site-Directed Active Site Mutagenesis to a Progesterone Dihydroxylase. *Arch. Biochem. Biophys.* **2003**, *409* (1), 113-126.
82. Halpert, J. R.; He, Y. A., Engineering of Cytochrome P450 2B1 Specificity. *J. Biol. Chem.* **1993**, *268* (6), 4453-4457.
83. Barka, E. A.; Vatsa, P.; Sanchez, L.; Gaveau-Vaillant, N.; Jacquard, C.; Meier-Kolthoff, J. P.; Klenk, H. P.; Clement, C.; Ouhdouch, Y.; van Wezel, G. P., Taxonomy, Physiology, and Natural Products of Actinobacteria. *Microbiol Mol Biol Rev* **2016**, *80* (1), 1-43.
84. Greule, A.; Stok, J. E.; De Voss, J. J.; Cryle, M. J., Unrivalled Diversity: The Many Roles and Reactions of Bacterial Cytochromes P450 in Secondary Metabolism. *Nat. Prod. Rep.* **2018**, *35* (8), 757-791.
85. Cheng, Q.; Lamb, D. C.; Kelly, S. L.; Lei, L.; Guengerich, F. P., Cyclization of a Cellular Dipentaenone by *Streptomyces coelicolor* Cytochrome P450 154A1 without Oxidation/Reduction. *J. Am. Chem. Soc.* **2010**, *132* (43), 15173-15175.
86. Podust, L. M.; Bach, H.; Kim, Y.; Lamb, D. C.; Arase, M.; Sherman, D. H.; Kelly, S. L.; Waterman, M. R., Comparison of the 1.85 Å Structure of CYP154A1 from *Streptomyces coelicolor* A3(2) with the Closely Related CYP154C1 and CYPs from Antibiotic Biosynthetic Pathways. *Protein Sci.* **2004**, *13* (1), 255-268.
87. Podust, L. M.; Kim, Y.; Arase, M.; Neely, B. A.; Beck, B. J.; Bach, H.; Sherman, D. H.; Lamb, D. C.; Kelly, S. L.; Waterman, M. R., The 1.92-Å Structure of *Streptomyces coelicolor* A3(2) CYP154C1. A New Monooxygenase That Functionalizes Macrolide Ring Systems. *J. Biol. Chem.* **2003**, *278* (14), 12214-12221.
88. Makino, T.; Katsuyama, Y.; Otomatsu, T.; Misawa, N.; Ohnishi, Y., Regio- and Stereospecific Hydroxylation of Various Steroids at the 16 α Position of the D Ring by the *Streptomyces griseus* Cytochrome P450 CYP154C3. *Appl. Environ. Microbiol.* **2014**, *80* (4), 1371-1379.
89. Bracco, P.; Janssen, D. B.; Schallmey, A., Selective Steroid Oxyfunctionalisation by CYP154C5, a Bacterial Cytochrome P450. *Microb. Cell Fact.* **2013**, *12* (95), 1-11.
90. Schallmey, A.; den Besten, G.; Teune, I. G.; Kembaren, R. F.; Janssen, D. B., Characterization of Cytochrome P450 Monooxygenase CYP154H1 from the Thermophilic Soil Bacterium *Thermobifida fusca*. *Appl. Microbiol. Biotechnol.* **2011**, *89* (5), 1475-1485.
91. Rühlmann, A.; Groth, G.; Urlacher, V. B., Characterization of CYP154F1 from *Thermobifida fusca* YX and Extension of Its Substrate Spectrum by Site-Directed Mutagenesis. *ChemBioChem* **2018**, *19* (5), 478-485.
92. von Bühler, C.; Le-Huu, P.; Urlacher, V. B., Cluster Screening: An Effective Approach for Probing the Substrate Space of Uncharacterized Cytochrome P450s. *ChemBioChem* **2013**, *14* (16), 2189-2198.

93. Bogazkaya, A. M.; von Buhler, C. J.; Kriening, S.; Busch, A.; Seifert, A.; Pleiss, J.; Laschat, S.; Urlacher, V. B., Selective Allylic Hydroxylation of Acyclic Terpenoids by CYP154E1 from *Thermobifida fusca* YX. *Beilstein J. Org. Chem.* **2014**, *10* (1), 1347-1353.
94. Dangi, B.; Lee, C. W.; Kim, K. H.; Park, S. H.; Yu, E. J.; Jeong, C. S.; Park, H.; Lee, J. H.; Oh, T. J., Characterization of Two Steroid Hydroxylases from Different *Streptomyces* spp. And Their Ligand-Bound and -Unbound Crystal Structures. *FEBS J.* **2019**, *286* (9), 1683-1699.
95. Herzog, K.; Bracco, P.; Onoda, A.; Hayashi, T.; Hoffmann, K.; Schallmeyer, A., Enzyme-Substrate Complex Structures of CYP154C5 Shed Light on Its Mode of Highly Selective Steroid Hydroxylation. *Acta Crystallogr. D Biol. Crystallogr.* **2014**, *70* (11), 2875-2889.
96. Whitehouse, C. J.; Bell, S. G.; Wong, L. L., P450_{BM3} (CYP102A1): Connecting the Dots. *Chem. Soc. Rev.* **2012**, *41* (3), 1218-1260.
97. Munro, A. W.; Daff, S.; Coggins, J. R.; Lindsay, J. G.; Chapman, S. K., Probing Electron Transfer in Flavocytochrome P-450 BM3 and Its Component Domains. *Eur. J. Biochem.* **1996**, *239* (2), 403-409.
98. Noble, M. A.; Miles, C. S.; Chapman, S. K.; Lysek, D. A.; Mackay, A. C.; Reid, G. A.; Hanzlik, R. P.; Munro, A. W., Roles of Key Active-Site Residues in Flavocytochrome P450 BM3. *Biochem. J.* **1999**, *339* (2), 371-379.
99. Miura, Y.; Fulco, A. J., (ω -2) Hydroxylation of Fatty Acids by a Soluble System from *Bacillus megaterium*. *J. Biol. Chem.* **1974**, *249* (6), 1880-1889.
100. Wong, L. L., P450(BM3) on Steroids: The Swiss Army Knife P450 Enzyme Just Gets Better. *ChemBioChem* **2011**, *12* (17), 2537-2539.
101. Weber, E.; Seifert, A.; Antonovici, M.; Geinitz, C.; Pleiss, J.; Urlacher, V. B., Screening of a Minimal Enriched P450 BM3 Mutant Library for Hydroxylation of Cyclic and Acyclic Alkanes. *Chem. Commun. (Camb.)* **2011**, *47* (3), 944-946.
102. Seifert, A.; Vomund, S.; Grohmann, K.; Kriening, S.; Urlacher, V. B.; Laschat, S.; Pleiss, J., Rational Resign of a Minimal and Highly Enriched CYP102A1 Mutant Library with Improved Regio-, Stereo- and Chemoselectivity. *ChemBioChem* **2009**, *10* (5), 853-861.
103. Watanabe, Y.; Laschat, S.; Budde, M.; Affolter, O.; Shimada, Y.; Urlacher, V. B., Oxidation of Acyclic Monoterpenes by P450 BM-3 Monooxygenase: Influence of the Substrate *E/Z*-Isomerism on Enzyme Chemo- and Regioselectivity. *Tetrahedron* **2007**, *63* (38), 9413-9422.
104. Schulz, S.; Girhard, M.; Gaßmeyer, S. K.; Jäger, V. D.; Schwarze, D.; Vogel, A.; Urlacher, V. B., Selective Enzymatic Synthesis of the Grapefruit Flavor (+)-Nootkatone. *ChemCatChem* **2015**, *7* (4), 601-604.
105. Lewis, J. C.; Mantovani, S. M.; Fu, Y.; Snow, C. D.; Komor, R. S.; Wong, C. H.; Arnold, F. H., Combinatorial Alanine Substitution Enables Rapid Optimization of Cytochrome P450_{BM3} for Selective Hydroxylation of Large Substrates. *ChemBioChem* **2010**, *11* (18), 2502-2505.
106. Kille, S.; Zilly, F. E.; Acevedo, J. P.; Reetz, M. T., Regio- and Stereoselectivity of P450-Catalysed Hydroxylation of Steroids Controlled by Laboratory Evolution. *Nat. Chem.* **2011**, *3* (9), 738-743.

107. Chen, W.; Fisher, M. J.; Leung, A.; Cao, Y.; Wong, L. L., Oxidative Diversification of Steroids by Nature-Inspired Scanning Glycine Mutagenesis of P450BM3 (CYP102A1). *ACS Catal.* **2020**, *10* (15), 8334-8343.
108. Salazar, O.; Cirino, P. C.; Arnold, F. H., Thermostabilization of a Cytochrome P450 Peroxygenase. *ChemBioChem* **2003**, *4* (9), 891-893.
109. Yun, C. H.; Kim, K. H.; Kim, D. H.; Jung, H. C.; Pan, J. G., The Bacterial P450 BM3: A Prototype for a Biocatalyst with Human P450 Activities. *Trends Biotechnol.* **2007**, *25* (7), 289-298.
110. Le-Huu, P.; Heidt, T.; Claasen, B.; Laschat, S.; Urlacher, V. B., Chemo-, Regio-, and Stereoselective Oxidation of the Monocyclic Diterpenoid β -Cembrenediol by P450 BM3. *ACS Catal.* **2015**, *5* (3), 1772-1780.
111. Le-Huu, P.; Petrović, D.; Strodel, B.; Urlacher, V. B., One-Pot Two-Step Hydroxylation of the Macrocyclic Diterpenoid β -Cembrenediol Catalyzed by P450 BM3 Mutants. *ChemCatChem* **2016**, *8* (24), 3755-3761.
112. Vottero, E.; Rea, V.; Lastdrager, J.; Honing, M.; Vermeulen, N. P.; Commandeur, J. N., Role of Residue 87 in Substrate Selectivity and Regioselectivity of Drug-Metabolizing Cytochrome P450 CYP102A1 M11. *J. Biol. Inorg. Chem.* **2011**, *16* (6), 899-912.
113. Sakaki, T., Practical Application of Cytochrome P450. *Biol. Pharm. Bull.* **2012**, *35* (6), 844-849.
114. Cook, D. J.; Finnigan, J. D.; Cook, K.; Black, G. W.; Charnock, S. J., Cytochromes P450: History, Classes, Catalytic Mechanism, and Industrial Application. *Adv. Protein Chem. Struct. Biol.* **2016**, *105*, 105-126.
115. Baran, P. S.; Ishihara, Y., Two-Phase Terpene Total Synthesis: Historical Perspective and Application to the Taxol® Problem. *Synlett* **2010**, *2010* (12), 1733-1745.
116. Le-Huu, P.; Rekow, D.; Krüger, C.; Bokel, A.; Heidt, T.; Schaubach, S.; Claasen, B.; Hölzel, S.; Frey, W.; Laschat, S.; Urlacher, V. B., Chemoenzymatic Route to Oxyfunctionalized Cembranoids Facilitated by Substrate and Protein Engineering. *Chem. Eur. J.* **2018**, *24* (46), 12010-12021.
117. Fessner, N. D., P450 Monooxygenases Enable Rapid Late-Stage Diversification of Natural Products via C-H Bond Activation. *ChemCatChem* **2019**, *11* (9), 2226-2242.
118. Martinez, C. A.; Rupasinghe, S. G., Cytochrome P450 Bioreactors in the Pharmaceutical Industry: Challenges and Opportunities. *Curr. Top. Med. Chem.* **2013**, *13* (12), 1470-1490.
119. Petzoldt, K.; Annen, K.; Laurent, H.; Wiechert, R. Process for the Preparation of 11- β -Hydroxy Steroids. 1982.
120. Suzuki, K.; Sanga, K.-i.; Chikaoka, Y.; Itagaki, E., Purification and Properties of Cytochrome P-450 (*P*-450_{lun}) Catalyzing Steroid 11 β -Hydroxylation in *Curvularia lunata*. *Biochim. Biophys. Acta* **1993**, *1203* (2), 215-223.
121. Hanson, F. R.; Maxon, W. D. Process for the Microbiological Oxygenation of Progesterone. 1965.

122. Hogg, J. A., Steroids, the Steroid Community, and Upjohn in Perspective: A Profile of Innovation. *Steroids* **1992**, *57* (12), 593-616.
123. Matsuoka, T.; Miyakoshi, S. Cytochrome P-450 Enzymes. 1993.
124. Watanabe, I.; Nara, F.; Serizawa, N., Cloning, Characterization and Expression of the Gene Encoding Cytochrome P-450_{sca-2} from *Streptomyces carbophilus* Involved in Production of Pravastatin, a Specific HMG-CoA Reductase Inhibitor. *Gene* **1995**, *163* (1), 81-85.
125. Tiwari, R.; Rana, C. S., Plant Secondary Metabolites: A Review. *Int. J. Eng. Res.Gen. Sci.* **2015**, *3* (5), 661-670.
126. Yarbrough, G. G.; Taylor, D. P.; Rowlands, R. T.; Crawford, M. S.; Lasure, L. L., Screening Microbial Metabolites for New Drugs-Theoretical and Practical Issues. *J. Antibiot.* **1993**, *46* (4), 535-544.
127. Paddon, C. J.; Westfall, P. J.; Pitera, D. J.; Benjamin, K.; Fisher, K.; McPhee, D.; Leavell, M. D.; Tai, A.; Main, A.; Eng, D.; Polichuk, D. R.; Teoh, K. H.; Reed, D. W.; Treynor, T.; Lenihan, J.; Fleck, M.; Bajad, S.; Dang, G.; Dengrove, D.; Diola, D.; Dorin, G.; Ellens, K. W.; Fickes, S.; Galazzo, J.; Gaucher, S. P.; Geistlinger, T.; Henry, R.; Hepp, M.; Horning, T.; Iqbal, T.; Jiang, H.; Kizer, L.; Lieu, B.; Melis, D.; Moss, N.; Regentin, R.; Secrest, S.; Tsuruta, H.; Vazquez, R.; Westblade, L. F.; Xu, L.; Yu, M.; Zhang, Y.; Zhao, L.; Lievens, J.; Covello, P. S.; Keasling, J. D.; Reiling, K. K.; Renninger, N. S.; Newman, J. D., High-Level Semi-Synthetic Production of the Potent Antimalarial Artemisinin. *Nature* **2013**, *496* (7446), 528-532.
128. Paddon, C. J.; Keasling, J. D., Semi-Synthetic Artemisinin: A Model for the Use of Synthetic Biology in Pharmaceutical Development. *Nat. Rev. Microbiol.* **2014**, *12* (5), 355-367.
129. Ro, D. K.; Paradise, E. M.; Ouellet, M.; Fisher, K. J.; Newman, K. L.; Ndungu, J. M.; Ho, K. A.; Eachus, R. A.; Ham, T. S.; Kirby, J.; Chang, M. C.; Withers, S. T.; Shiba, Y.; Sarpong, R.; Keasling, J. D., Production of the Antimalarial Drug Precursor Artemisinic Acid in Engineered Yeast. *Nature* **2006**, *440* (7086), 940-943.
130. Artemisinin & Synthetic Biology - a Case Study. *ETC Group* **2014**.
131. Peplow, M., Synthetic Biology's First Malaria Drug Meets Market Resistance. *Nature* **2016**, *530* (7591), 389-390.
132. Guengerich, F. P., Cytochrome P450s and Other Enzymes in Drug Metabolism and Toxicity. *AAPS Journal* **2006**, *8* (1), E101-E111.
133. Schroer, K.; Kittelmann, M.; Lütz, S., Recombinant Human Cytochrome P450 Monooxygenases for Drug Metabolite Synthesis. *Biotechnol. Bioeng.* **2010**, *106* (5), 699-706.
134. Obach, R. S., Pharmacologically Active Drug Metabolites: Impact on Drug Discovery and Pharmacotherapy. 2013; pp 580-605.
135. Friedberg, T.; Pritchard, M. P.; Bandera, M.; Hanlon, S. P.; Yao, D.; McLaughlin, L. A.; Ding, S.; Burchell, B.; Wolf, C. R., Merits and Limitations of Recombinant Models for the Study of Human P450-Mediated Drug Metabolism and Toxicity: An Intralaboratory Comparison. *Drug Metab. Rev.* **1999**, *31* (2), 523-544.

136. Hausjell, J.; Halbwirth, H.; Spadiut, O., Recombinant Production of Eukaryotic Cytochrome P450s in Microbial Cell Factories. *Biosci. Rep.* **2018**, *38* (2).
137. O'Reilly, E.; Kohler, V.; Flitsch, S. L.; Turner, N. J., Cytochromes P450 as Useful Biocatalysts: Addressing the Limitations. *Chem. Commun. (Camb.)* **2011**, *47* (9), 2490-2501.
138. Bernhardt, R.; Urlacher, V. B., Cytochromes P450 as Promising Catalysts for Biotechnological Application: Chances and Limitations. *Appl. Microbiol. Biotechnol.* **2014**, *98* (14), 6185-6203.
139. Yuryev, R.; Kasche, V.; Ignatova, Z.; Galunsky, B., Improved *A. faecalis* Penicillin Amidase Mutant Retains the Thermodynamic and pH Stability of the Wild Type Enzyme. *Protein J.* **2010**, *29* (3), 181-187.
140. Bouacem, K.; Bouanane-Darenfed, A.; Laribi-Habchi, H.; Elhoul, M. B.; Hmida-Sayari, A.; Hacene, H.; Ollivier, B.; Fardeau, M. L.; Jaouadi, B.; Bejar, S., Biochemical Characterization of a Detergent-Stable Serine Alkaline Protease from *Caldicoprobacter guelmensis*. *Int. J. Biol. Macromol.* **2015**, *81*, 299-307.
141. Ho, P. P. K.; Milikin, E. B.; Bobbitt, J. L.; Grinnan, E. L.; Burck, P. J.; Frank, B. H.; Boeck, L. V. D.; Squires, R. W., Crystalline L-Asparaginase from *Escherichia coli* B. *J. Biol. Chem.* **1970**, *245* (14), 3708-3715.
142. Guengerich, F. P., Cytochrome P450 Enzymes in the Generation of Commercial Products. *Nat. Rev. Drug Discov.* **2002**, *1* (5), 359-366.
143. Xu, L. H.; Du, Y. L., Rational and Semi-Rational Engineering of Cytochrome P450s for Biotechnological Applications. *Synth. Syst. Biotechnol.* **2018**, *3* (4), 283-290.
144. Cherry, J. R.; Fidantsef, A. L., Directed Evolution of Industrial Enzymes: An Update. *Curr. Opin. Biotechnol.* **2003**, *14* (4), 438-443.
145. Wahler, D.; Reymond, J.-L., High-Throughput Screening for Biocatalysts. *Curr. Opin. Biotechnol.* **2001**, *12* (6), 535-544.
146. Tee, K. L.; Schwaneberg, U., Directed Evolution of Oxygenases: Screening Systems, Success Stories and Challenges. *Combinatorial Chemistry & High Throughput Screen.* **2007**, *10* (3), 197-217.
147. Lutz, S., Beyond Directed Evolution - Semi-Rational Protein Engineering and Design. *Curr. Opin. Biotechnol.* **2010**, *21* (6), 734-743.
148. Gricman, L.; Vogel, C.; Pleiss, J., Identification of Universal Selectivity-Determining Positions in Cytochrome P450 Monooxygenases by Systematic Sequence-Based Literature Mining. *Proteins* **2015**, *83* (9), 1593-1603.
149. Carmichael, A. B.; Wong, L.-L., Protein Engineering of *Bacillus megaterium* CYP102: The Oxidation of Polycyclic Aromatic Hydrocarbons. *Eur. J. Biochem.* **2001**, *268* (10), 3117-3125.
150. Dill, K. A., Dominant Forces in Protein Folding. *Biochemistry* **1990**, *29* (31), 7133-7155.
151. Berry, M.; Fielding, B.; Gamielien, J., Practical Considerations in Virtual Screening and Molecular Docking. In *Emerging Trends in Computational Biology, Bioinformatics, and Systems Biology*, 2015; pp 487-502.

152. de Visser, S. P.; Ogliaro, F.; Sharma, P. K.; Shaik, S., What Factors Affect the Regioselectivity of Oxidation by Cytochrome P450? A DFT Study of Allylic Hydroxylation and Double Bond Epoxidation in a Model Reaction. *J. Am. Chem. Soc.* **2002**, *124* (39), 11809-11826.
153. Dietrich, J. A.; Yoshikuni, Y.; Fisher, K. J.; Woolard, F. X.; Ockey, D.; McPhee, D., J.; Renninger, N. S.; Chang, M. C. Y.; Baker, D.; Keasling, J. D., A Novel Semi-Biosynthetic Route for Artemisinin Production Using Engineered Substrate-Promiscuous P450_{BM3}. *ACS Chem. Biol.* **2009**, *4* (4), 261-267.
154. Meng, X. Y.; Zhang, H.-X.; Mezei, M.; Cui, M., Molecular Docking: A Powerful Approach for Structure-Based Drug Discovery. *Curr. Comput. Aided Drug Des.* **2011**, *7* (2), 146-157.
155. Morley, K. L.; Kazlauskas, R. J., Improving Enzyme Properties: When Are Closer Mutations Better? *Trends Biotechnol.* **2005**, *23* (5), 231-237.
156. Chica, R. A.; Doucet, N.; Pelletier, J. N., Semi-Rational Approaches to Engineering Enzyme Activity: Combining the Benefits of Directed Evolution and Rational Design. *Curr. Opin. Biotechnol.* **2005**, *16* (4), 378-384.
157. Kazlauskas, R. J.; Bornscheuer, U. T., Finding Better Protein Engineering Strategies. *Nat. Chem. Biol.* **2009**, *5* (8), 526-529.
158. Nguyen, K. T.; Virus, C.; Gunnewich, N.; Hannemann, F.; Bernhardt, R., Changing the Regioselectivity of a P450 from C15 to C11 Hydroxylation of Progesterone. *ChemBioChem* **2012**, *13* (8), 1161-1166.
159. Mildvan, A. S., Inverse Thinking About Double Mutants of Enzymes. *Biochemistry* **2004**, *43* (46), 14517-14520.
160. Reetz, M. T.; Bocola, M.; Carballeira, J. D.; Zha, D.; Vogel, A., Expanding the Range of Substrate Acceptance of Enzymes: Combinatorial Active-Site Saturation Test. *Angew. Chem. Int. Ed. Engl.* **2005**, *44* (27), 4192-4196.
161. Avi, M.; Wiedner, R. M.; Griengl, H.; Schwab, H., Improvement of a Stereoselective Biocatalytic Synthesis by Substrate and Enzyme Engineering: 2-Hydroxy-(4'-Oxocyclohexyl)Acetonitrile as the Model. *Chem. Eur. J.* **2008**, *14* (36), 11415-11422.
162. Xu, J.; Wang, C.; Cong, Z., Strategies for Substrate-Regulated P450 Catalysis: From Substrate Engineering to Co-Catalysis. *Chem. Eur. J.* **2019**, *25* (28), 6853-6863.
163. Braunegg, G.; de Raadt, A.; Feichtenhofer, S.; Griengl, H.; Kopper, I.; Lehmann, A.; Weber, H.-J., The Concept of Docking/Protecting Groups in Biohydroxylation. *Angew. Chem. Int. Ed. Engl.* **1999**, *38* (18), 2763-2766.
164. Landwehr, M.; Hochrein, L.; Otey, C. R.; Kasrayan, A.; Backvall, J. E.; Arnold, F. H., Enantioselective α -Hydroxylation of 2-Arylacetic Acid Derivatives and Buspirone Catalyzed by Engineered Cytochrome P450 BM-3. *J. Am. Chem. Soc.* **2006**, *128* (18), 6058-6059.
165. Vickers, C.; Backfisch, G.; Oellien, F.; Piel, I.; Lange, U. E. W., Enzymatic Late-Stage Oxidation of Lead Compounds with Solubilizing Biomimetic Docking/Protecting Groups. *Chem. Eur. J.* **2018**, *24* (68), 17936-17947.
166. Omura, T., Forty Years of Cytochrome P450. *Biochem. Biophys. Res. Commun.* **1999**, *266* (3), 690-698.

167. Francis, J. A.; Raja, S. N.; Nair, M. G., Bioactive Terpenoids and Guggulosteroids from *Commiphora mukul* Gum Resin of Potential Anti-Inflammatory Interest. *Chem. Biodivers.* **2004**, *1* (11), 1842-1853.
168. Rashid, M. A.; Gustafson, K. R.; Boyd, M. R., HIV-Inhibitory Cembrane Derivatives from a Philippines Collection of the Soft Coral *Lobophytum* Species. *J. Nat. Prod.* **2000**, *63* (4), 531-533.
169. Narisawa, T.; Takahashi, M.; Niwa, M.; Fukaura, Y.; Fujiki, H., Inhibition of Methylnitrosourea-Induced Large Bowel Cancer Development in Rats by Sarcophytol A, a Product from a Marine Soft Coral *Sarcophyton glaucum*. *Cancer Res.* **1989**, *49* (12), 3287-3289.
170. Otten, L. G.; Hollmann, F.; Arends, I. W., Enzyme Engineering for Enantioselectivity: From Trial-and-Error to Rational Design? *Trends Biotechnol.* **2010**, *28* (1), 46-54.
171. Kerdpin, O.; Elliot, D. J.; Boye, S. L.; Birkett, D. J.; Yoovathaworn, K.; Miners, J. O., Differential Contribution of Active Site Residues in Substrate Recognition Sites 1 and 5 to Cytochrome P450 2C8 Substrate Selectivity and Regioselectivity. *Biochemistry* **2004**, *43* (24), 7834-7842.
172. Dalton, J. A. R.; Jackson, R. M., An Evaluation of Automated Homology Modelling Methods at Low Target Template Sequence Similarity. *Bioinformatics* **2007**, *23* (15), 1901-1908.
173. Von Bühler, C. Development of Versatile Biocatalysts Based on P450 Monooxygenases from the CYP154 Family. Heinrich-Heine-University Düsseldorf, 2014.
174. Brunger, A. T.; DeLaBarre, B.; Davies, J. M.; Weis, W. I., X-Ray Structure Determination at Low Resolution. *Acta Crystallogr. D Biol. Crystallogr.* **2009**, *65* (2), 128-133.
175. Portmann, S.; Kwan, H. Y.; Theurillat, R.; Schmitz, A.; Mevissen, M.; Thormann, W., Enantioselective Capillary Electrophoresis for Identification and Characterization of Human Cytochrome P450 Enzymes Which Metabolize Ketamine and Norketamine *in vitro*. *J. Chromatogr. A* **2010**, *1217* (51), 7942-7948.
176. Desta, Z.; Moaddel, R.; Ogburn, E. T.; Xu, C.; Ramamoorthy, A.; Venkata, S. L.; Sanghvi, M.; Goldberg, M. E.; Torjman, M. C.; Wainer, I. W., Stereoselective and Regiospecific Hydroxylation of Ketamine and Norketamine. *Xenobiotica* **2012**, *42* (11), 1076-1087.
177. Krautwald, S.; Carreira, E. M., Stereodivergence in Asymmetric Catalysis. *J. Am. Chem. Soc.* **2017**, *139* (16), 5627-5639.
178. Shi, S. L.; Wong, Z. L.; Buchwald, S. L., Copper-Catalysed Enantioselective Stereodivergent Synthesis of Amino Alcohols. *Nature* **2016**, *532* (7599), 353-356.
179. Brooks, W. H.; Guida, W. C.; Daniel, K. G., The Significance of Chirality in Drug Design and Development. *Curr. Top. Med. Chem.* **2011**, *11* (7), 760-770.
180. Knight, A. M.; Kan, S. B. J.; Lewis, R. D.; Brandenburg, O. F.; Chen, K.; Arnold, F. H., Diverse Engineered Heme Proteins Enable Stereodivergent Cyclopropanation of Unactivated Alkenes. *ACS Cent. Sci.* **2018**, *4* (3), 372-377.

181. Zanos, P.; Moaddel, R.; Morris, P. J.; Georgiou, P.; Fischell, J.; Elmer, G. I.; Alkondon, M.; Yuan, P.; Pribut, H. J.; Singh, N. S.; Dossou, K. S.; Fang, Y.; Huang, X. P.; Mayo, C. L.; Wainer, I. W.; Albuquerque, E. X.; Thompson, S. M.; Thomas, C. J.; Zarate, C. A., Jr.; Gould, T. D., NMDAR Inhibition-Independent Antidepressant Actions of Ketamine Metabolites. *Nature* **2016**, *533* (7604), 481-486.
182. Schewe, H.; Kaup, B. A.; Schrader, J., Improvement of P450_{BM-3} Whole-Cell Biocatalysis by Integrating Heterologous Cofactor Regeneration Combining Glucose Facilitator and Dehydrogenase in *E. coli*. *Appl. Microbiol. Biotechnol.* **2008**, *78* (1), 55-65.
183. Takahashi, K.; Morita, T.; Kawazoe, Y., Mutagenic Characteristics of Formaldehyde on Bacterial Systems. *Mutat. Res.* **1985**, *156* (3), 153-161.
184. Auerbach, C.; Moutschen-Dahmen, M.; Moutschen, J., Genetic and Cytogenetical Effects of Formaldehyde and Related Compounds. *Mutat. Res.* **1977**, *39* (3-4), 317-362.
185. French, D.; Edsall, J. T., The Reactions of Formaldehyde with Amino Acids and Proteins. 1945; pp 277-335.
186. Hilberath, T.; Windeln, L. M.; Decembrino, D.; Le-Huu, P.; Bilsing, F. L.; Urlacher, V. B., Two-Step Screening for Identification of Drug-Metabolizing Bacterial Cytochromes P450 with Diversified Selectivity. *ChemCatChem* **2020**, *12* (6), 1710-1719.
187. Chakrabarty, S.; Wang, Y.; Perkins, J. C.; Narayan, A. R. H., Scalable Biocatalytic C-H Oxyfunctionalization Reactions. *Chem. Soc. Rev.* **2020**, *49* (22), 8137-8155.
188. Furuya, T.; Arai, Y.; Kino, K., Biotechnological Production of Caffeic Acid by Bacterial Cytochrome P450 CYP199A2. *Appl. Environ. Microbiol.* **2012**, *78* (17), 6087-6094.
189. Worsch, A.; Eggimann, F. K.; Girhard, M.; von Buhler, C. J.; Tieves, F.; Czaja, R.; Vogel, A.; Grumaz, C.; Sohn, K.; Lutz, S.; Kittelmann, M.; Urlacher, V. B., A Novel Cytochrome P450 Mono-Oxygenase from *Streptomyces platensis* Resembles Activities of Human Drug Metabolizing P450s. *Biotechnol. Bioeng.* **2018**, *115* (9), 2156-2166.
190. Brannigan, J. A.; Wilkinson, A. J., Protein Engineering 20 Years On. *Nat. Rev. Mol. Cell Biol.* **2002**, *3* (12), 964-970.
191. Hutchison, C. A.; Phillips, S.; Edgell, M. H.; Gillam, S.; Jahnke, P.; Smith, M., Mutagenesis at a Specific Position in a DNA Sequence. *J. Biol. Chem.* **1978**, *253* (18), 6551-6560.
192. Chen, K.; Arnold, F. H., Tuning the Activity of an Enzyme for Unusual Environments: Sequential Random Mutagenesis of Subtilisin E for Catalysis in Dimethylformamide. *PNAS* **1993**, *90* (12), 5618-5622.
193. Stemmer, W. P. C., Rapid Evolution of a Protein *in vitro* by DNA Shuffling. *Nature* **1994**, *370* (6488), 389-391.
194. Li, G.; Dong, Y.; Reetz, M. T., Can Machine Learning Revolutionize Directed Evolution of Selective Enzymes? *Adv. Synth. Catal.* **2019**, *361* (11), 2377-2386.

195. Acevedo-Rocha, C. G.; Gamble, C. G.; Lonsdale, R.; Li, A. T.; Nett, N.; Hoebenreich, S.; Lingnau, J. B.; Wirtz, C.; Fares, C.; Hinrichs, H.; Deege, A.; Mulholland, A. J.; Nov, Y.; Leys, D.; McLean, K. J.; Munro, A. W.; Reetz, M. T., P450-Catalyzed Regio- and Diastereoselective Steroid Hydroxylation: Efficient Directed Evolution Enabled by Mutability Landscaping. *ACS Catal.* **2018**, *8* (4), 3395-3410.
196. Denning, A.; Lülldorf, N.; Liu, H.; Schwaneberg, U., Regioselective *O*-Hydroxylation of Monosubstituted Benzenes by P450 BM3. *Angew. Chem.* **2013**, *52* (32), 8459-8462.
197. Feenstra, K. A.; Starikov, E. B.; Urlacher, V. B.; Commandeur, J. N.; Vermeulen, N. P., Combining Substrate Dynamics, Binding Statistics, and Energy Barriers to Rationalize Regioselective Hydroxylation of Octane and Lauric Acid by CYP102A1 and Mutants. *Protein Sci.* **2007**, *16* (3), 420-431.
198. Alogheli, H.; Olanders, G.; Schaal, W.; Brandt, P.; Karlen, A., Docking of Macrocycles: Comparing Rigid and Flexible Docking in Glide. *J. Chem. Inf. Model.* **2017**, *57* (2), 190-202.
199. Petrovic, D.; Bokel, A.; Allan, M.; Urlacher, V. B.; Strodel, B., Simulation-Guided Design of Cytochrome P450 for Chemo- and Regioselective Macrocyclic Oxidation. *J. Chem. Inf. Model.* **2018**, *58* (4), 848-858.
200. Meli, M.; Colombo, G., A Hamiltonian Replica Exchange Molecular Dynamics (MD) Method for the Study of Folding, Based on the Analysis of the Stabilization Determinants of Proteins. *Int. J. Mol. Sci.* **2013**, *14* (6), 12157-12169.
201. Qi, R.; Wei, G.; Ma, B.; Nussinov, R., Replica Exchange Molecular Dynamics: A Practical Application Protocol with Solutions to Common Problems and a Peptide Aggregation and Self-Assembly Example. *Methods Mol. Biol.* **2018**, *1777*, 101-119.
202. De Raadt, A.; Griengl, H., The Use of Substrate Engineering in Biohydroxylation. *Curr. Opin. Biotechnol.* *13* (6), 537-542.
203. Polic, V.; Auclair, K., Controlling Substrate Specificity and Product Regio- and Stereo-Selectivities of P450 Enzymes without Mutagenesis. *Bioorg. Med. Chem.* **2014**, *22* (20), 5547-5554.
204. Negretti, S.; Narayan, A. R.; Chiou, K. C.; Kells, P. M.; Stachowski, J. L.; Hansen, D. A.; Podust, L. M.; Montgomery, J.; Sherman, D. H., Directing Group-Controlled Regioselectivity in an Enzymatic C-H Bond Oxygenation. *J. Am. Chem. Soc.* **2014**, *136* (13), 4901-4904.
205. Li, S.; Chaulagain, M. R.; Knauff, A. R.; Podust, L. M.; Montgomery, J.; Sherman, D. H., Selective Oxidation of Carbolide C-H Bonds by an Engineered Macrolide P450 Mono-Oxygenase. *PNAS* **2009**, *106* (44), 18463-18468.
206. White, M. C.; Zhao, J., Aliphatic C-H Oxidations for Late-Stage Functionalization. *J. Am. Chem. Soc.* **2018**, *140* (43), 13988-14009.
207. Han, Y.; Mahender Reddy, K.; Corey, E. J., Simple Enantioselective Syntheses of (2*R*,6*R*)-Hydroxynorketamine and Related Potential Rapid-Onset Antidepressants. *Org. Lett.* **2017**, *19* (19), 5224-5227.
208. Tietze, L. F.; Brazel, C. C.; Holsken, S.; Magull, J.; Ringe, A., Total Synthesis of Polyoxygenated Cembrenes. *Angew. Chem. Int. Ed. Engl.* **2008**, *47* (28), 5246-5249.

209. Chen, K.; Baran, P. S., Total Synthesis of Eudesmane Terpenes by Site-Selective C-H Oxidations. *Nature* **2009**, *459* (7248), 824-828.
210. Wilde, N. C.; Isomura, M.; Mendoza, A.; Baran, P. S., Two-Phase Synthesis of (-)-Taxuyunnanin D. *J. Am. Chem. Soc.* **2014**, *136* (13), 4909-4912.
211. McKerrall, S. J.; Jorgensen, L.; Kuttruff, C. A.; Ungeheuer, F.; Baran, P. S., Development of a Concise Synthesis of (+)-Ingenol. *J. Am. Chem. Soc.* **2014**, *136* (15), 5799-5810.
212. Chen, M. S.; White, M. C., A Predictably Selective Aliphatic C–H Oxidation Reaction for Complex Molecule Synthesis. *Science* **2007**, *318* (5851), 783-787.
213. Gormisky, P. E.; White, M. C., Catalyst-Controlled Aliphatic C-H Oxidations with a Predictive Model for Site-Selectivity. *J. Am. Chem. Soc.* **2013**, *135* (38), 14052-14055.
214. Chen, M. S.; White, M. C., Combined Effects on Selectivity in Fe-Catalyzed Methylene Oxidation. *Science* **2010**, *327* (5965), 566-571.

5. Abbreviations

| | | | |
|------------------|--|-----------------|---|
| °C | degree Celsius | L | Leucine or Liter |
| A | alanine | LC-MS | liquid chromatography- mass spectrometry |
| <i>A. annua</i> | <i>Artemisia annua</i> | M | methionine |
| AG | Aktiengesellschaft | MD | molecular dynamics |
| C-H | carbon-hydrogen | mg | milligram |
| C-terminus | carboxy terminus | min | minute |
| CAST | combinatorial active-site saturation test | ml | milliliter |
| CO ₂ | carbon dioxide | mM | millimolar |
| CYP | cytochrome P450 monooxygenase | MM | molecular mechanics |
| Cys | cysteine | μM | micromolar |
| DNA | desoxyribonucleic acid | N | nitrogen |
| <i>E. coli</i> | <i>Escherichia coli</i> | NAD(P)H | nicotinamide adenine dinucleotide (phosphate) |
| EC | Enzyme Commission | nm | nanometer |
| e.g. | exempli gratia (for example) | NMR | nuclear magnetic resonance |
| et al. | et alia (and others) | N-terminus | amino terminus |
| ExxR | glutamate – any amino acid – any amino acid – arginine | O ₂ | molecular oxygen |
| F | phenylalanine | O | oxygen |
| FAD | Flavin adenine dinucleotide | P450 | cytochrome P450 monooxygenase |
| FDA | Food and Drug Administration | PCR | polymerase chain reaction |
| FDH | formaldehyde dehydrogenase | PDB | protein data bank |
| FdR | <i>E. coli</i> flavodoxin reductase | Phe | phenylalanine |
| Fe | iron | Q | glutamine |
| FMN | Flavin mononucleotide | S | serine |
| g | gram | SM | saturation mutagenesis |
| G | glycine | SRS | substrate recognition site |
| GC | gas chromatography | T | threonine |
| GC-MS | gas chromatography- mass spectrometry | <i>T. fusca</i> | <i>Thermobifida fusca</i> |
| Gly | glycine | TTN | total turnover number |
| H ₂ O | water | V | valine |
| HCl | hydrochloride | YkuN | <i>Bacillus subtilis</i> flavodoxin N |
| HNK | hydroxynorketamine | | |
| HPLC | High-performance liquid chromatography | | |
| HREX | Hamiltonian replica exchange | | |
| Inc. | Incorporation | | |
| ISM | iterative saturation mutagenesis | | |
| k _{cat} | turnover number | | |
| kDa | kilo Dalton | | |

6. Acknowledgments

This thesis has caused me some frustration and grey hair. Still, I don't regret a single day of this challenging time because otherwise, I would not have met so many wonderful people who have accompanied me on this journey. The time I have been privileged to spend with all of you made the last years unforgettable, and I would like to express my special thanks to a few people who have been particularly important to me.

First of all, I would like to thank Prof. Dr. Vlada B. Urlacher for allowing me to work for four years on the really appealing and exciting topic of engineering P450s for selective drug metabolism. You helped me work independently and reliably, and you gave me the freedom to pursue my own ideas. I really learned a lot at your institute, and I am very grateful for that.

Then, I am grateful to Prof. Dr. Karl-Erich Jäger, not only for accepting the co-opinion but also for all the meetings and advice throughout the last years and already before during my Master's thesis at evovx technologies GmbH.

I am deeply grateful to all the current and former members of the Institute of Biochemistry II. I really had unforgettable four years with you in and outside the lab. I have benefited a lot from all your experiences and knowledge, which definitively helped me finish this thesis. Even more important to me was to talk with you about anything but work. I really loved our evenings, at Schalander, Brückerbach, Kasette, Volksgarten, at the volleyball court, or anywhere else where we spent our evenings at that time. You were not just really lovely and fabulous colleagues, but you became true friends. Thank you!

I am incredibly grateful to my office crew Arsenij, Anne, Joost, Fabian (even though it was concise), Sebastian, and Niko. You made the days so much fun, and I cannot think of better office members than you. You helped me work-related when I got stuck about something in the lab, and you helped emotionally when I was down for any reason, always and whenever I needed it. Mainly, I would like to thank Niko. We were at the same wavelength directly from the start, and we share the same sense of humor

(especially when it comes to linguistic jokes). From the very first day, you made me feel welcome at the institute, and since then, many jokes and funny moments have followed. But also in more challenging times, you always listened to my problems and helped me or got my mind off with a good game of chess or simply a beer.

I thank the Paderborner Yetis. You might think that it is a bit exaggerated but I simply can't help feeling that without you, I probably would not have gotten to the point of starting this thesis. I spent so many great days on the training ground or at competition weekends (with unforgettable competition preparations), and I will never forget the time I spent with you. Alles ins Gold!

I am deeply grateful for all my friends but especially for Kai, Martin, Nina, and Vanessa from Düsseldorf for proving that the most important outcome from studying is friendship. Thank you for so many fabulous nights in the Altstadt, student residence parties, gaming nights, dart nights, ... and so much more. And Christian from Paderborn. We went through many ups and downs, and yet you never let me down. Thanks for being such a valuable friend over all these years.

Thanks to my family

To my brother, Kathrin, and the two best nieces in the world. You always considered me as part of your own little family.

To my mother and Bernard, who gave me many, many valuable advice. Not only on my way to the PhD but also on my way of growing up. I could and can always rely on you, and you always offered me a place to stay whenever I needed a break from my PhD.

To my father and Claudia, who supported me from the very first day as a student. You have always been a quiet voice in my head that had brought me back on track when I was on my way to get lost. Something that is not to be underestimated.

You all played such a significant part in this thesis, and I am so grateful to call all of you family.

Liliane Wulff. The day I am writing this, it has been more than ten and a half years. I can still feel the moment that started it all. Since then, our life was in permanent change, but you always remained my constant. I can't express how grateful I am that

6. Acknowledgements

you were always with me during these years, even though you couldn't always be with me. How fortunate can a person be to have met someone like you who enriches my life more and more every day? You have taught me that it's not what I have but who I have in my life that matters most, and if I had one wish, it would be that everyone found their own Lili. This thesis is dedicated to you, my love, my life.

7. Supplementary Data Chapter I-IV

Supporting Information

Enzyme-Mediated Two-Step Regio- and Stereoselective Synthesis of Potential Rapid Acting Antidepressant (2*S*,6*S*)-Hydroxynorketamine

Ansgar Bokel,[†] Ansgar Rühlmann,[†] Michael C. Hutter,[#] and Vlada B. Urlacher^{*†}

[†] *Institute of Biochemistry, Heinrich Heine University Düsseldorf, Universitätsstr. 1, 40225 Düsseldorf, Germany*

[#] *Center for Bioinformatics, Saarland University, Campus E2.1, 66123 Saarbruecken, Germany*

*Corresponding author, E-mail: Vlada.Urlacher@uni-duesseldorf.de

| | |
|---|----|
| Oligonucleotides..... | 2 |
| Cloning, Expression and Purification..... | 4 |
| Expression of YkuN in a 7.5 l Bioreactor..... | 4 |
| Enzyme Assays..... | 4 |
| GC/MS Screening Data | 5 |
| Rigid Docking of (<i>S</i>)-Ketamine and (<i>S</i>)-Norketamine | 6 |
| Further Mutagenesis | 6 |
| HPLC Data..... | 7 |
| CYP154E1 QAA Characterization..... | 9 |
| Substrate Binding Spectra for CYP154E1 QAA with (<i>S</i>)-Ketamine | 9 |
| Kinetics | 10 |
| Rigid Docking of (2 <i>S</i> ,6 <i>S</i>)-Hydroxyketamine..... | 11 |
| Preparative Scale Conversion..... | 12 |
| NMR Analysis..... | 13 |
| REFERENCES..... | 16 |

OLIGONUCLEOTIDES

Table S1. Oligonucleotides for the cloning and the quickchange mutagenesis. The mutated codon is marked by color and underline. Primer of for variants that were already available in our institute are not listed below. Fw: forward primer; Rev: reverse Primer.

| Primer QuickChange | Sequence (5' → 3') |
|---------------------|---|
| Fw: CYP154E1 T178F | CAGACGCTGGTGACGCGC <u>TTC</u> CTCTCCGGCACGGACCCTGAG |
| Rev: CYP154E1 T178F | CTCAGGGTCCGTGCCGGAGAG <u>GAA</u> GCGCGTCACCAGCGTCTG |
| Fw: CYP154E1 T178I | CAGACGCTGGTGACGCGC <u>ATC</u> CTCTCCGGCACGGACCCTGAG |
| Rev: CYP154E1 T178I | CTCAGGGTCCGTGCCGGAGAG <u>GAT</u> GCGCGTCACCAGCGTCTG |
| Fw: CYP154E1 L179F | GTGACGCGCACCC <u>TTT</u> TCCGGCACGGACCCTGAG |
| Rev: CYP154E1 L179F | CTCAGGGTCCGTGCCGGA <u>AAA</u> GGTGCGCGTCAC |
| Fw: CYP154E1 L179K | GTGACGCGCACCC <u>AAA</u> TCCGGCACGGACCCTGAG |
| Rev: CYP154E1 L179K | CTCAGGGTCCGTGCCGGA <u>TTT</u> GGTGCGCGTCAC |
| Fw: CYP154E1 L179R | GTGACGCGCACCC <u>CGC</u> TCCGGCACGGACCCTGAG |
| Rev: CYP154E1 L179R | CTCAGGGTCCGTGCCGGA <u>GCG</u> GGTGCGCGTCAC |
| Fw: CYP154E1 L234Q | CTGATCCACAACACG <u>CAG</u> CTGTCATCCAGGCG |
| Rev: CYP154E1 L234Q | CGCCTGGATGAGCAG <u>CTG</u> CGTGTTGTGGATCAG |
| Fw: CYP154E1 L235D | GAGCTGATCCACAACACGCTG <u>GAC</u> CTCATCATCGG |
| Rev: CYP154E1 L235D | CCGATGATGAG <u>GTC</u> CAGCGTGTTGTGGATCAGCTC |
| Fw: CYP154E1 L235E | GAGCTGATCCACAACACGCTG <u>GAA</u> CTCATCATCGG |
| Rev: CYP154E1 L235E | CCGATGATGAG <u>TTC</u> CAGCGTGTTGTGGATCAGCTC |
| Fw: CYP154E1 L235N | GAGCTGATCCACAACACGCTG <u>AAC</u> CTCATCATCGG |
| Rev: CYP154E1 L235N | CCGATGATGAG <u>GTT</u> CAGCGTGTTGTGGATCAGCTC |
| Fw: CYP154E1 L235Q | GAGCTGATCCACAACACGCTG <u>CAG</u> CTCATCATCGG |
| Rev: CYP154E1 L235Q | CCGATGATGAG <u>CTG</u> CAGCGTGTTGTGGATCAGCTC |
| Fw: CYP154E1 L235T | GAGCTGATCCACAACACGCTG <u>ACC</u> CTCATCATCGG |
| Rev: CYP154E1 L235T | CCGATGATGAG <u>GGT</u> CAGCGTGTTGTGGATCAGCTC |
| Fw: CYP154E1 I238D | GCTGCTGCTCATC <u>GAC</u> GGCGGGTTTCGAAACCAC |
| Rev: CYP154E1 I238D | GTGGTTTCGAACCCGCC <u>GTC</u> GATGAGCAGCAGC |
| Fw: CYP154E1 I238E | GCTGCTGCTCATC <u>GAG</u> GGCGGGTTTCGAAACCAC |
| Rev: CYP154E1 I238E | GTGGTTTCGAACCCGCC <u>CTC</u> GATGAGCAGCAGC |
| Fw: CYP154E1 I238N | GCTGCTGCTCATC <u>AAC</u> GGCGGGTTTCGAAACCAC |
| Rev: CYP154E1 I238N | GTGGTTTCGAACCCGCC <u>GTT</u> GATGAGCAGCAGC |
| Fw: CYP154E1 I238Q | GCTGCTGCTCATC <u>CAG</u> GGCGGGTTTCGAAACCAC |
| Rev: CYP154E1 I238Q | GTGGTTTCGAACCCGCC <u>CTG</u> GATGAGCAGCAGC |
| Fw: CYP154E1 I238T | GCTGCTGCTCATC <u>ACC</u> GGCGGGTTTCGAAACCAC |
| Rev: CYP154E1 I238T | GTGGTTTCGAACCCGCC <u>GGT</u> GATGAGCAGCAGC |
| Fw: CYP154E1 T243D | CAGGCGGGGTTTCGAA <u>GAC</u> ACCATGGGCATGATC |
| Rev: CYP154E1 T243D | GATCATGCCCATGGT <u>GTC</u> TTCGAACCCCGCCTG |
| Fw: CYP154E1 T243N | CAGGCGGGGTTTCGAA <u>AAC</u> ACCATGGGCATGATC |
| Rev: CYP154E1 T243N | GATCATGCCCATGGT <u>GTT</u> TTCGAACCCCGCCTG |
| Fw: CYP154E1 T243S | CAGGCGGGGTTTCGAA <u>AGC</u> ACCATGGGCATGATC |
| Rev: CYP154E1 T243S | GATCATGCCCATGGT <u>GCT</u> TTCGAACCCCGCCTG |

| | |
|--|--------------------------------------|
| Fw: CYP154E1 V286I | CGAATCAGCGATCGTCATGCTGCCGTTCC |
| Rev: CYP154E1 V286I | GGAACGGCAGCATGACGATCGCTGATTCCG |
| Fw: CYP154E1 V286N | CGAATCAGCGAACGTCATGCTGCCGTTCC |
| Rev: CYP154E1 V286N | GGAACGGCAGCATGACGTCGCTGATTCCG |
| Fw: CYP154E1 M388A | GACGCCGACCGTGTTCCGGAACCATCCGCTGAG |
| Rev: CYP154E1 M388A | CTCAGCGGATGGTTCGCGAACACGGTCGGCGTC |
| Fw: CYP154E1 M388G | GACGCCGACCGTGTTCCGGTAACCATCCGCTGAG |
| Rev: CYP154E1 M388G | CTCAGCGGATGGTTACCGAACACGGTCGGCGTC |
| Primer Cloning | |
| Fw: CYP154E1 QAA in pET22b (<i>Nde</i> I) | CAGCCATATGGGACAGTCCCGCCGACCC |
| Rev: CYP154E1 QAA in pET22b (<i>Eco</i> RI) | GCTCGAATTCTCAGGGTTTCGGGCGCAAG |
| Fw: YkuN in pCOLA Duet MCS I (<i>Nco</i> I) | TATACCATGGCTAAAGCCTTGATTACATATGC |
| Rev: YkuN in pCOLA Duet MCS I (<i>Bam</i> HI) | GATCGGATCCTCATGAAACATGGATTTTTTCCTTG |
| Fw: FdR in pCOLA Duet MCS II (<i>Bgl</i> II) | TATAAGATCTCATGGCTGATTGGGTAACAGGCAAAG |
| Rev: FdR in pCOLA Duet MCS II (<i>Xho</i> I) | GATCCTCGAGTTACCAGTAATGCTCCGCTGTC |
| Sequencing primer (pET vectors) | |
| T7 | TAATACGACTCACTATAGGG |
| pET-RP | CTAGTTATTGCTCAGCGG |
| Sequencing primer (pCOLA Duet vector) | |
| ACYC_Duet_Up1 | GGATCTCGACGCTCTCCCT |
| Duet_DOWN1 | GATTATGCGGCCGTGTACAA |
| Duet_Up2 | TTGTACACGGCCGCATAATC |

CLONING, EXPRESSION AND PURIFICATION

Construction of CYP154E1 mutants was carried out according to a modified quik-change mutagenesis protocol of Edelheit, Hanukoglu, and Hanukoglu (2009) using two separated single-primer reactions.¹

Expression of the redox partner FdR from *Escherichia coli*, and the NADPH regenerating glucose dehydrogenase (GDH) from *Bacillus megaterium* was performed as described elsewhere except for the expression vector pET11a for FdR.²⁻³ For screening, the genes coding for CYP154E1 wild type and mutants integrated into the pET28a+ vector were heterologously expressed in *E. coli* BL21(DE3). Expression was carried out in 50 ml TB medium in a 0.5 liter flask, initially at 37°C and 180 rpm until OD₆₀₀ of 0.6-0.8 was reached. After induction with 0.1 mM IPTG, 0.1 mM FeSO₄ and 0.5 mM 5-aminolevulinic acid, cultures were stirred for another 20 hours at 25°C and 140 rpm before cells were harvested. For protein purification, CYP154E1 wild type and mutants were expressed in 400 ml scale in 2 liter flasks under the same conditions as described above.

Purification was performed on an ÄKTApurifier (GE Healthcare) on a HisTrap FF crude 5 ml column (immobilized nickel affinity chromatography). Proteins were eluted using a buffer with 150 mM (FdR), 100 mM (CYP154E1) and 200 mM (YkuN) imidazole as the eluent. After subsequent desalting via size exclusion chromatography on a PD-10 column (GE Healthcare) proteins were stored in buffers containing 50 mM Tris-HCl, 50 mM NaCl, 5% (w/v) glycerol, pH 7.5 (YkuN) and 50 mM KPi, 50 mM NaCl, 5% (w/v) glycerol pH 7.5 (FdR and CYP154E1 variants). For CYP154E1 variants an additional heat precipitation step at 60°C for 15 min was included after sample desalting. After heat precipitation, target CYP154E1 enzymes were incubated on ice for another 20 min and precipitated proteins were removed via centrifugation.

EXPRESSION OF YKUN IN A 7.5 L BIOREACTOR

The vector pET16b carrying the gene for the electron transfer partner YkuN from *Bacillus subtilis* was already available in our laboratory. 10 ml LB pre-cultures containing *E. coli* transformants, hosting the YkuN-gene encoded vector pET16b, were grown over night at 37°C and 180 rpm. These pre-cultures were used to inoculate 500 ml TB medium starter cultures to an OD₆₀₀ of 0.05. After growth for several hours at 30°C and 180 rpm, the starter cultures were used onwards to inoculate a 7.5 l bioreactor (Infors, Bottmingen, Switzerland) containing 3.5 l fermentation basal salt medium (19.13 g l⁻¹ K₂HPO₄ · 3 H₂O, 4 g l⁻¹ NaH₂PO₄ · 2 H₂O, 2.47 g l⁻¹ (NH₄)₂SO₄, 2 g l⁻¹ Na₂SO₄, 0.5 g l⁻¹ NH₄Cl, 1 g l⁻¹ (NH₄)₂ citrate, 20 g l⁻¹ glycerol, 2 ml l⁻¹ 1 M MgSO₄, 1 ml l⁻¹ thiamine (100 mg ml⁻¹), 1 ml l⁻¹ ampicillin (100 mg ml⁻¹), 3.5 ml l⁻¹ trace metals (0.5 g l⁻¹ CaCl₂, 0.18 g l⁻¹ ZnSO₄ · 7 H₂O, 0.18 g l⁻¹ CoCl₂ · 6 H₂O, 0.16 g l⁻¹ CuSO₄ · 5 H₂O, 0.1 g l⁻¹ MnSO₄ · H₂O, 22.9 g l⁻¹ Na₂ EDTA · 2 H₂O, 16.7 g l⁻¹ FeCl₃ · 6 H₂O) to an OD₆₀₀ of 0.5. Temperature was maintained at 30°C until initial glycerol was exhausted (measurable by pO₂ increase). Afterwards expression was induced via addition of 0.1 mM IPTG. Temperature was decreased to 20°C and control of cell growth was maintained automatically by glycerol (50%) addition whenever the carbon source was consumed (again measurable by pO₂ increase).

ENZYME ASSAYS

Concentrations of cytochrome P450s (*E. coli* cell lysates and purified enzymes) were calculated via CO difference spectra using the extinction coefficient $\epsilon_{450-490} = 91 \text{ mM}^{-1}\text{cm}^{-1}$ as described elsewhere.⁴ The concentration of the purified redox proteins YkuN and FdR were determined spectroscopically as described elsewhere.⁵⁻⁸ The NADP⁺ reduction activity of the GDH was measured by increase of absorbance at 340 nm over time ($\epsilon_{340} = 6.22 \text{ mM}^{-1}\text{cm}^{-1}$). The reaction was set up with 0.1 M glucose, 100 μl of diluted GDH solution in 50 mM potassium phosphate buffer pH 7.5. The reaction was started by adding 0.1 mM NADP⁺.

GC/MS SCREENING DATA

Table S2. (S)-ketamine oxidation catalyzed by CYP154E1 variants. NK: norketamine; (2S,6)-HNK: (2S,6)-hydroxynorketamine. Conversion was estimated from the ratio of product peak areas only, compared to the sum of all peak areas (including the substrate peak area). *: CYP154E1 variants of our in-house collection.

| CYP154E1 variant | Conversion [%] | Product distribution [%] | | |
|------------------|----------------|--------------------------|------------|--------|
| | | NK | (2S,6)-HNK | Others |
| Wild Type | 1.8 | 100 | - | - |
| M87V | 0.0 | - | - | - |
| L94F* | 0.2 | 100 | - | - |
| T178F* | 1.1 | 100 | - | - |
| T178I* | 1.6 | 100 | - | - |
| L179F* | 1.7 | 100 | - | - |
| L179K* | 0.2 | 100 | - | - |
| L179R* | 0.6 | 100 | - | - |
| L235D | 0.0 | - | - | - |
| L235E | 0.0 | - | - | - |
| L235N | 0.0 | - | - | - |
| L235Q | 0.0 | - | - | - |
| L235T | 0.8 | 100 | - | - |
| I238D | 0.0 | - | - | - |
| I238E | 0.2 | 100 | - | - |
| I238N | 0.0 | - | - | - |
| I238Q | 21.9 | 58.1 | 7.1 | 34.8 |
| I238T | 2.4 | 100 | - | - |
| G239A* | 12.2 | 96.7 | 3.3 | - |
| V286A* | 0.3 | 100 | - | - |
| V286I | 0.6 | 100 | - | - |
| V286L* | 0.0 | - | - | - |
| V286N | 0.2 | 100 | - | - |
| M388A | 6.1 | 90.6 | 9.4 | - |
| M388G | 1.4 | 100 | - | - |
| M388Q* | 0.0 | - | - | - |

RIGID DOCKING OF (S)-KETAMINE AND (S)-NORKETAMINE

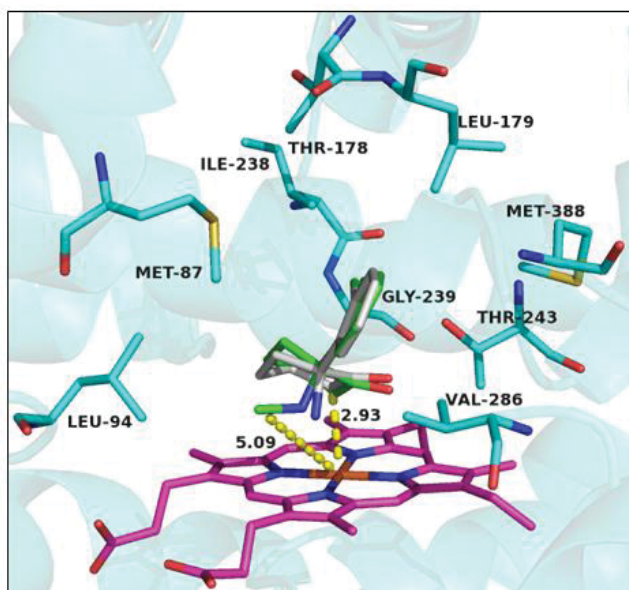


Figure S1. Best scored rigid docking poses of (*S*)-ketamine (green) and (*S*)-norketamine (grey) in the active site of CYP154E1 wild type. Dashed yellow lines indicate distances between atoms (5.09 Å between heme iron and aminomethyl group of (*S*)-ketamine and 2.93 Å between heme iron and C6 of (*S*)-norketamine).

FURTHER MUTAGENESIS

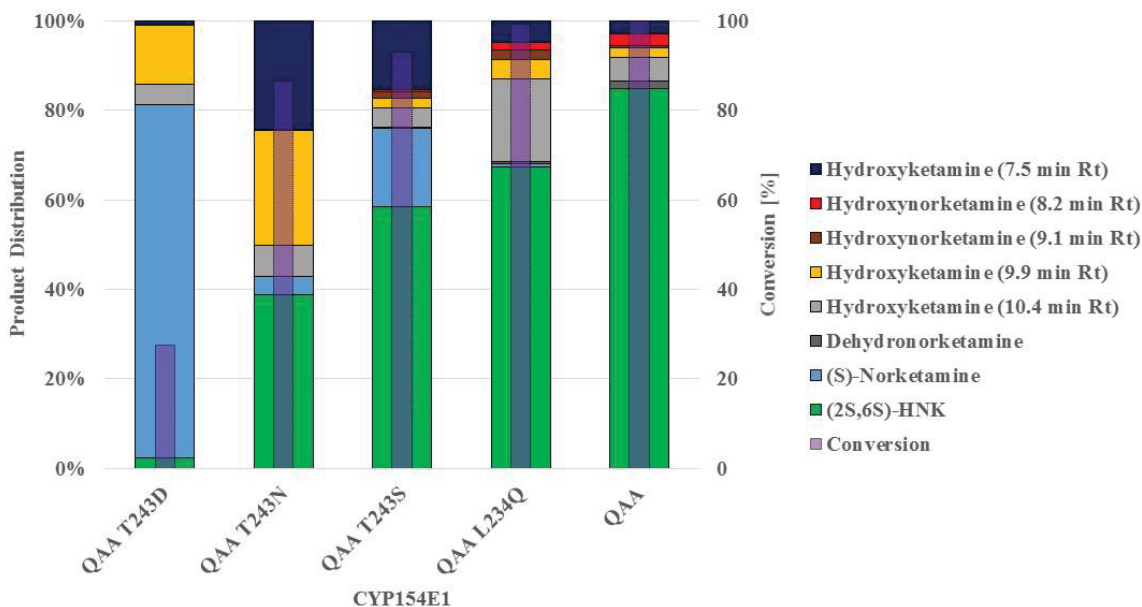


Figure S2. Product distribution and conversion of (*S*)-ketamine with CYP154E1 quadruple mutants in comparison to triple mutant QAA. Green columns represent desired products of (*2S,6S*)-hydroxynorketamine isomers. Mean values are calculated from three separate experiments.

HPLC DATA

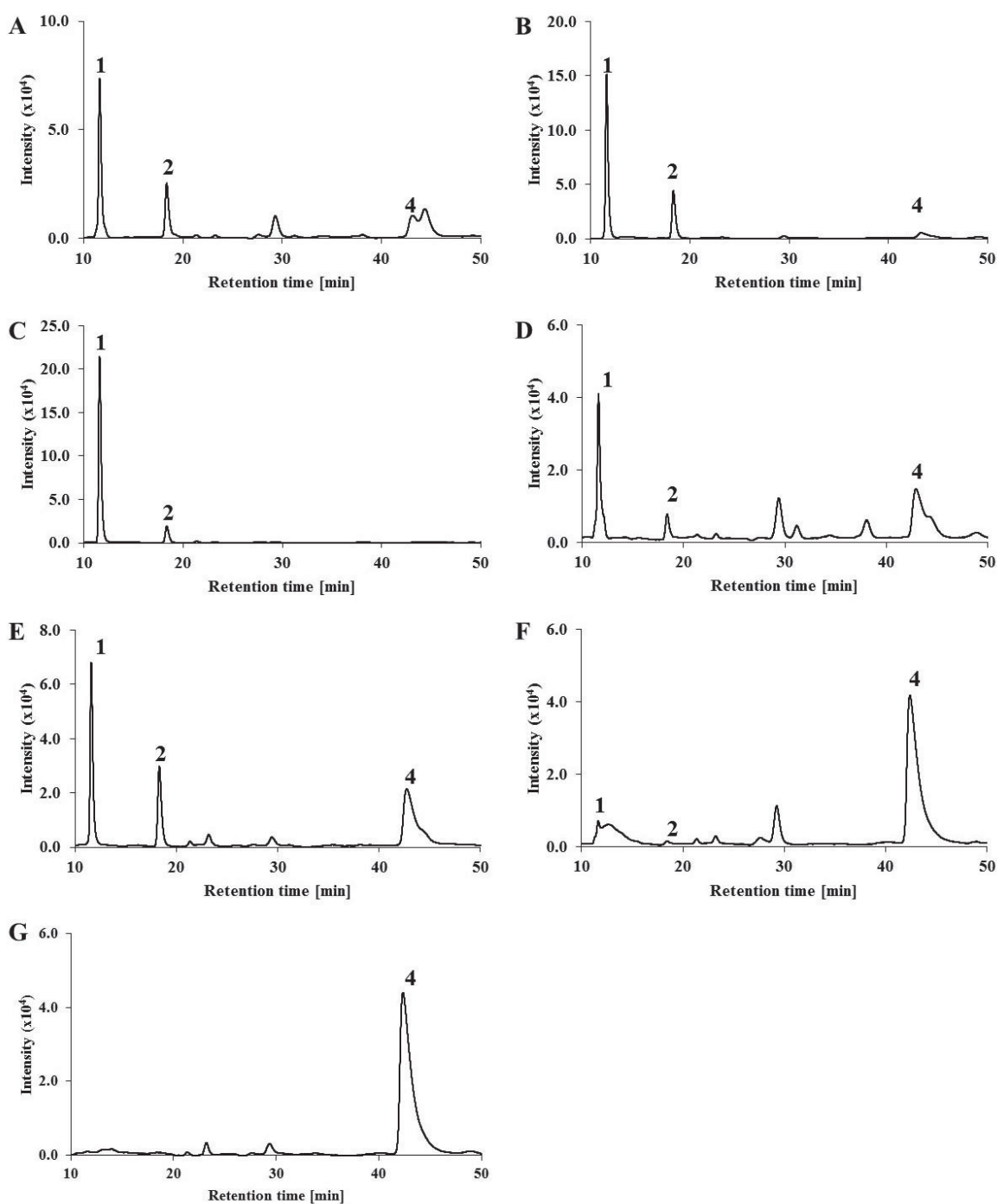


Figure S3. HPLC chromatograms of (*S*)-ketamine oxidation catalyzed by CYP154E1 I238Q (A), G239A (B), M388A (C), I238Q G239A (D), G239A M388A (E), I238Q M388A (F) and QAA (G) analyzed on a chiral Chiralpak IB (0.46 cm \varnothing x 25 cm, Chiral Technologies Europe) column. 1: (*S*)-ketamine, 2: (*S*)-norketamine, 4: (2*S*,6*S*)-hydroxynorketamine (identified by comparing with authentic standard).

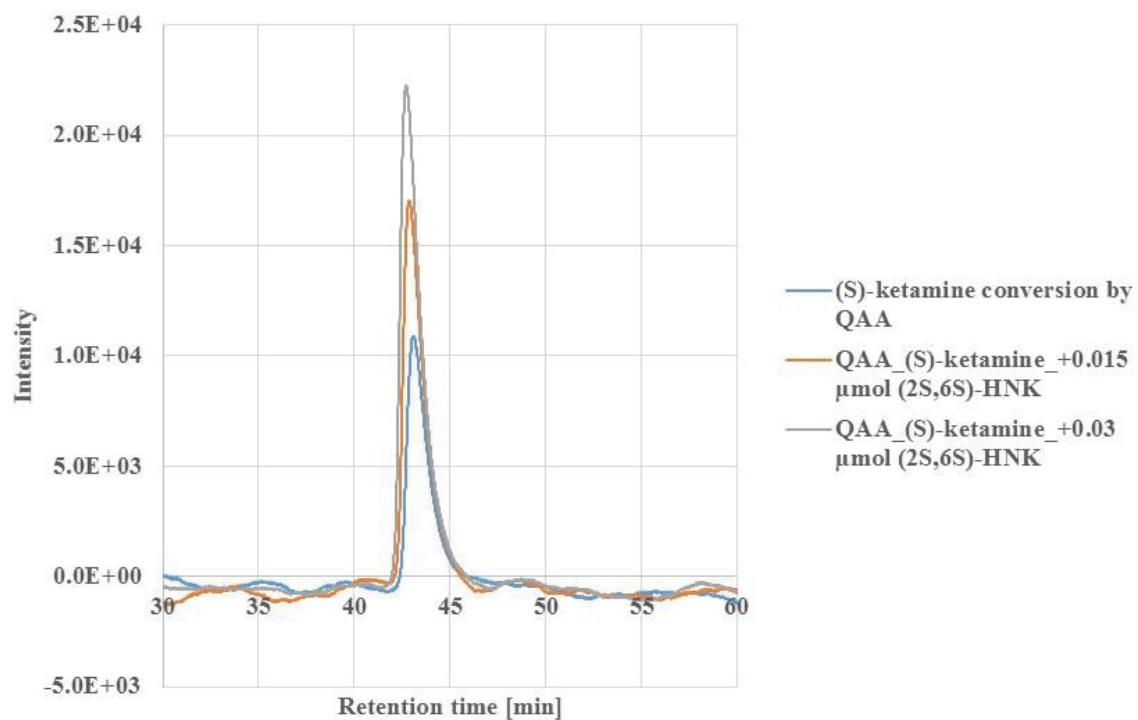


Figure S4. (2*S*,6*S*)-HNK product identification by spiking. Blue: Conversion of 500 μM (*S*)-ketamine by CYP154E1 QAA; orange: blue + 0.015 μmol (2*S*,6*S*)-HNK standard; grey: blue + 0.03 μmol (2*S*,6*S*)-HNK standard. Analytics were carried out with chiral column Chiralpak IB (0.46 cm \varnothing x 25 cm, Chiral Technologies Europe) on HPLC.

CYP154E1 QAA CHARACTERIZATION

SUBSTRATE BINDING SPECTRA FOR CYP154E1 QAA WITH (S)-KETAMINE

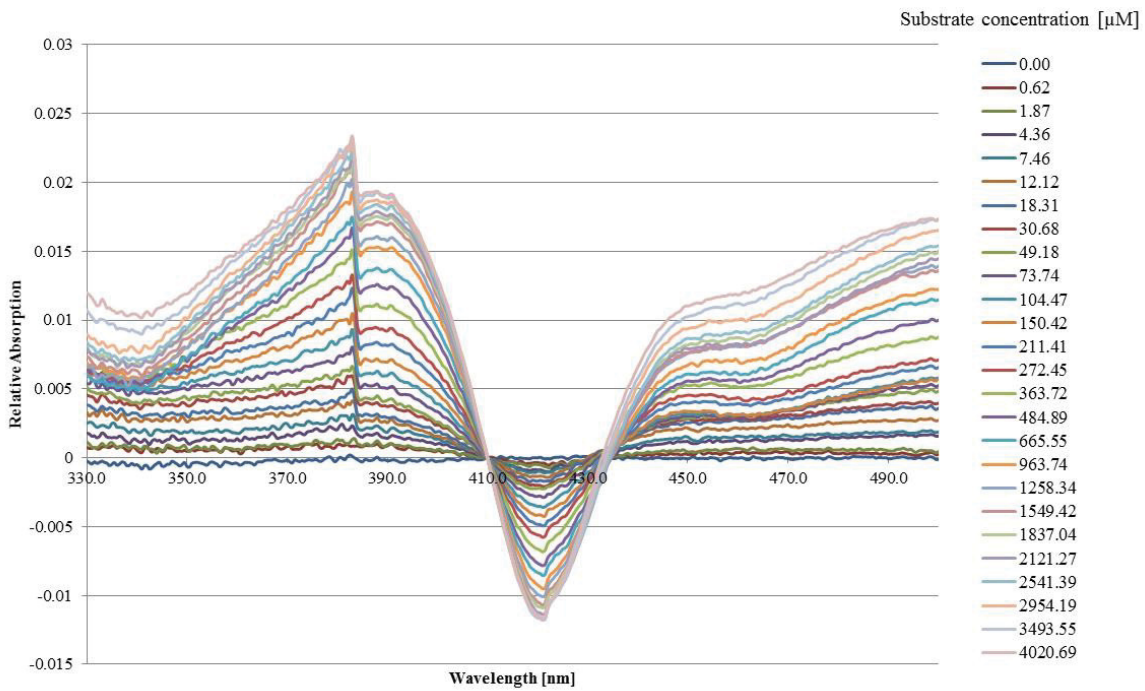


Figure S5. Substrate binding spectrum of CYP154E1 QAA with (S)-ketamine.

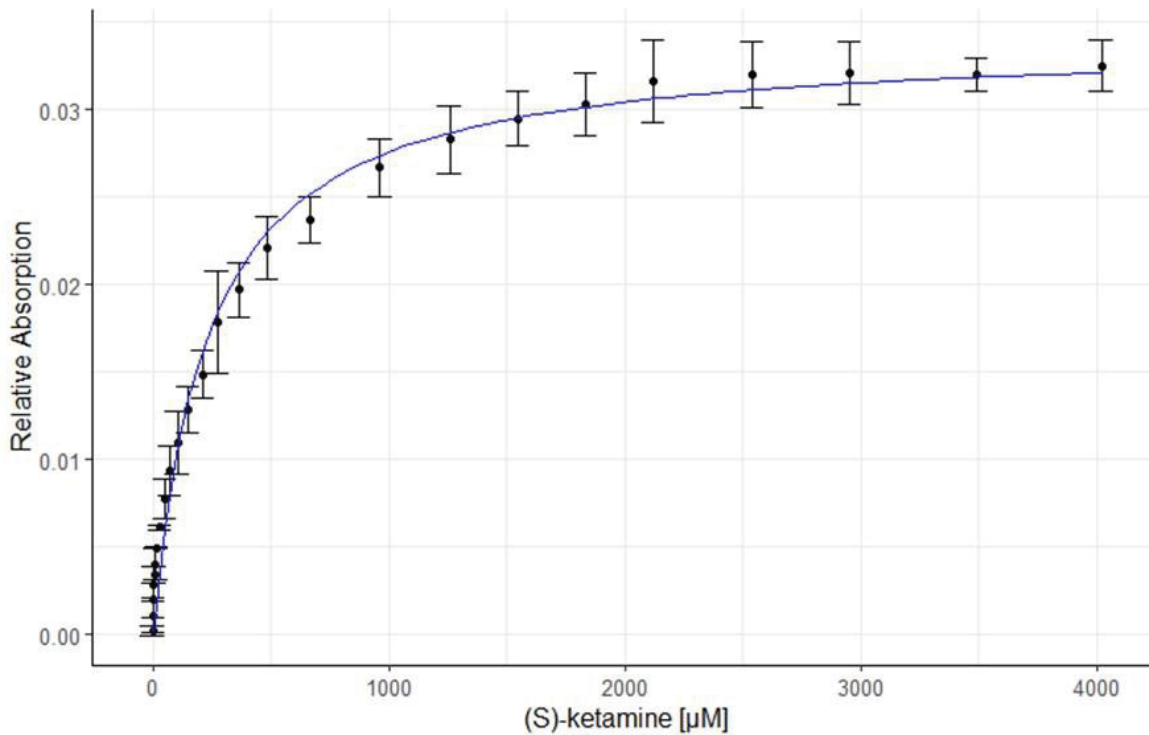


Figure S6. K_d -constant estimation. Plotting was done by using a Michaelis-Menten-like equation (see MM) using RStudio software (RStudio Team (2015). RStudio: Integrated Development for R. RStudio, Inc., Boston, MA URL <http://www.rstudio.com/>).

KINETICS

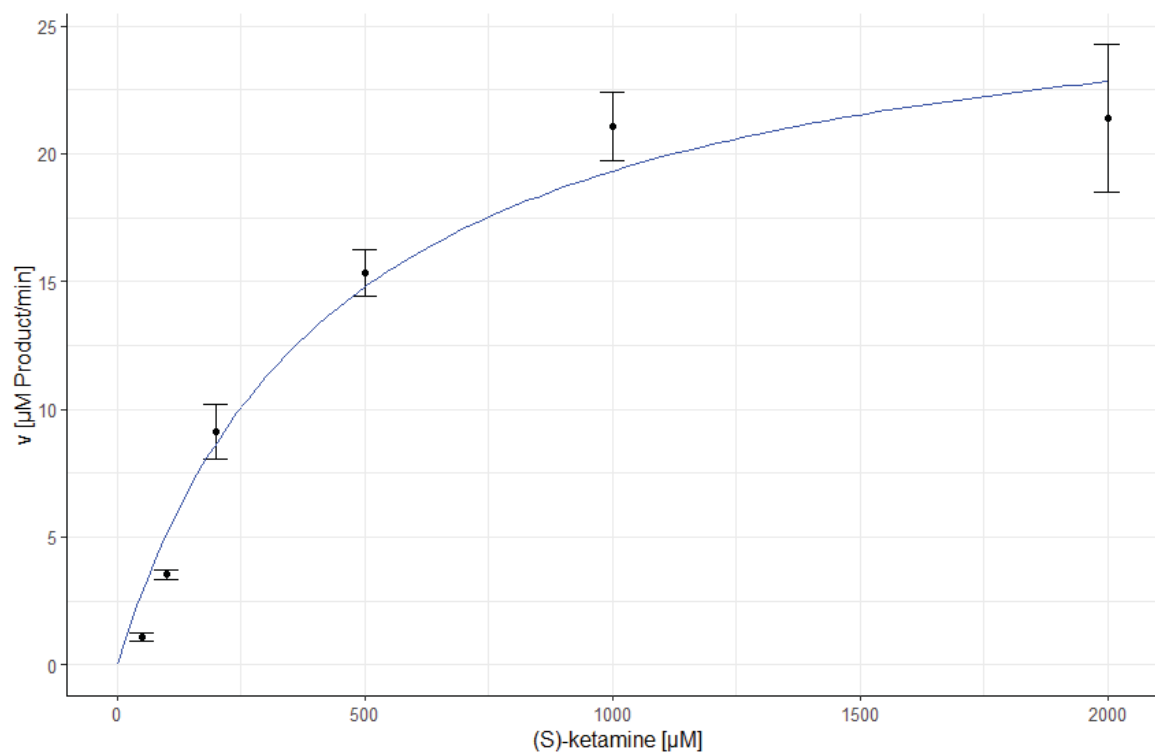


Figure S7. Reaction velocity depending on the (*S*)-ketamine concentration. Plotting was done by using the Michaelis-Menten equation using RStudio software (RStudio Team (2015). RStudio: Integrated Development for R. RStudio, Inc., Boston, MA URL <http://www.rstudio.com/>).

RIGID DOCKING OF (2*S*,6*S*)-HYDROXYKETAMINE

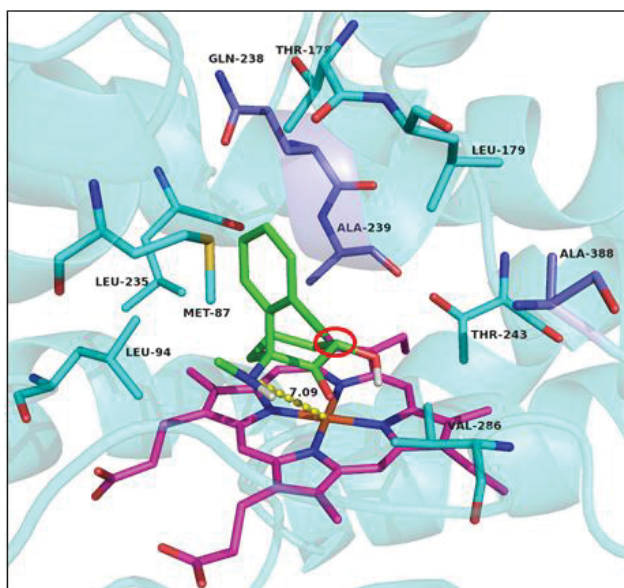


Figure S8. Best scored rigid docking poses of (2*S*,6*S*)-hydroxyketamine in the active site of CYP154E1 QAA. Position C6 of the cyclohexane ring is marked by red circle. Dashed yellow lines indicate distances between atoms. The numerical distance is given in Å.

PREPARATIVE SCALE CONVERSION

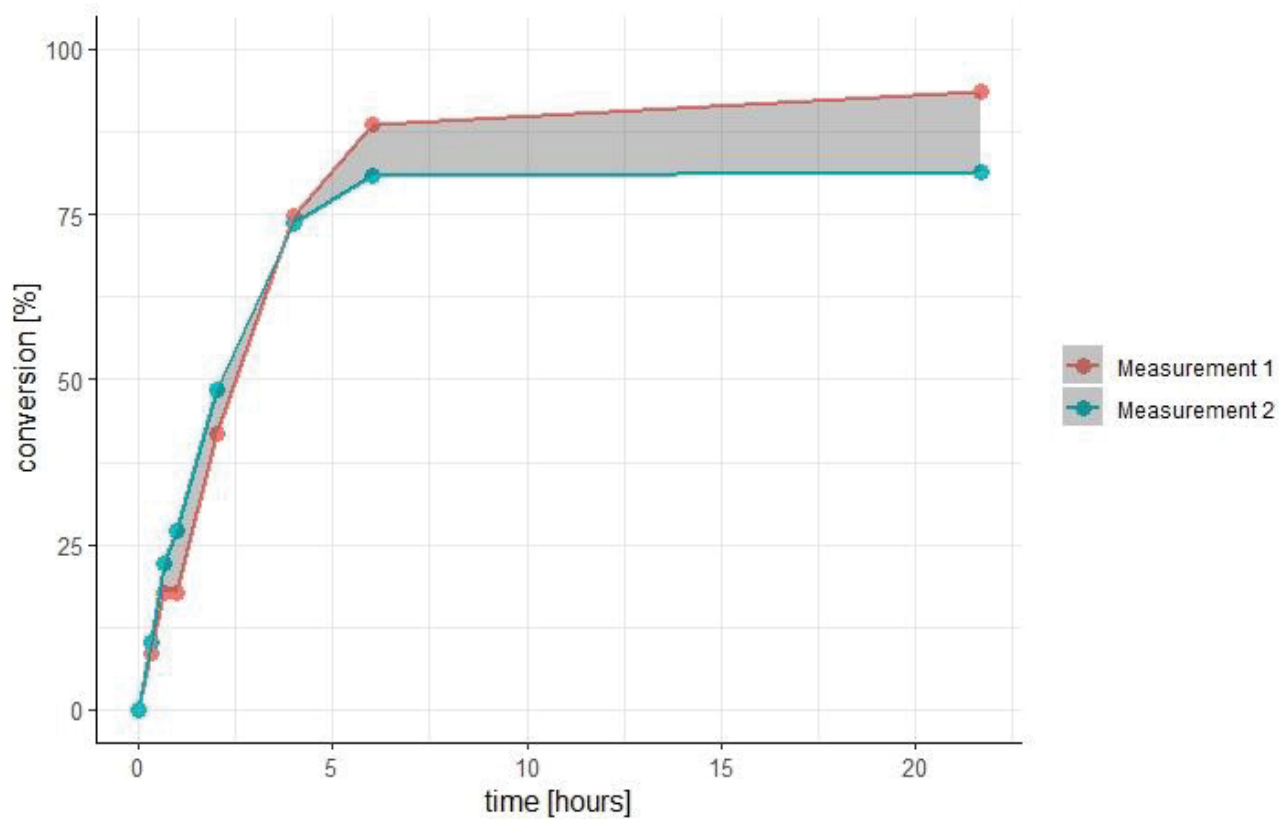


Figure S9. (*S*)-ketamine (5 mM) conversion in 10 ml whole cell biotransformation approach over a period of 21.67 hours in biological duplicate. Plotting was done using RStudio software (RStudio Team (2015). RStudio: Integrated Development for R. RStudio, Inc., Boston, MA URL <http://www.rstudio.com/>).

NMR ANALYSIS

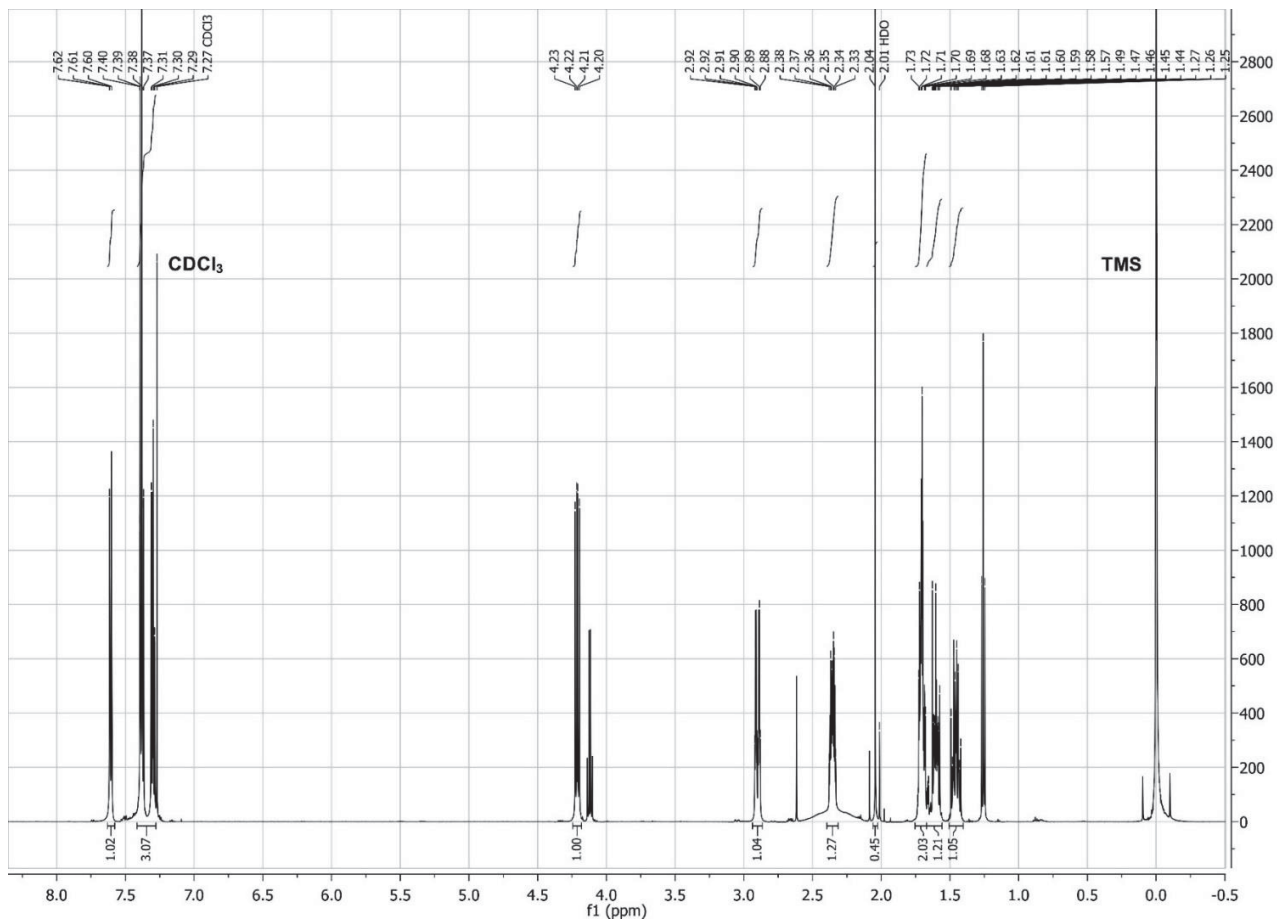


Figure S10. ¹H NMR of (2*S*,6*S*)-hydroxynorketamine in CDCl₃.

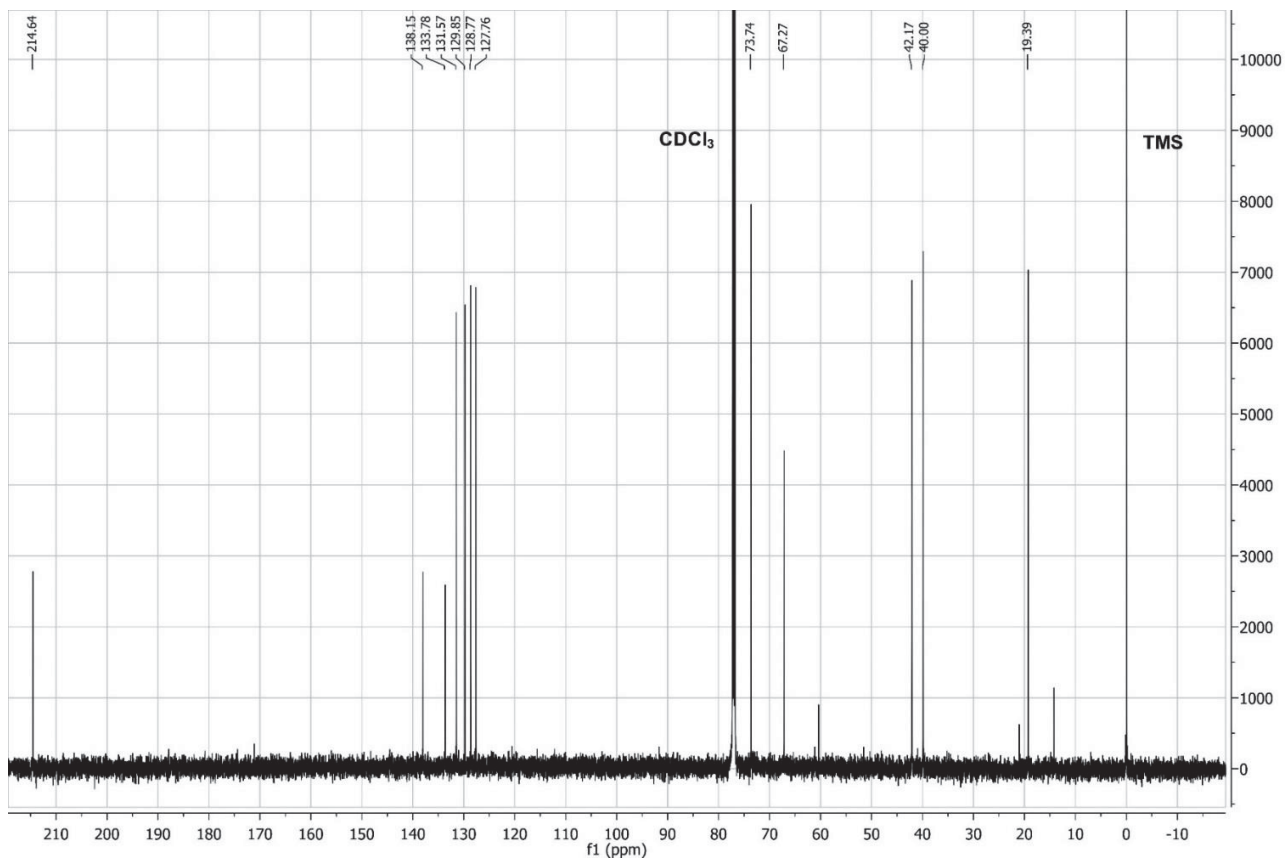


Figure S11. ^{13}C NMR of (2S,6S)-hydroxynorketamine in CDCl_3 .

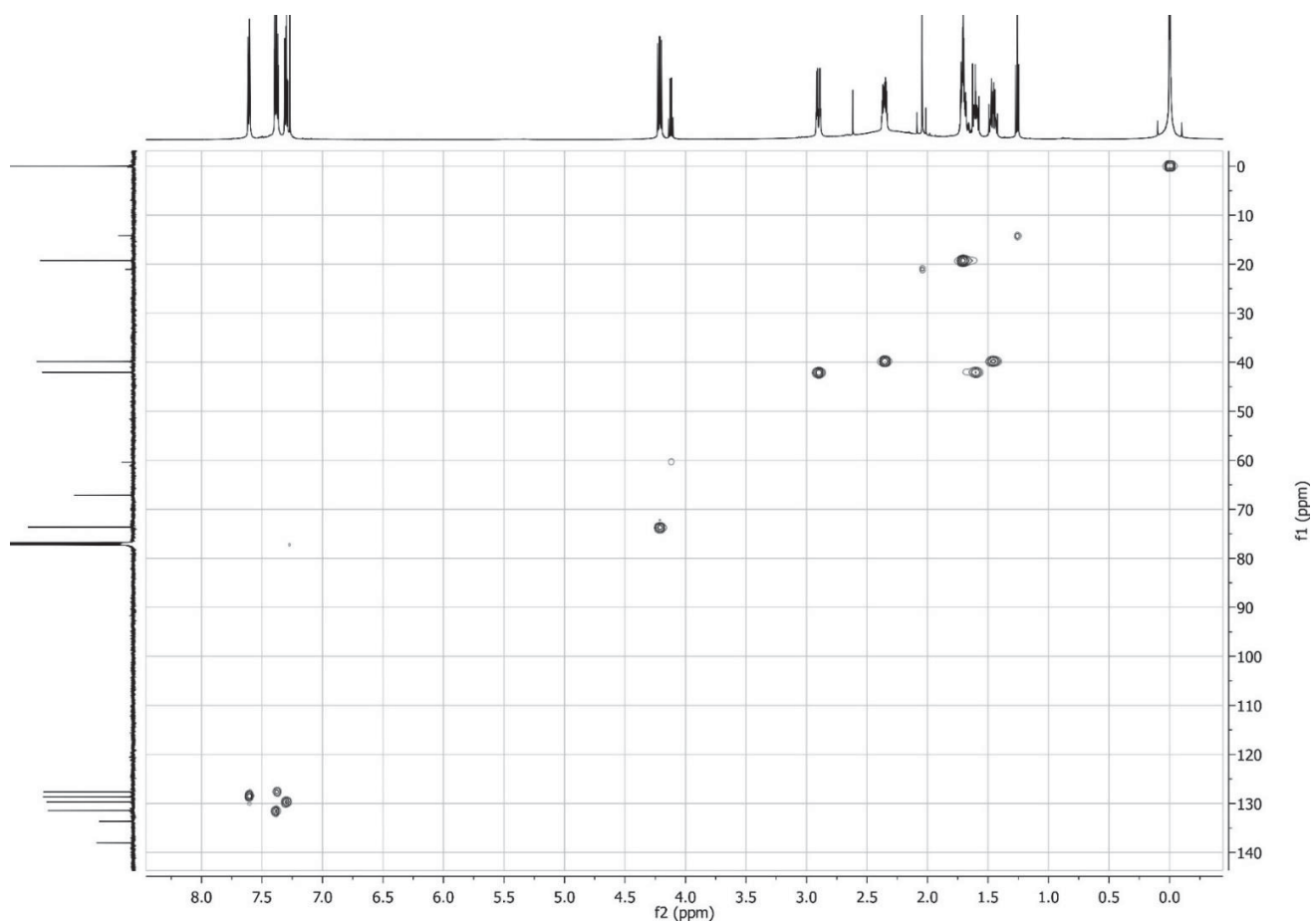


Figure S12. ^1H - ^{13}C HSQC spectrum of (2*S*,6*S*)-hydroxynorketamine in CDCl_3 .

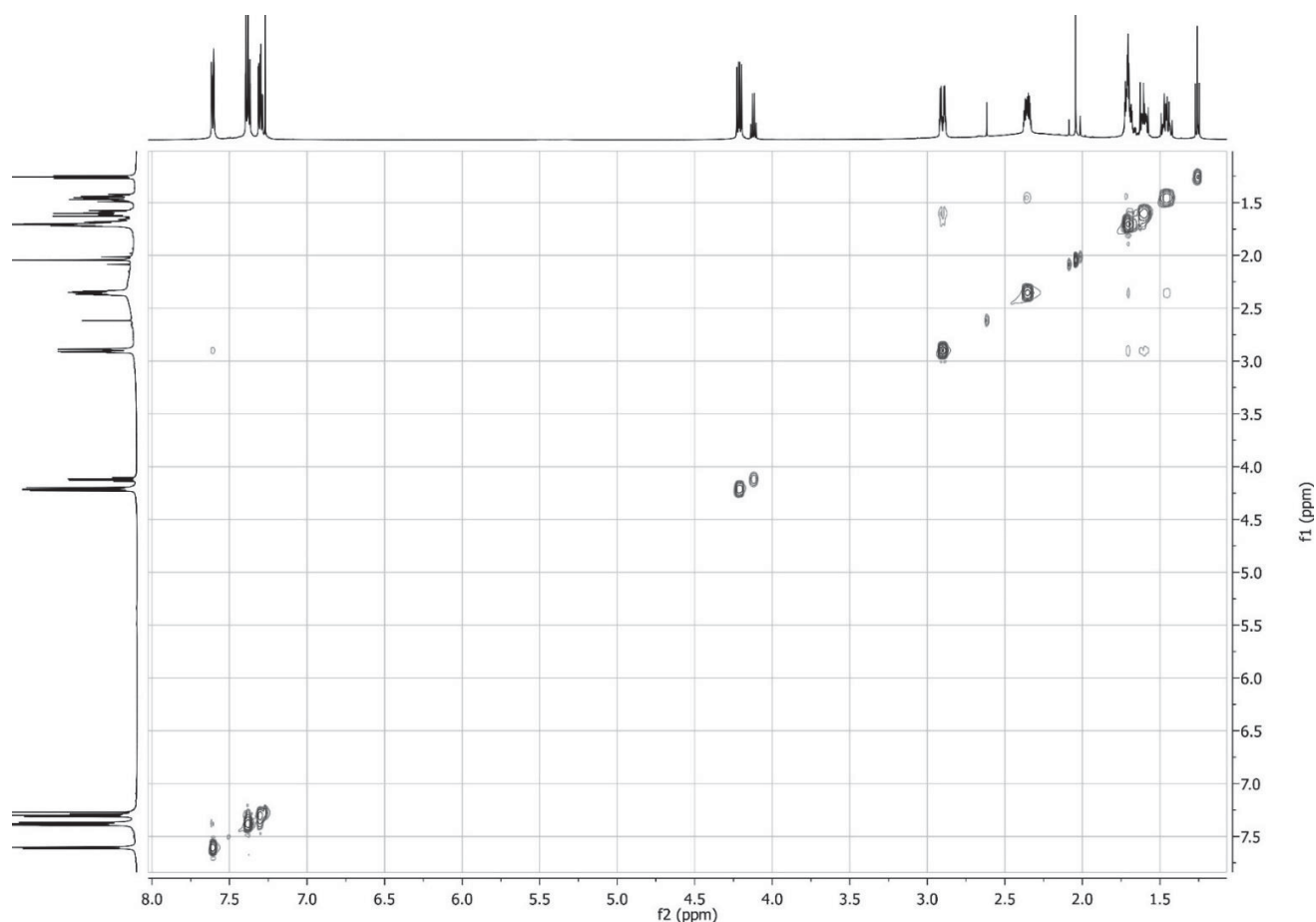


Figure S13. ^1H - ^1H NOESY spectrum of (2*S*,6*S*)-hydroxynorketamine in CDCl_3 .

REFERENCES

- (1) Edelheit, O.; Hanukoglu, A.; Hanukoglu, I. Simple and Efficient Site-Directed Mutagenesis Using Two Single-Primer Reactions in Parallel to Generate Mutants for Protein Structure-Function Studies. *BMC Biotechnol.* **2009**, *9*.
- (2) Girhard, M.; Klaus, T.; Khatri, Y.; Bernhardt, R.; Urlacher, V. B. Characterization of the Versatile Monooxygenase Cyp109b1 from *Bacillus Subtilis*. *Appl. Microbiol. Biotechnol.* **2010**, *87*, 595-607.
- (3) Le-Huu, P.; Heidt, T.; Claasen, B.; Laschat, S.; Urlacher, V. B. Chemo-, Regio-, and Stereoselective Oxidation of the Monocyclic Diterpenoid B-Cembrenediol by P450 BM3. *ACS Catalysis* **2015**, *5*, 1772-1780.
- (4) Omura, T.; Sato, R. The Carbon Monoxide-Binding Pigment of Liver Microsomes. *J. Biol. Chem.* **1964**, *239*, 2379-2385.
- (5) Fujii, K.; Huennekens, F. M. Activation of Methionine Synthetase by a Reduced Triphosphopyridine Nucleotide-Dependent Flavoprotein System. *The Journal of Biological Chemistry* **1974**, *249*, 6745-6753.
- (6) McIver, L.; Leadbeater, C.; Campopiano, D. J.; Baxter, R. L.; Daff, S. N.; Chapman, S. K.; Munro, A. W. Characterisation of Flavodoxin NADP⁺ Oxidoreductase and Flavodoxin; Key Components of Electron Transfer in *Escherichia Coli*. *Eur. J. Biochem.* **1998**, *257*, 577-585.
- (7) Wang, Z.-Q.; Lawson, R. J.; Buddha, M. R.; Wei, C.-C.; Crane, B. R.; Munro, A. W.; Stuehr, D. J. Bacterial Flavodoxins Support Nitric Oxide Production by *Bacillus Subtilis* Nitric-Oxide Synthase. *J. Biol. Chem.* **2007**, *282*, 2196-2202.
- (8) Lawson, R. J.; von Wachenfeldt, C.; Haq, I.; Perkins, J.; Munro, A. W. Expression and Characterization of the Two Flavodoxin Proteins of *Bacillus Subtilis*, Ykun and Ykup: Biophysical Properties and Interactions with Cytochrome P450 Bioi. *Biochemistry* **2004**, *43*, 12390-12409.

Electronic Supplementary Information

Molecular evolution of a cytochrome P450 for the synthesis of potential antidepressant (2*R*,6*R*)-hydroxynorketamine

Ansgar Bokel,^a Michael C. Hutter,^b and Vlada B. Urlacher^{*a}

^a Institute of Biochemistry, Heinrich-Heine University Düsseldorf, Universitätsstr. 1, 40225 Düsseldorf, Germany

^b Center for Bioinformatics, Saarland University, Campus E2.1, 66123 Saarbruecken, Germany

*E-mail: Vlada.Urlacher@uni-duesseldorf.de

Table of contents

| | |
|---|----|
| Oligonucleotides | 2 |
| Isolation of (<i>R</i>)-Ketamine from Racemic Ketamine | 3 |
| Enzyme Expression and Assays | 5 |
| Mutagenesis and Screening | 5 |
| Initial Screening for CYP154E1 Starting Variant..... | 10 |
| Kinetics | 11 |
| Identification of the Desired Product (2 <i>R</i> ,6 <i>R</i>)-Hydroxynorketamine by Spiking | 12 |
| LC/MS Analysis of (2 <i>R</i> ,4 <i>S</i>)-Hydroxyketamine Conversion | 13 |
| NMR Analysis | 14 |
| Docking of (<i>R</i>)-Ketamine and (<i>R</i>)-Norketamine | 20 |
| References | 20 |

Material and Methods

OLIGONUCLEOTIDES

Table S1. Oligonucleotides for cloning and site-saturation mutagenesis. The codons for mutated positions are underlined. Primers for the mutations that were already available in the lab are not listed below. Fw: forward primer; Rev: reverse primer. Sat_ultrashort: binds at the 5'-end of the gene; Sat_short: binds 354 bp upstream of the 5'-end; Sat_long: binds 4958 bp upstream of the 5' end.

| Primer for MegaPrimer PCR | Sequence (5'→ 3') |
|--|---|
| Rev: CYP154E1 I238Q M388A M87_NNK | GAT TCC ACG CGC AGM <u>NNG</u> TTG GCG ACC GGA TG |
| Rev: CYP154E1 I238Q M388A L94_NNK | TCC GGA GCG GGC <u>MNN</u> CAT GGA TTC CAC G |
| Rev: CYP154E1 I238Q M388A L235_NNK | CCG CCC TGG ATG AGM <u>NNC</u> AGC GTG TTG TGG |
| Rev: CYP154E1 I238Q M388A G239_NNK | TGG TTT CGA ACC <u>CMN</u> NCT GGA TGA GCA GC |
| Rev: CYP154E1 I238Q M388A T243_NNK | GCT GAT CAT GCC CAT GGT <u>MNN</u> TTC GAA CCC GCC CTG GAT GAG |
| Rev: CYP154E1 I238Q M388A V286_NNK | GAA CGG CAG CAT GAC <u>MNN</u> CGC TGA TTC GAA G |
| Rev: CYP154E1 I238Q M388A L289_NNK | CGT GGT GTA CAG GAA CGG <u>MNN</u> CAT GAC CAC CGC TGA TTC G |
| Fw: Sat_ultrashort | GGA GAT ATA CAT ATG GGA CAG TCC CGC CGA CC |
| Fw: Sat_short | CCT GCA TTA GGA AGC AGC CCA GTA GTA GGT TGA GGC CGT TG |
| Fw: Sat_long | TGG TTC ACG TAG TGG GCC ATC GCC CTG ATA GAC GG |
| Primer for QuikChange | |
| Fw: CYP154E1 L289T | CGA ATC AGC GGT GGT CAT <u>GAC</u> <u>GCC</u> GTT CCT GTA CAC CAC G |
| Rev: CYP154E1 L289T | CGT GGT GTA CAG GAA CGG <u>CGT</u> CAT GAC CAC CGC TGA TTC G |
| Fw: CYP154E1 L289T (I238Q M388A V286G) | CGA ATC AGC <u>GGG</u> <u>CGT</u> CAT <u>GAC</u> <u>GCC</u> GTT CCT GTA CAC CAC G |
| Rev: CYP154E1 L289T (I238Q M388A V286G) | CGT GGT GTA CAG GAA CGG <u>CGT</u> CAT GAC <u>GCC</u> CGC TGA TTC G |
| Fw: CYP154E1 I238A | CAA CAC GCT GCT GCT CAT <u>CGC</u> <u>GGG</u> CGG GTT CGA AAC C |
| Rev: CYP154E1 I238A | GGT TTC GAA CCC GCC <u>CGC</u> GAT GAG CAG CAG CGT GTT G |
| Fw: CYP154E1 I238C | CAA CAC GCT GCT GCT CAT <u>CTG</u> <u>CGG</u> CGG GTT CGA AAC C |
| Rev: CYP154E1 I238C | GGT TTC GAA CCC GCC <u>GCA</u> GAT GAG CAG CAG CGT GTT G |
| Fw: CYP154E1 I238D | GCT GCT GCT CAT <u>CGA</u> <u>CGG</u> CGG GTT CGA AAC CAC |
| Rev: CYP154E1 I238D | GTG GTT TCG AAC CCG <u>CCG</u> <u>TCG</u> ATG AGC AGC AGC |
| Fw: CYP154E1 I238E | GCT GCT GCT CAT <u>CGA</u> <u>GGG</u> CGG GTT CGA AAC CAC |
| Rev: CYP154E1 I238E | GTG GTT TCG AAC CCG <u>CCG</u> <u>TCG</u> ATG AGC AGC AGC |
| Fw: CYP154E1 I238F | GCT GCT GCT CAT <u>CTT</u> <u>CGG</u> CGG GTT CGA AAC CAC |
| Rev: CYP154E1 I238F | GTG GTT TCG AAC CCG <u>CCG</u> <u>AAG</u> ATG AGC AGC AGC |
| Fw: CYP154E1 I238G | CAA CAC GCT GCT GCT CAT <u>CGG</u> <u>CGG</u> CGG GTT CGA AAC C |
| Rev: CYP154E1 I238G | GGT TTC GAA CCC GCC <u>GCC</u> GAT GAG CAG CAG CGT GTT G |
| Fw: CYP154E1 I238H | CAA CAC GCT GCT GCT CAT <u>CCA</u> <u>CGG</u> CGG GTT CGA AAC C |
| Rev: CYP154E1 I238H | GGT TTC GAA CCC GCC <u>GTG</u> GAT GAG CAG CAG CGT GTT G |
| Fw: CYP154E1 I238K | CAA CAC GCT GCT GCT CAT <u>CAA</u> <u>AGG</u> CGG GTT CGA AAC C |
| Rev: CYP154E1 I238K | GGT TTC GAA CCC GCC <u>TTT</u> GAT GAG CAG CAG CGT GTT G |
| Fw: CYP154E1 I238L | CAA CAC GCT GCT GCT CAT <u>CCT</u> <u>GGG</u> CGG GTT CGA AAC C |

| | |
|---------------------|---|
| Rev: CYP154E1 I238L | GGT TTC GAA CCC GCC <u>CAG</u> GAT GAG CAG CAG CGT GTT G |
| Fw: CYP154E1 I238M | CAA CAC GCT GCT GCT CAT <u>CAT</u> <u>GGG</u> CGG GTT CGA AAC C |
| Rev: CYP154E1 I238M | GGT TTC GAA CCC GCC <u>CAT</u> GAT GAG CAG CAG CGT GTT G |
| Fw: CYP154E1 I238N | GCT GCT GCT CAT <u>CAA</u> <u>CGG</u> CGG GTT CGA AAC CAC |
| Rev: CYP154E1 I238N | GTG GTT TCG AAC CCG <u>CCG</u> <u>TTG</u> ATG AGC AGC AGC |
| Fw: CYP154E1 I238P | CAA CAC GCT GCT GCT CAT <u>CCC</u> <u>GGG</u> CGG GTT CGA AAC C |
| Rev: CYP154E1 I238P | GGT TTC GAA CCC GCC <u>CGG</u> GAT GAG CAG CAG CGT GTT G |
| Fw: CYP154E1 I238Q | GCT GCT GCT CAT <u>CCA</u> <u>GGG</u> CGG GTT CGA AAC CAC |
| Rev: CYP154E1 I238Q | GTG GTT TCG AAC CCG <u>CCC</u> <u>TGG</u> ATG AGC AGC AGC |
| Fw: CYP154E1 I238R | CAA CAC GCT GCT GCT CAT <u>CCG</u> <u>TGG</u> CGG GTT CGA AAC C |
| Rev: CYP154E1 I238R | GGT TTC GAA CCC GCC <u>ACG</u> GAT GAG CAG CAG CGT GTT G |
| Fw: CYP154E1 I238S | GCT GCT GCT CAT <u>CAG</u> <u>TGG</u> CGG GTT CGA AAC CAC |
| Rev: CYP154E1 I238S | GTG GTT TCG AAC CCG <u>CCA</u> <u>CTG</u> ATG AGC AGC AGC |
| Fw: CYP154E1 I238T | GCT GCT GCT CAT <u>CAC</u> <u>CGG</u> CGG GTT CGA AAC CAC |
| Rev: CYP154E1 I238T | GTG GTT TCG AAC CCG <u>CCG</u> <u>GTG</u> ATG AGC AGC AGC |
| Fw: CYP154E1 I238V | CAA CAC GCT GCT GCT CAT <u>CGT</u> <u>GGG</u> CGG GTT CGA AAC C |
| Rev: CYP154E1 I238V | GGT TTC GAA CCC GCC <u>CAC</u> GAT GAG CAG CAG CGT GTT G |
| Fw: CYP154E1 I238W | CAA CAC GCT GCT GCT CAT <u>CTG</u> <u>GGG</u> CGG GTT CGA AAC C |
| Rev: CYP154E1 I238W | GGT TTC GAA CCC GCC <u>CCA</u> GAT GAG CAG CAG CGT GTT G |
| Fw: CYP154E1 I238Y | CAA CAC GCT GCT GCT CAT <u>CIA</u> <u>CGG</u> CGG GTT CGA AAC C |
| Rev: CYP154E1 I238Y | GGT TTC GAA CCC GCC <u>GTA</u> GAT GAG CAG CAG CGT GTT G |

ISOLATION OF (*R*)-KETAMINE FROM RACEMIC KETAMINE

Isolation of (*R*)-ketamine from racemic ketamine hydrochloride was done according to patent DE60131397T2.¹ First, the free base form of racemic ketamine was generated. To this end, 4.97 g racemic ketamine hydrochloride were dissolved in 400 ml water; 1 M sodium carbonate was added till the pH of the solution reached pH 9.0. White sediment (freebase form of racemic ketamine) was filtrated under vacuum and dried at 37°C. Yield: 2.62 g. The filtrate containing remains of racemic ketamine freebase was extracted twice with 250 ml ethyl acetate. Organic phase was dried over sodium sulfate, filtered, and fully evaporated. Yield: 1.296 g. Combined isolated yield of racemic ketamine freebase was 3.916 g. In a two-necked flask, 4.93 g of ketamine freebase (additional ketamine freebase originates from a previous attempt) were dissolved in 63.1 ml acetone under constant stirring and heating. A reflux condenser was used to condense gaseous acetone. 1.89 g L-(+)-tartaric acid and 4.2 ml water were added and the solution was heated to 55°C. Temperature was hold for 15 minutes and afterwards the solution was cooled down to room temperatrue (RT) under stirring, which hold overnight. A white sediment occurred ((*S*)-ketamine tartrate), which was filtered under vacuum. The filtered white solid was stirred for 1.5 hours in 16 ml acetone - to remove remains of (*R*)-ketamine tartrate - and filtrated again (white solid was dried and stored at 4°C). The filtrates from both filtration steps were combined and evaporated to dryness ((*R*)-ketamine tartrate). Yield: 2.816 g. 2.816

g (*R*)-ketamine tartrate were dissolved in 28 ml 1 M HCl and a solution of 25% ammonium hydroxide was added until the pH reached 12. White precipitate ((*R*)-ketamine freebase) was filtered under vacuum and the purity was analyzed via chiral HPLC (Figure S1). Yield: 2.061 g; purity: ~90%. In order to increase the purity, the product was recrystallized: 2 g (*R*)-ketamine freebase were dissolved in 30 ml *n*-hexane under constant stirring and heated to the boiling point of *n*-hexane. A reflux condenser was used to condense gaseous *n*-hexane. More *n*-hexane was added stepwise until all (*R*)-ketamine was dissolved. The final solution was kept at boiling point for another 10 min before cooling down to RT overnight. Finally, the solution was cooled on ice and the white precipitate was filtered under vacuum and dried at 37°C. Yield: 1.82 g; Purity analyzed via chiral HPLC was ~99%. Finally, (*R*)-ketamine hydrochloride was synthesized. 1.8 g (*R*)-ketamine freebase were dissolved in 50 ml ethanol (HPLC grade). 37% HCl solution was added until the pH reached 2. The solution was cooled to 15°C before 51 ml diethyl ether were added and stirred for one hour at 15°C. Again, the precipitate was filtered under vacuum and the filtrate was saturated again with 37% HCl, stirred for another hour at 15°C and the precipitate again filtered under vacuum. The precipitates were combined, dissolved in 22 ml of a 1:1 mixture of ethanol and diethyl ether, stirred for 30 min and filtered under vacuum. The white powder was dried at 37°C. Yield: 1.04 g (37% yield when starting from 4.93 g ketamine freebase).

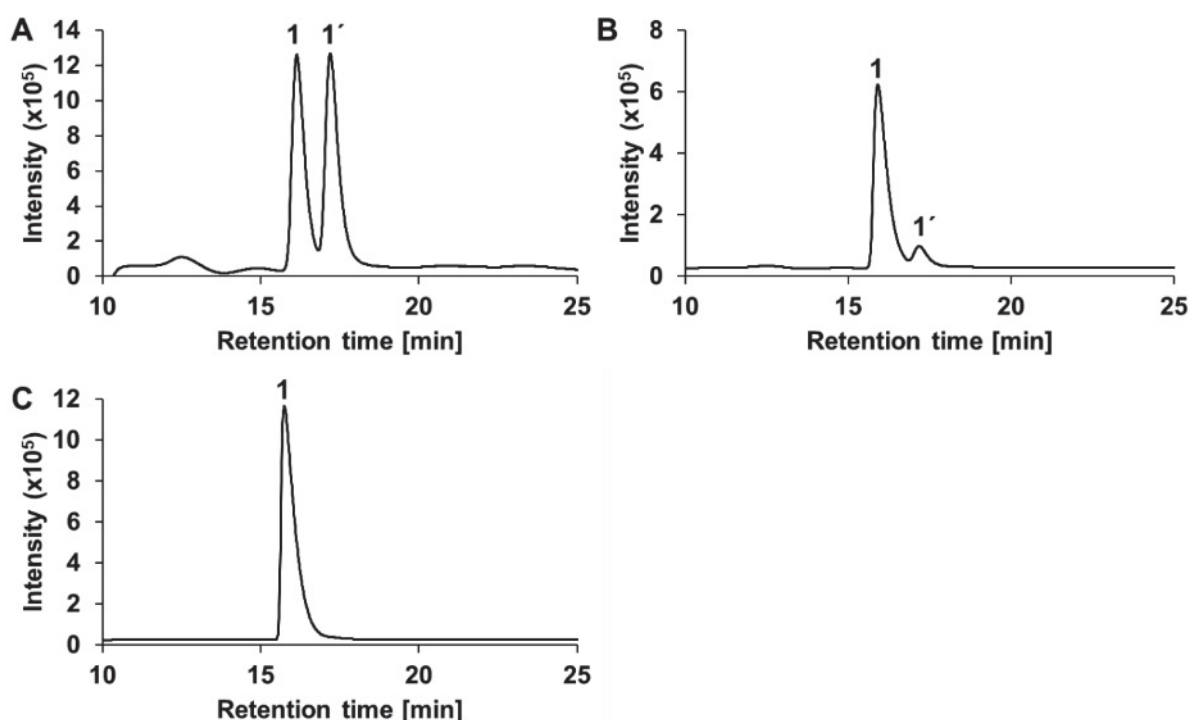


Fig. S1. Chiral HPLC analysis of the intermediates during (*R*)-ketamine isolation from racemic ketamine: Racemic ketamine (**A**); (*R*)-ketamine free base after isolation (**B**) and after recrystallization (**C**). Analysis was carried out using HPLC on a chiral column Chiralpak IB (0.46 cm Ø x 25 cm, Chiral Technologies Europe). **1**: (*R*)-ketamine, **1'**: (*S*)-ketamine (identified by comparing with authentic standard from Sigma Aldrich).

ENZYME EXPRESSION AND ASSAYS

Expression and purification of the redox proteins, the flavodoxin reductase FdR from *Escherichia coli* and the flavodoxin YkuN from *Bacillus subtilis*, as well as the expression of the NADPH regenerating glucose dehydrogenase (GDH) from *Bacillus megaterium* (vector pET22b) and the CYP154E1 variants (vector pET22b and pET28a) were performed as previously described.²

Concentrations of cytochrome P450 enzymes (in *E. coli* cell lysates) were determined based on the CO-difference spectra as previously described. Once a sample was saturated with CO and subsequently reduced with sodium dithionite (50 mM), absorption spectra were recorded between 400 and 500 nm. The P450 concentration was calculated using the extinction coefficient of $\epsilon_{450-490\text{ nm}} = 91\text{ mM}^{-1}\text{ cm}^{-1}$.³ Concentrations of the purified redox proteins YkuN and FdR, as well as the NADP⁺ reduction activity of the GDH were determined as described elsewhere.⁴

MUTAGENESIS AND SCREENING

Construction of the starting variant. Construction of CYP154E1 mutants was carried out according to a modified QuikChange mutagenesis protocol by Edelheit et al. (2009) using two separated single-primer reactions.⁵ Each PCR reaction contained ~500 ng of the template plasmid DNA, 4% DMSO, 0.2 mM dNTPs, 1 U Phusion DNA Polymerase, and either 2 μM forward or reverse primer in a total volume of 25 μl of HF Phusion buffer. Two PCR reactions were carried out in parallel, one with the forward and the other with the reverse primer. The PCR was carried out using the following program: denaturation step at 98°C for 2 min, followed by 30 cycles of 98°C 30 s, annealing for 60 s at 60°C (independent of the primer) and elongation at 72°C for 30 s/kb and a final extension at 72°C for 6 min. Subsequently, mixtures from both PCRs were combined and reannealing of the PCR products occurred according to the program reported by Edelheit et al.⁵ Template DNA was removed by *DpnI* digestion (addition of 1 μl FastDigest *DpnI* [Thermo Fisher Scientific] and incubation for 1 h at 37°C. Afterwards, another 1 μl FastDigest *DpnI* was added and the mixture was incubated overnight at 37°C) prior to transformation of chemically competent *E. coli* DH5 α cells.

Library construction. Construction of the site-saturation sub-libraries was carried out according to Sanchis et al 2008⁶ using primer shown in Table S1. Antiprimer were designed to first generate megaprimer of different length; the antiprimer for the ultrashort megaprimer anneals to the 5'-end of the gene (generating a megaprimer of 287 - 897 bp dependent on the mutation carrying forward primer); the antiprimer for the short megaprimer anneals 354 bp

upstream of the 5'-end of the gene (generating a megaprimer of 641 - 1251 bp dependent on the mutation carrying forward primer), and the antiprimer for the long megaprimer anneals 4958 bp upstream of the 5'-gene end (generating a megaprimer of 5245 - 5855 bp dependent on the mutation carrying forward primer). The first PCR cycle was used to generate the megaprimer and comprised of the following steps: initial denaturation at 98°C for 30 seconds, followed by five cycles at 98°C for 10 s, annealing for 30 s (temperature varied at this step and for all PCRs a temperature gradient was used) and elongation at 72°C for 20 s/kb (using Phusion DNA Polymerase) dependent on the megaprimer length. In the second PCR cycle the whole plasmid was amplified and program comprised of 20 cycles at 98°C for 30 s and at 72°C for 6 min, followed by a final extension at 72°C for 12 min. Each Megaprimer-PCR was controlled via agarose gel electrophoresis. Template DNA was removed by *DpnI* digestion (addition of 1 µl FastDigest *DpnI* [Thermo Fisher Scientific] and incubation for 1 h at 37°C. Afterwards, another 1 µl FastDigest *DpnI* was added and the mixture was incubated overnight at 37°C) prior to purification of the PCR sample and subsequent transformation of electrocompetent *E. coli* DH5α cells. After performing electroporation, one half of *E. coli* cells was spread on LB agar plates, whereas the other half was used to inoculate precultures, which were harvested the next day and used for plasmid preparation and subsequent sequencing. If the sequencing proved the NNK diversity at the desired positions and colony numbers were more than 100 colonies per plate, chemical competent *E. coli* BL21(DE3) pCOLA Duet YkuN (MCSI) FdR (MCSII) cells were transformed with the plasmids from the sub-libraries. Here again, the transformed cells were divided into two parts, and the quality of the library was checked again by sequencing.

Library screening. Colonies for each sub-library were toothpicked and used to inoculate 600 µl LB medium (containing 30 mg/ml kanamycin and 100 mg/ml ampicillin) in 96-deep well plates. After overnight incubation at 37°C and 600 rpm (TiMix 5 Control, Edmund Bühler GmbH), 20 µl of these precultures were used to inoculate expression cultures containing 980 µl autoinduction medium (supplemented with 30 mg/ml kanamycin, 100 mg/ml ampicillin, 100 µM FeSO₄ and 500 µM 5-aminolevulinic acid) per well. 300 µl 86% glycerin were added to the rest of the precultures and frozen at -80°C. The expression cultures were incubated at 37°C and 600 rpm till an OD₆₀₀ of ~ 1.0 was reached (wells A2 -A6 contained BL21(DE) pCOLA Duet YkuN (MCSI) FdR (MCSII) pET22b CYP154E1 I238Q M388A only and wells A2-A5 were used to measure the OD₆₀₀ whereas well A6 served as a control for the conversion of (*R*)-ketamine). After an OD₆₀₀ of ~1.0 was reached, the plates were incubated further at 25°C and 500 rpm overnight. The plates were centrifuged at 4500 rpm for 30 min at 4°C and the cells were washed once with 1 ml per well potassium phosphate buffer pH 7.5 containing sucrose and EDTA-Na₂. Cells were resuspended in 465 µl of the same potassium phosphate buffer; 25 µl

of a nutrient solution containing glucose, lactose and citrate, and 10 μ l of 25 mM (*R*)-ketamine were added. The reaction mixtures were shaken at 25°C and 1000 rpm. After 18 hours, the reactions were stopped by addition of 500 μ l 1 M sodium carbonate and extracted with 400 μ l ethyl acetate. After vigorous shaking and centrifugation, 100 μ l of the organic supernatant were directly transferred to GC/MS glass vials. The GC/MS analysis was done on a GC/MS QP-2010 Plus (Shimadzu, Duisburg, Germany) with a FS-Supreme-5ms (30 m x 0.25 mm x 0.25 μ m) column and helium as carrier gas as previously described.²

Verification of positive mutants. The variants performing better (higher amount of (2*R*,6)-hydroxynorketamine and middle to high conversion) than the CYP154E1 I238Q M388A control (well A6) were sequenced and their performance verified in an *in vitro* conversion of (*R*)-ketamine. To this end, positive mutants were streaked on LB plates containing ampicillin only to get rid of the pCOLA Duet YkuN (MCSI) FdR (MCSII) vector. Single colony was picked to inoculate LB precultures with ampicillin as the only antibiotic. After shaking at 37°C and 180 rpm overnight, 25 μ l of the precultures were used to inoculate new precultures containing again only ampicillin. This was repeated three times to get rid of most of the pCOLA Duet YkuN (MCSI) FdR (MCSII) plasmid (which impairs the *cyp154E1* expression). Further expression of the variants was carried out as described elsewhere.² After expression and cell lysis, oxidation reactions were performed with *E. coli* cell lysates in 100 mM potassium phosphate buffer pH 7.5 in a total reaction volume of 125 μ l at 25°C and 600 rpm. The reaction mixture contained 500 μ M (*R*)-ketamine HCl (dissolved in water), 2.5 μ M P450 (crude cell lysate), 2.5 μ M purified FdR, 25 μ M purified YkuN, 200 μ M NADPH, 5 U/ml GDH in the presence of 20 mM glucose for cofactor regeneration and 600 U/ml catalase. After 18 hours, reactions were stopped by addition of 125 μ l of 1 M Na₂CO₃ and 10 μ l of 5 mM xylazine hydrochloride as internal standard. Reactions were extracted twice with 200 μ l ethyl acetate and the combined organic phases were evaporated to dryness. Evaporated samples were resolved in a 1:1 mixture of acetonitrile and water (for LC/MS analysis) or 100 μ l ethanol (for HPLC analysis) respectively.

Kinetic constants were estimated under the same reaction conditions except for enzyme and substrate concentrations and reaction time. 0.5 μ M CYP, 0.5 μ M FdR and 40 μ M YkuN were used to convert 50 – 2000 μ M substrate, and reactions were stopped after 3 – 17 min. Kinetic data were fitted to the Michaelis-Menten equation using RStudio software (RStudio Team (2015)).⁷

LC/MS analysis was performed on a device consisting of a DGU-20A₃ Degaser, two LC-20AD modules (each for one solvent), a CBM-20A Communications Bus Module, a SPD-M20A Diode Array Detector, a SIL-20A HT Autosampler, and CTO-10AS VP column oven connected to LCMS-2020 (all from Shimadzu). A Chromolith® Performance RP-8e 100-4.6 mm column

(Merck Millipore), equipped with a Chromolith® RP-8e 5-4.6 mm guard cartridge was used. Elution occurred on a gradient between water (supplemented with 0.1% formic acid) and acetonitrile. Stereoselectivity was analyzed via HPLC (same equipment as for LC/MS except for the LCMS-2020 MS unit) equipped with the chiral column Chiralpak IB (0.46 cm Ø x 25 cm, Chiral Technologies Europe) and an isocratic elution mode consisting of 97% n-hexane and 3% ethanol.² Retention time and mass fragmentation patterns (GC/MS and LC/MS) compared to those of the corresponding authentic reference compounds and literature data⁸ were used to identify products and substrates. Conversions were determined via substrate depletion compared to the negative control. Xylazine served as an internal standard. All experiments were performed at least in triplicate.

Spiking experiment. The reaction was carried out as described in the section above. The reaction mixture contained 500 µM (*R*)-ketamine HCl (dissolved in water), 2.5 µM CYP154E1 L289T/I2238Q/M388A, 2.5 µM purified FdR, 25 µM purified YkuN, 200 µM NADPH, 5 U/ml GDH in the presence of 20 mM glucose for cofactor regeneration and 600 U/ml catalase. After 18 hours, reactions were stopped by addition of 125 µl of 1 M Na₂CO₃. The reaction was extracted twice with 200 µl ethyl acetate and the combined organic phases were evaporated to dryness. The evaporated sample was resolved in 100 µl ethanol and analyzed via HPLC equipped with the chiral column Chiralpak IB. After the HPLC analysis, 0.0167 µmol of authentic (*2R,6R*)-HNK (4.5 µl 3.7 mM freebase) were added to the same HPLC vial, which was then measured again. This procedure was repeated: 0.033 µmol of (*2R,6R*)-HNK standard was added to the same vial and measurement again.

Oxidation of (*2R,4S*)-hydroxyketamine. The reaction was carried out as described in the section “Verification of positive mutants”. The reaction mixture contained 500 µM (*2R,4S*)-hydroxyketamine freebase (dissolved in DMSO), 2.5 µM CYP154E1 V286G/I238Q/M388A (crude cell lysate), 2.5 µM purified FdR, 25 µM purified YkuN, 200 µM NADPH, 5 U/ml GDH in the presence of 20 mM glucose for cofactor regeneration and 600 U/ml catalase. After 18 hours, reactions were stopped by addition of 125 µl of 1 M Na₂CO₃ and 10 µl of 12 mM xylazine hydrochloride as internal standard. Reactions were extracted twice with 200 µl ethyl acetate and the combined organic phases were evaporated to dryness. Evaporated samples were resolved in a 1:1 mixture of acetonitrile and water and analyzed via LC/MS equipped with a Chromolith® Performance RP-8e 100-4.6 mm (Merck Millipore) column in combination with a Chromolith® RP-8e 5-4.6 mm guard cartridge.

Reactions at higher scale and product isolation. Reactions at higher scale were performed *in vivo* with *E. coli* carrying the pCOLA Duet vector with the genes of *ykun* and *fdr* in the first and respectively second multiple cloning site and a pET22b vector containing the gene of the CYP154E1 variant. Expression, cell preparation and reactions with 1 mM (*R*)-ketamine hydrochloride with the V286G/L289T/I238Q/M388A mutant and 5 mM (*R*)-ketamine with the L289T/I238Q/M388A triple mutant were carried out according to Bokel et al. 2020.² Isolation of (2*R*,6*R*)-HNK and (2*R*,6)-HK was carried out using semi-preparative HPLC (see section above) on a Eurospher II 100-10-C18 column (10.0µm, 300 x 8.0mm) using water (solvent A) and acetonitrile (solvent B) as solvents. The following gradient at a flow rate of 5 ml/min was applied for product separation: 20% B to 35% B in 10 min, increase to 90% B in 1 sec, holding 90% B for 3 min, decrease to 20% B again in 1 sec and holding 20% B for 4 min. Fractions were collected automatically.

Oxidation of in total 28.53 mg (*R*)-ketamine by CYP154E1 V286G/L289T/I238Q/M388A resulted in 7.62 mg (2*R*,6*R*)-hydroxynorketamine (26.6% isolated yield) and 9.50 mg (2*R*,6)-hydroxyketamine (31.3% isolated yield), both with >99% purity (HPLC). Oxidation of 11.86 mg (*R*)-ketamine by CYP154E1 L289T/I238Q/M388A resulted in quantitative conversion with 84% product selectivity. 5.96 mg (2*R*,6*R*)-hydroxynorketamine were isolated (49.8% isolated yield) and analyzed by NMR.

Results

INITIAL SCREENING FOR CYP154E1 STARTING VARIANT

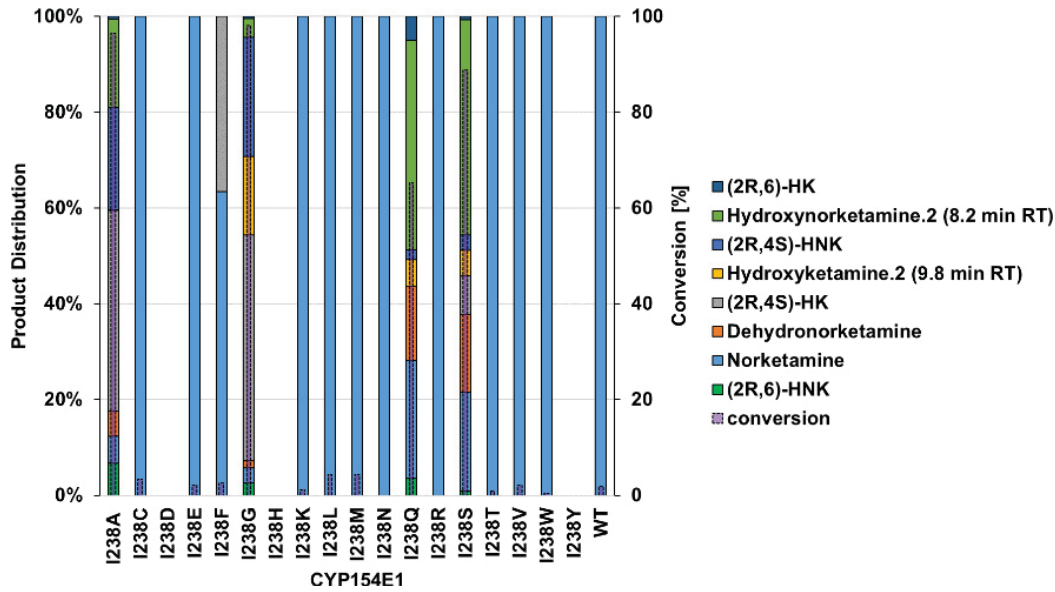


Fig. S2. Conversion of (*R*)-ketamine and product distribution observed with all possible I238 mutants of CYP154E1 except for I238P. Green columns represent the ratio of the desired (2*R*,6)-hydroxynorketamine. Conversion (secondary y-axis) is represented by transparent purple columns overlaid with the columns for the product distribution (primary y-axis). Mean values are calculated from three separate experiments. WT: wild type.

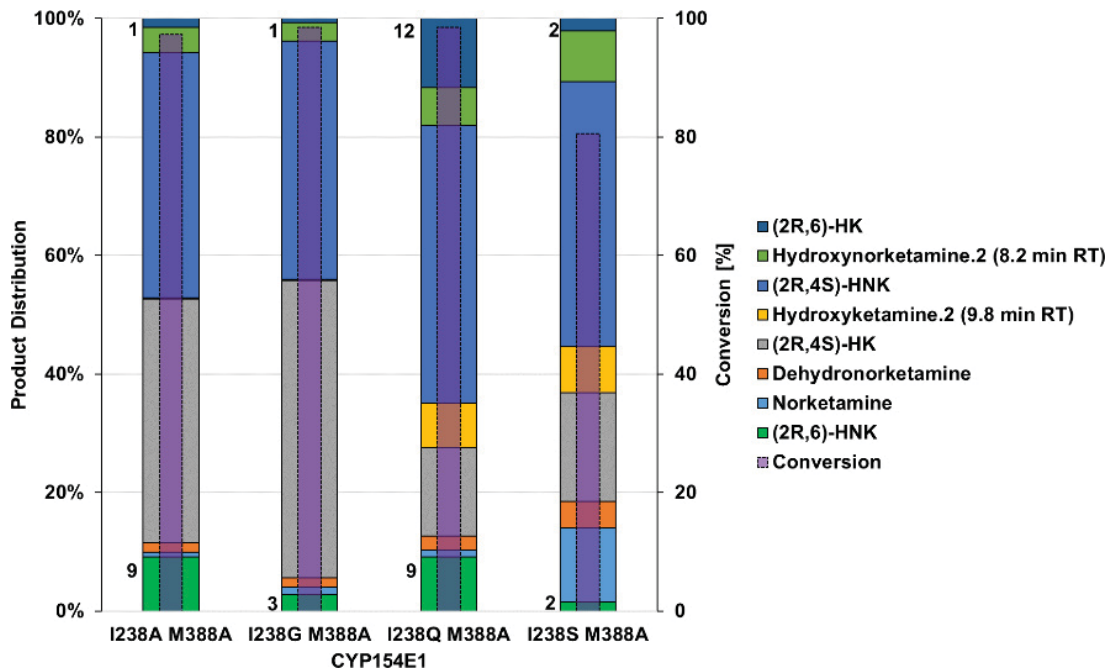


Fig. S3. Conversion of (*R*)-ketamine with CYP154E1 double mutants and product distribution. Mutation M388A was introduced to the best performing single mutants from Figure S1. Green columns represent (2*R*,6)-hydroxynorketamine and dark-blue columns represent (2*R*,6)-hydroxyketamine (percentage of (2*R*,6)-hydroxyketamine and (2*R*,6)-hydroxynorketamine are presented left of the respective column). Conversion (secondary y-axis) is represented by transparent purple columns overlaid with the columns for the product distribution (primary y-axis). Mean values are calculated from three separate experiments.

Table S2. Oxidation of (*R*)-ketamine catalyzed by CYP154E1 variants containing I238Q, L289T and M388A mutations and their combinations as well as by the quadruple mutant. (*R*)-NK: (*R*)-norketamine; (*2R,6*)-HNK: (*2R,6*)-hydroxynorketamine, (*2R,6*)-HK: (*2R,6*)-hydroxyketamine.

| CYP154E1 variants | Conversion [%] | Product distribution [%] | | | | | Others |
|--------------------------------|----------------|--------------------------|--------------------|---------------------|----------------------|-----------------|--------|
| | | (<i>2R,6</i>)-HNK | (<i>2R,6</i>)-HK | (<i>2R,4S</i>)-HK | (<i>2R,4S</i>)-HNK | (<i>R</i>)-NK | |
| L289T | 11 | - | - | - | - | 100 | - |
| L289T/I238Q | >99 | 61 | 30 | - | - | - | 9 |
| L289T/M388A | 55 | 14 | 4 | - | - | 76 | 5 |
| I238Q/M388A | 98 | 9 | 12 | 15 | 47 | 1 | 16 |
| L289T/I238Q/M388A | >99 | 85 | 10 | - | - | - | 5 |
| V286G/L289T/I238Q/M388A | >99 | 32 | 67 | - | - | - | 1 |

KINETICS

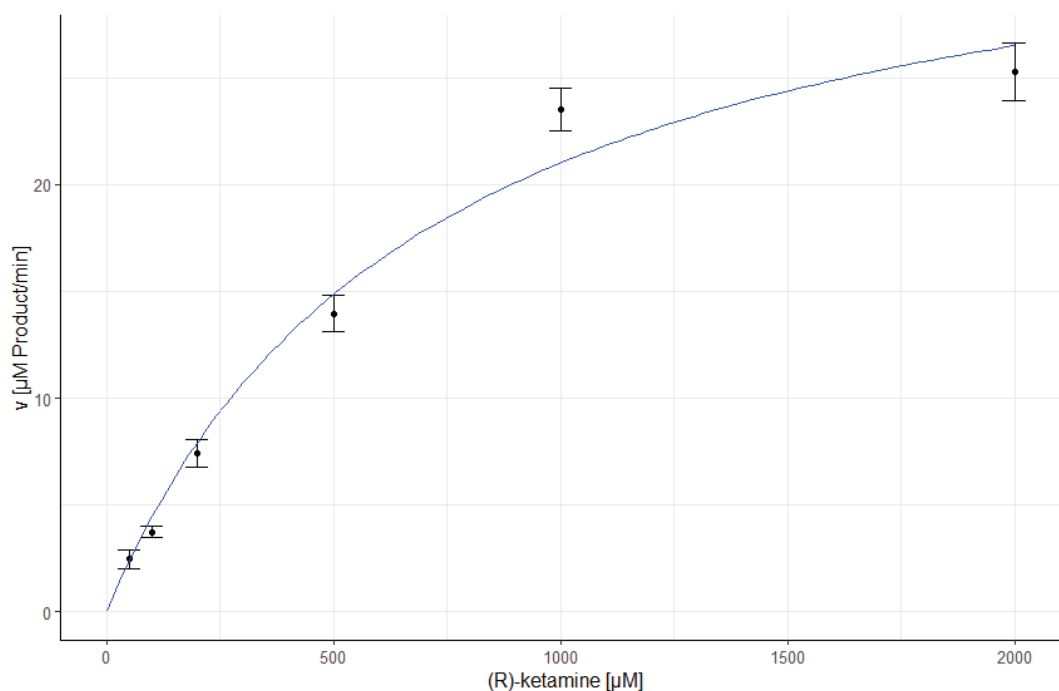


Fig. S4. Kinetics of the L289T/I238Q/M388A-catalyzed oxidation of (*S*)-ketamine. Reactions were carried out using 0.5 μ M P450, 0.5 μ M FdR and 40 μ M YkuN. Reactions were stopped after 3 – 17 min. Data were plotted to the Michaelis-Menten equation.

IDENTIFICATION OF THE DESIRED PRODUCT (2R,6R)- HYDROXYNORKETAMINE BY SPIKING

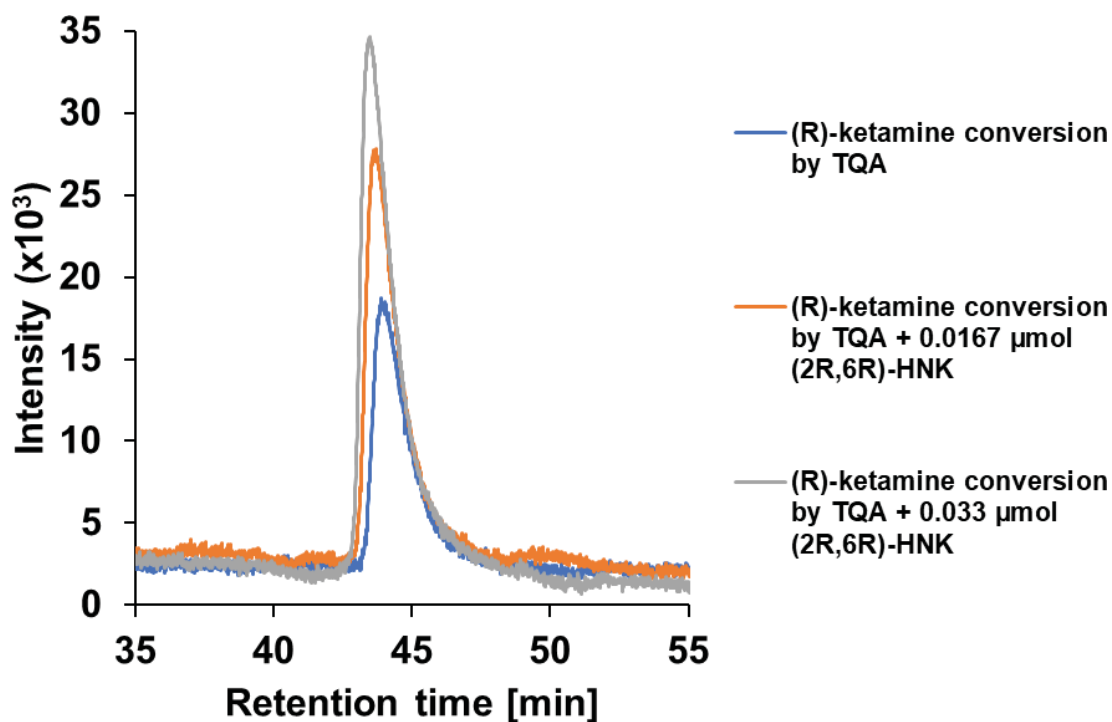


Fig. S5. HPLC analysis of the reaction catalyzed by the L289T/I238Q/M388A/ mutant (TQA). Blue: Conversion of 500 μM (R)-ketamine; orange: blue + 0.0167 μmol of authentic (2R,6R)-HNK; grey: blue + 0.033 μmol of authentic (2R,6R)-HNK. Analysis was carried out on the chiral column Chiralpak IB (0.46 cm \varnothing x 25 cm, Chiral Technologies Europe).

LC/MS ANALYSIS OF (2R,4S)-HYDROXYKETAMINE CONVERSION

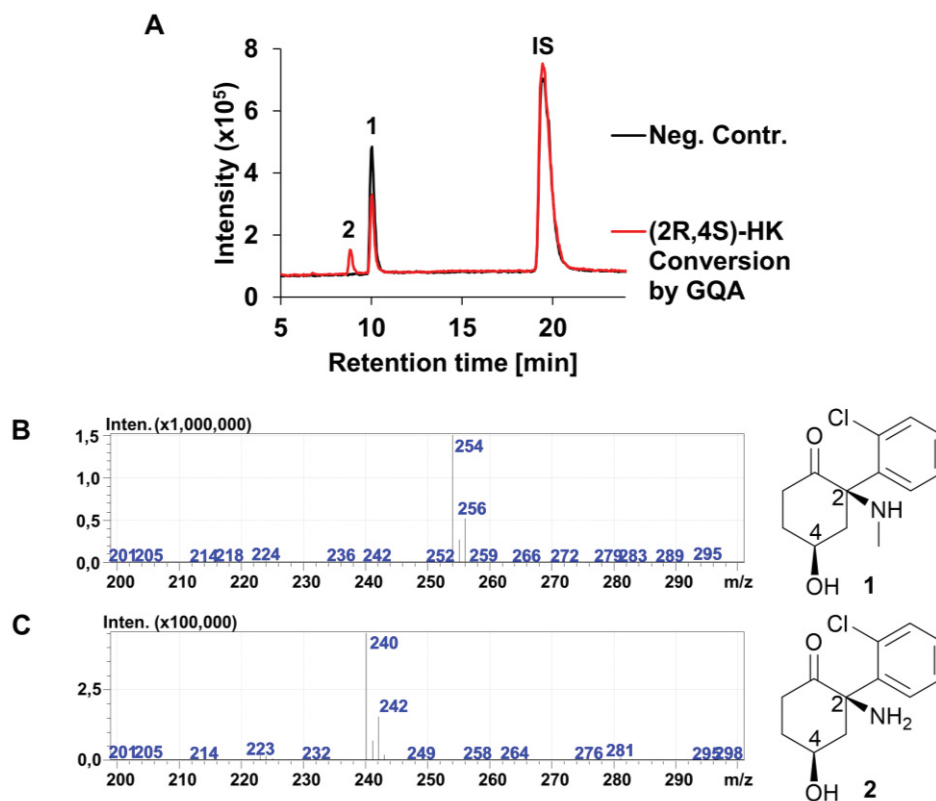


Fig. S6. LC/MS analysis of (2R,4S)-hydroxyketamine oxidation. **A**: LC/MS chromatogram of the conversion of (2R,4S)-hydroxyketamine (1) by CYP154E1 V286G/I238Q/M388A (GQA) compared to the negative control without P450. IS: internal standard xylazine. **B**: ESI MS spectrum of (2R,4S)-hydroxyketamine (1). 254 m/z corresponds to $[M+H]^+$; 256 m/z corresponds to $[M+H]^+$ and results from the ^{37}Cl isotope (compared to the ^{35}Cl isotope). **C**: ESI MS spectrum of (2). 240 m/z results from a loss of the methyl group ($\Delta 14$ m/z). 242 m/z is again attributes to the ^{37}Cl isotope (compared to the ^{35}Cl isotope). Therefore, the product of the (2R,4S)-hydroxyketamine oxidation must be (2R,4S)-hydroxynorketamine (demethylated product).

NMR ANALYSIS

(2R,6R)-HYDROXYNORKETAMINE

^1H NMR (600 MHz, MeOD) Δ 7.77 – 7.70 (M, 1H), 7.48 – 7.41 (M, 2H), 7.39 – 7.33 (M, 1H), 4.15 (DD, $J = 11.8, 6.6$ Hz, 1H), 2.93 (DDD, $J = 14.4, 3.1$ Hz, 1H), 2.27 – 2.19 (M, 1H), 1.79 – 1.68 (M, 2H), 1.66 – 1.57 (M, 1H), 1.57 – 1.48 (M, 1H).

^{13}C NMR (151 MHz, MeOD) Δ 214.00, 139.56, 134.80, 132.41, 131.03, 130.35, 128.97, 74.81, 68.12, 42.27, 40.36, 20.68.

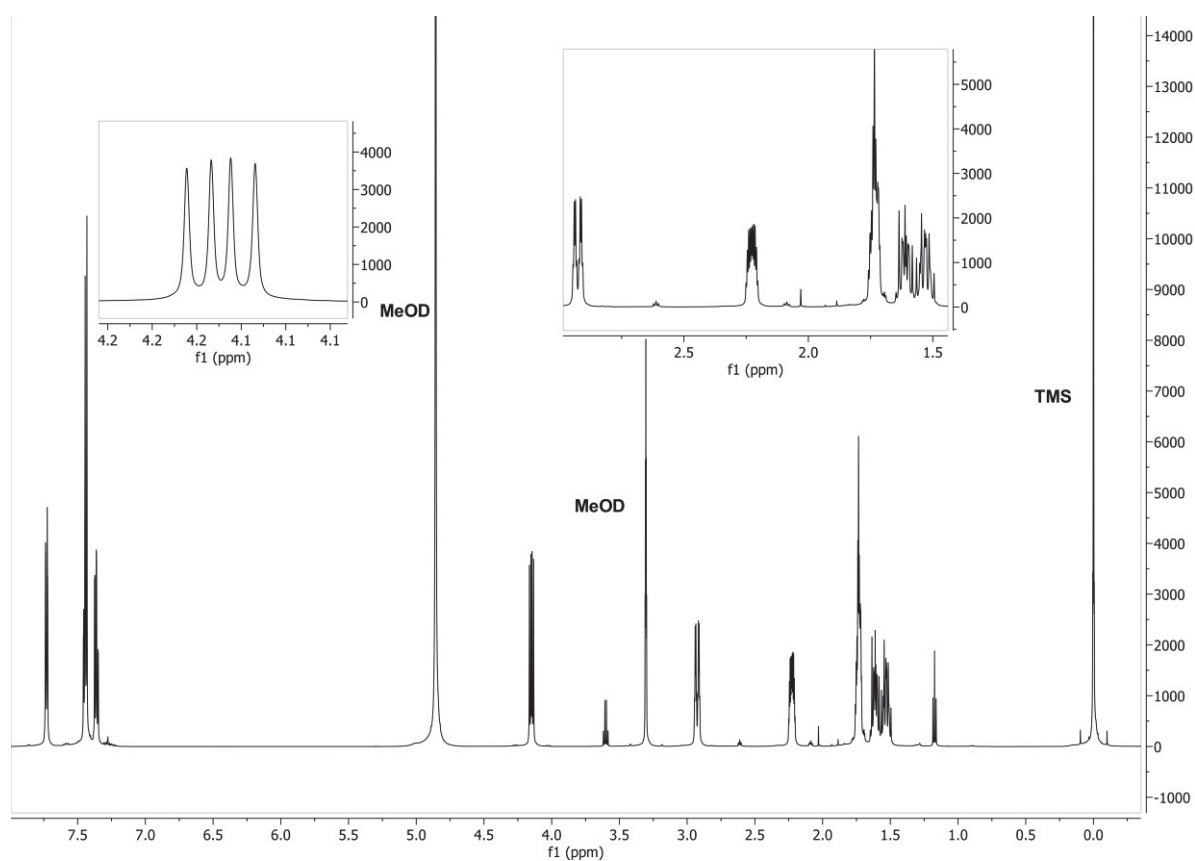


Fig. S7. ^1H NMR of (2R,6R)-hydroxynorketamine in MeOD. Enlargement of the doublet of doublets for the proton sitting at C6 with the hydroxyl group and the proton patterns of the cyclohexanone system.

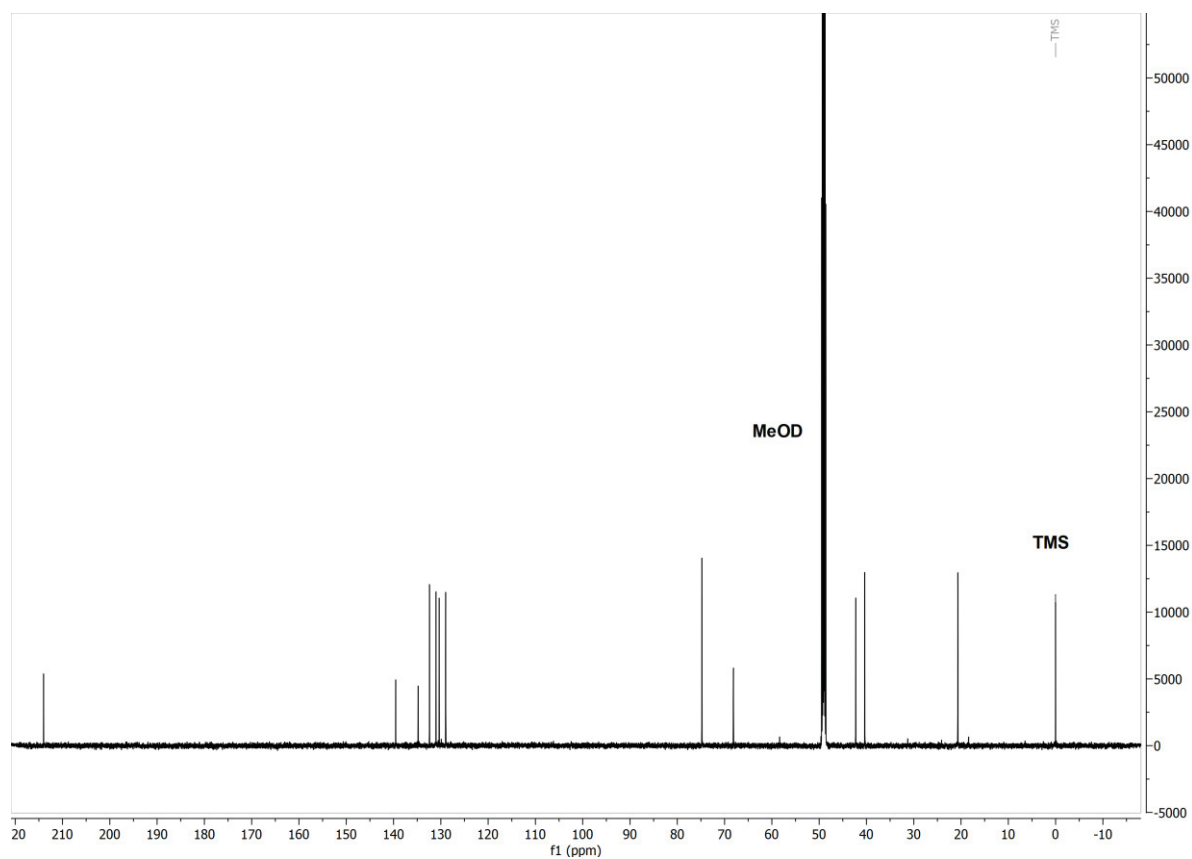


Fig.S8. ^{13}C NMR of (2R,6R)-hydroxynorketamine in MeOD.

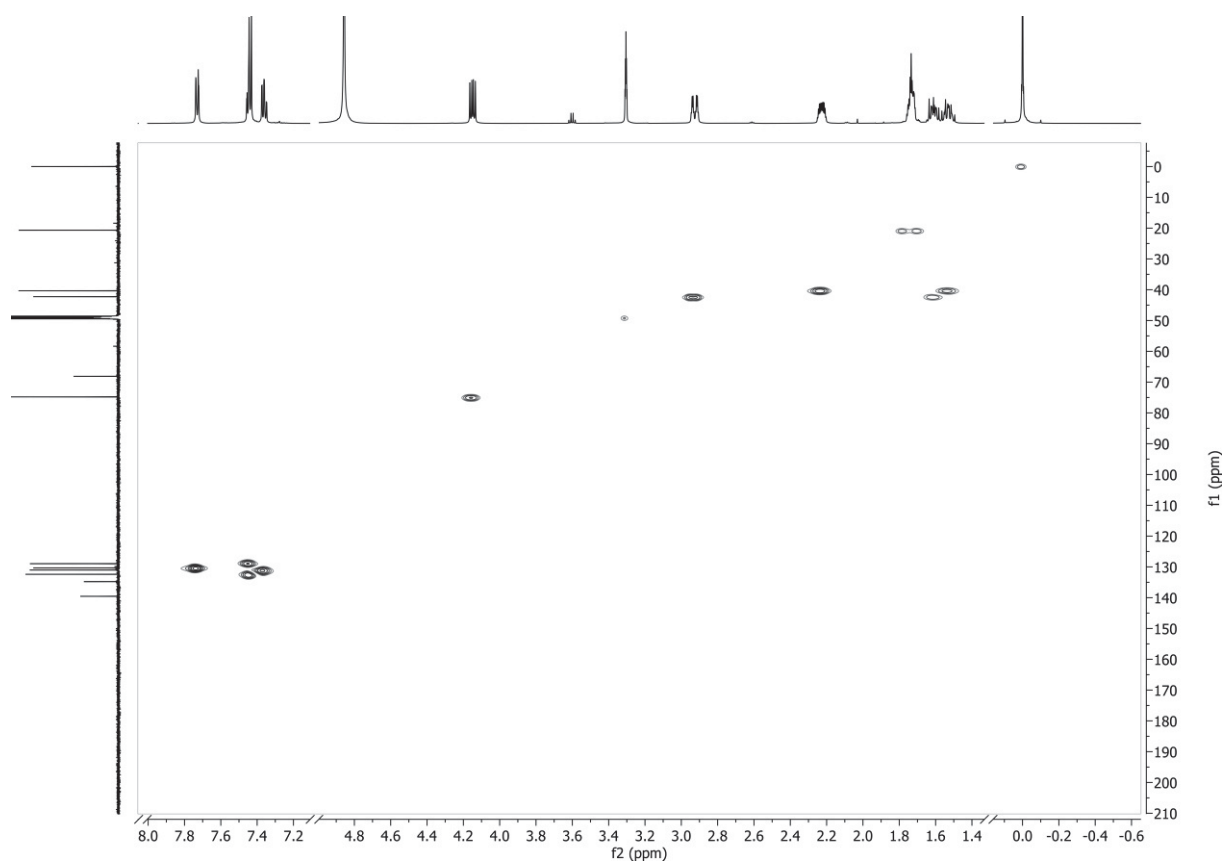


Fig. S9. ^1H - ^{13}C HSQC spectrum of (2R,6R)-hydroxynorketamine in MeOD. Signals of impurities were cut out for simplicity.

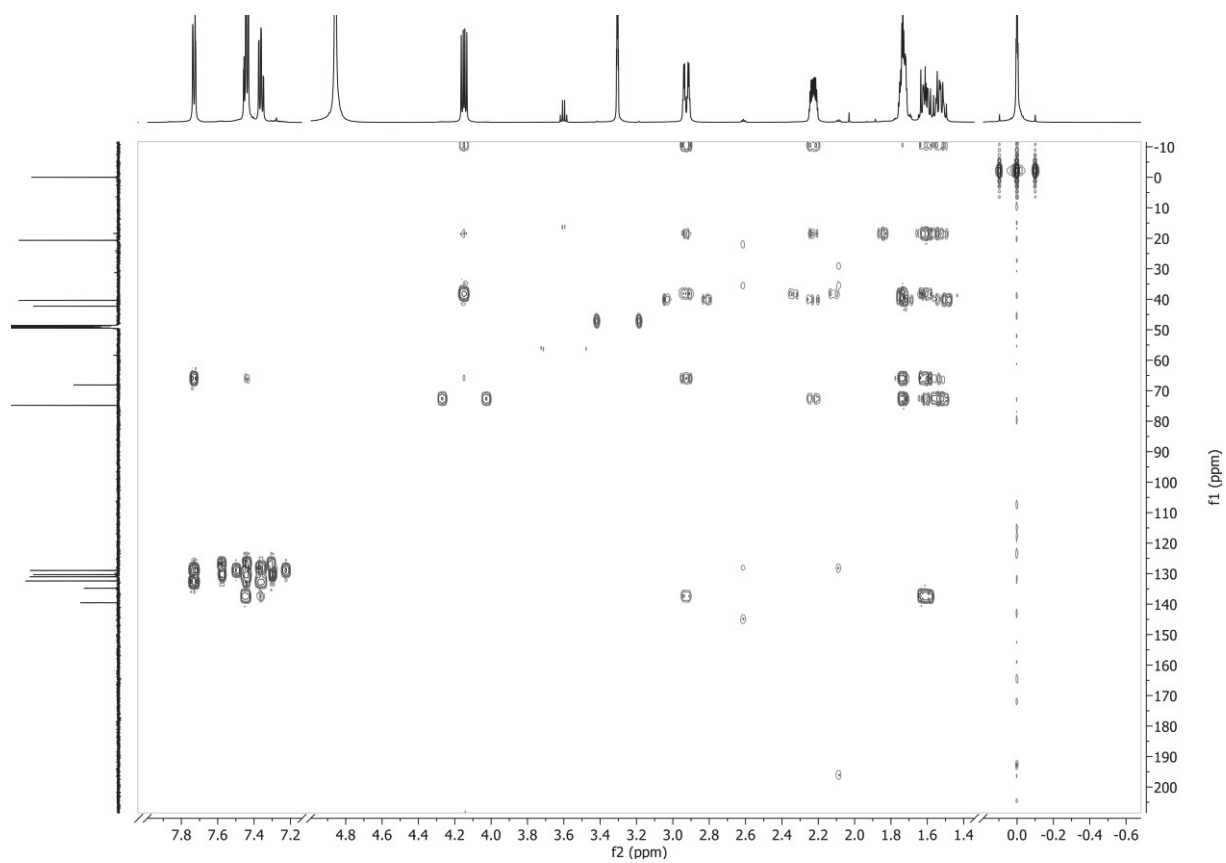


Fig. S10. ^1H - ^{13}C HMBC spectrum of $(2R,6R)$ -hydroxynorketamine in MeOD. Signals of impurities were cut out for simplicity.

(2*R*,6)-HYDROXYKETAMINE

^1H NMR (600 MHz, MeOD) Δ = 7.69 (DD, J =8.5, 1.6, 1H), 7.50 – 7.44 (M, 2H), 7.42 – 7.37 (M, 1H), 4.17 (DD, J =11.8, 6.6, 1H), 3.12 (DDD, J =14.2, 3.0, 1H), 2.27 – 2.21 (M, 1H), 1.81 – 1.75 (M, 1H), 1.72 – 1.62 (M, 1H), 1.61 – 1.54 (M, 2H).

^{13}C NMR (151 MHz, MeOD) Δ = 211.99, 135.67, 135.63, 132.55, 131.90, 131.34, 128.60, 75.08, 72.29, 40.35, 39.26, 28.79, 20.56.

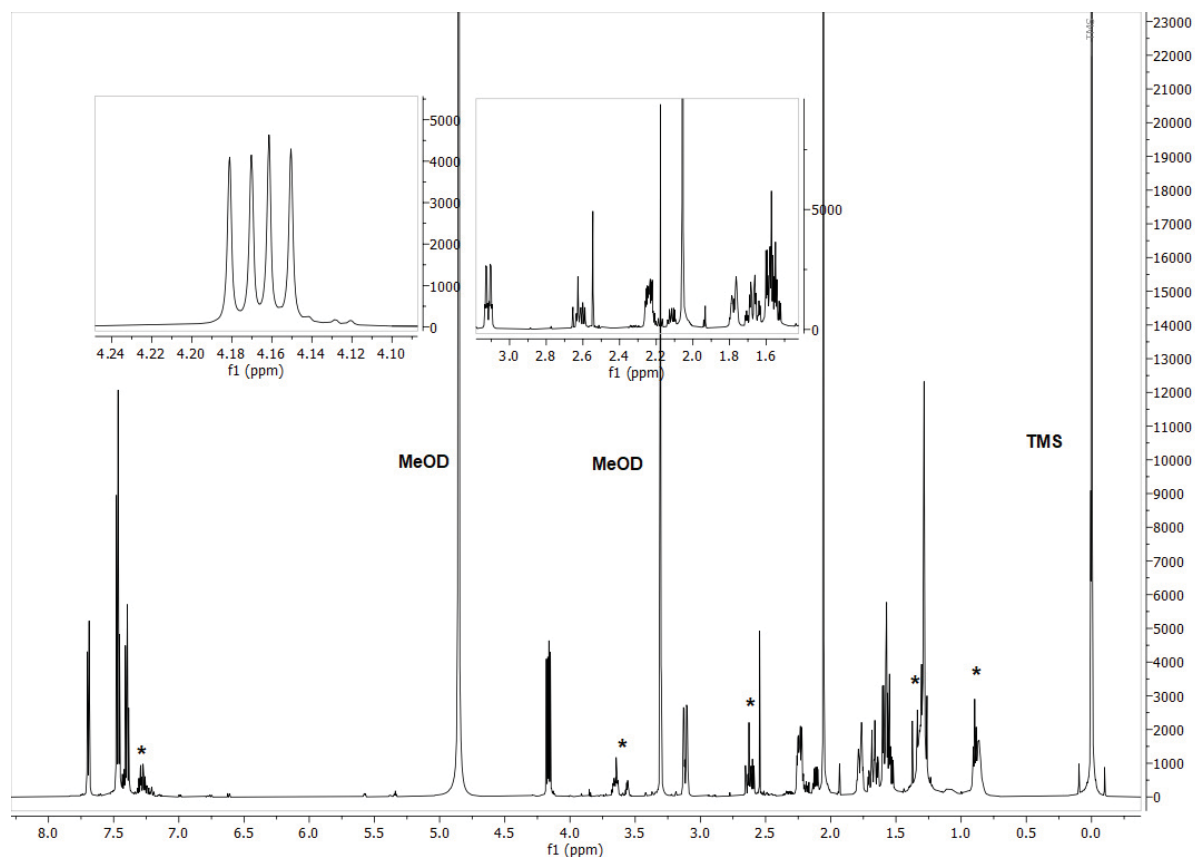


Fig. S11. ^1H NMR of (2*R*,6)-hydroxyketamine in MeOD. *: Solvent impurities. Enlargement of the doublet of doublets for the proton sitting at C6 with the hydroxy group and the proton patterns of the cyclohexanone system.

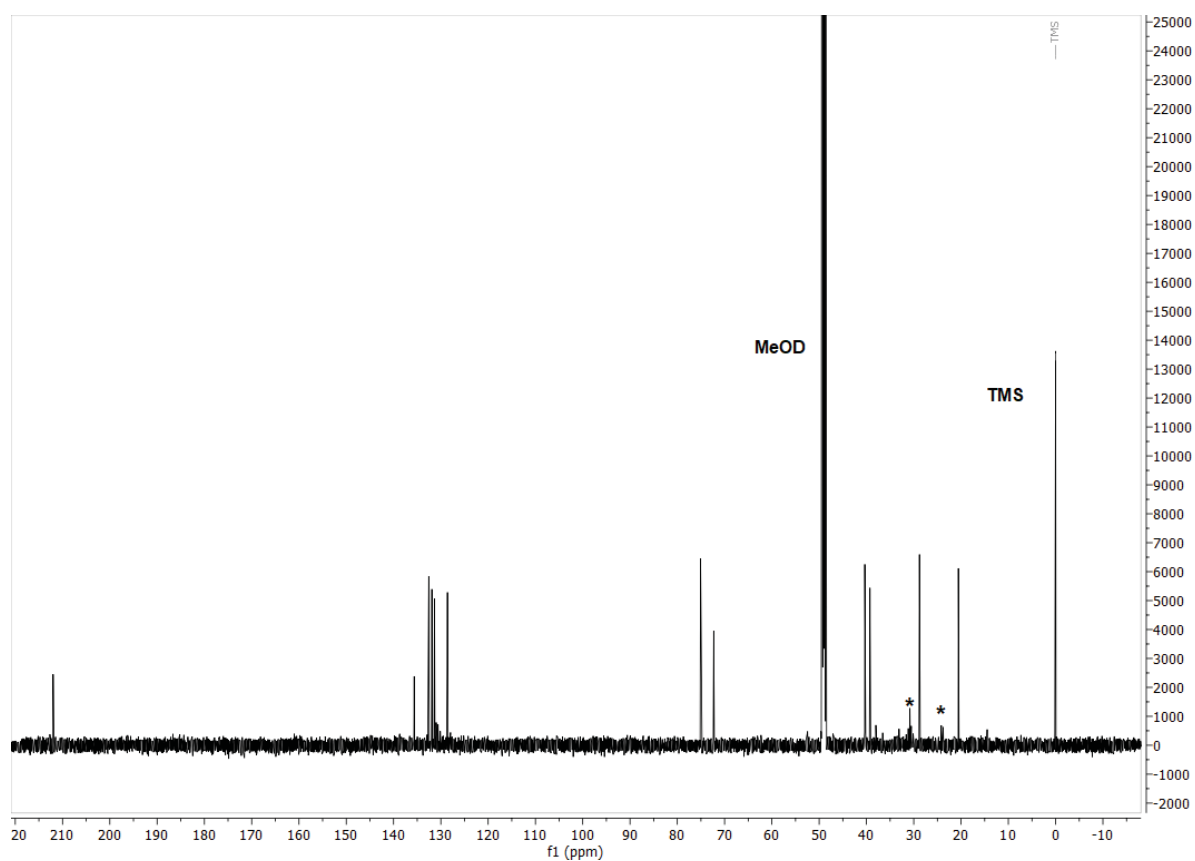


Fig. S12. ^{13}C NMR of (2R,6)-hydroxyketamine in MeOD. *: Solvent impurities.

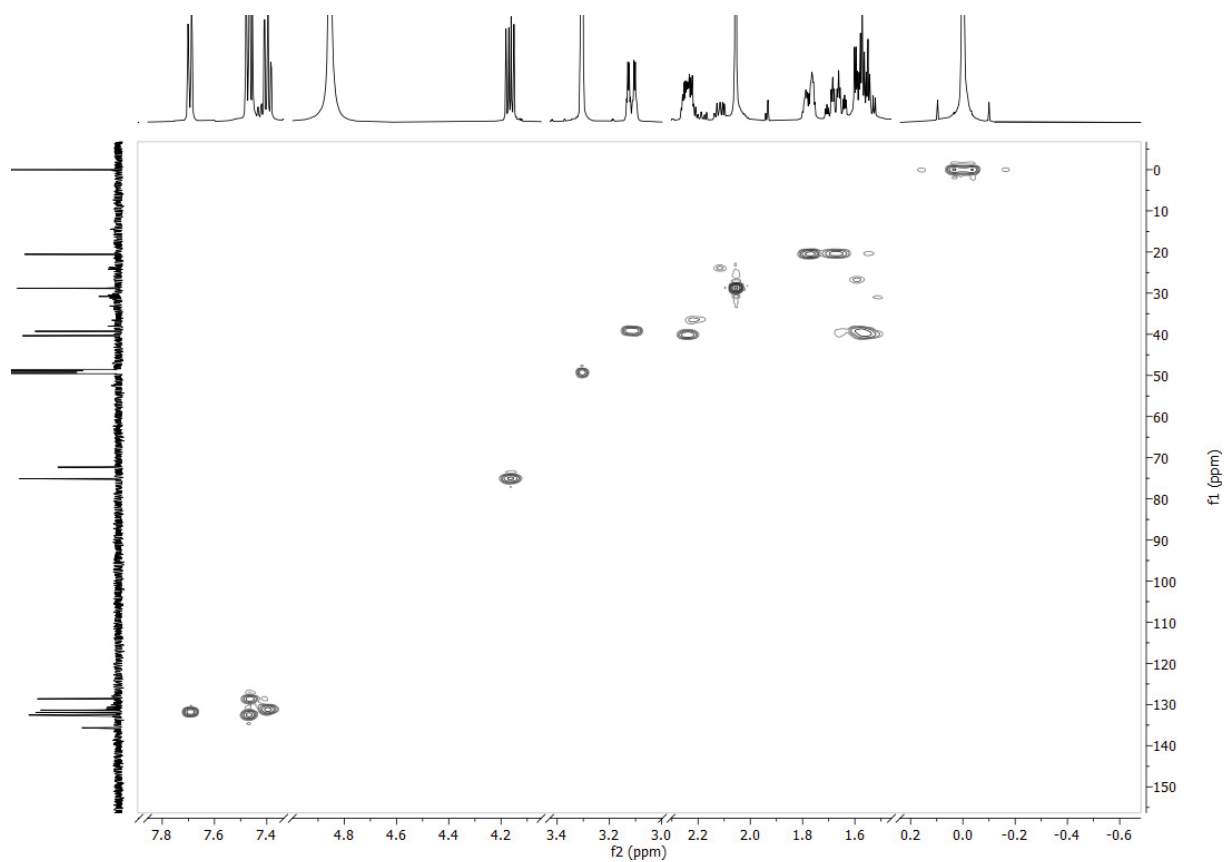


Fig. S13. ^1H - ^{13}C HSQC spectrum of (2R,6)-hydroxyketamine in MeOD. Signals of impurities were cut out for simplicity.

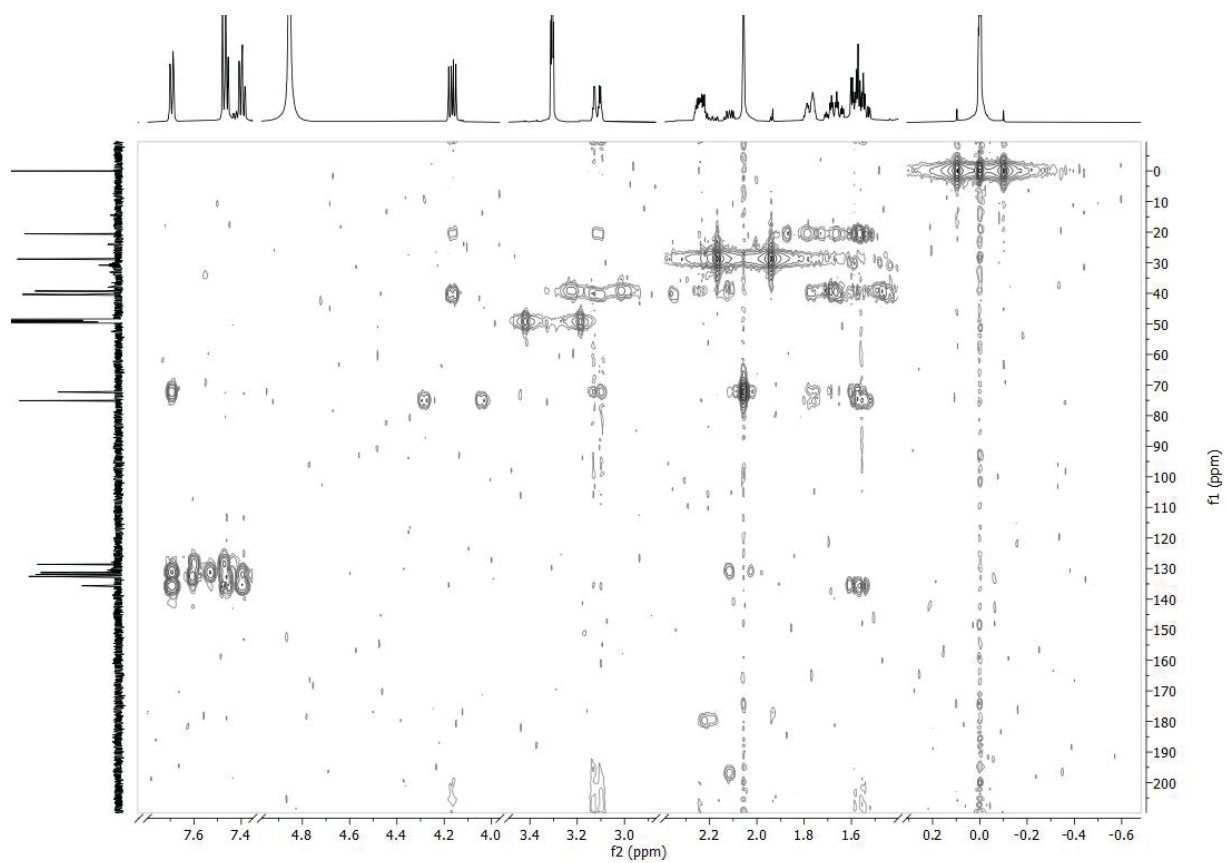


Fig. S14. ^1H - ^{13}C HMBC spectrum of (2R,6)-hydroxyketamine in MeOD. Signals of impurities were cut out for simplicity.

DOCKING OF (*R*)-KETAMINE AND (*R*)-NORKETAMINE

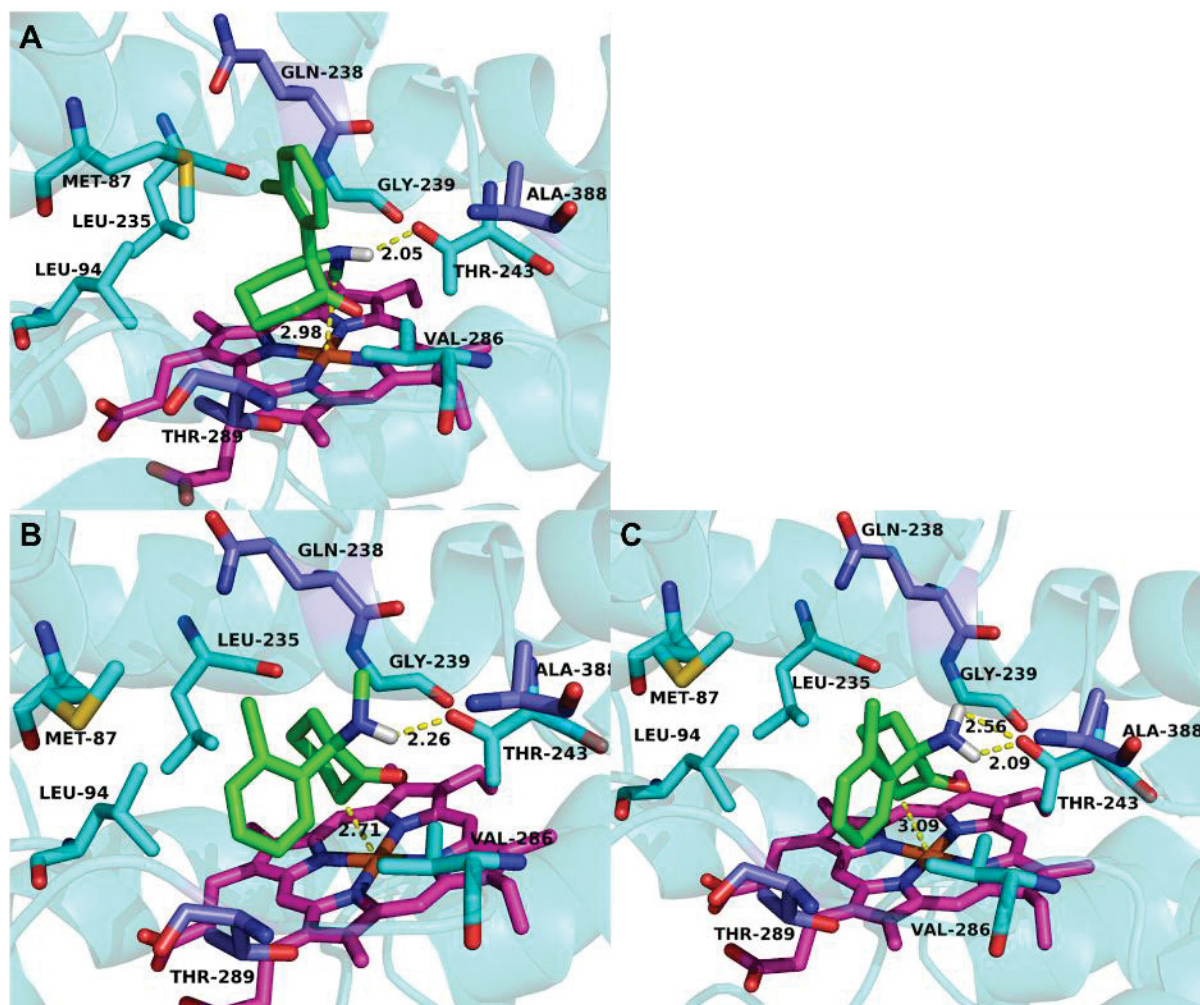


Fig. S15. Best scored rigid docking poses of (*R*)-ketamine in the model A (A) and model B (B) and of (*R*)-norketamine in the model B (C) of the active site of CYP154E1 L289T/I238Q/M388A. Dashed yellow lines indicate distances between atoms. Light-blue colored residues: residues of the first-sphere; dark-blue colored residues: first-sphere mutations I238Q, L289T and M388A. The numerical distance is given in Å.

REFERENCES

- 1 V. F. T. Russo and E. M. d. S. Russo, US6743949B2, 2004.
- 2 A. Bokel, A. Rühlmann, M. C. Hutter and V. B. Urlacher, *ACS Catal.*, 2020, **10**, 4151-4159.
- 3 T. Omura and R. Sato, *J. Biol. Chem.*, 1964, **239**, 2379-2385.
- 4 (a) K. Fujii and F. M. Huennekens, *The Journal of Biological Chemistry*, 1974, **249**, 6745-6753; (b) L. McIver, C. Leadbeater, D. J. Campopiano, R. L. Baxter, S. N. Daff, S. K. Chapman and A. W. Munro, *Eur. J. Biochem.*, 1998, **257**, 577-585; (c) Z.-Q. Wang, R. J. Lawson, M. R. Buddha, C.-C. Wei, B. R. Crane, A. W. Munro and D. J. Stuehr, *J. Biol. Chem.*, 2007, **282**, 2196-2202; (d) R. J. Lawson, C. von Wachenfeldt, I. Haq, J. Perkins and A. W. Munro, *Biochemistry*, 2004, **43**, 12390-12409.
- 5 O. Edelheit, A. Hanukoglu and I. Hanukoglu, *BMC Biotechnol.*, 2009, **9**.

- 6 J. Sanchis, L. Fernandez, J. D. Carballeira, J. Drone, Y. Gumulya, H. Hobenreich, D. Kahakeaw, S. Kille, R. Lohmer, J. J. Peyralans, J. Podtetenieff, S. Prasad, P. Soni, A. Taglieber, S. Wu, F. E. Zilly and M. T. Reetz, *Appl. Microbiol. Biotechnol.*, 2008, **81**, 387-397.
- 7 RStudio: Integrated Development for R. RStudio, Boston, MA URL <http://www.rstudio.com>.
- 8 C. H. Wu, M. H. Huang, S. M. Wang, C. C. Lin and R. H. Liu, *J. Chromatogr. A*, 2007, **1157**, 336-351.

Supporting Information

Simulation-Guided Design of Cytochrome P450 for Chemo- and Regioselective Macrocyclic Oxidation

Dušan Petrović,^{1,†,*} Ansgar Bokel,² Matthew Allan,^{1,3} Vlada B. Urlacher,² and Birgit Strodel^{1,4,*}

¹ Institute of Complex Systems: Structural Biochemistry, Forschungszentrum Jülich, 52425 Jülich, Germany

² Institute of Biochemistry, Heinrich-Heine University Düsseldorf, Universitätsstraße 1, 40225 Düsseldorf, Germany

³ Schreyer Honors College, The Pennsylvania State University, University Park, PA 16802, United States

⁴ Institute of Theoretical and Computational Chemistry, Heinrich-Heine University Düsseldorf, Universitätsstraße 1, 40225 Düsseldorf, Germany

[†] Present address: Department of Cell and Molecular Biology, Uppsala University, BMC Box 596, 751 24 Uppsala, Sweden

* E-mail: dusan.petrovic@icm.uu.se, b.strodel@fz-juelich.de

I Supporting Methods

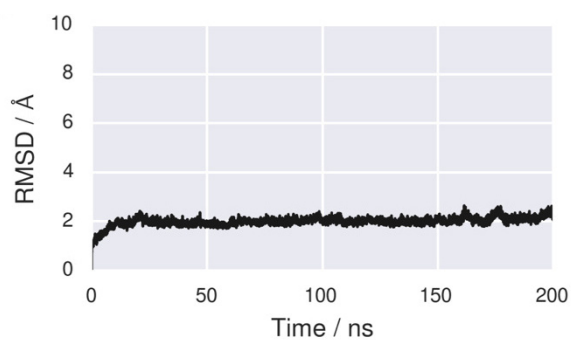


Figure S1. Protein backbone RMSD from the unliganded MD simulations of the V78A/F87A P450 BM3 mutant prepared from the 1JPZ crystal structure.

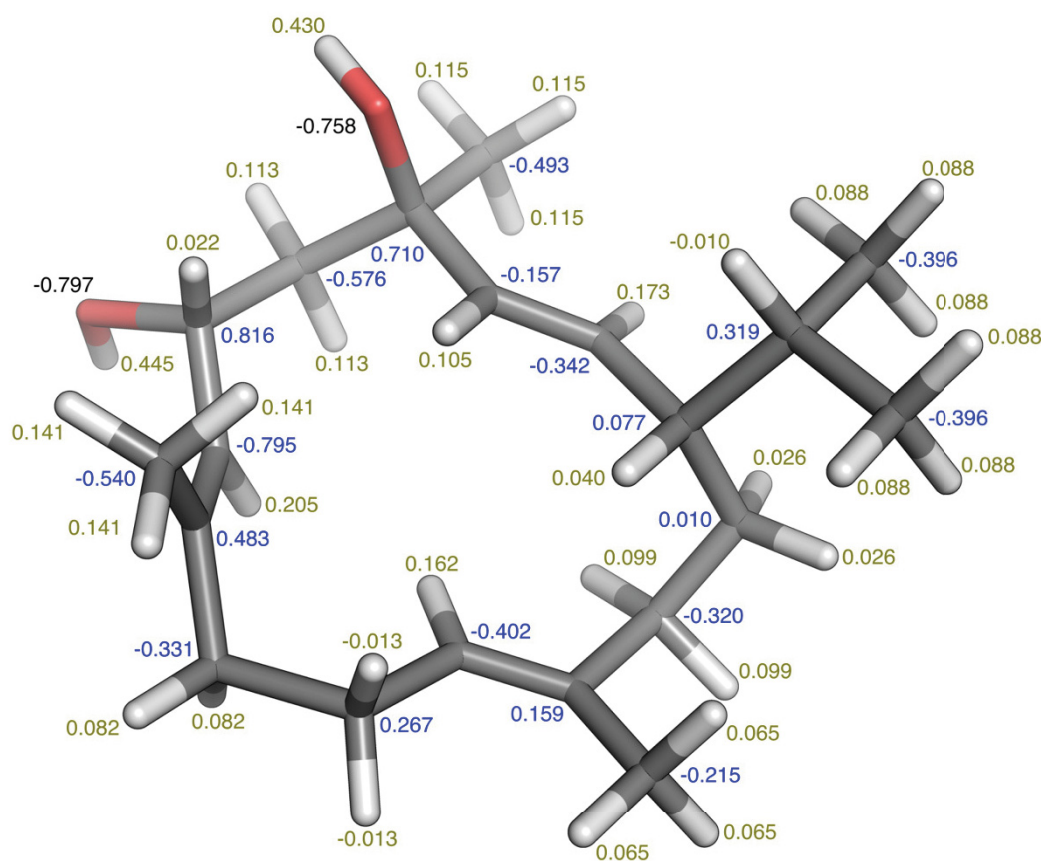


Figure S2. The HF/6-31G*//B3LYP/6-31G* level of theory RESP charges for β -cembrenediol, which are shown in blue for the C-atoms, in green for the H-atoms, and in black for the O-atoms.

II β -cembrenediol Docking

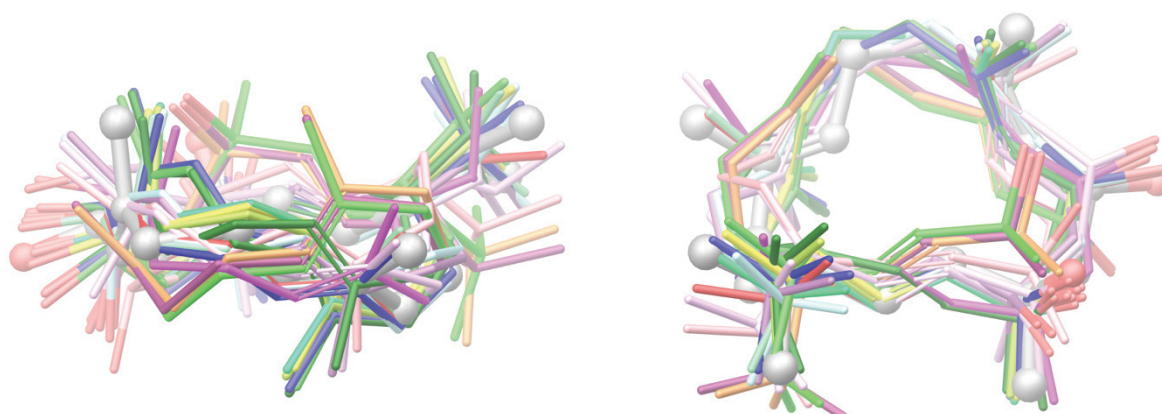


Figure S3. β -Cembrenediol conformational ensemble from OMEGA (in colored sticks), overlaid with the crystal structure (CCDC number: 1193351, in gray balls and sticks), shown from two different perspectives.

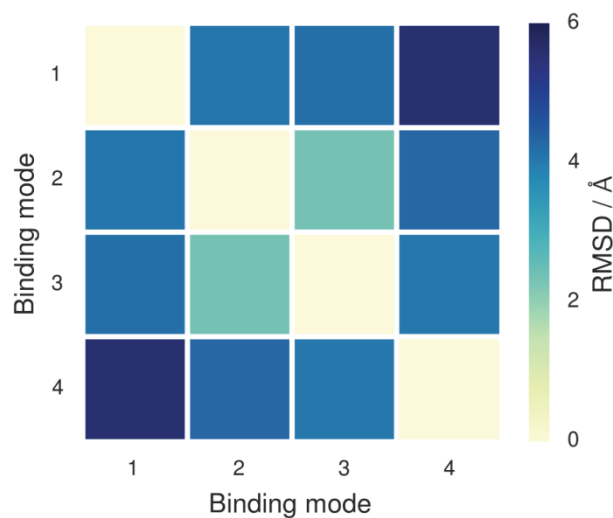


Figure S4. Pairwise RMSDs between the four binding modes of β -cembrenediol (from docking simulation) considered for MD and HREX-MD simulations. The RMSDs were calculated after structural alignment of the complexes to the positions of the heme atoms. The RMSD values between 2 and 6 Å indicate that the four binding modes of β -cembrenediol differ from each other.

For studying the binding of β -cembrenediol (**1**) to V78A/F87A P450 BM3 in more detail, we performed 200 ns MD simulations of the enzyme–ligand complex. The MD simulations showed that binding modes 1 and 3 are stable (substrate RMSD ~ 2 Å), while in modes 2 and 4 the substrate RMSD quickly jumps to values > 3 and 5 Å, respectively, and remains constant for the rest of the simulations (Figure S5).

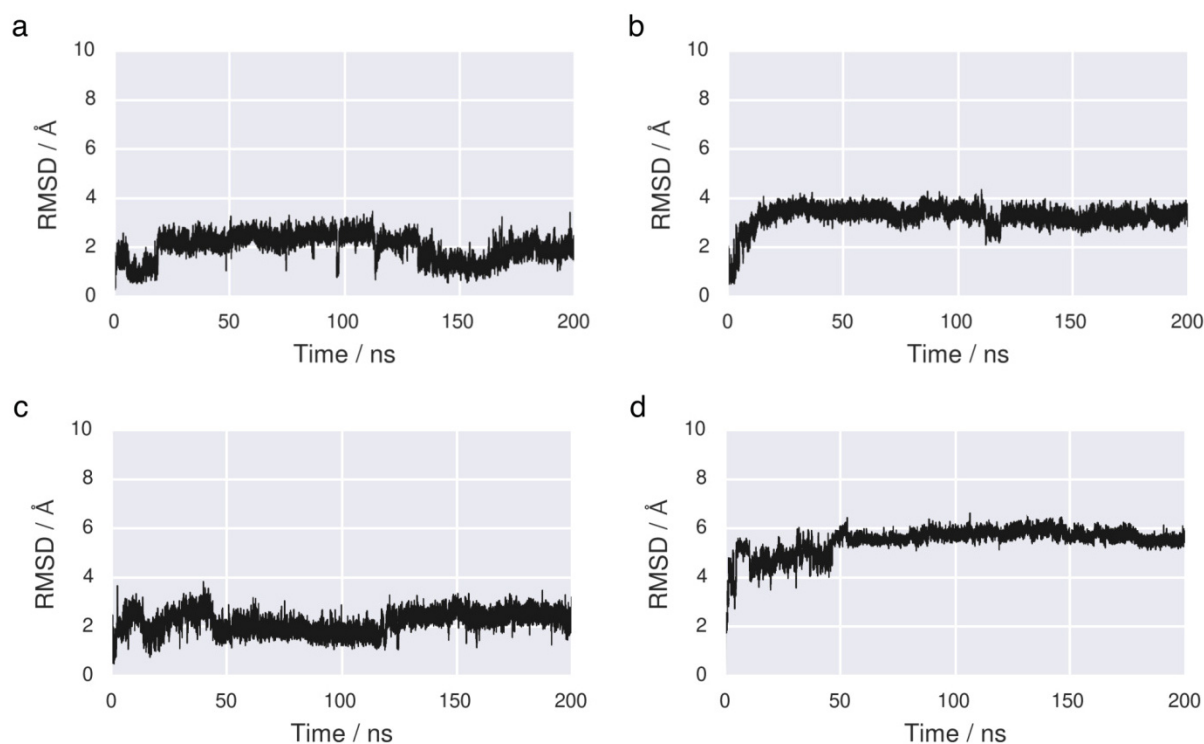


Figure S5. RMSD of the β -cembrenediol 14-membered macrocyclic ring, after protein backbone alignment, from the unbiased MD simulations. Panels a–d report values for the simulations initiated from the binding modes 1–4, described in Figure S4.

To better estimate the extent of the substrate sampling in the active site, we measured the distances between the axial oxygen of cI and several C atoms of **1**. Figure S6 shows that all atom pairs in simulations starting from binding modes 1, 2, and 4 sample a unimodal distance distribution. It should be noted, however, that the sampled modes in simulations 2 and 4 (with high RMSD values) are very far away from the initial ones, as indicated by the severe mismatch in the initial and the most-sampled distances. This means that after the substrate changed its initial binding mode in the first 10–50 ns, it finds a metastable position and does not sample any further conformations. In the simulation initiated from binding mode 3, however, narrow bimodal distance distributions can be observed for all investigated atoms of the substrate. This indicates that the substrate samples its initial and a geometrically close

conformation, typically within 2 Å. The distance analysis, together with the RMSD profiles, suggests an overall rigid behavior and not much conformational diversity within any single simulation. While the C9- and C10-atoms in binding modes 2 and 3 sample distances close to cI that could lead to chemical reactions, the C7/C8-atoms are rarely closer than 5 Å. Thus, the experimental presence of the epoxidation products cannot be explained with these MD simulations due to their limited sampling of the configuration space.

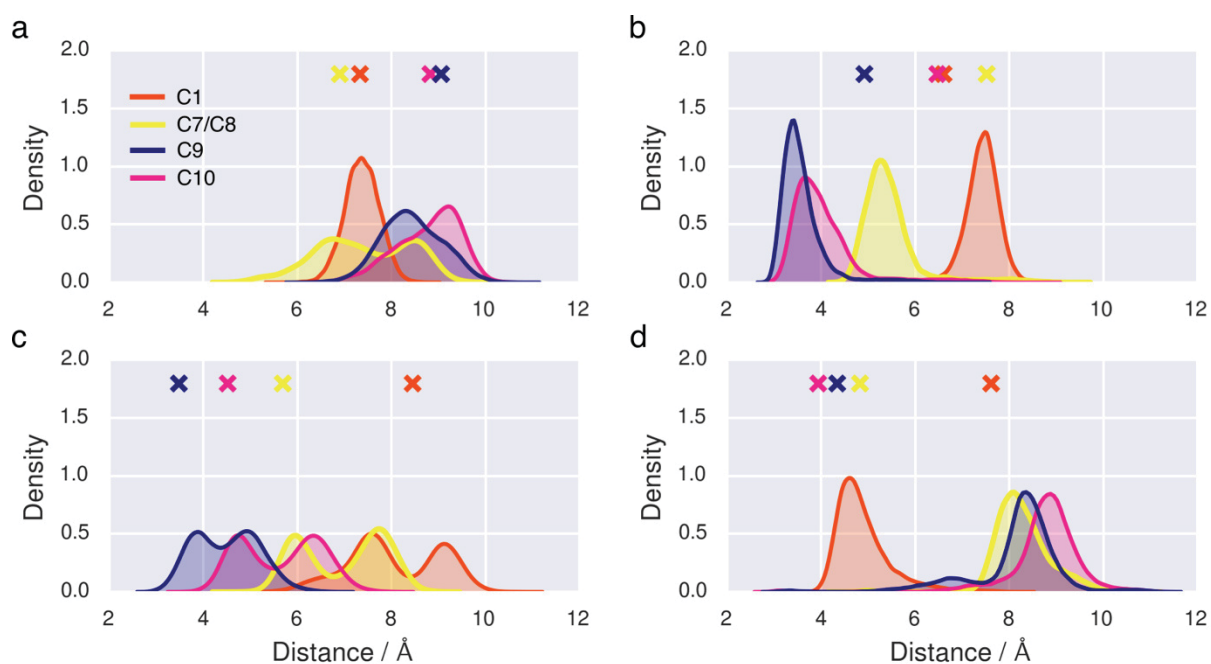


Figure S6. Distance distribution between the axial oxygen of cI and the selected β -cembrenediol C-atoms from the unbiased 200 ns MD simulations started from binding modes 1–4 (panels a–d). C7/C8 indicates the center of mass of the two atoms. The \times marks the initial distances in each of the simulations.

In HREX-MD simulations, a number of replicas is run with predefined Hamiltonians that typically scale down the intermolecular interactions.^{1,2} As neighboring replicas are allowed to exchange their coordinates according to the Metropolis criterion, the random walk through the Hamiltonian space allows for enhanced conformational sampling and calculation of thermodynamic properties. In addition, HREX-MD simulations were shown to be a good and inexpensive method to study protein–ligand interactions.³ The RMSD of **1** from HREX-MD simulations is shown in [Figure S7](#).

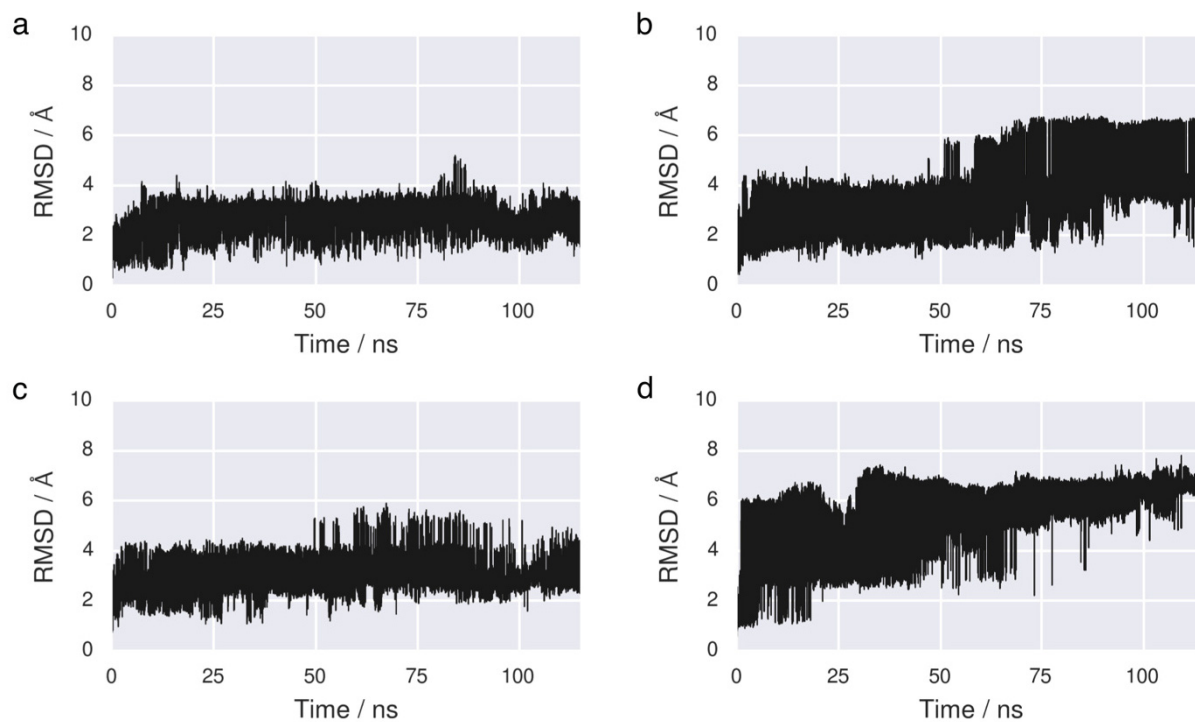


Figure S7. RMSD of the β -cembrene diol 14-membered macrocyclic ring, after protein backbone alignment, from 115 ns-long HREX-MD simulations. Panels a–d report values for simulations initiated from the binding modes 1–4, described in [Figure S3](#).

III Binding Density Surfaces

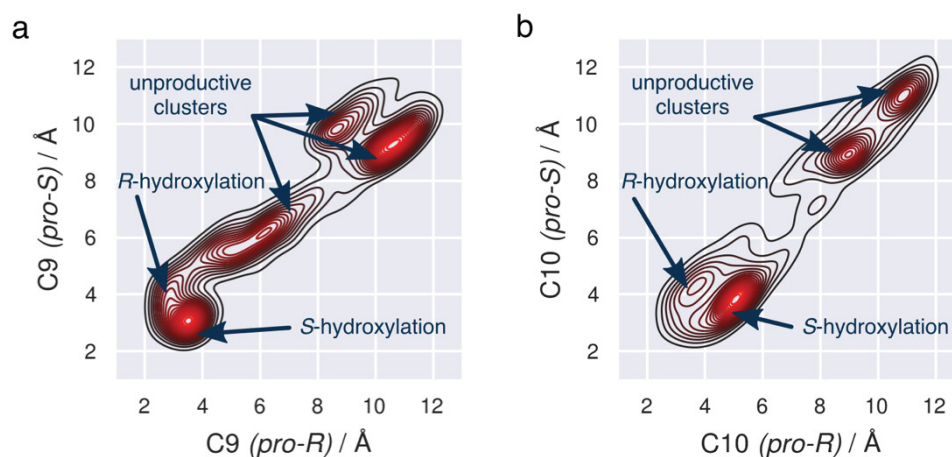


Figure S8. Binding density surfaces describing stereoselectivity of β -cembrenediol hydroxylation at positions (a) C9 and (b) C10. In case of the C9-hydroxylation, the *pro-R* maximum is less favorable than that of *pro-S*, which corresponds to an experimental ratio of 1:3 of the *R*- (**3a**) and *S*-products (**3b**). For the C10-hydroxylation, the *pro-R* maximum is also less prominent than the *pro-S* one, which contradicts experimental findings of 10*R* (**4a**) being a more dominant product than 10*S* (**4b**). This discrepancy in our model could be an artifact of generally sampling only a small number of conformations leading to C10-hydroxylation, which would prevent a reliable assignment of relative epimer stabilities.

IV Mutagenesis Hotspots

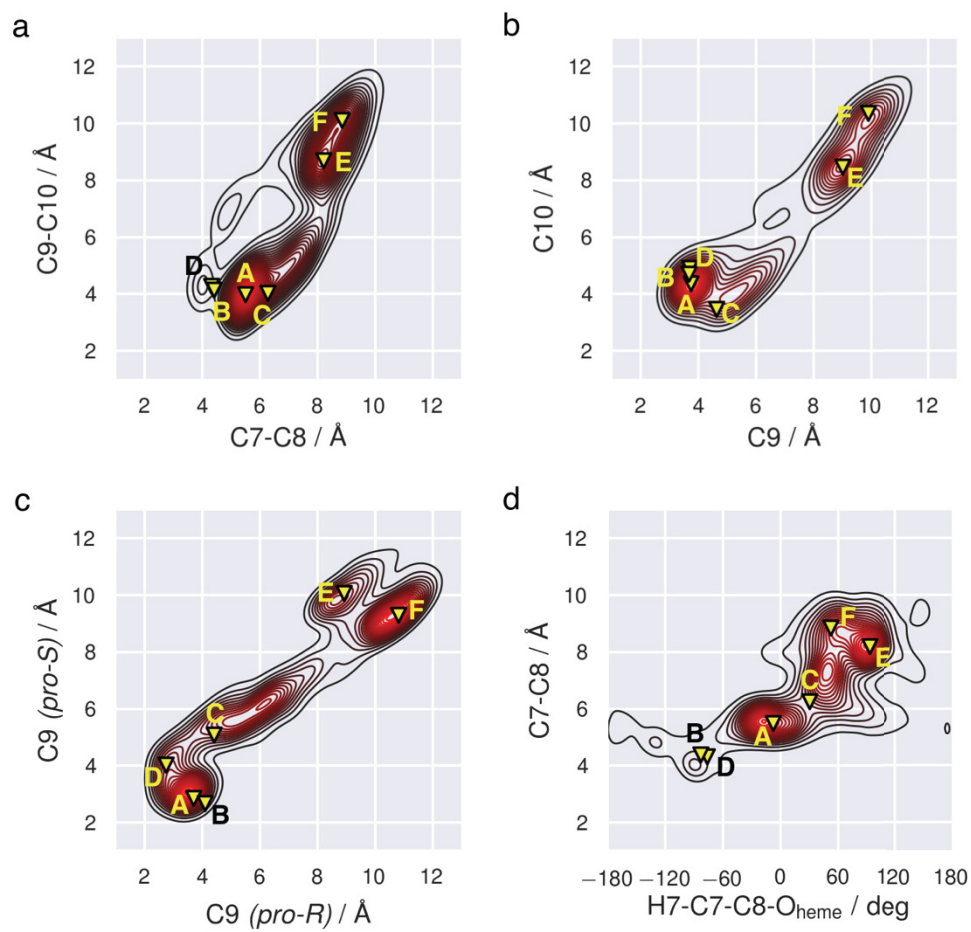


Figure S9. The six most populated structures, labeled A to F, obtained from clustering of the different binding modes of β -cembrenediol are mapped onto different binding density surfaces (a) to (d), which are described in detail in [Figures 3](#) and [S8](#).

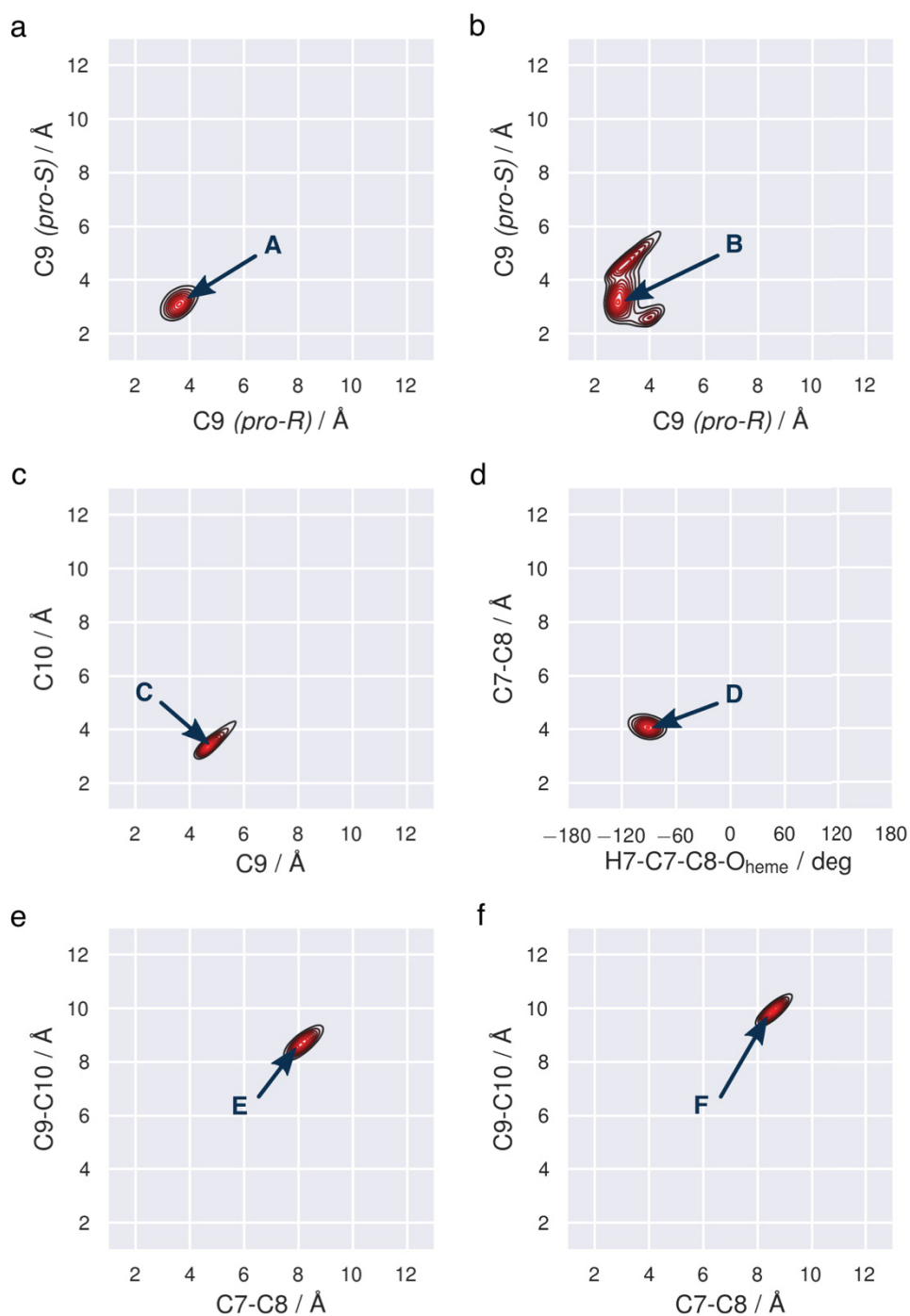


Figure S10. The conformations explored during short MD simulations performed for the MM/PBSA calculations are shown. The simulations were started from the six dominant clusters A to F shown in [Figures S9](#) and they sampled only a narrow conformational region around these binding modes. An exception is cluster B, which sampled three states, of which two correspond to 9*R*-hydroxylation.

Choosing mutagenesis hotspots requires first defining a goal G , such as increasing regioselective C10-hydroxylation. Based on our premise that the enzyme selectivity is linked to the amount of time that the substrate spends in an orientation proper for the reaction to occur, hotspot selection should aim to stabilize exclusively the productive substrate binding modes, p , and destabilize any unproductive binding modes, u . According to our formalism, a residue r is *stabilizing* for a goal $G(r)$ if it does not bind less tightly to the substrate in any p than in any u , and if it binds more tightly to the substrate in at least one p than in at least one u . That is, if all of the following are true:

$$E_r^p < E_r^u + c \quad (\text{S1})$$

and at least one of the following is true:

$$E_r^p \leq E_r^u - c \quad , \quad (\text{S2})$$

where E_r^p and E_r^u are the binding free energies of residue r to $\mathbf{1}$ in the productive and unproductive modes obtained from clusters A to F, respectively, and c is a small positive threshold (1 kcal mol⁻¹). This threshold is needed because MM/PBSA does not perfectly estimate substrate binding free energies, so there will be some error in each estimate. In a similar manner, a residue r is *destabilizing* for a goal $G(r)$ if all of the following are true:

$$E_r^p > E_r^u - c \quad (\text{S3})$$

and at least one of the following is true:

$$E_r^p \geq E_r^u + c \quad . \quad (\text{S4})$$

It should be noted that a residue can be neither stabilizing nor destabilizing if 1) it does not have any interaction energy whose absolute value is greater than the 1 kcal mol⁻¹ threshold, 2) it stabilizes some productive clusters but destabilizes others for the same goal, 3) it stabilizes both productive and unproductive clusters for the same goal, or 4) it destabilizes both productive and unproductive clusters for the same goal. Amino acid residues that are not near the active site fall into group 1) as they do not interact with the substrate and are neither stabilizing nor destabilizing for any goal.

To better understand our criteria for mutagenesis hotspot selection, let us consider a theoretical example with the binding energies (in kcal mol⁻¹) given in the table below. Let us further assume that clusters 1 and 2 are productive (the substrate is oriented so as to facilitate the reaction) and cluster 3 is unproductive for a certain goal.

| Residue | Cluster 1 | Cluster 2 | Cluster 3 |
|----------------|------------------|------------------|------------------|
| Ala1 | - 2.5 | - 2.0 | - 1.5 |
| Glu3 | - 5.5 | + 3.2 | - 5.4 |

Based on these numbers, Glu3 binds by $0.1 \text{ kcal mol}^{-1}$ more favorably to the ligand in the productive cluster 1 than in the unproductive cluster 3. If it would only be required that either $E_{Glu3}^{cl.1} < E_{Glu3}^{cl.3} + c$ or $E_{Glu3}^{cl.2} < E_{Glu3}^{cl.3} + c$ is true, then Glu3 would be stabilizing because the first of the two inequalities is fulfilled. However, Glu3 binds by $8.6 \text{ kcal mol}^{-1}$ less favorably in the productive cluster 2 than in cluster 3. Thus, it destabilizes the cluster 2 by a much greater amount than it stabilizes cluster 1. We therefore require for the binding free energies of a stabilizing residue to be lower in all the productive clusters than the energies (plus threshold c) in all the unproductive ones (inequality (S1)), and that at least one of the productive clusters does not have a higher energy for this residue than its energy (minus threshold c) in at least one unproductive cluster (equation (S2)). Both requirements are not fulfilled by Glu3, but Ala1 meets both inequalities. For a residue to be destabilizing, it would need to fulfill all requirements in (S3) and at least one in (S4). Therefore, Glu3 is a destabilizing residue as it meets the criteria (S3) and (S4).

V Experimental Confirmation

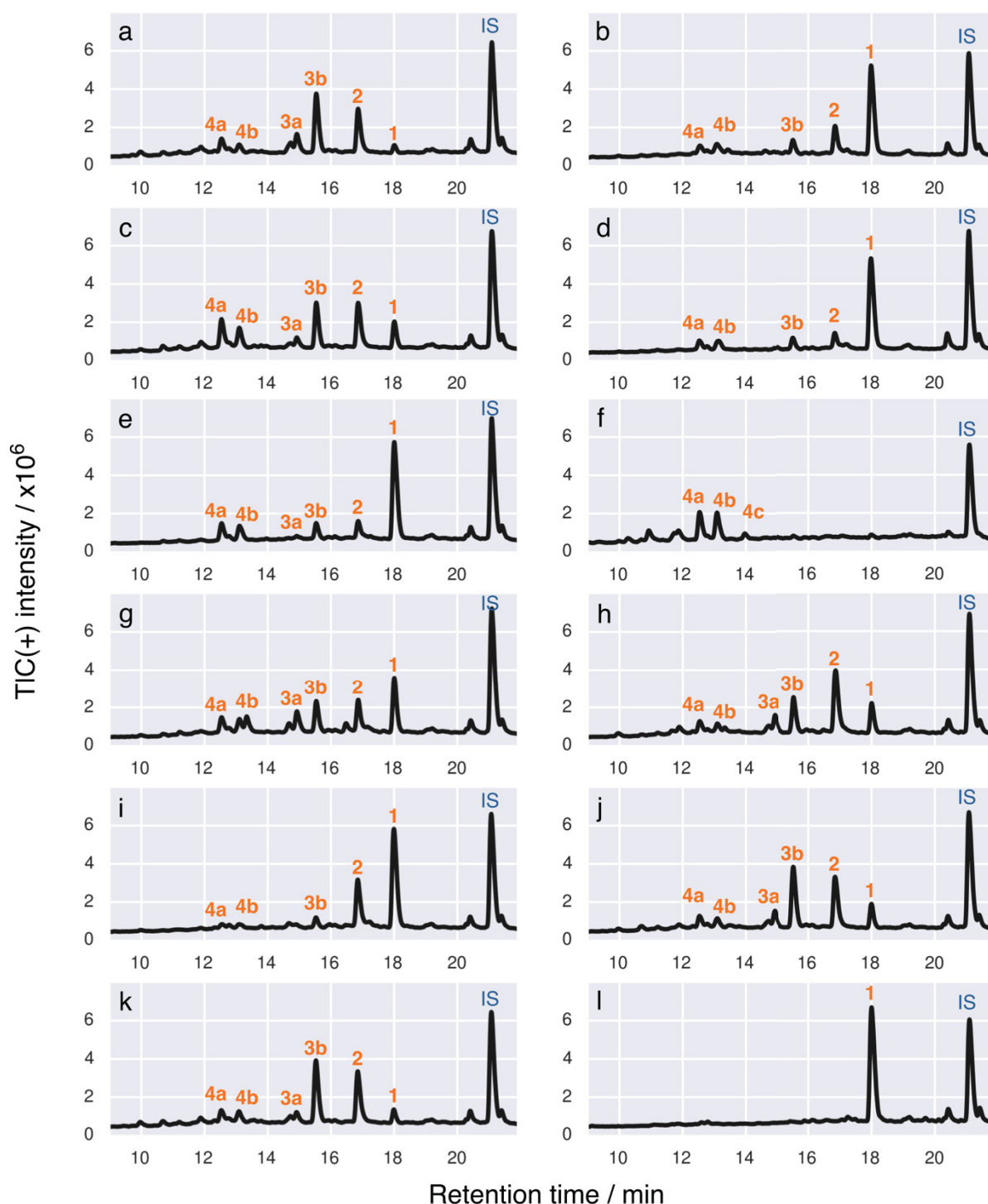


Figure S11. LC/MS-chromatograms of P450 BM3 oxidation products of β -cambrenediol (**1**). The parent mutant (a) bears two mutations (V78A and F87A) while the new engineered mutants (b–k) have an additional one: (b) K69R, (c) S72A, (d) S72I, (e) S72L, (f) L75A, (g) T268A, (h) T268S, (i) A328S, (j) F331Y, (k) F331T. The negative control (l) consisted of an empty pET28a vector, substrate **1**, and the internal standard (IS), i.e., dioctylphthalate.

Table S1. Product distribution of β -cembrenediol (**1**) oxidation by V78A/F87A P450 BM3 and its designed mutants.

| Mutation | Conversion (%) | Product distribution (%) ^{a,b} | | | | | | |
|----------|----------------|---|------|------|------|------|-----|-------|
| | | 2 | 3a | 3b | 4a | 4b | 4c | other |
| — | 98 | 23.8 | 10.4 | 31.9 | 7.6 | 4.7 | — | 21.6 |
| K69R | 13 | 35.6 | — | 17.2 | 12.4 | 16.0 | — | 18.9 |
| S72A | 92 | 26.3 | 5.8 | 23.7 | 15.8 | 11.4 | — | 17.1 |
| S72I | 17 | 23.3 | — | 19.3 | 16.0 | 20.0 | — | 21.5 |
| S72L | 24 | 23.6 | 3.0 | 18.4 | 21.9 | 20.5 | — | 12.5 |
| L75A | > 99 | — | — | — | 28.8 | 29.3 | 4.8 | 37.1 |
| T268A | 78 | 18.9 | 13.4 | 18.3 | 9.6 | 8.4 | — | 31.4 |
| T268S | 90 | 40.5 | 10.1 | 18.9 | 6.7 | 4.9 | — | 18.9 |
| A328S | 11 | 56.8 | — | 10.6 | 5.5 | 5.8 | — | 21.3 |
| F331Y | 90 | 30.4 | 9.3 | 34.0 | 6.5 | 5.4 | — | 14.4 |
| F331T | 96 | 28.9 | 5.4 | 33.3 | 7.1 | 6.7 | — | 18.6 |

^a Differences from 100% can occur due to rounding.

^b The product distribution was calculated based on the observed product peak areas under the assumption that the ionization of the metabolites is similar.

VI Supporting References

- (1) Bussi, G. Hamiltonian Replica Exchange in GROMACS: A Flexible Implementation. *Mol. Phys.* **2013**, *112*, 379–384.
- (2) Wang, L.; Friesner, R. A.; Berne, B. J. Replica Exchange with Solute Scaling: A More Efficient Version of Replica Exchange with Solute Tempering (REST2). *J. Phys. Chem. B* **2011**, *115*, 9431–9438.
- (3) Wang, K.; Chodera, J. D.; Yang, Y.; Shirts, M. R. Identifying Ligand Binding Sites and Poses Using GPU-Accelerated Hamiltonian Replica Exchange Molecular Dynamics. *J. Comput. Aided. Mol. Des.* **2013**, *27*, 989–1007.

CHEMISTRY

A **European** Journal

Supporting Information

Chemoenzymatic Route to Oxyfunctionalized Cembranoids Facilitated by Substrate and Protein Engineering

Priska Le-Huu^{+, [a]} Dominik Rekow^{+, [b]} Claudia Krüger,^[b] Ansgar Bokel,^[a] Tanja Heidt,^[b]
Sebastian Schaubach,^[b] Birgit Claasen,^[b] Sebastian Hölzel,^[a] Wolfgang Frey,^[b]
Sabine Laschat,^{*[b]} and Vlada B. Urlacher^{*[a]}

chem_201802250_sm_miscellaneous_information.pdf

Supporting Information

Chemoenzymatic route to oxyfunctionalized cembranoids facilitated by substrate and protein engineering

Priska Le-Huu,^{‡,[a]} Dominik Rekow,^{‡,[b]} Claudia Krüger,^[b] Ansgar Bokel,^[a] Tanja Heidt,^[b] Sebastian Schaubach,^[b] Birgit Claasen,^[b] Sebastian Hölzel,^[a] Wolfgang Frey,^[b] Sabine Laschat,^{*[b]} Vlada B. Urlacher^{*[a]}

^[a]Institute of Biochemistry, Heinrich-Heine University Düsseldorf, Universitätsstrasse 1, 40225 Düsseldorf, Germany

^[b]Institute of Organic Chemistry, University Stuttgart, Pfaffenwaldring 55, 70569 Stuttgart, Germany

Table of content

| | |
|---|----|
| Supporting experimental section..... | 2 |
| LC/MS analysis | 2 |
| NMR analysis | 2 |
| General procedure for the ring closing metathesis with Grubbs II catalyst [GP 1]..... | 2 |
| General procedure for esterification of alcohols with MTPA-Cl [GP 2] | 9 |
| General procedure for esterification of diols with MTPA-Cl [GP 3]..... | 9 |
| Mosher esters (S9) of menthol | 12 |
| Mosher esters (5) of cembranoid-ol (3d)..... | 15 |
| Mosher diesters (6) of cembranoid-diol (4)..... | 17 |
| Supporting results..... | 20 |
| Substrate screening | 20 |
| NMR studies with menthol..... | 22 |
| 2D-NMR assignment of the H signals of the (^{MTPA} S)-Mosher-diester (^{MTPA} S)-6..... | 26 |
| ¹ H, ¹ H-COSY, ¹ H, ¹³ C-HSQC, and ¹ H, ¹³ C-HMBC spectra | 27 |
| References | 55 |

Supporting experimental section

LC/MS analysis

Samples were analyzed on a Prominence/LC/MS 2020 (Shimadzu) using a Chromolith Performance RP-18e column 100 - 4.6 mm (Merck, Darmstadt, Germany). The column temperature was set to 30 °C and the flow rate was 1 mL/min. Gradient elution with 0.1 % formic acid in water and methanol was applied. Mass spectrometry was done in a dual ionization mode with ESI and APCI. Samples were detected in a positive scan mode.

NMR analysis

NMR spectra were recorded on a Bruker Avance 300, Avance 500 or Avance 700 spectrometer with TMS as internal standard. In the case of *E/Z*-isomers, data of the major isomer are given. IR spectra were recorded on a Bruker Vektor22 spectrometer equipped with an MKII golden gate single reflection diamond ATR system. Mass spectra were recorded with a Varian MAT 711 spectrometer (EI, 70 eV) and a Bruker Daltonics micrOTOF_Q (ESI) with nitrogen as carrier gas. Control of reactions and purity was performed with a Hewlett-Packard HP 6890 equipped with a HP-5 column (30 m × 0.32 mm). Chromatography was performed on silica gel (grain size 40–63 μm, Fluka). All reactions were performed under nitrogen in oven-dried glassware. All reagents were used as purchased unless otherwise noted. Solvents for chromatography were distilled prior to use. THF was distilled from potassium/benzophenone, Et₂O from sodium/benzophenone, CH₂Cl₂, Et₃N and DMF from CaH₂, and MeOH from magnesium. The reactions were monitored by TLC (Macherey-Nagel silica gel 60 F₂₅₄ plates) and visualized with an ethanolic solution of *p*-anisaldehyde and sulfuric acid or an aqueous solution of potassium permanganate, potassium carbonate and NaOH.

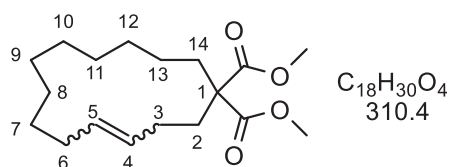
Dimethyl 2-(but-3-en-1-yl)-2-(undec-10-en-1-yl) malonate **S1** and 3-(but-3-en-1-yl)tetradec-13-en-2-one **S3** were prepared according ref.^[1]

General procedure for the ring closing metathesis with Grubbs II catalyst [GP 1]

In a dry Schlenk flask Grubbs II catalyst (1,3-bis-(2,4,6-trimethylphenyl)-2-imidazol-idinylidene)-dichloro-(tricyclohexylphosphin)-ruthenium (2.54 mg, 2.99 μmol) was dissolved in CH₂Cl₂ (12 mL). Then was added a solution of the diene (29.9 μmol) in CH₂Cl₂ (3 mL) and the mixture was refluxed for 14 h. After cooling to room temp. the catalyst was removed by filtration over silica and the solvent removed in vacuo. The crude product was purified by column chromatography on silica.

Dimethyl (*Z*)-cyclotetradec-4-ene-1,1-dicarboxylate (**1d**)

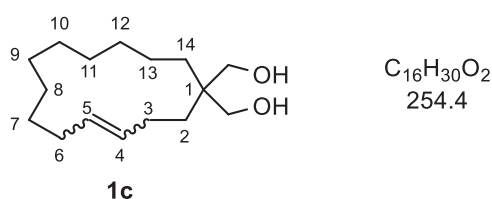
According to GP 1 dimethyl 2-(but-3-en-1-yl)-2-(undec-10-en-1-yl) malonate **S1** (80.0 mg, 240 μmol) was treated with Grubbs II (10.2 mg, 12.0 μmol). The crude product was purified by flash chromatography on silica (eluent: PE / Et₂O = 150 : 1 \rightarrow 100 : 1) to yield a pale yellow solid (34.0 mg, 110 μmol , 46 %) of an *E/Z* mixture (11 : 89 via ¹³C NMR).



$R_f = 0.44$ (PE / Et₂O = 4 : 1, KMnO₄); ¹H NMR (500 MHz, CDCl₃): $\delta = 1.05$ - 1.49 (m, 14H, 3-H, 4-H, 5-H, 6-H, 7-H, 8-H, 9-H), 1.79-2.15 (m, 8H, 2-H, 10-H, 13-H, 14-H), 3.71 (s, 6H, 2 x CO₂CH₃), 5.29-5.54 (m, 2H, 11-H, 12-H) ppm. ¹³C-NMR (125 MHz, CDCl₃): $\delta = 19.9$ (C-3), 21.5 (C-13), 23.8, 24.2, 25.4, 26.1, 26.9, 27.4 (C-4, C-5, C-6, C-7, C-8, C-9, C-10), 30.1 (C-2), 31.2 (C-14), 52.4 (2 x CO₂CH₃), 57.0 (C-1), 128.0, 130.5 (C-11, C-12), 172.2 (2 x CO₂CH₃) ppm. MS (ESI): $m/z = 333.2$ [M + Na]⁺, 254.9, 220.2, 202.2, 145.1. HRMS (ESI): C₁₈H₃₀NaO₄⁺ calcd. 333.2036 [M + Na]⁺, found 333.2028. FT-IR (ATR): $\tilde{\nu} = 2926$ (s), 2854 (m), 2260 (w), 1735 (vs), 1434 (m), 1262 (m), 1201 (s), 994 (w), 911 (m) cm⁻¹. CHN analysis: C₁₈H₃₀O₄ (310.4 g/mol), calcd. C 69.64 %, H 9.74 %; found C 69.40 %, H 9.73 %. The spectroscopic data are in accordance with ref.^[2]

Cyclotetradec-4-en-1,1-diyldimethanol (**1c**)

A solution of dimethyl (*E*)-cyclotetradec-4-ene-1,1-dicarboxylate **1d** (200 mg, 0.65 mmol) in CH₂Cl₂ (6 mL) was cooled to -78 °C and DIBAL-H (4.54 mL, 4.54 mmol, 1M in toluene) were dropwise added. The mixture was warmed to -25 °C and stirred for 2 h. Then the mixture was hydrolyzed with sat. Seignette salt solution (15 mL) and diluted with CH₂Cl₂ (60 mL). The gel like precipitate was removed by filtration via Celite and washed with CH₂Cl₂ (150 mL). The aqueous layer was extracted with CH₂Cl₂ (3 x 30 mL) and the combined organic layers were dried over MgSO₄ getrocknet. The crude product was purified by flash chromatography on silica (eluent: PE / Et₂O = 2 : 1) to yield a colorless solid (128 mg, 0.50 mmol, 78 %) as an *E/Z* mixture (17 : 83 by ¹H NMR).

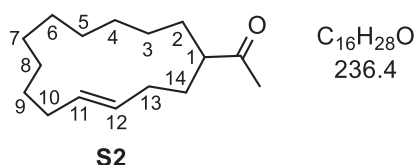


$R_f = 0.21$ (PE / Et₂O = 2 : 1, anisaldehyde). Mp.: 122 °C. ¹H NMR (500 MHz, CDCl₃): $\delta = 1.14$ - 1.23 (m, 2H, 13-H), 1.23-1.40 (m, 16H, 2-H, 7-H, 8-H, 9-H, 10-H, 11-H, 12-H, 14-H), 1.94-2.04

(m, 4H, 3-H, 6-H), 2.22-2.30 (m, 2H, OH), 3.57 (s, 4H, CH₂OH), 5.37 (dt, *J* = 10.8, 7.2 Hz, 1H, 4-H), 5.42 (dt, *J* = 10.8, 7.1 Hz, 1H, 5-H) ppm. ¹³C NMR (125 MHz, CDCl₃): δ = 19.2 (C-13), 20.6 (C-3), 23.6, 23.9, 26.0, 26.7, 27.1, 27.4, 29.3, 30.1 (C-2, C-7, C-8, C-9, C-10, C-11, C-12, C-14), 41.4 (C-1), 69.7 (CH₂OH), 129.4 (C-4), 129.7 (C-5) ppm. MS (EI): *m/z* (%) = 254.3 (1) [M]⁺, 236.2 (69) [M - H₂O]⁺, 218.2 (10) [M - 2 H₂O]⁺, 205.2 (52) [M - H₂O - CH₂OH]⁺, 191.2 (5) [C₁₄H₂₃]⁺, 175.2 (7) [C₁₃H₁₉]⁺, 161.1 (8) [C₁₂H₁₇]⁺, 149.1 (12) [C₁₁H₁₇]⁺, 135.1 (17) [C₁₀H₁₅]⁺, 123.1 (32) [C₉H₁₅]⁺, 109.1 (63) [C₈H₁₃]⁺, 95.1 (90) [C₇H₁₁]⁺, 81.0 (100) [C₆H₉]⁺, 67.0 (97) [C₅H₇]⁺, 55.0 (87) [C₄H₇]⁺, 41.0 (70) [C₃H₅]⁺. HRMS (EI): C₁₆H₃₀O₂⁺ calcd. 254.2246 [M]⁺, found 254.2251. FT-IR (ATR): $\tilde{\nu}$ = 3313 (s), 3002 (w), 2927 (vs), 2858 (s), 1686 (w), 1461 (m), 1258 (w), 1029 (s), 967 (w), 892 (w), 709 (m) cm⁻¹.

(*E*)-1-(Cyclotetradec-4-en-1-yl)ethan-1-one (S-HEI125c)

According to GP 1 3-(but-3-en-1-yl)tetradec-3-en-2-one **S3** (230 mg, 870 μmol) was treated with Grubbs II catalyst (37.0 mg, 43.5 μmol). The crude product was purified by flash chromatography on silica (eluent: PE / Et₂O = 125 : 1 → 100 : 1) to yield a colorless solid (42.0 mg, 178 μmol, 20 %) of an *E/Z* mixture (79 : 21 via ¹H NMR).

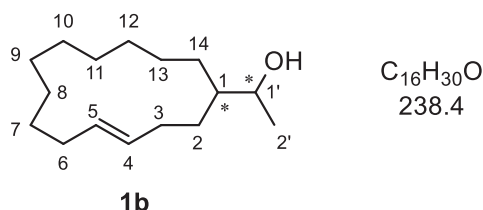


*R*_f = 0.65 (PE / Et₂O = 5 : 1, anisaldehyde). ¹H NMR (500 MHz, CDCl₃): δ = 1.13-1.50 (m, 16H, 2-H od. 14-H, 3-H, 4-H, 5-H, 6-H, 7-H, 8-H, 9-H), 1.57-1.65 (m, 2H, 2-H od. 14-H), 1.72-1.88 (m, 2H, 10-H od. 13-H), 2.14 (s, 3H, C(O)CH₃), 1.98-2.23 (m, 2H, 10-H od. 13-H), 2.70-2.81 (m, 1H, 1-H), 5.29-5.34 (m, 2H, 11-H, 12-H) ppm. ¹³C NMR (125 MHz, CDCl₃): δ = 23.4, 23.8, 24.2, 24.4, 24.5, 26.5, 27.1, 27.7, 29.7, 30.2, 31.1 (C-2, C-3, C-4, C-5, C-6, C-7, C-8, C-9, C-10, C-13, C-14), 28.9 (C(O)CH₃), 47.1 (C-1), 130.5, 132.4 (C-11, C-12), 213.4 (C(O)CH₃) ppm. MS (EI): *m/z* (%) = 236.2 (100) [M]⁺, 221.2 (4) [M - CH₃]⁺, 203.2 (1), 193.2 (7) [M - C(O)CH₃]⁺, 178.2 (19), 161.1 (4), 154.1 (8), 135.1 (10), 122.1 (10), 109.1 (16), 95.1 (24), 81.0 (25), 71.0 (53), 55.0 (31), 43.0 (44). HRMS (EI): C₁₆H₂₈O⁺ calcd. 236.2140 [M]⁺, found 236.2142. FT-IR (ATR): $\tilde{\nu}$ = 2923 (s), 2853 (s), 1715 (s), 1457 (m), 1376 (w), 1351 (w), 1245 (w), 1164 (w), 971 (m), 904 (vs), 727 (vs), 650 (s) cm⁻¹. CHN analysis: C₁₆H₂₈O (236.2 g/mol), calcd. C 81.29 %, H 11.94 %; found C 80.72 %, H 11.88 %.

1-(Cyclotetradec-4-en-1-yl)ethanol (1b)

A solution of (*E*)-1-(cyclotetradec-4-en-1-yl)ethan-1-one **S2** (100 mg, 0.63 mmol) in CH₂Cl₂ (6 mL) was cooled to -78 °C and DIBAL-H (1.40 mL, 1.40 mmol, 1M in toluene) were dropwise added. The mixture was stirred at -78°C for 2 h. Then the mixture was hydrolyzed with sat.

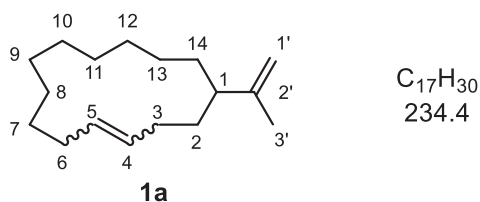
Seignette salt solution (15 mL) and diluted with CH₂Cl₂ (60 mL). The gel like precipitate was removed by filtration via Celite and washed with CH₂Cl₂ (150 mL). The aqueous layer was extracted with CH₂Cl₂ (3 × 30 mL) and the combined organic layers were dried over MgSO₄. The crude product was purified by flash chromatography on silica (eluent: PE / Et₂O = 5 : 1) to yield a colorless oil (147 mg, 0.62 mmol, 97 %) as (1 : 1) mixture of diastereomers.



R_f = (PE / Et₂O = 5 : 1, anisaldehyde). The marked signals (*) belong to one diastereomer. ¹H NMR (500 MHz, CDCl₃): δ = 1.13-1.19 (m, 4H, 13-H, 13-H*), 1.14 (d, *J* = 6.5 Hz, 3H, 2'-H), 1.16 (d, *J* = 6.7 Hz, 3H, 2'-H*), 1.19-1.47 (m, 32H, 2-H, 2-H*, 7-H, 7-H*, 8-H, 8-H*, 9-H, 9-H*, 10-H, 10-H*, 11-H, 11-H*, 12-H, 12-H*, 14-H, 14-H*), 1.56-1.65 (m, 2H, 1-H, 1-H*), 2.02-2.09 (m, 4H, 6-H, 6-H*), 2.09-2.18 (m, 4H, 3-H, 3-H*), 3.93-4.01 (m, 2H, 1'-H, 1'-H*), 5.24-5.41 (m, 4H, 4-H, 4-H*, 5-H, 5-H*) ppm. ¹³C NMR (125 MHz, CDCl₃): δ = 19.3 (C-2'), 19.9 (C-2'), 24.0, 24.2, 24.27, 24.33, 24.4, 24.6, 24.7, 24.80, 24.83, 25.7, 26.5, 26.93, 26.94, 27.0, 27.5 (C-2, C-2*, C-7, C-7*, C-8, C-8*, C-9, C-9*, C-10, C-10*, C-11, C-11*, C-12, C-12*, C-13, C-13*, C-14, C-14*), 29.6 (C-3), 30.0 (C-3), 30.9 (C-6), 31.1 (C-6), 37.6 (C-1), 38.1 (C-1), 68.2 (C-1'), 68.7 (C-1'), 131.1 (C-4), 131.3 (C-4), 131.5 (C-5), 131.6 (C-5) ppm. MS (EI): *m/z* (%) = 238.2 (41) [M]⁺, 220.2 (100) [M - H₂O]⁺, 205.2 (6) [M - H₂O - CH₃]⁺, 191.2 (15) [M - H₂O - C₂H₅]⁺, 177.2 (7) [C₁₃H₂₁]⁺, 163.1 (11) [C₁₂H₁₉]⁺, 149.1 (19) [C₁₁H₁₇]⁺, 135.1 (23) [C₁₀H₁₅]⁺, 121.1 (21) [C₉H₁₃]⁺, 109.1 (36) [C₈H₁₃]⁺, 95.1 (60) [C₇H₁₁]⁺, 81.0 (59) [C₆H₉]⁺, 67.0 (58) [C₅H₇]⁺, 55.0 (69) [C₄H₇]⁺, 41.0 (49) [C₃H₅]⁺. HRMS (EI): C₁₆H₃₀O⁺ calcd. 238.2297 [M]⁺, found 238.2298. FT-IR (ATR): $\tilde{\nu}$ = 3361 (m), 2925 (vs), 2856 (s), 1444 (m), 1371 (w), 1289 (w), 1096 (m), 967 (m), 880 (w), 708 (w) cm⁻¹.

5-(Prop-1-en-2-yl)cyclotetradec-1-ene (1a)

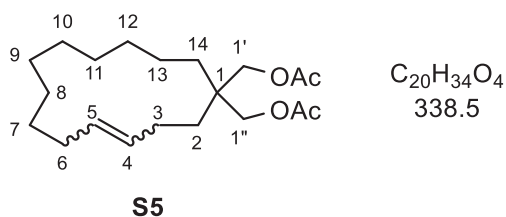
To a cooled solution of methyltriphenylphosphoniumbromide (911 mg, 2.55 mmol) in THF (10 mL) was added *n*BuLi (1.6 M in hexane, 1.59 mL, 2.55 mmol) at 0°C stirred for 30 min. Then was added a solution of (*E*)-1-(cyclotetradec-4-en-1-yl)ethan-1-one **S2** (120 mg, 510 μmol) in THF (5 mL) and the mixture was stirred for 40 h at room temp., followed by quenching with sat. NH₄Cl (10 mL), extraction with hexane (3 × 30 mL), drying over MgSO₄ and removal of the solvent in vacuo. Purification of the crude product by flash chromatography on silica (eluent: pentane) yielded a colorless oil (110 mg, 470 μmol, 92 %).



$R_f = 0.95$ (pentane, anisaldehyde). $^1\text{H NMR}$ (500 MHz, CDCl_3): $\delta = 1.09\text{--}1.52$ (m, 18H, 2-H, 7-H, 8-H, 9-H, 10-H, 11-H, 12-H, 13-H, 14-H), 1.56 (s, 3H, 3'-H), 1.91-1.98 (m, 1H, 3-H_a), 2.02-2.08 (m, 2H, 6-H), 2.08-2.14 (m, 1H, 3-H_b), 2.47 (dddd, $J = 11.2, 7.8, 6.9, 3.9$ Hz, 1H, 1-H), 4.85-4.87 (m, 1H, 1'-H_a), 4.89-4.91 (m, 1H, 1'-H_b), 5.23-5.34 (m, 2H, 4-H, 5-H) ppm. $^{13}\text{C NMR}$ (125 MHz, CDCl_3): $\delta = 17.8$ (C-3'), 23.4, 23.8, 24.6, 24.8, 25.5, 27.2, 28.0 (C-7, C-8, C-9, C-10, C-11, C-12, C-13), 29.5 (C-14), 29.8 (C-6), 31.5 (C-2), 32.0 (C-3), 40.4 (C-1), 112.6 (C-1'), 132.0, 132.1 (C-4, C-5), 147.6 (C-2') ppm. MS (EI): m/z (%) = 234.2 (100) $[\text{M}]^+$, 219.2 (8) $[\text{C}_{16}\text{H}_{27}]^+$, 205.2 (3) $[\text{C}_{15}\text{H}_{25}]^+$, 191.2 (10) $[\text{C}_{14}\text{H}_{23}]^+$, 177.2 (2) $[\text{C}_{13}\text{H}_{21}]^+$, 163.2 (3) $[\text{C}_{12}\text{H}_{19}]^+$, 149.1 (10) $[\text{C}_{11}\text{H}_{17}]^+$, 135.1 (13) $[\text{C}_{10}\text{H}_{15}]^+$, 121.1 (16) $[\text{C}_9\text{H}_{13}]^+$, 109.1 (29) $[\text{C}_8\text{H}_{13}]^+$, 95.1 (44) $[\text{C}_7\text{H}_{11}]^+$, 82.1 (55) $[\text{C}_6\text{H}_{10}]^+$, 69.1 (44) $[\text{C}_5\text{H}_9]^+$, 55.0 (36) $[\text{C}_4\text{H}_7]^+$, 41.0 (35) $[\text{C}_3\text{H}_5]^+$. HRMS (EI): $\text{C}_{17}\text{H}_{30}^+$ calcd. 234.2348 $[\text{M}]^+$, found 234.2345. FT-IR (ATR): $\tilde{\nu} = 2924$ (vs), 2852 (s), 1643 (w), 1441 (m), 1374 (w), 969 (m), 888 (m), 837 (w), 778 (w), 712 (w) cm^{-1} .

Cyclotetradec-4-en-1,1-diylbis(methylen)diacetate (S5)

To a solution of cyclotetradec-4-en-1,1-diylmethanol **1c** (90.0 mg, 0.35 mmol) in CH_2Cl_2 (5 mL) were added DMAP (2.20 mg, 18.0 μmol) and Ac_2O (288 mg, 2.83 mmol) and the resulting mixture was stirred for 18 h at room temp. Then was added MeOH (5 mL) and stirring was continued for 1 h. The mixture was diluted with hexanes (50 mL), the organic layer was washed with H_2O (2×10 mL) and brine (10 mL), dried over MgSO_4 and evaporated. Purification of the crude product by flash chromatography on silica (PE / EtOAc = 2 : 1) yielded colorless crystals (114 mg, 0.34 mmol, 95 %).



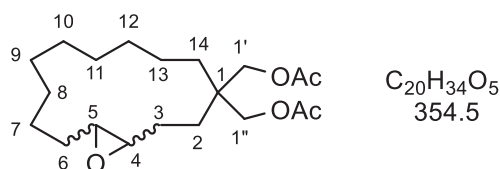
$R_f = 0.90$ (PE / EtOAc = 2 : 1, anisaldehyde). Mp.: 72 °C. $^1\text{H NMR}$ (500 MHz, CDCl_3): $\delta = 1.00\text{--}1.09$ (m, 2H, 13-H), 1.10-1.16 (m, 2H, 14-H), 1.19-1.37 (m, 14H, 2-H, 7-H, 8-H, 9-H, 10-H, 11-H, 12-H), 1.68 (s, 6H, CH_3), 1.83-1.90 (m, 2H, 3-H), 1.90-1.97 (m, 2H, 6-H), 3.97 (s, 4H, 1'-H, 1''-H), 5.35 (dt, $J = 10.7, 7.6$ Hz, 1H, 4-H), 5.45 (dt, $J = 10.7, 8.2$ Hz, 1H, 5-H) ppm.

$^{13}\text{C NMR}$ (125 MHz, CDCl_3): $\delta = 19.1$ (C-13), 20.4 (CH_3), 20.6 (C-3), 23.9, 24.2, 26.8, 27.4, 27.7, 30.6 (C-2, C-7, C-8, C-9, C-10, C-11), 25.7 (C-6), 26.3 (C-12), 29.7 (C-14), 39.9 (C-1), 65.9 (C-1', C-1''), 129.3 (C-4), 129.9 (C-5), 170.1 (C=O) ppm. MS (ESI): $m/z = 361.23$

[M + Na]⁺, 301.14, 279.23, 219.21. HRMS (ESI): C₂₀H₃₄NaO₄⁺ calcd. 361.2349 [M + Na]⁺, found 361.2346. FT-IR (ATR): $\tilde{\nu}$ = 2928 (m), 2860 (m), 1738 (s), 1462 (m), 1364 (m), 1226 (vs), 1041 (s), 983 (w), 710 (w) cm⁻¹.

15-Oxabicyclo[12.1.0]pentadecan-4,4-diylbis(methylene) diacetate (S6)

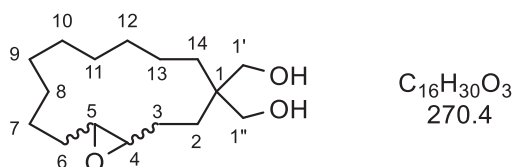
To a cooled solution of cyclotetradec-4-en-1,1-diylbis(methylen)diacetate **S5** (45.0 mg, 132 μ mol) in CH₂Cl₂ (6 mL) was added a solution of *m*CPBA (65.0 mg, 264 μ mol, 70 % pure) in CH₂Cl₂ (4 mL) at 0°C. The mixture was stirred for 20 h at 0°C and hydrolyzed with sat. K₂CO₃ (10 mL). The layers were separated and the aqueous layer was extracted with CH₂Cl₂ (3 \times 40 mL). The combined organic layers were washed with sat. NaHCO₃ (2 \times 20 mL), dried over MgSO₄ and evaporated. The purification of the crude product by flash chromatography on silica (PE / Et₂O = 5 : 2) yielded a colorless solid (45.0 mg, 126 μ mol, 96 %).



R_f = 0.27 (PE / Et₂O = 3 : 1, anisaldehyde). Mp.: 75 °C. ¹H NMR (500 MHz, CDCl₃): δ = 1.10-1.66 (m, 22H, 2-H, 3-H, 6-H, 7-H, 8-H, 9-H, 10-H, 11-H, 12-H, 13-H, 14-H), 2.07 (s, 6H, 3'-H, 3''-H), 2.91 (ddd, *J* = 7.8, 4.5, 4.0 Hz, 1H, 4-H), 2.99 (ddd, *J* = 7.9, 4.9, 4.0 Hz, 1H, 5-H), 3.85-3.99 (m, 4H, 1'-H, 1''-H) ppm. ¹³C NMR (125 MHz, CDCl₃): δ = 19.1 (C-13), 20.1 (C-3), 20.9 (C-3', C-3''), 22.6, 23.51, 23.53, 25.8, 26.2, 26.5, 26.9, 29.2 (C-2, C-7, C-8, C-9, C-10, C-11, C-12, C-14), 25.8 (C-6), 39.3 (C-1), 57.0 (C-4), 57.5 (C-5), 65.8, 65.9 (C-1', C-1''), 170.9, 171.0 (C-2', C-2'') ppm. MS (ESI): *m/z* = 377.23 [M + Na]⁺, 295.23, 277.22, 235.20, 217.19. HRMS (ESI): C₂₀H₃₄NaO₅⁺ calcd. 377.2298 [M + Na]⁺, found 377.2304. FT-IR (ATR): $\tilde{\nu}$ = 2930 (m), 2860 (m), 1737 (s), 1463 (m), 1365 (m), 1226 (vs), 1034 (s), 915 (w), 732 (w) cm⁻¹.

15-Oxabicyclo[12.1.0]pentadecane-4,4-diyl dimethanol (S7)

To a solution of 15-oxabicyclo[12.1.0]pentadecan-4,4-diylbis(methylene) diacetate **S6** (15.0 mg, 42.1 μ mol) in MeOH (5 mL) was added K₂CO₃ (10.0 mg, 71.4 μ mol) and the mixture was stirred for 18 h at room temp., followed by hydrolysis with sat. NH₄Cl (5 mL). The layers were separated and the aqueous layer was extracted with Et₂O (2 \times 20 mL). The organic layers were dried over MgSO₄, evaporated and the crude product was purified by flash chromatography on silica (hexane / EtOAc = 3 : 2) to yield a colorless solid (11.0 mg, 40.7 μ mol, 97 %).

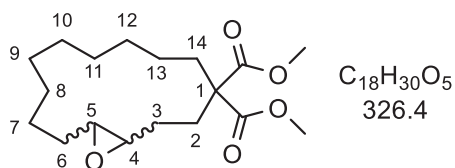


S7

$R_f = 0.12$ (PE / EtOAc = 1 : 1, anisaldehyde). Mp.: 125 °C. $^1\text{H NMR}$ (500 MHz, CDCl_3): $\delta = 1.09$ -1.68 (m, 22H, 2-H, 3-H, 6-H, 7-H, 8-H, 9-H, 10-H, 11-H, 12-H, 13-H, 14-H), 2.29-2.49 (br, 2H, OH), 2.94 (dt, $J = 8.0, 4.0$ Hz, 1H, 4-H or 5-H), 2.97 (dt, $J = 8.5, 4.0$ Hz, 1H, 4-H or 5-H), 3.56-3.59 (m, 4H, 1'-H, 1''-H) ppm. $^{13}\text{C NMR}$ (125 MHz, CDCl_3): $\delta = 19.4, 20.4, 22.6, 23.5, 23.6, 25.7, 25.86, 25.93, 26.6, 27.1, 29.3$ (C-2, C-3, C-6, C-7, C-8, C-9, C-10, C-11, C-12, C-13, C-14), 41.0 (C-1), 57.4, 57.6 (C-4, C-5), 69.1, 69.4 (C-1', C-1'') ppm. MS (ESI): $m/z = 293.21$ [$\text{M} + \text{Na}$] $^+$, 253.22, 235.21, 217.19, 135.12, 121.10, 109.10. HRMS (ESI): $\text{C}_{16}\text{H}_{30}\text{NaO}_3^+$ calcd. 293.2087 [$\text{M} + \text{Na}$], found 293.2074. FT-IR (ATR): $\tilde{\nu} = 3420$ (br), 2929 (s), 2853 (m), 2361 (w), 2245 (w), 1462 (m), 1260 (w), 1052 (m), 1002 (m), 906 (s), 799 (m), 728 (vs), 647 (w) cm^{-1} .

Dimethyl-15-oxabicyclo[12.1.0]pentadecane-4,4-dicarboxylate (S4)

To a cooled solution of dimethyl (*Z*)-cyclotetradec-4-ene-1,1-dicarboxylate **1d** (10.0 mg, 32.2 μmol) in CH_2Cl_2 (3 mL) was added a solution of *m*CPBA (15.0 mg, 60.9 μmol , 70% pure) in CH_2Cl_2 (2 mL) at 0°C. The mixture was stirred 20 h bei 0 °C and hydrolyzed by addition of sat. K_2CO_3 (5 mL). The layers were separated and the aqueous layer was extracted with CH_2Cl_2 (3 \times 10 mL) extrahiert. The combined organic layers were washed with sat. NaHCO_3 (2 \times 10 mL), dried over MgSO_4 and evaporated. Purification of the crude product by flash chromatography on silica (eluent: PE / $\text{Et}_2\text{O} = 5 : 1$) yielded a colorless solid (9.10 mg, 27.8 μmol , 88 %).



S4

$R_f = 0.20$ (PE / $\text{Et}_2\text{O} = 5 : 1$, anisaldehyde). Mp.: 109 °C. $^1\text{H NMR}$ (500 MHz, CDCl_3): $\delta = 0.91$ -0.99 (m, 1H, 13-H), 1.14-1.52 (m, 17H, 3-H, 6-H_a, 7-H, 8-H, 9-H, 10-H, 11-H, 12-H, 13-H), 1.65-1.73 (m, 1H, 6-H_b), 1.78 (ddd, $J = 14.5, 13.7, 3.3$ Hz, 1H, 14-H_a), 1.90-1.99 (m, 2H, 2-H_a, 14-H_b), 2.15 (ddd, $J = 14.4, 13.7, 4.4$ Hz, 1H, 2-H_b), 2.94 (ddd, $J = 8.9, 3.8, 3.5$ Hz, 1H, 4-H), 2.98 (ddd, $J = 8.7, 4.5, 3.8$ Hz, 1H, 5-H), 3.72 (s, 3H, CH_3), 3.74 (s, 3H, CH_3) ppm. $^{13}\text{C NMR}$ (125 MHz, CDCl_3): $\delta = 20.1$ (C-13), 21.5 (C-3), 22.7, 23.0, 25.2, 26.9, 31.6 (C-8, C-9, C-10, C-11, C-12), 24.1 (C-7), 26.3 (C-6), 27.4 (C-2), 30.0 (C-14), 52.5, 52.6 (CH_3, CH_3), 56.9 (C-1), 56.6 (C-4), 57.4 (C-5), 171.8, 172.0 (C=O) ppm. MS (ESI): $m/z = 349.20$ [$\text{M} + \text{Na}$] $^+$, 327.22 [M

+ H]⁺, 295.19 [M - OCH₃]⁺, 267.19 [M - CO₂CH₃]⁺, 235.17, 207.17, 189.16. HRMS (ESI): C₁₈H₃₀NaO₅⁺ calcd. 349.1985 [M + Na]⁺, found 349.1985. FT-IR (ATR): $\tilde{\nu}$ = 2925 (s), 2858 (m), 1733 (vs), 1461 (m), 1434 (m), 1254 (m), 1220 (m), 1196 (s), 1161 (m), 1120 (w), 1094 (w), 1006 (w), 881 (w), 829 (w), 797 (w), 749 (w), 724 (w) cm⁻¹.

General procedure for esterification of alcohols with MTPA-Cl [GP 2]

The reaction was carried out in accordance with the literature.^[3] A solution of the alcohol (1.0 equiv.) in dry CH₂Cl₂ was prepared and cooled to 0 °C in an ice bath for 20 min. Dry pyridine (4.0 equiv.), a solution of (S)-(+)- or (R)-(-)- α -methoxy- α -trifluoromethylphenylacetyl chloride (2.5 equiv.) in dry CH₂Cl₂ (1 mL) and DMAP (0.5 equiv.) were added successively at 0 °C. The mixture was warmed to room temperature and stirred for 22 h before being quenched with saturated NaHCO₃ solution (5 mL). The aqueous phase was extracted with CH₂Cl₂ (3 x 15 mL) and the combined organic fractions were dried with MgSO₄ and evaporated under reduced pressure. The intense yellow crude product was then purified using column chromatography on silica (eluent: PE / EtOAc = 5 : 1) to give the MTPA ester as a slightly yellow oil.

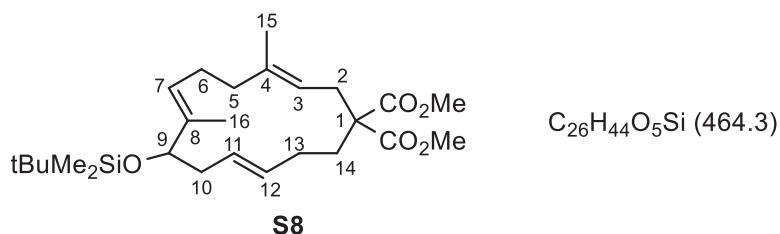
General procedure for esterification of diols with MTPA-Cl [GP 3]

The reaction was carried out in accordance with the literature.^[3] A solution of the diol (1.0 equiv.) in dry CH₂Cl₂ was prepared and cooled to 0 °C in an ice bath for 20 min. Dry pyridine (4.0 equiv.), a solution of (S)-(+)- or (R)-(-)- α -methoxy- α -trifluoromethylphenylacetyl chloride (3.5 equiv.) in dry CH₂Cl₂ (1 mL) and DMAP (0.5 equiv.) were added successively at 0 °C. The mixture was warmed to room temperature and stirred for 22 h before being quenched with saturated NaHCO₃ solution (6 mL). The aqueous phase was extracted with CH₂Cl₂ (3 x 20 mL) and the combined organic fractions were dried with MgSO₄ and evaporated under reduced pressure. The intense yellow crude product was then purified using column chromatography on silica PE / EtOAc = 3 : 1) to give the MTPA diester as a slightly yellow oil.

Dimethyl (3*E*,7*E*,11*E*)-9-[(*tert*-butyldimethylsilyl)oxy]-4,8-dimethylcyclotetradeca-3,7,11-trien-1,1-dicarboxylate (S8)

The reaction was carried out in accordance with our previously published method.^[4] Grubbs II catalyst ((1,3-bis(2,4,6-trimethylphenyl)-2-imidazolidinylidene)-dichloro(phenylmethylene)-(tricyclohexylphosphine)-ruthenium) (11.7 mg, 14.0 μ mol, 0.05 equiv.) was suspended in dry CH₂Cl₂ (140 mL) under a nitrogen atmosphere. The acyclic precursor^[4] dimethyl 2-(2*E*,6*E*)-8-[(*tert*-butyldimethylsilyl)oxy]-3,7-dimethylundeca-2,6,10-trien-1-yl)-2-((*E*)-4-methylhex-3-en-1-yl)malonate **S9** (150 mg, 280 μ mol) was diluted in dry CH₂Cl₂ (4 mL)

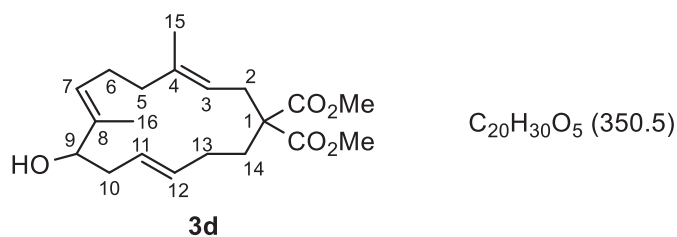
and added to the Grubbs II catalyst. The mixture was stirred for 48 h under reflux. The reaction mixture was filtered through silica and evaporated under reduced pressure. The crude product was purified by column chromatography on silica (PE / EtOAc = 50 : 1 → 25 : 1) to yield a colorless oil (87.0 mg, 187 μ mol, 66 %) as an *E/Z* mixture (*E* / *Z* = 86 : 14 according to GC).



R_f = 0.33 (PE / Et₂O = 8 : 1, phosphomolybdic acid). R_t = 23.76 min. ¹H NMR (500 MHz, CDCl₃): δ = -0.02 (s, 3H, Si(CH₃)), 0.02 (s, 3H, Si(CH₃)), 0.87 (s, 9H, C(CH₃)₃), 1.52 (s, 3H, 16-H), 1.56 (s, 3H, 15-H), 1.61-1.70 (m, 3H, 14-H_a, 13-H), 2.02-2.15 (m, 5H, 5-H_a, 6-H_a, 10-H, 14-H_b), 2.20-2.27 (m, 1H, 5-H_b), 2.32-2.41 (m, 1H, 6-H_b), 2.52-2.58 (m, 1H, 2-H_a), 2.86 (dd, *J* = 15.8, 10.1 Hz, 1H, 2-H_b), 3.71 (s, 3H, CO₂CH₃), 3.73 (s, 3H, CO₂CH₃), 3.84 (t, *J* = 7.4 Hz, 1H, 9-H), 4.76-4.82 (m, 1H, 3-H), 4.91-4.96 (m, 1H, 7-H), 4.96-5.02 (m, 1H, 11-H), 5.33-5.42 (m, 1H, 12-H) ppm. ¹³C NMR (175 MHz, CDCl₃): δ = -4.9 (Si(CH₃)), -4.7 (Si(CH₃)), 10.5 (C-16), 14.9 (C-15), 18.2 (C(CH₃)₃), 24.4 (C-6), 25.9 (C(CH₃)₃), 26.4 (C-13), 29.8 (C-2), 32.0 (C-14), 37.4 (C-10), 38.8 (C-5), 52.5 (CO₂CH₃), 52.6 (CO₂CH₃), 56.5 (C-1), 79.9 (C-9), 118.9 (C-3), 126.2 (C-7), 127.6 (C-11), 130.7 (C-12), 135.7 (C-8), 137.8 (C-4), 171.8 (CO₂CH₃), 172.3 (CO₂CH₃) ppm. HRMS (ESI): calcd. for [C₂₆H₄₄O₅SiNa]⁺ 487.2850, found 487.2831 [M + Na]⁺. FT-IR (ATR): $\tilde{\nu}$ = 2953 (m), 2929 (m), 2894 (w), 2856 (m), 1736 (vs), 1602 (w), 1471 (w), 1453 (w), 1435 (w), 1388 (w), 1361 (w), 1295 (w), 1270 (m), 1250 (m), 1237 (m), 1217 (m), 1201 (m), 1173 (m), 1065 (s), 1006 (w), 960 (w), 890 (w), 864 (w), 836 (m), 811 (w), 776 (m), 670 (w), 558 (w) cm⁻¹.

Dimethyl (3*E*,7*E*,11*E*)-9-((*tert*-butyldimethylsilyl)oxy)-4,8-dimethylcyclotetradeca-3,7,11-triene-1,1-dicarboxylate (**3d**)

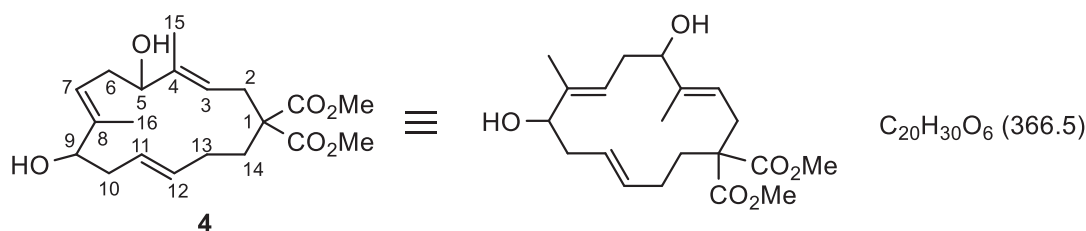
A solution of dimethyl (3*E*,7*E*,11*E*)-9-[(*tert*-butyldimethylsilyl)oxy]-4,8-dimethylcyclotetradeca-3,7,11-trien-1,1-dimalonate **S8** (100 mg, 215 μ mol) in dry THF (30 mL) was cooled to 0 °C for 30 min. TBAF (301 μ L, 79.6 mg, 301 μ mol, 1 M in THF) was added dropwise and the reaction mixture was stirred for 48 h at room temp. before being diluted with sat. NaHCO₃ (30 mL). The aqueous phase was extracted with Et₂O (3 × 30 mL) and the combined organic layers were dried over MgSO₄. The solvent was evaporated and the crude product was purified using column chromatography on silica (PE / EtOAc = 5 : 1) to give a colorless solid (56.0 mg, 160 μ mol, 74 %, >95 % GC purity).



$R_f = 0.41$ (PE / EE = 3 : 1, phosphomolybdic acid). $R_t = 24.62$ min. $^1\text{H NMR}$ (700 MHz, CDCl_3): $\delta = 1.56$ (s, 3H, 15-H), 1.58 (s, 3H, 16-H), 1.64-1.74 (m, 2H, 13-H), 1.80-1.85 (m, 1H, 14- H_a), 1.91-1.97 (m, 1H, 14- H_b), 2.11-2.19 (m, 3H, 5- H_a , 6- H_a , 10- H_a), 2.20-2.26 (m, 1H, 5- H_b), 2.28-2.35 (m, 2H, 6- H_b , 10- H_b), 2.64 (dd, $J = 15.7, 5.4$ Hz, 1H, 2- H_a), 2.77 (dd, $J = 15.7, 8.3$ Hz, 1H, 2- H_b), 3.72 (s, 3H, CO_2CH_3), 3.73 (s, 3H, CO_2CH_3), 3.98 (dd, $J = 8.8, 4.5$ Hz, 1H, 9-H), 4.78-4.82 (m, 1H, 3-H), 5.02 (dt, $J = 15.4, 7.7$ Hz, 1H, 11-H), 5.04-5.08 (m, 1H, 7-H), 5.46 (dt, $J = 14.8, 6.8$ Hz, 1H, 12-H) ppm. $^{13}\text{C NMR}$ (175 MHz, CDCl_3): $\delta = 11.2$ (C-16), 14.9 (C-15), 24.4 (C-6), 26.5 (C-13), 29.9 (C-2), 32.1 (C-14), 35.8 (C-10), 38.8 (C-5), 52.5 (CO_2CH_3), 52.6 (CO_2CH_3), 56.5 (C-1), 77.8 (C-9), 119.1 (C-3), 126.5 (C-11), 126.8 (C-7), 131.9 (C-12), 135.1 (C-8), 137.6 (C-4), 171.8 (CO_2CH_3), 172.1 (CO_2CH_3) ppm. HRMS (ESI): calcd. for $[\text{C}_{20}\text{H}_{30}\text{O}_5\text{Na}]^+$ 373.1985, found 373.1983 $[\text{M} + \text{Na}]^+$. FT-IR: $\tilde{\nu} = 3535$ (br, w) 3427 (br, w), 2951 (m), 2920 (m), 2852 (w), 1732 (vs), 1436 (m), 1295 (w), 1271 (m), 1202 (m), 1173 (m), 1099 (w), 1020 (w), 974 (w) cm^{-1} .

Dimethyl (3*E*,7*E*,11*E*)-5,9-dihydroxy-4,8-dimethylcyclotetradeca-3,7,11-triene-1,1-dicarboxylate (**4**)

Compound **4** was obtained from the cytochrome P450 monooxygenase-catalyzed oxidation of cembranoid-ol **3d**. For details see below.



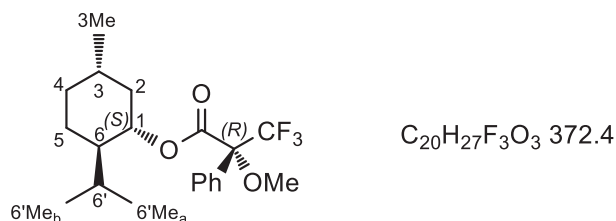
$R_t = 26.62$ min. $^1\text{H NMR}$ (500 MHz, CDCl_3): $\delta = 1.48$ -1.55 (m, 1H, 14- H_a), 1.55-1.63 (m, 1H, 13- H_a), 1.59 (s, 6H, 15-H, 16-H), 1.63-1.71 (m, 1H, 13- H_b), 2.03-2.16 (m, 2H, 14- H_b , 10- H_a), 2.20-2.26 (m, 1H, 10- H_b), 2.26-2.33 (m, 1H, 6- H_a), 2.47-2.54 (m, 1H, 6- H_b), 2.54-2.59 (m, 1H, 2- H_a), 2.89 (dd, $J = 16.5, 10.4$ Hz, 1H, 2- H_b), 3.70 (s, 3H, CO_2CH_3), 3.72 (s, 3H, CO_2CH_3), 3.87 (dd, $J = 10.6, 5.1$ Hz, 1H, 9-H), 4.13 (dd, $J = 10.6, 4.4$ Hz, 1H, 5-H), 4.89-5.00 (m, 2H, 11-H, 7-H) 5.04 (dd, $J = 5.3, 2.5$ Hz, 1H, 3-H), 5.41 (ddd, $J = 15.1, 8.8, 4.5$ Hz, 1H, 12-H) ppm. $^{13}\text{C NMR}$ (125 MHz, CDCl_3): $\delta = 10.3$ (C-16), 10.5 (C-15), 26.4 (C-13), 29.6 (C-2), 31.9 (C-14), 32.6 (C-6), 35.9 (C-10), 52.6 (CO_2CH_3), 52.8 (CO_2CH_3), 56.3 (C-1), 78.0 (C-5), 79.6 (C-9),

122.7 (C-3), 122.9 (C-7), 126.8 (C-11), 131.4 (C-12), 136.4 (C-8), 139.7 (C-4), 171.4 (CO₂CH₃), 172.0 (CO₂CH₃) ppm. HRMS (ESI): calcd. for [C₂₀H₃₀O₆Na]⁺ 389.1935, found 389.1904 [M + Na]⁺. FT-IR (ATR): $\tilde{\nu}$ = 3389 (br, m), 2922 (s), 2851 (m), 1732 (vs), 1453 (m), 1365 (w), 1272 (m), 1239 (m), 1206 (m), 1175 (m), 1016 (m), 856 (w), 732 (w), 554 (w) cm⁻¹.

Mosher esters (S9) of menthol

D-menthyl-(^{MTPA}R)-ester [(^{MTPA}R,D)-S9]

| | |
|---------------------------------|---|
| Method | GP 2 |
| D-menthol | 9.00 mg (57.6 μmol) |
| CH ₂ Cl ₂ | 1 mL |
| abs. pyridine | 18.6 μL (18.2 mg, 230 μmol) |
| (S)-MTPA-Cl | 26.9 μL (36.4 mg, 144 μmol) |
| DMAP | 3.52 mg (28.8 μmol) |
| Yield | 22 mg (57.6 μmol, >99 %), slightly yellow oil |



R_f = 0.86 (PE : EtOAc = 3 : 1, anisaldehyde). ¹H NMR (500 MHz, CDCl₃): δ = 0.67 (d, J = 6.9 Hz, 3H, 6'Me_a), 0.74 (d, J = 6.9 Hz, 3H, 6'Me_b), 0.84-0.89 (m, 1H, 1H, 4-H_a), 0.94 (d, J = 6.5 Hz, 3H, 3Me), 1.04 (dq, J = 39.6, 26.7, 13.7, 3.4 Hz, 1H, 5-H_a), 1.11 (q, J = 23.4, 11.6 Hz, 1H, 2-H_a), 1.40-1.45 (m, 1H, 6-H), 1.49-1.60 (m, 2H, 3-H, 6'-H), 1.64-1.72 (m, 2H, 5-H_b, 4-H_b), 2.10-2.16 (m, 1H, 2-H_b), 3.58 (s, 3H, OCH₃), 4.90 (td, J = 22.3, 11.3, 4.5 Hz, 1H, 1-H), 7.35-7.42 (m, 3H, Ph), 7.52-7.56 (m, 2H, Ph) ppm. ¹³C NMR (125 MHz, CDCl₃): δ = 15.6 (6'Me_a), 20.6 (6'Me_b), 22.0 (3Me), 22.8 (C-5), 25.3 (C-6'), 34.1 (C-4), 40.5 (C-2), 46.7 (C-6), 55.5 (OCH₃), 77.1 (C-1), 84.3 (q, J(¹⁹F) = 29.7 Hz, CCF₃), 123.5 (q, J = 289 Hz, CF₃), 127.1 (CH_{Ar}), 128.3 (CH_{Ar}), 129.5 (CH_{Ar}), 132.7 (C_{Ar}), 166.1 (CO) ppm. HRMS (ESI): calcd. for [C₂₀H₂₇F₃O₃Na]⁺ 395.1805, found 395.1921 [M + Na]⁺. FT-IR: $\tilde{\nu}$ = 2956 (br, m), 2872 (w), 1831 (w), 1741 (s), 1497 (w), 1452 (m), 1389 (w), 1371 (w), 1260 (s), 1167 (vs), 1121 (s), 1081 (m), 1018 (s), 994 (s), 964 (m), 909 (m), 846 (w), 819 (w), 805 (w), 764 (w), 732 (m), 719 (s), 967 (s), 648 (m), 542 (w), 507 (w), 467 (w)cm⁻¹.

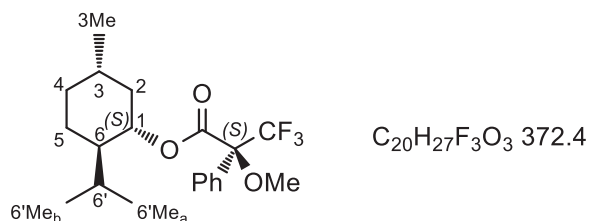
The spectroscopic data are in accordance with ref.^[5]

D-menthyl-(^{MTPA}S)-ester [(^{MTPA}S,D)-S9]

| | |
|-----------|---------------------|
| Method | GP 2 |
| D-menthol | 9.00 mg (57.6 μmol) |

CH₂Cl₂ 1 mL
 abs. pyridine 18.6 μL (18.2 mg, 230 μmol)
 (*R*)-MTPA-Cl 26.9 μL (36.4 mg, 144 μmol)
 DMAP 3.52 mg (28.8 μmol)

Yield 22 mg (57.6 μmol, >99 %), slightly yellow oil

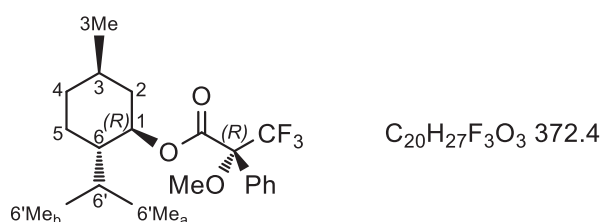


$R_f = 0.86$ (PE : EtOAc = 3 : 1, anisaldehyde). ¹H NMR (700 MHz, CDCl₃): δ = 0.77 (d, $J = 6.9$ Hz, 3H, 6'Me_a), 0.86 (ddd, $J = 38.4, 26.1, 12.5$ Hz, 1H, 4-H_a), 0.87 (d, $J = 6.9$ Hz, 3H, 6'Me_b), 0.91 (d, $J = 6.5$ Hz, 3H, 3Me), 0.98 (q, $J = 23.3, 11.7$ Hz, 1H, 2-H_a), 1.06 (dq, $J = 39.5, 25.9, 12.9, 3.5$ Hz, 1H, 5-H_a), 1.42-1.48 (m, 1H, 6-H), 1.48-1.55 (m, 1H, 3-H), 1.67-1.72 (m, 2H, 5-H_b, 4-H_b), 1.88 (dq, $J = 28.1, 21.3, 13.8, 6.9, 2.8$ Hz, 1H, 6'-H), 2.06-2.10 (m, 1H, 2-H_b), 3.53 (s, 3H, OCH₃), 4.88 (td, $J = 22.1, 11.1, 4.6$ Hz, 1H, 1-H), 7.39-7.42 (m, 3H, Ph), 7.51-7.55 (m, 2H, Ph) ppm. ¹³C NMR (175 MHz, CDCl₃): δ = 14.5 (6'Me_a), 19.8 (6'Me_b), 20.9 (3Me), 21.8 (C-5), 24.8 (C-6'), 30.4 (C-3), 33.0 (C-4), 39.0 (C-2), 45.6 (C-6), 54.3 (OCH₃), 76.4 (C-1), 83.7 (q, $J^{19F} = 27.8$ Hz, CCF₃), 122.4 (q, $J = 291$ Hz, CF₃), 126.4 (CH_{Ar}), 127.3 (CH_{Ar}), 128.5 (CH_{Ar}), 131.3 (C_{Ar}), 165.3 (CO) ppm. HRMS (ESI): calcd. for [C₂₀H₂₇F₃O₃Na]⁺ 395.1805, found 395.1939 [M + Na]⁺. FT-IR: $\tilde{\nu} = 2956$ (br, m), 2872 (w), 1832 (w), 1742 (s), 1452 (m), 1371 (w), 1261 (s), 1169 (vs), 1122 (m), 1081 (m), 1020 (s), 994 (s), 909 (m), 845 (w), 805 (w), 764 (w), 719 (s), 967 (m), 648 (m), 508 (w), 470 (w)cm⁻¹.

The spectroscopic data are in accordance with ref.^[5]

L-menthyl-(^{MTPA}*R*)-ester [(^{MTPA}*R,L*)-S9]

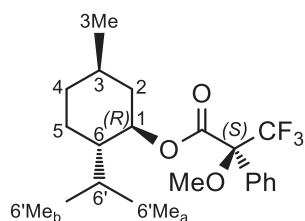
Method GP 2
 L-menthol 10.0 mg (64.0 μmol)
 CH₂Cl₂ 1 mL
 abs. pyridine 19.80 μL (20.2 mg, 256 μmol)
 (*S*)-MTPA-Cl 54.6 μL (40.4 mg, 160 μmol)
 DMAP 3.91 mg (32.0 μmol)
 Yield 24 mg (64.0 μmol, >99 %), slightly yellow oil



$R_f = 0.86$ (PE : EtOAc = 3 : 1, anisaldehyde). ^1H NMR (500 MHz, CDCl_3): $\delta = 0.77$ (d, $J = 6.9$ Hz, 3H, $6'\text{Me}_a$), 0.86 (ddd, $J = 38.4, 26.1, 12.5$ Hz, 1H, 4-H_a), 0.87 (d, $J = 6.9$ Hz, 3H, $6'\text{Me}_b$), 0.91 (d, $J = 6.5$ Hz, 3H, 3Me), 0.98 (q, $J = 23.3, 11.7$ Hz, 1H, 2-H_a), 1.06 (dq, $J = 39.5, 25.9, 12.9, 3.5$ Hz, 1H, 5-H_a), 1.42-1.48 (m, 1H, 6-H), 1.48-1.55 (m, 1H, 3-H), 1.67-1.72 (m, 2H, $5\text{-H}_b, 4\text{-H}_b$), 1.88 (dq, $J = 28.1, 21.3, 13.8, 6.9, 2.8$ Hz, 1H, $6'\text{-H}$), 2.06-2.10 (m, 1H, 2-H_b), 3.53 (s, 3H, OCH_3), 4.88 (td, $J = 22.1, 11.1, 4.6$ Hz, 1H, 1-H), 7.39-7.42 (m, 3H, Ph), 7.51-7.55 (m, 2H, Ph) ppm. ^{13}C NMR (125 MHz, CDCl_3): $\delta = 14.5$ ($6'\text{Me}_a$), 19.8 ($6'\text{Me}_b$), 20.9 (3Me), 21.8 (C-5), 24.8 (C-6'), 30.4 (C-3), 33.0 (C-4), 39.0 (C-2), 45.6 (C-6), 54.3 (OCH_3), 76.4 (C-1), 83.7 (q, $J(^{19}\text{F}) = 27.8$ Hz, CCF_3), 122.4 (q, $J = 291$ Hz, CF_3), 126.4 (CH_{Ar}), 127.3 (CH_{Ar}), 128.5 (CH_{Ar}), 131.3 (C_{Ar}), 165.3 (CO) ppm. HRMS (ESI): calcd. for $[\text{C}_{20}\text{H}_{27}\text{F}_3\text{O}_3\text{Na}]^+$ 395.1805, found 395.1776 $[\text{M} + \text{Na}]^+$. FT-IR: $\tilde{\nu} = 2956$ (br, m), 2872 (w), 1832 (w), 1740 (s), 1497 (w), 1452 (m), 1389 (w), 1372 (w), 1359 (s), 1167 (vs), 1120 (s), 1081 (m), 1017 (s), 993 (s), 964 (s), 909 (m), 846 (w), 820 (w), 764 (w), 719 (s), 967 (s), 648 (m), 597 (w), 542 (w), 507 (w), 468 (w) cm^{-1} . The spectroscopic data are in accordance with ref.^[5]

L-menthyl-(^{MTPA}S)-ester [(^{MTPA}S,L)-S9]

| | |
|--------------------------|---|
| Method | GP 2 |
| L-menthol | 10.0 mg (64.0 μmol) |
| CH_2Cl_2 | 1 mL |
| abs. pyridine | 19.80 μL (20.2 mg, 256 μmol) |
| (<i>R</i>)-MTPA-Cl | 54.6 μL (40.4 mg, 160 μmol) |
| DMAP | 3.91 mg (32.0 μmol) |
| Yield | 24 mg (64.0 μmol , >99 %), slightly yellow oil |



$R_f = 0.86$ (PE : EtOAc = 3 : 1, anisaldehyde). ^1H NMR (500 MHz, CDCl_3): $\delta = 0.67$ (d, $J = 7.1$ Hz, 3H, $6'\text{Me}_a$), 0.74 (d, $J = 6.8$ Hz, 3H, $6'\text{Me}_b$), 0.84-0.89 (m, 1H, 1H, 4-H_a), 0.94 (d, $J = 6.8$ Hz, 3H, 3Me), 1.04 (dq, $J = 39.8, 27.2, 14.3, 3.4$ Hz, 1H, 5-H_a), 1.11 (q, $J = 23.1, 11.2$ Hz, 1H, 2-H_a), 1.40-1.45 (m, 1H, 6-H), 1.49-1.60 (m, 2H, 3-H, $6'\text{-H}$), 1.64-1.72 (m, 2H, $5\text{-H}_b, 4\text{-H}_b$), 2.10-2.16 (m, 1H, 2-H_b), 3.58 (s, 3H, OCH_3), 4.90 (td, $J = 22.3, 11.3, 4.5$ Hz, 1H, 1-H), 7.35-7.42 (m, 3H, Ph), 7.52-7.56 (m, 2H, Ph) ppm. ^{13}C -NMR (125 MHz, CDCl_3): $\delta = 15.6$ ($6'\text{Me}_a$), 20.6 ($6'\text{Me}_b$), 22.0 (3Me), 22.8 (C-5), 25.3 (C-6'), 34.1 (C-4), 40.5 (C-2), 46.7 (C-6), 55.5 (OCH_3), 77.1 (C-1), 84.3 (q, $J(^{19}\text{F}) = 29.7$ Hz, CCF_3), 123.5 (q, $J = 289$ Hz, CF_3), 127.1 (CH_{Ar}), 128.3 (CH_{Ar}), 129.5 (CH_{Ar}), 132.7 (C_{Ar}), 166.1 (CO) ppm. HRMS (ESI): calcd. for

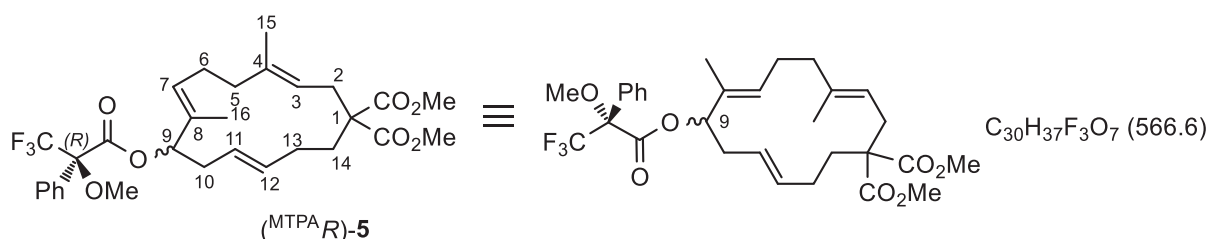
$[\text{C}_{20}\text{H}_{27}\text{F}_3\text{O}_3\text{Na}]^+$ 395.1805, found 395.1755 $[\text{M} + \text{Na}]^+$. FT-IR: $\tilde{\nu} = 2956$ (br, m), 2872 (w), 1742 (s), 1494 (w), 1452 (m), 1389 (w), 1371 (w), 1261 (s), 1166 (vs), 1122 (s), 1081 (m), 1020 (s), 994 (s), 948 (m), 909 (m), 845 (w), 820 (w), 765 (w), 719 (s), 967 (m), 647 (w), 596 (w), 558 (w), 509 (w), 466 (w) cm^{-1} .

The spectroscopic data are in accordance with ref.^[5]

Mosher esters (5) of cembranoid-ol (3d)

(^{MTPA}R)-Ester [(^{MTPA}R,9R)-5], [(^{MTPA}R,9S)-5]

| | |
|--------------------------|---|
| Method | GP 2 |
| Alcohol 3d | 15.0 mg (42.6 μmol) |
| CH_2Cl_2 | 2 mL |
| abs. pyridine | 6.90 μL (6.70 mg, 85.2 μmol) |
| (S)-MTPA-Cl | 19.9 μL (26.9 mg, 107 μmol) |
| DMAP | 2.60 mg (21.3 μmol) |
| Yield | 24 mg (42.4 μmol , >99 %), slightly yellow oil |
| Isomer ratio | (9R) : (9S) = 1 : 1 |

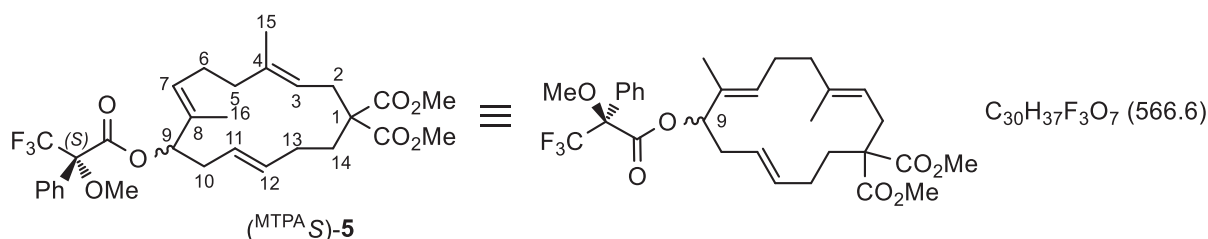


$R_f = 0.54$ (PE / EtOAc = 5 : 1, anisaldehyde). ^1H NMR (700 MHz, CDCl_3): $\delta = 1.45$ (s, 3H, 16- $\text{H}_{(9S)}$), 1.55 (s, 3H, 15- $\text{H}_{(9S)}$), 1.56 (s, 3H, 15- $\text{H}_{(9R)}$), 1.57 (s, 3H, 16- $\text{H}_{(9R)}$), 1.62-1.68 (m, 2H, 13- H_a), 1.68-1.75 (m, 4H, 13- H_b , 14- H_a), 2.01-2.06 (m, 2H, 14- H_b), 2.09-2.18 (m, 4H, 5- H_a , 6- H_a ($_{(9R) / (9S)}$), 2.18-2.27 (m, 3H, 5- H_b , 10- H_a ($_{(9R)}$), 2.29-2.40 (m, 5H, 6- H_b ($_{(9R) / (9S)}$), 10- H_a ($_{(9R)}$), 10- H_b ($_{(9R) / (9S)}$), 2.58 (d, $J = 15.6$ Hz, 2H, 2- H_a ($_{(9R) / (9S)}$), 2.82 (dd, $J = 15.6, 9.6$ Hz, 1H, 2- H_b ($_{(9R) / (9S)}$), 3.52 (s, 3H, OCH_3 ($_{(9R)}$), 3.56 (s, 3H, OCH_3 ($_{(9S)}$), 3.72 (s, 6H, CO_2CH_3), 3.74 (s, 6H, CO_2CH_3), 4.77-4.83 (m, 2H, 3-H), 4.96-5.04 (m, 2H, 11- $\text{H}_{(9R) / (9S)}$), 5.17-5.20 (m, 1H, 7- $\text{H}_{(9S)}$), 5.22-5.27 (m, 3H, 7- $\text{H}_{(9R)}$, 9-H), 5.45-5.54 (m, 2H, 12- $\text{H}_{(9R) / (9S)}$), 7.37-7.41 (m, 6H, Ph), 7.48-7.53 (m, 4H, Ph) ppm. ^{13}C -NMR (175 MHz, CDCl_3): $\delta = 10.9$ (C-16($_{(9S)}$), 11.2 (C-16($_{(9R)}$), 15.0 (C-15($_{(9S)}$), 15.0 (C-15($_{(9R)}$), 24.5 (C-6($_{(9S)}$), 24.6 (C-6($_{(9R)}$), 26.4 (C-13), 29.8 (C-2), 31.6 (C-14), 33.0 (C-10($_{(9R)}$), 33.2 (C-10($_{(9S)}$), 38.5 (C-5), 52.5 (CO_2CH_3), 52.6 (CO_2CH_3), 55.3 (OCH_3), 55.4 (OCH_3), 56.5 (C-1), 82.7, 82.7 (C-9), 84.5, 84.6 (2 x q, $J^{(19\text{F})} = 28.1$ Hz, CCF_3), 119.2 (C-3), 123.4 (2 x q, $J^{(19\text{F})} = 288.9$ Hz, CF_3), 124.8 (C-11($_{(9R)}$), 124.9 (C-11($_{(9S)}$), 127.3, 127.5 (CH_{Ar}), 128.3, 128.4

(CH_{Ar}), 129.5, 129.5 (CH_{Ar}), 129.9 (C-8_(9S)), 130.1 (C-8_(9R)), 131.1 (C-7_{(9R)/(9S)}), 132.5, 132.5 (C_{Ar}), 133.1 (C-12_{(9R)/(9S)}), 137.3 (C-4), 165.4, 165.6 (CO), 171.7 (CO₂CH₃), 172.0 (CO₂CH₃) ppm. HRMS (ESI): calcd. for [C₃₀H₃₇F₃O₇Na]⁺ 589.2384, found 589.2317 [M + Na]⁺. FT-IR: $\tilde{\nu}$ = 2953 (br, w), 2850 (w), 1831 (m), 1734 (s), 1496 (w), 1452 (m), 1270 (s), 1168 (vs), 1121 (m), 1095 (s), 1081 (m), 1017 (w), 992 (m), 962 (s), 887 (w), 848 (w), 764 (w), 749 (w), 719 (m), 698 (s), 648 (m), 543 (w), 510 (w) cm⁻¹.

(^{MTPA}S)-Ester [(^{MTPA}S,9R)-5], [(^{MTPA}S,9S)-5]

| | |
|---------------------------------|---|
| Method | GP 2 |
| Alcohol 3d | 15.0 mg (42.6 μmol) |
| CH ₂ Cl ₂ | 2 mL |
| abs. pyridine | 6.90 μL (6.70 mg, 85.2 μmol) |
| (R)-MTPA-Cl | 19.9 μL (26.9 mg, 107 μmol) |
| DMAP | 2.60 mg (21.3 μmol) |
| Yield | 24 mg (42.4 μmol, >99 %), slightly yellow oil |
| Isomer ratio | (9R) : (9S) = 1 : 1 |



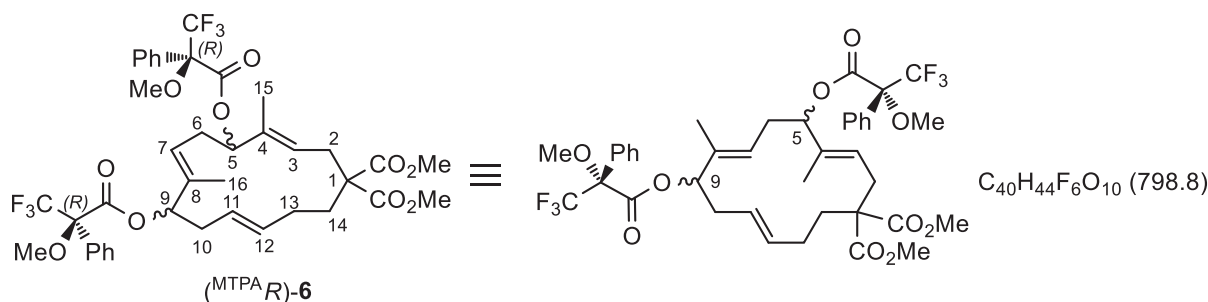
R_f = 0.54 (PE / EtOAc = 5 : 1, anisaldehyde). ¹H-NMR (700 MHz, CDCl₃): δ = 1.45 (s, 3H, 16-H_(9R)), 1.55 (s, 3H, 15-H_(9R)), 1.56 (s, 3H, 15-H_(9S)), 1.57 (s, 3H, 16-H_(9S)), 1.62-1.68 (m, 2H, 13-H_a), 1.68-1.75 (m, 4H, 13-H_b, 14-H_a), 2.01-2.06 (m, 2H, 14-H_b), 2.09-2.18 (m, 4H, 5-H_a, 6-H_a_{(9R)/(9S)}), 2.18-2.27 (m, 3H, 5-H_b, 10-H_a_(9S)), 2.29-2.40 (m, 5H, 6-H_b_{(9R)/(9S)}, 10-H_a_(9S), 10-H_b_{(9R)/(9S)}), 2.58 (d, *J* = 15.6 Hz, 2H, 2-H_a_{(9R)/(9S)}), 2.82 (dd, *J* = 15.6, 9.6 Hz, 1H, 2-H_b_{(9R)/(9S)}), 3.52 (s, 3H, OCH₃_(9S)), 3.56 (s, 3H, OCH₃_(9R)), 3.72 (s, 6H, CO₂CH₃), 3.74 (s, 6H, CO₂CH₃), 4.77-4.83 (m, 2H, 3-H), 4.96-5.04 (m, 2H, 11-H_{(9R)/(9S)}), 5.17-5.20 (m, 1H, 7-H_(9R)), 5.22-5.27 (m, 3H, 7-H_(9S), 9-H), 5.45-5.54 (m, 2H, 12-H_{(9R)/(9S)}), 7.37-7.41 (m, 6H, Ph), 7.48-7.53 (m, 4H, Ph) ppm. ¹³C NMR (175 MHz, CDCl₃): δ = 10.9 (C-16_(9R)), 11.2 (C-16_(9S)), 15.0 (C-15_(9R)), 15.0 (C-15_(9S)), 24.5 (C-6_(9R)), 24.6 (C-6_(9S)), 26.4 (C-13), 29.8 (C-2), 31.6 (C-14), 33.0 (C-10_(9S)), 33.2 (C-10_(9R)), 38.5 (C-5), 52.5 (CO₂CH₃), 52.6 (CO₂CH₃), 55.3 (OCH₃), 55.4 (OCH₃), 56.5 (C-1), 82.7, 82.7 (C-9), 84.5, 84.6 (2 x q, *J*^{19F} = 28.1 Hz, CCF₃), 119.2 (C-3), 123.4 (2 x q, *J*^{19F} = 288.9 Hz, CF₃), 124.8 (C-11_(9S)), 124.9 (C-11_(9R)), 127.3, 127.5 (CH_{Ar}), 128.3, 128.4 (CH_{Ar}), 129.5, 129.5 (CH_{Ar}), 129.9 (C-8_(9R)), 130.1 (C-8_(9S)), 131.1 (C-7_{(9R)/(9S)}), 132.5, 132.5 (C_{Ar}), 133.1 (C-12_{(9R)/(9S)}), 137.3 (C-4), 165.4, 165.6 (CO), 171.7 (CO₂CH₃), 172.0 (CO₂CH₃)

ppm. HRMS (ESI): calcd. for $[C_{30}H_{37}F_3O_7Na]^+$ 589.2384, found 589.2340 $[M + Na]^+$. FT-IR: $\tilde{\nu}$ = 2953 (br, w), 2851 (w), 1832 (m), 1735 (s), 1497 (w), 1452 (m), 1271 (s), 1171 (vs), 1121 (m), 1096 (s), 1081 (m), 1017 (w), 992 (m), 963 (s), 850 (w), 764 (w), 749 (w), 719 (m), 699 (m), 648 (m), 543 (w), 508 (w) cm^{-1} .

Mosher diesters (6) of cembranoid-diol (4)

(^{MTPA}R)-Diester [(^{MTPA}R,5R,9R)-6], [(^{MTPA}R,5S,9S)-6]

| | |
|---------------------------------|--|
| Method | GP 3 |
| Diol 4 | 15.0 mg (40.9 μ mol) |
| CH ₂ Cl ₂ | 1 mL |
| abs. pyridine | 13.2 μ L (13.0 mg, 163 μ mol) |
| (S)-MTPA-Cl | 26.8 μ L (36.2 mg, 143 μ mol) |
| DMAP | 2.50 mg (20.5 μ mol) |
| Yield | 33 mg (40.9 μ mol, >99 %), slightly yellow oil |
| Isomer ratio | (5S,9S) : (5R,9R) = 1 : 0.75 |

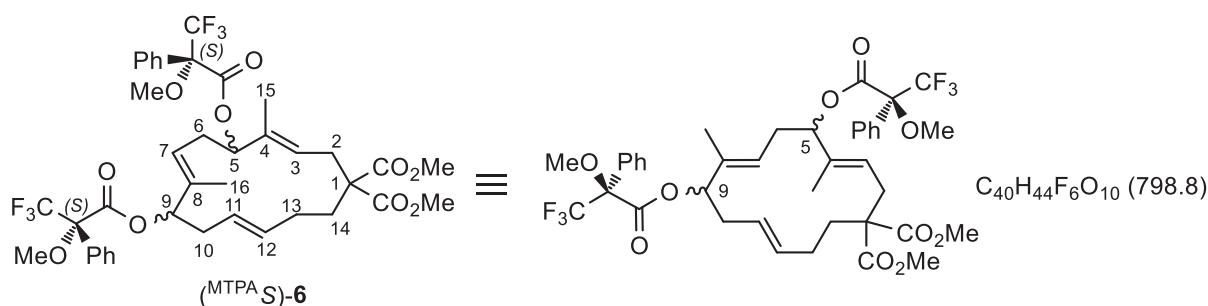


R_f = 0.57 (PE / EtOAc = 3 : 1, anisaldehyde). ¹H-NMR (700 MHz, CDCl₃): δ = 1.43 (s, 3H, 15-H_(5S,9S)), 1.45 (s, 3H, 16-H_(5S,9S)), 1.50-1.56 (m, 2H, 14-H_a), 1.57 (s, 3H, 16-H_(5R,9R)), 1.59-1.63 (m, 2H, 13-H_a), 1.61 (s, 3H, 15-H_(5R,9R)), 1.70-1.79 (m, 2H, 13-H_b), 2.11-2.18 (m, 2H, 14-H_b), 2.22 (dt, J = 11.7, 6.6 Hz, 1H, 10-H_{a(5R,9R)}), 2.31 (dt, J = 11.7, 6.6 Hz, 1H, 10-H_{a(5S,9S)}), 2.34-2.44 (m, 4H, 6-H_{a(5S,9S)/(5R,9R)}, 10-H_{b(5S,9S)/(5R,9R)}), 2.58-2.65 (m, 2H, 2-H_{a(5S,9S)/(5R,9R)}), 2.63 (dt, J = 14.8, 11.0 Hz, 1H, 6-H_{b(5R,9R)}), 2.69 (dt, J = 14.8, 11.0 Hz, 1H, 6-H_{b(5S,9S)}), 2.88 (dd, J = 15.8, 11.1 Hz, 1H, 2-H_{b(5S,9S)}), 2.93 (dd, J = 15.8, 11.1 Hz, 1H, 2-H_{b(5R,9R)}), 3.50 (s, br, 6H, OCH₃), 3.53 (s, 3H, OCH₃), 3.54 (s, 3H, OCH₃), 3.71 (s, 3H, CO₂CH₃), 3.72 (s, 3H, CO₂CH₃), 3.78 (s, 3H, CO₂CH₃), 3.79 (s, 3H, CO₂CH₃), 4.92-4.99 (m, 1H, 11-H), 5.19-5.25 (m, 4H, 9-H, 7-H_{(5S,9S)/(5R,9R)}), 5.29-5.33 (m, 1H, 3-H_(5S,9S)), 5.33-5.36 (m, 1H, 3-H_(5R,9R)), 5.48-5.56 (m, 4H, 5-H, 12-H_{(5S,9S)/(5R,9R)}), 7.36-7.43 (m, 6H, Ph), 7.44-7.50 (m, 4H, Ph) ppm. ¹³C NMR (175 MHz, CDCl₃): δ = 10.6 (C-16_(5S,9S)), 10.9 (C-15_(5S,9S)), 11.0 (C-16_(5R,9R)), 11.3 (C-15_(5R,9R)), 26.3, 26.3 (C-13), 29.7 (C-2_(5S,9S)), 29.8 (C-2_(5R,9R)), 30.0 (C-6_(5R,9R)), 30.2 (C-6_(5S,9S)), 31.7, 31.7 (C-14), 32.9 (C-10_(5R,9R)), 33.1 (C-10_(5S,9S)), 52.6, 52.6 (CO₂CH₃), 52.9 (CO₂CH₃), 55.3 (br,

OCH₃), 55.4, 55.4 (OCH₃), 56.2, 56.2 (C-1), 81.0, 81.1 (C-5), 82.8, 82.9 (C-9), 84.5 (4 x q, $J(^{19}\text{F}) = 27.9$ Hz, CCF₃), 123.3 (4 x q, $J(^{19}\text{F}) = 288.9$ Hz, CF₃), 124.6, 124.7 (C-11), 124.7 (C-7_(5R,9R)), 124.8 (C-7_(5S,9S)), 127.0 (C-3_(5R,9R)), 127.1 (C-3_(5S,9S)), 127.2, 127.3, 127.3, 127.4 (CH_{Ar}), 128.4 (br), 128.4, 128.4 (CH_{Ar}), 129.6, 129.6, 129.6, 129.6 (CH_{Ar}), 132.3 (br), 132.4, 132.4 (C_{Ar}), 132.9, 132.9 (C-8), 133.1 (C-12_(5R,9R)), 133.1 (C-12_(5S,9S)), 134.1, 134.3 (C-4), 165.2 (br), 165.4, 165.5 (CO), 171.2, 171.2 (CO₂CH₃), 171.6, 171.6 (CO₂CH₃) ppm. HRMS (ESI): calcd. for [C₄₀H₄₄F₆O₁₀Na]⁺ 821.2731, found 821.2759 [M + Na]⁺. FT-IR: $\tilde{\nu} = 2953$ (br, w), 2850 (w), 1732 (vs), 1496 (w), 1452 (m), 1373 (w), 1270 (s), 1238 (vs), 1165 (vs), 1121 (s), 1081 (m), 1015 (s), 990 (s), 963 (m), 912 (s), 856 (w), 828 (w), 765 (m), 731 (vs), 719 (vs), 697 (s), 648 (m), 547 (w), 510 (w) cm⁻¹.

(^{MTPA}S)-Diester [(^{MTPA}S,5R,9R)-6], [(^{MTPA}S,5S,9S)-6]

| | |
|---------------------------------|--|
| Method | GP 3 |
| Diol 4 | 15.0 mg (40.9 μmol) |
| CH ₂ Cl ₂ | 1 mL |
| abs. pyridine | 13.2 μL (13.0 mg, 163 μmol) |
| (<i>R</i>)-MTPA-Cl | 26.8 μL (36.2 mg, 143 μmol) |
| DMAP | 2.50 mg (20.5 μmol) |
| Yield | 32 mg (40.0 μmol, 98 %), slightly yellow oil |
| Isomer ratio | (5S,9S) : (5R,9R) = 1 : 0.75 |



R_f = 0.57 (PE / EtOAc = 3 : 1, anisaldehyde). ¹H-NMR (700 MHz, CDCl₃): δ = 1.43 (s, 3H, 15-H_(5R,9R)), 1.45 (s, 3H, 16-H_(5R,9R)), 1.50-1.56 (m, 2H, 14-H_a), 1.57 (s, 3H, 16-H_(5S,9S)), 1.59-1.63 (m, 2H, 13-H_a), 1.61 (s, 3H, 15-H_(5S,9S)), 1.70-1.79 (m, 2H, 13-H_b), 2.11-2.18 (m, 2H, 14-H_b), 2.22 (dt, $J = 11.7, 6.6$ Hz, 1H, 10-H_a_(5S,9S)), 2.31 (dt, $J = 11.7, 6.6$ Hz, 1H, 10-H_a_(5R,9R)), 2.34-2.44 (m, 4H, 6-H_a_{(5S,9S) / (5R,9R)}, 10-H_b_{(5S,9S) / (5R,9R)}), 2.58-2.65 (m, 2H, 2-H_a_{(5S,9S) / (5R,9R)}), 2.63 (dt, $J = 14.8, 11.0$ Hz, 1H, 6-H_b_(5S,9S)), 2.69 (dt, $J = 14.8, 11.0$ Hz, 1H, 6-H_b_(5R,9R)), 2.88 (dd, $J = 15.8, 11.1$ Hz, 1H, 2-H_b_(5R,9R)), 2.93 (dd, $J = 15.8, 11.1$ Hz, 1H, 2-H_b_(5S,9S)), 3.50 (s, br, 6H, OCH₃), 3.53 (s, 3H, OCH₃), 3.54 (s, 3H, OCH₃), 3.71 (s, 3H, CO₂CH₃), 3.72 (s, 3H, CO₂CH₃), 3.78 (s, 3H, CO₂CH₃), 3.79 (s, 3H, CO₂CH₃), 4.92-4.99 (m, 1H, 11-H), 5.19-5.25 (m, 4H, 9-H, 7-H_{(5S,9S) / (5R,9R)}), 5.29-5.33 (m, 1H, 3-H_(5R,9R)), 5.33-5.36 (m, 1H, 3-H_(5S,9S)), 5.48-5.56

(m, 4H, 5-H, 12-H_{(5S,9S) / (5R,9R)}), 7.36-7.43 (m, 6H, Ph), 7.44-7.50 (m, 4H, Ph) ppm. ¹³C NMR (125 MHz, CDCl₃): δ = 10.6 (C-16_(5R,9R)), 10.9 (C-15_(5R,9R)), 11.0 (C-16_(5S,9S)), 11.3 (C-15_(5S,9S)), 26.3, 26.3 (C-13), 29.7 (C-2_(5R,9R)), 29.8 (C-2_(5S,9S)), 30.0 (C-6_(5S,9S)), 30.2 (C-6_(5R,9R)), 31.7, 31.7 (C-14), 32.9 (C-10_(5S,9S)), 33.1 (C-10_(5R,9R)), 52.6, 52.6 (CO₂CH₃), 52.9 (CO₂CH₃), 55.3 (br, OCH₃), 55.4, 55.4 (OCH₃), 56.2, 56.2 (C-1), 81.0, 81.1 (C-5), 82.8, 82.9 (C-9), 84.5 (4 x q, $J(^{19}\text{F}) = 27.9$ Hz, CCF₃), 123.3 (4 x q, $J(^{19}\text{F}) = 288.9$ Hz, CF₃), 124.6, 124.7 (C-11), 124.7 (C-7_(5S,9S)), 124.8 (C-7_(5R,9R)), 127.0 (C-3_(5S,9S)), 127.1 (C-3_(5R,9R)), 127.2, 127.3, 127.3, 127.4 (CH_{Ar}), 128.4 (br), 128.4, 128.4 (CH_{Ar}), 129.6, 129.6, 129.6, 129.6 (CH_{Ar}), 132.3 (br), 132.4, 132.4 (C_{Ar}), 132.9, 132.9 (C-8), 133.1 (C-12_(5S,9S)), 133.1 (C-12_(5R,9R)), 134.1, 134.3 (C-4), 165.2, 165.4 (br), 165.5 (CO), 171.2, 171.2 (CO₂CH₃), 171.6, 171.6 (CO₂CH₃) ppm. HRMS (ESI): calcd. for [C₄₀H₄₄F₆O₁₀Na]⁺ 821.2731, found 821.2716 [M + Na]⁺. FT-IR: $\tilde{\nu}$ = 2953 (br, w), 2850 (w), 1733 (vs), 1496 (w), 1452 (m), 1373 (w), 1270 (s), 1239 (vs), 1167 (vs), 1122 (s), 1082 (m), 1016 (s), 991 (s), 964 (m), 919 (m), 857 (w), 827 (w), 765 (w), 720 (s), 698 (m), 649 (w), 548 (w), 510 (w) cm⁻¹.

Supporting results

Substrate screening

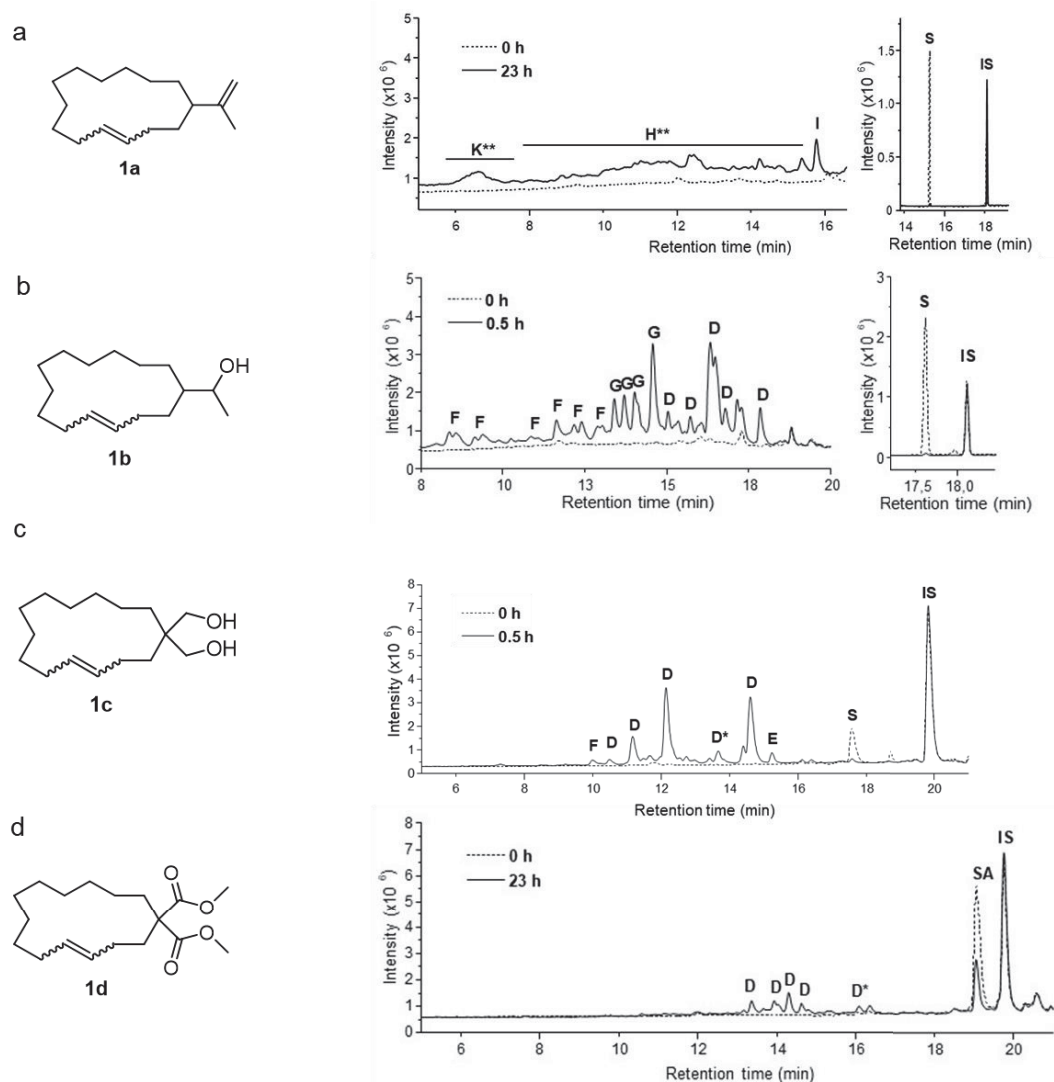


Figure S1. LC/MS chromatograms of P450 BM3 F87G catalyzed oxidations of macrocycles **1a** (a), **1b** (b), **1c** (c), and **1d** (d). Reaction time was set to 23 h with **1a** and **1d**, and 0.5 h with **1b** and **1c**. S: corresponding substrates; IS: internal standard. Products were identified by MS-analysis, with mass differences to the respective substrates of +14 m/z (C), +16 m/z (D), +30 m/z (E), +32 m/z (F), +34 m/z (G), +48 m/z (H), +62 m/z (I), +64 (K). Products (D) marked with an asterisk (*) could be identified by comparison with reference compounds as (11,12)-epoxides of the respective substrates. ** Products of **1a** could be determined by mass, but their separation was not possible.

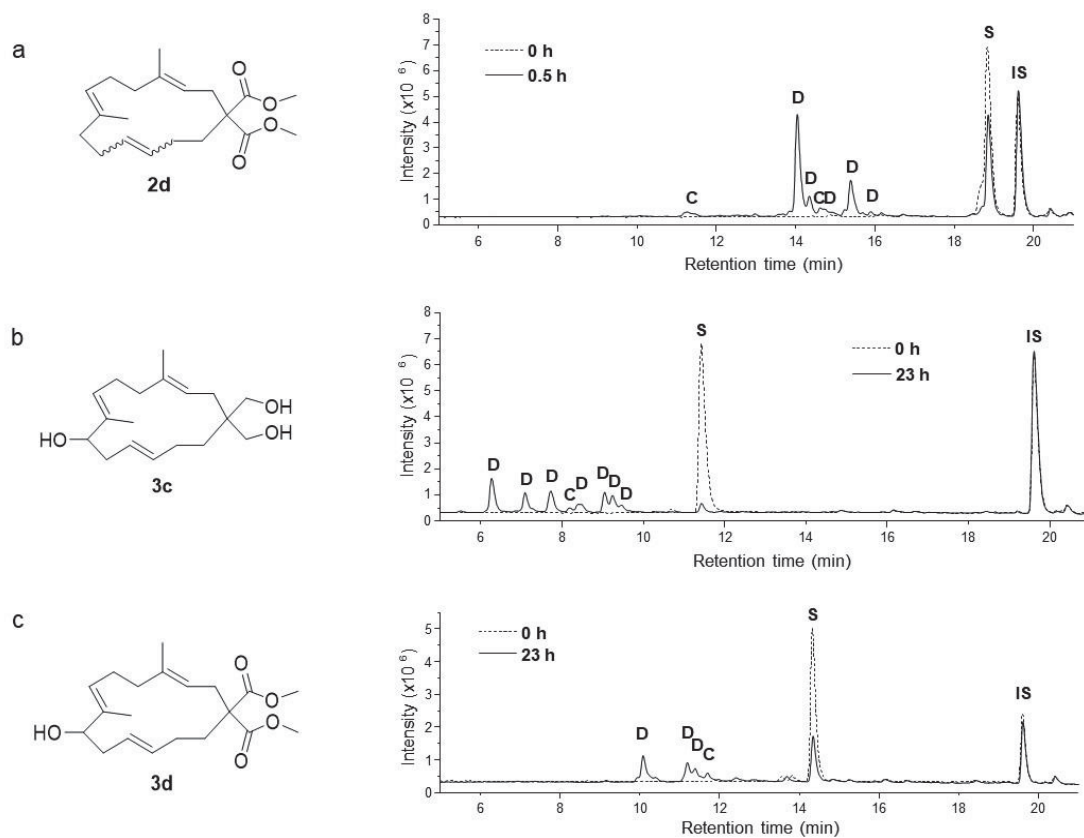
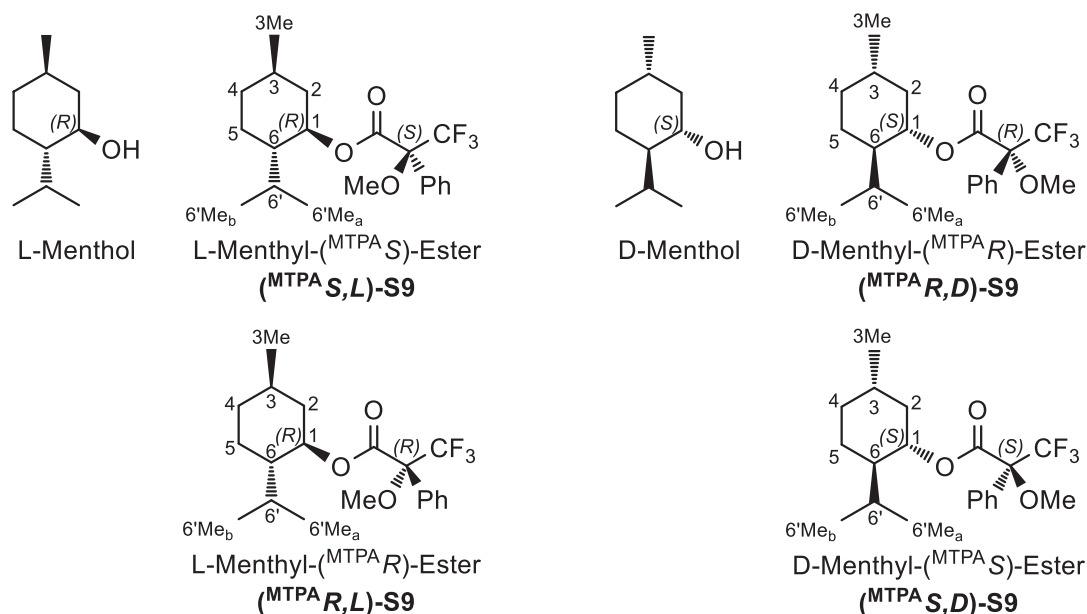


Figure S2. LC/MS chromatograms of the P450 BM3 F87G catalyzed oxidations of macrocycles **2d** (a), **3c** (b), and **3d** (c). Reaction time was set to 0.5 h with **2d** and 23 h with **3c** and **3d**. **S**: corresponding substrates; **IS**: internal standard. Products were identified by MS-analysis, with mass differences to the respective substrates of +14 m/z (**C**) and +16 m/z (**D**)

NMR studies with menthol

As described in the manuscript enantiomerically pure L- and D-menthol and a (1 : 0.75) mixture of L- and D-menthol were treated with (*R*)- and (*S*)-MTPA-Cl in parallel experiments. The starting materials and the corresponding products are shown in Scheme S1. In order to simplify the spectral assignment no racemic mixtures of L- and D-menthol were used.



Scheme S1. L- and D-menthol and the corresponding (^{MTPA}R)- and (^{MTPA}S)-Mosher esters.

¹H NMR spectra of the Mosher esters **S9** could be fully assigned based on literature precedence.^[3, 5, 6] As shown in Figure S3 the ¹H NMR spectra of Mosher ester (^{MTPA}R,L)-**S9** derived from L-menthol and (*S*)-MTPA-Cl (Figure S3a) and Mosher ester (^{MTPA}S,D)-**S9** derived from D-menthol and (*R*)-MTPA-Cl (Figure S3b) are identical. Accordingly, the ¹H NMR spectra of (^{MTPA}S,L)-**S9** derived from L-menthol and (*R*)-MTPA-Cl (Figure S3c), and (^{MTPA}R,D)-**S9** derived from D-menthol and (*S*)-MTPA-Cl (Figure S4d) are identical as well.

The chemical shifts δ [ppm] of the signals shown in Figure 34 are listed in Table S1. Comparison of the chemical shift difference $\Delta\delta^{\text{SR}} = (\delta_{\text{S}} - \delta_{\text{R}})$ [Hz] of L- and D-menthol revealed a sign inversion, which can be explained by the Mosher theory (Scheme S2).^[7] The phenyl group results in an upfield shift, while the methylester leads to a downfield shift.^[7] Protons which are located below the plane of the Mosher ester, i.e. protons of R² display values $\Delta\delta^{\text{SR}} < 0$, whereas protons located above the the plane of the Mosher ester, i.e. protons of R¹ display values $\Delta\delta^{\text{SR}} > 0$ (Table S1).

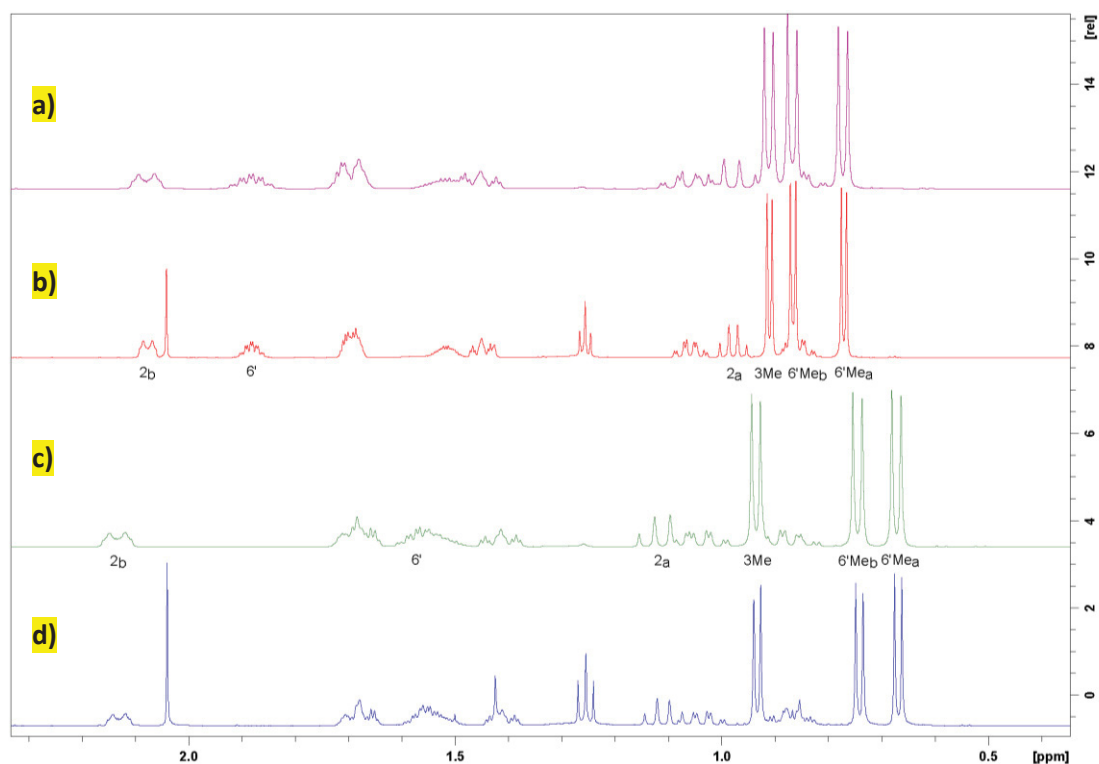
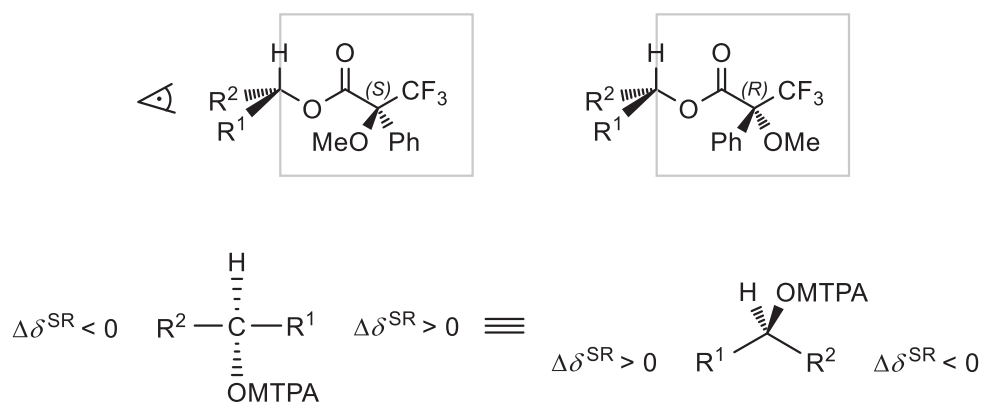


Figure S3. Characteristic section of the ^1H NMR spectra (700 MHz, CDCl_3) of the Mosher esters **S9** derived from the reactions of D- and L-menthol with (*R*)- and (*S*)-MTPA-Cl respectively.



Scheme S2. Schematic drawing of the plane dissecting the Mosher ester with substituents R^1 located above and R^2 located below the plane. Positive and negative values $\Delta\delta^{\text{SR}}$ for the chemical shift differences can be explained by the relative orientation of the phenyl and methoxy units with respect to R^1 , R^2 . When H signals with positive $\Delta\delta^{\text{SR}}$ value belong to R^1 and H signals with negative $\Delta\delta^{\text{SR}}$ belong to R^2 , the absolute configuration according to the CIP nomenclature can be assigned.

Table S1 Chemical shifts δ [ppm] of characteristic H signals of the Mosher esters **S9** and their difference $\Delta\delta^{\text{SR}}$ [Hz].

| ¹ H NMR signal | L-Menthol [ppm] | | $\Delta\delta^{\text{SR}} = (\delta_{\text{S}} - \delta_{\text{R}})$ [Hz] | D-Menthol [ppm] | | $\Delta\delta^{\text{SR}} = (\delta_{\text{S}} - \delta_{\text{R}})$ [Hz] |
|---------------------------|-------------------------------|-------------------------------|---|-------------------------------|-------------------------------|---|
| | δ (^{MTPA} S) | δ (^{MTPA} R) | | δ (^{MTPA} S) | δ (^{MTPA} R) | |
| 6'Me _a | 0.67 | 0.77 | - 50 | 0.77 | 0.67 | + 50 |
| 6'Me _b | 0.74 | 0.87 | - 61 | 0.87 | 0.74 | + 61 |
| 6' | 1.56 | 1.88 | -162 | 1.88 | 1.56 | +162 |
| 2 _a | 1.11 | 0.98 | + 67 | 0.98 | 1.11 | - 67 |
| 2 _b | 2.14 | 2.08 | + 30 | 2.08 | 2.14 | - 30 |
| 3Me | 0.94 | 0.91 | + 14 | 0.91 | 0.94 | - 14 |

Treatment of a (1 : 0.75) mixture of L- and D-menthol with (*R*)- and (*S*)-MTPA-Cl in parallel runs revealed NMR spectra with identical chemical shifts, but different intensities (Figure S4a,b). The relative signal intensities correlate with the ratio of L- and D-menthol in the mixture as can be seen most obviously for methyl groups 6'-Me_a and 6'-Me_b (green frame) as well as 3-Me (red frame). For comparison the ¹H NMR spectra of the Mosher ester (^{MTPA}*R,D*)-**S9** derived from D-menthol and (*R*)-MTPA-Cl and the Mosher ester (^{MTPA}*S,L*)-**S9** derived from L-menthol and (*S*)-MTPA-Cl respectively are shown in Figure S4c,d respectively.

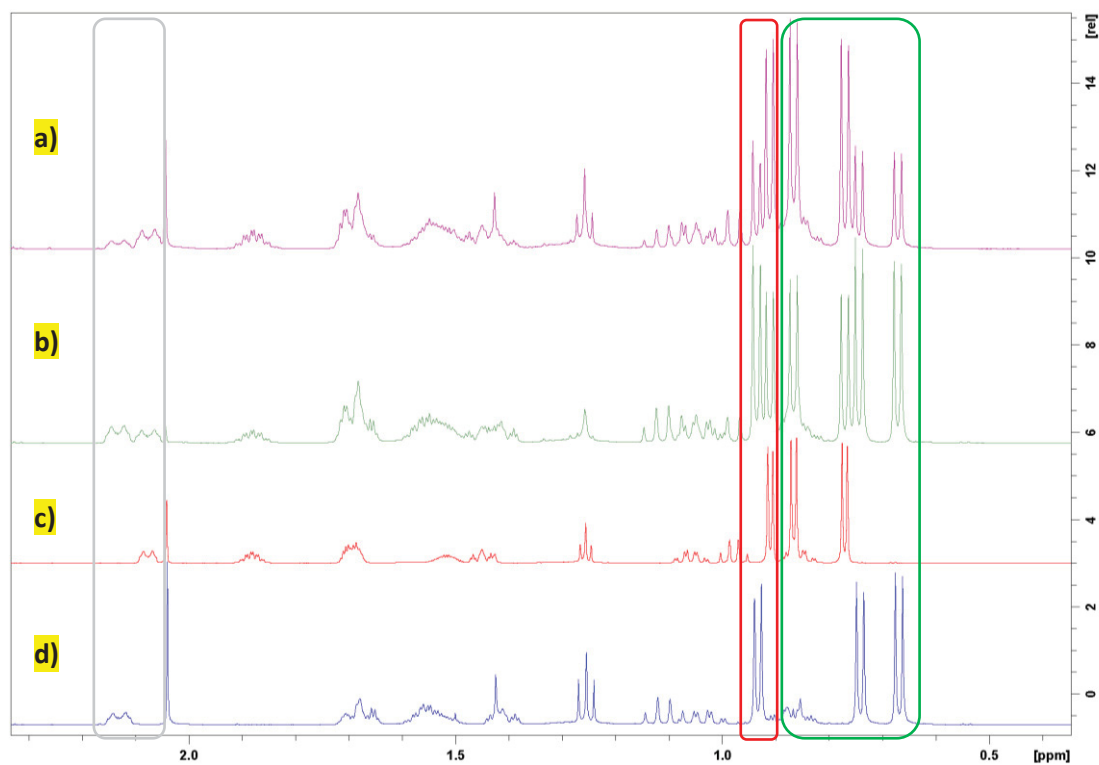


Figure S4 Characteristic section of the ^1H NMR spectra of the Mosher esters **S9** derived from the reaction of a) a (1 : 0.75) mixture of L- and D-menthol with (*S*)-MTPA-Cl, b) a (1 : 0.75) mixture of L- and D-menthol with (*R*)-MTPA-Cl, c) D-menthol with (*R*)-MTPA-Cl and d) D-menthol with (*S*)-MTPA-Cl.

In case of menthol a complete assignment of all NMR signals for the respective menthyl-MTPA ester is possible via HSQC and COSY NMR. Thus configurational assignment should be also possible in a racemic mixture (displaying equal signal intensities).

2D-NMR assignment of the H signals of the (^{MTPA}S)-Mosher-diester (^{MTPA}S)-6

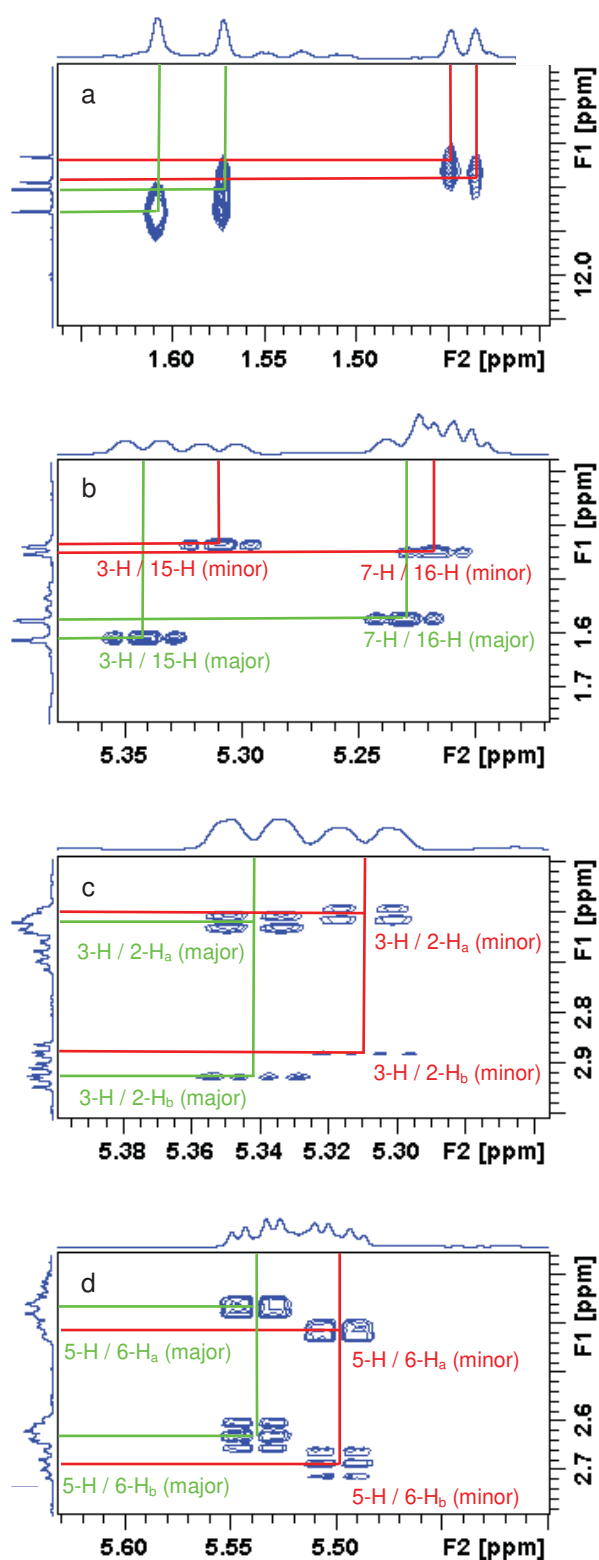
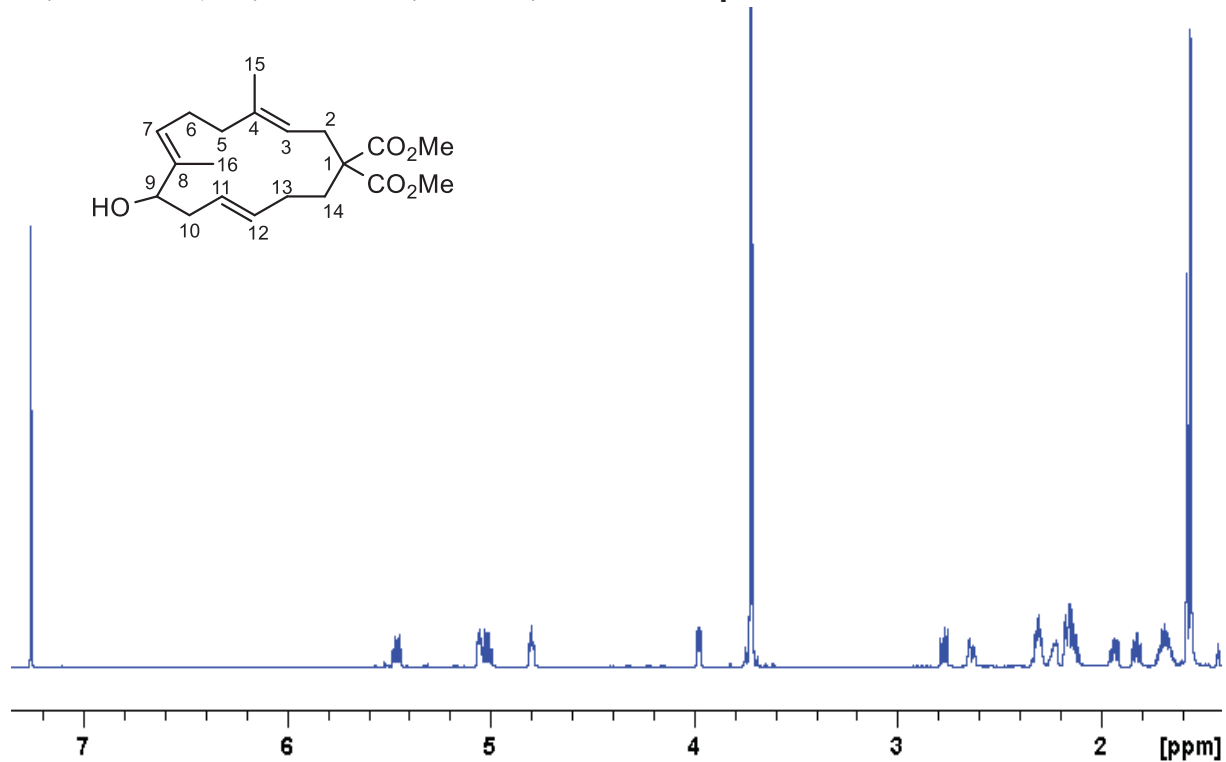
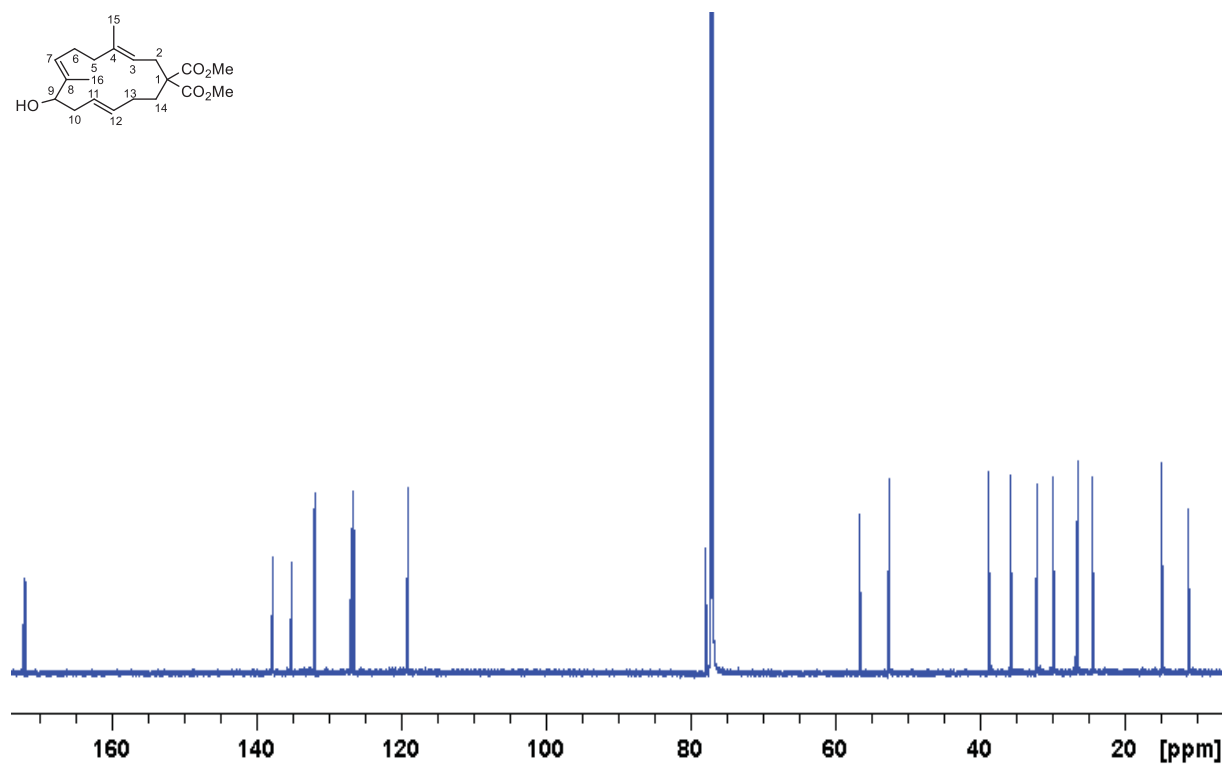


Figure S5. a) Section of the HSQC NMR spectrum (700 MHz, CDCl₃) of the (^{MTPA}S)-Mosher diester (^{MTPA}S)-6 showing the methyl signals 15-H, 16-H; b) Section of the COSY NMR spectrum (700 MHz, CDCl₃) of the (^{MTPA}S)-Mosher diester (^{MTPA}S)-6 showing the coupling pattern of 3-H / 15-H and 7-H / 16-H; c) the coupling pattern of 3-H / 2-H of major and minor isomer; d) the coupling pattern of 5-H / 6-H.

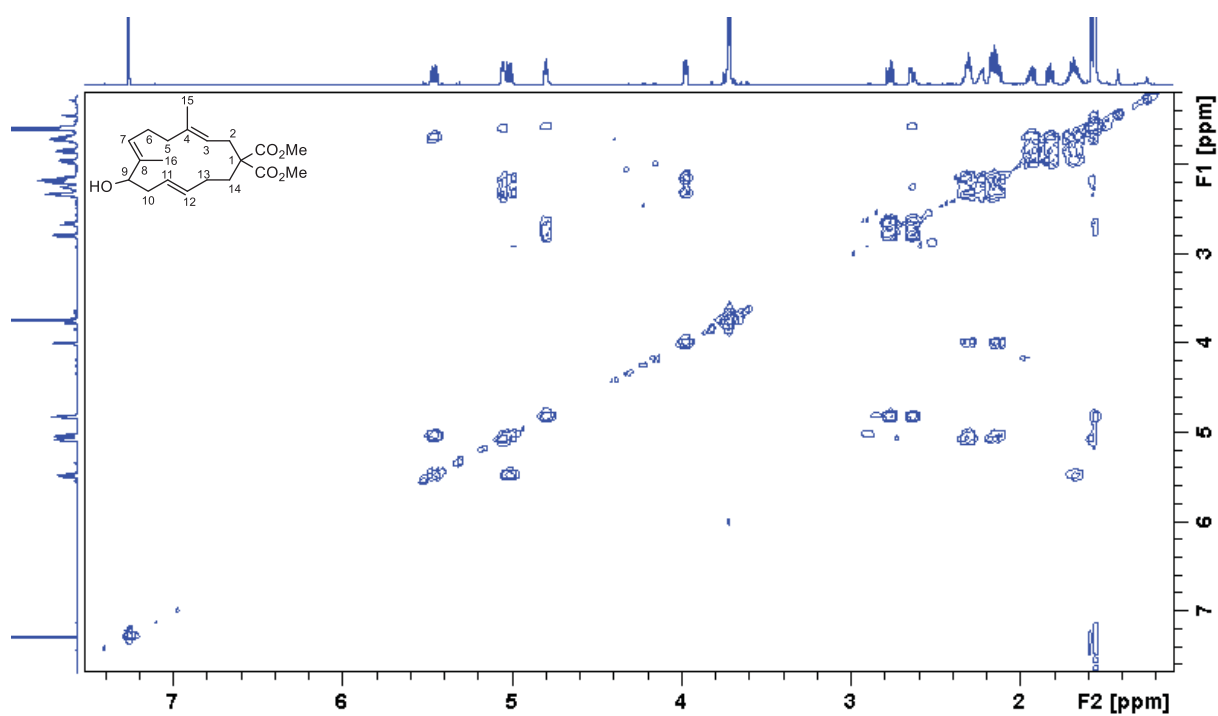
^1H , ^1H -COSY, ^1H , ^{13}C -HSQC, and ^1H , ^{13}C -HMBC spectra



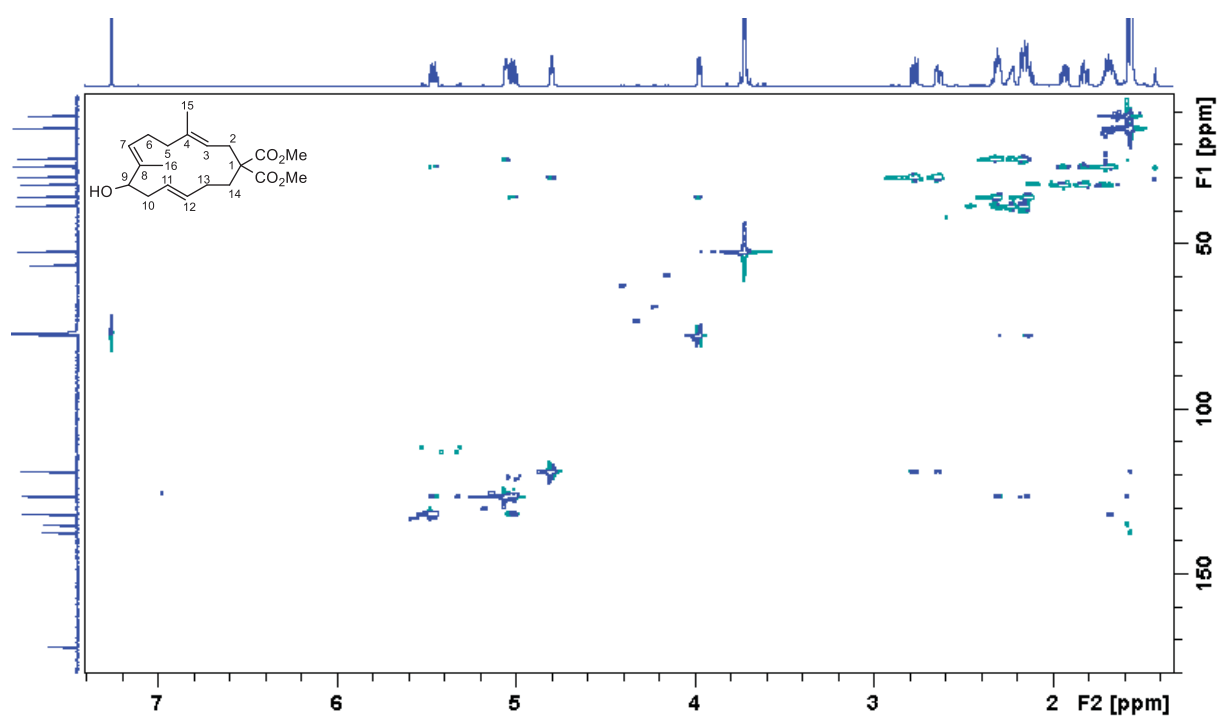
^1H NMR Cembranol 3d



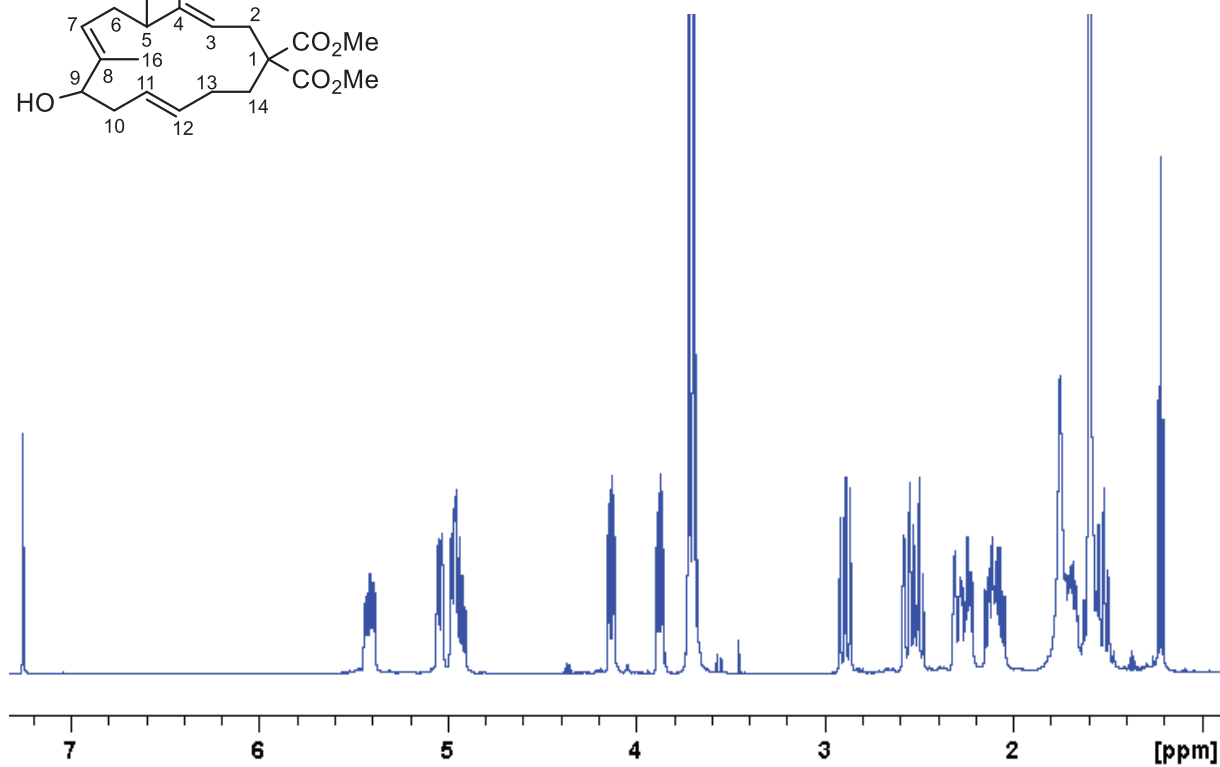
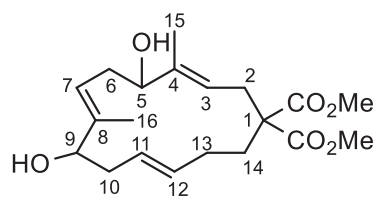
^{13}C NMR Cembranol 3d



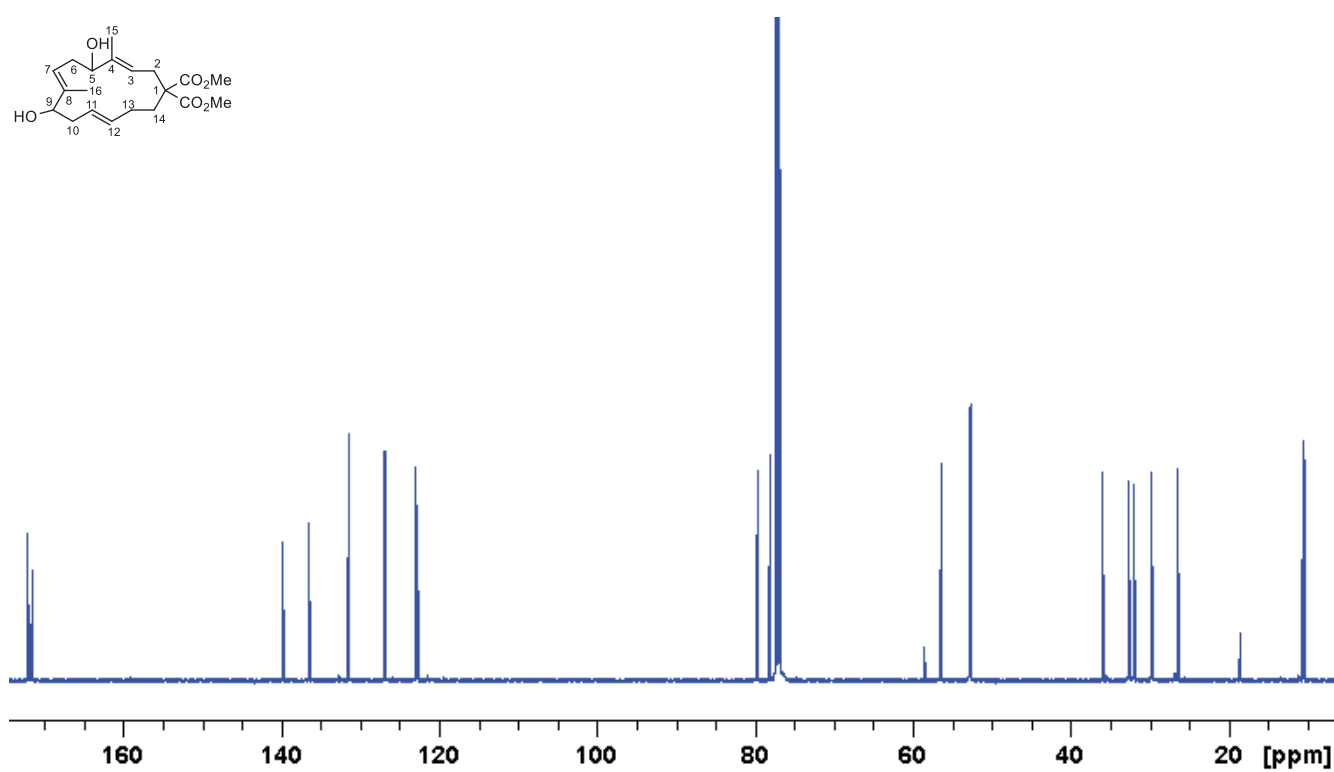
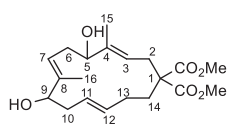
$^1\text{H}, ^1\text{H}$ COSY NMR Cembranol **3d**



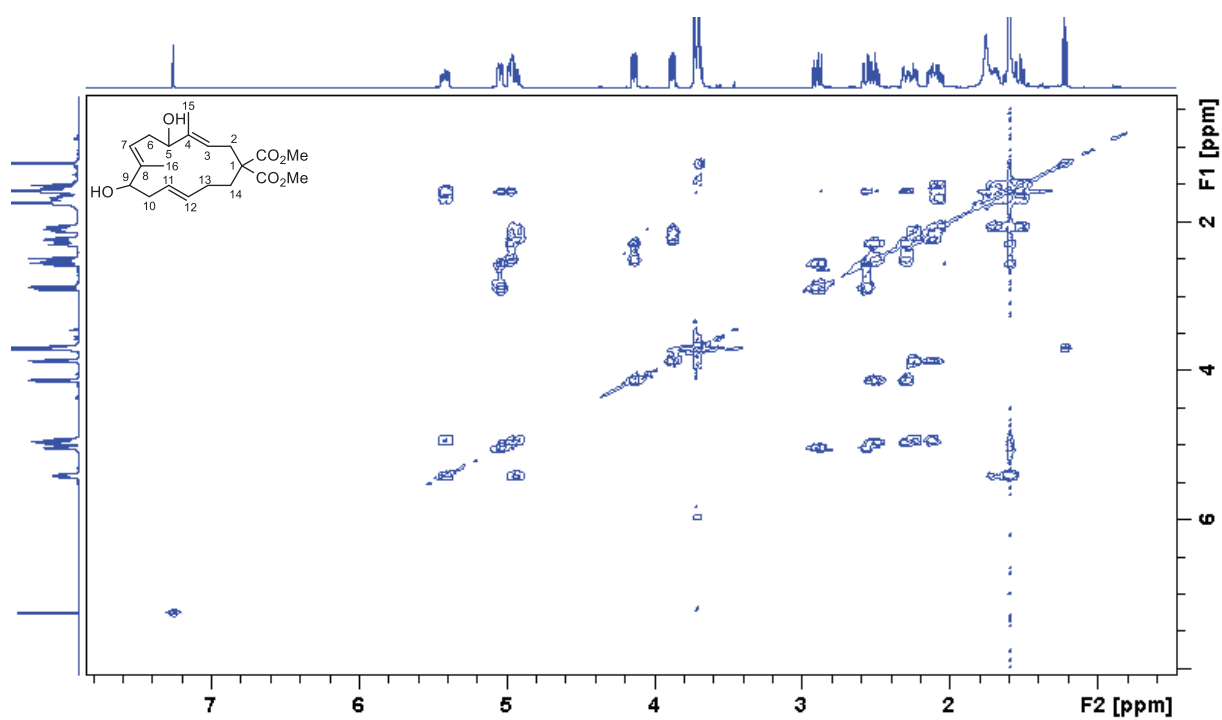
$^1\text{H}, ^{13}\text{C}$ HSQC NMR Cembranol **3d**



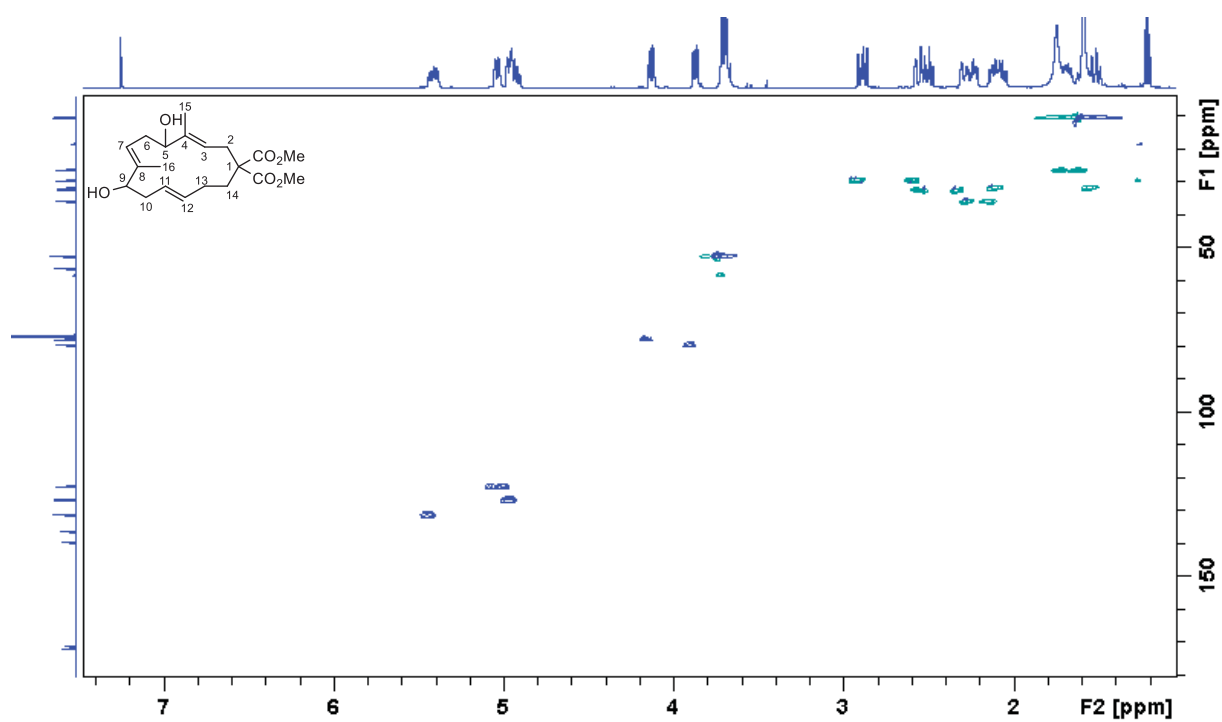
¹H NMR Diol 4



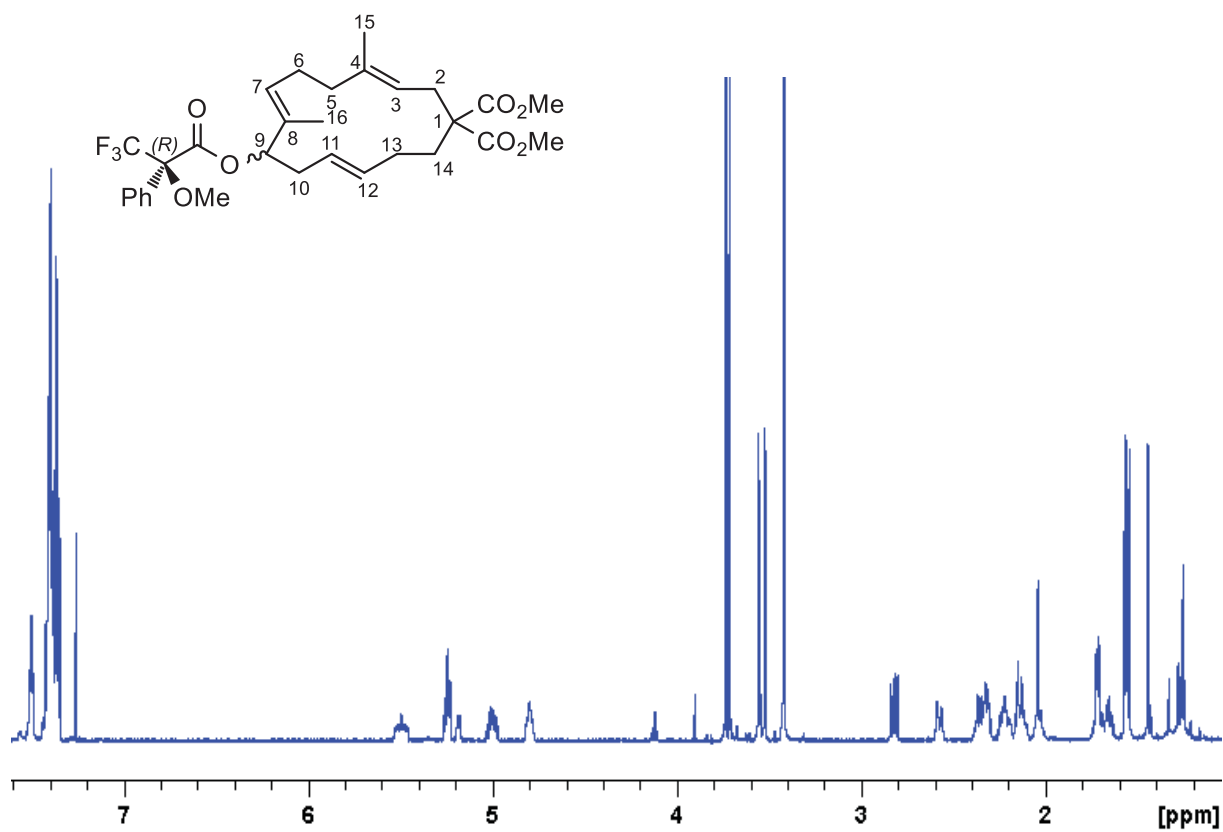
¹³C NMR Diol 4



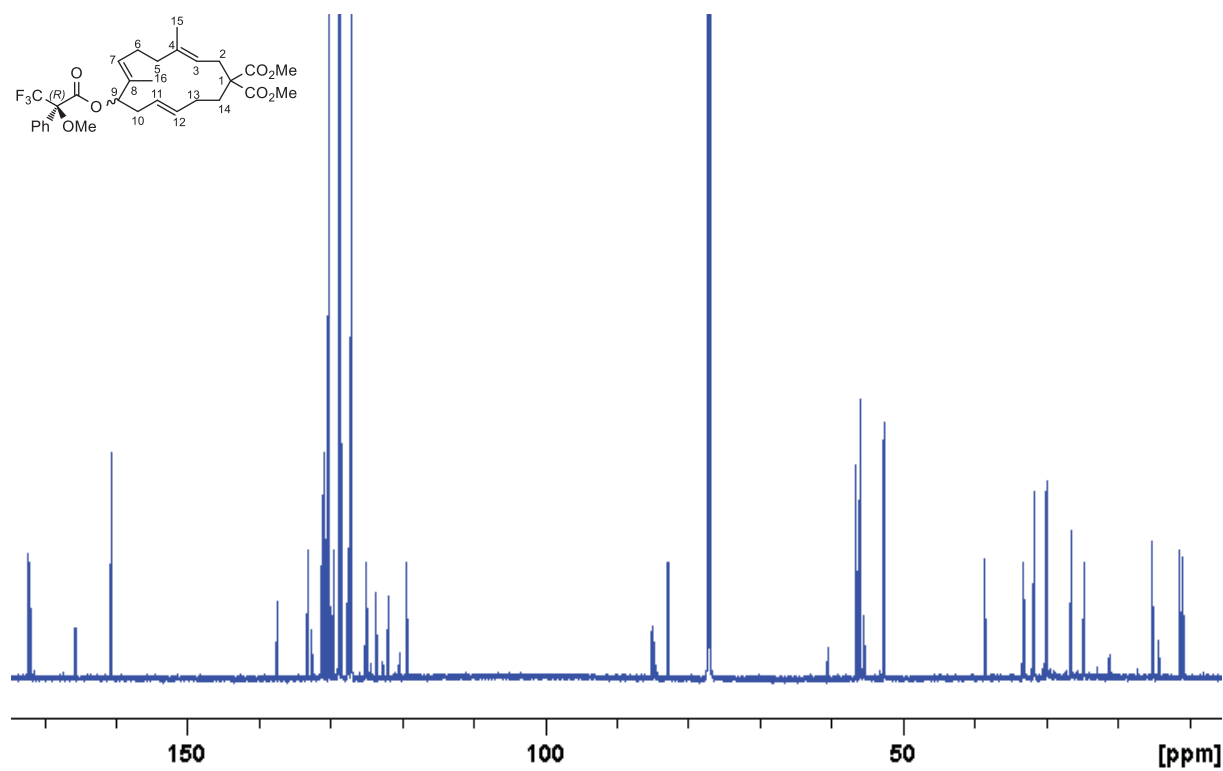
$^1\text{H}, ^1\text{H}$ COSY NMR Diol 4



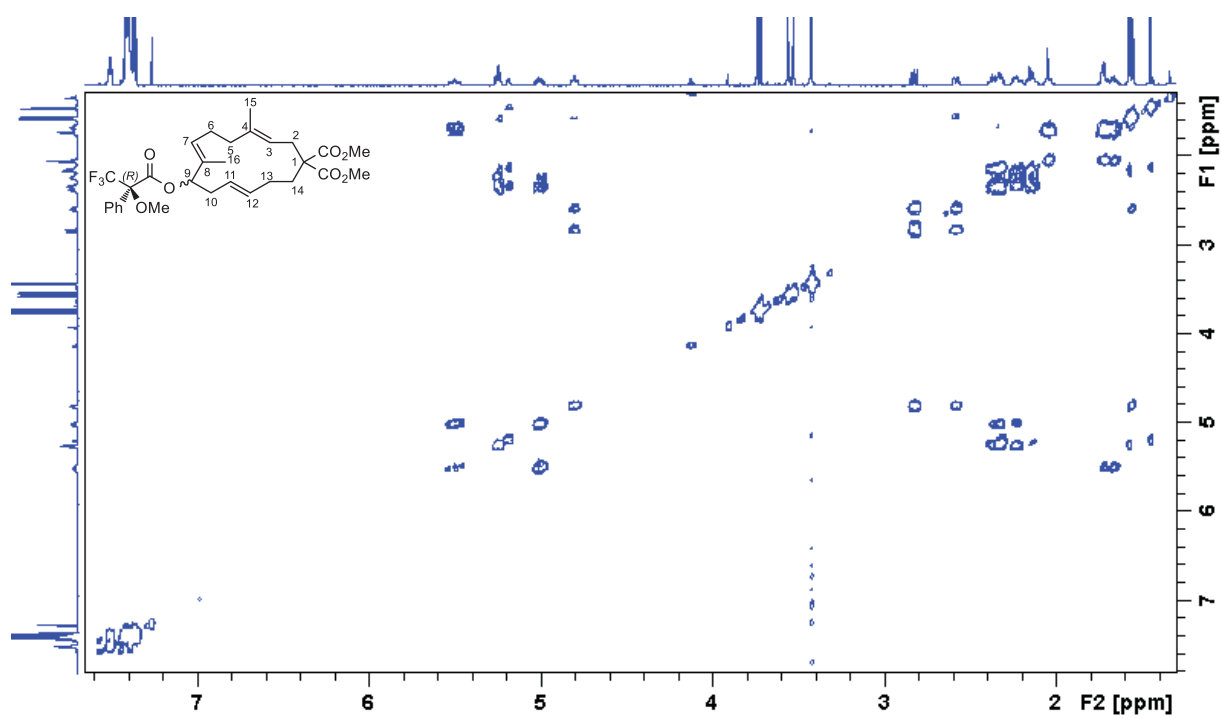
$^1\text{H}, ^{13}\text{C}$ HSQC NMR Diol 4



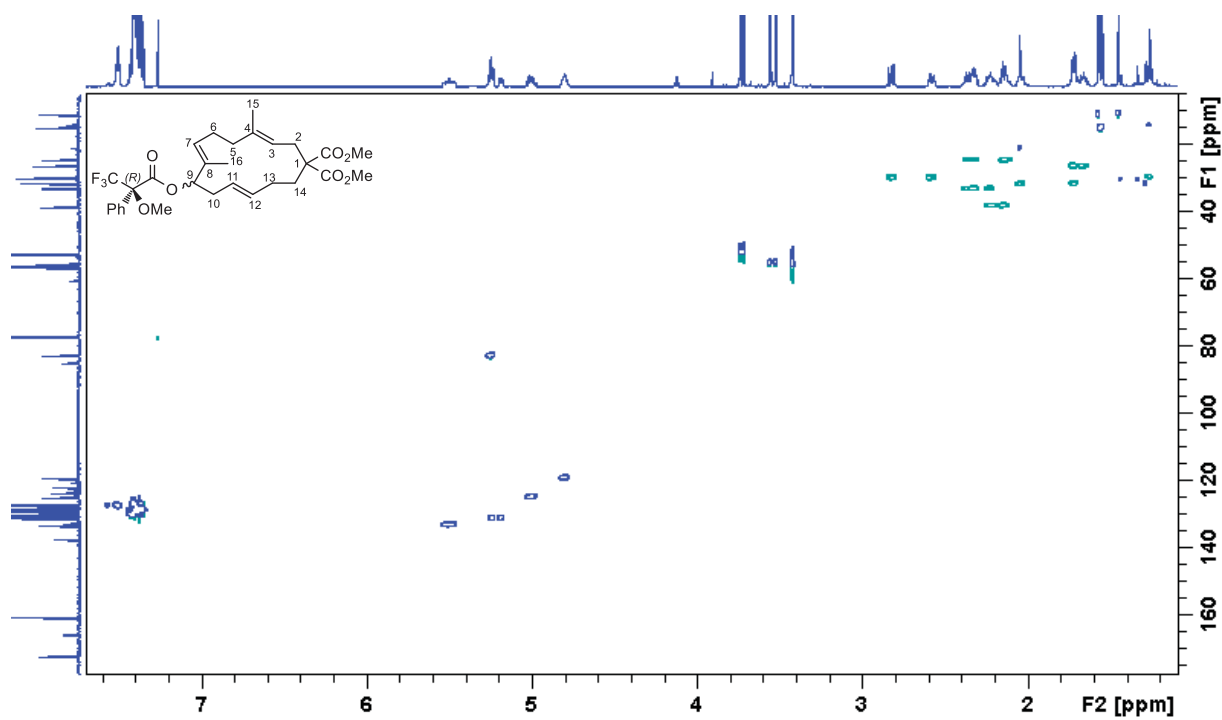
¹H NMR (MTPA *R*)-Ester 5



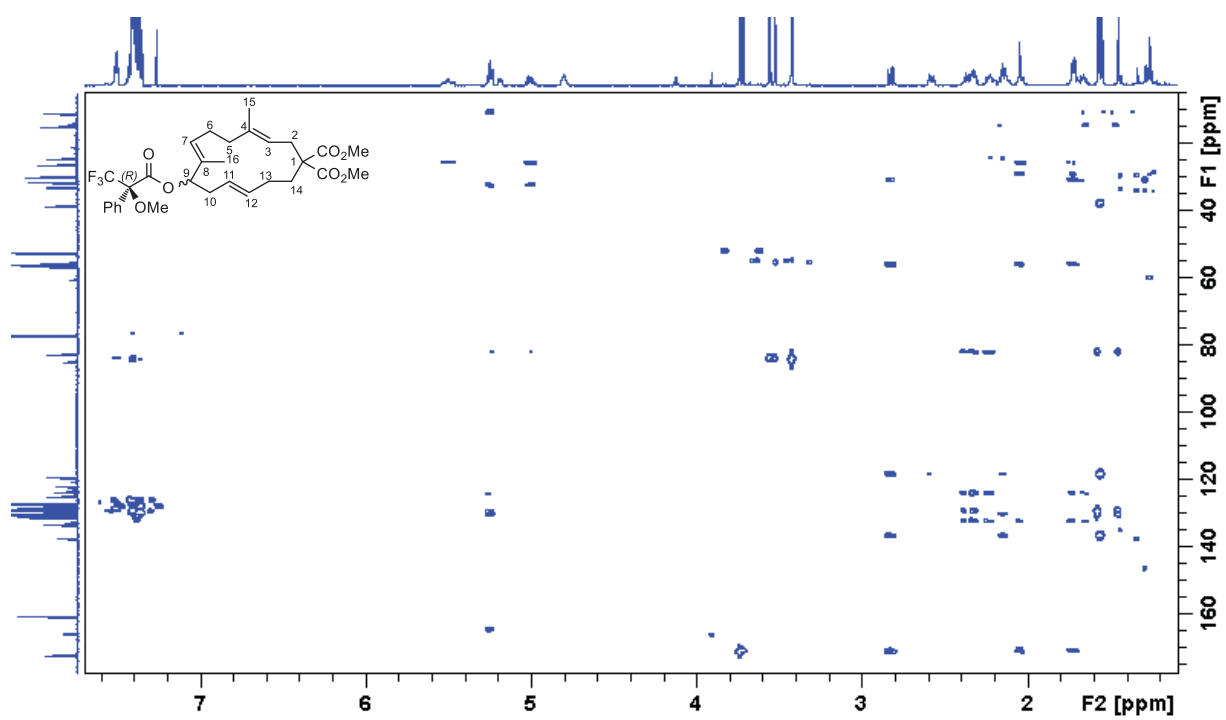
¹³C NMR (MTPA *R*)-Ester 5



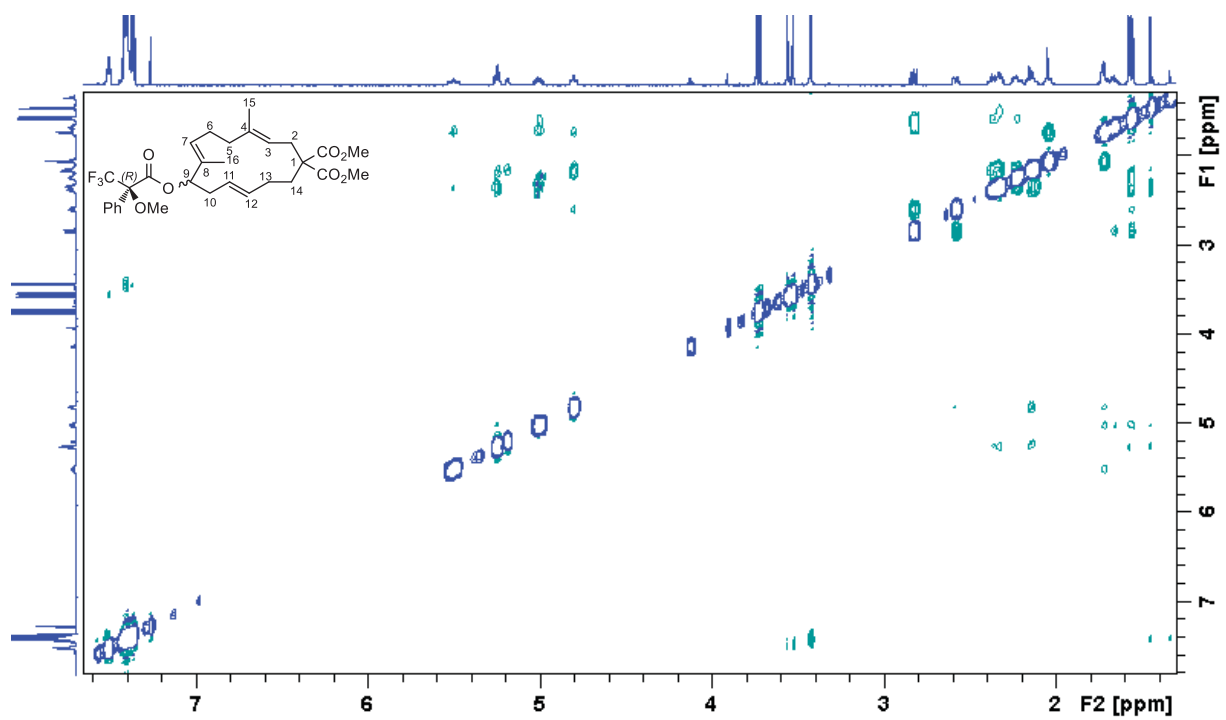
$^1\text{H}, ^1\text{H}$ COSY NMR ($M^{TPA}R$)-Ester 5



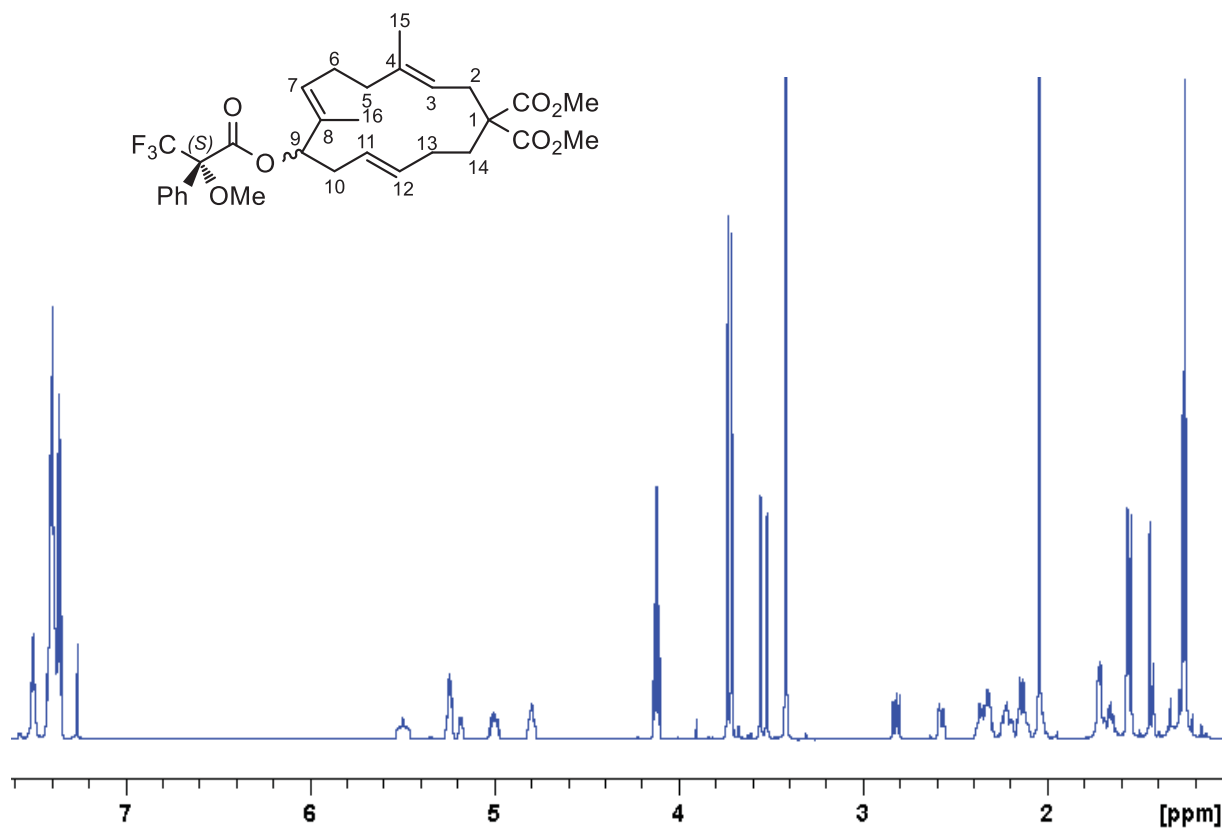
$^1\text{H}, ^{13}\text{C}$ HSQC NMR ($M^{TPA}R$)-Ester 5



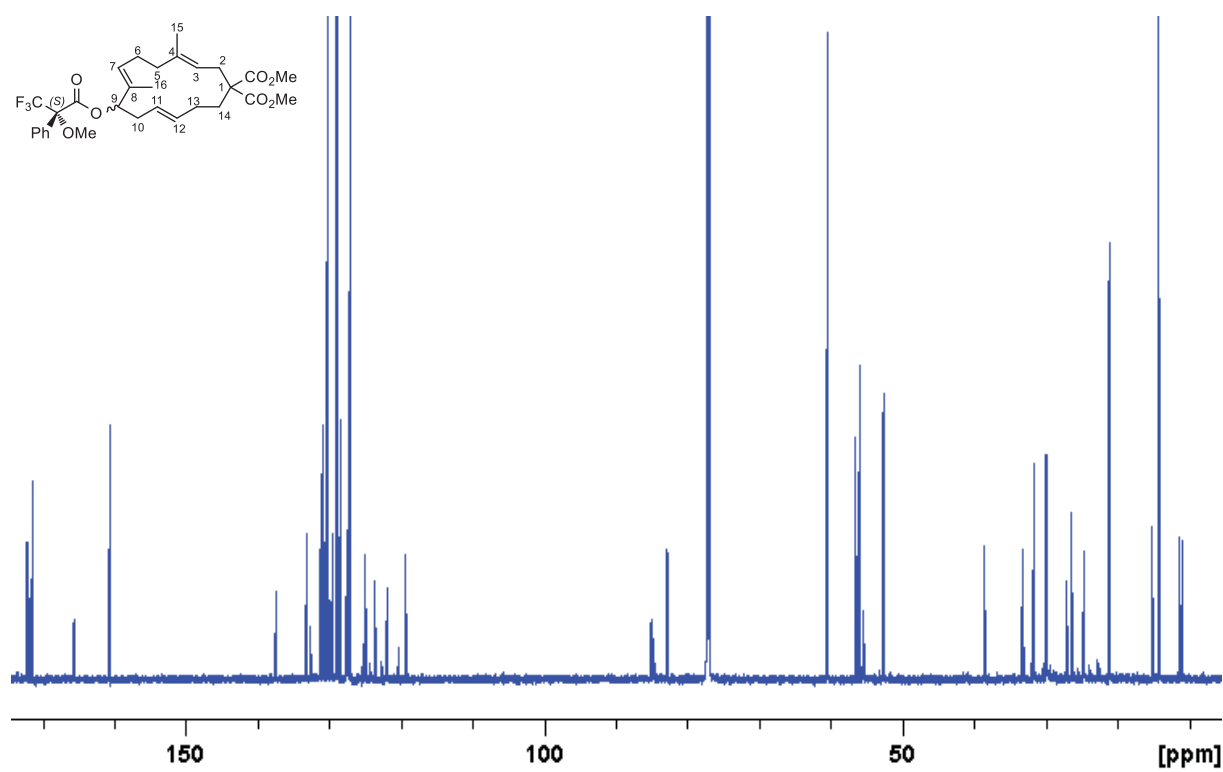
$^1\text{H}, ^{13}\text{C}$ HMBC NMR ($MTPA R$)-Ester 5



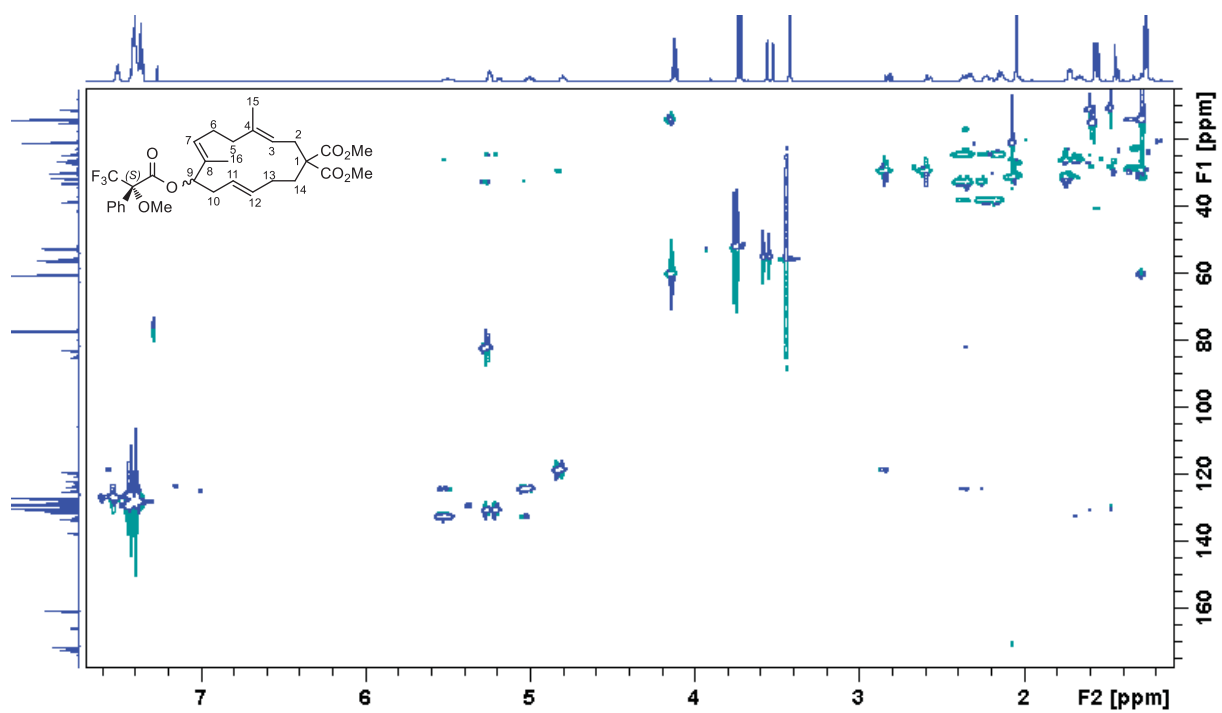
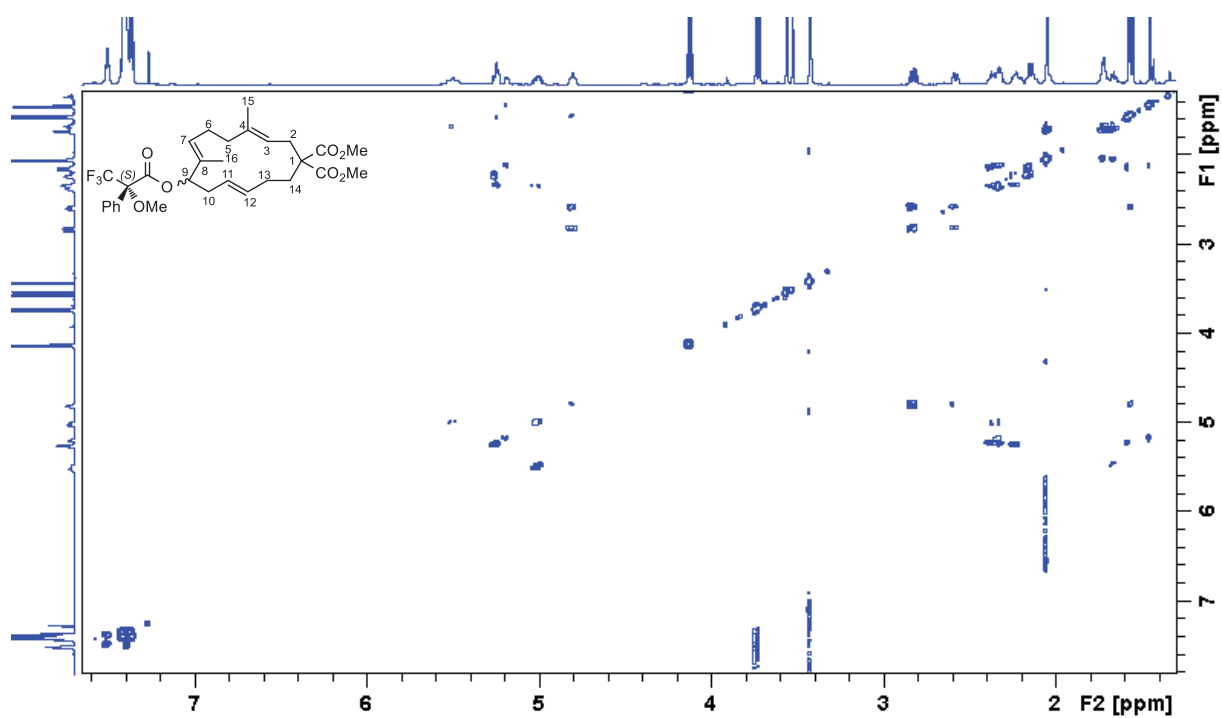
$^1\text{H}, ^1\text{H}$ NOESY NMR ($MTPA R$)-Ester 5

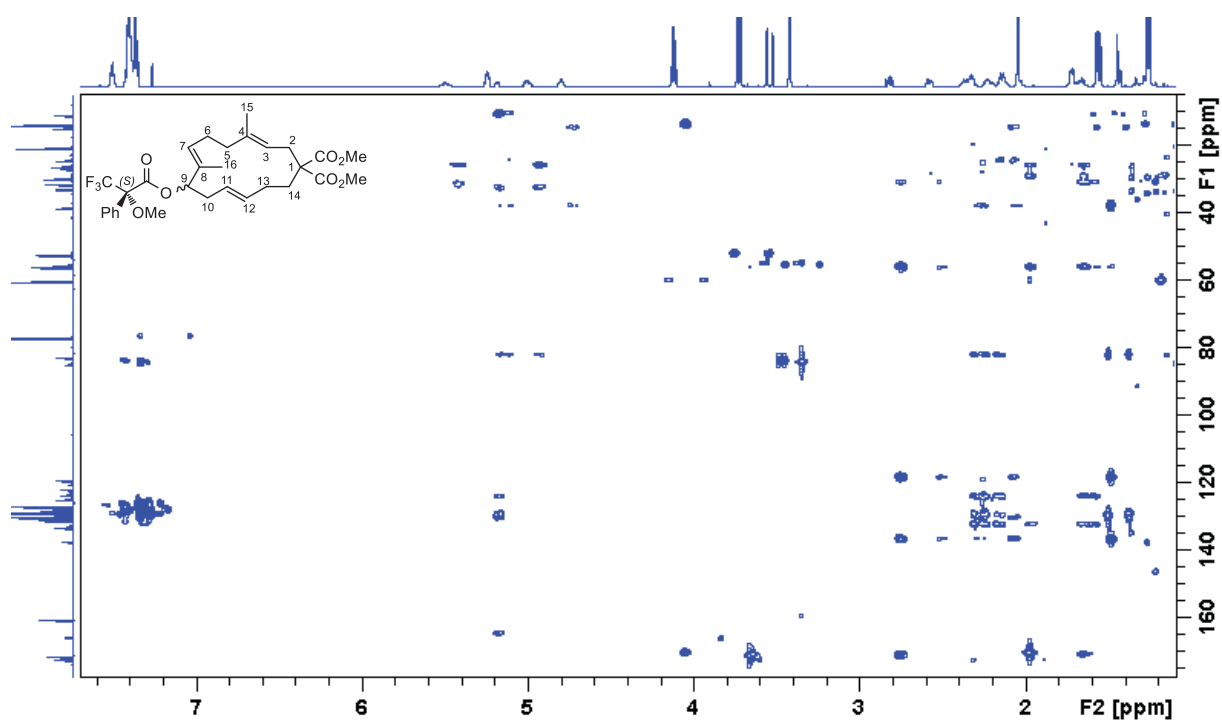


¹H NMR (MTPA S)-Ester 5

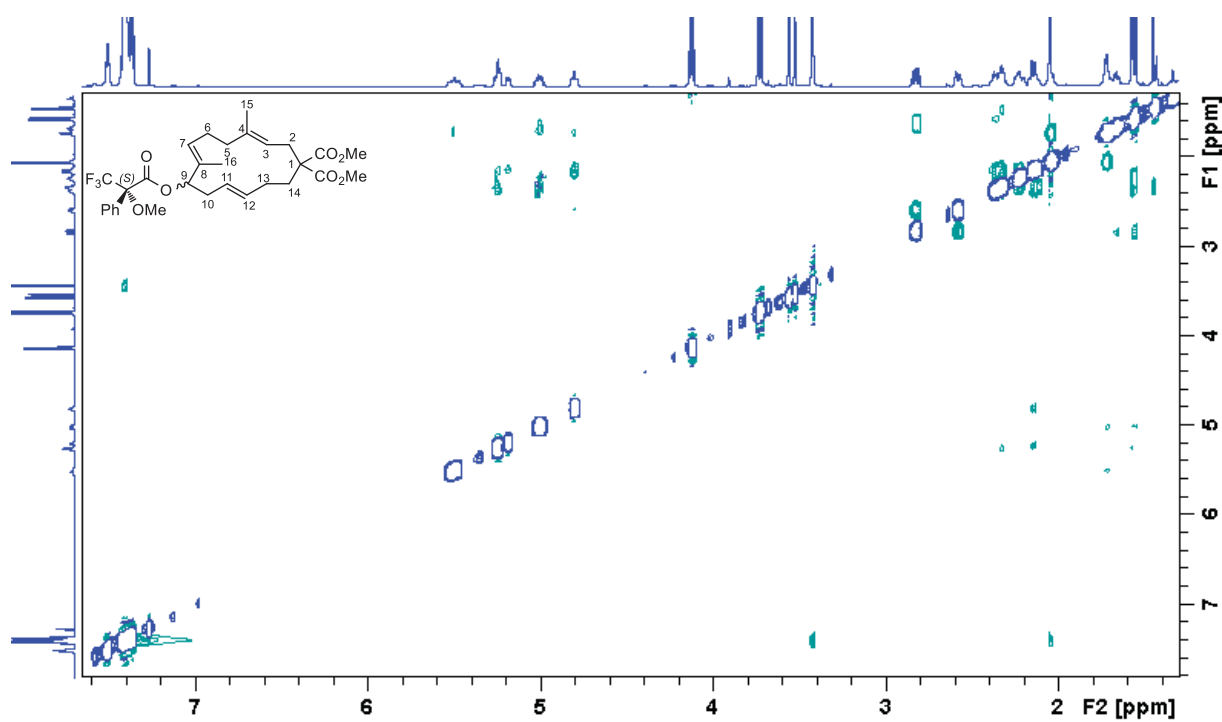


¹³C NMR (MTPA S)-Ester 5

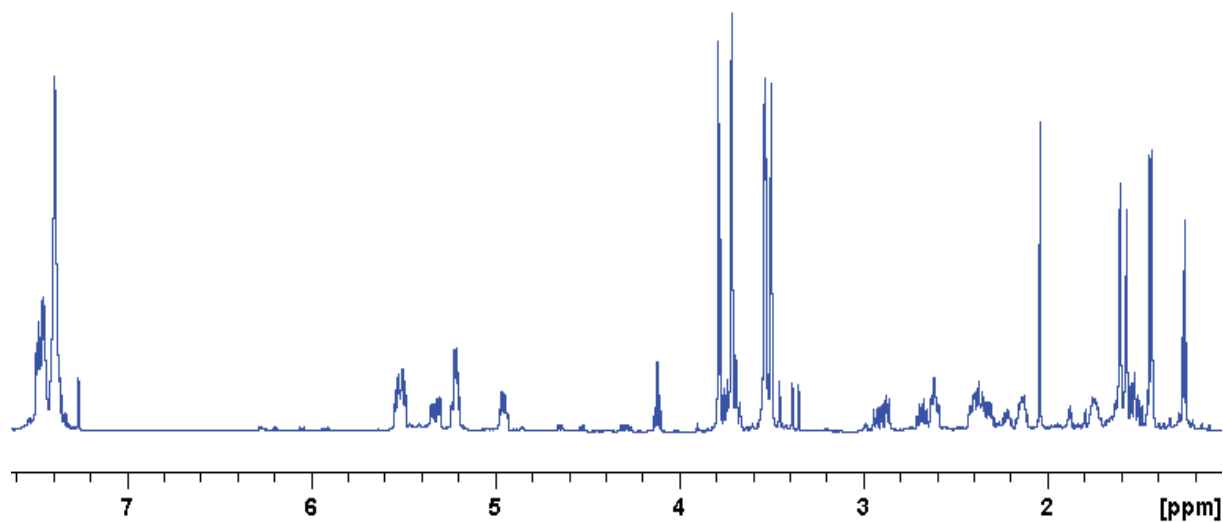
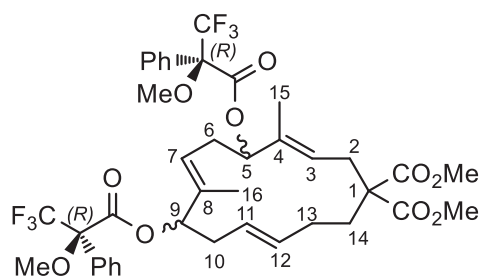




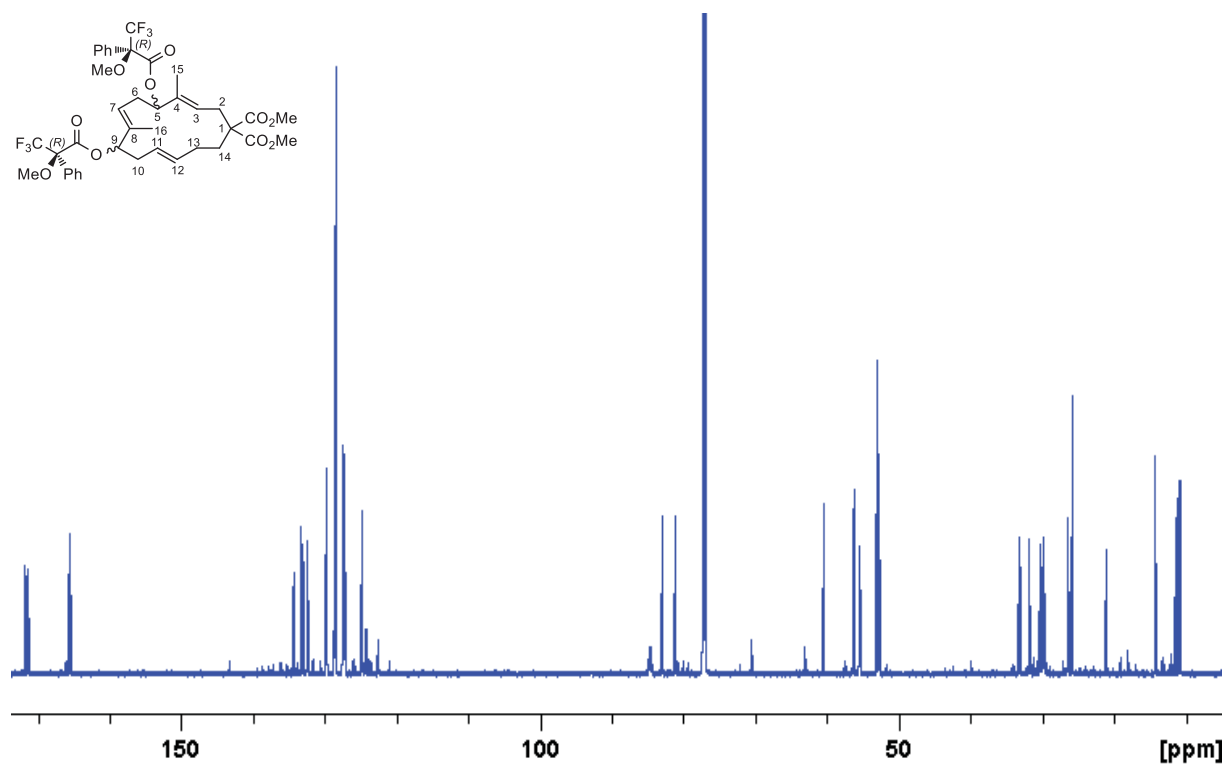
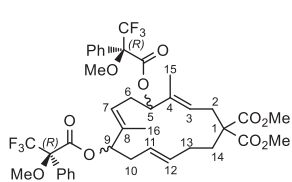
$^1\text{H},^{13}\text{C}$ HMBC NMR (MTPA-S)-Ester 5



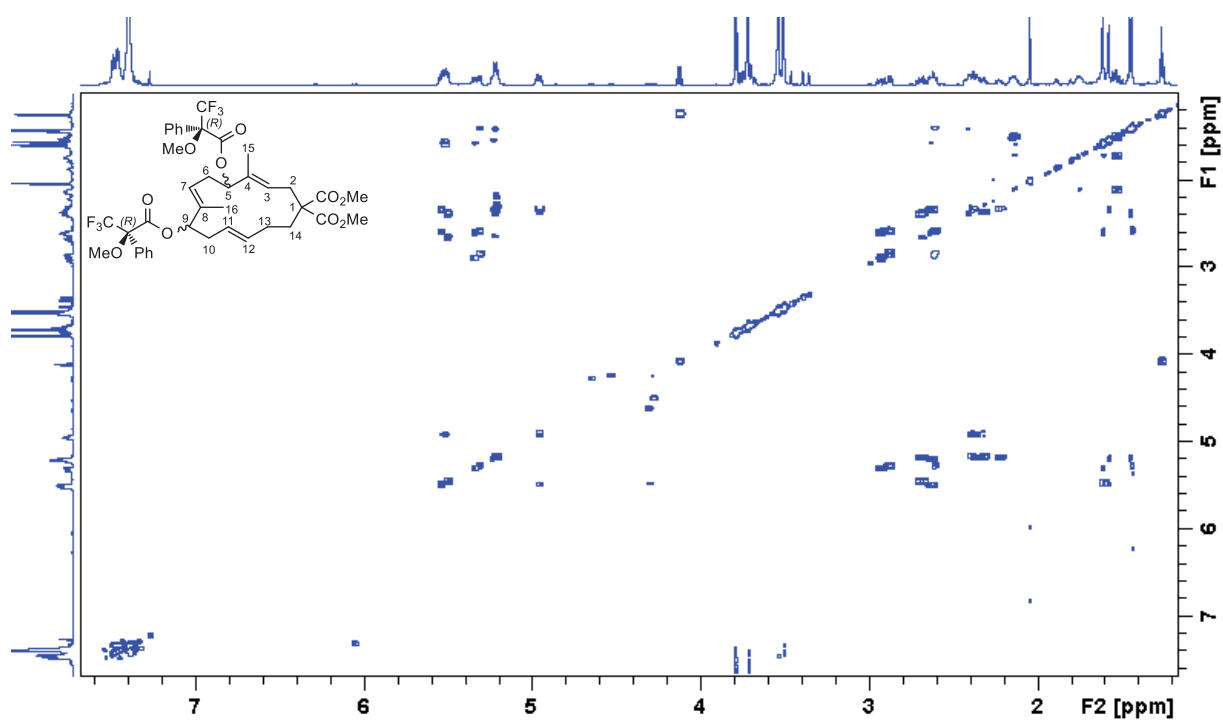
$^1\text{H},^1\text{H}$ NOESY NMR (MTPA-S)-Ester 5



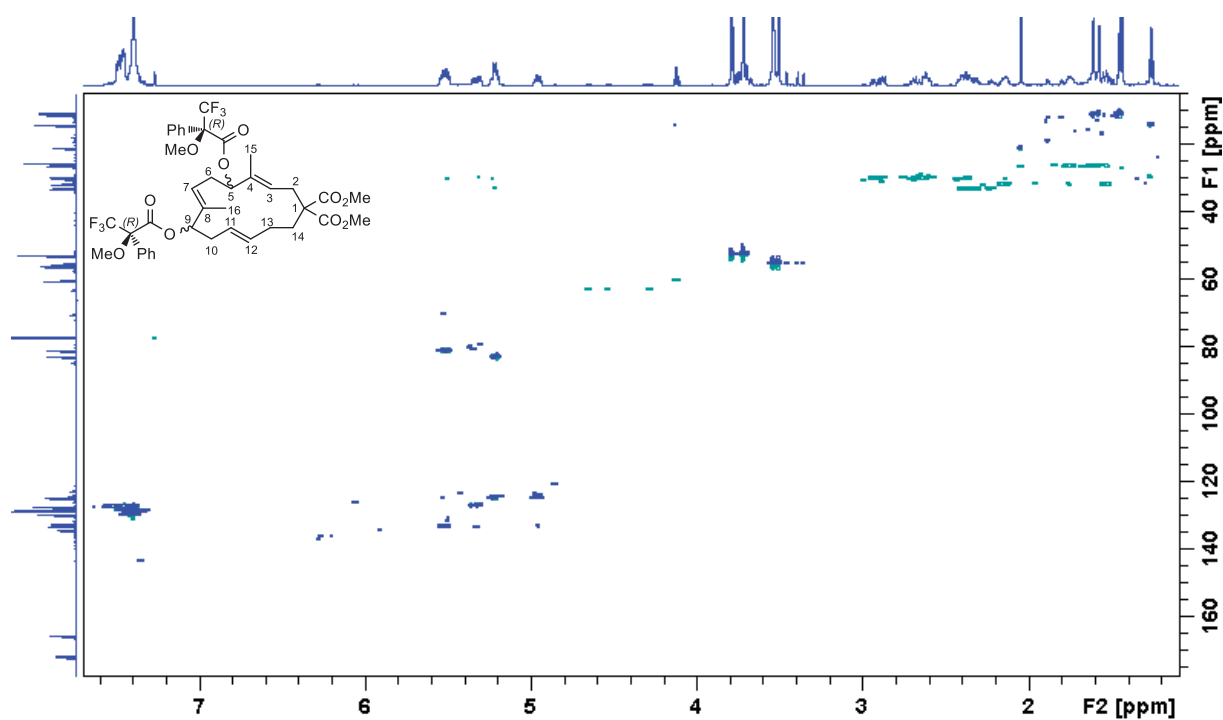
^1H NMR NMR (5- MTPA *R*, 9- MTPA *R*)-Ester 6



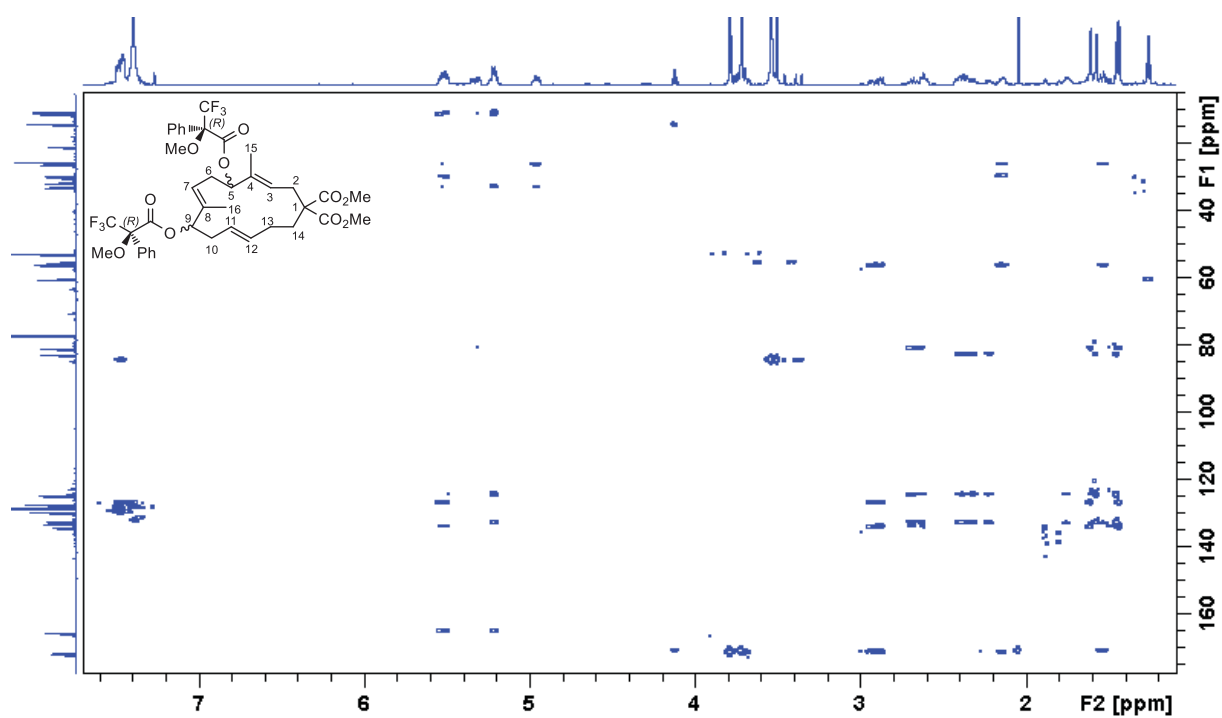
^{13}C NMR NMR (5- MTPA *R*, 9- MTPA *R*)-Ester 6



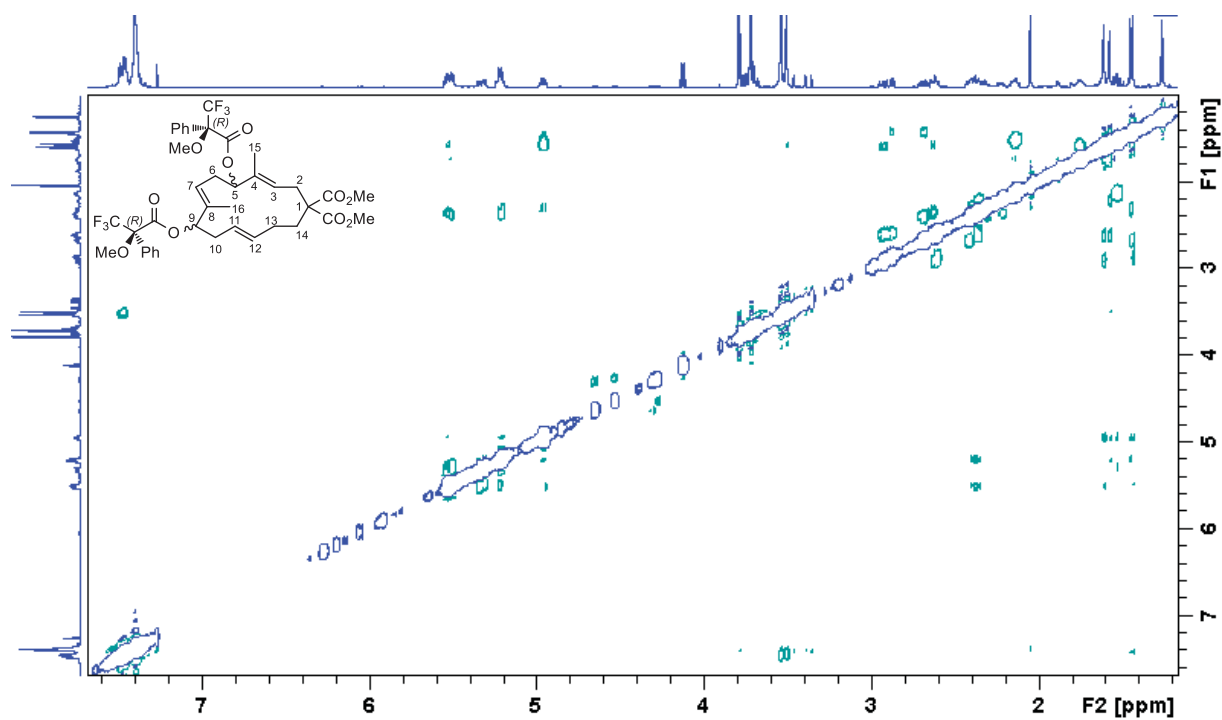
$^1\text{H}, ^1\text{H}$ COSY NMR (5-*MTPA* *R*,9-*MTPA* *R*)-Ester **6**



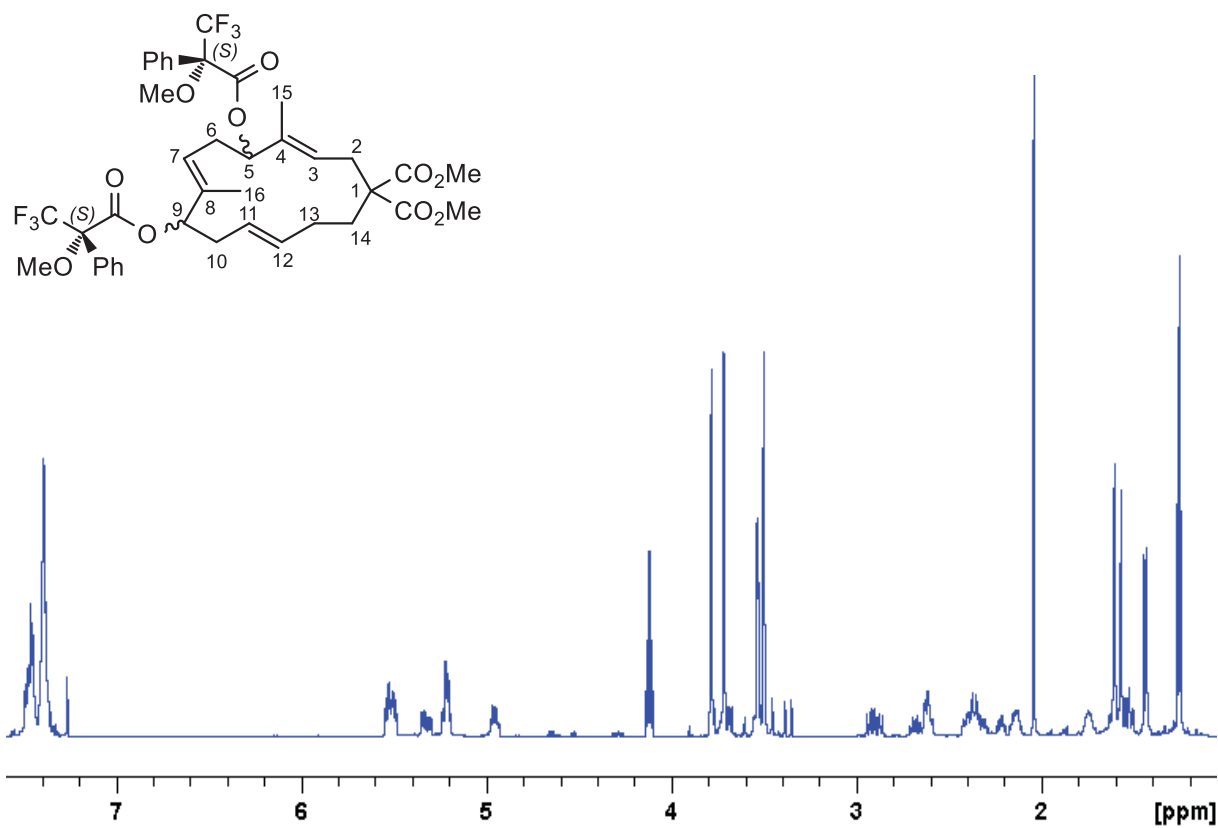
$^1\text{H}, ^{13}\text{C}$ HSQC NMR (5-*MTPA* *R*,9-*MTPA* *R*)-Ester **6**



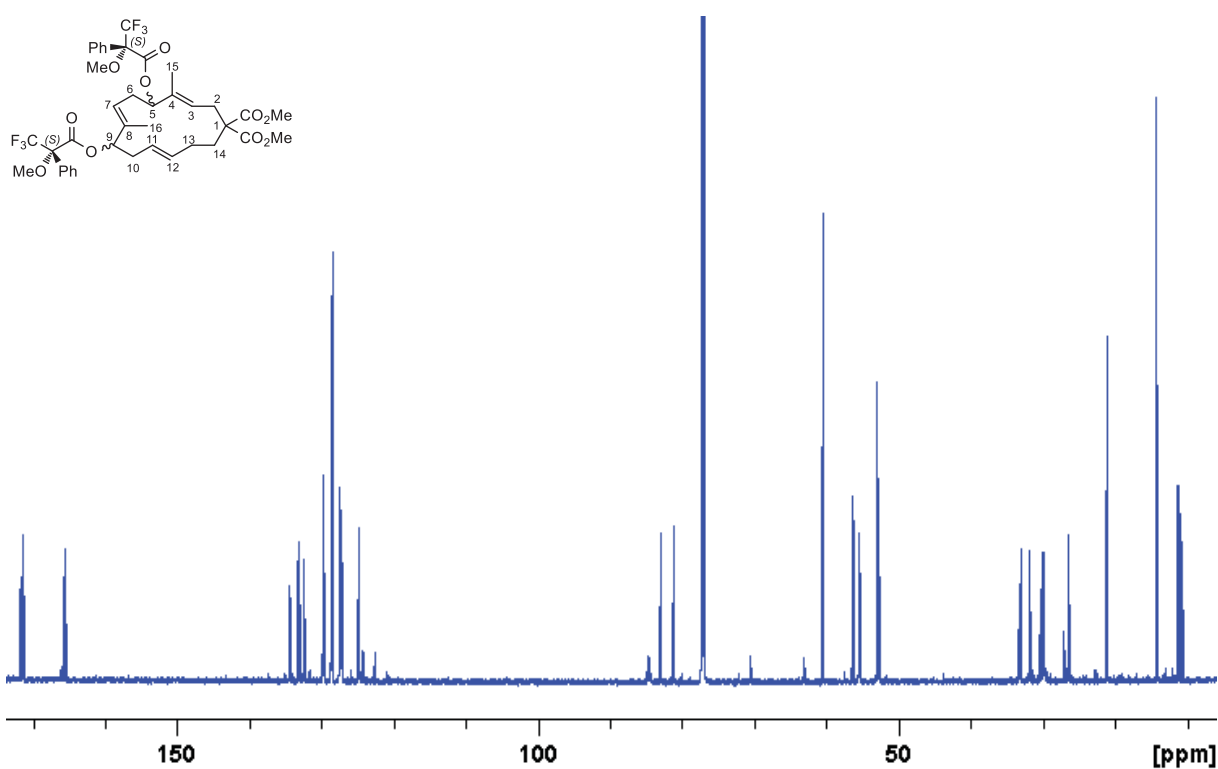
$^1\text{H},^{13}\text{C}$ HMBC NMR (5-MTPA *R*,9-MTPA *R*)-Ester **6**



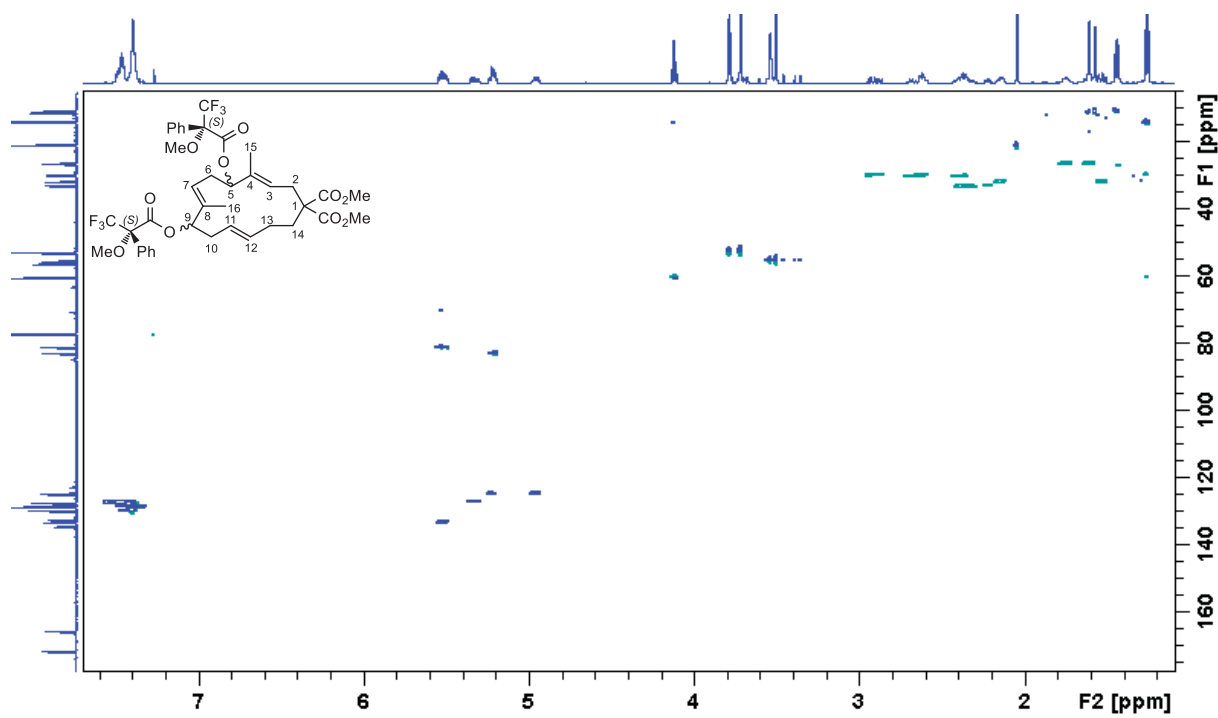
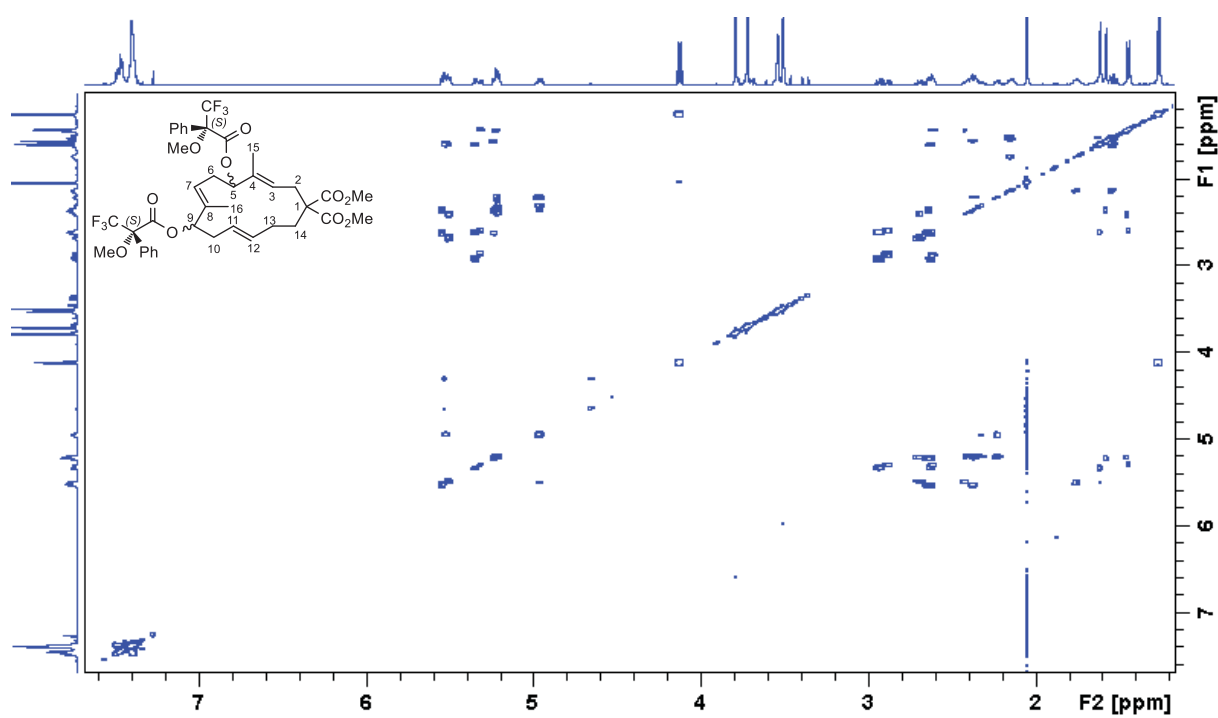
$^1\text{H},^1\text{H}$ NOESY NMR (5-MTPA *R*,9-MTPA *R*)-Ester **6**

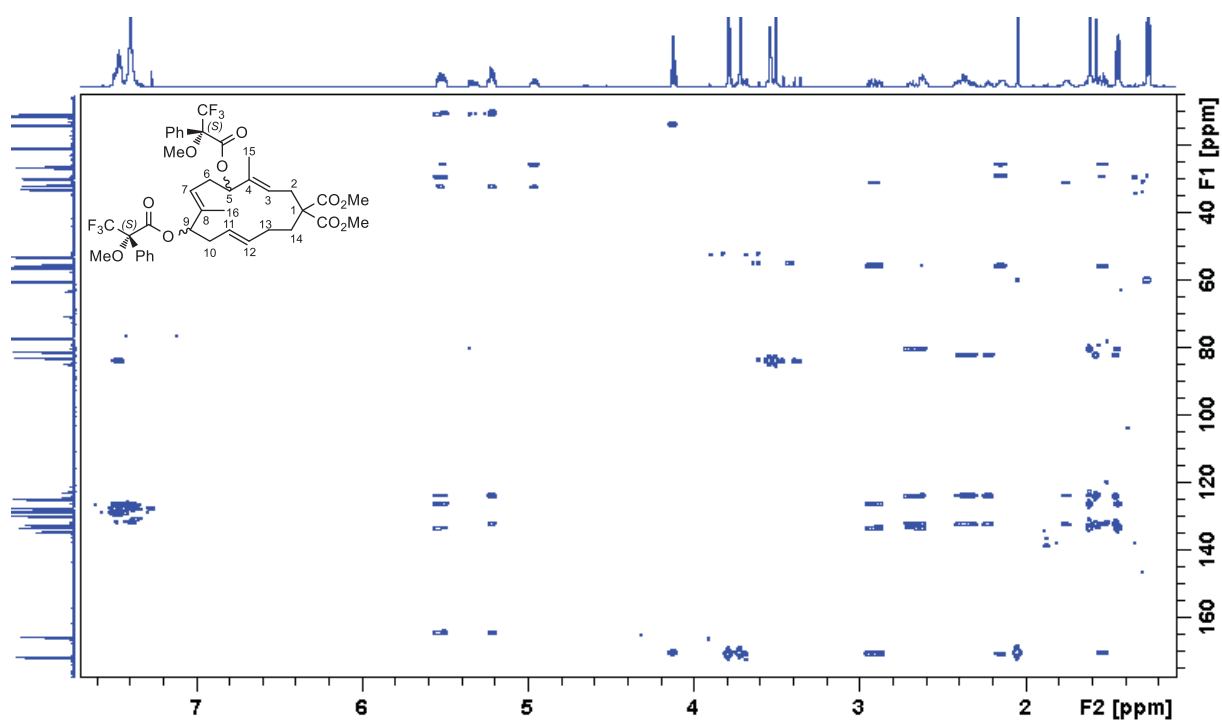


¹H NMR (5-MTPA,S,9-MTPA,S)-Ester 6

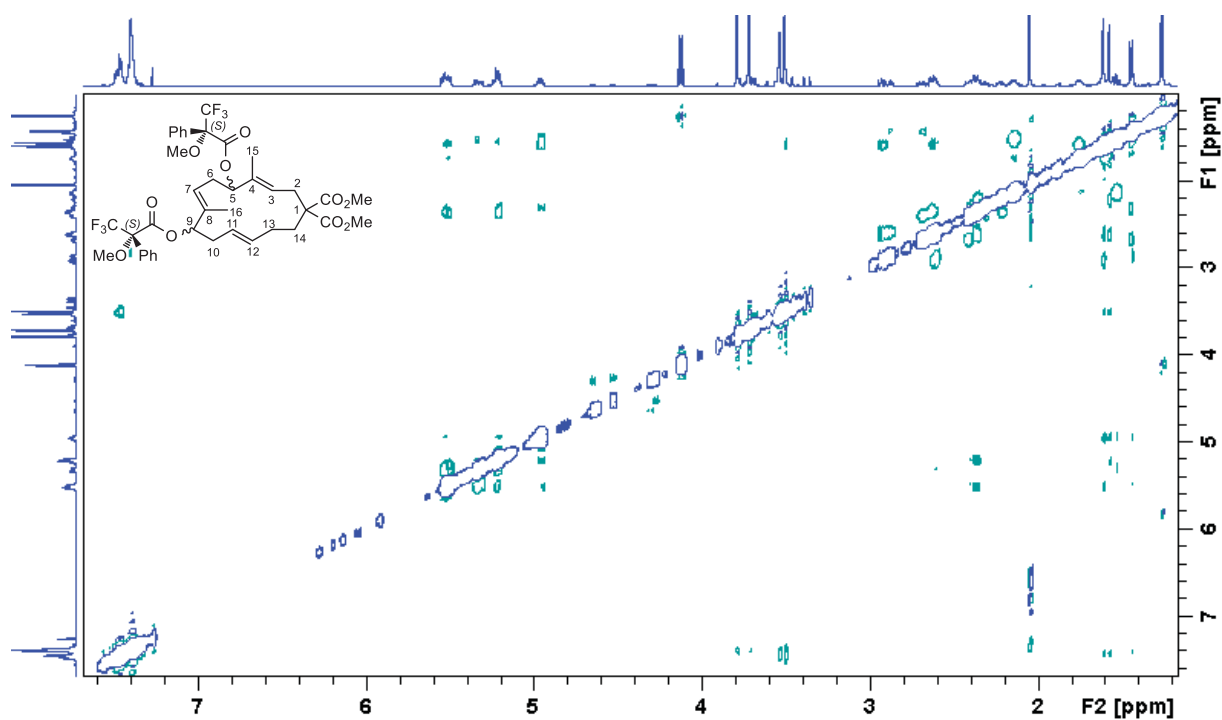


¹³C NMR (5-MTPA,S,9-MTPA,S)-Ester 6

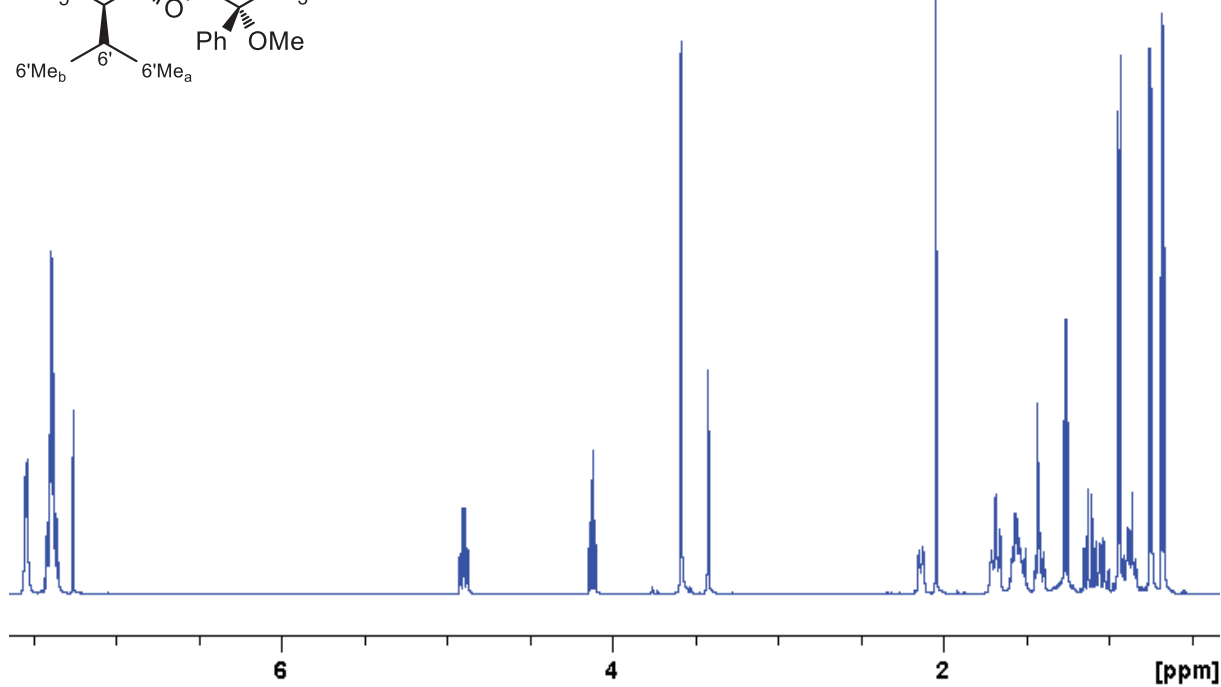
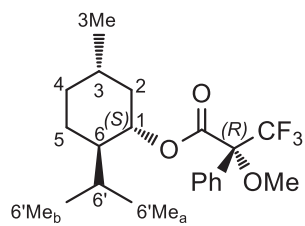




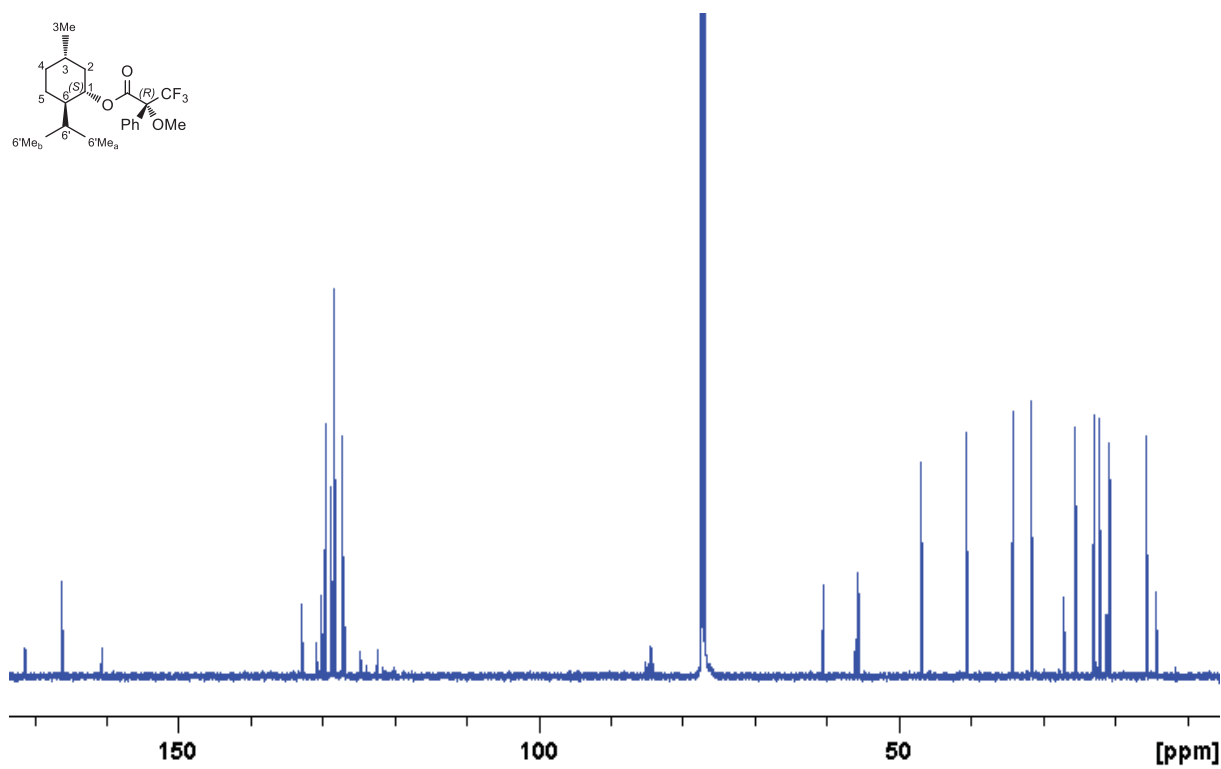
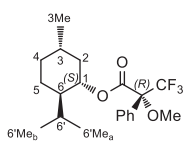
$^1\text{H},^{13}\text{C}$ HMBC NMR (5-MTPA_S,9-MTPA_S)-Ester 6



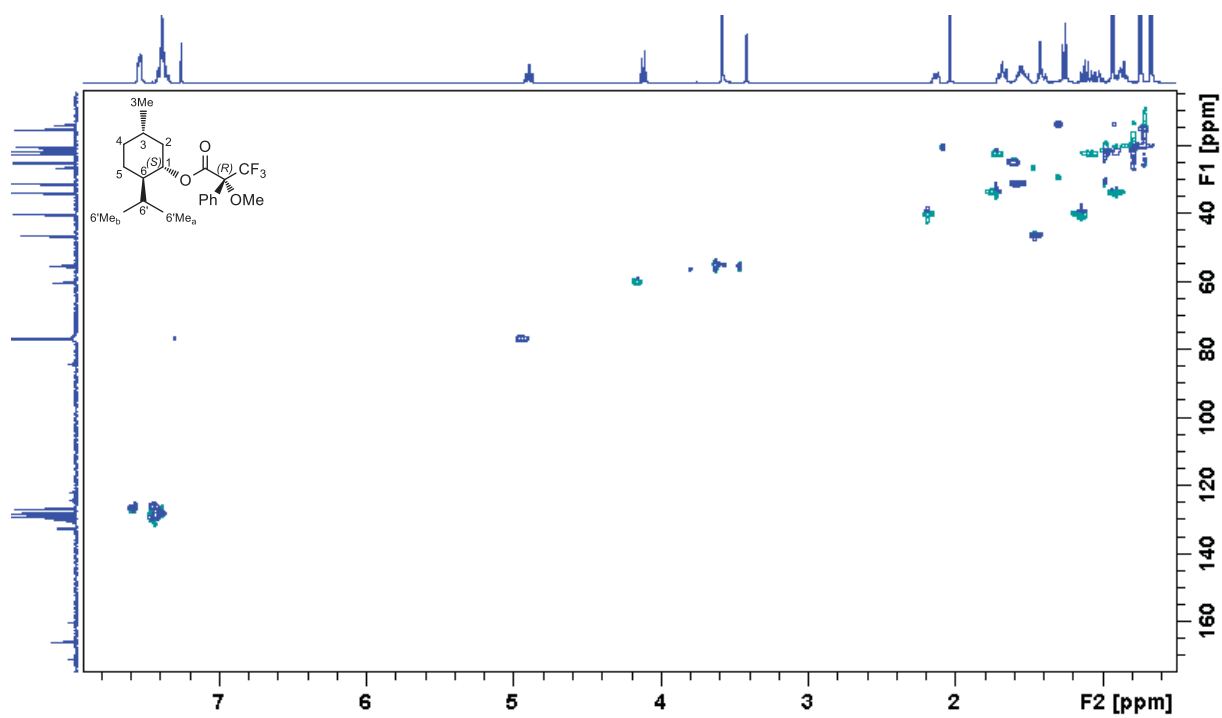
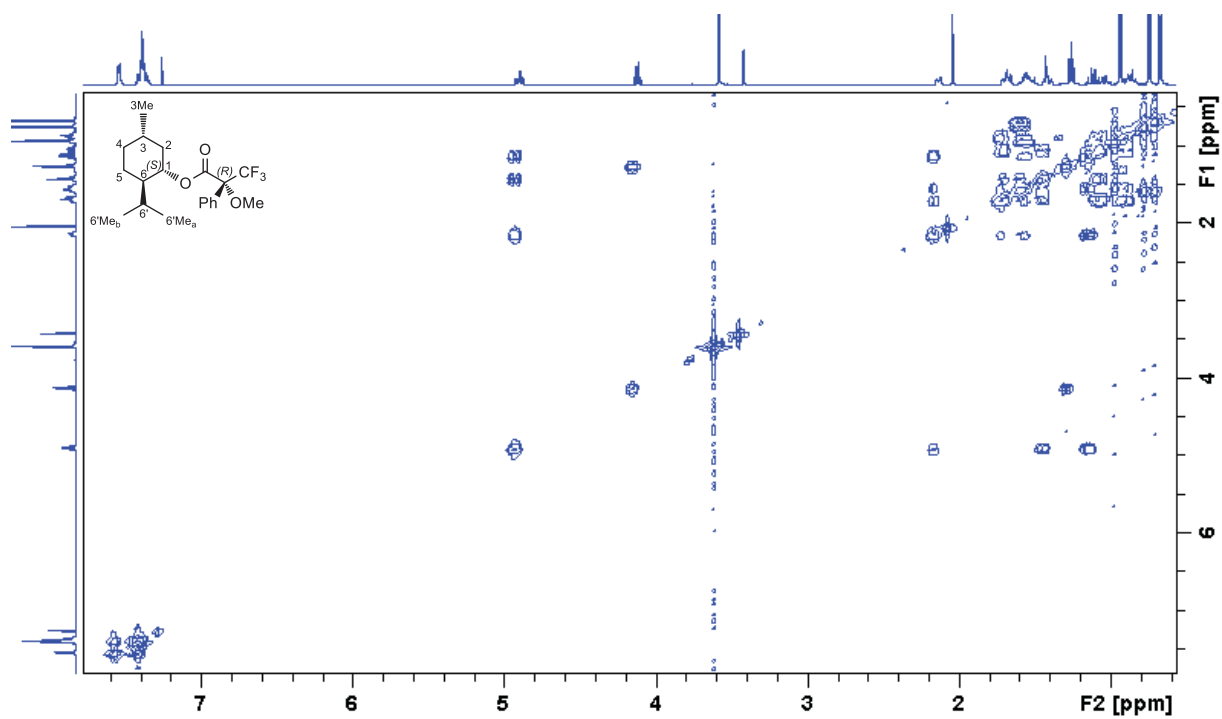
$^1\text{H},^1\text{H}$ NOESY NMR (5-MTPA_S,9-MTPA_S)-Ester 6

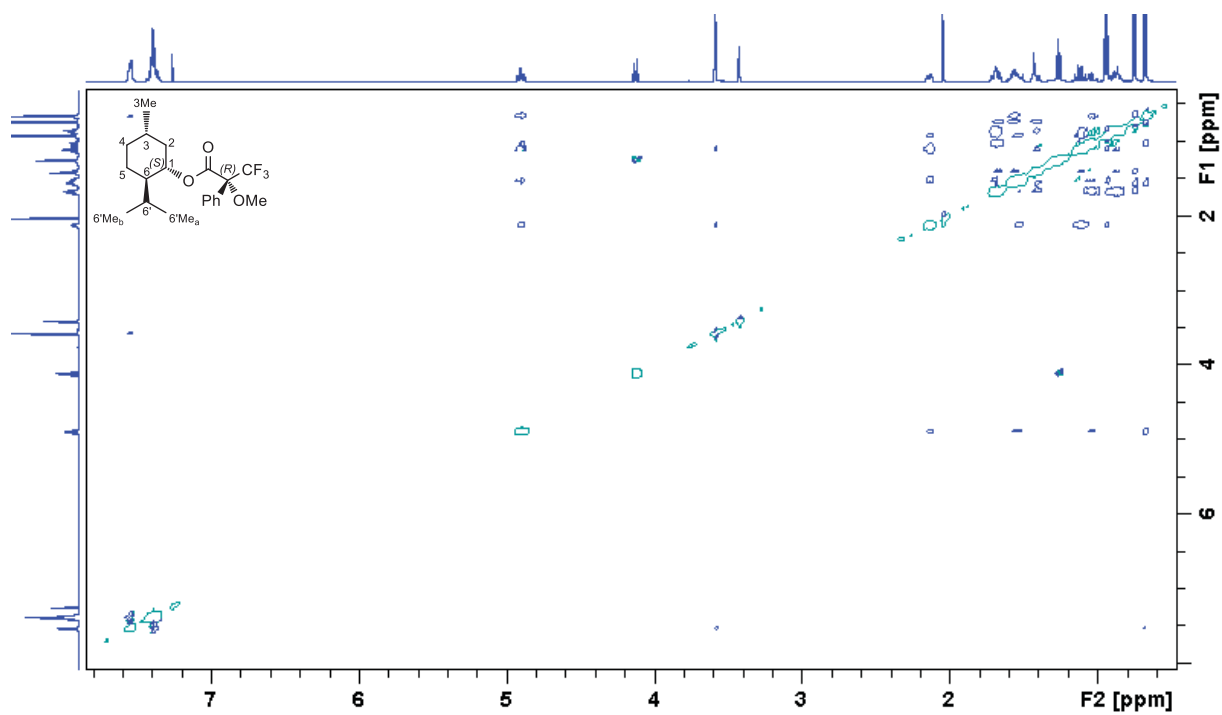
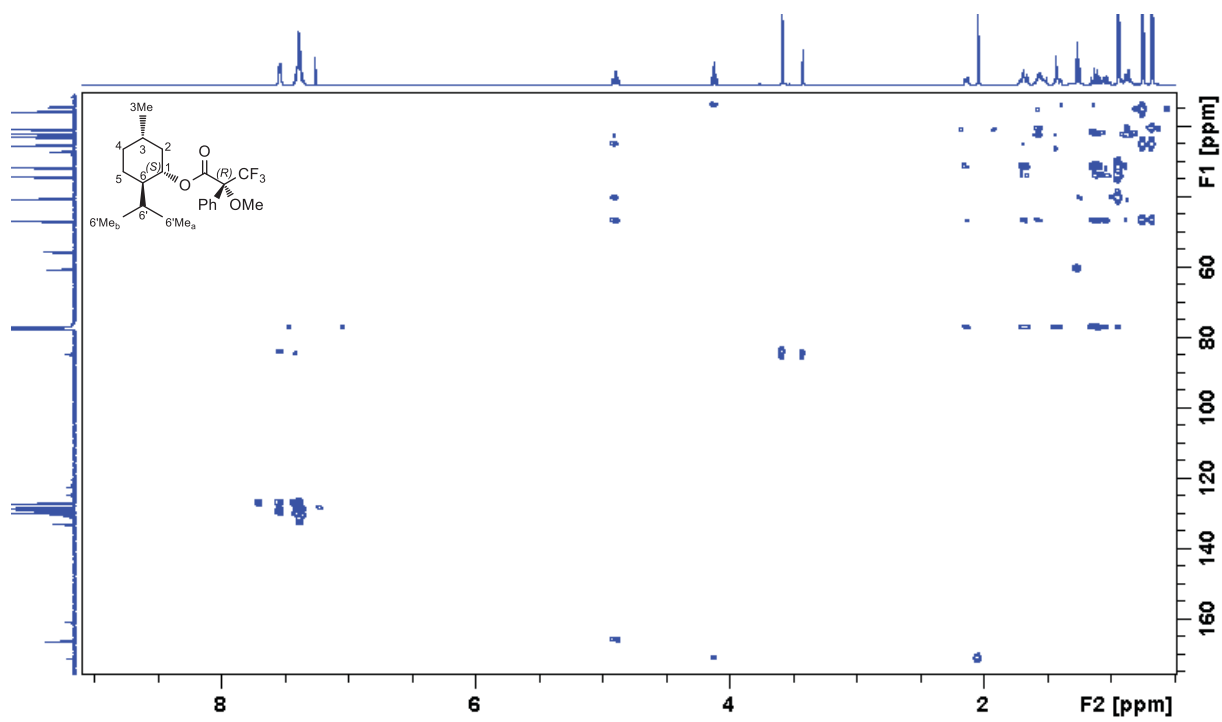


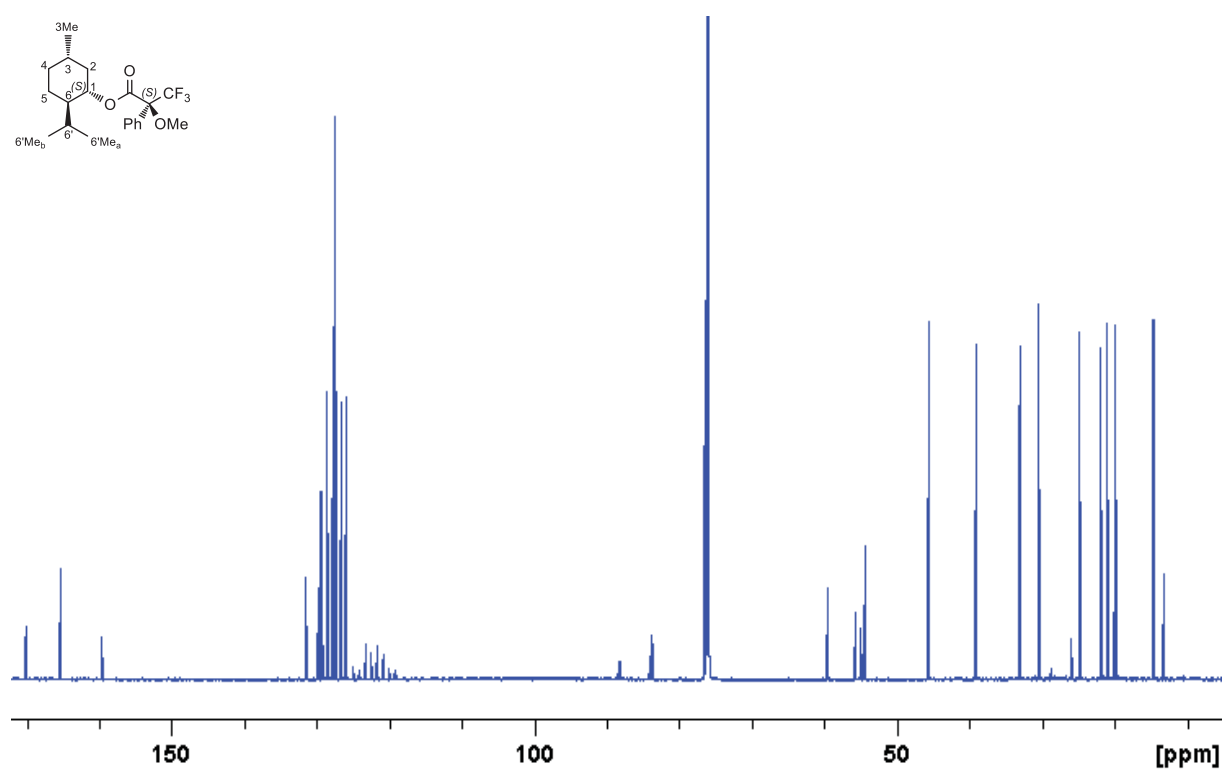
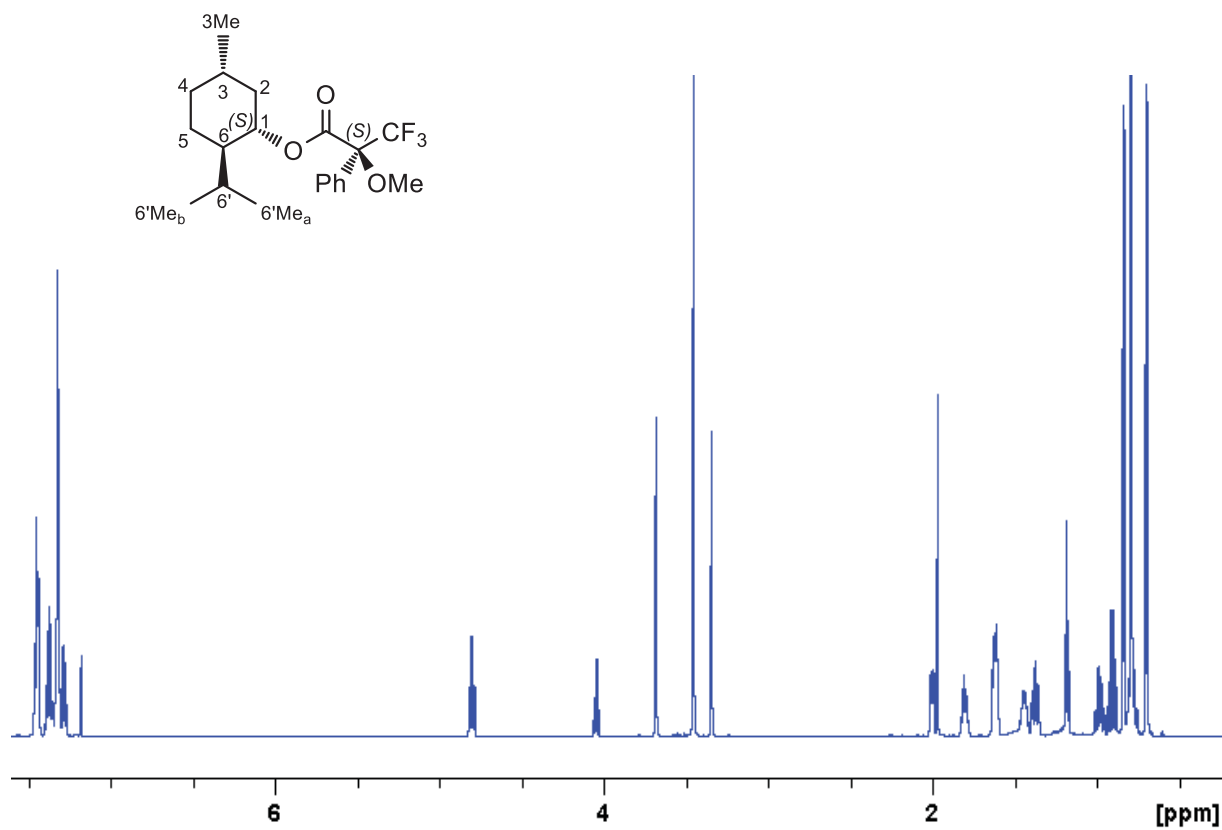
^1H NMR *D*-menthyl-(^{MTPA}*R*)-ester **S9**

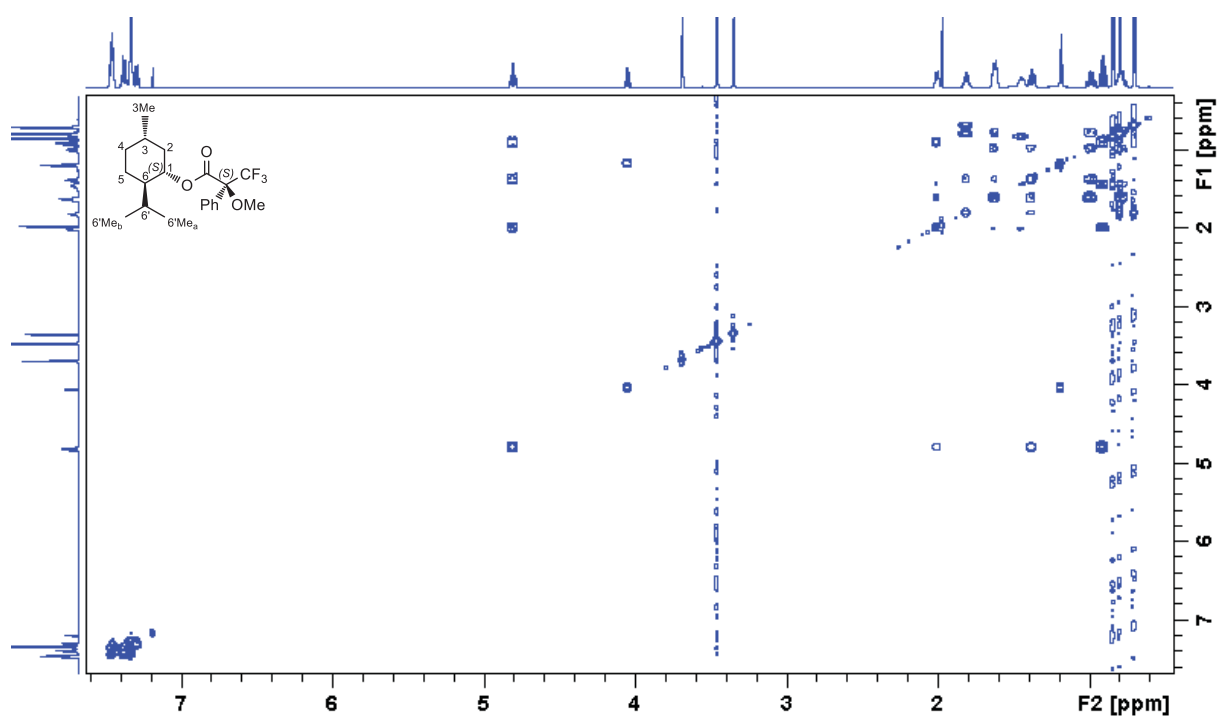


^{13}C NMR *D*-menthyl-(^{MTPA}*R*)-ester **S9**

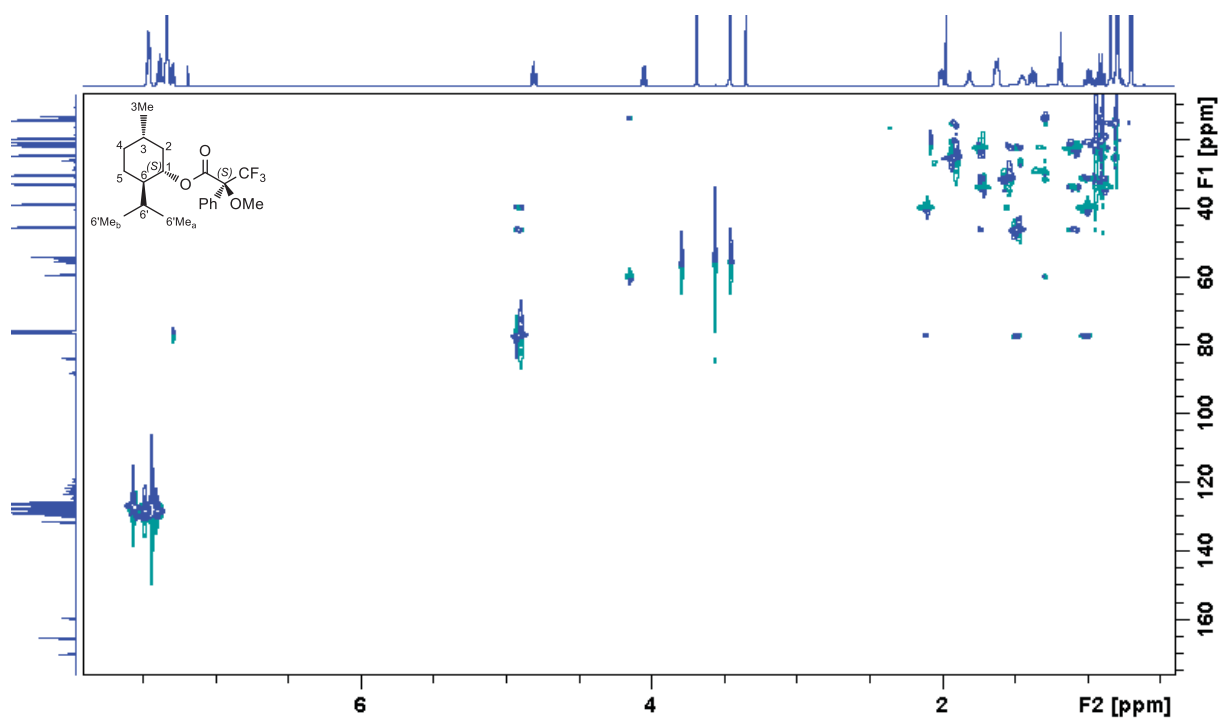




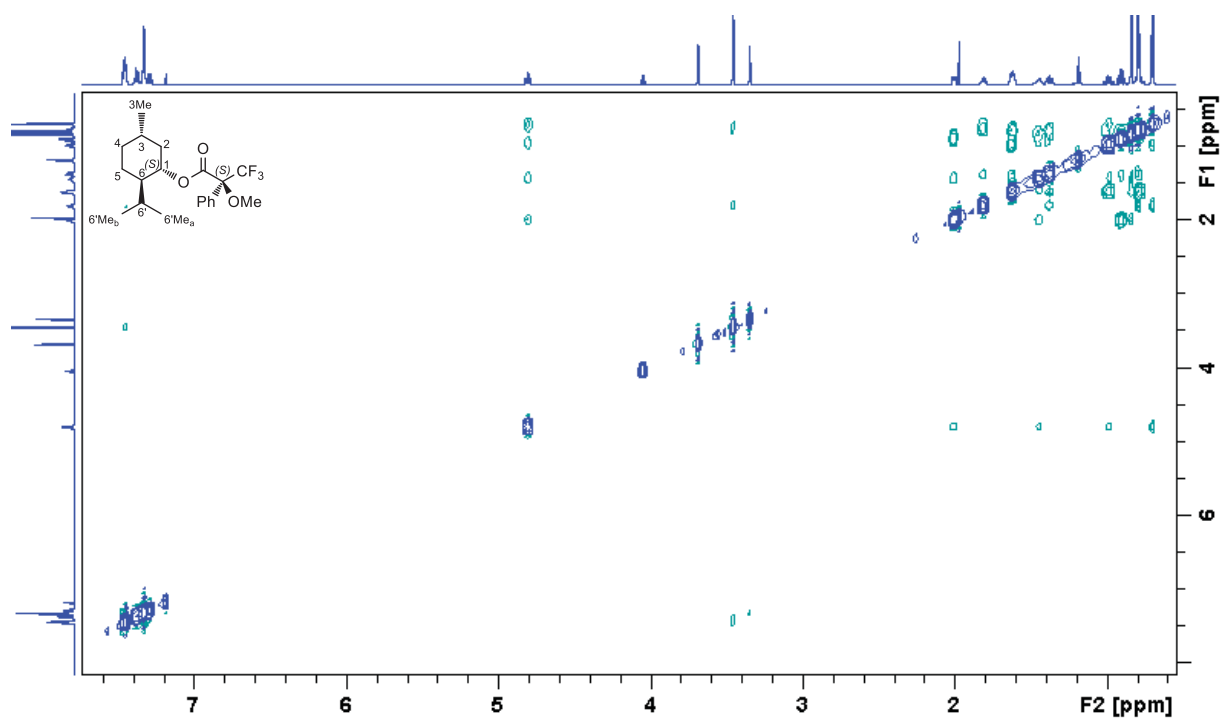
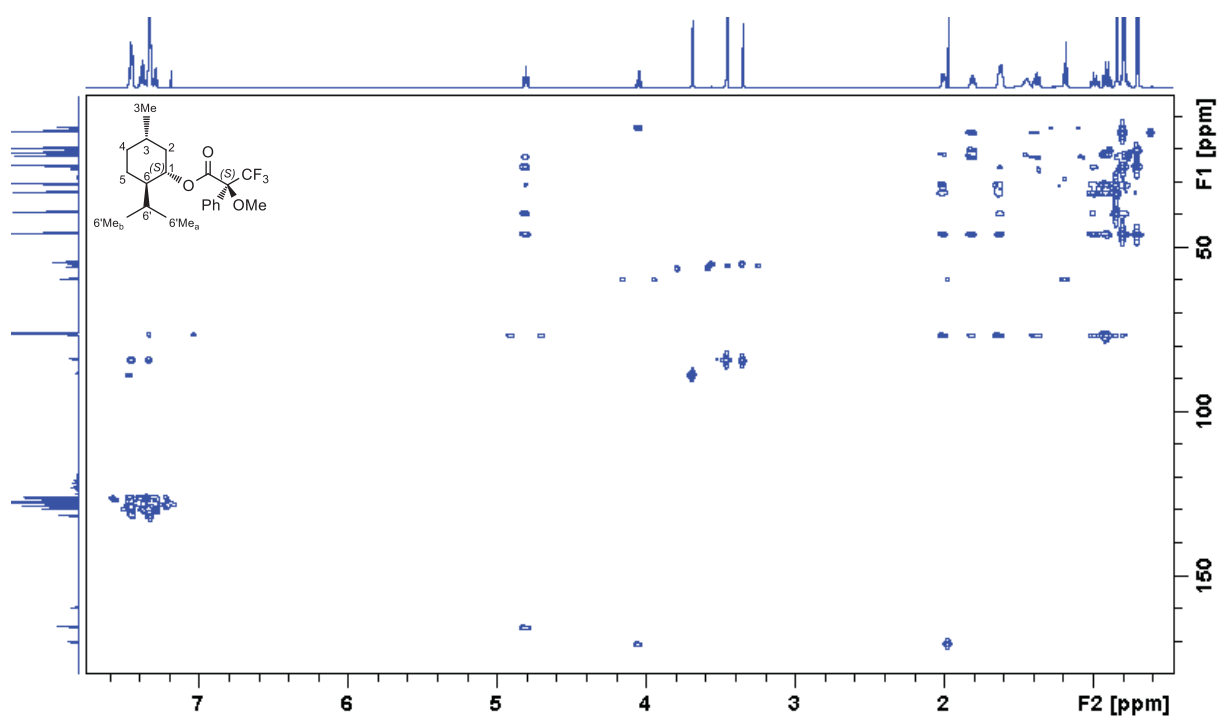


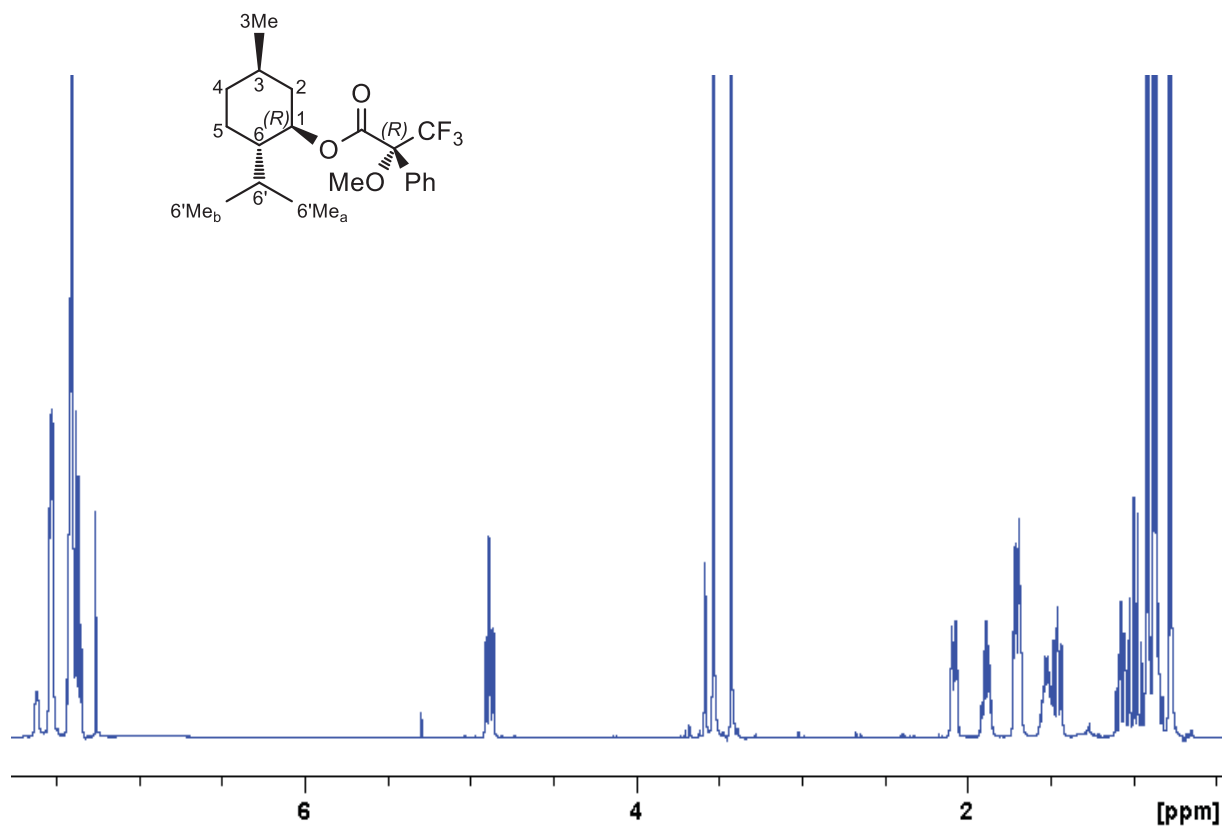


¹H,¹H COSY NMR *D*-menthyl-(^{MTPA(S)})-ester **S9**

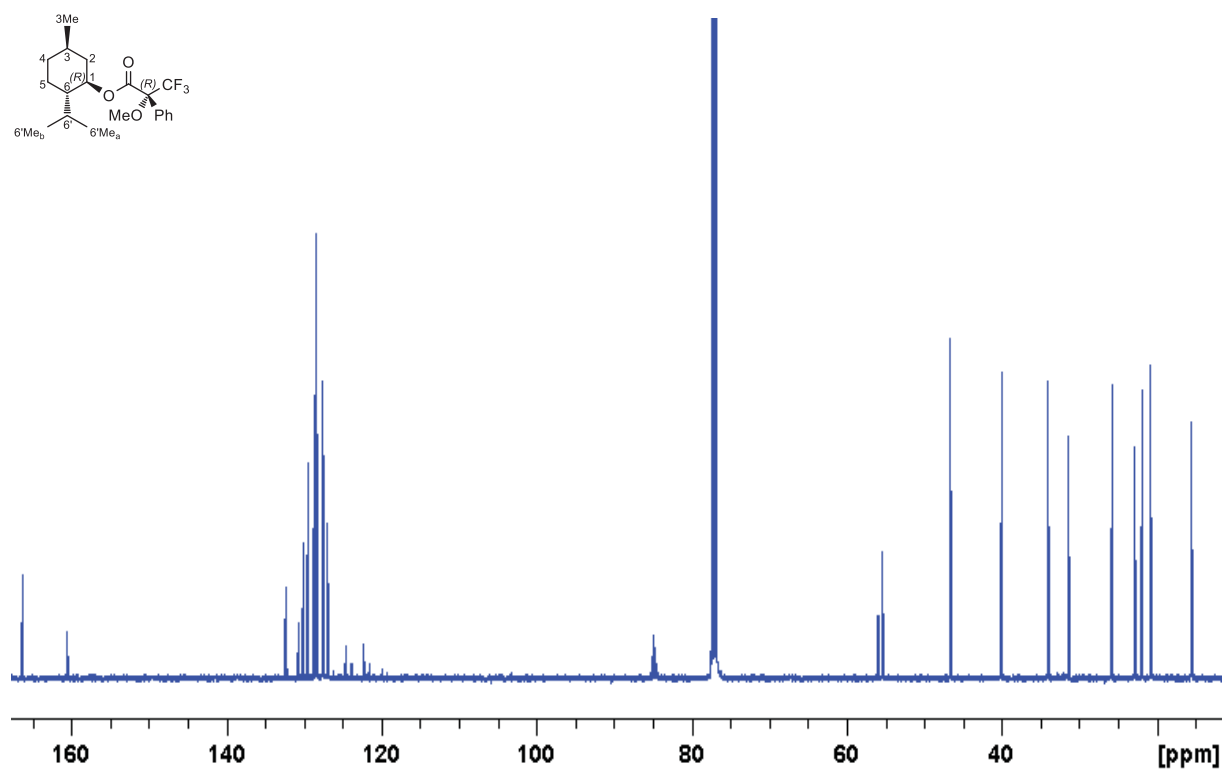


¹H,¹³C HSQC NMR *D*-menthyl-(^{MTPA(S)})-ester **S9**

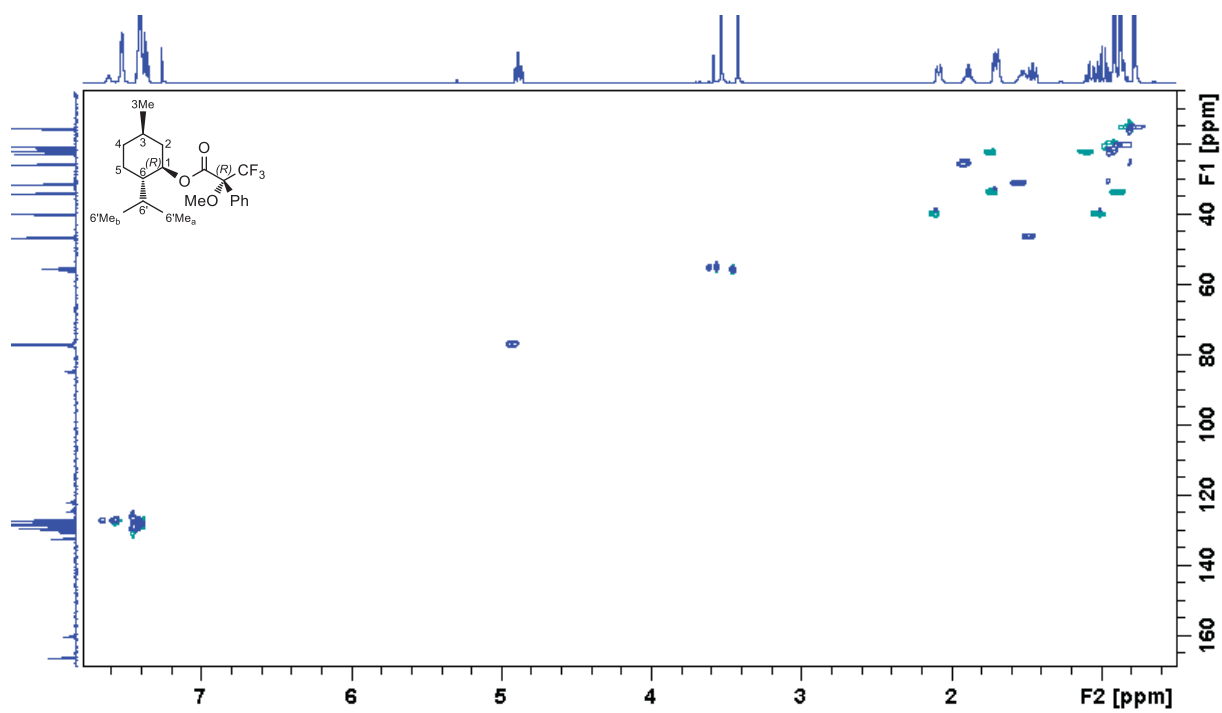
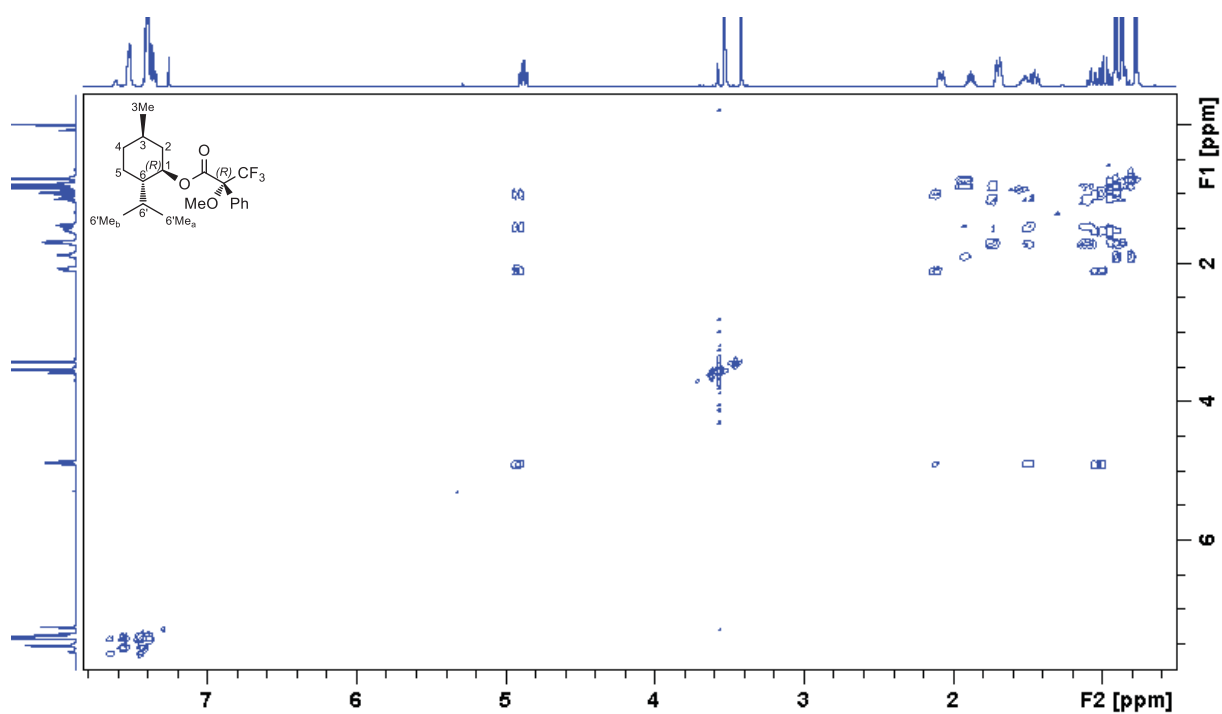


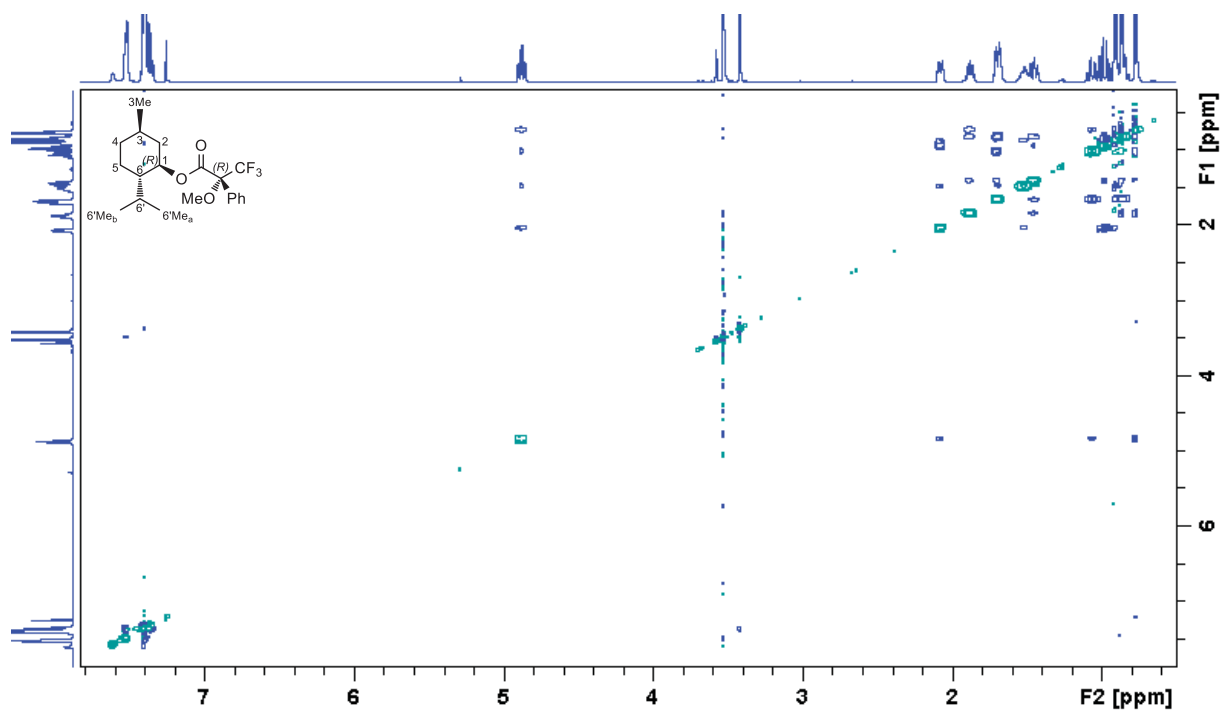
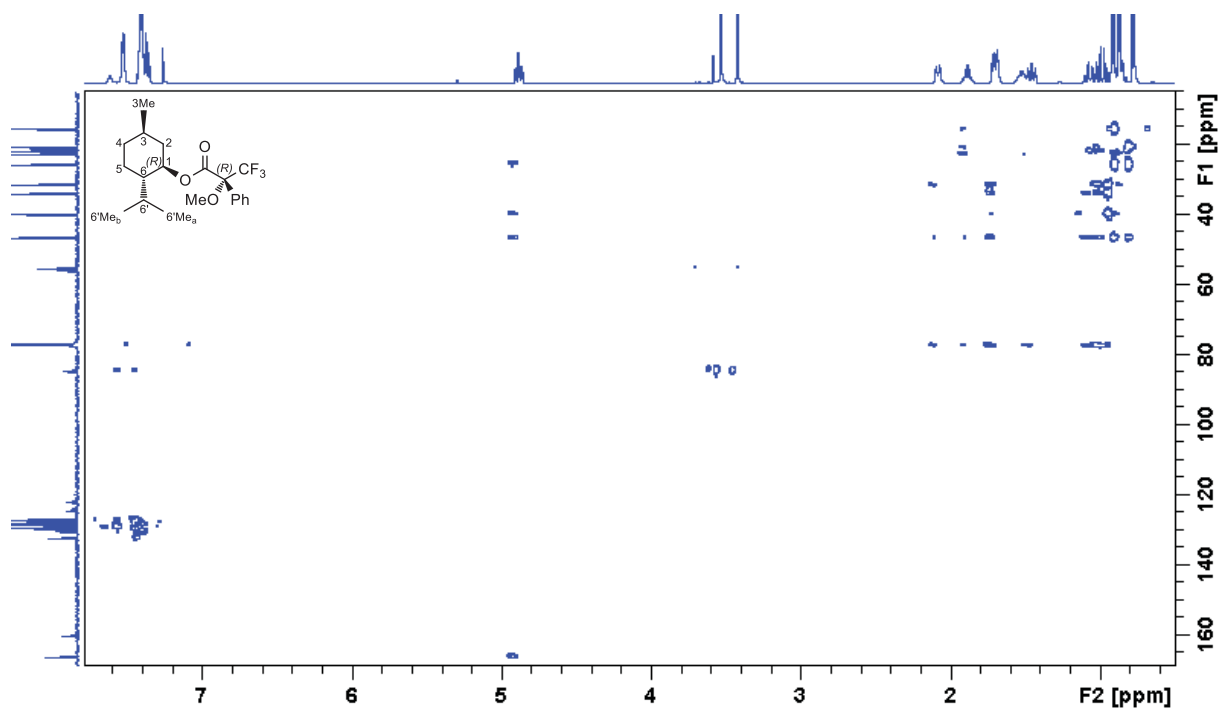


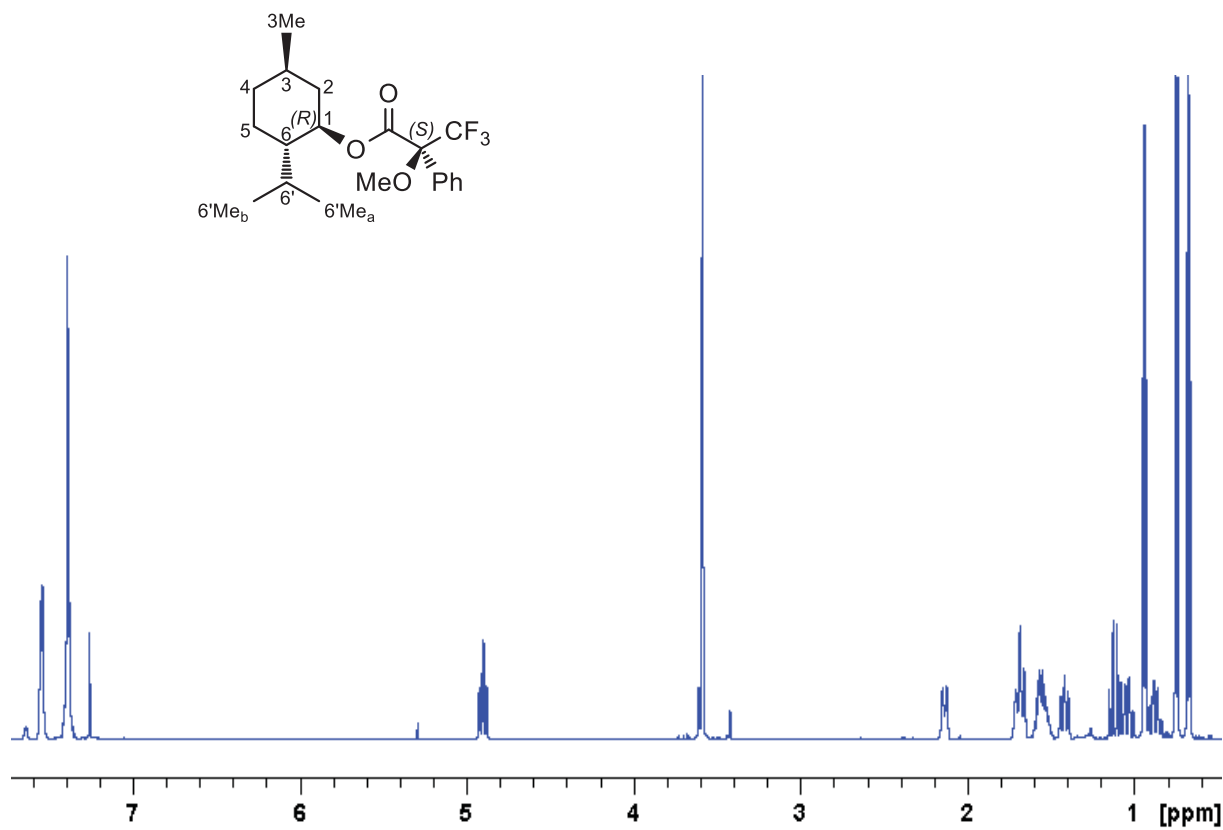
¹H NMR *L*-menthyl-(^{MTPA}*R*)-ester **S9**



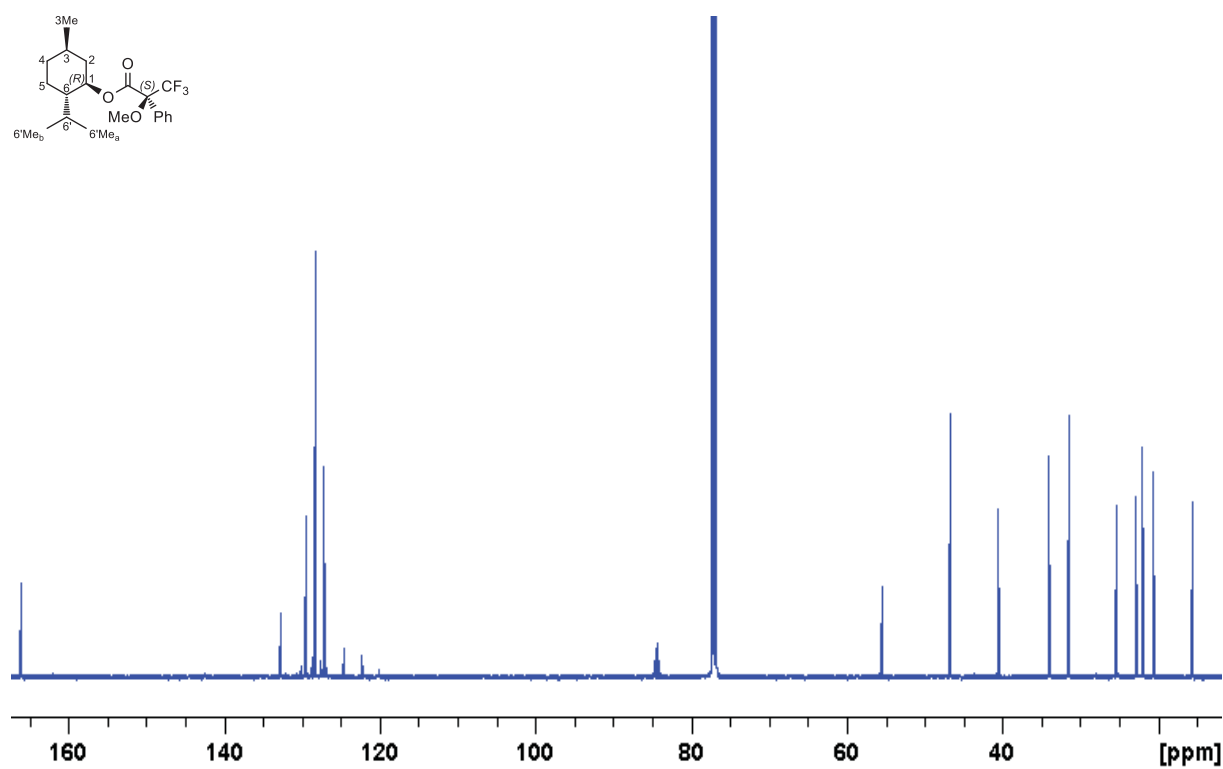
¹³C NMR *L*-menthyl-(^{MTPA}*R*)-ester **S9**



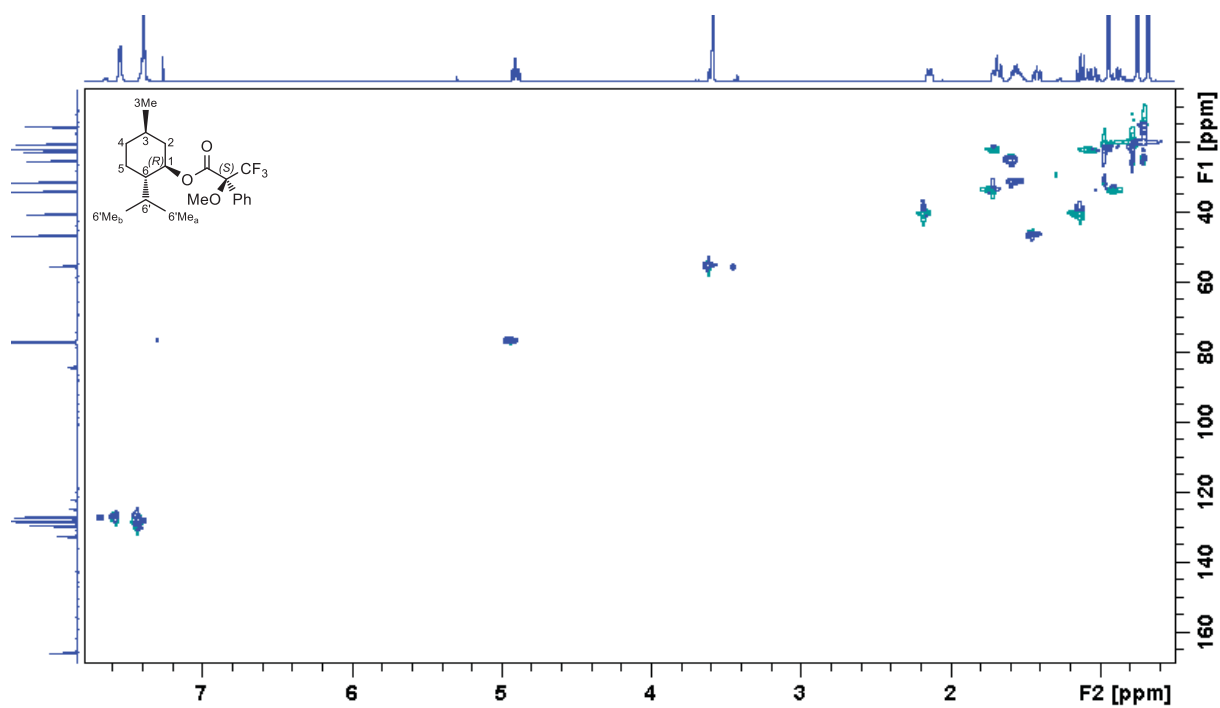
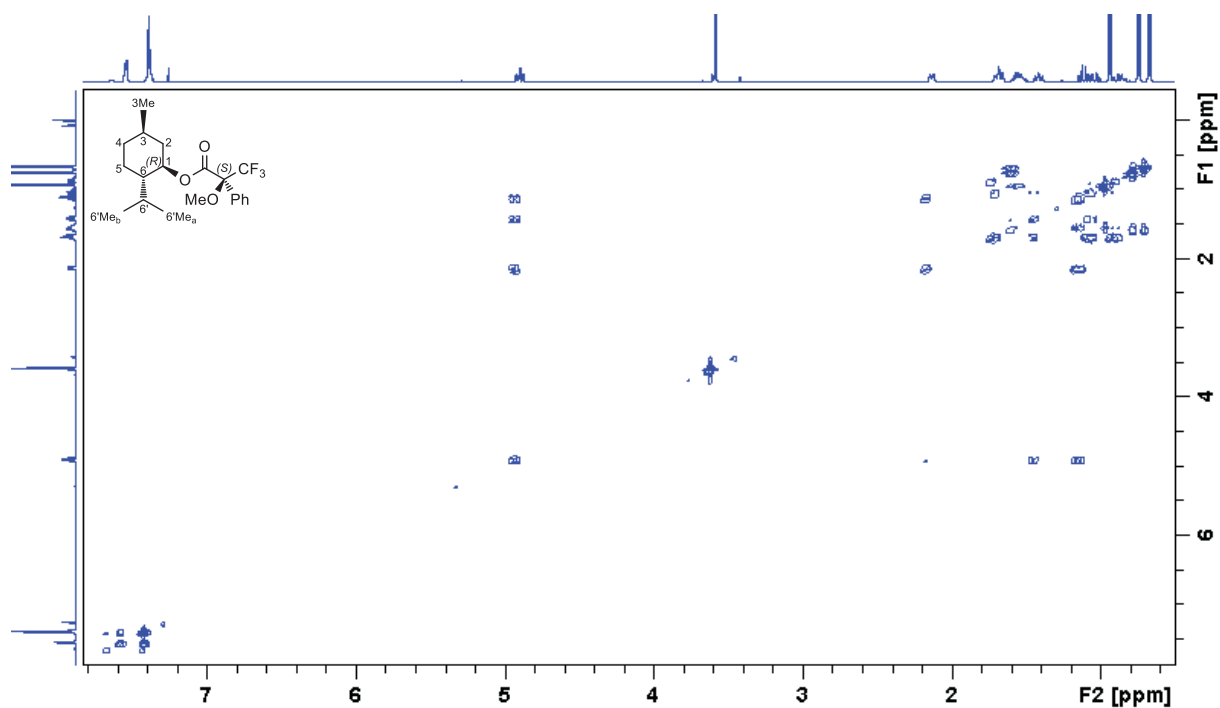


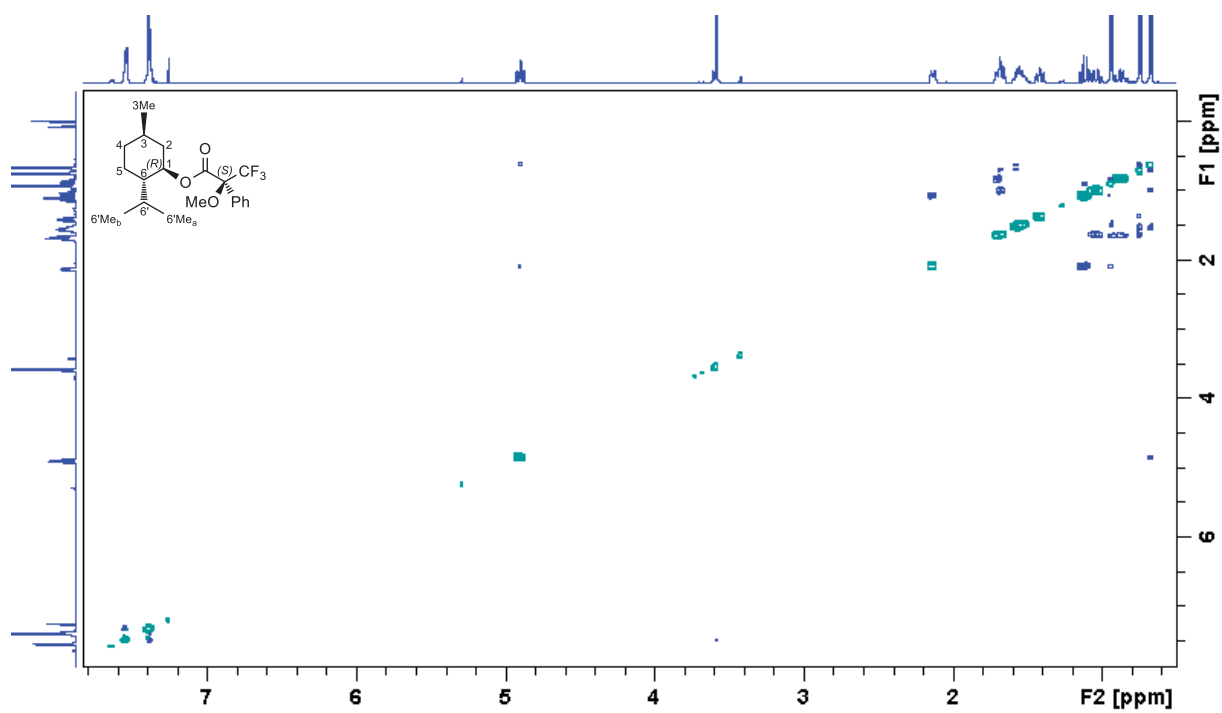
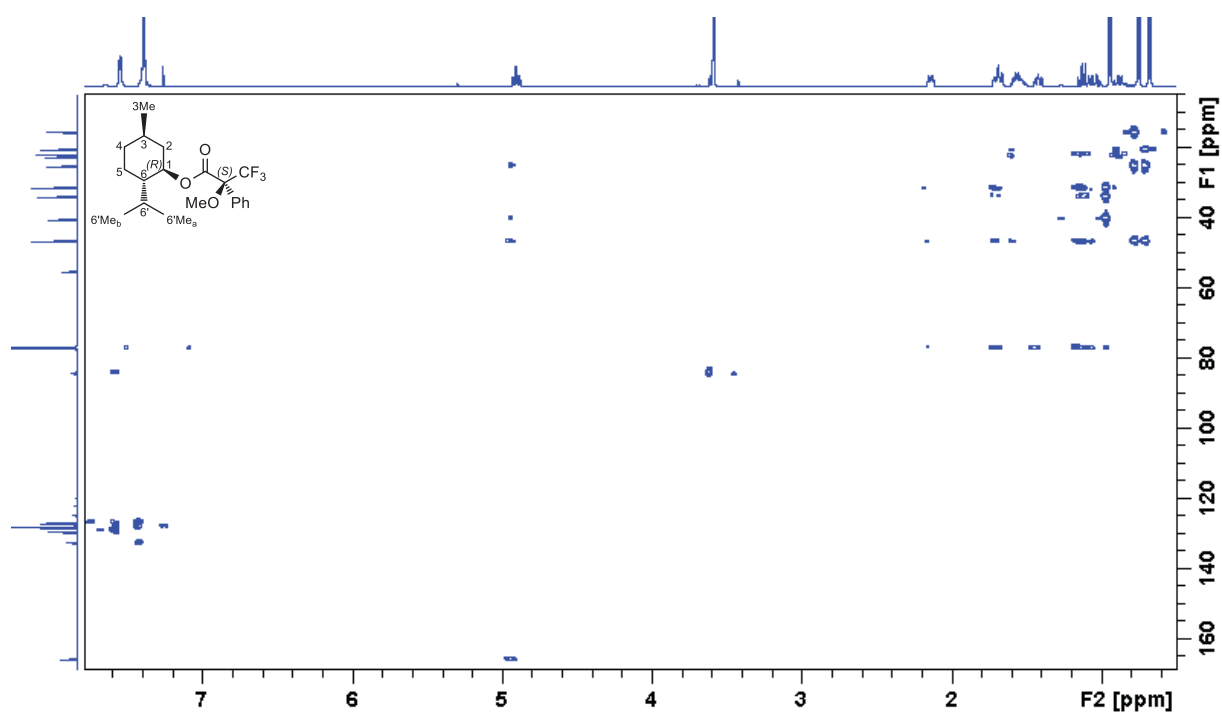


¹H NMR *L*-menthyl-(^{MTPA}*S*)-ester **S9**



¹³C NMR *L*-menthyl-(^{MTPA}*S*)-ester **S9**





References

- [1] T. Ohwada, D. Kojima, T. Kiwada, S. Futaki, Y. Sigiura, K. Yamaguchi, Y. Neshi, Y. Kobayashi, *J Org Chem* **2007**, *72*, 7750-7756.
- [2] T. A. Evans, L. J. Kennedy, *Tetrahedron Lett* 2001, *42*, 7015-7078.
- [3] T. R. Hoye, C. S. Jeffrey and F. Shao, *Nat Protoc* **2007**, *2*, 2451-2458.
- [4] T. Heidt, A. Baro, A. Kohn and S. Laschat, *Chemistry* **2015**, *21*, 12396-12404.
- [5] S. K. Latypov, J. M. Seco, E. Quiñoá, R. Riguera, *J Org Chem* **1996**, *61*, 8569-8577]
- [6] K. Omata, T. Fujiwara, K. Kabuto, *Tetrahedron: Asymm* **2002**, *13*, 1655-1662
- [7] a) J. A. Dale, D. L. Dull, H. S. Mosher, *J Org Chem* **1969**, *34*, 2543-2549; b) G. R. Sullivan, J. A. Dale, H. S. Mosher, *J Org Chem* **1973**, *38*, 2143-2147; c) J. A. Dale, H. S. Mosher, *J Am. Chem Soc* **1973**, *95*, 512-519; d) J. M. Seco, E. Quiñoá, R. Riguera, *Chem Rev* **2004**, *104*, 17-117; e) T. Kusumi, T. Ooi, Y. Ohkubo, T. Yabuuchi, *Bull Chem Soc Jpn* **2006**, *79*, 965-980; f) I. Ohtani, T. Kusumi, Y. Kashman, H. Kakisawa, *J Am Chem Soc* **1991**, *113*, 4092-4096; g) D. P. Curran, B. Sui, *J Am Chem Soc* **2009**, *131*, 5411-5413.

*Baker, M., Protein engineering: Navigating Between Chance and Reason. *Nat. Methods* **2011**, *8*, 623–626.

© Cover image Designed by rawpixel.com / Freepik